Structure and function studies on the Calcitonin Receptor, a Class B1 GPCR

Emma Dal Maso

Bachelor Pharmaceutical Sciences (Hons)

A thesis submitted for the degree of Doctor of Philosophy

September 2017

Monash Institute of Pharmaceutical Sciences

Copyright notice

Table of Contents

ABSTRACT

The calcitonin receptor (CTR) belongs to Class B1 G protein-coupled receptors (GPCRs). The CTR has been identified in several tissues where it has a wide range of physiological roles from bone and calcium homeostasis to cell proliferation and differentiation. In humans, there are at least two common CTR splice variants (CTR_a, CTR_b), that have unique expression patterns in different tissues, and two polymorphisms (a Leu/Pro substitution in the C-terminal tail) have also been identified. The CTR is activated by the calcitonin peptide , a 32 amino acid peptide identified in different species. In addition, an endogenous peptide structurally related to VIP, PHM-27, has been reported to act as an agonist to this receptor. Upon activation, the CTR pleiotropically couples to Gαs, Gαq and also potentially Gαi proteins.

This thesis examines how natural changes in the receptor structure (splice and polymorphic receptor variants) affect intracellular signalling and receptor trafficking, and identifies unique signalling patterns for the different splice variants of the CTR. In addition, constitutive internalisation of the hCTR was demonstrated in multiple cell systems. Furthermore, the availability of multiple ligands and the promiscuous coupling of this receptor allowed for exploration of biased agonism at the CTR. Assessment of three distinct signalling pathways (cAMP formation, calcium mobilisation and ERK1/2 phosphorylation) in presence of multiple ligands for each of the four CTR variants revealed biased agonism exists at the CTR.

To further explore at a molecular level how different agonists engage with the CTR_aLeu variant and how this may be linked to biased agonism, Ala scanning mutagenesis was performed on ECL2, ECL3 and adjacent TMs. For each receptor mutant, ligand affinity and three distinct signalling pathways were assessed and the pharmacology was assessed using advanced analytical models. Results were mapped onto a 3D model of the CTR, identifying distinct networks or residues for driving CTR ligand binding, and additionally, distinct residues that were important for intracellular signalling. The use of five different CTR agonists revealed that each receptor-ligand pair established unique interactions that may, in part, be linked to the observed biased agonism of these ligands. Additionally, comparison of our

results with literature on other Class B1 GPCRs revealed that these key networks are only partially conserved across receptors of this sub-Class.

This thesis extends knowledge of the influence of natural CTR variants on intracellular signalling and provides key insights into networks of residues important for ligand affinity and activation of distinct signalling pathways. This study also highlights that distinct biased CTR agonists differentially engage with the receptor to modulate its function. Despite limited structural similarities, different Class B1 GPCRs engage with the same intracellular signalling effectors (predominantly through Gαs), despite engaging with their ligands in a unique manner. However, the overall profile of signalling differs for different receptors, and even for the same receptor when in complex with distinct ligands. This knowledge could aid rational design of novel therapeutics, and may allow the identification of new biased compounds that selectively target specific signalling outputs that may result in more effective beneficial ligands in terms of physiological outcomes.

GENERAL DECLARATION

In accordance with Monash University Doctorate Regulation 17.2 Doctor of Philosophy and Research Master's regulations the following declarations are made:

I hereby declare that this thesis contains no material which has been accepted for the award of any other degree or diploma at any university or equivalent institution and that, to the best of my knowledge and belief, this thesis contains no material previously published or written by another person, except where due reference is made in the text of the thesis.

This thesis includes 1 original paper published in peer reviewed journals. The core theme of the thesis is "Structure and function studies on the calcitonin receptor, a Class B1 GPCRs". The ideas, development and writing up of all the papers in the thesis were the principal responsibility of myself, the candidate, working within the Department of Pharmacology under the supervision of Denise Wootten, Dr. Sebastian Furness, Prof. Patrick Sexton, and Dr. David Thal.

	Publication title	Publication status	Nature and extent of candidate's contribution
Appendix 2	Ligand-Dependent Modulation of G Protein Conformation Alters Drug Efficacy	Published	Performed experiments 10%

I have not renumbered Sections of submitted or published papers in order to generate a consistent presentation within the thesis.

Student signature: [redacted] **Date:** 21/09/2017

The undersigned hereby certify that the above declaration correctly reflects the nature and extent of the student's and co-authors' contributions to this work. In instances where I am not the responsible author I have consulted with the responsible author to agree on the respective contributions of the authors.

Main Supervisor signature: [redacted] **Date:** 21/09/2017

ACKNOWLEDGEMENTS

First and foremost, I'd like to thank my supervirors. Thanks to Denise for always being present and finding time to help when I needed it most, for showing me the right path but letting me develop my skills independently, and for finding the fun part about my Yoda-like English skills. To Sebastian for always challenging my knowledge and keeping my brain fit. To Patrick for his constant guidance, for reminding me to always consider the bigger picture, and for the opportunity to be part of his group. Thanks to David for showing me that science is also fun.

Thanks to Yue Zhu for her invaluable contribution towards this project, and to Prof. Christopher Reynolds for the almost immediate delivery of a 3D modelling of CTR. Thanks to everyone at MIPS, especially the people from DDB, which in one way or another have had an impact on this project. Thank you all for the endless hours spent in and out of the lab, and for making this whole experience unforgettable. I would also like to thank Mark Wheatley and his lab for the opportunity to visit their lab and sharing their knowledge and enthusiasm.

Thanks to my family and friends, near and far, for always being there. A special thank you to the "hens of the coop" for their unwavering presence through good and bad times.

One final thank you to Monash for this fantastic opportunity, and more importantly to the taxpayers for providing the financial support that kept me and this project running.

PUBBLICATIONS AND COMMUNICATIONS

Peer reviewed articles

Furness, S.G.B., Liang, Y.L., Nowell, C.J., Halls. M.L., Wookey, P.J., **Dal Maso, E.**, Inoue, A., Christopoulos, A., Wootten, D. AND Sexton, P.M. (2016). *Ligand-Dependent modulation of G Protein conformation alters drug efficacy.* Cell 167, 739–749. (Appendix 2)

Published abstracts

Emma Dal Maso, Sebastian Furness1, Denise Wootten1, Patrick Sexton. (2014). *Functional expression of modified calcitonin receptor in nanodiscs for biophysical measurements of family B GPCR conformational changes.* Poster presentation. Molecular Pharmacology of G Protein Coupled Receptors (MPGPCR) meeting. Melbourne, Australia.

Dal Maso, E., Furness, S.G.B., Thal, D., Sexton, P.M., and Wootten, D. (2015). *Characterisation of signalling and regulation of common calcitonin receptor splice variants and polymorphisms.* Poster presentation. GPCR workshop. Hawaii, USA.

Dal Maso, E., Furness, S.G.B., Thal, D., Sexton, P.M., and Wootten, D. (2016). *Characterisation of signalling and regulation of common calcitonin receptor splice variants and polymorphisms.* Poster presentation. Molecular Pharmacology of G Protein Coupled Receptors (MPGPCR) meeting. Melbourne, Australia.

Invited seminars

Dal Maso, E., Furness, S.G.B., Thal, D., Sexton, P.M., and Wootten, D. (2016). *Characterisation of signalling and regulation of common calcitonin receptor splice variants and polymorphisms.* Pharmacogenomics Special Interest Group Workshop, Molecular Pharmacology of G Protein Coupled Receptors (ASCEPT-MPGPCR) meeting. Melbourne, Australia.

ABBREVIATIONS

9E10	Anti-Myc antibody
α	Intrinsic activity
β_2AR	Beta 2 adrenergic receptor
Δ(1-47)CTR	Calcitonin receptor lacking the first 47 at the N-terminus residues
ε	Intrinsic efficacy
A_{2A}R	Adenosine A2A receptor
ACTH	Adrenocorticotropic hormone
AF	Alexa Fluor dye
AM	Adrenomedullin
AMY	Amylin receptor
Amy	Amylin peptide
ANOVA	Analysis of variance
ATP	Adenosine triphosphate
AT1R	Angiotensin 1 receptor
BEN	Human lung cancer cells
B_{max}	Receptor density
Bpa	p- benzoyl-L-phenylalanine
BSA	Bovine serum albumin
BRET	Bioluminescence resonance energy transfer
CALCR	Calcitonin receptor protein coding gene
cAMP	3’,5’-cyclic adenosine monophosphate
cCT	Chicken calcitonin peptide
CGRP	Calcitonin-like receptor peptide
CHO	Chinese hamster ovary cells
CLR	Calcitonin-like receptor
COS-7	Monkey kidney tissue fibroblast-like cell
CRFR	Corticotrophin-releasing hormone receptors
cpm	Counts per minute
CREB	cAMP response element-binding protein
CTR	Calcitonin receptor
CV-1	Cercopithecus aethiops kidney cells
DAG	Diacylglycerol
DMEM	Dulbecco’s modified eagle medium
ECL	Extracellular loop
EM	Electron microscopy
EMA	European Medicines Agency
E_{max}	Maximal response
ER	Endoplasmic reticulum
Epac	Exchange protein directly activated by cAMP
ERK	Extracellular signal–regulated kinase
Eu-SA	Europium-streptavidin
FBS	Foetal bovine serum
FDA	US Food and Drug Administration
Forskolin	(3*R*,4a*R*,5*S*,6*S*,6a*S*,10*S*,10a*R*,10b*S*)-6,10,10b-Trihydroxy-3,4a,7,7,10a-pentamethyl-1-oxo-3-vinyldodecahydro-1*H*-benzo[*f*]chromen-5-yl acetate
FRET	Förster resonance energy transfer

Gα	Alpha (α) subunit of the G-protein heterotrimer
Gαi	Adenylyl cyclase inhibitor G-protein heterotrimer
Gαq	Phospholipase C activating G-protein heterotrimer
Gαs	Adenylyl cyclase activating G-protein heterotrimer
Gβγ	Beta (β) and gamma (γ) subunits of the G-protein heterotrimer
GCGR	Glucagon receptor
GHRHR	Growth hormone releasing hormone receptor
GIPR	Gastric inhibitor peptide receptor
GLP	Glucagon-like peptide
GLP-1R and GLP-2R	Glucagon-like peptide 1 and 2 receptors
GPCR	G protein-coupled receptor
GRAFS	Glutamate, rhodopsin, adhesion, frizzled/taste2, and secretin classification system
GRK	G protein-coupled receptor kinase
GDP	Guanosine diphosphate
GEF	Guanine-nucleotide exchange factor
GIRK	G protein-coupled inwardly-rectifying potassium channel
GTP	Guanosine triphosphate
HBSS	Hank's balanced salt solution
hCT	Human calcitonin peptide
Hx8	C-terminus α-helix 8
CTR	Calcitonin receptor
$hCTR_a$, CTR_{I1-}, $hCTR_2$ or hCT_a	Human calcitonin receptor variant, lacking a 16 amino acid insertion in the first intracellular loop (ICL1)
$hCTR_b$, CTR_{I1+}, $hCTR_1$, hCT_b	Human calcitonin receptor variant, including a 16 amino acid insertion in the first intracellular loop (ICL1)
IBMX	3-isobutyl-1-methylxanthine
$_iCa^{2+}$	Intracellular calcium
ICL	Intracellular loop
IP_1	Inositol-1-phosphate
IP_3	Inositol-3-phosphate
LOI	Line of identity
M3 mAChR	Muscarinic receptor subtype 3
MAPK	Mitogen-activated protein kinase
MCF7	Human breast cancer cells
NF-κB	Nuclear factor
NMR	Nuclear magnetic resonance spectroscopy
NTD	N-terminus domain
OCL	Osteoclasts-like cells
PACAP	Pituitary adenylate cyclase-activating peptide
pCT	Porcine calcitonin peptide
PACAPR	Pituitary adenylate cyclase-activating polypeptide receptor
PCR	Polymerase chain reaction
PDB	Protein Data Bank
PDZ	Discs-large homologous domain
pEC_{50}	Half maximal effective concentration
PFA	Paraformaldehyde
PHM-27	Human peptide histidine-methionine 27
PI_1	Inositol 1 phosphate
PI_3	Phosphatidylinositol (3,4,5)-trisphosphate

PI3K	Phosphoinositide 3-kinase
PIP_2	Phosphatidylinositol 4,5-bisphosphatecAMP response element-binding protein
pK_A	Functional affinity, derived from operational model of agonism
PKA	Protein kinase A
PKC	Protein kinase C
pK_i	Equilibrium affinity defined by competition radioligand binding
PLC	Phospholipase C
PLD	Phospholipase D
PTX	Pertussis toxin
PTH	Parathyroid hormone
R*	Active form of receptor
R*E	Active form of receptor coupled to an effector
Raf	Mitogen-activate protein kinase
RAMP	Receptor activity-modifying protein
ROX	Carboxy-X-rhodamine
rAmy	Rat amylin peptide
rCT	Rat calcitonin peptide
sAC	Soluble adenylyl cyclase
sCT	Salmon calcitonin peptide
SCTR	Secretin receptor
SNP	Single nucleotide polymorphism
TIP39	Tuberoinfundibular peptide
TM	Transmembrane domain of GPCR
tmAC	Transmembrane adenylyl cyclase
VIP	Vasoactive intestinal peptide
VPACR	Vasoactive intestinal peptide receptors
V2R	Vasopressin V2 receptor
WT	Wild type

CHAPTER 1

General introduction

1.1 G protein-coupled receptors (GPCRs)

1.1.1 General introduction

G Protein-Coupled Receptors (GPCRs) are the largest family of integral membrane proteins in eukaryote genome (Bjarnadottir et al., 2006, Fredriksson et al., 2003, Takeda et al., 2002, Venter et al., 2001). In humans, the family consists of 826 receptors that can recognise diverse ligands including ions, pheromones, light-sensitive compounds, odours and molecules connected to taste, neurotransmitters, hormones and other small molecules, small peptides and even large proteins and fatty acids (Lagerstrom and Schioth, 2008). With such a plethora of stimuli involved, GPCRs can be found in all organs and tissues regulating a multitude of physiological functions, making them important therapeutic targets. Currently they are the target for over 30% of the drugs on the market (Rask-Andersen et al., 2014, Overington et al., 2006, Tyndall and Sandilya, 2005).

1.1.2 Classification of GPCRs

Despite low overall sequence homology, GPCRs can be phylogenetically grouped into 5 Classes (or Families) that form the GRAFS classification system (Glutamate, Rhodopsin, Adhesion, Frizzled/Taste2 and Secretin) (*Figure 1.1.**1***) (Fredriksson et al., 2003), or A to F in the Kolakowski system (Kolakowski Jr, 1993). Both classifications are based solely on the transmembrane (TM) core of the protein, without taking into account the N-termini or the C-termini.

Rhodopsin-like receptors (or Class A in the A-F classification) comprises approximately 80% of all GPCRs. Receptors of this class bind biogenic amines, neurotransmitters, fatty acids, chemokines, neuropeptides, opioids, light sensitive compounds, olfactory and several other small molecules (reviewed in (Wolf and Grunewald, 2015, Attwood and Findlay, 1994)).

Secretin-Family receptors (also known as Class B1) are an evolutionarily ancient group that arose prior to the most recent common metazoan ancestor (de Mendoza et al., 2014). The 15 members that constitute this family in human, are involved in the physiology and pathophysiology of cardiovascular system function, bone homeostasis, glucose regulation, satiety and food intake, migraine, depression, stress and anxiety (summarised in (Culhane et al., 2015, Harmar, 2001)). Receptors belonging to this

class are characterised by a large extracellular N-termini and are activated by endogenous peptides (Harmar, 2001).

Adhesion receptors (or Class B2) share limited sequence similarities with secretin-like receptors and are characterised by a very large extracellular N-termini which contain several domains known to facilitate matrix and cell to cell interactions (Hamann et al., 2015, Pisegna et al., 1996).

Metabotropic glutamate/pheromone group (or Class C) receptors comprise receptors for taste, glutamate, calcium and GABA, and play a major role in the nervous system. These receptors form obligate dimers and contain several distinct features, including a cysteine rich domain that connect the TMs to the N-termini, and a large extracellular N-terminal domain often referred to as the Venus Fly Trap domain (VFT). It is the latter that binds the orthosteric ligand (Hampson et al., 2008, Cao et al., 2009).

Frizzled/smoothened receptors (or Class F) are involved in cell proliferation, migration and polarity, and development of tissues and organs in both embryos and adult. This class is the least studied, with limited information known about these receptors (reviewed (Huang and Klein, 2004, Schulte and Bryja, 2007, Schulte, 2010)).

To date, endogenous ligands for over 140 GPCRs, referred to as orphans, have yet to be identified (Civelli et al., 2013). Thus the physiological role for most of these receptors, which are spread across all the different GPCR Classes, remains unknown.

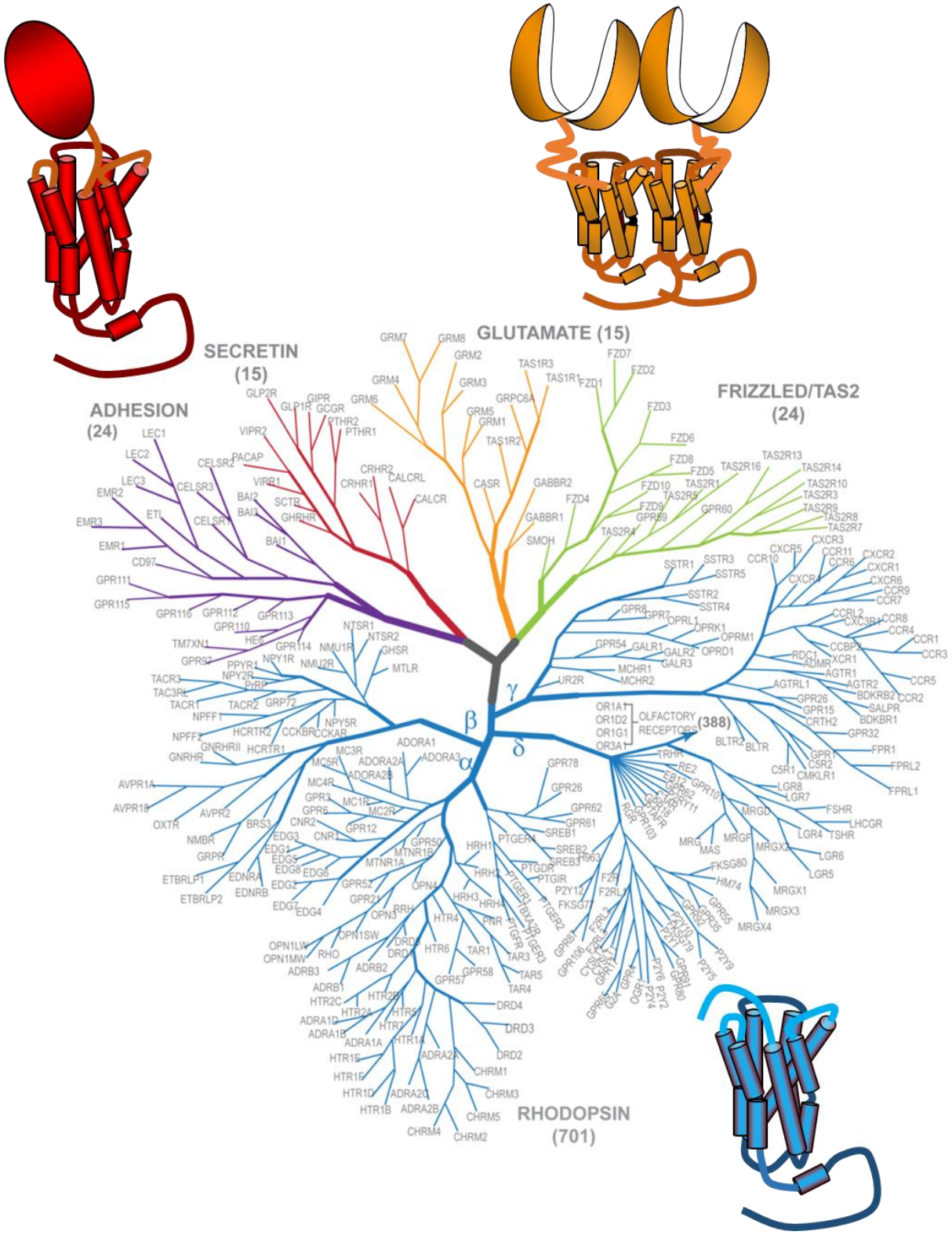

Figure 1.1 Phylogenetic tree representation of GPCRs using the GRAFS system, from original work of Fredriksson et al. (2003) and modified by Stevens et al. (2013)*. At the bottom right (blue) the cartoon representing a rhodopsin-like Class A GPCR. At the top left (red) the cartoon of a secretin-like receptor, Class B1 with the characteristic large extracellular N-terminus. At the top right the representation of glutamate Class C (orange), obligate dimers with the Venus fly trap domain at the N-termini.*

1.2 Structure-function of GPCRs

1.2.1 Structure and activation

All GPCRs share common structural features, including an extracellular N-terminus of varied length, 7 transmembrane spanning α-helices (TM1-TM7) tightly organised in a bundle and connected by alternating loops, 3 intracellular (ILC1, ICL2 and ICL3) and 3 extracellular (ECL1, ECL2 and ECL3), and an intracellular C-terminus that may also include an additional amphipathic α-helix (Rosenbaum et al., 2009).

Numerous biophysical and biochemical methods extensively applied to Class A GPCRs have highlighted specific arrangement of the TM domain, confirming predictions that the ligands interact with their receptors between the juxta membranous region and the upper portion of the TM bundle (Rasmussen et al., 2011a, Rasmussen et al., 2011b). Additionally, these studies revealed that receptor activation via ligand engagement triggers substantial structural rearrangements at the intracellular face of GPCRs that promote specific interactions between receptor and effectors (Kobilka, 2013). These include canonical interactions with guanine-nucleotide binding proteins (G proteins), but also G protein-coupled receptor kinases (GRK) and β-arrestins. In 1996, Zn^{2+}-crosslinking investigated the regions involved in the activation of rhodopsin, identifying relative movements of TM3 and TM6 (Sheikh et al., 1996) to transition from an inactive receptor to an active state. A similar observation was made through cysteine cross-linking and electron paramagnetic resonance by Farrens *et. al*. (1996). In addition, cysteine-crosslinking studies confirmed that similar movements occur in the muscarinic receptor subtype 3 (M3 mAChR), showing that full agonist binding resulted in a change of TM6 orientation (Ward et al., 2006) with TM5 moving closer to TM6 (Ward et al., 2002) and movements of the outward face of TM7 towards TM3 in regions that were within close proximity to the orthosteric binding pocket (Han et al., 2005). These relative rearrangements are further supported by NMR studies (Kim et al., 2013, Nygaard et al., 2013). Other approaches involved the use of environmentally sensitive probes that can selectively label accessible residues or groups in a protein structure. The fluorescence emission of these compounds depends on the polarity of the environment surrounding the probe and

provided information about proximity of residues in helices (Gether et al., 1995, Gether et al., 1997, Dunham and Farrens, 1999, Jensen et al., 2001, Ghanouni et al., 2001, Yao et al., 2006, Yao et al., 2009). In the past decade, numerous crystal structures have been solved providing information on structural features of these receptors in their different states of activation. However, GPCRs are highly dynamic proteins and these structures represent a small proportion (the most stable) of the ensemble of conformations that these receptors can adopt. 211 GPCR crystal structures are currently available, covering approximately 45 GPCRs. The majority of these belong to the largest and most studied Rhodopsin, Class A GPCR subfamily. Of these, majority receptors have been crystallized bound to inverse agonists or antagonists in their inactive conformations, while only few receptors have also been refined in complex with agonists to give insight into partly and fully active conformations. In 2008, a partially active structure of opsin was also resolved in complex with a fragment of a G-protein α-subunit (Scheerer et al., 2008). In 2011 the partially active structure of A2 adrenergic receptor (A_{2A}-R) was crystallised in complex with an agonist (Lebon et al., 2011). The same year, the agonist-bound β2-adrenergic receptor (β2A-R) in complex with a nanobody, that mimics a G protein, supplied the first fully active conformation of a GPCR in complex with an effector (Rasmussen et al., 2011a). In 2013, the crystal structure of the fully active ternary complex of β2-adrenoreceptor, in complex with its agonist and a nucleotide free Gαs heterotrimer, provided insight into structure of a fully active conformation (Ring et al., 2013). In 2015, rhodopsin was solved in complex with another effector (β-arrestin) (Kang et al., 2015), and in 2017 two Class B1 GPCR were solved with heterotrimeric Gαs protein (Zhang et al., 2017b, Liang et al., 2017).

1.2.2 G protein dependent signalling

GPCRs are very versatile signalling proteins that can modulate the activity of more than one intracellular effector. These receptors couple to G proteins, with many having the ability to interact to multiple different types of G proteins. Receptor activation and coupling to the G protein heterotrimer (α, β and γ subunit) leads to a rearrangement of the G protein structure (Janz and Farrens, 2004), exchange of GDP for GTP at the α subunit of the G-protein (Oldham and Hamm, 2008), promoting either dissociation of the α subunit from the βγ heterodimer (Lambright et al., 1994) or sufficient

rearrangement of the αβγ heterotrimer to allow downstream effector engagement (Bunemann et al., 2003) (***Figure 1.2***). Both α and βγ complex regulate the activity of various secondary effectors (***Figure 1.3***). Termination of the stimuli occur when the GTP bound to the G_α subunit is hydrolysed to GDP. This promotes conformational rearrangements in the G_α subunit and the re-association of the βγ dimer (***Figure 1.2***).

Multiple Gα subunits have been cloned, and these govern distinct signalling pathways. These can be broadly grouped into four main families that primarily differ in their C-terminus sequence. This sequence is the primary is the primary region that interacts with GPCRs, and is the major contributor to receptor selectivity. The Gαs family acts to activate transmembrane adenylyl cyclase (tmAC), which converts ATP into cAMP (Sunahara et al., 1996). The increase in intracellular cAMP activates protein kinase A (PKA) and exchange protein directly activated by cAMP (Epac) (Cheng et al., 2008), which in turn regulate ion channel opening (Scheuer, 2011), sugar and lipid metabolism (Rui, 2014), promote formation of cell junction (Kooistra et al., 2007, Fukuhara et al., 2005), cell adhesion (De Rooij et al., 1998, Rangarajan et al., 2003, Qiao et al., 2002, Bos et al., 2003), exocytosis and secretion of neurotransmitters, hormones and other biologically active molecules (Hatakeyama et al., 2007), and activate cAMP response element-binding protein (CREB) that modulates gene transcription (Shaywitz and Greenberg, 1999). Gαi/o proteins inhibit tmAC activity and decrease intracellular cAMP production (Taussig et al., 1993). Additionally Gαi proteins activate the Src- family tyrosine kinases (Src) (Ma et al., 2000) and control gene transcription, cell differentiation, proliferation and survival (Stork and Schmitt, 2002, Thomas and Brugge, 1997). Gαq/11 regulates Ca^{2+} entry and phospholipase C (PLC) activity (Rhee and Choi, 1992, Macrez-Leprêtre et al., 1997), that catalyses the conversion of phosphatidylinositol (PIP_2) into diacylglycerol (DAG) and inositol 1,4,5-triphosphate (IP_3) (Axelrod et al., 1988); DAG remains within the membrane while IP_3 diffuses through the cytosol and binds to calcium channels (known as IP_3 receptors) on the endoplasmic reticulum (ER) to stimulate release of calcium from intracellular stores. Both Ca^{2+} and DAG activate protein kinase C (PKC) (Nishizuka, 1992, Nishizuka, 1995), which in turn influences gene expression, cell secretion, proliferation and immune response via activation of nuclear factor (NF-κB) and mitogen-activated protein kinase

(MAPK) pathways (Ueda et al., 1996, Moscat et al., 2003). Gα12/13 controls cell cytoskeleton remodelling and regulates cell migration through the activation of Rho guanine-nucleotide exchange factors (GEFs) (Kozasa et al., 1998, Hart et al., 1998).

The βγ dimer is also important for signalling: the complex comprises one of the five isoforms of Gβ subunit and one of the 12 isoforms of the Gγ, and is tethered to the plasma membrane through prenylation at the C-termini of the Gγ subunit. The dissociation from the G_{α} subunit allows the βγ-complex to directly interact with AC, inwardly rectifying K^{+} channels (GIRKs) and Ca^{2+} channels, GPCR kinase 2 and 3 (GRK2/GRK3), multiple isoforms of PLC_{β}, phosphoinositide 3 kinase γ ($PI3K_{\gamma}$) and activation of MAPK pathways (Pitcher et al., 1992, Boyer et al., 1992, Camps et al., 1992, Smrcka and Sternweis, 1993, Stephens et al., 1994, Ikeda, 1996, Smrcka, 2008, Sunahara et al., 1996, Wickman et al., 1994, Clapham and Neer, 1993). Additionally, depending on which isoforms of the two subunits constitute the βγ complex, the βγ dimer can mediate additional, selective downstream responses (Smrcka, 2008).

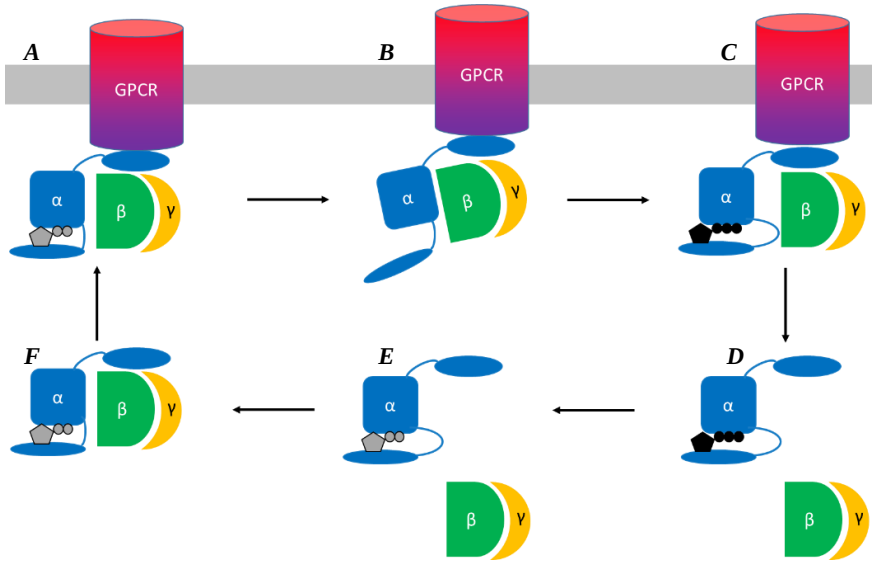

Figure 1.2 G protein activation cycle. *(A) Activation of a GPCR causes conformational changes in the receptor that reveal the binding pocket for GDP-bound G protein. (B) Interaction with the receptor causes rearrangement of the G_α subunit of the G protein that promotes release of GDP and binding of GTP (C). Binding of GTP causes further rearrangement in the G protein subunits that leads to the dissociation of the GTP- bound G protein from the receptor (D). Additionally, the conformational changes due to the presence of GTP in the α subunit can also promote dissociation from the βγ dimer. In both cases (GTP-αβγ trimer, or GTP- α subunit and βγ dimer) the GTP-bound G protein is now in its active conformation and is capable of activating secondary effectors. (E) G_α subunit inherent GTPase activity hydrolyses GTP to GDP, terminating the signal and promoting re-association of βγ dimer into the inactive GDP-bound αβγ G protein heterotrimer (F).*

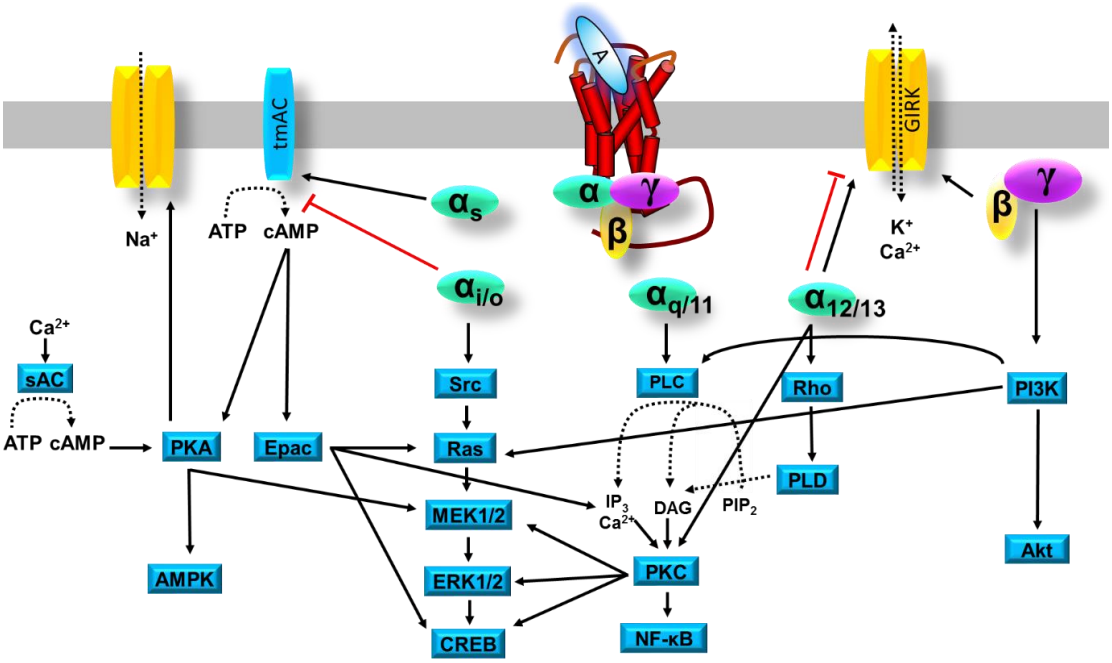

Figure 1.3 Schematic representation of the signalling pathways downstream of G protein activation caused by interaction with GPCRs*. Gαs family activates transmembrane adenylyl cyclase (tmAC), to generate cAMP, which regulates the activity of protein kinase A (PKA) and exchange protein directly activated by cAMP (Epac). PKA activates ion channels and AMP kinases to regulate energy homeostasis, whilst both PKA and Epac can both regulate MAP kinase (MAPK) pathways and control gene regulation, cell survival, metabolism and motility. Gαi/o family inhibits tmAC, while it can also active MAPK pathways. Both Gαq/11 and Gα12/13 can control protein kinase C (PKC) activity; the former through the activation of phospholipase C (PLC), the latter through activation of phospholipase D (PLD). Downstream of PKC are MAPK and nuclear factor (NF-κB) that regulate immune response, gene expression and cell remodelling. Gα12/13 also regulate the activity of Rho, which regulates the cytoskeleton, and is thus upstream of cell shape and motility. Additionally Gα12/13 can control the activity of inwardly rectifying K^+ channels (GIRKs) and Ca^{2+} channels. Similarly βγ dimer can act on GIRK as well as AC, PLC_β, $PI3K_\gamma$ and MAPK.*

1.2.3 GPCR internalisation and regulation

Multiple mechanisms are involved in modulating the intensity and duration of GPCR cellular responses; these include desensitisation, internalisation, degradation and downregulation. The fastest mechanism of modulation is desensitization, which involves uncoupling of the receptor from its intracellular effectors and may take place within seconds from the application of a stimuli. Internalization occurs within minutes and employs scaffolding proteins to remove receptors from the cell surface and segregate them into intracellular compartments (Ferguson, 2001). Once inside the cell, the receptor may initiate signalling from intracellular compartments (Calebiro et al., 2010), can be degraded in lysosomes, or be recycled to the cell surface for sequential rounds of activation (Dale et al., 2004). Downregulation of receptors can be achieved by degradation of existing protein, reduction of trafficking of receptors to the plasma membrane, or diminished protein or mRNA synthesis.

1.2.4 GPCR desensitisation mechanisms

Two independent mechanisms of desensitization can modulate GPCR signalling (Kelly et al., 2008, Ferguson, 2001) (*Figure 1.4*).

Heterologous desensitization refers to the loss of response of GPCRs (either ligand-bound or in their apo form), caused by the activation of a different receptor, through either direct receptor phosphorylation or to changes in downstream signalling events (Steele et al., 2002). Stimuli that increase intracellular cAMP or diacylglycerol have the potential to activate protein kinases, such as PKA (Benovic et al., 1985, Hausdorff et al., 1990, Clark et al., 1988) or PKC (Murthy et al., 2000); these can phosphorylate the intracellular domain of an apo GPCR to reduce the coupling of G protein to that receptor and terminate its ability to signal.

Homologous desensitization occurs at an activated receptor, whereby a ligand-bound GPCR is phosphorylated at threonine or serine residues within its intracellular face by GRKs (Freedman and Lefkowitz, 1995, Gurevich et al., 2012). This phosphorylation produces high affinity sites for scaffolding proteins, such as β-arrestin1 or β-arrestin2, which translocate from the cytosol to the plasma membrane. Interaction with the receptor promotes conformational change within β-arrestin, exposing

binding sites for clathrin and AP-2 adaptor complex at the C-terminus of β-arrestin that initiates the internalization processes (reviewed by (Gurevich and Gurevich, 2013)). Homologous desensitization not only allows the cells to tune G protein dependent signalling by reducing the number of receptors at the plasma membrane available for interaction with ligand, but can also have an effect on gene transcription, apoptosis and cell motility, as scaffolding proteins such as β-arrestins can also act as signalling effectors (Lefkowitz and Shenoy, 2005, Luttrell and Gesty-Palmer, 2010).

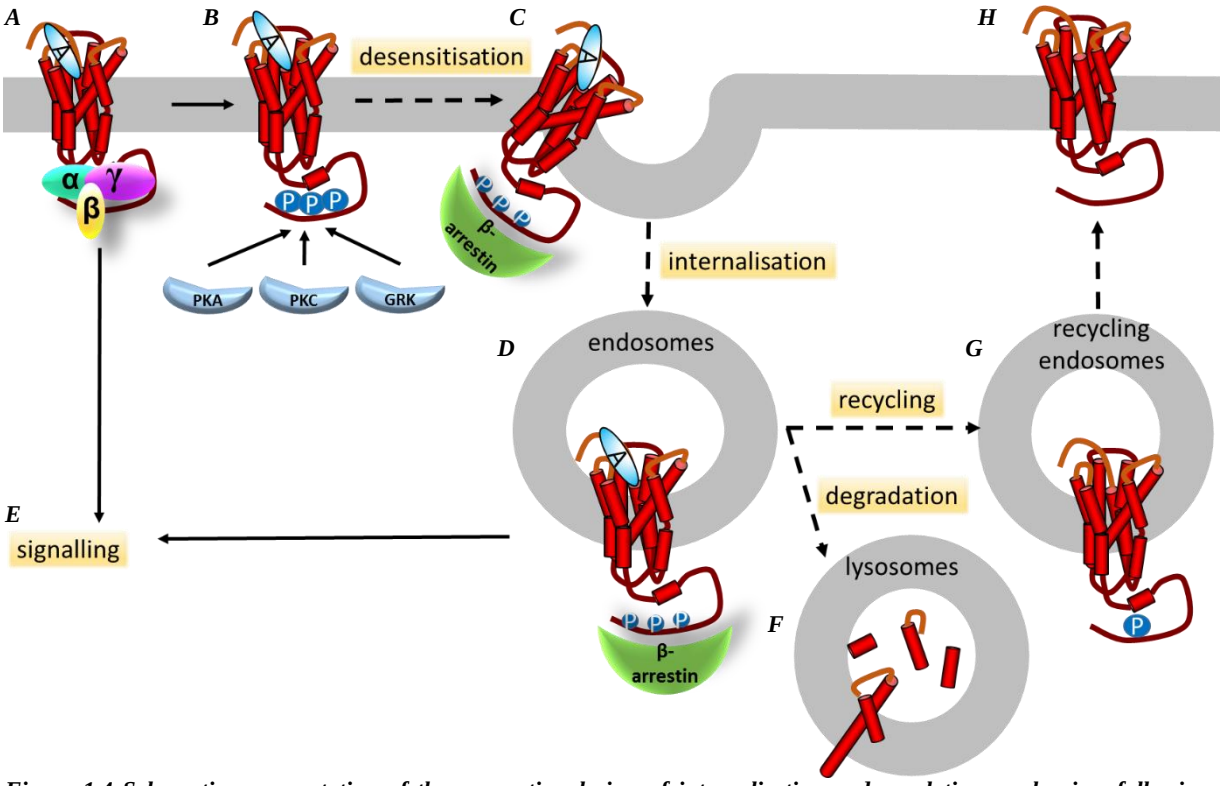

Figure 1.4 Schematic representation of the conventional view of internalisation and regulation mechanism following GPCR activation. *(A) A GPCR binding an agonist A recruits G protein and triggers intracellular signalling. (B) GPCR can be phosphorylated by GRK (homologous desensitisation) or PKA/PKC (heterologous mechanism). (C) This causes uncoupling and termination of G protein dependent signalling and exposes high affinity sites for β-arrestins. (D) The coupling of the latter promotes internalisation of the receptor into endosomal compartments. Recent data reveal GPCRs can also signal from these intracellular compartments (E). Internalised receptors can be then sorted toward lysosome for degradation (F) or uncoupled from the extracellular stimuli (G) and recycled to the cell surface (H) for further activation from the ligand.*

1.2.5 G protein independent signalling

It is becoming increasingly evident that, in addition to performing regulatory functions, a ligand bound-GPCR-β-arrestin complex is also able to independently signal through multiple mechanisms, including promotion of phosphorylation of MAP kinases such as ERKs (Luttrell et al., 2001), c-Jun N-terminal kinase 3 (JNK3) and several other proteins such as phosphatases, ubiquitin ligases and transcription factors (Luttrell and Gesty-Palmer, 2010, DeWire et al., 2007). The intensity and duration of this signalling cascade can also depend on the strength of the interaction between receptor and the adaptor protein: β-arrestin1 and 2 can make either transient or stable interactions with a GPCR, causing distinct conformational changes in the arrestin structure, that can lead to specific downstream signalling via distinct interactions of these scaffolding β-arrestin proteins with numerous signalling molecules (Lee et al., 2016a).

1.2.6 Biased agonism

GPCRs are highly dynamic structures that can shift between multiple conformations. Distinct ligands can interact with the same GPCR and stabilise distinct ensembles of receptor conformations with each different conformational state of the receptor modulating affinity and activation for different effectors (Kim et al., 2013). Thus a ligand, through the stabilisation of distinct receptor conformations, has the potential to promote differential activation of effectors promoting distinct signalling profiles (***Figure 1.5***). This phenomenon is called ligand-directed signalling bias or biased agonism (Kenakin, 2011, Kenakin and Christopoulos, 2013).

There are many examples of different ligands acting at the same GPCR that produce a unique signalling fingerprint. One of the first examples reported was PAC1R, where PACAP(1-38) peptide is more potent than PACAP(1-27) in cAMP production, whereas the opposite is true in IP production (Spengler et al., 1993). Since then, examples of biased agonism have been reported for many different GPCRs of all classes, and this includes differential engagement and activations of G protein subtypes as well as β-arrestins (Bologna et al., 2017, Rajagopal et al., 2010).

The concept of signalling bias is extremely important when we consider the physiological implication of the simultaneous activation of multiple signalling pathways. Theoretically, activation of one effector pathway could lead to beneficial effects that are desirable in therapy (***Figure 1.5, signal 1***), whereas the activation of a second pathway could translate into side effects (***Figure 1.5, signal 2***). In this scenario, a ligand that can specifically activate the signalling pathways leading to beneficial effects, while inhibiting, or sparing, those that elicit adverse effects would be an exemplary therapeutic compound. Some examples of this can be found for the β_2AR and angiotensin II type 1 receptor (AT1-R) where agonists that specifically activate the β-arrestin pathways over the G protein axis produce cardio protective effects (Galandrin et al., 2016, Noma et al., 2007, Kim et al., 2008, Whalen et al., 2011).

To design better therapeutics it is therefore of extreme importance to understand, for a defined receptor, which pathway activation profile leads to beneficial effects or adverse ones, and what structural determinants give rise to this biased agonism.

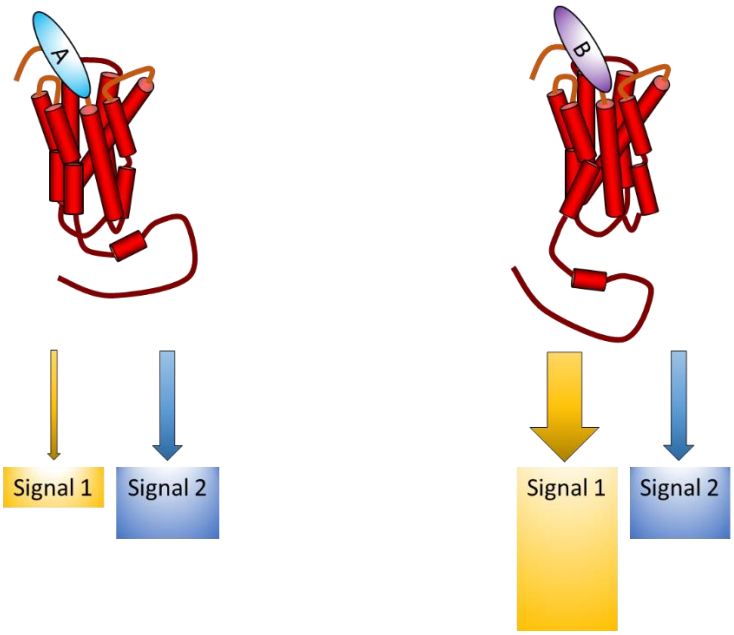

Figure 1.5 Schematic representation of biased agonism. *GPCR (represented in red) can pleiotropically couple to more than one intracellular effector and trigger multiple cellular responses (signal 1 and 2). Distinct ligands (A and B) have the potential to modulate the efficacy of coupling of the receptor to the effectors (arrows), and control the physiological outcome of a specific GPCR activation.*

1.3 Drug-receptor theory and pharmacological quantification of efficacy using operational models

1.3.1 Drug-receptor theory

In 1957 Del Castillo & Katz (Del Castillo and Katz, 1957) described a mechanism of action for ion channels (later applied to receptors) by combining enzyme theory, whereby an enzymatic reaction requires the formation of substrate-enzyme complex to proceed, with their observations that ion channels could bind several compounds but only some produced tissue depolarization. They proposed that ion channels could exist in two states, inactive (R) or active depolarizing (R*) forms, and a ligand (A) could interact with the inactive state of the receptor to form an intermediate state (AR); agonists can promote conformational changes in the receptor (from R to R*), and the process is a reversible mechanism that is governed by affinity/isomerisation constants.

Equation 1:

$$A + R \rightleftharpoons AR$$

Subsequent improvements of this two-state theory introduced several additional concepts: to explain the constitutive activity of receptors. Wyman and Allen proposed that the receptors could exist in an active conformation (R*) in the absence of the ligand (A) (Wyman and Allen, 1951). Agonists have higher affinity for the R* state over R and can shift the equilibrium toward the active state (Karlin, 1967), while antagonist would not differentiate between the two states of the receptor (Gaddum et al., 1955, Gaddum, 1957). Compounds such as inverse agonists, that preferentially bind R over R*, shift the equilibrium toward R and reduce spontaneous basal activity of the receptor (Thron, 1973).

Equation 2:

$$\begin{array}{ccc} A+R & \rightleftharpoons & A+R^* \\ \uparrow\downarrow & & \uparrow\downarrow \\ AR & \rightleftharpoons & AR^* \end{array}$$

While the two state model can be applied to enzymes, ion channels and also GPCRs, it became clear that for the latter group, an additional level of complexity was required. In order to elicit a cellular response, GPCRs recruit intracellular effectors (E) such as G protein, arrestins and kinases. DeLean et al. (1980) extended the two state model into the ternary complex model, to include the recruitment of the intracellular effector, postulating that E has to couple to the R* (R*E) to produce a cellular response. In presence of receptors that require agonists to elicit an intracellular signal, A would form a ternary complex (AR*E), while it is possible that this complex can exist independently of A and would be responsible for agonist-independent basal activity (Samama et al., 1993).

Equation 3:

$$\begin{array}{ccccc} A+R & \rightleftharpoons & A+R^* & \rightleftharpoons & A+R^*E \\ \Updownarrow & & \Updownarrow & & \Updownarrow \\ AR & \rightleftharpoons & AR^* & \rightleftharpoons & AR^*E \end{array}$$

1.3.2 The operational model of agonism

The first attempt to mathematically quantify how a stimuli drives a cellular response was proposed in the early 20th century by Clark (Clark, 1933), where the law of mass-action was incorporated into a function that correlated the cellular effect to concentration of agonist and occupied receptor. This model was based on the assumptions that the response was proportional to the amount of receptor occupied, and that the maximal response to an agonist corresponds to the maximal response of the tissue itself.

As such, the model could not explain the effect of partial agonists, only capable of triggering submaximal response even at saturating concentrations. Ariëns (Ariens, 1954) therefore introduced the concept of intrinsic activity α, a proportionality factor characteristic of a specific ligand, that allows for scaling of the amplitude of the response elicited. $\alpha=1$ for full agonists, $1<\alpha<0$ for partial agonists and $\alpha=0$ for antagonists.

Based on Nickerson's observations that some agonists can trigger maximal tissue response while occupying only a fraction of available receptors (Nickerson, 1956), Stephenson improved the model to introduce the concept of efficacy (Stephenson, 1956): defined as the strength of a stimulus in triggering a tissue response. Furchgott then further revised this model to separate tissue-dependent parameters and

ligand-specific parameters, and introduce the concept of intrinsic efficacy (ε) of a ligand that is the part of efficacy purely dependent on the agonist and independent from tissue properties (Furchgott, 1966). At this point, the theory was then composed of two parts: properties related solely to the ligand-receptor interaction (such as affinity of a ligand for the receptor and intrinsic efficacy) and tissue-dependent properties (comprising receptor expression and efficiency of coupling of the tissue effector to active receptor to produce a response (β)).

In 1983 Black and Leff (Black and Leff, 1983) revised the previous theories proposing a new model where tissue response was described by 3 parameters: receptor expression [R_t], the disassociation constant of the agonist-receptor complex (K_A), and efficiency of the response upon coupling of the effector to activated receptor (K_E). A new term τ (transducer ratio) was introduced to define agonist efficiency, which is the ratio [R_t]/K_E and corresponds to the amount of receptor that needs to be occupied to obtain half maximal response in the tissue. Defined as such, τ is independent from ligand affinity, but is correlated to intrinsic efficacy of the ligand and tissue-specific parameters, allowing the relative comparison of different agonists (either full or partial agonists) within the same system.

Equation 4:

$$E = \frac{E_{max} * \tau * [A]}{K_A + (1 + \tau) * [A]}$$

The Black and Leff operational model is commonly applied to measure biased agonism (Kenakin et al., 2012). Concentration-response curves for different ligands and pathways define the maximal response (E_{max}) that can be obtained in a specific cell system. The Black and Leff operational model uses E_{max} and concentration of agonist [A] to derive, for each ligand and pathway, the transduction ratio τ/ K_A. This ratio can be compared to a reference ligand, for each compound and pathway investigated, allowing quantification of bias (Kenakin and Christopoulos, 2013).

1.4 Secretin-like, Class B1 GPCRs

1.4.1 Class B1 subfamily

Secretin-like receptors (Class B1) bind peptides, which range in length from 26 to 114 amino acids. Class B1 GPCRs are characterised by a large extracellular N-terminus domain (NTD), the typical 7TM

bundle, and an intracellular C-terminus. Despite these common features, the 15 GPCRs that constitute this class of receptors share no more than 50% sequence homology. Based on structural similarities, Class B1 GPCRs can be further subdivided into 5 groups.

Vasoactive intestinal peptide receptors (VPAC1 and VPAC2) are associated with vasodilation, cardiac function and regulation of gastrointestinal tone and secretion. Structurally similar to the VPACs, pituitary adenylate cyclase-activating polypeptide receptor (PAC1) (Ng et al., 2012) plays a role in brain development, neurotransmission and neuromodulation (Vaudry et al., 2000, Shen et al., 2013). Pathologies associated with this receptor include neurodevelopment disorders, schizophrenia and post-traumatic stress disorder (Ressler et al., 2011).

Corticotrophin-releasing hormone receptors ($CRFR_1$ and $CRFR_2$) play a role in the stress response and are potential targets for the treatment of anxiety, depression, anorexia nervosa, stroke and neurodegenerative disorders such as Huntington's disease, Alzheimer's and Parkinson's (Schank et al., 2012).

The glucagon-related receptor subfamily consists of 6 GPCRs involved in glucose homeostasis (secretin receptor SCTR, glucagon receptor GCGR, gastric inhibitory polypeptide receptor GIPR and glucagon-like peptide 1 receptor GLP-1R), intestinal function and nutrient intake (GLP-1R and GLP-2R), gastric emptying and secretion (GLP-1R, GIPR and SCTR), and growth and development (growth hormone-releasing hormone receptor GHRHR). These functions make this subclass or receptors appealing targets for the treatment of type II diabetes and obesity (Drucker, 2006, Cho et al., 2012).

Parathyroid hormone receptors (PTHR) regulate calcium homeostasis ($PTHR_1$) and are involved in neurotransmission of pain ($PTHR_2$) (Gensure et al., 2005). Pathologies associated with these receptors include Jansen's metaphyseal chondrodysplasia (a form of dwarfism), and other forms of skeletal development (Schipani et al., 1996, Jobert et al., 1998).

Calcitonin (CTR) and calcitonin receptor-like receptor (CLR) share about 50% sequence identity. CTR is involved in bone homeostasis and remodelling (Dacquin et al., 2004), while CLR plays a role in cardiovascular homeostasis and nociception (Poyner et al., 2002). Both receptors form heterocomplexes with receptor activity modifying proteins (RAMPs), which modify receptor function (discussed in

Section 1.4.6). Calcitonin-like receptors bind to peptides that are characterised by a disulphide bond at the N-terminus (between Cysteine 1 and 7 in calcitonin peptide (CT), 2 and 7 in amylin(AMY) and calcitonin gene-related peptide (CGRP), 16 and 21 for adrenomedullin (AM)) (Routledge et al., 2017).

1.4.2 Class B1 structure

The NTD that distinguishes the class B1 sub-group of GPCRs is a ~15kDa structure (~100-200 residues) with an overall common architecture, whereby one α-helical domain and two antiparallel β-sheets are linked by three completely conserved disulphide bonds and five loops. This region contains a highly conserved hydrophobic groove that forms part of the binding site for the orthosteric peptide (Section 1.4.3 for the binding-activation mechanism). Crystal and NMR structures of the isolated NTD, both apo and/or bound to their physiological peptides have been solved for the majority of the secretin-like receptors (Culhane et al., 2015, Parthier et al., 2009, Lee et al., 2016b, Hennen et al., 2016, Dong et al., 2014, Booe et al., 2015, Kusano et al., 2012, Johansson et al., 2016). The common structure of this domain is shown in (***Figure 1.6***).

The NTD is connected to the 7TM bundle through TM1, which for some receptors extends above and away from the plasma membrane (Hennen et al., 2016, Liang et al., 2017, Siu et al., 2013). This region of the receptor is referred to as the stalk (historically named J junction), but is not present in the recently solved structure of GLP-1R (Song et al., 2017).

Crystal structures of the isolated 7TM bundle of the GCGR (Siu et al., 2013) and CRF-1R (Hollenstein et al., 2013) were solved in 2013, both in complex with an antagonist. This year five new Class B1 structures were published: a EM structure of hCTR bound to an agonist and $G_{\alpha}s$ protein heterotrimer (Liang et al., 2017) (***Figure 1.7***), a full length inactive crystal structure of GCGR, bound to an antagonist antibody and a small molecule negative allosteric modulator (Zhang et al., 2017a), a highly modified isolated TM bundle domains of GLP-1R bound to two small molecule allosteric modulators (Song et al., 2017), and a full-length active GLP-1R bound to an agonist and G protein (Zhang et al., 2017b).

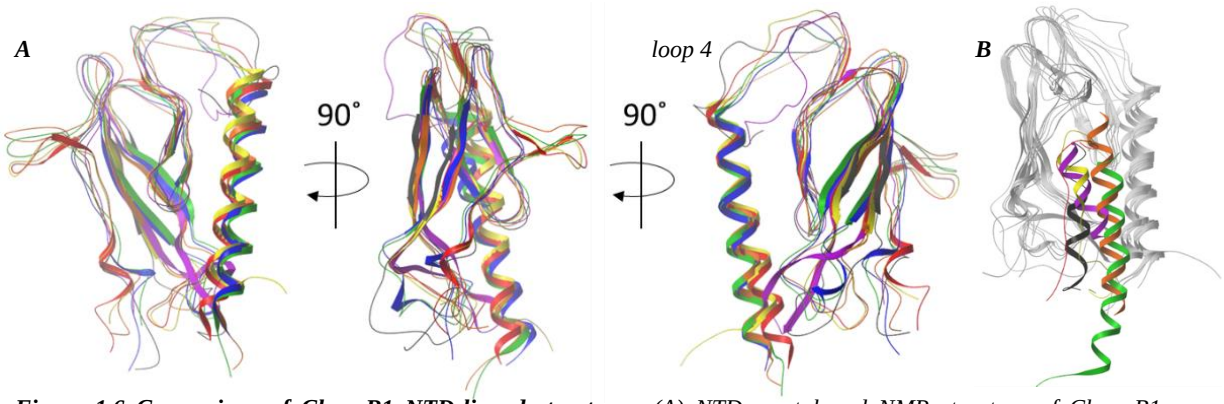

Figure 1.6 Comparison of Class B1 NTD-ligand structures. *(A) NTD crystal and NMR structure of Class B1 were superimposed using Molsoft ICM and coloured as follows: (A) in red CTR (pdb 5II0), in orange PTH-1R (pdb 3C4M), in yellow CLR (pdb 4RWF), in green GLP-1R (pdb 3IOL), in blue GIP (pdb 4HJ0), in purple CRF-1R (pdb 3EHT) and in black CRF-2R (pdb 2JND). (B) Comparison of ligands binding poses: when co-crystallised with the NTD, ligands were coloured according to their receptor.*

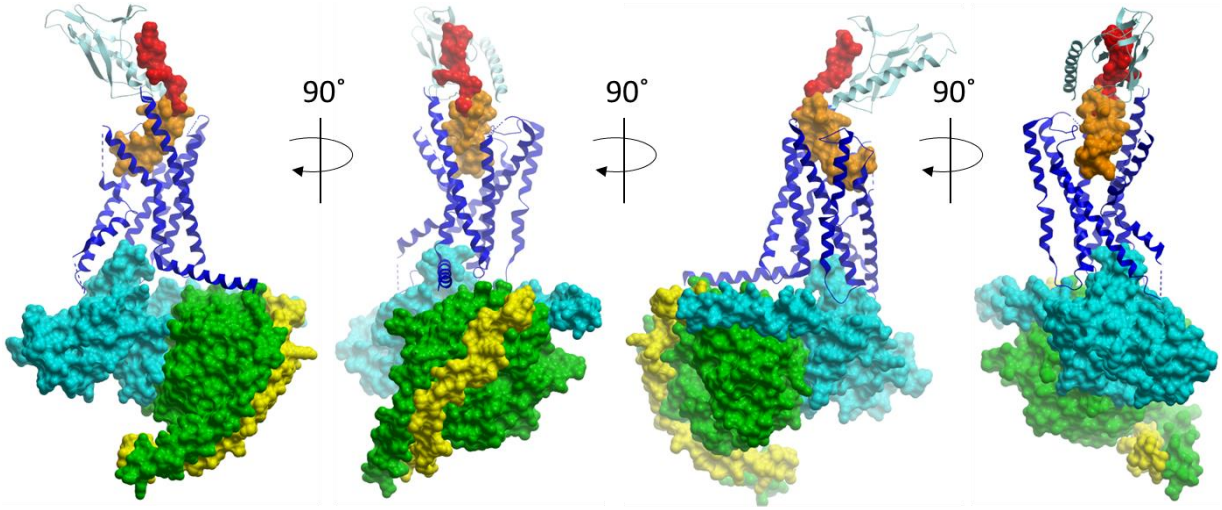

Figure 1.7 Active hCTR in complex with sCT and G_{α}s protein heterotrimer (5UZ7) (Liang et al., 2017). *Cryo-EM structure of the TM of hCTR (blue ribbon) in complex with the αβγ Gαs protein heterotrimer (azure, green and yellow surface respectively). The NTD of hCTR is highly flexible and was only refined at lower resolution with Cryo-EM. However, the crystal structure of the N-termini of hCTR in complex with sCT has been recently solved (Johansson et al., 2016) (5II0) and could be fitted into the CTR EM density (light blue ribbon). The C-termini of sCT (red balloon) and was present in the NTD crystal structure, whereas the extreme N-termini of the peptide was not resolved. Nonetheless, the Cryo-EM data shows density for the peptide backbone at the top of TM bundle and the N-termini could be modelled (orange balloon). Images were generated using ICM Molsoft.*

1.4.3 The peptide ligand binding site and two domain model of Class B1 GPCR binding and activation

The juxta membrane portion of the GPCRs consisting of the NTD, the extracellular portion of TM bundle and the ECLs contain distinct features for each Class of GPCR. Each ligand-receptor pair may couple with a distinct mode, due to the size and position of the binding pockets and nature of the physiological ligands. For Class B1 GPCRs, a two-domain mechanism (Hoare, 2005, Hollenstein et al., 2014) of interaction between orthosteric ligand and receptors has been proposed (***Figure 1.8***). According to this model, the C-terminus of the peptide ligand initially forms a high affinity interaction with the NTD (Figure 1.8 B). These interactions then orientate the N-terminus of the peptide toward the top of the TM domain and the extracellular loops of the receptor (Figure 1.8 C) (Al-Sabah and Donnelly, 2003, Neumann et al., 2008, Dong et al., 2014, Wootten et al., 2016, Dong et al., 2016, Koole et al., 2012b). The peptide N-terminus then interacts with the TM bundle triggering conformational changes within the receptor TM bundle that expose the binding sites for intracellular effectors (***Figure 1.8 D***).

Mutagenesis and crosslinking studies support the initial interaction between the NTD and the peptide C-terminus, and truncation of the C-termini of the peptides or generation of hybrid ligands dramatically impairs ligand affinity, but only partially affects receptor activation (Holtmann et al., 1995, Laburthe et al., 2007, Bergwitz et al., 1996, Runge et al., 2003b, Runge et al., 2003a, Stroop et al., 1995). Furthermore, in all the available structures of isolated NTD-ligand complexes (Pal et al., 2012, Parthier et al., 2009, Bergwitz et al., 1996, Barwell et al., 2010, Booe et al., 2015, Liang et al., 2017) (with the exception of PAC-1R-PACAP NMR structure (Sun et al., 2007)), ligands of Class B1 receptors show similar binding poses within the NTD domain (Parthier et al., 2009, Hollenstein et al., 2014, Pal et al., 2012) (***Figure 1.8 B***). The peptide C-terminus fold into an amphipathic α-helix that establishes hydrophobic and hydrophilic interactions within the hydrophobic cleft of the NTD. Similarly, the alignment of available NTD structures of Class B1 GPCRs (Parthier et al., 2009, Hollenstein et al., 2014) (***Figure 1.6 A***) highlights a completely conserved folding of the NTD, with the exception of the loops (in particular loop 4). Despite the similar binding mode, the ligands of Class B1 have generally

low affinity for the other receptors of this Class besides their own (Runge et al., 2003a, Bergwitz et al., 1996, Runge et al., 2003b, Stroop et al., 1995, Holtmann et al., 1995, Laburthe et al., 2007). Such specificity is attributed to three factors: the ligand sequence that is only partly conserved across different peptides (Pal et al., 2012) , the extremely low sequence homology between NTDs of receptors of Class B1 (Pal et al., 2012), and the small changes in orientation of the loops in the NTD between different receptors. These three factors contribute to determine unique interactions that allow the sorting of ligand-receptor pairs. There is also a second network of interactions between the N-terminus of the ligand and receptor, which is important for receptor activation and that will be discussed in Section 1.4.5.

The second step of the two-domain model is the re-orientation of the NTD to correctly position the N-terminus of the peptide towards the top of support the TM bundle (***Figure 1.8 C***). The unavailability of high resolution full length apo structures and the availability of two low resolution EM structures of full length Class B1 GPCRs bound to peptide ligand (Liang et al., 2017, Zhang et al., 2017b) high flexibility of the NTD. Further evidence also comes from the full length GCGR X-ray structure, which was achieved only by using an antibody that stabilises the NTD (Zhang et al., 2017a). It has been proposed that the reorientation of the NTD relative to the TM bundle is promoted by specific interaction between the mid-region of the peptide ligand. These interactions are confirmed by numerous crosslinking and mutagenesis studies (Dong et al., 2014, Zhao et al., 2016) and by the recently solved structures of the full length CTR and GLP-1R in complex with an agonist and Gαs protein heterotrimer (Liang et al., 2017, Zhang et al., 2017b). This conformational rearrangement is of extreme importance for quiescence/activation of some (glucagon-like sub-class (Koth et al., 2012, Mukund et al., 2013, Yin et al., 2016, Zhao et al., 2016)) but not all (corticotrophin- and parathyroid-hormone-like sub-class (Nielsen et al., 2000)) Class B1 receptors: for glucagon-like receptors, the quiescent state would be maintained by interaction between NTD and the ECLs. The ligand forms interactions with the stalk, forcing the NTD away from the TM bundle to reveal the peptide N-terminus binding site in the receptor core (Zhao et al., 2016, Koth et al., 2012). This model is also supported by the full length structure of the GPL-1R in complex with GLP-1 agonist, where ligand forms a rigid body that stabilises the NTD

(Zhang et al., 2017b). For corticotrophin- and parathyroid-hormone-like receptors the NTD freely exchanges between conformations in absence of the ligand. Thus far evidences have shown that the NTD for these receptors functions as a high affinity trap for the ligand, while an effect on receptor quiescence have not yet been observed (Nielsen et al., 2000).

The final step in the two domain model proposes specific interactions between the N-termini of the ligands with juxta membrane portion of the TM bundle (***Figure 1.8 D***). The importance of these interactions for receptor activation is widely supported by truncation of ligand N-terminus of various Class B1 receptor peptides that produce competitive antagonists (Rivier et al., 1984, Hinke et al., 2001, Donnelly, 2012, Gardella and Juppner, 2001, Bergwitz et al., 1996). A plethora of information involving chimeric receptors and hybrid ligands, mutagenesis and photo-crosslinking studies, and the recent ligand-bound fully active receptor complexes of two Class B1 structures highlight specific residues in all the three ECLs and the top of the TM helices bundle (except TM4) that define the peptide binding pocket (Dong et al., 2014, Wootten et al., 2016, Dods and Donnelly, 2015). However, in spite of these similarities, there are also differences across Class B1 sub-families: corticotrophin-like ligand N-termini are significantly longer than the other peptides for this Class. Additionally, the calcitonin-like ligands are characterised by a cyclic ring that provides wider steric hindrance compared to the linear features of the other peptides. These factors translate to structural difference in the binding pockets, with calcitonin binding in a slightly different position in the CTR (Liang et al., 2017) compared to GLP-1 bound to the GLP-1R (Zhang et al., 2017b) and that predicted for other ligands of Class B1 (Siu et al., 2013, Wootten et al., 2016, Dods and Donnelly, 2015, Weaver et al., 2017) (***Figure 1.9***). From mutagenesis studies, it is also becoming evident that different orthosteric ligands can establish distinct interaction with the residues that line the binding pocket of the receptor, and therefore trigger biased signalling (discussed in Section 1.4.5).

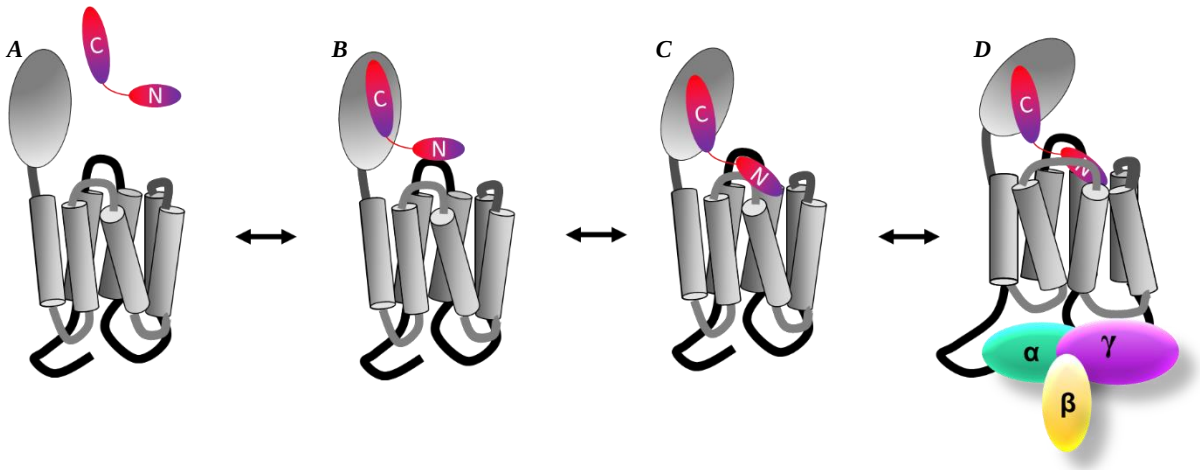

Figure 1.8 Two domain model representation of ligand-receptor interaction of class B1 GPCRs. *(A) Apo receptor in grey and ligand in warm colours. (B) The C-terminus of the endogenous ligand makes contacts with NTD of the receptor. This interaction orientates N-termini of the peptides toward the extracellular domain of the TM bundle (C) to promote conformational changes of the receptor structure and intracellular recruitment of intracellular effectors, in this diagram represented by the G protein heterotrimer (D).*

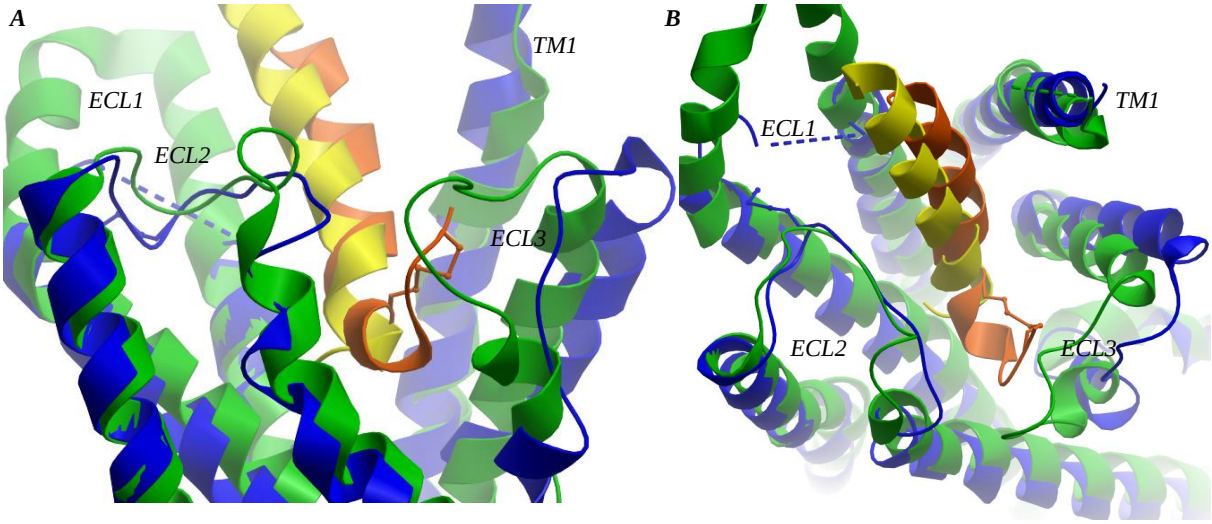

Figure 1.9 Superimposition of Cryo-EM structure of agonist-bound GLP-1R (Zhang et al., 2017b) and CTR (Liang et al., 2017). *Ribbon representation of CTR and GLP-1R (in blue and green, respectively) bound to sCT and GLP-1 (in orange and yellow, respectively) were superimposed using ICM Molsoft to show differences in binding mode of these two agonists with their receptors. Despite poor electron density for the side chains of the sCT peptide, there was enough density to model the backbone of this peptide within the CTR groove (Liang et al., 2017). (A) Side view and (B) top view of the N-terminus of these peptides interacting with their receptor binding cavity. While there is partial alignment of the peptide ligands, the N-termini ring bounding the last 6 residues of sCT provides additional steric hindrance when compared to the linear GLP-1, dictating a different binding pose for the CT peptide.*

1.4.4 Similarities between Class A and B1 GPCRs

The large NTD characteristic of Class B1 GPCRs is not present in Class A, whereas the GPCR structures available for both Classes show a conserved overall organization of the 7 helices that constitute the TM bundle. When compared with inactive crystal structures of Class A GPCRs (***Figure 1.10 A***), the extracellular region of the TM bundle displayed a very different orientation between Class A and B, with Class B1 adopting a more open V-shaped conformation, probably due to their very different binding modes for their endogenous ligands (***Figure 1.10 B and E***). However these structures revealed also a conserved orientation of the cytoplasmic face on the TMs (***Figure 1.10 C and F***) and patterns that may extend across different families of GPCRs. The structure of the transmembrane domain of the metabotropic glutamate receptor 5 (mGlu5, a Class C GPCR) was also solved in 2014 (Dore et al., 2014), and confirms again a more divergent than structure at the extracellular face of the bundle and a similar orientation of the helices at the intracellular face.

Analogies between Classes extend beyond the general architecture of secondary structure. Although Class A and B1 GPCRs share little sequence homology (less than 12%), specific residues or networks of residues, that are known to be important for receptor activation, are conserved. A conserved disulphide connecting ECL2 and the top of TM3 confers structural constraint in all GPCRs.

Upon ligand binding, GPCRs undergo rearrangement of the 7TM bundle. Although the conformational changes within the receptor that lead to recruitment of intracellular effectors are largely unknown for Class B1, there is limited evidence to support the hypothesis that part of the activation mechanism may be conserved across Class A and B1. Despite the low sequence conservation, the overall organisation of the TM grove in the cytosolic face of GPCRs is clearly maintained in all the available structures of GPCRs, both in the inactive (***Figure 1.10 C***) and the active conformations (***Figure 1.10 F***). Besides the structural organisation, the cytosolic face of the receptor (intracellular portion of the TM bundle, ILCs and C-terminus) also acts as interaction site for the same repertoire of intracellular effectors. Additionally, for Class A GPCRs, it is known that ligand binding leads to the sharp outward slant of TM6 (Lee et al., 2015) , which allows the opening of the binding sites for intracellular effectors. A similar motion in the cytoplasmic portion of TM6 relative to TM3 is required for receptor activation for

both Class A (rhodopsin (Sheikh et al., 1996) and β2-AR) and a member of Class B1 (PTHR (Sheikh et al., 1999)). A highly conserved proline residue in TM6 was shown to be the hinge that allows this tilt of the α-helix upon activation in both Class A (Shi et al., 2002) and B1 (Conner et al., 2005, Bailey and Hay, 2007, Knudsen et al., 2001, Conner et al., 2007, Barwell et al., 2013, Dong et al., 2012). However, a much greater kink occurs around this Pro present in TM6 of Class B1 (as evident from the recently published active state structures of CTR [125] and GLP-1R (Zhang et al., 2017b)) relative to the active state Class A structures (β_2AR, A_{2A}R and rhodopsin) (***Figure 1.10 D, E and F***). Such difference may be linked to the larger structure of Class B1 ligands compared to β_2AR, A_{2A}R and rhodopsin ligands (***Figure 1.10 E***).

Deeply embedded within the TM bundle, GPCRs are characterised by a network of polar residues connecting TM 2, 3, 6 and 7. Ligand binding causes the reorientation of these residues, driving structural reorganization along the TM grove and opens the binding pocket for intracellular effectors. The residues that constitute this network are less conserved across Classes, but their organisation is preserved in both Class A and B1 (Angel et al., 2009, Venkatakrishnan et al., 2013, Wootten et al., 2015, Hollenstein et al., 2013, Wootten et al., 2013, Siu et al., 2013, Liang et al., 2017, Song et al., 2017, Zhang et al., 2017a, Zhang et al., 2017b). In Class A, the D(E)$R^{3.50}$Y motif forms an ionic lock at the base of TM2, TM3 and TM6 in the inactive state (Rovati et al., 2007, Ballesteros et al., 2001). Re-orientation of the residues of the DRY motif allows the outward movement of TM6, exposing a cavity within the receptor where the C-terminal α5- helix of the G protein makes contacts (Lebon et al., 2011, Scheerer et al., 2008, Rasmussen et al., 2011a, Ring et al., 2013) (Figure 1.10 F). This DRY motif is absent in class B1, however the $H^{2.50}E^{3.50}T^{6.42}$,$Y^{7.57}$ motif (Class B1 numbering based on (Wootten et al., 2013)), located one turn above in the secretin-like compared to the rhodopsin-like receptors, has been proposed to play a similar role (Barwell et al., 2013, Vohra et al., 2013, Kirkpatrick et al., 2012, Wootten et al., 2013, Chugunov et al., 2010, Gaudin et al., 1998, Couvineau et al., 2003, Turner et al., 1996, Schipani et al., 1996, Tseng and Lin, 1997, Conner et al., 2006b). This hypothesis is supported by the recently published GLP-1R and CTR active structures (Liang et al., 2017, Zhang et al., 2017b) which show that the $H^{2.50}E^{3.50}T^{6.42}Y^{7.57}$ is also disrupted upon receptor activation, leading to the analogous outward

movement of TM6. The residues one turn below the HETY motif of Class B1 ($R^{2.46}$, $R/L^{6.37}$, $N^{7.61}$ and $G^{8.41}$) establish an additional polar network between TM2, 6, 7 and Hx8 (discussed below) that holds the Class B1 in the inactive conformation (Song et al., 2017, Zhang et al., 2017a, Siu et al., 2013) (not visible in CRF-1R structure (Hollenstein et al., 2013) due to absence of Hx8). Upon activation, this second lock is also disrupted to allow rearrangement of the TM bundle (Liang et al., 2017, Zhang et al., 2017b).

A second conserved motif of Class A is $NPXXY^{7.53}$ (in TM7) important for receptor packing and activation. The motif is also absent in Class B1, but based on mutagenesis studies and molecular simulation $VXXXY(/F)^{7.53}$ has been proposed to be the equivalent in the secretin-like receptors (Vohra et al., 2013, Wootten et al., 2013, Conner et al., 2007, Langer and Robberecht, 2007).

The TM proximal terminal of the intracellular C-terminal tail of GPCRs is organised in an 8th amphipathic α-helix (Hx8) (***Figure 1.10 C and F***) that sits parallel and partially embedded in the plasma membrane. In Class A and B1, Hx8 and ICL3 have similar functions and are known to be involved in receptor expression, G protein recruitment and internalisation (Krishna et al., 2002, Tetsuka et al., 2004, Santos et al., 2006, Aratake et al., 2012, Kirchberg et al., 2011, Conner et al., 2008, Seck et al., 2003, Conner et al., 2006a). In fact, sequential truncation of Hx8 causes reduction of cell surface expression and receptor function in both CTR and CLR (Liang et al., 2017, Conner et al., 2008). Hx8 is visible in several published structures of Class A (Moreira, 2014) and 2(3) Class B1 (Siu et al., 2013, Liang et al., 2017, Song et al., 2017, Zhang et al., 2017a, Zhang et al., 2017b). However, Hx8 appears to be longer in the secretin-like receptors than the rhodopsin-like receptors (***Figure 1.10 C and F***). Cryo-EM structures, crosslinking and mutagenesis studies in Class B1 GPCRs have demonstrated that the binding domain for G proteins includes the 3 ICLs (particularly ICL2 and ICL3), TM6 and the Hx8, where Hx8 appears to establish interactions with ICL1 and Gβ, interactions that are not present in the published Class A structures (Liang et al., 2017, Zhang et al., 2017b, Moreira, 2014).

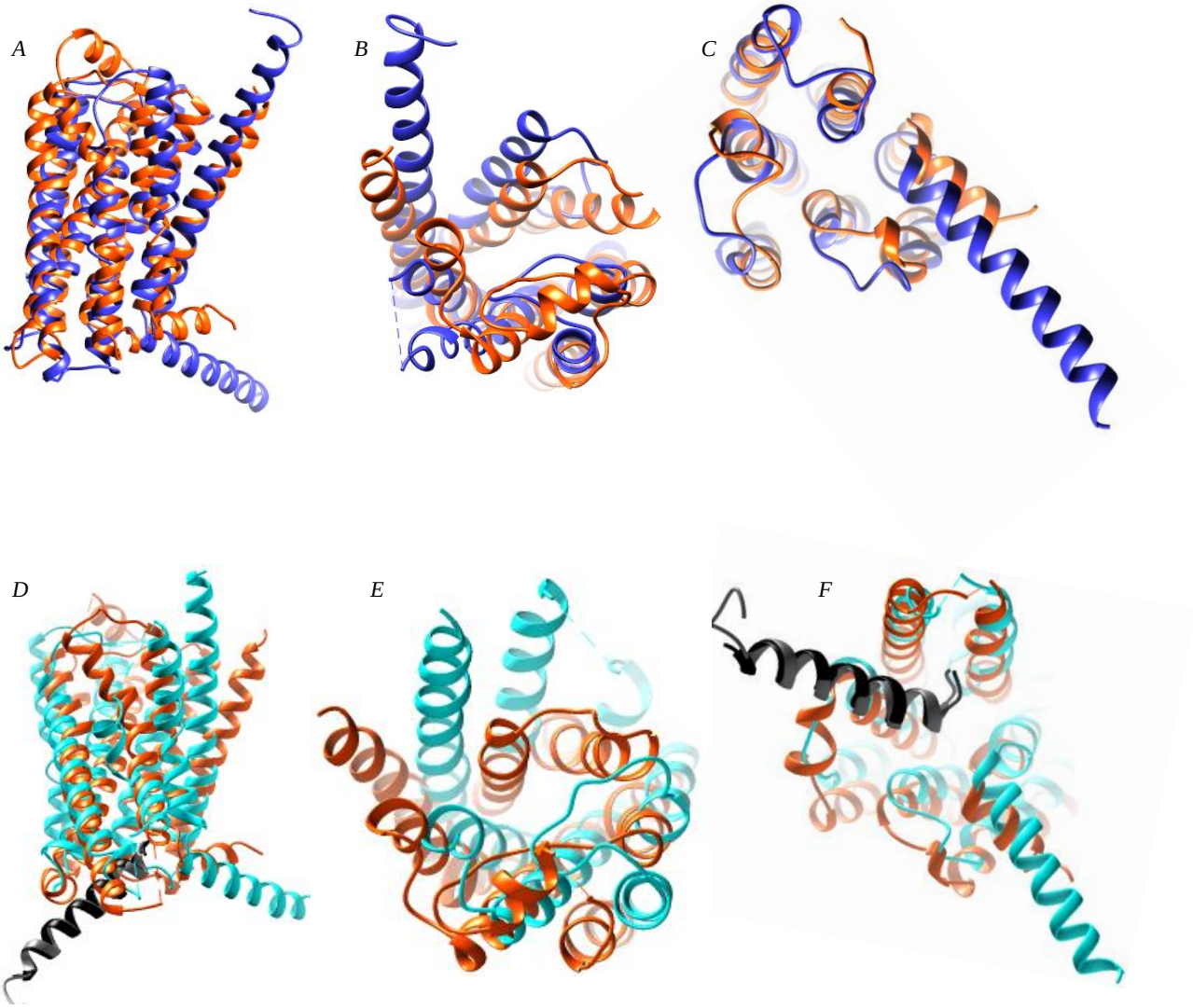

Figure 1.10 Schematic representation of available Class B1 structures and comparison with Class A β2-AR. *(A) Inactive β2-AR structure (pdb structure 2RH1 in orange) superimposed with the inactive GCGR (4L6R in blue); top (B) and bottom (C) prospect of the TM bundle. (D) Side view of the active crystal structures of β2-AR (3SN6, orange) superimposed to active CTR (5UZ7, azure), C-terminus αhelix 5 of Gαs protein is represented in grey and black; top (E) and bottom (F) prospect of the TM bundle. Images were generated using ICM Molsoft or UCSF Chimera 1.8.1*

1.4.5 Biased agonism at Class B GPCRs

Many Class B1 receptors are known to pleiotropically couple with more than one G protein (Pisegna et al., 1996, Segre and Goldring, 1993, Nabhan et al., 1995) and most also recruit β-arrestins (Sonoda et al., 2008, Zindel et al., 2016, Shetzline et al., 2002, Oakley et al., 2007). Additionally, most Class B1 receptors bind more than one ligand. It is therefore not surprising that biased agonism is evident for this Class of receptors. The first reported example of this was seen for PACAP(1-38) and PACAP(1-27), which bind to PAC-1R. These ligands produce a more potent Gαs dependent cAMP signal with the former ligand, and a more potent IP signal with the latter (Spengler et al., 1993). TIP39 and PTH are both agonists of the PTH-2R, but can differentially modulate G protein and β-arrestin signalling (Appleton et al., 2013, Gesty-Palmer et al., 2006). Mutagenesis studies on PTH-2R and GLP-1R revealed that biased signalling can be linked to specific interactions between the peptide and residues deeply embedded within the TM bundle of the receptor (Weaver et al., 2017, Wootten et al., 2015).

Increasing body of information is available about the importance of distinct residues within ECLs and TMs of the Class B1 receptors in defining intracellular signalling and specific interactions that are important in triggering biased agonism (Dong et al., 2014, Wootten et al., 2016). Good examples are the extensive mutagenesis studies on GLP-1R and how these mutations affect the binding and signalling of different known biased agonists: specific residues in ECL2, ECL3, TM5, TM6, TM2 and adjacent portion of ECL1 are important for cAMP and Ca^{2+} signalling, whereas interactions with ECL3 (but not ECL2) trigger ERK1/2 signalling (Wootten et al., 2016, Koole et al., 2012b). Additionally, these studies have revealed that different ligands establish unique interactions with the receptor that likely promote distinct receptor conformational changes and cause biased signalling (Wootten et al., 2016, Koole et al., 2012b, Wootten et al., 2015, Weston et al., 2014).

The understanding of which residues in the receptor structure trigger the activation of one pathway over another can significantly aid the design of new therapeutic compounds, by potentially promoting the activation of ideally only beneficial pathways, and avoiding those predicted to lead to on-target adverse effects.

1.4.6 Accessory proteins and GPCR heterocomplexes with RAMPs

First described in 1998 (McLatchie et al., 1998), receptor activity-modifying proteins (RAMPs) are a class of three membrane integral proteins (RAMP1, RAMP2 and RAMP3) characterised by a large extracellular N-terminal domain, a single pass transmembrane α helix and a short intracellular C-terminus. Ten Class B1 GPCRs (VPAC1, VPAC2, PTHR1, PTHR2, CRF1R , CLR, CTR, GCGR, GLP-2R , SCTR) as well as the calcium sensing receptor (Class C), the oestrogen receptor GRP30 (Class A) and non-GPCR proteins such as β-tubulin can interact with RAMPs (Routledge et al., 2017).

The interaction with RAMPs has the potential to alter receptor trafficking, ligand binding and receptor signalling. The best characterised examples are CTR and CLR, where formation of heterocomplexes with RAMPs selectively alters trafficking, ligand specificity and signalling (Poyner et al., 2002, Hay et al., 2006). Specifically, the CTR can traffic on its own to the cell surface in the absence of RAMPs, whereas CLR requires the interaction with one of the three RAMPs for efficient expression at the plasma membrane (McLatchie et al., 1998, Bühlmann et al., 1999). The presence of RAMPs also expands the range of physiological activities of these receptor, with dramatic changes in both affinity, specificity and/or activation of downstream signalling profile. Coexpression of CLR with RAMP1 results in a receptor phenotype with high affinity for calcitonin gene-related peptide (CGRP) that is involved in pain modulation (Benemei et al., 2009), whereas the interaction with RAMP2 or RAMP3 generates an adrenomedullin receptor type (AM) (Hilairet et al., 2001), which regulates the tone of the cardiovascular system (Taylor et al., 2005). Although RAMPs are not required for CTR trafficking, complexes between CTR and RAMP1 generate receptors with high affinity for CGRP, whereas complex between CTR and with any one of the three RAMPs forms an amylin (AMY) receptor, involved in glucose homeostasis and food intake (Reda et al., 2002). The CTR variant involved in the formation of heterocomplex with RAMPs, the subtype of RAMP as well as cell backgorund change both AMY affinity and receptor function (Christopoulos et al., 1999, Tilakaratne et al., 2000, Zumpe et al., 2000, Christopoulos et al., 2003, Poyner et al., 2002, Dacquin et al., 2004, Hay et al., 2005, Morfis et al., 2008). Additionally, the three RAMPs contribute to the coupling efficiency of the AMY, CGRP and AM receptors to G protein (Morfis et al., 2008, Weston et al., 2016).

1.5 The calcitonin receptor (CTR)

1.5.1 Physiological role of the CTR

The calcitonin receptor (CTR) belongs to the calcitonin subfamily of the secretin GPCRs. In the absence of RAMPs, its predominant physiological agonist is calcitonin, a 32 amino acid peptide secreted by the thyroid gland in response to increases in the circulating calcium concentration.

The CTR is expressed in multiple tissues. It is highly expressed in osteoclasts (Fujikawa et al., 1996b, Nicholson et al., 1986) where it reduces their bone remodelling activity (Kallio et al., 1972), promotes cell survival (Selander et al., 1996) and differentiation from the bone marrow precursors (Cornish et al., 2001, Quinn et al., 1998, Fujikawa et al., 1996a, Wookey et al., 2010). Similarly, it regulates differentiation of leucocytes and their precursors (Wookey et al., 2010, Marx et al., 1974, Perry III et al., 1983). In kidneys, the CTR is localized in the thick ascending limb of the loop of Henle and in the distal convoluted tubule (Sexton et al., 1987, Marx et al., 1972) where it influences the excretion of calcium and stimulates diuresis (Carney, 1996). The CTR has been identified in different organs of the gastrointestinal system where it reduces gastric function (DuBay et al., 2003), gastric acid and pepsin secretion and release of amylase (Goebell et al., 1979, Hotz and Goebell, 1975), and its activation reduces food intake in rodents (Eiden et al., 2002) and primates (Bello et al., 2010) through a direct action in the CNS. In different areas of the brain (Hilton et al., 1995, Liberini et al., 2016, Fabbri et al., 1985, Bower et al., 2016) CTR activation also increases secretion of endorphins, cortisol and ACTH (Shah et al., 1990, Rohner and Planche, 1985, Laurian et al., 1986). In lungs CT receptor activation blocks bronco-constriction by reducing the release of thromboxane and prostaglandins and inhibiting the effect of substance P (Becker, 1993). High expression of the CTR in sperm, the uterus and placenta (Kuestner et al., 1994) suggests a role in fertilisation and placental function. Additionally, elevated levels of CT during the early stages of gestation reveal a potential role in the development of the blastocyst and facilitation of implantation (Wang et al., 1998). Although the CTR has been identified in several cancer tissues and may offer a new therapeutic target, studies have been inconsistent, with opposing effects on cell proliferation depending on the type of tumour or tumour derived cell line

studied (Mould and Pondel, 2003, Thomas and Shah, 2005, Thomas et al., 2007, Thomas et al., 2006, Lacroix et al., 1998, Sabbisetti et al., 2005).

1.5.2 CTR as therapeutic target

Although not the first therapeutic choice, the CTR is currently targeted for the treatment of severe, well-established osteoporosis (Cosman et al., 2014), due to its inhibitory effects on osteoclast activity that leads to the reduction of bone remodelling and resorption (Yamamoto et al., 2005a). However, due to this action, agonists of the CTR (human and salmon calcitonins) are more commonly used in the treatment of diseases of high bone turnover such as Paget's disease and osteogenesis imperfecta (DeRose et al., 1974, Castells et al., 1979, Langston and Ralston, 2004): the first involves an excessive bone resorption while the latter is a congenital disorder characterised by impaired development of the bone matrix that translates into brittle bones and predisposition to fractures.

CTR agonists are also used as an adjunct therapy in the treatment of hypercalcemia of malignancy, which is a frequent complication of melanoma, breast and lung cancers. In these pathologies, the tumour often releases parathyroid hormone-like factors to promote osteolysis. Treatment with CTR agonists aims to reduce bone resorption, as well as to increase the excretion of blood calcium (Minhas and Virdi, 2017).

Additionally, several *in vivo* and clinical studies report calcitonin peptides can be used to modulate pain (Blanchard et al., 1990, Jaeger and Maier, 1992, Eskola et al., 1992, Miralles et al., 1987, Gennari et al., 1986, Micieli et al., 1988). Although the mechanism is still largely unknown, CTR ligands potentially have both central and peripheral analgesic effects: CT administered by nasal spray or subcutaneously passes the blood-brain barrier and accumulates in the central nervous system (CNS) where it induces a direct analgesic effect through increasing the release of endorphins. Peripherally, the activation of CTR reduces inflammation by inhibiting the release of inflammatory mediators, reducing blood vessels permeability and modulating calcium flux (Azria, 2002).

CTR stimulation also produces opposing effects in several cancerous tissues, increasing proliferation of some, while reducing it in others. Calcitonin treatment of breast cancer cell lines reduced tumour proliferation (Lacroix et al., 1998, Nakamura et al., 2007), whereas it promoted proliferation in prostate

cancer cell lines (Sabbisetti et al., 2005, Thomas and Shah, 2005, Thomas et al., 2006, Thomas et al., 2007). This suggests that in some tumours CTR agonists may be beneficial therapeutics, while in other forms of cancer CTR antagonists may be a better treatment of the disease. The studies on prostate cancer cell lines have opened a debate about pharmacological use of commercial CTR agonists. Although no strong correlation has been identified between the use of CTR agonists and increased risk of cancer development, the European Medicines Agency (EMA) in 2012 and the Food and Drug Administration (FDA) in 2013-2014 revised the guidelines for the prescription of CTR agonists to include a boxed warning in case of patients with prostate cancer.

1.5.3 Natural occurring CTR isoforms and splice variants

The CTR has been identified throughout the vertebrate phylum (Arlot-Bonnemains et al., 1983, Lasmoles et al., 1985) and in other organisms of the animal kingdom (Sekiguchi et al., 2009, Coast et al., 2001, Zandawala et al., 2013). In humans, alternative splicing of the calcitonin receptor gene (CALCR) located on chromosome 7 (Yamin et al., 1994) produces multiple splice variants of the receptor. The first isoform to be cloned, in 1992, contains a 16 amino acid insert in ICL1 and is now named $CTR_{b,}$ (previously termed CTR_{I1+} or $hCTR_1$ (Gorn et al., 1992)). A second isoform was later isolated from mammary carcinoma and is termed CTR_a (CTR_{I1-} or $hCTR_2$) (Kuestner et al., 1994). Analysis of expression in tissues where the CTR_a and CTR_b isoforms have been identified shows significant variation in relative expression of CTR_b compared to the CTR_a (Kuestner et al., 1994, Frendo et al., 1994, Gorn et al., 1995, Gorn et al., 1992).

In 1995, Albrandt et al. (1995) reported a third isoform of human CTR (Δ(1-47)CTR_a) from human breast carcinoma MCF-7 . Sequencing of RT-PCR product revealed identity with the $hCTR_a$ clone except for the deletion of the first 47 residues at the N-term of the receptor. Recombinant expression in COS-7 cells of the Δ(1-47)CTR clone demonstrated binding of sCT with similar affinity as displayed for CTR_a. Although protein expression has not been confirmed in non-transformed cell lines, Δ(1-47)CTR mRNA is co-expressed with the other 2 splice variants in skeletal muscle, kidney, lung and brain cell lines (Albrandt et al., 1995). PCR analysis indicates that the two splice variants are expressed at different levels in different tissues and the differential physiological responses observed to CTR

activation *in vitro*/*in vivo* may be due to the prevalence of one isoform over the other (Kuestner et al., 1994).

Single-nucleotide polymorphisms (SNP) are defined as variations in the genome of individuals of a species that are present in at least 1% of the population. It is not surprising that SNP are also present in GPCRs (Small et al., 2003, Lee et al., 2003) and the CTR has a common polymorphism, where the substitution of a single nucleotide at the 3' end of the CALCR gene (within the sequence encoding residue 447 at the CTR_a) leading to either a Proline (CCG) or a Leucine (CTG) residue (Egerton et al., 1995, Gorn et al., 1995). The Pro residue is conserved throughout vertebrates, while the Leu variant found in humans seems to be a variation correlated to the ethnicity. Asian background, in particular in the Japanese population, have genotypes that code predominantly for the proline variant (Nakamura et al., 1996) while Caucasians, Hispanics and African-Americans tend to be either leucine (homozygous) or leucine/proline (heterozygous) (Wolfe et al., 2003).

Albrandt et al. (1995) also reported a polymorphism where threonine 347 (in TM6) is substituted by isoleucine. This variant is not properly classified as a SNP, nor can numerous other polymorphisms found in the pfSNP (potentially functional SNP search engine), because, as per the definition, they have not been reported in at least 1% of the population.

In some cases, GPCR SNPs are associated with increased risk of disease, in particular when present in the TM bundle (Balasubramanian et al., 2005, Jaing et al., 2003). In the CTR, the T347I polymorphism does not affect cAMP formation in recombinant cells (Qi et al., 2013). The P447L polymorphism is extremely common and contradictory evidence exists that leave an open discussion on whether a correlation exists between disease and polymorphism can be associated with ethnic background. Clinical studies where patients with different ethnic background were genotyped indicated a potential correlation between an increase in osteoporosis and kidney stone disease incidence and people expressing the leucine variant (Masi et al., 1998a, Braga et al., 2002, Masi et al., 1998b, Mitra et al., 2017). A comparable number of clinical analyses, also suggest no statistical correlation exists between disease and the polymorphisms (Dehghan et al., 2016, Wolfe et al., 2003).

1.5.4 Calcitonin ligands

The endogenous ligand of the CTR (CTR) is a 32 amino acid peptide named calcitonin . CT peptides have been cloned from several species and all are characterised by a disulphide bond between Cysteines 1 and 7, a highly conserved amidated proline at the carboxyl-termini, but a divergent sequence in the mid-region of the peptide, between residues 10 and 27.

Human CTR (hCTR) can bind different CTs with distinct affinities; salmon calcitonin (sCT), for instance, has highest affinity, followed by porcine CT (pCT), with the endogenous ligand, human CT (hCT), having lower affinity. In addition, the kinetics of binding also differ, with sCT capable of establishing pseudo-irreversible interactions with the receptor, whereas the hCT peptide has a binding t½ of between 10 and 30 minutes (Hilton et al., 2000, Moore et al., 1995, Furness et al., 2016). The C-terminus and mid region of these peptides are the least conserved and are known to be responsible for these differences in both affinity and binding kinetics (Hilton et al., 2000, Furness et al., 2016). Nevertheless, all these ligands have similar efficacy in cAMP signalling, although not in all cell backgrounds (Kuestner et al., 1994, Wolfe et al., 2003, Moore et al., 1995).

In 2004, Ma et al. reported a 27 residue endogenous peptide that also acts as an agonist at the CTR (Ma et al., 2004). The peptide, named PHM-27, is not structurally related to the CT peptides and originates from the same precursor of the endogenous vasointestinal peptide (VIP) (Bodner et al., 1985, Itoh et al., 1983, Bloom et al., 1983), which binds to VPAC1 and VPAC2 receptors. To date this peptide has not been widely characterised.

Most CTR ligands are peptides, including all the ones used therapeutically. As medications, peptides have no oral bioavailability (unless appropriately formulated (Karsdal et al., 2015)) and their administration via injection or nasal spray has low compliance (Karsdal et al., 2015). Additionally, long term treatment with CT agonists, such as sCT, can lead to development of antibodies and resistance to therapy. There has therefore been interest in developing small molecules that act as a calcitonin mimetic and that could be orally administered (Boros et al., 2005, Katayama et al., 2001, Dong et al., 2009). When compared to hCT, one of these compounds (SUN B8155) appeared to be a low potency, full agonist for CTR in both rodent and human cell lines (CHO, UMR106-06, T47D and SaSO2) and,

similarly to CT, lowered Ca^{2+} blood levels in rats (Katayama et al., 2001). In the same study, data suggested that this compound could be an allosteric agonist of the CTR receptor, as it was unable to compete with the physiological agonist hCT at concentrations up to 100 µM in all hCTR transfected cells. Importantly, its signalling was not abolished in presence of up to 1 µM of the orthosteric antagonist sCT(8-32). Similar results were also obtained by Dong et al. (2009). However, these compounds were not very efficacious and were therefore abandoned.

```
cCT      CASLSTCVLGKLSQELHKLQTYPRTDVGAGTP
sCT      CSNLSTCVLGKLSQELHKLQTYPRTNTGSGTP
pCT      CSNLSTCVLSAYWRNLNNFHRFSGMGFGPETP
hCT      CGNLSTCMLGTYTQDFNKFHTFPQTAIGVGAP
         └──────┘

PHM-27   HADGVFTSDFSKLLGQLSAKKYLESLM
```

Table 1.1: Sequence comparison of more commonly studied CT and PHM-27 peptides. *The CTs have been aligned and residues highlighted in* ***green*** *are identical amino acids, those in* ***blue*** *are conservative substitutions, those in* ***orange*** *are semi-conservative substitutions, and those in* ***black*** *non-conserved. Due to low homology PHM-27 has not been aligned with the CTs.*

1.5.5 CTR signalling

Ligand binding promotes coupling of the hCTR to several G proteins, but as with all Class B1 GPCRs, the predominant interaction is with $G_{\alpha}s$ protein, to activate tmACs and increase intracellular cAMP levels. This has been reported in several endogenous and recombinant systems expressing hCTR (Chabre et al., 1992, Raggatt et al., 2000, Nicholson et al., 1986, Kuestner et al., 1994, Moore et al., 1995, Gorn et al., 1995, Wolfe et al., 2003, Findlay et al., 1980, Gorn et al., 1992, Frendo et al., 1994). Despite their distinct affinity, all CT peptides described in Section 1.5.4 can trigger a similar cAMP response upon binding to the hCTR, suggesting that lower affinity ligands such as hCT are more efficacious in activating Gαs protein at this receptor. This hypothesis has recently been supported by Furness et al. (2016), hCT promotes a ternary complex with higher affinity for GTP, a faster G protein turnover resulting in a faster production of cAMP at sub-saturating concentration of agonist compared to sCT. This study also revealed faster kinetics of G protein activation. These distinct effects were dependent on distinct conformations of the G protein that were dependent on the ligand bound to the receptor.

The CTR can also couple to Gαq, activating the phospholipase C (PLC) pathway and triggering a rapid mobilisation of intracellular Ca^{2+} from the endoplasmic reticulum (ER) (Chabre et al., 1992). While the $hCTR_a$ splice variant is able to elicit this iCa^{2+} response, the $hCTR_b$ does not produce this response (Kuestner et al., 1994, Moore et al., 1995).

There is limited evidence that the CTR also promotes activation of Gαi proteins (Chen et al., 1998, Lacroix et al., 1998), however this interaction between receptor and Gαi protein may be temporally limited to the S phase (but not G1/G0 or G2) of the cell cycle at least in some cell types (Chakraborty et al., 1991).

Phosphorylation of extracellular regulated kinases 1 and 2 (pERK1/2) and protein kinase B (PKB, also known as Akt) also occurs downstream of CTR activation (Raggatt et al., 2000, Thomas and Shah, 2005), and activation of those pathways is generally involved in cell survival and apoptosis (Nakamura et al., 2007). ERK phosphorylation also increases expression of urokinase plasminogen activation (uPA), an important factor in tumour invasion (Han et al., 2006). CTR stimulation can suppress cell growth in breast cancer cells line that present constitutive activation of ERK1/2 pathway, but not in cells where pERK1/2 is not constitutive (Nakamura et al., 2007). Additionally, activation of the $hCTR_a$ but not $hCTR_b$ inhibits cell proliferation in transfected HEK293 (Raggatt et al., 2000).

β-arrestin recruitment can promote intracellular signalling independently of G protein for GPCRs (Kendall and Luttrell, 2009). Only one study to date has investigated the interaction between these effector proteins and the $hCTR_a$, through a complementation-based arrestin recruitment assay (Andreassen et al., 2014). The study revealed a transient interaction of the receptor stimulated with hCT compared to a sustained interaction with sCT, consistent with the different kinetics of binding of the two ligands. Transient vs sustained interaction with β-arrestins may lead to a distinct temporal intracellular signalling or even biased agonism (Shukla et al., 2011, Lee et al., 2016a). However, it is important to note that the specific arrestin recruitment assay used had a CTR with a modified (V2 receptor) C-terminus, and thus it is not clear if this arrestin interaction is physiological. To date, other signalling events have not been extensively studied.

It is important to understand whether there are distinct signalling profiles triggered by different ligands, and to understand the mechanisms of activation of the CTR family as it has therapeutic implications for development of therapeutics. As the CTR promiscuously couples to multiple intracellular effectors, and multiple ligands can activate the receptor, there is potential for CTR to display biased agonism. However, to date this concept has not been explored for this receptor.

1.5.6 CTR trafficking

T47D (human breast cancer derived cells) endogenously co-express the $hCTR_a$ and $hCTR_b$ and display internalisation of the receptor when incubated at 37℃ (Findlay et al., 1982). Similar observations could be made for MCF7 (human breast cancer), BEN (human lung cancer) and OCL (osteoclasts-like cells) (Lamp et al., 1981, Wada et al., 1995, Findlay et al., 1980, Michelangeli et al., 1982). The presence of the 16 amino acids insertion in ICL1 was reported to impede the internalization of the hCTR transfected in BHK recombinant cells (Moore et al., 1995). Both Michelangeli et al. (1982) and Schneider et al. (1988) used protein synthesis or trafficking inhibitors and concluded that, in several cancer cell lines, the internalised receptor is degraded while new receptor is continuously synthesized and transported to the plasma membrane. Seck et al. (2003) followed the constitutive internalisation of CTR in HEK293, M2 and A7 cell lines and reported that the receptor can recycle to the plasma membrane from endosomal compartments when it associates with acting-binding protein filamin, and that agonist stimulation prevents receptor degradation and promotes recycling over degradation by inhibiting calpin protease activity (Seck et al., 2003). Besides the observation that hCTR does internalises in several cellular backgrounds, it has yet to be determined the mechanism behind CTR trafficking, whether receptor variants (splices and polymorphisms) internalise at different rates, if distinct ligands affect the mechanism or kinetic of internalisation. Additionally, the possibility of constitutive trafficking has yet to be explored.

1.6 Structure-function studies on the CTR: ligand interaction and receptor activation

1.6.1 NTD-ligand interactions

As discussed in Section 1.4.4, the NTD of Class B1 GPCRs is the principle binding site for the C-termini of orthosteric ligands. In the absence of ligand, the NTD has the potential to exchange between closed states, where NTD may interact with the ECL3 for some Class B1 receptors (***Figure 1.11 B***), and a more open conformation, with the NTD moving away from the TM bundle (***Figure 1.11 A***) (Yang et al., 2015). The binding of the ligand could stabilise a subset of these conformations (***Figure 1.11 C***). For CTR however, it is unlikely that ligand would promote a completely open conformation, because the use of a ligand with a rigid α-helical structure that would stabilise the open conformation inhibits both affinity and signalling (Andreotti et al., 2006). Additionally the Cryo-EM structure of the full length CTR in complex with the ligand shows a tilted orientation of the NTD relative to the TM bundle, and a degree of flexibility that was evident in low resolution 3D class averages (Liang et al., 2017).

Specific interactions are established between the C-termini of CT ligands and the NTD was originally proposed based on experiment testing chimeras of (PTHR/CTR) exchanging the NTD and stimulation by CT/PTH ligands (Bergwitz et al., 1996). Sequence 22-32 appears to be the minimal requirement for high affinity CT binding at the NTD, and T25, T27, G28 and P32 of the sCT are fundamental for the interaction with the receptor NTD (Lee et al., 2016b).

Chimeric receptors between CTR/SECR or CTR/GCGR confirm that the CTR NTD is required for high affinity ligand binding and downstream signalling (Dong et al., 2009, Stroop et al., 1995). Deletion of the first 47 residues of the human receptor (Δ(1-47)hCTR_a) leads to reduced potency in CT-mediated cAMP response when compared to the full length CTR_a, potentially due to the loss in affinity (Qi et al., 2013). Truncation of residues 1-53 causes a 30-fold loss of potency in a cAMP accumulation assay with no change in E_{max}; further deletion of 5 residues Δ(1-58) produces a functional receptor with 2000-fold lower potency for CT-mediated cAMP accumulation, while truncation beyond residue 73 generates a completely inactive receptor (Dong et al., 2009).

Cross-linking of photolabile amino acids incorporated into CT peptides has also been used to identify proximity of peptide and CTR and insight into binding between CT peptides and the NTD of hCTR. Bpa (p- benzoyl-L-phenylalanine) inserted in position 14 of the ligand crosslinks to the NTD of the hCTR between Y41 and M48, while residue 26 crosslinks to T30 (Dong et al., 2004a).

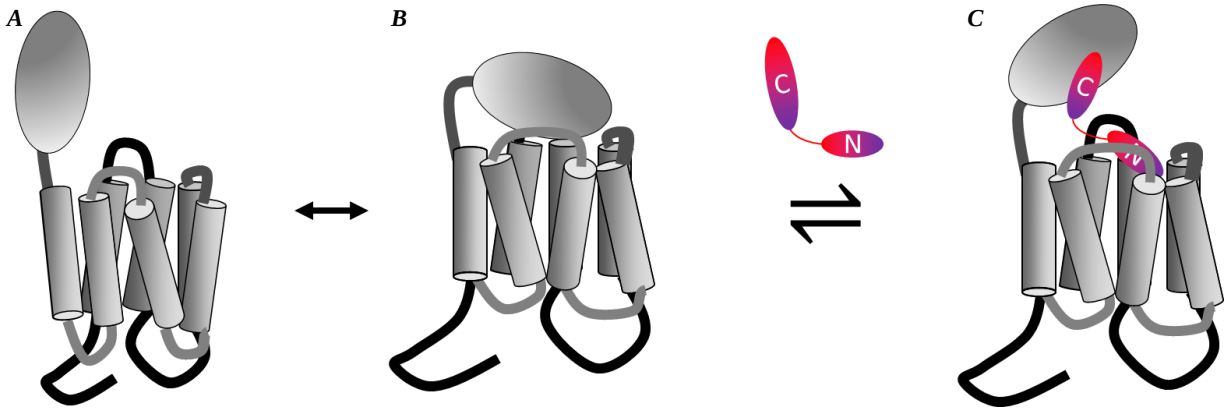

Figure 1.11: Schematic representation of the different conformational states of NTD of Class B1 GPCRs. *In absence of ligand (A and B), the NTD of Class B1 receptor may exchange between an open (A) or closed (B) conformation. The binding of a ligand (C) could stabilise an ensemble of these conformations.*

1.6.2 Ligand interactions with TM1/NTD interface

Residues in the mid-region of the hCT peptide make contact with the TM1/NTD interface (***Figure 1.12***). Deletion of CTR residues 150-151 produces a fully active receptor, however potency in cAMP response is reduced by over 1000-fold. Δ(150-154) is completely inactive (Dong et al., 2009).

Through cross-linking studies, L16 of CT peptides was reported to interact with F137 (Dong et al., 2004a), while L19 crosslinked in a region bounded by C134 and L141 (Pham et al., 2004, Pham et al., 2005) of the TM1 stalk/NTD interface. The published structure of sCT-CTR complex (Liang et al., 2017), confirms potential proximity of L19 and L141 (ligand and receptor respectively). However, L16 of sCT in this structure was not in close proximity of F137. Pham et al. (2004) mutated several residues of TM1 (133-141) and found that the majority of these mutations impaired cAMP signalling with no effect on affinity of the ligand (with the exception of C134, where mutation to alanine that also dramatically reduced expression). The low resolution of this region in the Cryo-EM structure of sCT-CTR complex and the inability to identify specific interactions between ligand and TM1 further supports the flexibility of both stalk and mid-region of the CT ligands.

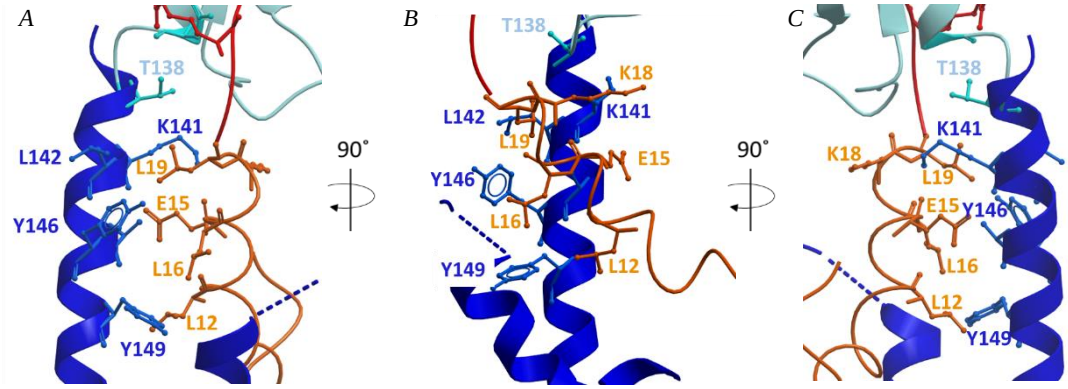

Figure 1.11 Representation of the TM1 stalk of the CTR in complex with the mid-region of the sCT peptide. *Similar to Figure 1.6, the crystal structure of the NTD of CTR in complex with the C-terminus of sCT (pdb EII0, in light blue and red respectively) was rigid-body fitted into the electron density of the Cryo-EM structure of the CTR in complex with the ligand (pdb EUZ7, blue). Due to the lack density side chains of the ligand (orange), this portion of the peptide was modelled by Christopher Reynolds (university of Essex) into the published sCT-CTR Cryo-EM structure (Liang et al., 2017). Images were generated using ICM Molsoft.*

1.6.3 The TMs-ligand interactions

In the two domain model, the N-terminus of the ligand interacts with the TM and ECLs of Class B1 GPCRs. Evidence supporting this model includes data from generation of chimeric receptors containing the NTD-GCGR and TM bundle of the CTR. This chimera had a cAMP response (albeit low potency) to sCT despite no detectable binding, whereas the complementary chimera showed binding but no cAMP response (Stroop et al., 1995). The reduced affinity of the former is likely attributable to the lack of specific interaction between the C-terminus of the peptide and the NTD of the receptor, but the N-terminus of the peptide still retains the ability to activate the receptor. A different study using CTR/SECR chimeras revealed that ECL2 and ECL3 are also required for ligand binding and signalling (Dong et al., 2009), and similar observation were also made for SCTR and GLP-1R (Dong et al., 2016, Wootten et al., 2016, Koole et al., 2012b). Lastly, ligand crosslinking studies of the CTR, where Bpa was introduced in position 8 of the antagonist sCT(8-32) or in the full agonist hCT, showed that the antagonist crosslinks with M49 in the NTD (Pham et al., 2005) while the agonist crosslinks to residue L368 in ECL3 (Dong et al., 2004b). This further supports that the NTD of CTR has altered position in presence of the full length peptide.

The calcitonin-like subclass of ligands (CGRP, CTR, AMY and AM) have a characteristic disulphide ring bridge at the N-terminus, which can be removed without affecting the pharmacology of the sCT

agonist both *in vitro* and *in vivo* (Feyen et al., 1992, Orlowski et al., 1987, Hilton et al., 2000), suggesting that the cyclic structure of the peptide is not a requirement for biological activity. However, the first 6 residues that make the N- terminus are essential for receptor activation. For instance, progressive truncation of the N-termini of the CT peptides impairs intracellular signalling while causing little to no effect on binding. Removal of the first 2 residues of the CT ligand has no effect on signalling, while truncation between residues 3 and 6 produces partial agonists with increasing loss of efficacy determined by cAMP accumulation assay. Further truncation beyond residue 6 generates antagonists in HEK-293 (Hilton et al., 2000). Truncation beyond residue 9 also impairs affinity (Feyen et al., 1992, Hilton et al., 2000). Additionally, unpublished data from our group (Vi Pham 2004, PhD thesis, Monash University), where Bpa moiety was inserted in position 2, 3 and 4 of the sCT ligand, caused little to no reduction in affinity and only limited reduction of cAMP response of these agonists. These three agonists crosslinked weakly with the receptor, but their site of interaction could not be identified, suggesting potential introduction of steric hindrance (of the reactive Bpa group) that would not allow correct orientation of the moiety towards the receptor. Alternatively, the side chains of the residues within the cyclic ring in the N-terminus of the peptide were either not oriented towards the receptor side chains or retain a degree of flexibility. Both hypothesises would be supported by the low resolution structure of the CTR in complex with sCT (Liang et al., 2017), where only the backbone of the sCT peptide showed sufficient density to be modelled, whereas the side chains of the residues remained too flexible to provide sufficient density.

1.7 Scope of the thesis

Class B1 receptors are involved in metabolism and homeostasis, cardiovascular, stress and pain response, and associated pathologies. Their importance as drug targets is well established. There is currently a great deal of interest in explaining the promiscuous coupling of these receptors, as it opens up the possibility of generating biased compounds that selectively target a subset of signalling pathways that trigger beneficial physiological effects while avoiding those that lead to on-target side effects. However, to be able to specifically target one (or more) signal over others, we need to fully understand the profile of signalling of distinct ligands, and the molecular details of how this is achieved. In this

context, large knowledge gaps are evident in our understanding of some receptors. For some Class B1 receptors, such as GLP-1R, VPAC/PAC1R, biased agonism is well established, but the physiological implications are still not well understood. For the other receptors, biased agonism is less well established, however most are known to pleiotropically couple to many signalling pathways. In addition, mechanistic details into how biased agonism occurs at the molecular level for Class B1 receptors is limited to some mutagenesis and photo-crosslinking studies, and a handful of Class B1 structures that are partially incomplete and/or modified, or are bound to one (or few) of the several known ligands and effectors.

This thesis focuses on expanding the knowledge on a specific Class B1 GPCR, the CTR. In humans, the CTR is expressed in several variants; alternative splicing of the CTR gene produces two common splice variants of CTR. The expression pattern of these two splice variants alters significantly in different tissues, and there is some evidence that these variants can differentially couple to different intracellular effectors. A second common variant is the Leu/Pro polymorphism in the C-terminus of CTR (residue 447/463 in the $hCTR_a$/$hCTR_b$ variants, respectively), but little is known on the functional significance (if any) of this polymorphism. Additionally, the CTR shares less than 50% homology (in the TM bundle) with other Class B1 receptors, and structural differences across receptors are likely to be present. Each one of these factors can contribute to generation of unique receptor conformations that would impact on the selectivity, affinity and binding mode of the ligand, as well as in the repertoire of intracellular effectors that can be recruited to the receptor that in turn could trigger ligand or receptor-dependent physiological effects or pathologies.

In Chapter 3, extensive pharmacological characterisation of the four most common variants of hCTR was performed to examine how natural changes in the receptor sequence and/or structure affect ligand affinity, intracellular signalling and receptor trafficking. Using multiple ligands, including some that are approved therapeutics, I aimed to understand the contribution of these differences in the receptor to CTR function. The use of different ligands enabled exploration of the concept of biased agonism for this receptor, and the influence of splice/polymorphism on this phenomenon.

Chapter 4 and 5 investigate, at a molecular level, how ligands engage with the CTR to trigger intracellular signalling. At the commencement of these studies, there was no structure of CTR, and very little was known about how the orthosteric agonists interact with the CTR to activate intracellular signalling. Limited mutagenesis and photo-crosslinking studies on other Class B1 receptors highlighted distinct networks of residues within Class B1 receptor structure differentially modulate ligand binding or activation of distinct intracellular signalling pathways. However, ligands of the CTR family are structurally different to those of other Class B1, and there is evidence that they could interact with their receptors in unique ways. In Chapters 4 and 5 I have used Ala mutagenesis explore the role of residues within ELC2 and ECL3 (and adjacent TMs) of the CTR to determine the influence of those domains in engagement of different agonist with the receptor, and to map key networks within those loops that are important for driving ligand binding and intracellular signalling. Ligand affinity and multiple signalling pathways were assessed in presence of five different CTR agonists. I identified that each receptor-ligand pair established unique interactions with these domains, which were mapped onto a 3D model of the CTR. The mapping revealed different networks involved in activation of distinct signalling pathways, and these were not always correlated to those involved in binding. Moreover, these networks differed depending of the bound ligand. Furthermore, these networks are only partially conserved across different receptors of Class B1 GPCRs.

This study extends knowledge of the influence of how natural receptor variants, and distinct ligands modify CTR signalling, and identifies, for the first time, biased agonism at the CTR. Furthermore, it provides insight into which receptor residues are important for ligand binding, and activation of distinct signalling pathways. This knowledge will help to understand CTR activation, and will aid in rational design of novel potentially biased agonists.

CHAPTER 2

Materials and methods

2.1 Materials

2.1.1 Media and tissue culture reagents

Dulbecco's Modified Eagle's Medium (DMEM) and heat-inactivated foetal bovine serum (FBS) were purchased form GIBCO.

Selection antibiotics puromycin, zeocin and hygromycin B were provided respectively by Integrated Sciences, Sigma-Aldrich and Thermofisher Scientific.

2.1.2 Peptides

PHM-27, salmon (sCT or sCT(1-32)) and sCT(8-32), human (hCT), porcine (pCT) and chicken (cCT) calcitonins were purchased from Mimotopes Pty Ltd. Rat amylin (rAmy) and human calcitonin gene-related peptide (hαCGRP) were acquired from Bachem. sCT(8-32)-AF548 was labelled in house with 3 fold molar excess of AF568 succinimidyl-NHS-ester (Life technologies) at pH 8.3 and free dye removed using a 3 kDa molecular weight cut off centrifugal concentrator (Amicon). Labelled peptide was separated from unlabelled peptide by reverse phase HPLC and buffer exchanged into PBS before storing at -80°C. sCT(1-32)-ROX (rhodamine) and sCT(8-32)-ROX were synthesised and labelled by Mimotopes.

2.1.3 Antibodies

Mouse anti-human-cMyc 9E10 (IgG_1) was harvested from hybridoma supernatant, (ATCC cell line number CRL-1729, https://www.atcc.org/Products/All/CRL-1729.aspx) and purified in house over protein G sepharose by standard methods. 46/08-2C4 (IgG_1) and 31/01-1H10 (IgG_{2A}) anti-CTR antibodies were kindly provided by Peter Wookey (University of Melbourne) and are commercially available from Welcome Receptor Antibodies (WRA, Melbourne, Victoria). Rabbit anti-caveolin 1 (cat. ab2910) was purchased from Abcam. Goat Anti-mouse AF647 (cat. A-21235), goat anti-rabbit AF532 (cat. A-11009) were purchased from Thermofisher (formerly Invitrogen^{TM}).

2.1.4 General reagents

MycoAlert® Mycoplasma Detection kit for detection of mycoplasma infection was from Lonza.

Protease inhibitors cocktail (cat. P8340) and PMSF were purchased from Sigma-Aldrich. Acrylamide:bis (30% 37.5:1, cat. 1610158) and PVDF membrane for western blotting (cat.162-0177) were purchased from Bio-Rad.

2.1.5 Plasmids and primers

pEF5/FRT/V5 DEST, pOG44 and pENTR11 were from Thermofisher, while pENTR-SF1 was modified from pENTR-11. pEF-IRES-puro6 was modified from pEF-IRES-puro (Hobbs et al., 1998): the reference cDNA encoding human CTR in pcDNA3.1 had the cMyc epitope (encoding EQKLISEEDL) inserted immediately downstream of the predicted signal peptide (Signal P 4.1) by overlap extension PCR. The resulting cDNA was cloned as a NheI/XhoI fragment into pENTR-SF1 to generate pENTR-cMychCTR$_a$Leu.

Sequencing primers such as pENTR forward and reverse, BHG and T7 were synthesised by GeneWorks.

2.2 Molecular biology

2.2.1 Generation of single alanine point mutation of the cMycCTR$_a$Leu in pENTR vector

Quikchange Lightning Site-directed mutagenesis kit (Agilent) was used to introduce single alanine substitutions in cMycCTR$_a$Leu sequence (***Table S1, Appendix 1***) in pENTR vector. Primers listed in (***Table S4 and S5, Appendix 1***) were designed with PrimerX (www.bioinformatics.org) and were purchased from Bioneer Pacific. Parameters of the thermal cycle, digestion and amplification of the products were indicated in the protocol provided with the kit, in short: 50 ng of DNA template and 100 ng of primer were added into a PCR tube containing DNA polymerase and ligase, deoxy ribonucleotide triphosphates (dNTP) and buffer provided with the kit. 30 PCR cycles (denaturation 1 min at 95℃; annealing 1 min at 55℃; polymerisation 17 min at 65℃) produced novel double strand DNA (ds-DNA) that was digested with Dpn I (10 U/µl) overnight at 37℃.

2.2.2 Transformation

Amplification of plasmid DNA for transfection into mammalian cells was conducted in *E. coli* as follows. 2.5 µl of in-vitro PCR product or 1 to 10 ng of ds-DNA were pre-incubated for 30 min on ice with 30 µl of XL10-Gold Ultracompetent or DH5α cells. Transformation occurred by heat-shock of bacteria for 40 sec at 42℃, followed by 2 min incubation on ice. Transformed bacteria were left to recover and proliferate at 37℃ for 1 h in 250 µl of LB before being plated on agar plate containing antibiotic for the selection of the resistant plasmid vectors (pENTR, 50 µg/ml Kanamycin; pEF5/FRT/V5 and pIRESpuro6, 100 µg/ml Ampicillin). All selection plates were incubated at 37℃ for 12 to 16 h to allow colonies to form.

2.2.3 DNA amplification, extraction

Single colonies grown on agar selection were expanded for 12 to 16 h at 37℃ in LB media containing relevant antibiotic indicated in the previous Section (5 ml of broth for Miniprep DNA extraction, 250 ml for Maxiprep). Culture broth was pelleted for 15 min at 4℃, 1000 g and plasmids extracted using Wizard Plus SV Minipreps DNA Purification System kit (Promega) or QIAGEN® Plasmid Maxi Kits, following manufacturer instructions.

2.2.4 Sequence confirmation

In order to confirm the correct insertion of single alanine substitution, cMycCTR$_a$leu gene was sequenced and analysed as follows. 1 µl of sequencing primers corresponding to ~10 ng or 10pM (BGH, T7 for pEF5/FRT/V5 or pENTR forward and reverse for pENTR vector) (***Table S3 Appendix***) was added to ~400 ng of plasmid DNA and sent for automated sequencing at the Australian Genome Research Facility Ltd. Chromatographic sequences obtained were uploaded onto Biology WorkBench (http://workbench.sdsc.edu) and aligned with wild type (WT) cMycCTR$_a$leu gene.

2.2.5 Recombination into destination vector

Gateway® LR Clonase® II Enzyme mix (Life Technologies) was used to transfer the inserts from pENTR vectors into pEF5/FTR/V5 destination vector. In short, pENTR containing either WT CTR or relevant mutant, naïve pEF5/FRT/V5 destination vector and LR clonase were mixed following

manufacturer instructions and reaction was left to proceed overnight at room temperature (RT). DNA was then transformed into competent cells, expanded, extracted and sequenced as previously described.

2.3 Tissue culture

2.3.1 Mammalian cell culture

Cells were grown as a monolayer and maintained at 37℃, 85% humidity and 5% CO_2 in a water jacket incubator (Forma Scientific, Oh, USA) unless specified otherwise. Cells were maintained in sterile 175 cm^2 flasks and passaged at 95% confluency by Versene (PBS, 0.5mM EDTA, pH 7.4) treatment for approximately 5-15 min at 37 ℃. Cells were centrifuged at 350g for 3 min and resuspended in media into a new flask, discarded or counted and plated for assay.

Parental cell lines and transiently transfected African Green Monkey kidney fibroblast-like kidney cells (COS-7 (Gluzman, 1981)) were cultured in DMEM containing 5 % FBS. COS-7 cells stably expressing the four CTR variants/isoforms were transfected and FACS sorted by Dr. Sebastian Furness to select a polyclonal sub-population that highly expresses the four isoforms of hCTR. Cells cultured in media supplemented with 10 μg/ml puromycin.

African Green Monkey kidney Flp-In CV-1 cells stably expressing either WT or single alanine point mutation of the CTR_aLeu were cultured in DMEM, 5% FBS and 300 μg/ml hygromycin B.

2.3.2 Transient transfection of mammalian cells

To achieve transient expression of CTR receptor, naïve cells were seeded at $2x10^6$ cells/10 cm petri dish and cultured overnight at 37℃ in 5% CO_2 to 70-80% confluency. Each dish was transfected with DNA using PEI in a 1:6 DNA to PEI ratio: 5 μg of plasmid DNA in 250 μl sterile 150 mM NaCl was combined with 30 μl of 1 μg/μl of sterile polyethylenimine (PEI) diluted to 250 μl in sterile 150 mM NaCl. PEI/DNA solution was incubated at RT for at least 10 min. Culture media was replaced with fresh media and the PEI/DNA complex was added dropwise onto the cells. Dishes were incubated overnight at 37℃ in CO_2 humidified incubator prior to plating at the concentration required for each assay 24 h after transfection. Cells were further cultured for 24 h before assaying.

2.3.3 Stable transfection of mammalian FlpIn cells

In order to obtain stable expression of CTR (either WT or alanine mutants), Flp-In-CV-1 cells were seeded in 25 cm^2 flasks in DMEM, 5% FBS, 100 µl zeocin and allowed to reach 70-80 % confluency. Media was replaced with DMEM, 5% FBS and cells were transfected using PEI and 5 µg of DNA mix (prepared at the ratio 1:10 of pEFS/FTR/V5-dest and pOG44). 48 h after transfection cells were detached with Versene and re-plated in the same flask in presence of DMEM, 5% FBS, 300 µg/ml hygromycin B for selection of stably expressing cells.

2.4 Functional Assays

2.4.1 Iodination of sCT(8-32)

To perform whole cell binding assays, sCT(8-32) was iodinated in house to obtain mono-iodo-tyrisyl ^{125}I-sCT(8-32). In a 1.7 ml Eppendorf tube the following solutions were added in order: 5 µl of 1 mg/ml chloramine T (freshly prepared in PBS, pH 7.4) and 10 µl of ^{125}I (~350 mCi/ml, Perkin Elmer) were incubated at RT for 60 sec. 20 µl of PBS and 5 µl of 0.1 mM sCT(8-32) were then added and iodination was left to proceed at room temperature for 10 sec. Reaction was quenched by addition of 200 µl of KI (5 mg/ml prepared in PBS) and diluted with an additional 260 µl of PBS to the final volume of 500 µl. Excess of ^{125}I was separated from peptide by reverse phase HPLC on a C-18 column using a gradient from 0.1% TFA in H_2O to 0.1% TFA in acetonitrile. BSA (final 0.1 %) was added to fractions containing iodinated peptide and stored at -20℃.

2.4.2 Whole cell radioligand binding assay

To determine both receptor expression and affinity for ligands used in this study, cells were seeded overnight in DMEM, 5% FBS in a 96 wells plate. On the day of the assay, cells were incubated with 80 µl of binding buffer (DMEM, 25 mM HEPES, 0.1% BSA, pH 7.4) and chilled at 4℃ for at least 1 h to inhibit internalization. Approximately 10,000 to 50,000 cpm/well (corresponding to 25-100 pM) of ^{125}I-sCT(8-32) were diluted in 10 µl and added to wells, followed by 10 µl of relevant dilution of competing non-iodinated ligand. Plates were incubated overnight a 4℃ to reach equilibrium. Binding buffer was then removed and wells washed 2x with ice cold PBS. Bound ligand was stripped with 50 µl of 0.1 M

NaOH, transferred into scintillation tubes and γ radiation detected using a γ-counter (Wallac Wizard 1470 Gamma Counter, Perkin Elmer, 80% counter efficiency). Data was analysed in Graphpad Prism 7 and normalized to total level of bound ligand and non-specific binding, defined by saturating concentration of sCT(8-32) (1 μM) and vehicle.

2.4.3 cAMP accumulation Assay

cAMP production was assessed in 96 well clear culture plates, 48 h following transient transfection of cells (30,000 cells/well) or 12-16 h after seeding stable cell lines (10,000 cells/well for COS-7 or 25,000 cells/well for CV-1 FlpIn). Culture media was replaced with 90 μl of Stimulation Buffer (phenol red free DMEM, 0.1% BSA, 0.5 mM IBMX, 5 mM HEPES, pH 7.4) and incubated for 30 min at 37℃, 5% CO_2. Cells were stimulated with either forskolin (10^{-4} M final), vehicle or relevant concentrations of ligands for 30 min at 37℃, 5% CO_2, media was then removed and cells were lysed with ice-cold 100% (v/v) ethanol. After ethanol was evaporated, 75 μl of lysis buffer, containing 0.3% Tween20 (v/v), 5 mM HEPES and 0.1% BSA (w/v), pH7.4 was added. Endogenously produced cAMP was measured using a Lance cAMP detection kit (PerkinElmer) as follows: 5 μl of cell lysate were transferred into a 384 well optiplate (Perkin Elmer). A cAMP standard curve ranging between 0.1nM and 10μM was prepared in lysis buffer and transferred in the same plate. 5μl of anti-cAMP antibody mixture (Alexa fluor-647 anti-cAMP diluted in detection buffer supplied by the manufacturer) were added to each wells of the optiplate and incubated for 30 min at RT in reduced lighting conditions. Subsequently, 10 μl of Eu-SA and biotinylated cAMP mix (EuW8044 labelled streptavidin (Eu-SA) and biotinylated cAMP diluted in kit detection buffer and pre-incubated for a minimum of 15 min) was added to each well and incubated at RT for 12-16 h before signal was measured using a top read on the Envision plate reader system. In Graphpad Prism 7, raw RFU data were interpolated to the cAMP standard curve performed in parallel to give absolute cAMP values and normalized to forskolin and vehicle.

2.4.4 iCa^{2+} mobilization Assay

Stably expressing cell lines were seeded at 10,000 cells/well for COS-7 or 25,000 cells/well for CV-1 FlpIn in 96 wells plates and incubated overnight at 37℃, 5% CO_2 in DMEM, 5% FBS. Cells were

washed twice with Ca^{2+} Buffer (150 mM NaCl, 10 mM HEPES, 10 mM D-glucose, 2.6 mM KCl, 1.18 mM $MgCl_2$, 2.2 mM $CaCl_2$, 0.5% BSA, 4 mM probenecid, pH 7.4) before addition of 1 μM Fluo4-AM diluted in Ca^{2+} buffer. Cells were incubated at 37℃ for 45-60 min (no CO_2) before stimulation and detection of Ca^{2+} mobilisation in a FlexStation 3 (Perkin Elmer Molecular Devices) using following parameters: 37℃, excitation 485 nm, emission 525 nm, baseline reads of 15 sec before drug addition, fast drug dispense, and 120 sec reading. All data were extracted as the peak Ca^{2+} response and normalised to ATP (10^{-4} M) and vehicle.

2.4.5 IP_1 assay

25,000 cells/well of CTR stable CV-1 FlpIn were plated in 96 well plates and cultured overnight in DMEM, 5% FBS in a humidified incubator at 37℃ and 5% CO_2. Culture media was replaced with 90 μl of Stimulation Buffer (1 mM $CaCl_2$, 0.5 mM $MgCl_2$, 4.2 mM KCl, 146 mM NaCl, 5.5 mM D-glucose, 50 mM LiCl, 0.1% BSA, 10 mM HEPES, pH 7.4) and incubated for 40 min at 37 ℃, 5% CO_2. Cells were stimulated with either relevant ligands dilutions, ATP (10^{-4} M final) or vehicle for 60 min at 37℃, 5% CO_2 and then lysed with 20 μl of lysis buffer (50 mM HEPES pH 7, 15 mM KF, 1.5% (v/v) TritonX-100, 3% (v/v) FBS, 0.2% (w/v) BSA). Endogenous IP_1 was measured using an IP-One HTRF® assay kit (CisBio) as follows: 7 μl of cell lysate or IP_1 standard curve (ranging between 38.5 and 2.4 μM, prepared in lysis buffer, was transferred into a 384 well proxiplate (Perkin Elmer). 3μl of beads mix (1:20 parts of terbium cryptate-labelled anti-IP_1 and 1:20 parts d2-labelled IP_1 diluted in lysis buffer supplied with the kit) were added to each wells and plate was incubated for 60 min at 37℃ in reduced lighting conditions before reading on the Envision. Similar to cAMP accumulation assay, raw data obtained were interpolated to standard curve and normalised to ATP and vehicle.

2.4.6 ERK1/2 Phosphorylation Assay

Stably expressing cell lines were seeded at 10,000 cells/well for COS-7 or 25,000 cells/well for CV-1 FlpIn in 96 wells plates and incubated overnight at 37℃ with 5% CO_2 in DMEM, 5% FBS. Culture media was replaced with FBS-free DMEM, 0.1% BSA incubated for a further 12-16 h. An initial time-course was performed for each ligand to assess the maximum peak of ERK1/2 phosphorylation, using

relevant drugs at 1 μM (final concentration). Subsequently, concentration-response curves were performed for each drug at the time point of maximum ERK1/2 phosphorylation. In both cases, after stimulation, media was removed and cells were lysed in lysis buffer (TGR Bioscience). ERK1/2 phosphorylation was detected using an Alphascreen kit (TGR Bioscience) as previously described (Koole et al., 2010). All data were normalised to vehicle and 10% FBS.

2.4.7 β-arrestin recruitment by BRET assays

24 h post transient transfection (each CTR variant was encoded in the dual vector BIVISTI in combination with either β-arrestin1 or 2), cells were seeded in a white 96 wells plate (PerkinElmer) at 30,000 cells/well and incubated overnight in DMEM, 5% FBS at 37℃ in 5% CO_2. Cells were washed twice with buffer (HBSS, 0.05% BSA, pH 7.4) and incubated for 30 min at 37℃. Coelenterazine (5 μM final) was added and incubated for another 10 min before BRET measurement using a LUMIstar (BMG LABTECH GmbH, Ortenberg, Germany) that allows for simultaneous reading of signals at 475 nm (Rluc8) and 535 nm (Venus). Wells were read for 4 cycles before addition of 10 μl of ligand (final concentration 1 μM) or negative control (vehicle) and read every 10 sec for a further 12 min. The BRET signal was calculated by dividing ratio of emission at 535 nm by 475 nm. After baseline correction, the vehicle ratio was then subtracted to give the ligand-induced BRET signal.

2.5 Imaging

2.5.1 Internalisation and β-arrestin recruitment

To identify the redistribution of β-arrestins upon ligand stimulation, CTR stable COS-7 cells were transiently transfected with the either β-arrestin 1 or β-arrestin 2 labelled with a Venus-tag at the C-termini. Cells plated at 30,000 cells/well in 96 wells plates and cultured overnight at 37℃ in 5% CO_2 in DMEM, 5% FBS to be assessed 48 h after transfection. On the day of the assay, cells were serum starved in DMEM for 2 h, 1 μM of relevant drugs were added at the varies time-points and stimulation continued at 37℃. Media was then removed and cell were fixed for 15 min in 4% PFA in PBS at 4℃, followed by 3x PBS washes. Images were collected with Operetta (PerkinElmer), objectives: 20x/Olympus LUCPlanFLN, 0.45 NA or 10x/Olympus U Plan FLN, 0.3 NA.

2.5.2 Internalization of fluorescent ligand and tagged-receptor.

To follow the internalization of the ligand, COS-7 cells stably expressing the 4 isoforms of the CTR were plated at 10,000 cells/well in a 96 wells/plate and stimulated with 1 or 0.1 μM of either sCT(8-32)-AF548 or sCT(1-32)-ROX for 5, 10, 15, 30 or 60 min at 37℃. Cells were subsequently fixed and imaged as described in Section 2.5.1 using the Operetta. Fluorophores were excited at 550-570 nm and emission was acquired at 570-620 nm.

2.5.3 Internalization of fluorescent antibody and tagged receptor

To determine internalization of receptor, cMycCTRLeu (either a or b variants) stably expressed in COS-7 cells were seeded overnight at 10,000 cells/well on μ-ibidi 8 wells slide (DKSH Australia Pty Ltd.) and cultured overnight at 37 ℃, 5% CO_2. On the day of the assay, media was replaced with phenol red free DMEM, 0.1% BSA. Cells were chilled to 4℃ for 1 h and relevant compounds were added: anti-cMyc antibody 9E10-AF647 (1 ug/ml), sCT(1-32)-ROX (100 nM) or sCT(8-32)-ROX (100 nM) (fluorescently-conjugated ligands) or a combination of antibody and ligands. Cells were then incubated at 4℃ for 1 h to allow binding without internalization. Wells were washed 2x with ice cold PBS and 200 μl of cold media were added to each well. Slide was incubated in a 37 ℃ chamber built into a SP8 confocal microscope (Leica TCS SP8, LASX v2.1), using a 63x/U Plan APO CS2, 1.43 NA and imaged every 1 min for 1 h (561 nm BP 570-610 and 633 nm BP 640-700).

2.5.4 9E10 mouse anti-cMyc antibody purification

In house antibody purification was required to obtain anti-cMyc antibody (9E10) from the supernatant of mouse hybridoma, using a Protein G conjugated agarose resin. In short: supernatant from hybridoma culture was loaded onto Protein G-agarose column (HiTrap 1 ml column, GE Healthcare) at a rate of 1 ml/min to allow antibody binding to the resin. Extensive wash with PBS was performed to eliminate contaminated protein. Antibody was eluted in 0.1 M glycine buffer, pH 2.7. Fractions containing protein were neutralised with Tris-HCl, pH 9 upon collection. For storage, 9E10 was dialysed in PBS, 0.02% azide and concentrated to 1 mg/ml by centrifugation at 4,000 g, 4℃ on 100 kDa Amicon centrifugal filter unit (Merck).

2.7 Data analysis

2.7.1 Equations

Data analysis was performed in GraphPad Prism 7.

Homologous competition binding was used to derive B_{max} and quantify receptor expression in whole cell binding assay calculated as follows.

Equation 1:

$$y = \frac{Bmax * [Hot]}{[Hot] + [A] + Kd} + Bottom$$

$$sites/cell = \frac{Bmax * 6.02 * 10^8}{SA * CN}$$

where B_{max} corresponds to the maximal binding capacity of the system; *[Hot]* is the concentration (expressed in nM) of ^{125}I-sCT(8-32) and [*A]* is the molar concentration of competing ligand; K_d is the equilibrium dissociation constant of ^{125}I-sCT(8-32) in nM; *SA* is the specific activity of ^{125}I-sCT(8-32) and equals to 3907.2 cpm/fmol; *CN* is the cell number plated for each replicate.

Affinity (Ki) for each of the ligand used was also measured in heterologous competition binding assay.

Equation 2:

$$a = -(NS + 1)$$

$$b = \left(1 + [A] - 10^{logKi}\right) * Kd * SA * 100 + [\mathrm{Hot}]$$

$$c = (NS + 1) * b + NS * [Hot] + Bmax$$

$$d = -[Hot] * (NS * b + Bmax)$$

$$y = \frac{-c + \sqrt{c^2 - 4ad}}{2a}$$

where *NS* stands for non-specific binding of ^{125}I-sCT(8-32).

Concentration-response curves were analysed using three parameter fit.

Equation 3:

$$y = Bottom + \frac{(Top - Bottom)}{1 + 10^{(logEC_{50} - \log(A))}}$$

cAMP accumulation response in Chapter 3 were fitted more accurately using a biphasic curve, when compared to a three parameter fitting, as determined by a F-test in Graphpad Prism 7.

Equation 4:

$$Span = Top - Bottom$$

$$Section1 = (Top - Bottom) * \frac{Frac}{1 + 10^{(LogEC50_1 - \log[A]) * nH1}}$$

$$Section2 = (Top - Bottom) * \frac{(1 - Frac)}{1 + 10^{(LogEC50_2 - \log[A]) * nH2}}$$

$$Y = Bottom + Section1 + Section2$$

where 1 and 2 represent the 2 phases of the curve; *bottom* and *top* represent the plateau *y* values at the left and right ends of the curve, that are respectively the basal and maximum response to stimulation; $LogEC_{50}$ is the concentration of ligand that produce a half-maximal response; *nH1* and *nH2* are the Hill slopes factors values and have been constrained 1; *Frac* is the proportion of maximal response of the more robust phase.

In order to define the contribution of a specific residues to signalling bias of the receptor, operational model of partial agonism was applied to derive the τ values, which accounts for receptor expression and is a measurement of efficacy of a ligand in a specific system. τ expresses the inverse of the fraction of receptor that have to be occupied to produce 50% of the maximal response in a defined signalling pathway.

Equation 5:

$$y = Bottom + \frac{Emax - Bottom}{1 + \frac{10^{logKa} + 10^{log[A]}}{10^{log\tau + log[A]}}}$$

where E_{max} represents the maximal response in the system and K_a is the equilibrium dissociation constant of an agonist.

2.7.2 Error propagation

Each instrumental measurement is associated to an uncertainty ∂ (SEM or SD). When instrumental data are mathematically processed and combined, it is necessary to propagate their uncertainty in a manner that reflects the manipulation of the original data.

If an equation is calculated as the sum or difference between data ($y = a \pm b$), than the error has to be propagated as equation 6:

$$\partial y = \sqrt{\partial a^2 + \partial b^2}$$

In case of functions such as $y = a \times b$ or $y = a \div b$, error propagation is defined as equation 7:

$$\partial y = |y| \sqrt{\left(\frac{\partial a}{a}\right)^2 + \left(\frac{\partial b}{b}\right)^2}$$

2.7.3 Statistics

Data and estimated parameters were assessed by one way analysis of variance (one-way ANOVA). Dunnetts post-hoc test was used to assess significance relative to the control ligand hCT or the receptor variant CTR_aleu in Chapter 3, or to the wild type receptor (WT) in Chapters 4 and 5. Additionally, Bonferroni post-hoc test was used in Chapter 3 to perform multiple comparisons across all ligands or receptor variant.

Significance was taken as $p<0.05$.

CHAPTER 3

Characterisation of signalling and regulation of common calcitonin receptor splice variants and polymorphisms

3.1 Introduction

The calcitonin receptor (CTR), a class B GPCR, is highly expressed in osteoclasts where it is involved in the physiology of bone remodelling and homeostasis by reducing osteoclast activity, and differentiation from precursors (Fujikawa et al., 1996b). The CTR is therapeutically targeted for the treatment of osteoporosis, Paget's disease and severe hypercalcemia (Minhas and Virdi, 2017, Langston and Ralston, 2004, Cosman et al., 2014). The receptor is also expressed in multiple other tissues including within the kidneys, gastrointestinal system (Goebell et al., 1979), brain (Shah et al., 1990, Rohner and Planche, 1985, Laurian et al., 1986), leucocytes and their precursors (Fujikawa et al., 1996b), lungs, placenta, uterus, sperm (Kuestner et al., 1994), and in several types of cancer (Egerton et al., 1995). However, the physiological role of CTR expression in most of these cells and tissues is poorly understood.

The primary endogenous ligand for the CTR is a 32 amino acid peptide named calcitonin, and this peptide contains a disulphide bond between Cys residues 1 and 7. Calcitonin peptides from different species vary in sequence ***Table 1.1***, but all maintain the cyclic N-terminal structure through the formation of the disulphide bond (Hilton et al., 2000). Both hCT and sCT are currently used clinically, but the majority of the formulations incorporate sCT (Miacalcic, Fortical, Calcimar, Cibacalcin ®) (Plosker and McTavish, 1996) due to its higher *in vivo* efficacy (40-50 fold), compared to the human analogue, in reducing bone resorption and hypercalcaemic effects. In 2004 Ma *et al.* (2004) reported that PHM-27, an endogenous 27 amino acid peptide closely related to the vasoactive intestinal peptide, can also activate the CTR, promoting cAMP formation.

Upon activation, the CTR primarily couples to the adenylate cyclase stimulatory G protein isoform, Gαs, promoting the formation of intracellular cAMP. However, the receptor is pleiotropically coupled, with evidence for activation of Gαq and Gαi G protein isoforms (Chabre et al., 1992, Chen et al., 1998, Chakraborty et al., 1991). CTR activation also promotes fast transient Ca^{2+} mobilization from intracellular stores and ERK1/2 phosphorylation (Raggatt et al., 2000). CT can induce CTR downregulation and cell remodelling via PKA (and perhaps PKC) (Wada et al., 1995, Suzuki et al.,

1996), whereas secretion of HCl and other bone remodelling factors from osteoclasts is inhibited by PKC activation (Sørensen et al., 2010).

The CTR is also reported to internalise following receptor activation (Schneider et al., 1988, Findlay et al., 1994, Seck et al., 2003); however, to date, there is limited evidence for the recruitment of β-arrestins to the CTR (Andreassen et al., 2014), despite these proteins being involved in the process of desensitization and internalization for many other GPCRs (Luttrell and Lefkowitz, 2002, Ferrari et al., 1999, Jorgensen et al., 2005, Reiter and Lefkowitz, 2006).

The CTR can be identified in animals down to the simplest chordates (Lin et al., 1991, Albrandt et al., 1993, Sexton et al., 1993, Gorn et al., 1992, Yamin et al., 1994, Shyu et al., 1996) and in humans the CTR is expressed in at least 2 major variants as the result of alternative splicing. These variants differ by the presence or absence of a 16 amino acid insertion in the first intracellular loop, and are termed $hCTR_a$ (or hCT_a, the insert negative) and $hCTR_b$ (or hCT_b, the insert positive) (Kuestner et al., 1994). When compared to the $hCTR_a$ splice variant, $hCTR_b$ shows more restricted expression (Kuestner et al., 1994). For instance, high levels of both splice variants are identified (via PCR) in the reproductive system, whereas $hCTR_b$ expression was lower than $hCTR_a$ or could not be detected in gut, lungs, kidney, bones and brain. $hCTR_b$ is reported to be unable to trigger a Ca^{2+} response when activated (Gorn et al., 1992, Kuestner et al., 1994, Nakamura et al., 1995, Chen et al., 1997, Moore et al., 1995, Raggatt et al., 2000). In 1994, Kuestner *et al.* (1994) reported a polymorphism of the insert negative hCALCR in which position 1377, with respect to the start codon, was either a C or T nucleotide encoding either a Pro or Leu, respectively. While in other mammals the Pro codons is completely conserved at this position and Kuestner *et al.* (1994) speculated that this may be a cloning artefact, the widespread occurrence of this polymorphism in humans was confirmed by others (Nakamura et al., 1996, Wolfe et al., 2003). Prevalence of the specific polymorphic variant is related to ethnic background; Caucasians, Hispanics and Afro-Americans predominantly have a genotype encoding the Leu variant or are heterozygous (Wolfe et al., 2003), while Asians, in particular the Japanese population, are predominantly homozygous for the Pro variant (Nakamura et al., 1996). Some clinical studies have reported a potential correlation between a genotype encoding the Leu polymorphism and an increased

incidence of osteoporosis and kidney stone disease (Masi et al., 1998a, Braga et al., 2002, Masi et al., 1998b, Mitra et al., 2017); these have low power and other studies have failed to confirm these findings (Dehghan et al., 2016, Wolfe et al., 2003).

Many factors influence the observed pharmacology and tissue responses upon CTR activation. First of all, two different ligands are used clinically, each one potentially stabilizing distinct receptor conformations. This could give rise to biased agonism, but biased agonism has yet to be explored at this receptor. Additionally, different splice or polymorphic variants could display distinct signalling profiles that may also differ in the presence of different ligands. To date, this has also not been extensively studied. Differences in the relative expression of $hCTR_a$ and $hCTR_b$ splice variants may influence tissue response, resulting in different outcomes of CTR activation in distinct tissue beds. Hence, ligand-dependent biased agonism, type of receptor variant expressed and other components of the cellular background could all influence outcomes of CTR activation. This likely contributes to observed differences in agonist, for example, in proliferative versus apoptotic actions that have been observed in *in vitro* studies in breast cancer and prostate cancer cell lines (Thomas and Shah, 2005, Thomas et al., 2006, Thomas et al., 2007, Lacroix et al., 1998). Currently, there are only limited studies comparing the cellular response of either receptor variant or different ligands in different cellular backgrounds. To our knowledge robust, direct comparison of the most common splice and polymorphic variants, for their ability to activate distinct signalling pathways in response to different CTR ligands, has not be performed. Therefore, in this study, we have characterised the cellular responses triggered by a variety of agonists (four CT peptides derived from different species and PHM-27) at the 2 most common hCTR splice variants ($hCTR_a$, or $hCTR_b$), each with the 2 human polymorphisms (Leu or Pro) following heterologous expression in COS-7 cells. These tools allow us to evaluate if ligands with distinct sequence can elicit biased agonism at the CTR and to assess if signalling profiles vary substantially between the different hCTR variants. Finally, we have followed the hCTR internalisation and investigated the ability of the distinct peptides to recruit β-arrestin1 or β-arrestin2 to the hCTR variants.

3.2 Results

To compare the signalling profiles of different CTR variants when activated by distinct ligands, $hCTR_aLeu$, $hCTR_bLeu$, $hCTR_aPro$ and $hCTR_bPro$ were stably expressed in COS-7 cells and pharmacologically assessed. COS-7 cells do not endogenously express either CTR, CLR or RAMPs that could alter the response observed. Throughout, an N-terminally cMyc tagged CTR was used. This construct has been previously tested in the laboratory and does not alter receptor expression, binding or cAMP signalling.

3.2.1 Cell surface expression of hCTR variants

Analysis of cell surface expression of each of the four different receptor variants was assessed using both FACS and radioligand binding (***Figure 3.1***). Homologous competition for ^{125}I-sCT(8-32) revealed that the $hCTR_bLeu$, $hCTR_aPro$, $hCTR_bPro$ variant were expressed at similar levels (0.83±0.33 x10^6, 0.92±0.22 x10^6, 0.64±0.31 x10^6 receptors/cell, respectively), while the $hCTR_aLeu$ had ~4 fold higher expression (3.57±0.81 x10^6 receptors/cell).

One-way ANOVA comparison between $hCTR_aLeu$ and all other splice/polymorphic variants showed statistically significant difference in expression by radioligand binding (Dunnett's post-test $p<0.01$). No statistically significant difference in expression between the other variants was observed (***Figure 3.1 B***).

Expression of the different CTR variants was also assessed by flow cytometry of using an anti-mouse AF-488 secondary antibody for detection of anti-cMyc binding to cMyc-tag introduced at the extreme N-terminus of these receptors (***Figure 3.1 C***). Compared to unstranfected COS-7 cells (in black), $hCTR_aLeu$ variant showed higher expression. Interestingly, $hCTR_bLeu$ variant also appeared to be expressed at a similar level, whereas both splice variants of the Pro polymorphism were expressed at a lower level than the $hCTR_a$ splice variants. This contrasted with binding estimates with the antagonist ^{125}I-sCT(8-32), and may imply alterations of the equilibrium between conformational states of the $hCTR_aLeu$ and $hCTR_aPro$ variants.

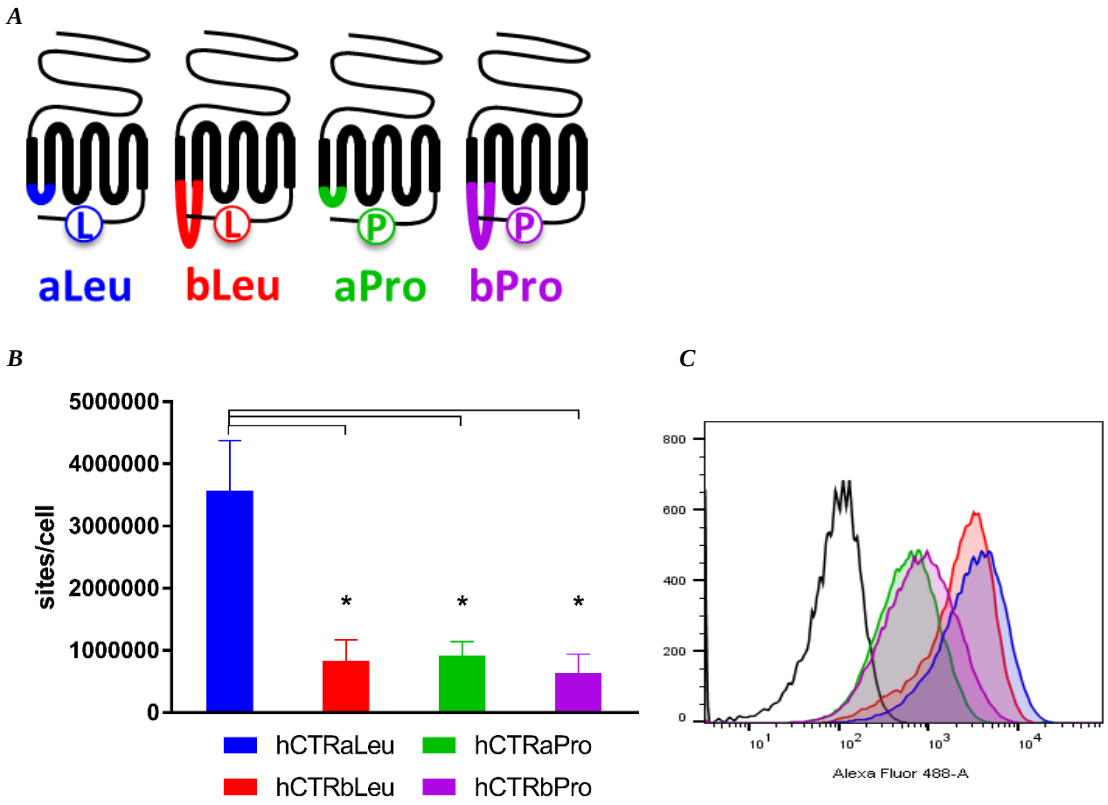

Figure 3.1 Cell surface expression of the 4 hCTR variants stably expressed in COS-7 cells. *(A) Schematic representation of the four CTR variants assessed in this study. 16 amino acid instert in intracellular loop 1 (ICL1) and Leu/Pro polymorphism at residues 447/463 (in the hCTR$_a$/ hCTR$_b$ splice variant, respectively) are highlighted in the same colour code used throughout this Chapter. (B) Homologous competition radioligand binding was performed in presence of 3 concentrations of ^{125}I-sCT(8-32), to derive B_{max}, thus sites/cell. All values are mean+S.E.M. of 4 independent experiments conducted in duplicate. Statistical significance of differences in expression of splice/polymorphic variant in comparison to the hCTR$_a$Leu was determined by a one-way analysis of variance and Dunnett's post-test ($p<0.05$ represented by *). (C) Representative flow cytometry of more than 5 experiments. COS-7 cells stained with anti-cMyc antibody and goat anti-mouse AF488 secondary. CTR variants are represented with the same colour scheme used in panel (A), while control, naïve COS-7 cells are represented in black (flow cytometry experiments were performed by Dr. S. Furness).*

3.2.2 Ligand affinity at the hCTR variants

Homologous competition of ^{125}I-sCT(8-32) binding with sCT(8-32) was used to assess the affinity of the antagonist sCT(8-32). To assess the affinity of the other peptides ***(Table 1.1)***, heterologous competition radioligand binding was used to determine peptide pK$_d$, following correction of pK$_i$ values using the Cheng-Prusoff equation (Equation 4 Section 2.6.1) ***Table 3.1***.

Consistent with previous literature (Kuestner et al., 1994, Wolfe et al., 2003, Moore et al., 1995, Hilton et al., 2000, Furness et al., 2016), each receptor variant showed a similar trend in their binding profiles for the different CT ligands with sCT, sCT(8-32) and cCT having higher affinity compared to pCT (20-100 fold) and hCT (150-1000 fold) (***Figure 3.2 A-D, Table 3.1***).

To determine the effect of differences in receptor sequence (i.e. splicing and polymorphism) on affinity, statistical analysis of the same ligand across receptor variants was performed, using $hCTR_a$Leu as the reference (***Table 3.1***). This revealed that both sCT and cCT had a significantly higher affinity at the $hCTR_b$ variants with increased affinity (3-10 fold) for both $hCTR_b$ polymorphism compared to both polymorphisms at the $hCTR_a$ splice. In addition, both sCT and cCT had significantly higher affinity for the Pro polymorphism compared to the Leu, when compared to the $hCTR_a$ variant (4-5 fold), but not at the $hCTR_b$ variant. sCT(8-32), hCT and pCT did not show significant differences in affinity between hCTR splice or polymorphic variants.

PHM-27 displayed only partial competition of the radiolabelled sCT(8-32) (***Figure 3.2 A-D***). This may be due to low affinity or to binding to a distinct binding site to that of ^{125}I-sCT(8-32), such that it doesn't fully compete with the radioligand. A robust pK_i value, therefore, could not be determined for this peptide.

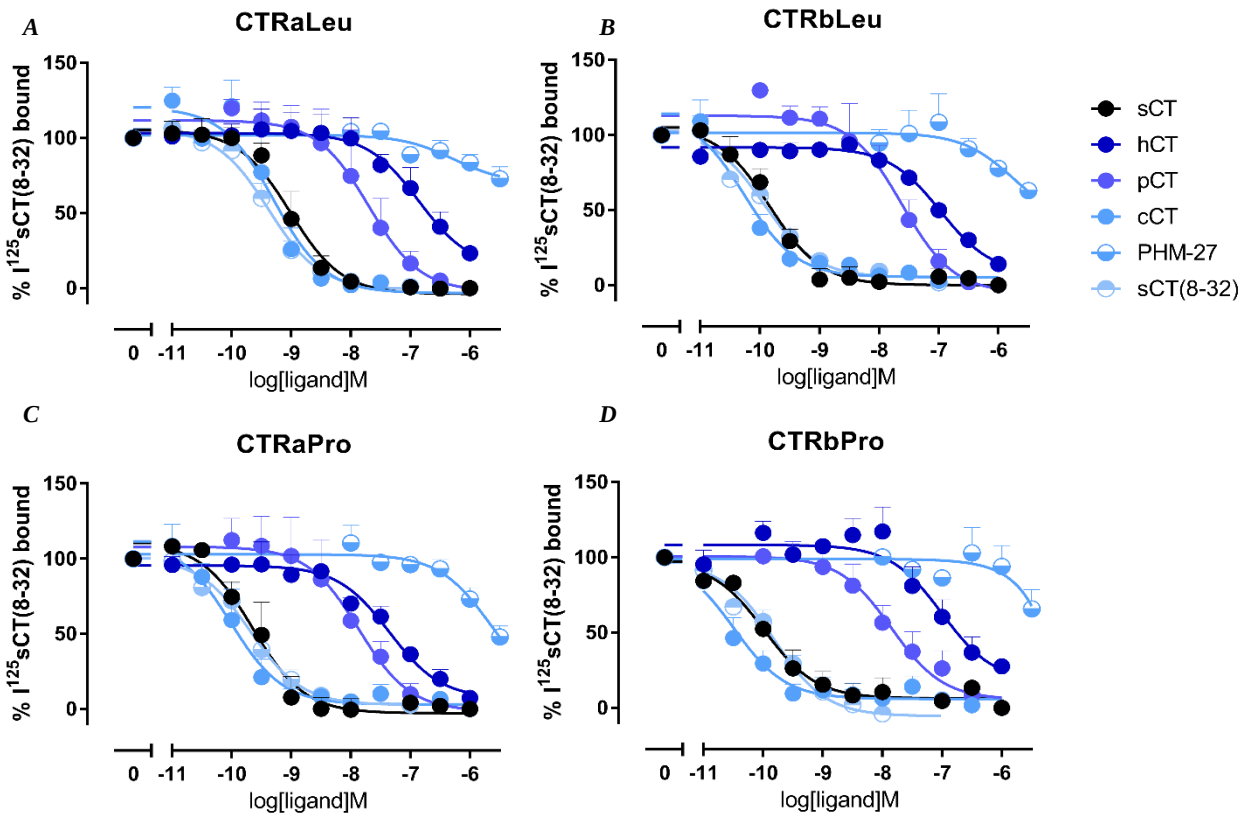

Figure 3.2 Homologous and heterologous competition binding profiles. *Whole cell radioligand competition binding studies of the 6 ligands at hCTR$_a$Leu (A), hCTR$_b$Leu (B), hCTR$_a$Pro (C), hCTR$_b$Pro (D) stably expressed in COS-7 cells were performed using the radioligand ^{125}I-sCT(8-32). All values are mean+S.E.M. of 3 to 4 independent experiments conducted in duplicate.*

	hCTR$_a$Leu	hCTR$_b$Leu	hCTR$_a$Pro	hCTR$_b$Pro
sCT(8-32)	9.49±0.19	10.17±0.22	9.73±0.30	9.87±0.29
sCT	9.10±0.11	10.11±0.09*	9.69±0.13*	10.11±0.11*
hCT	6.83±0.19	7.19±0.12	7.2±0.13	7.12±0.21
pCT	7.78±0.20	8.02±0.16	7.95±0.23	7.97±0.16
cCT	9.37±0.16	10.53±0.12*	10.06±0.14*	10.61±0.11*
PHM-27	N.D.	N.D.	N.D.	N.D.

Table 3.1 Ligand affinity expressed as** pK_i **for the peptides used in this study at each of the hCTR variants stably expressed in COS-7 cells. *Whole cell radioligand binding was performed for each ligand and receptor variant using ^{125}I-sCT(8-32). All values are mean±S.E.M. of 3 to 4 independent experiments conducted in duplicate. Significant differences in affinity of each ligand was determined by multiple comparisons across receptor variants in a one-way analysis of variance and Bonferroni post-test ($p<0.05$ represented by *).*

3.2.3 Assessment of intracellular signalling induced by CT peptide ligands at the four hCTR variants

cAMP accumulation, pERK1/2 and intracellular calcium mobilisation were determined for each individual splice/polymorphic variant of the hCTR stably expressed in COS-7 cells. Cells were stimulated with each of the 4 CT peptides (human (hCT), salmon (sCT), porcine (pCT), chicken (cCT)) or PHM-27. Concentration response curves were generated for each ligand and pEC_{50} values and maximal response (E_{max}) were calculated. In all the statistical analysis, responses for $hCTR_a$Leu were used as a reference to compare ligand responses between receptor variants, while hCT was used as the reference ligand for the comparison between different ligands at individual receptor variants.

3.2.3.1 cAMP signalling

cAMP accumulation profiles in response to CT peptides were initially analysed using an F-test to compare a biphasic curve fit and a three-parameter logistic curve fit. The $hCTR_a$ splice variant concentration-response curve was best described by a two phase curve fit, whereas the $hCTR_b$ splice variant for all CT ligands favoured a three-parameter logistic curve fit (***Figure 3.3***).

One-way ANOVA comparison of the same ligand across different $hCTR_a$ polymorphic variants revealed there was no statistical difference between the fraction of cAMP response that constituted the high potency site for any ligand at any variant (***Table 3.2***). Similarly, there was no significant difference in potency for any CT peptide at the high affinity site, or lower affinity site for either polymorphisms of the $hCTR_a$ splice. In addition, the potency for cAMP response for each ligand at the $hCTR_b$ splice variants was the same for both polymorphisms. When comparing E_{max}, the $hCTR_b$ splice variant showed reduced maximal response compared to the $hCTR_a$ splice in presence of any of the peptides assessed, although comparison between $hCTR_b$Leu and $hCTR_a$Pro showed significant differences only in presence of cCT peptide. When $hCTR_a$Leu E_{max} was compared to the $hCTR_b$ variants, all ligands showed reduced E_{max}, while only hCT and cCT showed statistical difference between $hCTR_a$ polymorphic variants (Pro/Leu) (***Figure 3.3***, ***Table 3.2***). The $hCTR_a$Pro variant showed significantly higher E_{max} than $hCTR_b$Pro (but not $hCTR_b$Leu) for all CT peptides.

Comparison of distinct CT peptide ligand responses at the same receptor variant showed that sCT, pCT and cCT had no significant differences in potency when compared to hCT for all variants. However, cCT had a higher E_{max} than the other peptides at both polymorphisms in the $hCTR_a$ splice variant, although statistical significance was only evident for the $hCTR_a$Pro variant.

Assessment of PHM-27 revealed a different cAMP profile to that of the CT peptides. Here, for all four receptor variants, the data fit to a three parameter linear regression curve revealing only a one site fit. PHM-27 was a weak partial agonist, with a statistically lower E_{max} and pEC_{50} in comparison to hCT at all variants assessed. In addition, PHM-27 was a weaker potency agonist at all hCTR variants (> 10 fold), with statistical significance observed relative to hCT of all variants with the exception of $hCTR_a$Pro, where however there was a similar trend. When comparing PHM-27 responses across different receptor variants, similar to that observed with the CT peptides, the maximal response to PHM-27 was significantly lower at the $hCTR_b$ splice variants in comparison to the $hCTR_a$ variant.

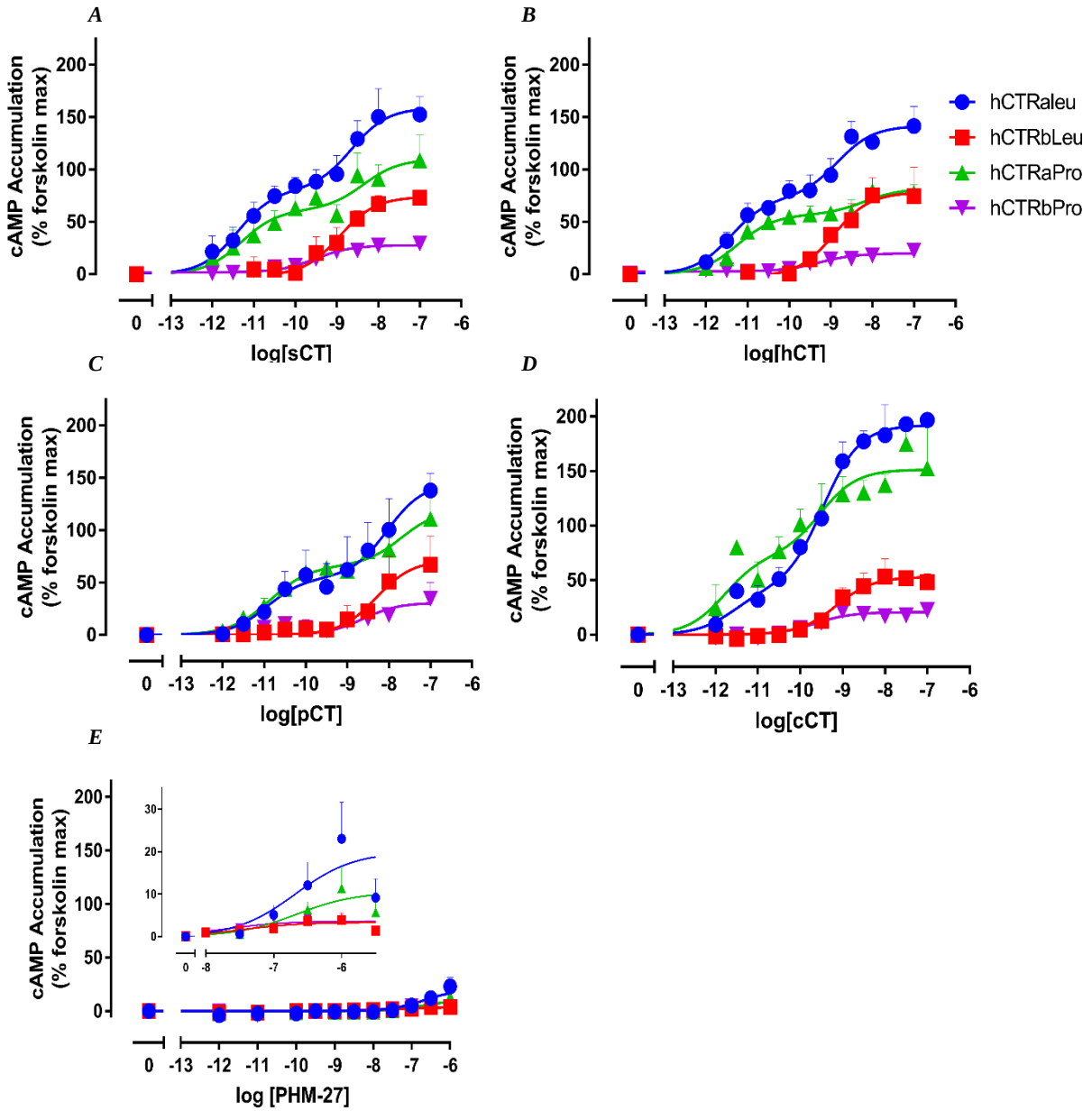

Figure 3.3 Agonist-dependent cAMP accumulation at the four hCTR variants. *Characterization of cAMP formation elicited by sCT (A), hCT (B), pCT (C), cCT (D) or PHM-27(E) in COS-7 cells stably expressing each of the four splice/polymorphic variants of hCTR. Data are analysed by either a three-parameter or a biphasic logistic curve where the Hill slopes have been constrained to 1. In (E), the cAMP data is shown on the same scale as (A-D). The insert shows the cAMP response on a different scale, revealing weak responses, at all variants, to the PHM-27 peptide. All values are mean+S.E.M. of 3 to 4 independent experiments conducted in duplicate.*

	hCTR$_a$Leu					hCTR$_b$Leu				
	pEC$_{50}$(1)	fraction	pEC$_{50}$(2)	E$_{max}$		pEC$_{50}$(1)	fraction	pEC$_{50}$(2)	E$_{max}$	
hCT	11.4±0.24	0.51±0.08	8.84±0.32	141.8±9.4**/***/****	(4)	-	-	8.93±0.22	78.2±8.7*/****	(4)
sCT	11.39±0.28	0.51±0.08	8.64±0.37	158.9±13.5**/****	(4)	-	-	8.94±0.21	74±7.7*	(4)
pCT	10.93±0.59	0.37±0.14	8.04±0.51	145.3±23.8**/****	(3)	-	-	8.3±0.26	71.4±12.5*	(3)
cCT	11.58±0.64	0.22±0.08	9.47±0.18	192.1±8.5**/***/****	(3)	-	-	9.15±0.18	52.9±4.3*	(4)
PHM-27	-	-	6.68±0.33†	20±4.5**/****/†	(4)	-	-	7.46±0.32†	3.3±0.5*/†	(4)

	hCTR$_a$Pro					hCTR$_b$Pro				
	pEC$_{50}$(1)	fraction	pEC$_{50}$(2)	E$_{max}$		pEC$_{50}$(1)	fraction	pEC$_{50}$(2)	E$_{max}$	
hCT	11.23±0.17	0.7±0.08	8.21±0.56	81.7±7.7*/****	(4)	-	-	9.27±0.28	19.9±2.1*/**/***	(4)
sCT	11.3±0.37	0.56±0.12	8.36±0.67	109.9±16.6****	(4)	-	-	9.52±0.17	27.7±1.8*/***	(4)
pCT	10.86±0.23	0.56±0.08	7.7±0.34	119.5±15.4****	(3)	-	-	8.62±0.31	30.9±5.8*/***	(3)
cCT	11.79±0.48	0.48±0.13	9.52±0.43	151.3±9.6*/**/****/†	(3)	-	-	9.65±0.29	20.6±2.5*/**/***	(4)
PHM-27	-	-	6.78±0.31	10.5±2.3†	(4)	-	-	7.7±0.46†	3.6±0.8*/†	(4)

Table 3.2 cAMP accumulation mediated by distinct agonists in COS-7 cells stably expressing four splice/polymorphic variants of hCTR. *Data in Figure 3.3 (A), (B), (C) and (D) were fitted with either a biphasic curve (CTR$_a$ variants) or a three-parameter curve (CTR$_b$ variants), constraining Hill slopes for both sites to 1; while Figure 3.3 (E) was analysed by a three-parameter logistic curve. pEC$_{50}$ is the negative logarithm of the concentration of agonist that produces half the maximal response. (1) and (2) are the high and low potency pEC$_{50}$ values of the biphasic curve, respectively (CTR$_a$ variants), or calculated pEC$_{50}$(2) calculated by the three-parameter logistic curve fit (hCTR$_b$ variants). E$_{max}$ is the maximal response expressed as % of 10^{-5}M forskolin response. Fraction refers to the % of the response that is from the higher potency site. All values are mean±S.E.M. of 3 to 4 independent experiments conducted in duplicate. Statistical significance of changes in pEC$_{50}$, fraction or E$_{max}$ of each ligands in comparison to hCT were determined for each receptor variant by a one-way analysis of variance and Dunnett's post-test ($p<0.05$ represented by †).Multiple comparison one-way analysis of variance and Bonferroni's post-test was also used to identify significant changes ($p<0.05$) in pEC$_{50}$, fraction or E$_{max}$ of each splice/polymorphic variant (in comparison to the hCTR$_a$Leu represented by *; hCTR$_b$Leu represented by **, hCTR$_a$Pro represented by ***, hCTR$_b$Pro represented by ****) were determined for each ligand.*

3.2.3.2 Ca^{2+} signalling

Consistent with previous reports, the $hCTR_a$ variant elicited strong intracellular calcium mobilization in response to all CT peptides, while there was no detectable response at the concentration range tested for any of the peptides at either polymorphic variants of the $hCTR_b$ variant (***Figure 3.4 A-D***, ***Table 3.3***). These concentration-response profiles fit a three-parameter logistic curve. There was no difference in E_{max} or potency for hCT, pCT or cCT to elicit a calcium response at either Leu or Pro polymorphism of the CTR_a splice.

In contrast to the CT peptides, no calcium signalling could be detected within the concentration range used for PHM-27 at any of the receptor variants (***Figure 3.4 E***, ***Table 3.3***).

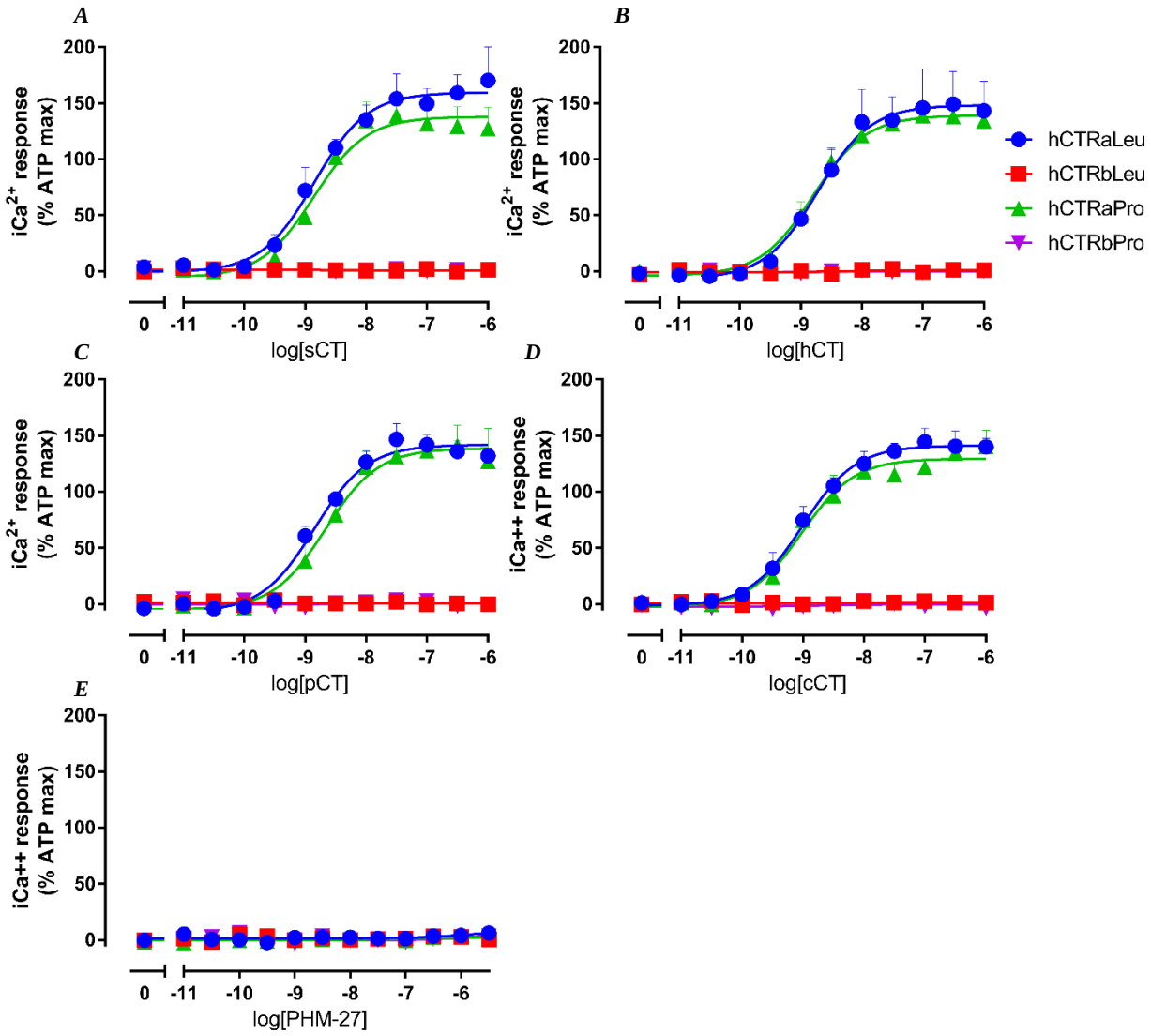

Figure 3.4 Intracellular calcium mobilisation by hCTR variants activated by distinct peptides. *Characterisation of the calcium mobilization profile elicited by sCT (A), hCT (B),pCT (C), cCT (D) and PHM-27 (E) in COS-7 cells stably expressing the four splice/polymorphic variants of hCTR. Concentration-response data was calculated at the peak of calcium mobilisation response. Data were analysed by non-linear regression using a three-parameter logistic curve. All values are mean+S.E.M. of 3 to 4 independent experiments conducted in duplicate.*

	$hCTR_aLeu$			$hCTR_bLeu$		$hCTR_aPro$			$hCTR_bPro$	
	pEC_{50}	E_{max}		pEC_{50}	E_{max}	pEC_{50}	E_{max}		pEC_{50}	E_{max}
hCT	8.73±0.16	148.2±8.7	(3)	-	-	8.8±0.08	139.1±3.9	(3)	-	-
sCT	8.85±0.12	159.5±6.6	(4)	-	-	8.86±0.12	137.9±6	(4)	-	-
pCT	8.85±0.08	141.8±3.9	(3)	-	-	8.67±0.13	138.7±6.6	(3)	-	-
cCT	9.01±0.08	141.1±3.8	(4)	-	-	9.03±0.11	129.5±4.4	(4)	-	-

Table 3.3 Effect of peptide agonists in calcium mobilisation in COS-7 cells stably expressing the four splice/polymorphic variants of hCTR. *Concentration response data were analysed by non-linear regression with a three-parameter logistic curve to derive $pEC_{50}$and E_{max} values. pEC_{50} is the negative logarithm of the estimated concentration of agonist that produces half the maximal response and is plotted as a % of the response elicited by ATP (100 μM). E_{max} is the maximal response. All values are mean±S.E.M. of 3 to 4 independent experiments conducted in duplicate. No statistically significant difference in pEC_{50} or E_{max} across the splice/polymorphic variants (one-way analysis of variance).*

3.2.3.3 ERK1/2 phosphorylation

In response to the CT peptide ligands, all hCTR variants triggered a fast, transient, ERK1/2 phosphorylation at saturating ligand concentrations that returned towards baseline within 30-60 min of stimulation (***Figure 3.5 A-D***). As such, concentration response curves to peptides were established at the approximate time of peak stimulation (4 min for sCT and hCT, 5 min for pCT, 9 min for cCT). Data were analysed by non-linear regression using a three parameter curve (***Figure 3.6 A-D***). Similar to cAMP responses, the $hCTR_b$ variants produced a significantly lower maximal response in comparison to the $hCTR_a$ variants for all CT peptides assessed. The polymorphisms had no effect on maximal response. In addition, all variants ($hCTR_a$ and $hCTR_b$, Leu and Pro) exhibited a similar potency in response to each CT peptide analysed (***Figure 3.6 A-D***, ***Table 3.4***).

Comparison across peptides using hCT as reference ligand revealed that, for the $hCTR_b$ splice variants, sCT and cCT produced a significantly lower maximal response.

Time-courses for hCTR activation by PHM-27 revealed a different kinetic profile to that of the CT peptides, with a slow onset, sustained ERK1/2 phosphorylation that was more prolonged than that produced by CT peptides (***Figure 3.5 E***). Due to the distinct kinetic profile of PHM-27, concentration response curves were generated at both 9 (***Figure 3.6 E***) and 30 min time points (***Figure 3.6 F***). These data revealed that PHM-27 was a partial agonist in comparison to CT peptides in this signalling pathway for all variants assessed. In addition, PHM-27 at 9 min displayed a statistically significant lower potency than hCT and other peptide ligands for the $hCTR_a$ variants, whereas the $hCTR_b$ variants had potencies similar to hCT. Similar to that observed with the CT peptides (and in cAMP), PHM-27 had a statistically significant lower E_{max} for the $hCTR_b$ polymorphisms in comparison to the $hCTR_a$Leu variant at 9 min. Despite lower E_{max}, at the 9 min time point, PHM-27 had also a higher potency (~10 fold) at the $hCTR_b$ variant relative to the CTR_a splice, albeit this failed to reach statistical significance for $hCTR_b$Leu ($p=0.06$) (***Table 3.4***). Comparison of potency and maximal responses of PHM-27 across different time points (9 and 30 min) revealed that at 30 min, the potency of this peptide decreases significantly for all CTR variants, with the exception of $hCTR_a$Leu where pEC_{50} remained unaltered (***Table 3.4***). Analysis of the magnitude of response showed that at both splice variants of the Pro polymorphism PHM-27 did

not change significantly between 9 and 30 min stimulation. Interestingly, at the Leu polymorphism, the maximal response was significantly lower at 30 min (when compared to 9 min time point) for the $hCTR_a$ variant, whereas was significantly higher at the $hCTR_b$ splice variant.

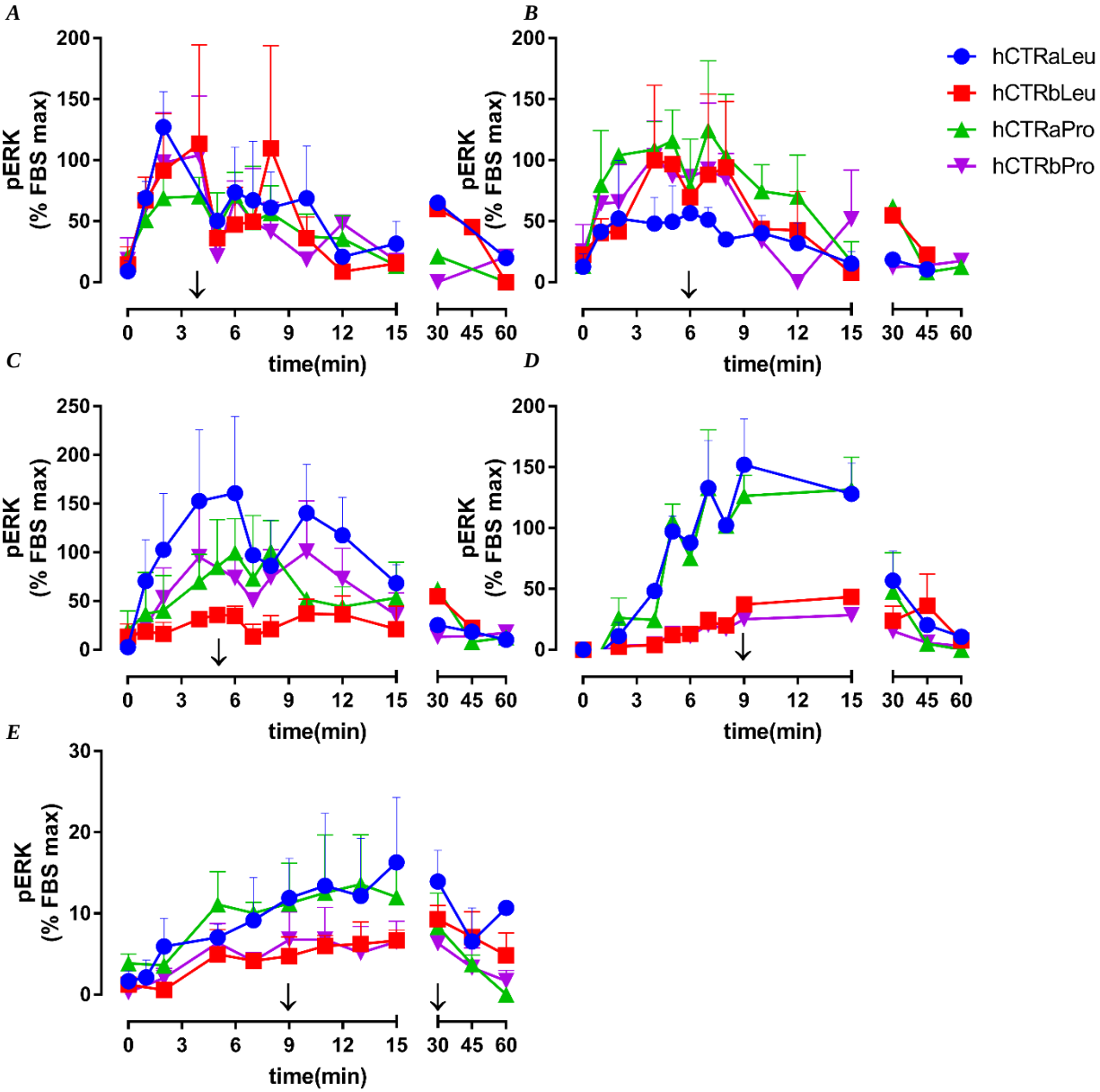

Figure 3.5 ERK1/2 phosphorylation time-courses at the hCTR variants when stimulated by distinct ligands. *Phosphorylation of ERK1/2 was assessed in the presence of 1 µM of sCT (A), hCT (B), pCT (C), cCT (D) or 10 µM of PHM-27 (E) in COS-7 cells stably expressing four splice/polymorphic variants of hCTR. Data represent mean+S.D or S.E.M. of 2 to 3 independent experiments conducted in duplicate. Arrows identify time chosen for concentration-response analysed.*

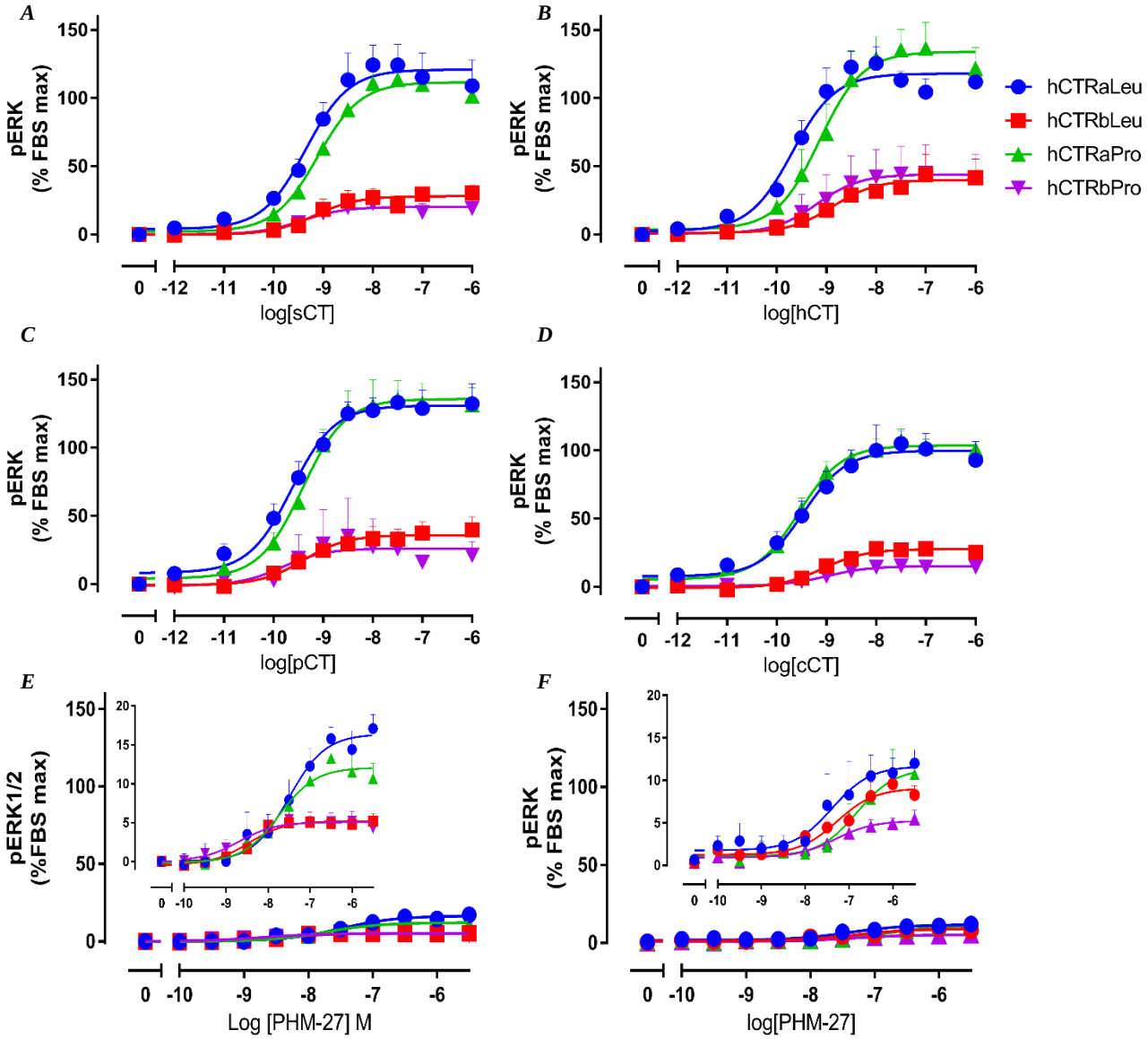

Figure 3.6 ERK1/2 phosphorylation at the four hCTR variants. *Characterization of the agonist-mediated phosphorylation of ERK 1/2 elicited by sCT (A) and hCT (B) at 4 min, pCT (C) at 5 min, cCT (D) and PHM-27 at 9 min (E) and PHM-27 at 30 min (F) in COS-7 cells stably expressing four splice/polymorphic variants of hCTR. Data were analysed by a three-parameter logistic curve. All values are mean+S.E.M. of 3 to 6 independent experiments conducted in duplicate at the peak of maximum phosphorylation determined by a time course experiment.*

	hCTR$_a$Leu			hCTR$_a$Pro			hCTR$_b$Leu			hCTR$_b$Pro		
	pEC$_{50}$	E$_{max}$		pEC$_{50}$	E$_{max}$		pEC$_{50}$	E$_{max}$		pEC$_{50}$	E$_{max}$	
hCT	9.69±0.12	118±4.2**/****	(3)	9.14±0.15	134.1±6.9**/****	(3)	8.87±0.32	40±4.6*/***	(3)	9.19±0.46	44.1±6.8*/***	(3)
sCT	9.35±0.15	120.9±5.7**/****	(3)	9.12±0.08	111.7±3.2†/**/****	(3)	9.17±0.23	28.1±2.2†/*/***	(3)	9.42±0.35	20.2±2.3†/*/***	(3)
pCT	9.64±0.11	131±4.1**/****	(3)	9.42±0.11	135.8±4.7**/****	(3)	9.4±0.25	35.9±3*/***	(3)	9.82±0.76	26.2±6.1†/*/***	(3)
cCT	9.48±0.16	99.8±4.7†/**/****	(4)	9.56±0.09	103.6±2.7†/**/****	(4)	9.07±0.16	27.6±1.6†/*/***	(4)	8.99±0.15	15.1±0.8†/*/***	(4)
PHM-27 (9 min)	7.5±0.19†/****	16.39±1.28†**/***/****	(6)	7.73±0.19†	12.08±0.89†/*/**/****	(5)	8.46±0.3	5.21±0.52†/*/***	(5)	8.7±0.34*	5.07±0.5†/*/***	(6)
PHM-27 (30 min)	7.38±0.33	11.66±1.41‡/****	(6)	6.82±0.26‡	11.38±1.44****	(6)	7.27±0.2‡	9.01±0.7‡	(6)	7.31±0.25‡	5.23±0.47*/***	(6)

Table 3.4 Effect of peptide agonists in ERK 1/2 phosphorylation in COS-7 cells stably expressing the four splice/polymorphic variants of hCTR. *Concentration response curves were analysed using non-linear regression fitted with a three-parameter logistic curve. pEC$_{50}$ is the negative logarithm of the estimated concentration of agonist that produces half the maximal response. E$_{max}$ is the maximal response expressed as a % of the 10% FBS response. All values are mean±S.E.M. of 3 to 6 independent experiments conducted in duplicate. Statistical significance of changes in pEC$_{50}$ or E$_{max}$ of each ligands in comparison to hCT were determined for each receptor variant by a one-way analysis of variance and Dunnett's post-test (p<0.05 represented by †). Differences in PHM-27 pEC$_{50}$ and E$_{max}$ between 9min and 30 min were also analysed using a t-test (p<0.05 represented by ‡).Multiple comparison one-way analysis of variance and Bonferroni's post-test was also used to identify significant changes (p<0.05) in pEC$_{50}$, fraction or E$_{max}$ of each splice/polymorphic variant (in comparison to the hCTR$_a$Leu represented by *; hCTR$_b$Leu represented by **, hCTR$_a$Pro represented by ***, hCTR$_b$Pro represented by ****) were determined for each ligand.*

3.2.3.4 Signalling bias

In order to quantify biased agonism, the Black/Leff operational model of agonism (Black and Leff, 1983) is commonly applied to calculate the transduction ratio that provides a measure of the efficiency of a ligand to activate a specific signalling pathway. Through this factor it is therefore possible to statistically compare the relative efficacies of distinct ligands for the same receptor and quantify whether these ligands have differential signalling. However, application of the operational model to biphasic pharmacological responses such as observed for the cAMP accumulation data is problematic; the operational model can only be readily applied to responses that fit a hyperbolic function and is much more complex for data such as described here for cAMP, where the best fit for CT peptides at the CTR_a variants was a biphasic curve. Therefore, to determine if biased agonism occurred at any (or all) of the hCTR splice/polymorphic variants, bias plots were generated by interpolating the response obtained from equioccupant concentration of ligand in one pathway against the second pathway. In this analysis, the % of response for one pathway is plotted against a second pathway for each ligand at equipotent concentrations for each receptor variant. While these derived plots do not allow statistical comparison, they allow the identification of potential biased agonism between distinct ligands, and if any observed bias is consistent or different between receptor variants.

When comparing cAMP to pERK1/2 (***Figure 3.7***), hCT, sCT and pCT had similar profiles in both polymorphic variants of the $hCTR_a$ splice variant, lower concentrations of ligand produced more cAMP than pERK1/2, whereas at higher concentrations, greater pERK1/2 was produced. Relative to the reference ligand (hCT), there was no obvious bias of the sCT relative to hCT. pCT displayed apparent bias toward pERK1/2, an observation that was more evident in the $hCTR_a$Pro than $hCTR_a$Leu (***Figure 3.7 A and C***). cCT produced more cAMP than pERK1/2 at all concentrations though its overall profile was similar to that of hCT and sCT. As observed at the $hCTR_a$ variant, hCT and sCT had similar signalling profiles, while pCT exhibited bias towards pERK1/2 relative to hCT. In contrast, the cCT profile was particularly interesting. In both $hCTR_b$ variants, this peptide showed a biased profile, but the direction of the bias differed depending on the polymorphism. The Pro polymorphism drove the

bias of cCT towards cAMP (relative to hCT), whereas the direction of the bias was towards ERK1/2 phosphorylation at the $hCTR_b$Leu variant.

In contrast to the CT peptides, that displayed variable levels of bias dependent on receptor polymorphism and splice variant, PHM-27 (compared to hCT) was biased towards pERK1/2 relative to cAMP at all CTR variants, although the relationship between cAMP and pERK1/2varied according to receptor variant.

Bias plots comparing calcium mobilisation and cAMP or pERK1/2 were prepared only for the $hCTR_a$ splices, as $hCTR_b$ variants did not produce a detectable signal for Ca^{2+} mobilisation.

In accord with patterns observed for cAMP:pERK1/2, hCT, sCT and cCT had similar profiles, with greater cAMP response. pCT, however, exhibited relative bias towards Calcium mobilisation compared to reference hCT peptide.

When comparing the calcium mobilisation and pERK1/2 pathways (***Figure 3.9***), all the CT peptides generated more pERK1/2 relative to Ca^{2+}, and there was no obvious bias in the profile of these peptides, although subtle variances may exist.

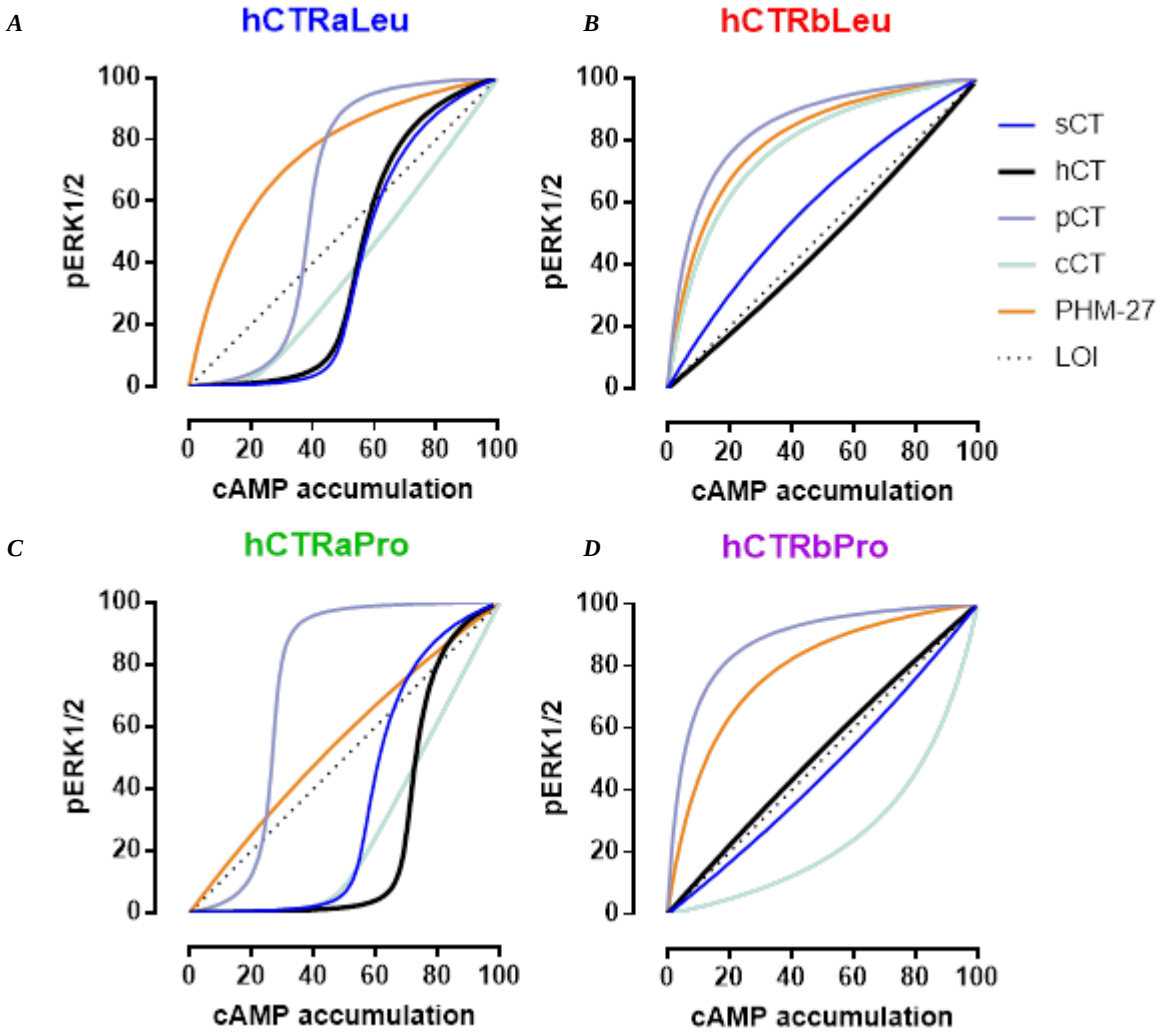

Figure 3.7 Bias plots comparing cAMP-pERK1/2 pathways activated by distinct peptides acting at the hCTR variants. *Each ligand response at each receptor variant was normalised to its own E_{max}. Equi-occupant concentrations of response for cAMP pathway were plotted against pERK1/2 pathway for each ligand at the $hCTR_aLeu$ (A), $hCTR_bLeu$ (B), $hCTR_aPro$ (C) or $hCTR_bPro$ (D). For PHM-27, data relative to pERK1/2 response at 9 min have been used.*

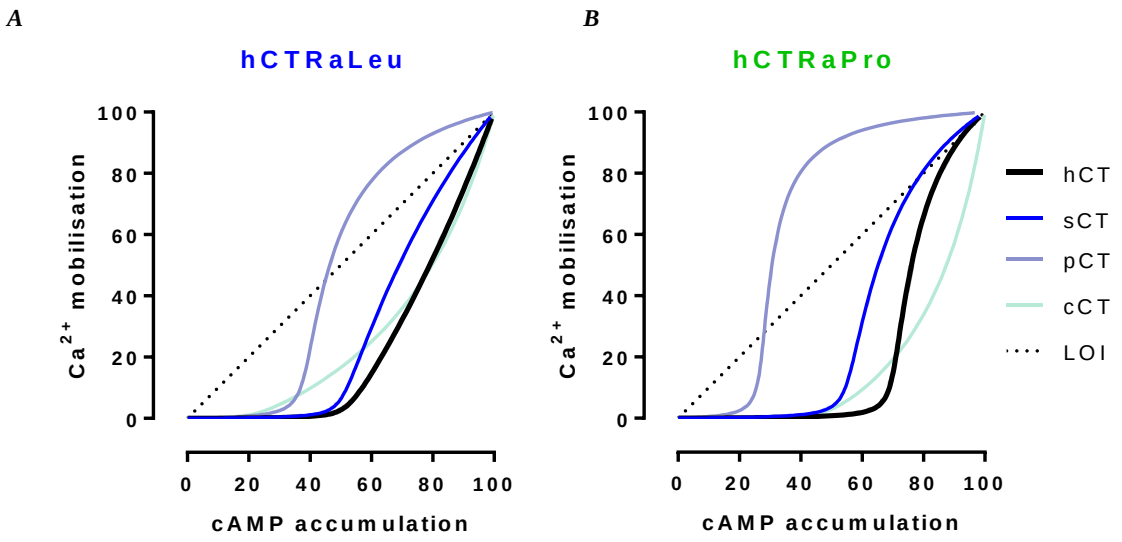

Figure 3.8 Bias plots comparing cAMP-Ca^{2+} pathways activated by distinct peptides acting at the hCTR variants. *Each ligand response at each receptor variant was normalised to its own E_{max}. Equi-occupant concentrations of response for cAMP pathway were plotted against Ca^{2+} pathway for each CT ligand at the $hCTR_aLeu$ (A) or $hCTR_aPro$ (B).*

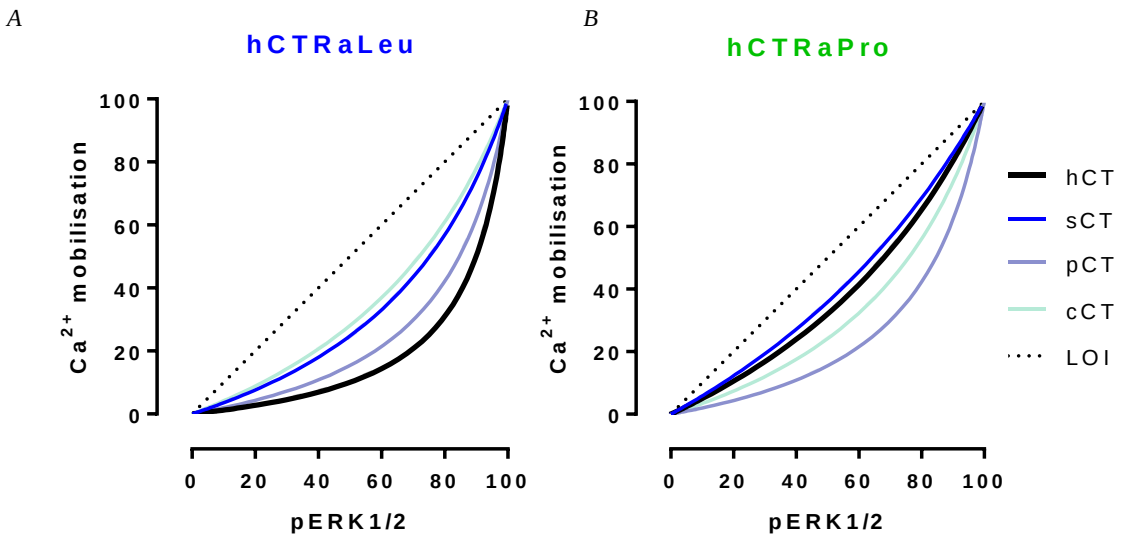

Figure 3.9 Bias plots comparing Ca^{2+}-pERK1/2 pathways activated by distinct peptides acting at the hCTR variants. *Each ligand response at each receptor variant was normalised to its own E_{max}. Equi-occupant concentrations of response for pERK1/2 pathway were plotted against Ca^{2+} pathway for each CT ligand at the $hCTR_aLeu$ (A) or $hCTR_aPro$ (B).*

3.2.4 β-arrestin 1/2 recruitment

A BRET assay was used to assess the ability of different hCTR variants to recruit β-arrestins following agonist stimulation. A bicistronic vector was used to co-express either β-arrestin 1 or β-arrestin 2-Venus and each of the four hCTR splice/polymorphism variants tagged at the C-terminal tail with Rluc8. cAMP accumulation measured 48 h post transient transfection of the vector expressing these proteins in COS-7 cells confirmed that the introduction of the Rluc8 tag to the receptor C-terminus and the overexpression of the β-arrestin-Venus did not affect the pharmacology of the hCTR variants of the hCTR-tagged variants when compared to the transiently transfected untagged hCTR (at least in terms of cAMP) (***Figure 3.10***). Interestingly, due to the limited number of replicates and the larger error, cAMP concentration-response curves of our constructs were fit to a three-parameter logistic curve, but we cannot exclude that further replicates would reveal a biphasic fit for the $hCTR_a$ polymorphism even in a transient setting.

None of the hCTR variants, in response to saturating concentrations of any of the CT peptides elicited a significant increase in BRET over a 10 min time period (***Figure 3.12***). The GLP-1R that is known to recruit both β-arrestin 1 and β-arrestin 2 was assessed in parallel as a positive control to confirm that the assay could robustly detect the recruitment of arrestins to a receptor (***Figure 3.11***).

To ensure that the absence of observed β-arrestin recruitment was not due to low expression of GRKs in the cell system, GRK 2, 3, 5 or 6 were co-transfected with the bicistronic vector and the assay was repeated. Despite the overexpression of GRKs, no BRET signal profile was observed for the recruitment of tagged β-arrestin to any of the tagged hCTR variants (data not shown).

To check that the addition of the Rluc8 tag does not interfere with any potential β-arrestin 1 or 2 recruitment to the various forms of hCTR, COS-7 cells stably expressing hCTR variants (without the Rluc8 tag) were transiently transfected with varying level of the Venus tagged β-arrestins and stimulated with either sCT, sCT(8-32) or vehicle. No specific redistribution of either of the Venus tagged β-arrestins could be observed in wide field images up to 60 min stimulation, supporting the BRET data that no ligand assessed in this study was able to promote recruitment of β-arrestin 1 or 2 to any of the variants of the hCTR (***Figure 3.13***).

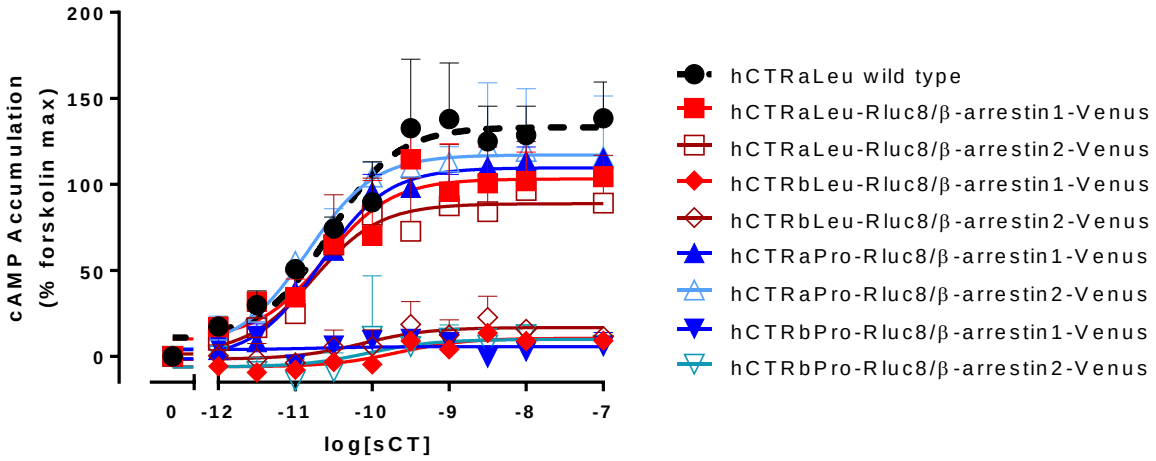

Figure 3.10 cAMP formation in COS-7 cells transiently expressing four splice/polymorphic variants of hCTR containing a C-teminal-Rluc8 tag and overexpressing β-arrestin 1 or β-arrestin 2. *COS-7 cells were transfected and plated at 30.000 cells/well and stimulated with sCT. Data are analysed by non-linear regression with a three-parameter logistic curve. All values are mean+S.D. of 2 independent experiments conducted in duplicate.*

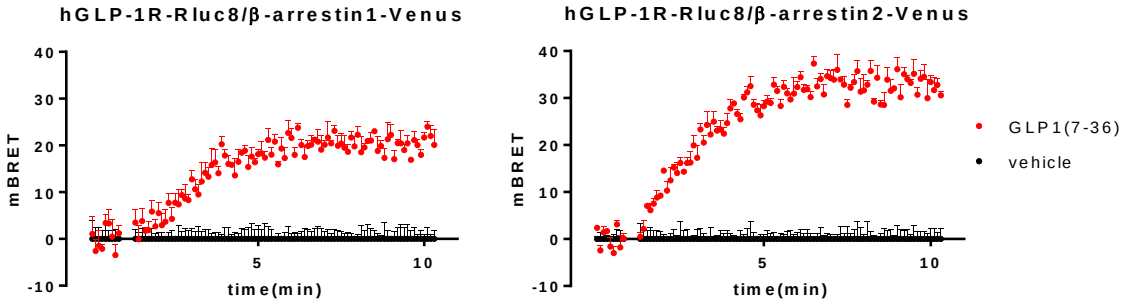

Figure 3.11 BRET characterization of the recruitment of β-arrestins 1/2-Venus to hGLP-1R-Rluc8 co-expressed in COS-7 cells. *48 h transient transfection of the bicistronic vector containing either of β-arrestin 1-Venus or β-arrestin 2-Venus and the GLP-1R-Rluc8. Cells were stimulated with 1 μM of ligand and BRET was measured over 10 min. Data represent mBRET ratio corrected for vehicle. All values are mean+S.D. of 2 independent experiment conducted in triplicate.*

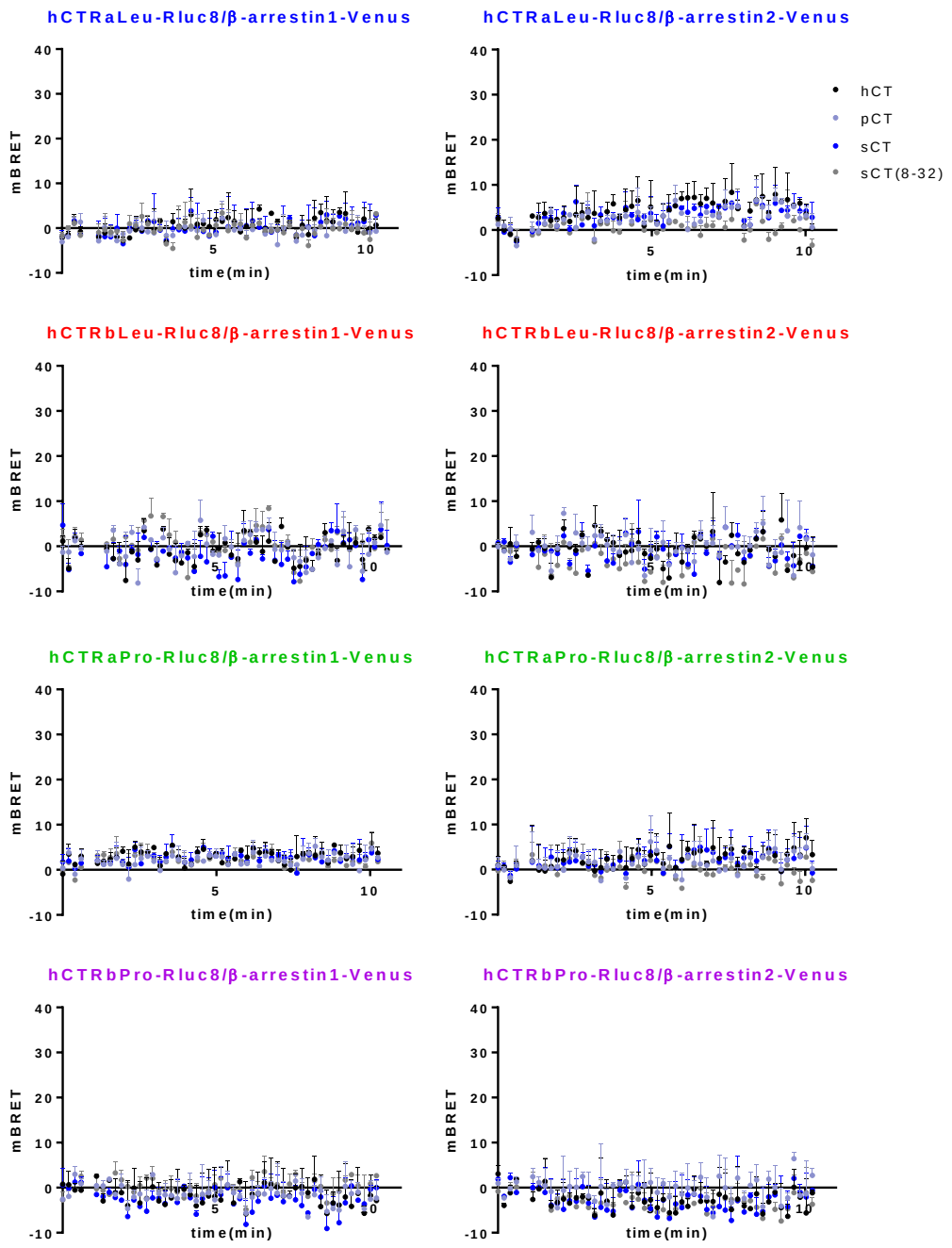

Figure 3.12 BRET characterization of the recruitment of β-arrestins 1/2-Venus to hCTR-Rluc8 variants co-expressed in COS-7 cells. *Assays were performed 48 h following transient transfection of the bicistronic vector containing either of the β-arrestin 1-Venus or the β-arrestin 2-Venus and different hCTR variants tagged with Rluc8 at the C-terminal tail. Cells were stimulated with 10 μM of ligand and ligand-induced BRET was measured over 10 min. Data represent mBRET ratio corrected for vehicle. All values are mean+S.D. of 2 independent experiments conducted in triplicate.*

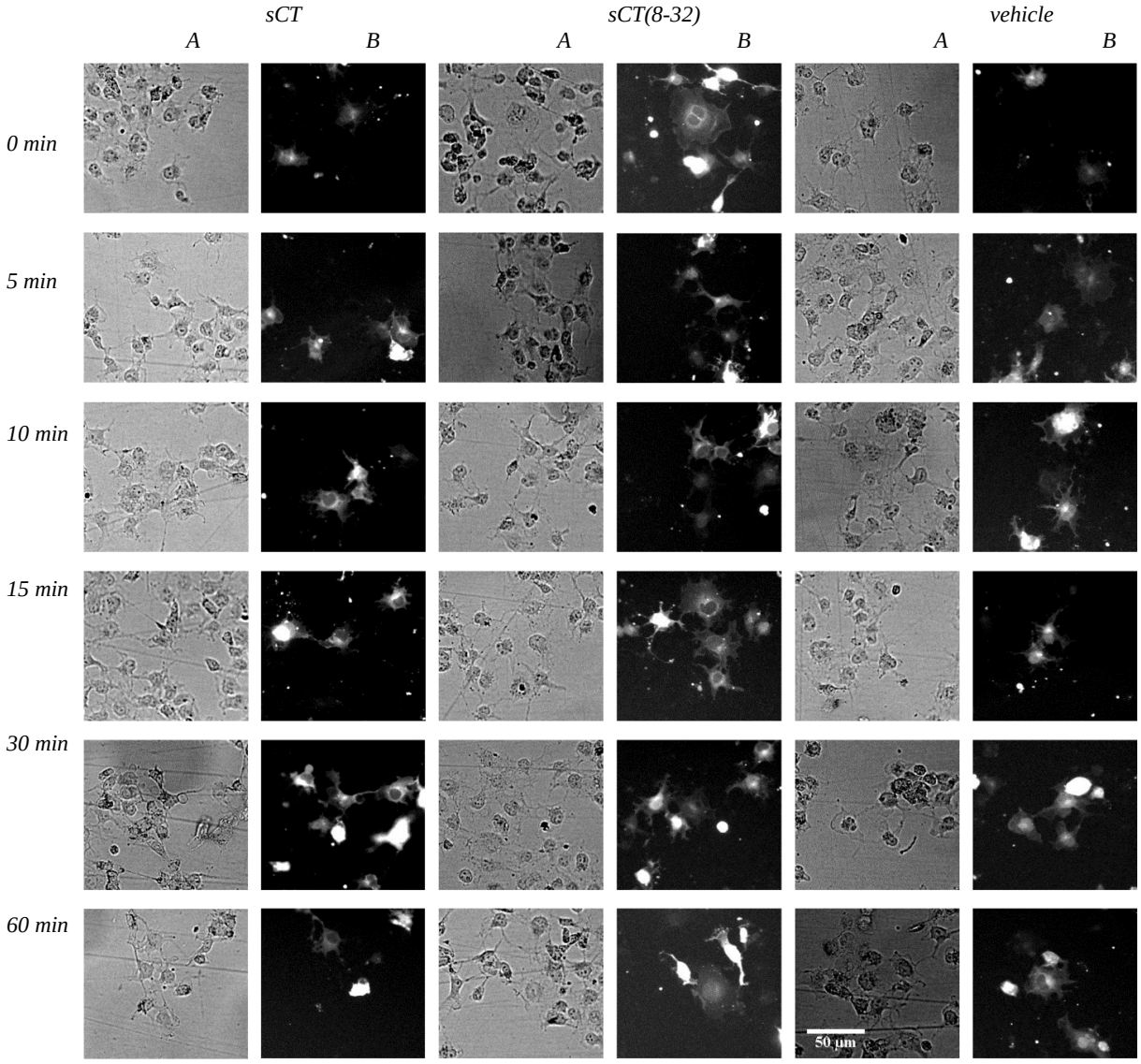

Figure 3.13: The hCTR does not recruit β-arrestin 1 to the cell surface upon ligand stimulation in Cos7 cells. *Wide-field representative images of COS-7 cells stably expressing hCTR$_a$Leu and transiently transfected with β-arrestin 1-Venus. Cells were stimulated with 1 µM of sCT, sCT(8-32) or vehicle and imaged at 0 min (A, D), 5 min (B, E) and 60 min (C, F) post ligand stimulation. Images were collected when the same cells were transfected with β-arrestin 2-Venus or with different splice variants of the receptor, with similar findings.*

3.2.5 Receptor internalisation

Internalisation of the hCTR was determined by confocal imaging. COS-7 cells stably expressing $hCTR_aLeu$, $hCTR_bLeu$, $hCTR_aPro$ or $hCTR_bPro$ were stimulated with either sCT-ROX or sCT(8-32)-AF568. The fluorescent probes did not alter the pharmacology of these ligands (***Figure 3.14*** for sCT-ROX, sCT(8-32)-AF568 (Furness et al., 2016).

Wide-field images of cell stimulated with each of the two fluorescent ligands revealed ligand internalization within 5 minutes from application of the stimuli in cells expressing hCTR variants, but not in naïve COS-7 cells that do not express the receptor (***Figure 3.15*** and ***Figure 3.16***).

Similarly, fluorescently conjugated antibody that selectively labels the cMyc tag at the extreme N-termini of the hCTR variants (9E10-AF647) revealed a rapid internalisation of the receptor in the absence of any stimulating ligand (***Figure 3.17*** 10.4225/03/59c1f93681dc4 10.4225/03/59c1fa9625067). Treatment of naïve COS-7 cells with the fluorescently conjugated antibody did not result in internalisation of the antibody, confirming a receptor mediated internalisation. Co-treatment of hCTR-expressing cells with fluorescent antibody and fluorescent ligand (sCT-ROX) showed rapid co-localisation of the two probes in intracellular compartments (within seconds/minutes). The rate of internalisation of the receptor did not visually appear to be altered by the addition of either sCT-ROX or sCT(8-32)-AF568 (***Figure 3.18***. 10.4225/03/59c1f2ea9d402, and ***3.19*** 10.4225/03/59c1f6998fedb).

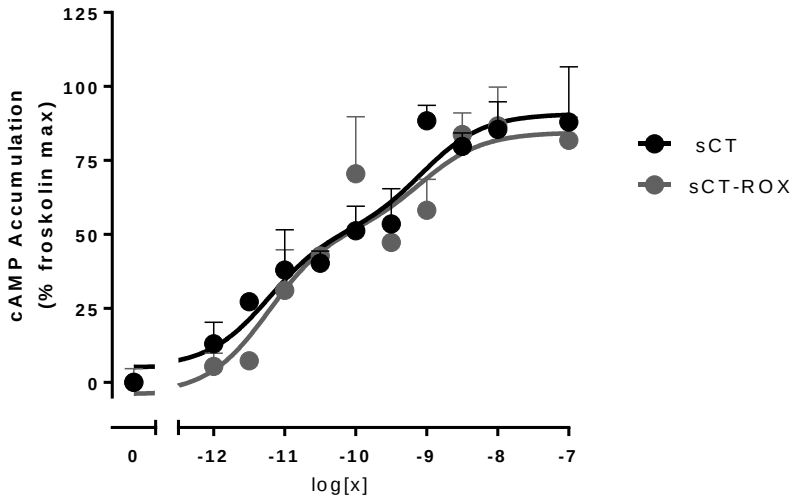

Figure 3.14: cAMP formation in COS-7 cells stably expressing $hCTR_aLeu$ variant in presence of sCT or sCT-ROX. *Stable COS-7 cells were stimulated with either sCT or sCT-rhodamine (sCT-ROX). Data were analysed by non-linear regression with a three-parameter logistic curve. All values are mean+S.D. of 1 experiment conducted in duplicate.*

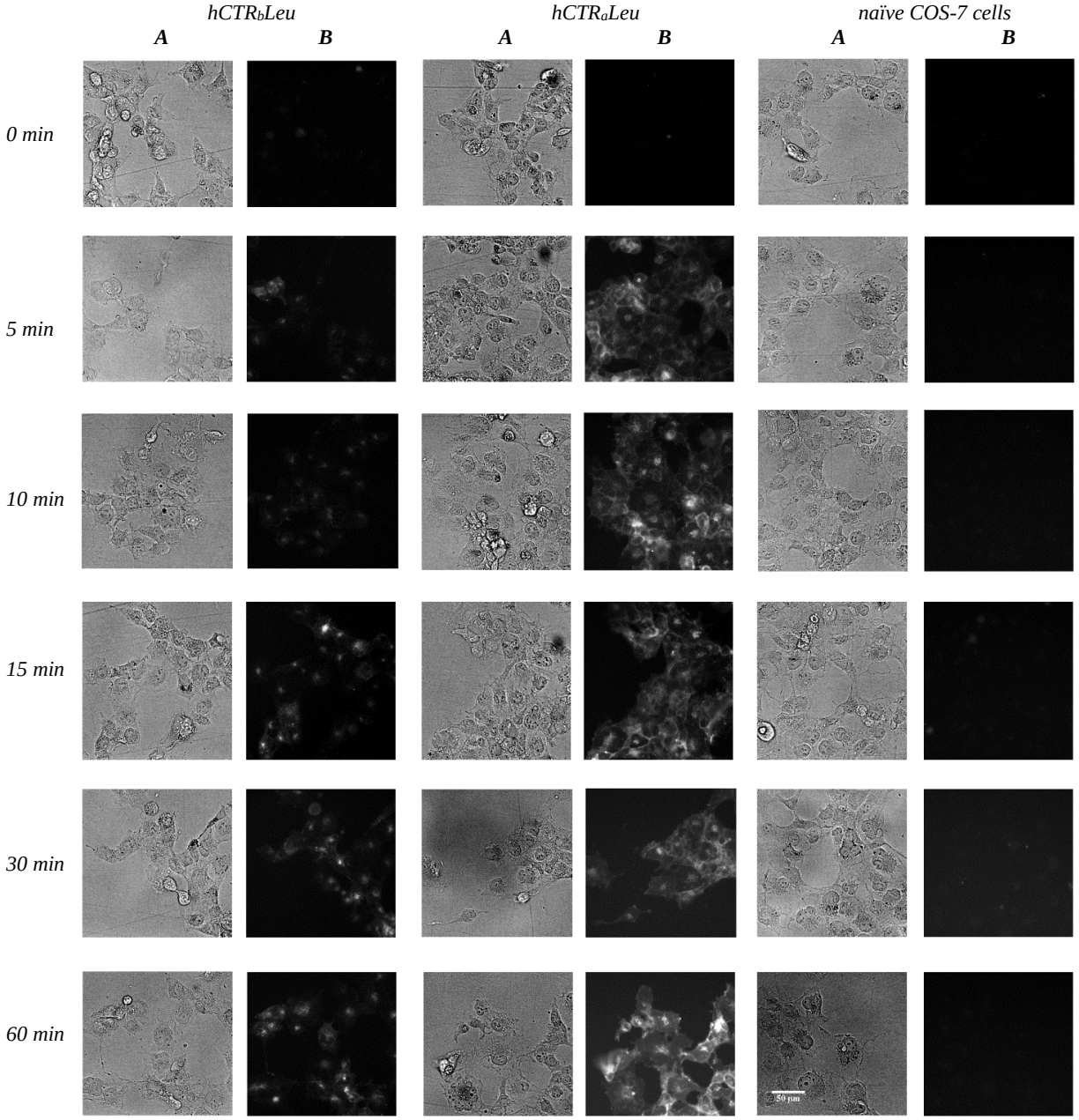

Figure 3.15 Internalisation of sCT(8-32)-AF568 in COS-7 cells stably expressing the hCTR. *Wide-field images of COS-7 cells stably expressing hCTR$_a$Leu, hCTR$_b$Leu or naïve COS-7 cells. Cells were stimulated with 1 µM sCT(8-32)-AF568 for 0 min, 5 min, 10min, 15 min, 30 min and 60 min. (A) bright field images, (B) AF568 emission.*

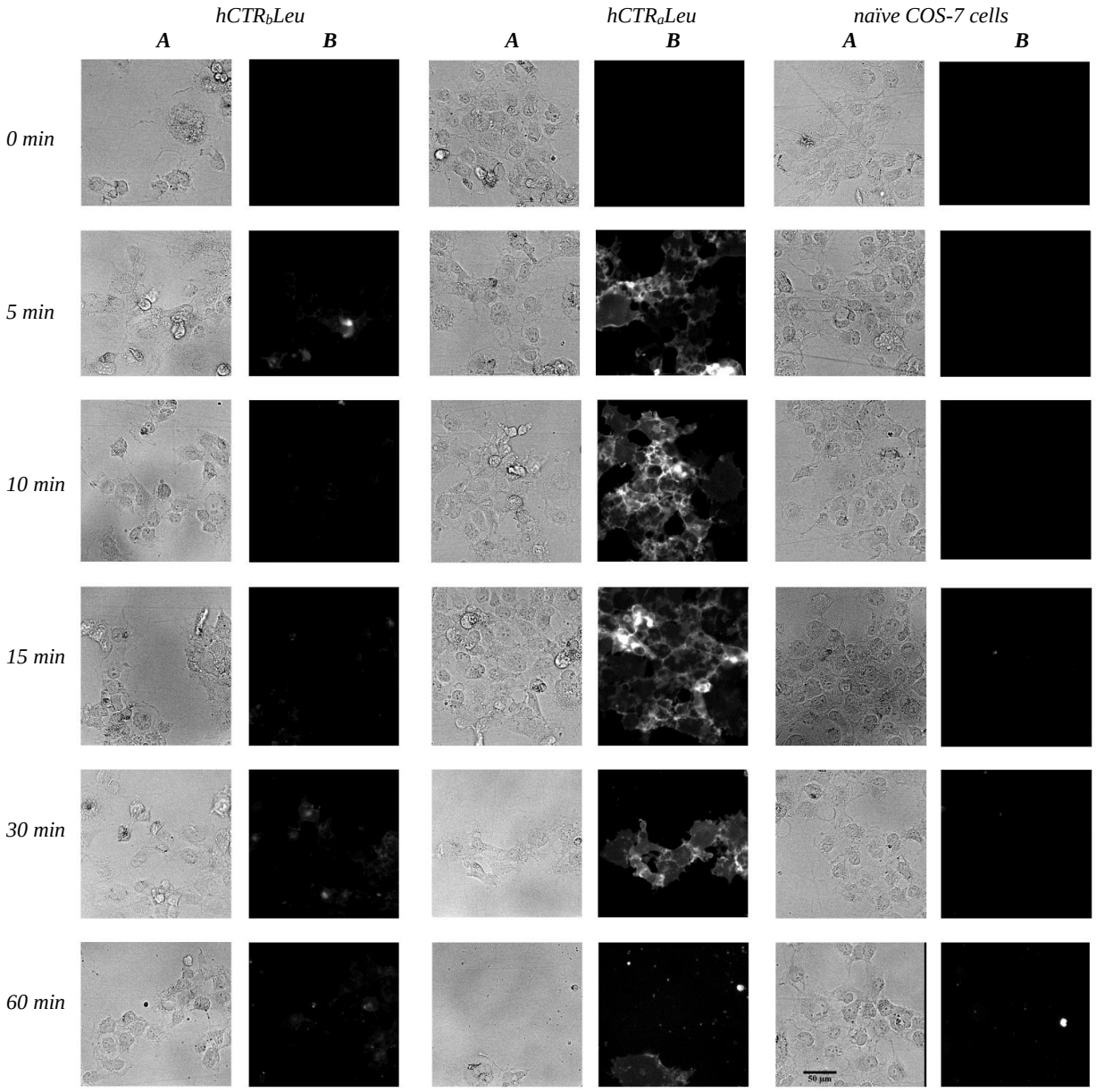

Figure 3.16 Internalisation of sCT-ROX in COS-7 cells stably expressing the hCTR. *Wide-field images of COS-7 cells stably expressing hCTR$_a$Leu, hCTR$_b$Leu and naïve COS-7 cells. Cells were stimulated with 1 µM sCT-ROX for 0 min, 5 min, 10 min, 15 min, 30 min and 60 min. (A) bright field images, (B) Rhodamine emission.*

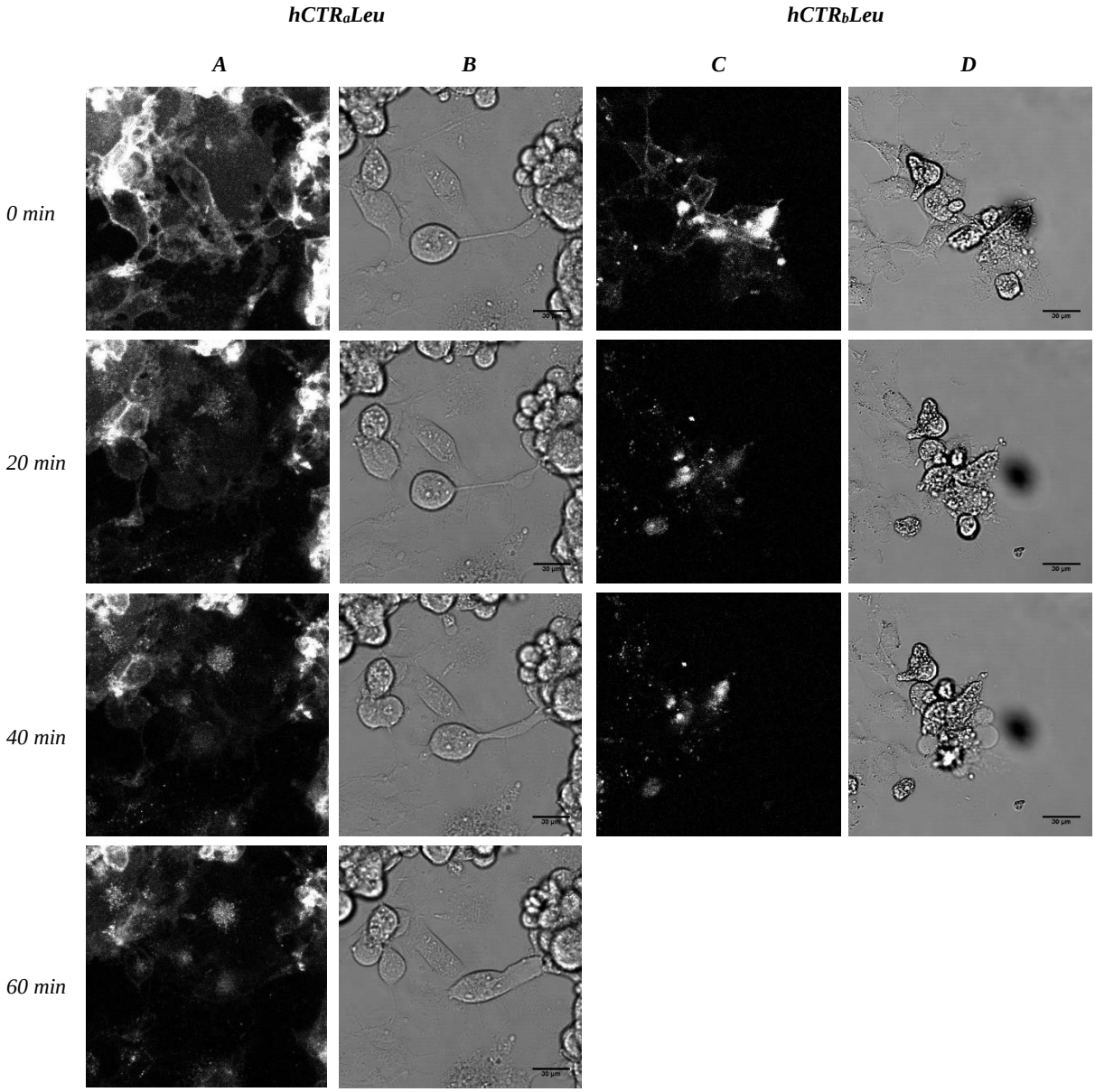

Figure 3.17 Internalisation of 9E10-AF647 in COS-7 cells stably expressing the hCTR. *Confocal field images of COS-7 cells stably expressing hCTR$_a$Leu (A and B) or hCTR$_b$Leu (C and D) variants were incubated with 1 µg/ml anti-cMyc antibody (9E10-AF647) for 60 to 100 min on ice. Cells were extensively washed with cold PBS before imaging in SP-8 for 60 min at 37 ℃. Four focal planes were acquired every 1 min for 60 min. Images presented are stacking three to four planes elaborated in Fiji ImageJ for (A) and (C) 9E10-AF647 emission, (B) and (D)bright field images. Representative images of 2 independent experiments. Scale bar represents 30 µm.*

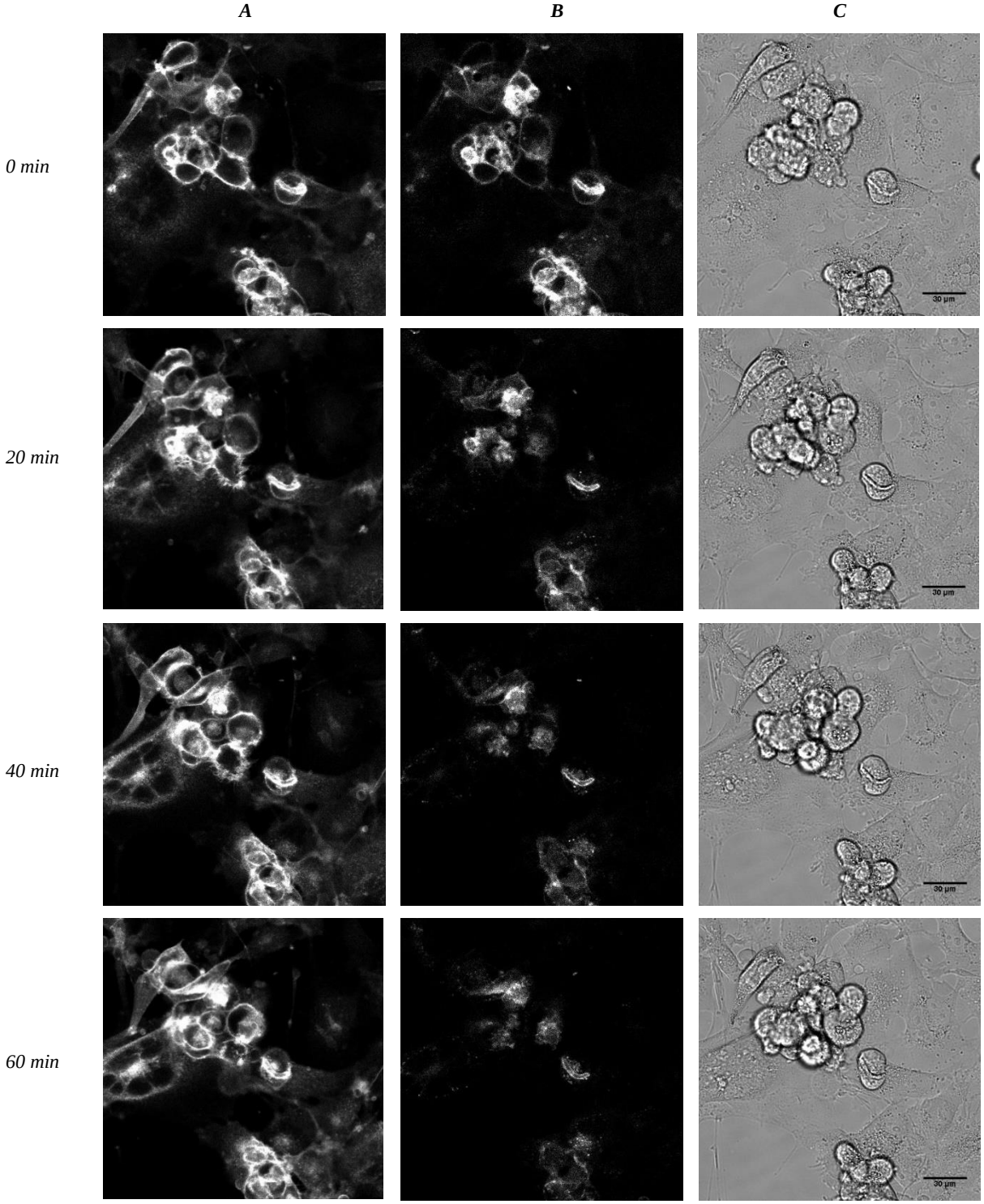

Figure 3.18 Internalisation of sCT(1-32)-ROX and 9E10-AF647 in COS-7 cells stably expressing the hCTR$_a$Leu. *Confocal field images of COS-7 cells stably expressing hCTR$_a$Leu were incubated with 1 µM sCT-ROX and 1 µg/ml anti-cMyc antibody (9E10-AF647) for 60 to 100 min on ice. Cells were extensively washed with cold PBS before imaging in SP-8 for 60 min at 37 ℃. Four focal planes were acquire every 1 min for 60 min. Images are presented as maximum intensity projections of the four planes (processed in the Fiji distribution of ImageJ) for (A) 9E10-AF647 emission, (B) sCT-ROX emission and (C) bright field images. Representative images of 2 independent experiments. Scale bar represents 30 µm.*

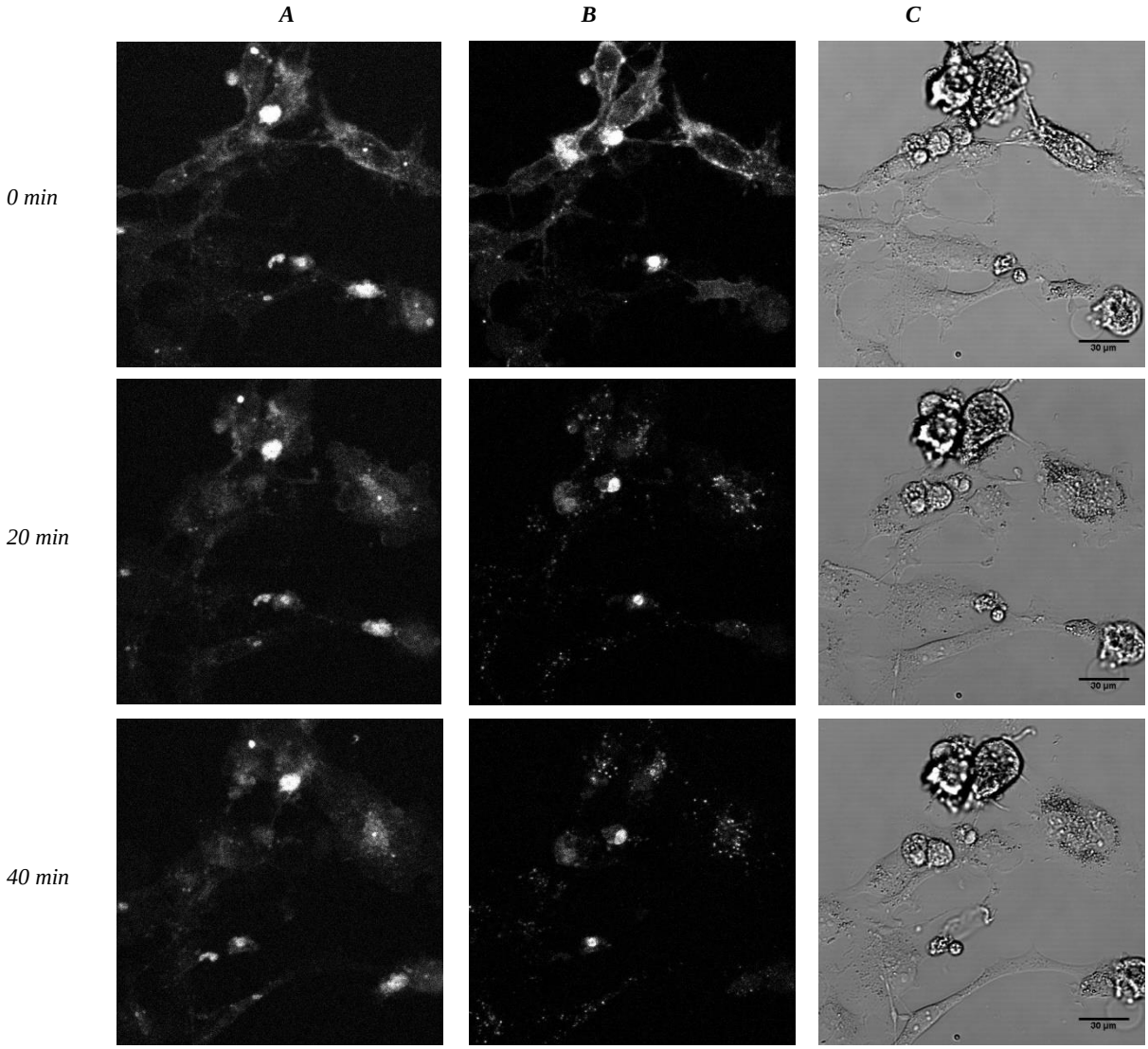

Figure 3.19 Internalisation of sCT(8-32)-AF568 and 9E10-AF647 in COS-7 cells stably expressing the hCTR$_a$Leu. *Confocal field images of COS-7 cells stably expressing hCTR$_a$Leu were incubated with 1 µM sCT(8-32)-AF568 and 1 µg/ml anti-cMyc antibody (9E10-AF647) for 60 to 100 min on ice. Cells were extensively washed with cold PBS before imaging in SP-8 for 60 min at 37 ℃. Three focal planes were acquired every 1 min for 40 min. Images are presented as maximum intensity projections of the four planes (processed in the Fiji distribution of ImageJ) for (A) 9E10-AF647 emission, (B) sCT(8-32)-AF568 emission and (C) bright field images. Scale bar represents 30 µm.*

3.3 Discussion

In humans, two splice variants of the CTR are expressed at different levels, depending on the tissue in which the receptor is expressed. Additionally, individuals from different ethnic backgrounds carry differing genotypes with respect to the common coding polymorphism of the CTR. These different receptor variants can be activated by distinct ligands and/or produce divergent responses, and ultimately trigger different physiological outcomes. Thus, it is important to understand the pharmacological profile these natural splice/polymorphic variants of the CTR, because these may impact on how patients with distinct genotypes respond to the same therapeutics.

In this study we have performed a comparative analysis of the signalling output of four common splice/polymorphic variants of the hCTR expressed in COS-7 cells. We show consolidated evidence that the activation of the hCTR triggers cAMP production, calcium mobilisation and downstream phosphorylation of ERK1/2, and that receptor splicing alters the signalling profile of the CTR. In this study we also showed that different variants of the CTR can have differential impacts on the efficacy of individual agonists. Using distinct ligands, we have revealed the first evidence for biased agonism at the CTR. In addition, we have identified an unusual trafficking profile for this receptor. We have determined that, in the COS-7 recombinant cell system, the CTR shows constitutive internalisation with ligand addition having no apparent effect on the kinetics of this process. In this cell system, the receptor activation and trafficking does not appear to involve β-arrestin recruitment or redistribution of these regulatory proteins.

3.3.1 Ligand affinity is dependent on receptor polymorphism and splicing

Consistent with previous studies, sCT and cCT have higher affinity for the hCTR compared to hCT and pCT (Kuestner et al., 1994). However, both sCT and cCT show enhanced affinity for the $hCTR_b$ variant irrespective of the polymorphism. At the $hCTR_a$ variant the Pro polymorphism displayed higher affinity for these 2 ligands compared with the Leu polymorphism, however there was no difference in apparent affinity of the polymorphic variants at the $hCTR_b$ variant. Despite these differences in affinity, both between ligands and across variants, all four ligands revealed a similar profile for stimulation of cAMP

accumulation (Wolfe et al., 2003). Previous studies using CT chimeric peptides had already highlighted that the mid-region and C-terminal residues of the CT ligands (residues 13-32) (***Table 1.1***), that are the least conserved across CT peptides, are the key to the distinct observed affinity and binding kinetics of the different CT peptides (Hilton et al., 2000, Furness et al., 2016).

Our study also shows that changes in the receptor at the intracellular face has an impact on the signalling pathway triggered following receptor activation (i.e. differences in peptide-mediated Ca^{2+} mobilisation signalling between $hCTR_a$ and $hCTR_b$ splice variants) and also an effect on the observed affinity of a subset of the agonists.

It is possible that changes in the observed affinity of the ligands across splice variants could be affected by differential engagement with G proteins. However, this is unlikely to be the case, as all the CT ligands had similar affinities at the other receptor variants despite large differences in signalling, particularly between the $hCTR_a$Pro and $hCTR_b$Pro. Moreover, Hilton et al. (2000) also observed that binding kinetics of different CT agonists remain unchanged in membranes containing CTR treated with or without GTP. Altogether this suggests that the G protein interaction with the receptor has limited impact on ligand affinity under the conditions of assay.

In this study we could not observe recruitment of β-arrestins to ligand-activated receptor, however the fact that CTR constitutively internalises (discussed in Section 3.3.5) suggests that other scaffolding partners do interact with the receptor. For instance, the CTR contains a highly conserved PDZ domain at the extreme C-terminus of the receptor, although the role of this domain has yet to be investigated. As such, the CTR may differentially engage with, as yet, unidentified partners that could impact on ligand affinity.

3.3.2 The different components of CTR signalling

Similar to previous reports, we observed pleiotropically coupling of the hCTR to multiple intracellular effectors. Its activation elicits cAMP production and ERK phosphorylation for all receptor splice/polymorphic variants, while the transient calcium mobilisation from intracellular stores is only detectable for the $hCTR_a$ splice variants.

All CT peptides stimulate biphasic cAMP responses with the $hCTR_a$ variant but not the $hCTR_b$ variants. The first hypothesis that could explain this profile is the possibility of compartmentalised signalling. It is becoming evident that GPCRs can signal from within endosomes (Vilardaga et al., 2011, Kuna et al., 2013), however to date this has not been explicitly shown for CTR. Our data has shown a rapid receptor internalisation of both $hCTR_a$ and $hCTR_b$ splice variants, that drives the receptor towards perinuclear compartments. Using a radioligand approach, Schneider et al. (1988) showed that in T47D cells (which expresses both receptor splice variants) internalised CTR is transferred to lysosome for degradation without recycling, while new receptor is continuously resynthesized and transported to the plasma membrane. This may not be the case in our COS-7 cells, as our data and other published data clearly reveal that CTR trafficking differs in different cellular backgrounds. For instance, Moore *et al.* (1995) used a radioligand binding approach on BHK cells transfected with the either of the two CTR splice variant to show appreciable internalization of the radiolabelled ligand when the $hCTR_a$, but not of the $hCTR_b$ splice variant is expressed, whereas in our COS-7 cells both splice variants internalise and traffic both agonist and antagonist ligands into the cell. It therefore possible that in our COS-7 cells, once internalised, different CTR variants traffic to distinct sub-compartments (i.e. Golgi), a hypothesis that has yet to be addressed. Additionally, it would be interesting to determine if different receptor variants signal in the same way from distinct cellular compartments, and/or if they recruit a different subset of effectors. We have yet to examine the impact of inhibition of receptor internalisation on signalling of the different hCTR variants or to explore inhibition of the various components of the signalling cascade. This could be addressed by knocking down scaffolding proteins involved in trafficking, such as caveolin or dynamin, and measuring if receptor still traffics and/or if its signalling function is altered.

A second hypothesis for the observed biphasic response could attribute the distinct cAMP profile to different isoforms of G proteins coupling to the receptor with distinct affinities. It is known that each subunit of the G protein heterotrimer can exist in several isoforms and splice variants (Hildebrandt, 1997, Downes and Gautam, 1999), each one with a potentially different affinity for the active hCTR. To investigate this hypothesis, G protein knock-out cells could be used to co-transfected CTR and the individual isoforms of G protein. Also, a BRET or FRET approach (similar to that what was used

recently by our lab (Furness et al., 2016)) may be helpful; by tagging both receptor and the G protein it would be possible to measure (upon ligand addition) the kinetic and affinity of different G protein binding to the receptor. By tagging two distinct subunits of the G protein (α and βγ), it would be possible to measure the kinetics of G protein rearrangement upon ligand addition. These experiments could (i) reveal if distinct isoforms of G protein are activated in a distinct manner, (ii) by conducting these experiments in presence of different receptor variants, they could reveal if different receptor splice or polymorphic variants activate the G protein in a different manner, (Perry III et al.) by using different ligands to stimulate the receptor, it could be possible to identify whether different ligands cause distinct conformational changes in the effector structure (potentially leading to signalling bias as discussed in Section 3.3.3).

As the $hCTR_a$ and $hCTR_b$ splice variants differ by the presence or absence of the 16 amino acid insertion in ICL1, this may modulate either the coupling affinity and/or kinetics of activation of different Gα proteins. For example, Kleinau et al. (2010) have systematically mutated residues in ICL1 in the thyrotropin receptor (THSR, a class A GPCR) and shown that the cytosolic portions of TM1 and TM2 are important for interaction with G_α proteins, and that their mutation drastically impairs the downstream signalling, in particular of Gαq. Despite the low sequence homology, experiments on similar results were also obtained for Class B1 GPCRs: Bavec et al. (2003) have shown that ICL3 of the GLP-1R is important for Gαs and Gαq protein coupling while ICL1 and ICL2 seem to play a sorting role to differentiate which G protein the receptor couples to. The importance of the first 2 ICLs has also been shown for the PTH-1R (Iida-Klein et al., 1997), CGRP (Cypess et al., 1999) and secretin receptors (Garcia et al., 2012). For CTR, helix 8 at the C-terminus are also important for receptor interaction with G proteins, in particular Gαs and Gαq (Seck et al., 2005). More recently, our group has solved the near-atomic resolution structure of sCT-$hCTR_a$Leu-Gαs heterotrimer complex, showing that the intracellular portion of the TM bundle makes extensive contacts with the Gαs protein. In this structure ICL1 is located above the WD40 repeats 1 and 7 of the β subunit and close to the N-terminal alpha-helical domain of Gαs (Liang et al., 2017). Therefore, it is not surprising that the 16 amino acid insertion in ICL1 modulates coupling of signalling effectors to the hCTR, as it would sterically hinder the observed

interactions of the $hCTR_a$ receptor variant. In functional data this would translate in a shift to the right of the concentration-response curves for the $hCTR_b$ variant. Nonetheless, this does not provide a clear molecular mechanism for the biphasic response seen with the $hCTR_a$ variant.

It is possible that the Ca^{2+} response could also contribute to one of the two phases of the cAMP response as this is observable solely in the $hCTR_a$ splice variant that is competent for calcium signalling. Increases in intracellular calcium can activate soluble adenylyl cyclase (sAC) and produce additional cAMP (Jaiswal and Conti, 2003), and current study confirmed previous reports of a divergent calcium response between the 2 splice variants, where the $hCTR_b$ splice is not capable of producing a detectable Ca^{2+} response in the presence of up to 1 μM of agonist (Moore et al., 1995, Kuestner et al., 1994). Preliminary data support Gαq-dependence of the Ca^{2+} response in our stable COS-7 cells as UBO-QIC (FR900359), a Gαq inhibitor, completely blocked the Ca^{2+} response (***Figure S1 A, Appendix 1***). Further experiments with the Gαq protein inhibitor should identify if one of the two phases of the cAMP response has a Ca^{2+} component, as well as the involvement of the Gαq protein in other signalling pathways downstream of CTR activation.

pERK1/2 can be modulated by numerous upstream signalling pathways, including those initiated by Gαs, Gαi and Gαq (Pitcher et al., 1992, Boyer et al., 1992, Camps et al., 1992, Smrcka and Sternweis, 1993, Stephens et al., 1994, Ikeda, 1996, Smrcka, 2008, Sunahara et al., 1996, Wickman et al., 1994, Clapham and Neer, 1993, Ueda et al., 1996, Moscat et al., 2003). For the CTR, pERK1/2 is a convergent endpoint of multiple pathways, as illustrated by Morfis *et al.* (2008), where several inhibitors were used to tease apart contribution of different components of the signalling cascade mediated by the $hCTR_aLeu$, leading to pERK1/2, when expressed in the same cellular background used in the current study. In the Morfis *et al.* (2008) study, inhibition of PLC, PI3K, PKC, Raf and MAPK (but not PKA) all reduced or completely abolished pERK1/2, consistent with convergent activation, and this likely varies between splice variants, due to the absence of Gαq-mediated iCa^{2+} mobilisation. To further investigate the contribution of different upstream effectors to the pERK1/2 signalling, different inhibitors could be used to tease apart the different components that produce this response. Additionally, by performing signalling assays in presence of the different hCTR variants and various inhibitors, it may be possible

to identify the effect that polymorphism and splicing has on the specific pathways driving the pERK1/2 response.

Another important aspect of pERK1/2 signalling is that different cell compartments, such as nucleus and cytosol, have localised ERK that can be phosphorylated in a distinct spatiotemporal manner. Examples of this are the μ-opioid receptor (Halls et al., 2016), and the neurokinin 1 receptor (Jensen et al., 2014) where different ligands produce distinct outcomes because of the origin of the pERK1/2 signalling within the cell. In our study we have measured the overall cellular pERK1/2 (however, concentration response curves are at single time points), and we are yet to tease apart whether the origin of the pERK1/2 response differs for different variants or in response to different ligands. FRET sensors tethered to different cell compartments (nucleus or cytosol) are available for assessing compartmentalised-pERK1/2 signal and could help to elucidate the origin of ERK1/2 responses and the potential for differences in signal location with the different receptor variants, or in response to the different peptide ligands.

3.3.3 Biased agonism of the CT ligands

3.3.3.1 Receptor variants have an effect on maximal responses of CT peptides

Both polymorphism and receptor splicing play a role in defining the differential efficacies observed for agonists between different receptor variants. Our data would suggest that the efficiency of coupling of the Pro polymorphism variants to the pathways analysed could be stronger than the Leu variants, and for cAMP formation, this is principally reflected in the magnitude of the second phase of signalling. Due to lower expression levels of the Pro variant, our data may also suggest that the Pro polymorphism promotes higher efficacy of all CT agonist peptides towards pERK1/2 and Ca^{2+} mobilisation when compared to the Leu variant.

Intriguing differences were observed in cAMP E_{max} across the different variants (***Figure 3.3, Table 3.2***). While a component of this variance may arise from differences in receptor expression, limited differences were observed in E_{max} for the other pathways, at least within the same splice variant. Moreover, the extent of difference was, in part, peptide dependent, suggesting that the differences were likely due to properties of the receptor.

3.3.3.2 Biased agonism at the hCTR$_a$Leu variant

When the other CT peptides are compared to the reference ligand hCT, differences in signalling profiles become evident. sCT showed a signalling profile analogous to the reference peptide hCT. On the other hand, pCT and cCT displayed biased agonism at the hCTR$_a$Leu compare to hCT. Specifically pCT showed bias towards Ca^{2+} and pERK1/2, and away from cAMP compared to hCT, suggesting that potentially pCT-dependent pERK1/2 signalling bias may be related to altered Ca^{2+} signalling relative to cAMP (when compared to hCT), and this is reflected in equivalence of pCT to hCT in bias plots comparing iCa^{2+} to pERK1/2 (***Figure 3.9***). cCT has more sequence similarity to sCT than to pCT or hCT, yet the pattern of its response differs from that of the other CTs, showing a stronger cAMP response than the other two pathways assessed, and a bias away from pERK1/2, when compared to the reference hCT ligand.

The N-terminus of the CT peptide is critical for initiation of signalling (at least for cAMP), and the N-terminal 7 amino acids are highly conserved. Furness *et al.* (2016) have demonstrated that CT peptides with distinct affinity for the hCTR (such as sCT and hCT) can be equipotent in cAMP response by promoting different ensembles of active states in the G protein. Specifically, hCT is less potent than the sCT in recruiting G protein to the ligand-bound receptor, however, it triggers a faster exchange of GDP for GTP and a faster turnover of G protein. This ultimately induces an initial higher activation of adenylyl cyclase and faster production of cAMP. The use of chimeric peptides exchanging N-terminal (13-16) amino acids between sCT and hCT has also highlighted the role of the ligand N-termini in promoting distinct G protein conformational changes, while the potency at which the conformational rearrangement in G protein occur depends on the mid-C-terminal region of the peptide. These fine differences are likely to require kinetic analysis of response to distinguish ligand behaviour, while the accumulation experiment performed in this study cannot capture changes that occur within minutes of ligand interaction with the receptor. Of interest for our study is the observation that the mid-region of cCT is absolutely conserved when compared to sCT, while the N-termini differs from all the other CT ligands at residues 2 and 3, being Ala or Ser, respectively for cCT and Ser/Gly2 and Asn3 in the other CT peptides. We speculate that these two residues could contribute to formation of a distinct ensemble

of conformations in receptor and in G protein relative to those observed for hCT, sCT and pCT. Experiments to confirm this hypothesis would involve assessing receptor conformations by advanced methods that include BRET, single molecule FRET, NMR and other spectroscopic methods (for instance DEER), or assessing effector conformations such as those already performed by Furness *et al.* (2016) for hCT and sCT, utilising BRET sensors inserted in distinct subunits of the G protein. Comparison between sCT, cCT and unique chimeric peptides altering the N-terminus of these ligands would confirm if those two residues have a differential effect in promoting distinct G protein conformational changes.

3.3.3.3 Effect of receptor splicing on biased CT signalling

The analysis of the shapes of the curves in the bias plots that compare Ca^{2+} (or cAMP) and pERK1/2 pathways show that for the $hCTR_a$ variant reflect the ability of this splice variant to couple to more downstream pathways. On the other hand, profiles of sCT and hCT at the $hCTR_b$ splice variants in the bias plots comparing cAMP and pERK1/2 pathways (that lacks Ca^{2+} response due to only limited interaction with Gαq protein) tend to the line of identity (LOI), suggesting that the Gαq coupling to hCTR variants could be one of the main drive for the downstream pERK1/2. Interesting in this case is the bias displayed by pCT and cCT away from the LOI when compared to hCT. It is possible that the bias observed for pCT and cCT could be attributed to the differential activation of this signalling pathway by these two ligands when compared to hCT and sCT. Additionally, as mentioned previously, we have to consider that other effectors (besides those investigated in this study) and scaffolding proteins interacting at the intracellular face of the CTR could subtly alter receptor conformation and therefore selectively alter signalling of these ligands.

3.3.3.4 Effect of receptor polymorphism on biased agonism

Different clinical studies show contradicting evidence about the potential role of the Leu polymorphism in increasing osteoporotic risk (Braga et al., 2002, Masi et al., 1998b, Dehghan et al., 2016). *In vitro* experiments conducted by Wolfe *et al.* (2003) showed that, in the presence of equimolar concentration of ligand, neither of the two polymorphisms stimulated with sCT, hCT or pCT showed a statistical difference in affinity or signalling (cAMP). Similarly in our cAMP signalling experiments, all receptor

polymorphic variants show no major statistical differences in potency for any of the CT peptides attributable to polymorphism, and the difference in maximal response could be attributed to changes in expression, although this appears unlikely, as discussed above.

This is highlighted by interesting differences were observed in our bias plots when comparing cAMP and pERK1/2 responses. At the $hCTR_a$ variants cCT had a similar signalling profile regardless of polymorphism. However, at the $hCTR_b$ splice variants, cCT displayed a distinct signalling profile when comparing the two polymorphisms with enhanced pERK1/2 at the Leu variant, and enhanced cAMP for the Pro variant relative to the reference ligand hCT.

This is the first pharmacological demonstration of an effect of this polymorphism on hCTR function. It would also be interesting to assess if this polymorphism has an effect on other signalling pathways besides those assessed in this study, to both identify how the different biased agonists, identified in this study, activate other potentially physiologically relevant pathways.

3.3.5 PHM-27 is a weak partial agonist of hCTR

The identification of an endogenous peptide that is not closely related to calcitonin but that activates the receptor would imply a distinct physiological role for the receptor.

PHM-27 has been reported to be a full agonist of hCTR in triggering intracellular cAMP production and cell proliferation in both HEK293 and 3T3 transfected cell lines (Ma et al., 2004).

In our stable COS-7 cells, PHM-27 does not fully compete with ^{125}I-sCT(8-32) at the concentrations tested, and appears to show very low affinity for the hCTR, which could potentially represent binding to a different site. From this assay it is not possible to define whether this ligand is an orthosteric or an allosteric agonist of the hCTR. We can speculate that due to low similarity to the CTs, this peptide establishes different interactions with the receptor and potentially binds with a different mode than the other orthosteric peptides. To determine if this is the case, additional experiments would need to be performed. These could include radioligand binding experiments with labelled PHM-27 as well as cross-linking experiments that may information about the binding pocket(s) for CT and PHM-27. For these studies, ligand modification would be required to insert a photoaffinity group in the ligand (or the receptor) that does not have a significant on the affinity/signalling of the ligand-receptor pair.

In our cell line PHM-27 is also only a partial agonist in triggering cAMP formation relative to CTs. Differences in cAMP profiles in our COS-7 cells, compared with previous studies using different cell backgrounds, could be due to many factors. In our experiments, the hCTR variants were expressed in COS-7 cells, while previous studies used NIH3T3 and HEK293 cells. It is not uncommon to observe different response to the same ligand and receptor depending on the cell system used in the assay (Ertel et al., 2006). Different tissues can express distinct isoforms and levels of effectors, each with a distinct affinity or apparent efficacy at the same receptor. In addition, compartmentalisation could differentially affect signalling (discussed above) in different cell lines due to different concentrations of lipids, cholesterol and caveolae in cell membranes, different internalisation machinery and receptor trafficking profiles (Halls et al., 2016).

Alternatively, the different responses to PHM-27 may be due to the presence or absence of accessory proteins present in different cell backgrounds. For example HEK cells (used in previously published studies) express RAMPs that alter the pharmacology of the hCTR. hCTR in complex with RAMP1 generates a receptor for amylin (Amy) and calcitonin-gene related peptide (CGRP), while a complex with RAMP2 or RAMP3 produces Amy receptors with lower affinity for CGRP. Some strains of HEK293 are reported to express RAMPs (Uhlen et al., 2015). For the CTR, it is unclear whether RAMPs directly interact with the ligand. RAMPs have been postulated change the conformation of the extracellular portion of the receptor to expose a distinct network of residues capable to interact with AMY or CGRP (Gingell et al., 2016). The hCTR appears to have low affinity and efficacy for PHM-27 in our system. Differences in efficacy between our study and the previous reports may suggest that PHM-27 actually activates an Amy or CGRP receptor, formed by a CTR-RAMP complex, although it may alternatively reflect differences in the assay. Complexing the hCTR with RAMP may provide a higher affinity binding site for PHM-27, or alternatively may result in more efficacious signalling for PHM-27 (Christopoulos et al., 2003). Future experiments could assess the ability of RAMPs to influence PHM-27 pharmacology by co-transfecting our COS-7 cells with both the hCTR variants and RAMPs.

We further assessed PHM-27 signalling in our stable COS-7 cells expressing hCTR, identifying that it does not produce a detectable Ca^{2+} response up to 3 μM of peptide, and like cAMP, is only a partial agonist in pERK1/2. It is important to consider that the phosphorylation of ERK1/2 is a converging point of multiple upstream signalling pathways and the profile observed with this peptide could be explained by a distinct spatial-temporal activation of diverse upstream effectors. Interestingly, bias plots suggest that PHM-27 is a biased agonist toward pERK1/2 and away from cAMP relative to hCT. Though it is important to note that bias plots do not quantify relative efficacy. Moreover, our bias plots were generated at single time points of ERK1/2 phosphorylation. PHM-27 generates a very sustained pERK1/2 response relative to hCT, and full kinetic measures of activation in both assay would be require to more fully understand the relative signalling of these peptides.

3.3.6 β-arrestin recruitment and trafficking of hCTR

In the COS-7 recombinant cells system, both a proximity assay and a microscopy-based approach failed to demonstrate any ligand induced recruitment of β-arrestins, suggesting that hCTR internalization and/or ligand-induced signalling does not involve the recruitment of β-arrestins to the receptor. To our knowledge, only one study had previously reported interaction between $hCTR_aLeu$ variant and β-arrestins (Andreassen et al., 2014). This study showed that sCT induces a prolonged interaction between receptor and β-arrestins, while hCT produced only a transient interaction with the effector. The differences in our observations could reflect cell-type differences in β-arrestin recruitment profiles for CTR. However, the results of the previous study may have been influenced by the experimental design of the assay. In the previously reported study, both the hCTRaLeu and the β-arrestins were tagged with two fragments of the β-galactosidase enzyme, which, upon interaction between the two binding partners, promote reconstitution of the active enzyme. This system can provide very amplified responses and could even result in artefacts, as the complementation is essentially irreversible. Of greater relevance, the receptor was modified by fusing, the C-terminus of the vasopressin V2 receptor (V2R) to the receptor. The V2R is known to strongly promote recruitment of β-arrestins (Oakley et al., 1999). Nevertheless, the different profiles observed in the published study between hCT and sCT their complementation assay suggest distinct conformational rearrangements in the receptor that may be

induced by the two ligands. That study also reported ligand-induced internalisation of the receptor, in contrast to the ligand independent constitutive internalisation profile observed in the current experiments. However again, presence of V2R tail likely impacts broadly on receptor function and would have disrupted the PDZ domain discussed above.

In our study both splice variants internalise constitutively and independently of the presence of ligand. Both the full agonist sCT and the putative antagonist sCT(8-32) are internalised in presence of all hCTR splice and polymorphic variants but not in untransfected cells, confirming that this process is receptor-dependent. Real time imaging experiments revealed that ligand interaction (either an agonist or a reported antagonist/partial agonist sCT(8-32)) did not appear to visually alter the rate or speed of internalisation (although this was not quantified), clearly indicating that in COS-7 cells all variants constitutively internalise independent of ligand, and accumulate our probes in perinuclear compartment. Despite our observations, studies by other groups reported ligand-dependent receptor internalisation, however, these studies follow internalisation of ligand rather than receptor. For example internalisation of ^{125}I-sCT has been identified to occur in cancer cell lines (T47D and BEN) (Lamp et al., 1981, Findlay et al., 1982, Wada et al., 1995) that endogenously express both hCTR splice variants, while Moore *et al.* (1995) used a similar radioligand binding approach on transfected BHK cells to show internalization of the radioligand with the $hCTR_a$, but not the $hCTR_b$ splice variant. These latter studies are particularly intriguing as they are indicative of cell-dependent processes in receptor trafficking.

Our lab has recently generated preliminary data suggesting the constitutive, rapid internalisation of the hCTR also occurs in human osteoclasts (S. Furness, personal communication), a physiologically relevant system that naturally expresses both CTR splice variants, (the $hCTR_a$ at higher levels) (Kuestner et al., 1994). These findings support our identification of a novel trafficking of the CTR that occurs in osteoclasts, and this warrants further exploration.

The physiological role of this process and the potential for differences in trafficking with different splice variants observed in previous studies (Schneider et al., 1988, Lamp et al., 1981, Findlay et al., 1982, Wada et al., 1995) is still unclear, but the fast and continuous internalisation of the receptor may be a mechanism of acute down-regulation adopted by the cell. The mechanistic basis behind CTR trafficking

also remains unclear at this stage, though the PDZ domain is unexplored. The potential ubiquitination of the CTR has yet to be explored, which could be assessed by immunoprecipitation or by western blotting using commercially available anti-ubiquitin antibodies (Sigismund and Polo, 2016). It is possible to speculate that CTR may produce downstream signalling from intracellular compartments, as continual removal of receptor from the cell surface could also deliver the activated receptor to internal sites of action and thus promote compartmentalised signalling.

We have yet to prevent receptor internalisation of the hCTR or block various components of the signalling cascade to explore these possibilities in the different hCTR variants, and these studies are required to better understand its role in receptor function.

3.3.7 Physiological implications of our findings

Despite several studies in whole animals, primary and recombinant cells, only limited evidence is available regarding signalling pathways that are important for physiological function mediated by the CTR. In murine osteoclasts, prolonged CT treatment causes PKA activation and downregulation of CTR (Takahashi et al., 1995, Wada et al., 1996, Wada et al., 1995). In these cells, the formation of actin rings and cytoskeleton remodelling is controlled by PKA (with some potential involvement of PKC) (Suzuki et al., 1996), whilst rise of intracellular calcium and PKC activation blocks lysosome acidification, pit formation (via inhibition of actin-ring formation) and release of hydrochloric acid that dissolves the bone matrix (Yamamoto et al., 2005b, Sørensen et al., 2010). The CTR may also function as calcium sensing receptor (Stroop et al., 1993) and may provide *in situ* feedback to inhibit excessive bone resorption in osteoclasts or excretion in kidneys. However to our knowledge there are no data addressing whether there are differences between receptor polymorphisms or splice variants relevant to these different functions. These signalling mechanisms may be particularly important in tissue-dependent responses, especially when we consider the modulatory role played by the 16 amino acid insertion and also that the expression of the $hCTR_b$ splice variant is more selective that the $hCTR_a$ (Kuestner et al., 1994). It is therefore likely that the unique signalling profiles of the different splice variants may contribute to different functional roles of these receptors in different tissues.

Of particular note, the CTR appears to play an important role in implantation and development of the embryo in the placenta, and the increase in progesterone level following ovulation is known to increase CTR expression. Activation of the CTR can activate PKA and Ca^{2+} pathways, leading to increase expression of transglutaminase (tTGase) (Li et al., 2006), an enzyme involved in stabilisation of extracellular matrix, cell adhesion, motility and proliferation. CT treatment of murine endometrium alone favours implant of the trophoblast (outer layer of the embryo which will develop into majority of the placenta) and this is reported to be dependent on intracellular Ca^{2+} mobilisation and PKC activation (Li et al., 2008). Moreover, CT treatment of murine trophoblasts enhances expression of adhesion proteins, again favouring implantation and expansion in endometrium (Xiong et al., 2012). In later stages of gestation, the human syncytiotrophoblast brush border (part of the foetal placenta facing the mother) is known to express higher levels of CTR than the foetus, and potentially helps the transport of calcium, against gradient, to the foetus (Lafond et al., 1994). Although to our knowledge no evidence is available in humans, these data would suggest that if CTR agonist may play a role in fertility and foetus development, and patterns of $hCTR_a$ and $hCTR_b$ likely contribute to how these tissue respond.

Several epidemiological studies have linked the common Leu/Pro polymorphism to risk of developing osteoporosis and kidney stone disease (Masi et al., 1998a, Braga et al., 2002, Mitra et al., 2017). Although this link is based on limited patient numbers, it is possible that changes in signalling patterns downstream of CTR activation could change tissue response and predispose and a patient towards a pathology. In this context, our data provide evidence that polymorphism does indeed affect CTR function. If a relationship between the polymorphism and pathology is eventually established, the genotype of the patient could be used as a diagnostic of early onset of disease, as well as informing treatment, as our data support ligand dependent differences in response depending on their genotype.

Both pCT and cCT display biased agonism relative to hCT in a receptor-variant dependent manner. The unique cCT signalling profiles that we have determined may suggest that the two divergent residues at the N-terminus of this peptide, that are known to interact with the core of the hCTR (Liang et al., 2017), may contribute to the differences observed in signalling. Although we have yet to clearly understand how each signalling pathways correlates to a tissue effect, this knowledge may help to develop biased

agonists if further exploration reveals that selective CTR-mediated signalling would be beneficial for treatment of specific pathological conditions. In addition, these biased ligands may help to tease apart the importance of the different signalling, or to distinguish pathological from physiological effects of hCTR activation.

To conclude, the existence of multiple splice and polymorphic variants, expressed at different levels in different tissues, is likely to promote distinct physiological outcomes in tissues and organs. Therefore, understanding the role of different agonists, their signalling profiles and whether these agonist are biased may help in defining treatment regimens and eventually (with more data) to predict patient-specific treatments. Understanding how a specific pathway links to specific tissue responses may unveil new therapeutic targets or additional uses of current therapeutics.

CHAPTER 4

Structure-function study of extracellular loop 2 (ECL2) of the human calcitonin receptor (hCTR)

4.1 Introduction

Orthosteric ligands of Class B1 GPCRs are proposed to interact with their receptors via a two-domain mechanism whereby the C-terminus of the ligand first interacts with the NTD of the receptor. Subsequently the N-terminus of the peptide re-orientates toward the juxta membrane portion of the receptor, where specific interactions with the top of the TM bundle and connecting ECLs trigger conformational changes in the receptor structure that subsequently result in intracellular signalling (Hoare, 2005, Hollenstein et al., 2014). To date, the specific interactions between the ligand N-terminus and the ECLs-TM bundle that drive receptor activation are still not well defined for the majority of Class B1 GPCRs. The three ECLs, in particular, are highly flexible, and are not fully resolved in the available crystal and Cryo-EM structures (Zhang et al., 2017b, Zhang et al., 2017a, Song et al., 2017, Liang et al., 2017, Hollenstein et al., 2013). Mutagenesis and crosslinking studies have shown that, despite significant heterogeneity, the 3 ECLs are involved to different extents in ligand selectivity, affinity and binding kinetics across different Class B1 GPCRs (Dong et al., 2016, Wootten et al., 2016, Dong et al., 2014, Woolley and Conner, 2017, Weaver et al., 2017). Additionally, some of these studies have identified how specific residues of the three ECLs also play a role in controlling intracellular signalling (Dong et al., 2016, Wootten et al., 2016, Woolley et al., 2017, Woolley and Conner, 2017, Dong et al., 2014). The physiological orthosteric ligands that activate Class B1 are also structurally diverse with the N-terminus of calcitonin-like ligands (CT, CGRP, CTR, Amy and AM), characterised by a cyclic ring that is essential for receptor activation, whereas the other peptides of this Class share a linear structure (Dods and Donnelly, 2015). This may translate into structural differences in both the features of the receptor binding pocket and in the network of interactions that ligand and receptor establish. This hypothesis is supported by the recently solved structures of peptide agonist-bound GLP-1R (Zhang et al., 2017b) and CTR (Liang et al., 2017) where the cyclic ring of the calcitonin peptide has additional steric constraints when compared to the linear N-terminus of GLP-1, dictating a different orientation of the first 6 residues of sCT.

ECL2 is the most structurally diverse across all GPCR classes in terms of length, sequence and conformation (in the available structures to date), and is important for ligand selectivity and binding for

all Class A, B1 and C receptors, where it has been studied to date (Woolley and Conner, 2017). Like Class A GPCRs, the Class B1 ECL2 has a completely conserved Cys residue, involved in a disulphide bond with TM3 that stabilises receptor structure. This Cys is part of a completely conserved Class B1 "CW" motif. Also conserved in Class B1 receptors are basic residues adjacent to the top of TM4 (***Figure 4.1 A***).

Mutagenesis and crosslinking studies performed in several of the Class B1 GPCRs have identified specific residues within ECL2 that establish distinct interactions with different orthosteric ligands of the same receptor (Dong et al., 2016, Wootten et al., 2016, Woolley et al., 2017, Dong et al., 2014). This has also identified differences in residues important for affinity and efficacy of different known biased agonists of the GLP-1R (Koole et al., 2012b, Wootten et al., 2016, Mann et al., 2010), a receptor that pleiotropically couples to multiple signalling pathways including Gαs, Gαi, Gαq and β-arrestins (Fletcher et al., 2016). In particular, while ECL2 is important for ligand affinity, cAMP production and calcium mobilisation, it has a limited role in coupling ligand binding to ERK1/2 phosphorylation. Moreover, despite a common domain for coupling to cAMP and Ca^{2+} mobilisation, distinct residues within ECL2 are of differential importance for coupling different biased agonists to these different signalling pathways.

Due to the limited sequence homology between receptors of Class B1 (***Figure 4.1 A***), we were interested in determining the importance of ECL2 in affinity and coupling to distinct signalling pathways in other Class B1 GPCRs, and whether the observations made for GLP-1R are conserved across different receptors. We have investigated the human calcitonin receptor (hCTR), which is involved in bone remodelling, calcium homeostasis, food intake, gastric motility, modulation of pain transmission in the CNS, fertility and cancer proliferation (Egerton et al., 1995, Goebell et al., 1979, Shah et al., 1990, Rohner and Planche, 1985, Laurian et al., 1986, Fujikawa et al., 1996b, Kuestner et al., 1994). Little to no evidence is available regarding the role of ECL2 in CTR binding and activation. However information on the related calcitonin-like receptors suggest that this domain is important for coupling to cAMP in the calcitonin receptor family.

The recently published Cryo-EM structure of the hCTR-sCT complex has poor resolved density within the EM map for the ECLs and the top of TM6 and TM7, due to their high flexibility (Liang et al., 2017). This receptor structure, obtained in complex with the pseudo-irreversible agonist sCT, revealed the location of the agonist binding site with the backbone of the N-terminus of sCT clearly resolved. However, peptide side chains were not visible in the EM map, and this limited the modelling of the specific interactions between receptor and agonist. The location of this peptide backbone suggest ECL2 is likely to be important for sCT binding, and this will likely extend to other peptide ligands that bind to CTR. Among calcitonin ligands, there are known differences in ligand pharmacology. hCT has lower affinity and faster off rate in its binding kinetics, while showing similar potency for cAMP accumulation when compared to sCT (Andreassen et al., 2014, Hilton et al., 2000, Moore et al., 1995). Porcine CT (pCT) shows an intermediate binding affinity, when compared to hCT and sCT, and cell-dependent signalling efficacy (Kuestner et al., 1994, Wolfe et al., 2003, Moore et al., 1995). Additionally, CTR can also bind calcitonin gene-related peptide (CGRP) and amylin (Amy) with low affinity, however upon formation of heterocomplex between receptor and RAMPs the affinities and efficacies for these two ligands are enhanced (Routledge et al., 2017). Of note, the signalling efficacy of sCT and hCT is different, with these two ligands differentailly activating $G_{\alpha}s$ protein, by promoting different conformations in the G protein structure (Furness et al., 2016). To date, how this is linked with receptor structure is unknown. Altogether, the published data suggests that these agonists could establish distinct interactions with the receptor upon binding, and that these interactions may trigger specific conformational changes in the receptor and/or G protein that alter effector/regulatory protein recruitment and differential activation of downstream signalling pathways.

In this Chapter an extensive alanine substitution study on ECL2 of the hCTR was performed to determine its role in binding and signalling of five known CTR orthosteric agonists (hCT, sCT, pCT, Amy and CGRP), to determine the network of interaction between the ligand and receptor and how these alanine mutations alter efficacy in a global or ligand-specific manner. Residues that form ECL2 and adjacent portions of TM4 and TM5 (residues I279 to I300) (***Figure 4.1 B***) were individually substituted to alanine, and receptors were stably expressed in CV-1-FlpIn cells. Both binding and

intracellular signalling (cAMP, IP_1 formation and pERK1/2) were assessed as measure of receptor activation.

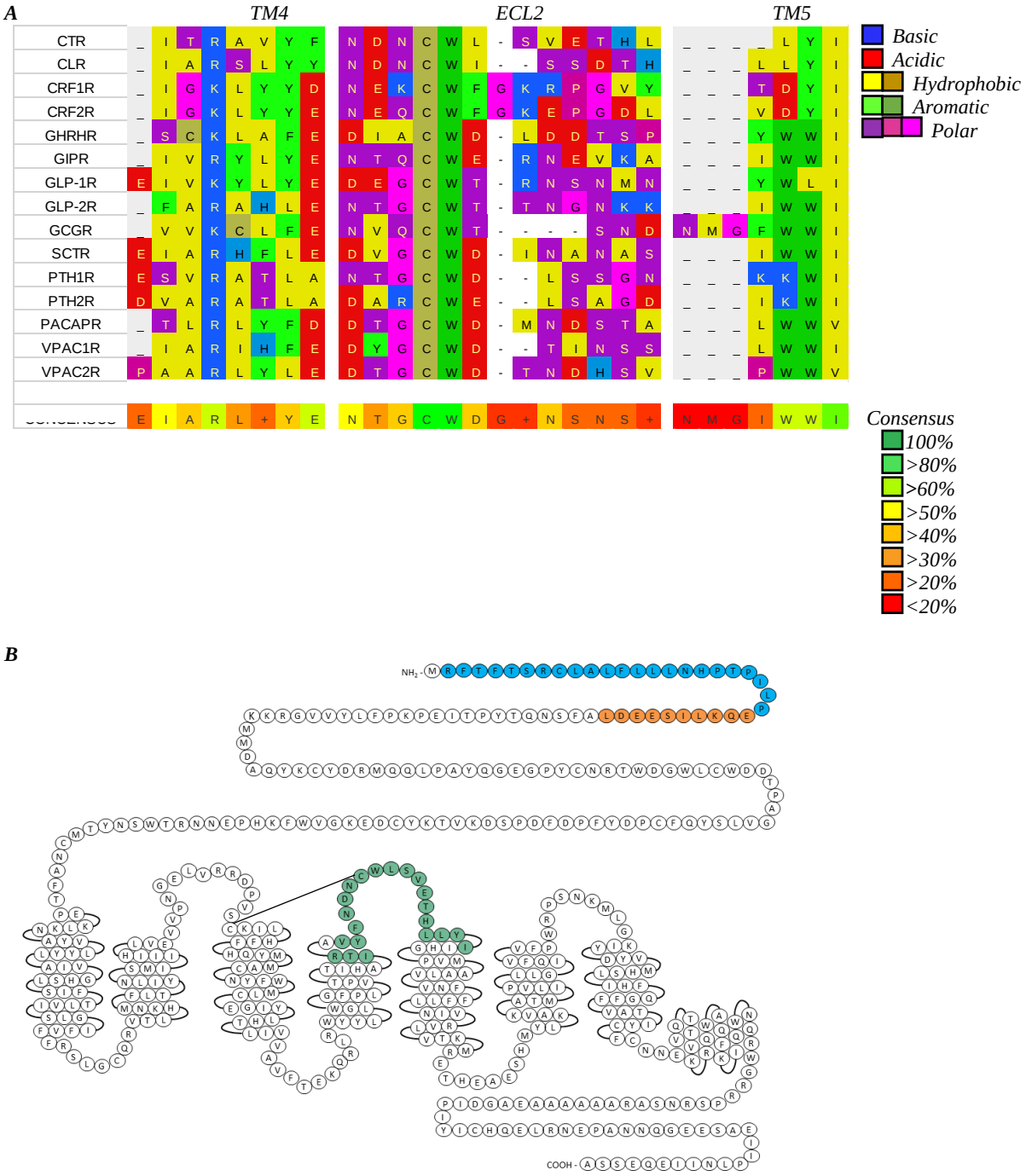

Figure 4.1 Sequence alignment of human Class B1 GPCRs, diagram and model of the hCTR$_a$Leu receptor used in this study. *(A) Sequence alignment of TM4-ECL2-TM5 of the 15 human Class B1 GPCRs. Receptors sequences were aligned and exported from gpcrdb.org. (B) Snake diagram of the hCTR: highlighted in blue are the residues that constitute the signal peptide of the receptor, in orange the cMyc tag, and in green the residues that have been mutated to alanine.*

4.2 Results

The residues in ECL2 and the extracellular portion of TM4 and TM5 (I279 to I300) (***Figure 4.1 B and C***) of the hCTR$_a$Leu were individually mutated to alanine and stably expressed in CV-1-FlpIn cells. Wild type (WT) or mutant receptor surface expression and affinity for all peptides were measured. Statistical analysis was performed for each assay and ligand used, by comparing data obtained from the mutant receptors to WT in a one-way ANOVA followed by Dunnett's post-test with a cut-off of $p<0.05$ as significant.

4.2.1 Cell surface expression of CTR variants

Receptor expression at the plasma membrane was determined by performing heterologous competition in the presence of two different concentrations of the radioligand ^{125}I-sCT(8-32), for both WT and mutant receptors (***Figure 4.2, Table 4.2***). B_{max} was derived using Equation 5 (Section 2.6.1) and converted to sites/cell (Equation 6, Section 2.6.1). No radioligand binding was detectable for mutations N286A, D287A, C289A, W290A and I300A and their expression could therefore not be determined. When compared to WT, T280A, N286A and H296 mutants had significantly higher surface expression. Although not significant, V293, E294 and residues throughout top of TM4 and adjacent residues of ECL2 (I279-F285, with the exception of R281) also trended towards increased expression compared to WT, whilst the mutation of residues in the distal part of ECL2 and proximal of TM5 reduced receptor surface expression, although this did not achieve significance.

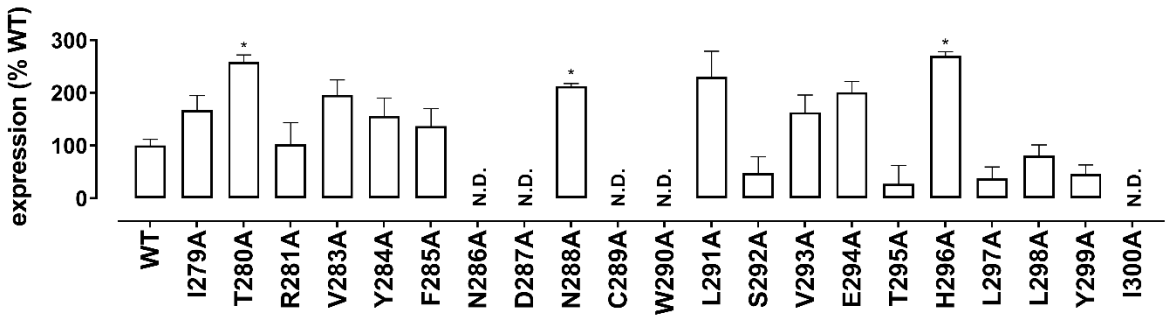

Figure 4.2 Cell surface expression of the hCTR$_a$Leu mutants stably expressed in CV-1-FlpIn cells. *Homologous competition of radioligand binding was performed in the presence of 2 concentrations of ^{125}I-sCT(8-32), with concentrations of the competing sCT(8-32) ranging between 1 µM and 1 pM. CPM data were converted to sites/cell and then normalized to WT and non-specific binding. All values are mean+S.E.M. of 3 to 5 independent experiments conducted in duplicate. (N.D.) affinity not determined as no radioligand binding was detected.*

4.2.2 Ligand affinity

Whole cell radioligand competition binding assays employing ^{125}I-sCT(8-32) were used to determine affinity of the CT peptides for all the hCTR$_a$Leu receptors (WT and mutants) used in this study (summarised in ***Table 4.1*** and ***4.2***). Affinity for sCT(8-32) was determined via homologous competition binding (***Figure 4.3***), whereas heterologous inhibition binding was performed for hCT (***Figure 4.4***), sCT (***Figure 4.5***) and pCT (***Figure 4.6)***. For heterologous competition, the affinity of the radioligand, determined for each mutant via homologous competition, was used and data for radioligand occupancy were corrected using the Cheng-Prusoff equation (Equation 7, Section 2.6.1) to calculate pK$_i$. Changes in affinity relative to WT for all CT ligands and receptors (ΔpK$_i$) are represented as bar graph in (***Figure 4.7***).

Consistent with published literature and data in Chapter 3, sCT and sCT(8-32) had pK$_i$ values of 9.87±0.04 and 9.82±0.05, respectively for the WT receptor, while the measured affinities for pCT and hCT were 8.25±0.10 and 6.84±0.14, respectively. The N286A, D287A, C289A, W290A and I300A mutants showed no detectable binding for ^{125}I-sCT(8-32), hence peptide affinities could not be measured for these five mutants. Mutant R281A showed a significant reduction in affinity (5-12 fold) for all CT peptides. Conversely, L291A showed a significant reduction in affinity for hCT and pCT (12-27 fold), but no change in sCT affinity. Despite having no effect on sCT affinity, T295A significantly enhanced affinity for sCT(8-32) (3-fold), while reducing hCT (6-fold) and pCT (9-fold) affinity. sCT and sCT(8-32) affinities were not affected by any other mutations, whereas hCT and pCT affinity were selectively altered: I279A, V293A L297A and L298A reduced the affinity for hCT, whereas L298A and Y299A reduced the affinity of pCT (***Figure 4.3 to 4.7***, ***Table 4.2 and 4.3***).

rAmy and hαCGRP are known to bind with low affinity to the hCTR and their affinity could not be determined, as up to 1 μM of peptide did not fully compete for ^{125}I-sCT(8-32) binding.

```
sCT(8-32)          VLGKLSQELHKLQTYPRTNTGSGTP
sCT        CSNLSTCVLGKLSQELHKLQTYPRTNTGSGTP
pCT        CSNLSTCVLSAYWRNLNNFHRFSGMGFGPETP
hCT        CGNLSTCMLGTYTQDFNKFHTFPQTAIGVGAP

rAmy       KCNTATCATQRLANFLVRSSNNLGPVLPPTNVGSNTY
hαCGRP     ACDTATCVTHRLAGLLSRSGGVVKNNFVPTNVGSKAF
```

Table 4.1 Sequence comparison of the peptides studied in this Chapter. *Alignment of the CTs was performed using Biology WorkBench (workbench.sdsc.edu). Identical residues have been highlighted in* ***green****, conservative substitutions are coloured* ***blue****, and semi- conservative substitutions are in* ***orange****.* ***Black*** *text indicates the non-conserved. Due to limited homology, rAmy, hαCGRP have been aligned with the CT peptides, using the N-terminal loop as reference.*

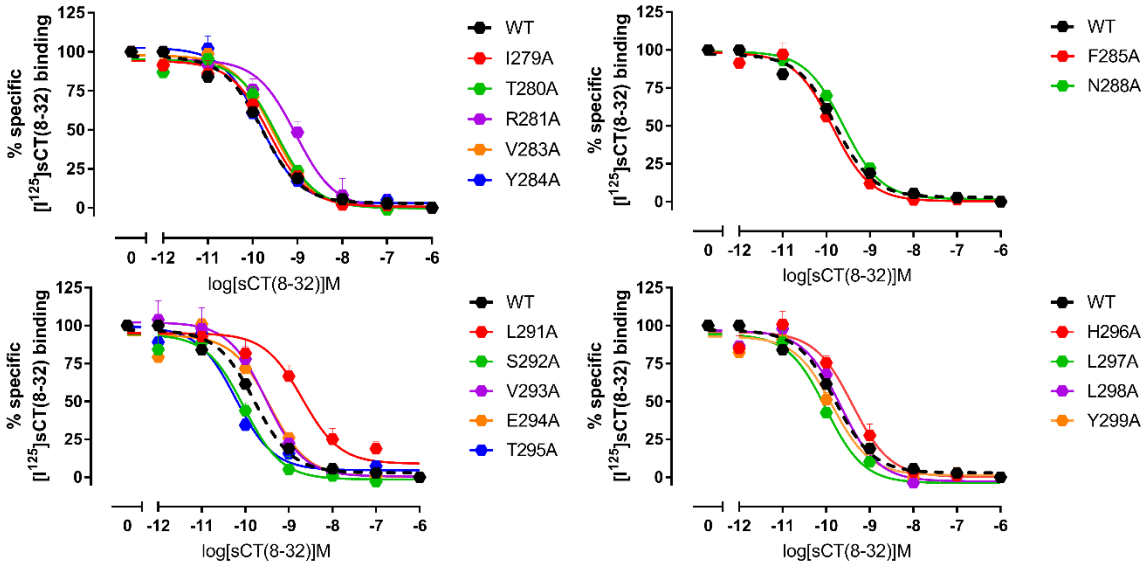

Figure 4.3 Homologous competition of ^{125}I-sCT(8-32) binding for each of the hCTR$_a$Leu mutants stably expressed in CV-1-FlpIn cells. *Whole cell radioligand binding was performed for each receptor mutant in presence of ^{125}I-sCT(8-32) and competing sCT(8-32) ranging in concentration between 1 μM and 1 pM. Non-specific binding was determined in the presence of 1 μM of sCT(8-32) and was used to calculate % of specific binding. Data were fit with a three parameter logistic equation. All values are mean+S.E.M. of 8 to 10 independent experiments, conducted in duplicate.*

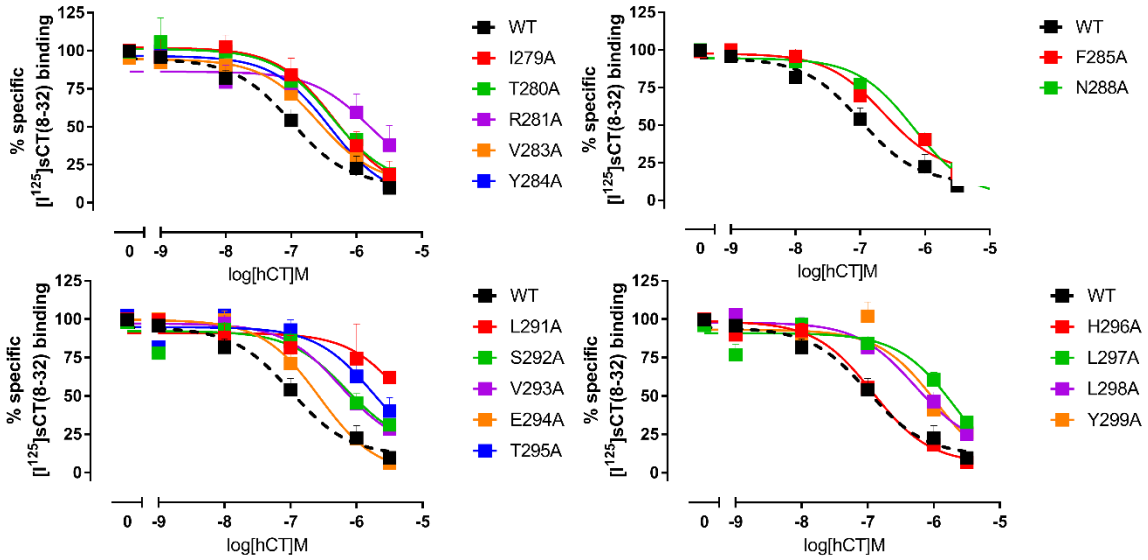

Figure 4.4 Heterologous competition binding of hCT for each of the hCTR$_a$Leu mutants stably expressed in CV-1-FlpIn cells. *Whole cell radioligand binding was performed for each receptor mutant in the presence of ^{125}I-sCT(8-32) and competing hCT ranging in concentration between 3 μM and 1 nM. Non-specific binding was determined in the presence of 1 μM of sCT(8-32) and was used to calculate % of specific binding. Data were fit with a three parameter logistic equation. All values are mean+S.E.M. of 4 to 5 independent experiments, conducted in duplicate.*

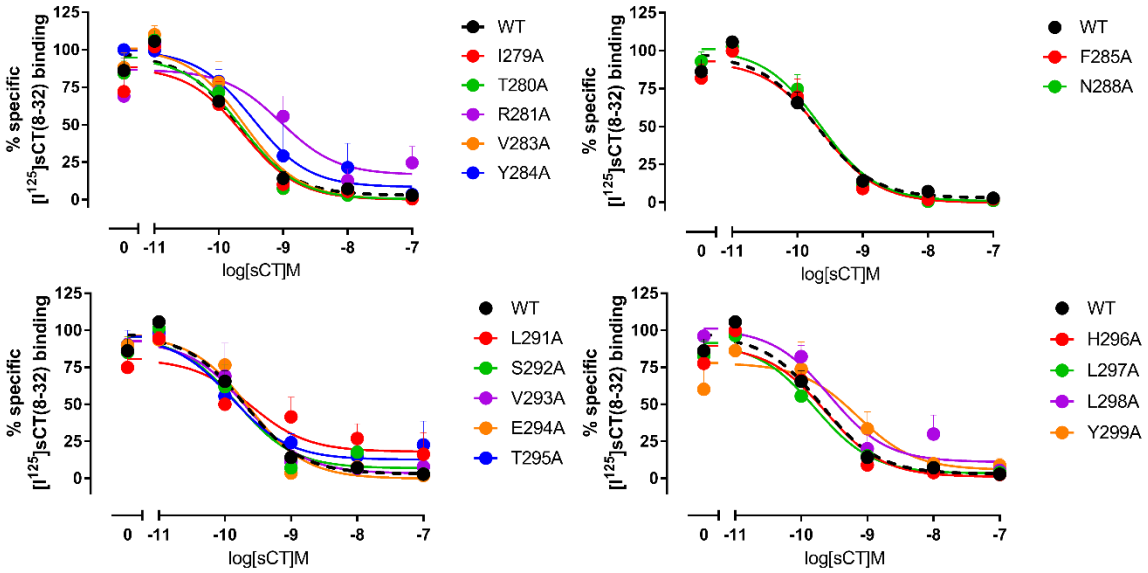

Figure 4.5 Heterologous competition binding of sCT for each of the hCTR$_a$Leu mutants stably expressed in CV-1-FlpIn cells. *Whole cell radioligand binding was performed for each receptor mutant in the presence of ^{125}I-sCT(8-32) and competing sCT ranging in concentration between 1 μM and 10 pM. Non-specific binding was determined in the presence of 1 μM of sCT(8-32) and was used to calculate % of specific binding. Data were fit with a three parameter logistic equation. All values are mean+S.E.M. of 3 to 6 independent experiments, conducted in duplicate.*

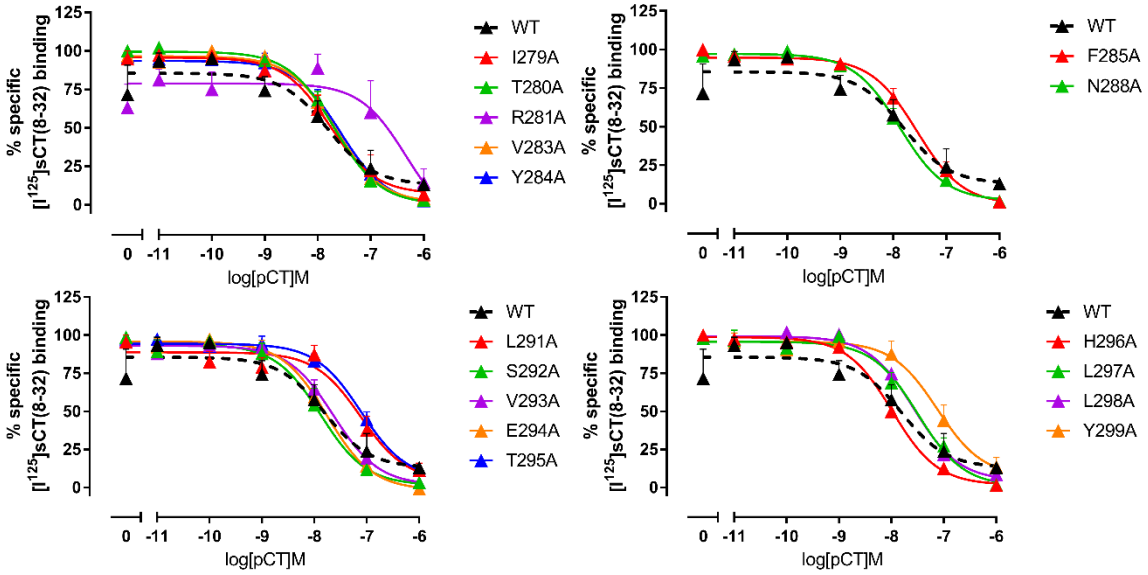

Figure 4.6 Heterologous competition binding of pCT for each of the hCTR$_a$Leu mutants stably expressed in CV-1-FlpIn cells. *Whole cell radioligand binding was performed for each receptor mutant in the presence of ^{125}I-sCT(8-32) and competing pCT ranging in concentration between 1 µM and 10 pM. Non-specific binding was determined in the presence of 1 µM of sCT(8-32) and was used to calculate % of specific binding. Data were fit with a three parameter logistic equation. All values are mean+S.E.M. of 4 to 6 independent experiments, conducted in duplicate.*

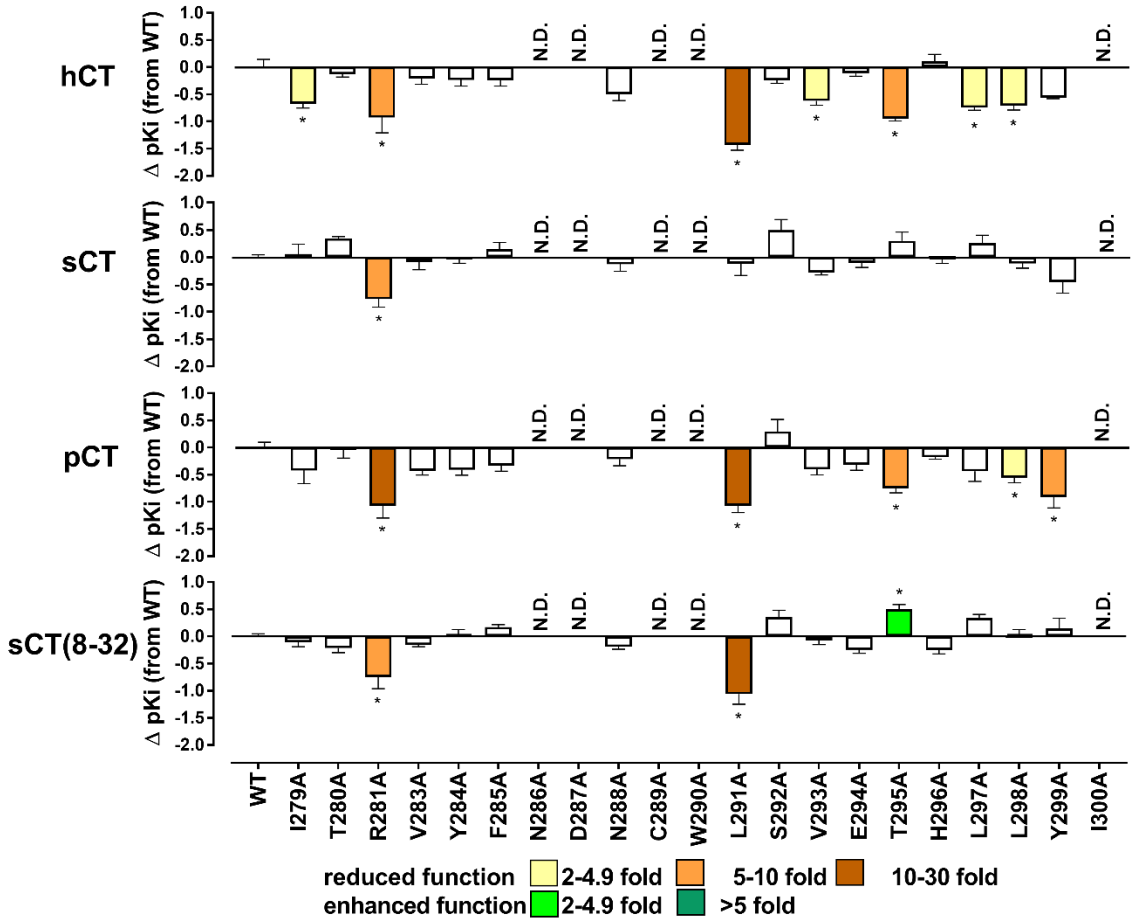

Figure 4.7 Effect of single alanine mutations in ECL2 of hCTR$_a$Leu on ligand affinity. *pK$_i$ were derived for each ligand and mutant receptor from analysis of data in Figure 4.3-6. Changes in affinity (Δ pK$_i$) for each mutant relative to WT (on a log scale) for hCT, sCT, pCT or sCT(8-32) are represented as bars. All values are mean+S.E.M. of 3 to 10 independent experiments conducted in duplicate. Significance of changes in affinity of each ligand was determined by comparison of the WT by a one-way analysis of variance and Dunnett's post-test (p<0.05 represented by *). (N.D.) affinity not determined as no radioligand binding was detected.*

	hCT pK_i		sCT pK_i		pCT pK_i		sCT(8-32) pK_i		Whole cell binding sites/cell	
WT	6.84±0.14	(9)	9.87±0.04	(8)	8.25±0.1	(9)	9.82±0.05	(8)	24,200±2,900	(5)
I279A	6.16±0.08*	(4)	9.93±0.18	(4)	7.83±0.24	(4)	9.72±0.08	(8)	40,500±11,300	(5)
T280A	6.71±0.05	(4)	10.22±0.03	(4)	8.2±0.15	(4)	9.61±0.08	(8)	62,600±8,700*	(4)
R281A	5.92±0.28*	(5)	9.1±0.15*	(6)	7.18±0.23*	(5)	9.07±0.21*	(10)	24,900±10,200	(3)
V283A	6.63±0.11	(4)	9.78±0.14	(4)	7.82±0.08	(4)	9.67±0.03	(8)	47,600±13,600	(4)
Y284A	6.61±0.11	(5)	9.83±0.07	(3)	7.84±0.1	(4)	9.85±0.1	(8)	37,800±12,800	(4)
F285A	6.6±0.11	(4)	10.02±0.12	(4)	7.92±0.11	(4)	9.99±0.05	(8)	33,200±11,000	(4)
N286A	N.D.		N.D.		N.D.		N.D.		N.D.	
D287A	N.D.		N.D.		N.D.		N.D.		N.D.	
N288A	6.35±0.12	(4)	9.74±0.13	(4)	8.03±0.12	(5)	9.63±0.04	(8)	51,600±2,600*	(4)
C289A	N.D.		N.D.		N.D.		N.D.		N.D.	
W290A	N.D.		N.D.		N.D.		N.D.		N.D.	
L291A	5.41±0.1*	(3)	9.75±0.21	(5)	7.17±0.12*	(6)	8.76±0.19*	(9)	55,700±27,400	(3)
S292A	6.6±0.05	(4)	10.36±0.2	(4)	8.54±0.22	(4)	10.18±0.13	(8)	11,600±3,600	(4)
V293A	6.22±0.08*	(4)	9.59±0.05	(4)	7.85±0.1	(4)	9.75±0.08	(8)	39,500±13,000	(4)
E294A	6.73±0.06	(5)	9.77±0.08	(4)	7.93±0.1	(4)	9.58±0.07	(8)	48,700±10,100	(4)
T295A	5.9±0.05*	(4)	10.17±0.16	(4)	7.49±0.08*	(4)	10.33±0.09*	(8)	6,600±2,300	(4)
H296A	6.95±0.13	(4)	9.84±0.09	(4)	8.07±0.03	(4)	9.57±0.07	(8)	65,500±5,100*	(4)
L297A	6.09±0.05*	(4)	10.12±0.15	(4)	7.81±0.19	(4)	10.17±0.07	(8)	9,200±2,000	(4)
L298A	6.13±0.08*	(4)	9.76±0.09	(4)	7.69±0.1*	(4)	9.83±0.12	(8)	19,600±4,000	(4)
Y299A	6.28±0.02	(4)	9.41±0.2	(4)	7.33±0.2*	(4)	9.97±0.18	(8)	11,100±1,900	(4)
I300A	N.D.		N.D.		N.D.		N.D.		N.D.	

Table 4.2 Effect of single alanine mutations in ECL2 of hCTR$_a$Leu on ligand affinity and cell surface expression. *pIC_{50} (negative logarithm of the concentration of ligand that produces half the maximal displacement of the iodinated radioligand). Data were obtained by fitting a three parameter logistic equation and data for radioligand occupancy were corrected using the Cheng-Prusoff equation (Equation 7, Section 2.6.1) to calculate pK_i. All values expressed as pK_i are mean±S.E.M. of 3 to 10 independent experiments conducted in duplicate. Homologous whole cell binding was used to determine B_{max} values by fitting (Equation 5, Section 2.6.1) to concentration-response data performed in presence of two different concentrations of the radioligand ^{125}I-sCT(8-32). B_{max} values were converted to sites/cell (Equation 6, Section 2.6.1). Significance of changes in affinity of each ligand was determined by comparison of the WT to the other receptor mutants in a one-way analysis of variance and Dunnett's post-test (p<0.05 represented by *). (N.D.) affinity or expression not determined as no radioligand binding was detected.*

	hCT				sCT				pCT				sCT(8-32)		rAmy		hαCGRP	
	ΔpK_i		ΔpK_A		ΔpK_i		ΔpK_A		ΔpK_i		ΔpK_A		ΔpK_i		ΔpK_A		ΔpK_A	
WT	0.0±0.14	(9)	0.0±0.16	(20)	0.0±0.04	(8)	0.0±0.13	(25)	0.0±0.1	(9)	0.0±0.16	(15)	0.0±0.05	(8)	0.0±0.19	(11)	0.0±0.28	(8)
I279A	-0.68±0.08*	(4)	0.45±0.39	(4)	0.06±0.18	(4)	0.45±0.31	(5)	-0.42±0.24	(4)	0.11±0.24	(6)	-0.11±0.08	(8)	-0.55±0.34	(5)	-0.39±0.28	(4)
T280A	-0.13±0.05	(4)	0.49±0.37	(4)	0.35±0.03	(4)	0.69±0.33	(4)	-0.04±0.15	(4)	0.01±0.24	(5)	-0.22±0.08	(8)	-0.56±0.45	(4)	-0.25±0.39	(4)
R281A	-0.92±0.28*	(5)	-2.73±0.26*	(7)	-0.77±0.15*	(6)	-0.43±0.17	(10)	-1.07±0.23*	(5)	-1.57±0.21*	(6)	-0.75±0.21*	(10)	0.62±0.45	(5)	0.73±0.38	(4)
V283A	-0.21±0.11	(4)	0.6±0.39	(4)	-0.09±0.14	(4)	0.34±0.25	(5)	-0.43±0.08	(4)	0.16±0.25	(5)	-0.16±0.03	(8)	-0.27±0.37	(5)	0.14±0.33	(4)
Y284A	-0.23±0.11	(5)	0.24±0.3	(5)	-0.04±0.07	(3)	0.25±0.26	(5)	-0.41±0.1	(4)	-0.13±0.23	(6)	0.03±0.1	(8)	0.1±0.28	(5)	0.41±0.33	(4)
F285A	-0.24±0.11	(4)	0.1±0.29	(5)	0.15±0.12	(4)	0.34±0.27	(5)	-0.33±0.11	(4)	0.0±0.29	(6)	0.17±0.05	(8)	-0.16±0.31	(5)	0.2±0.35	(4)
N286A	N.D.		-0.64±0.27	(5)	N.D.		0.01±0.28	(5)	N.D.		-0.58±0.3	(5)	N.D.		0.68±0.3	(5)	0.09±0.8	(4)
D287A	N.D.		-2.98±0.26*	(6)	N.D.		-0.52±0.18	(10)	N.D.		-1.51±0.4*	(4)	N.D.		N.D.		N.D.	
N288A	-0.5±0.12	(4)	0.03±0.26	(5)	-0.13±0.13	(4)	0.46±0.36	(6)	-0.22±0.12	(5)	-0.14±0.25	(5)	-0.19±0.04	(8)	-0.64±0.43	(5)	0.11±0.36	(4)
C289A	N.D.		-2.47±0.2*	(8)	N.D.		-0.63±0.16	(10)	N.D.		-1.44±0.31*	(3)	N.D.		0.92±0.36	(4)	N.D.	
W290A	N.D.		-3.48±0.26*	(10)	N.D.		-0.67±0.15*	(11)	N.D.		-2.19±0.24*	(4)	N.D.		1.12±0.41*	(5)	N.D.	
L291A	-1.43±0.1*	(3)	-1.74±0.2*	(10)	-0.12±0.21	(5)	0.07±0.2	(9)	-1.08±0.12*	(6)	-0.92±0.24*	(6)	-1.06±0.04*	(9)	0.42±0.31	(5)	N.D.	
S292A	-0.24±0.05	(4)	-0.16±0.21	(6)	0.49±0.2	(4)	0.3±0.24	(5)	0.3±0.22	(4)	0±0.19	(6)	0.35±0.13	(8)	-0.33±0.28	(6)	0.48±0.43	(4)
V293A	-0.62±0.08*	(4)	0.11±0.25	(5)	-0.28±0.05	(4)	0.09±0.25	(5)	-0.4±0.1	(4)	-0.02±0.22	(6)	-0.07±0.08	(8)	-0.11±0.28	(6)	0.22±0.3	(3)
E294A	-0.11±0.06	(5)	0.32±0.3	(5)	-0.1±0.08	(4)	0.31±0.28	(5)	-0.32±0.1	(4)	0.04±0.25	(5)	-0.25±0.07	(8)	0.12±0.31	(5)	0.74±0.33	(4)
T295A	-0.94±0.05*	(4)	-0.62±0.27	(5)	0.3±0.16	(4)	-0.530.25	(4)	-0.76±0.08*	(4)	-0.93±0.23*	(5)	0.5±0.09*	(8)	0.72±0.39	(5)	1±0.61*	(4)
H296A	0.11±0.13	(4)	0.54±0.26	(10)	-0.02±0.09	(4)	0.25±0.23	(9)	-0.18±0.03	(4)	0.14±0.27	(5)	-0.25±0.07	(8)	-0.17±0.27	(5)	0.2±0.35	(5)
L297A	-0.75±0.05*	(4)	-0.18±0.39	(4)	0.26±0.15	(4)	0.03±0.31	(4)	-0.44±0.19	(4)	-0.46±0.19	(6)	0.34±0.07	(8)	0.15±0.33	(5)	0.56±0.52	(4)
L298A	-0.71±0.08*	(4)	-0.46±0.32	(5)	-0.11±0.09	(4)	-0.14±0.26	(5)	-0.55±0.1*	(4)	-0.23±0.22	(5)	0.01±0.12	(8)	-0.1±0.25	(5)	0.57±0.44	(4)
Y299A	-0.56±0.02	(4)	-0.74±0.26	(5)	-0.46±0.2	(4)	0.04±0.28	(5)	-.092±0.2*	(4)	-0.58±0.2	(6)	0.15±0.18	(8)	0.43±0.3	(4)	0.4±0.69	(4)
I300A	N.D.		-0.18±0.27	(5)	N.D.		-0.09±0.26	(5)	N.D.		-0.22±0.22	(5)	N.D.		0.51±0.26	(5)	0.18±0.54	(4)

Table 4.3 Comparison of the effect of single alanine mutation in ECL2 of hCTR$_a$Leu on equilibrium affinity and functional affinity. *Functional affinity (pK_A) was derived by applying the operational model of agonism (Black and Leff, 1983) to the cAMP concentration-response curves (Section 4.3.2.1). Data reported in this table (and represented in Figure 4.7) are the change from WT of functional affinity (ΔpK_A). For comparison, equilibrium affinity (calculated as described in Table 4.2) are also reported in this table as change from WT (ΔpK_i). All values are mean±S.E.M. Significance of changes in affinity of each ligand was determined by comparison of the WT to receptor mutants by one-way analysis of variance and Dunnett's post-test ($p<0.05$ represented by *). (N.D.) affinity not determined as no radioligand binding was detected.*

4.2.3 Assessment of intracellular signalling by calcitonin receptor peptides

The hCTR most strongly couples to Gαs and elicits the production of intracellular cAMP (Chabre et al., 1992, Raggatt et al., 2000, Nicholson et al., 1986, Kuestner et al., 1994, Moore et al., 1995, Gorn et al., 1995, Wolfe et al., 2003, Findlay et al., 1980, Gorn et al., 1992, Frendo et al., 1994). The receptor also couples to other G proteins, including Gαq, triggering the generation of IP_3 (Chabre et al., 1992, Kuestner et al., 1994, Moore et al., 1995), and promotes phosphorylation of ERK1/2, which is likely to be a convergent pathway (Raggatt et al., 2000, Thomas and Shah, 2005, Nakamura et al., 2007, Han et al., 2006). In this study, activation and intracellular signalling of hCTR was measured through the assessment of cAMP or IP_1 accumulation (a stable downstream metabolite IP_3), and peak ERK1/2 phosphorylation. Each receptor, stably expressed in CV-1 FlpIn cells was assessed 24 h after plating. Cells were stimulated with relevant concentrations of human (hCT), salmon (sCT), or porcine calcitonin (pCT), rat amylin (rAmy) or human calcitonin gene related peptide alpha (hαCGRP). The resulting concentration response curves were fit to a three-parameter logistic equation, from which estimates of potency (pEC_{50}) and maximal response (E_{max}) were derived.

To compare the effect of the different mutations on receptor function, pEC_{50} cannot be used to compare across different receptors as it is a function of receptor expression, ligand affinity and efficacy. Therefore, coupling efficacy ($\log(\tau)$) was derived for each receptor, ligand and pathway using the operational model of agonism proposed by Black and Leff (Black and Leff, 1983) (Equation 7, Section 2.6.1). In the operational model, τ represents the amount of receptor that needs to be occupied to obtain half maximal response; it is a value independent of affinity and can be corrected for expression to obtain $\log(\tau_c)$(Kenakin and Christopoulos, 2013). Due to difficulties in the assessment of expression by radioligand binding, expression data could be calculated for four mutants, and only three mutants had significantly different expression. Therefore only T280A, N288A and H296A, which showed significant increase in surface expression when compared to WT (Section 3.3.1), were corrected for expression. Independent measurement of surface expression of our receptors by ELISA was trialled, but no robust window was observed. A more sensitive flow cytometry assay is currently in development in the laboratory. In absence of this data the calculated efficacy needs to be interpreted with caution.

Nonetheless this study focuses mainly on differences observed across peptides at the same receptor, which are independent of expression.

4.2.3.1 cAMP signalling

cAMP accumulation profiles were obtained after 30 min stimulation in presence of hCT (***Figure 4.8***), sCT (***Figure 4.9***), pCT (***Figure 4.10***), rAmy (***Figure 4.11***) or hαCGRP (***Figure 4.12***). In CV-1 FlpIn cells, cAMP responses fitted a 3 parameter logistic curve fit. pEC_{50}, E_{max} and log(τ) values are reported in (***Table 4.4 and 4.5***). Functional pK_A values were also calculated and used to compare to values of observed pK_i assessed by binding (***Table 4.2***). Additionally, we were able to evaluate the effect of our mutagenesis on rAmy and hαCGRP, low affinity agonists of the CTR, where pK_i were not able to be robustly defined.

4.2.3.1.1 CT peptides

The functional pK_A values describe the affinity of the ligand for the receptor complex (ligand/receptor/effector(s)) upstream of the measured signalling. In contrast, K_i or K_d are equilibrium values that can arise from multiple interchanging states (complexes). Thus the two affinities do not necessarily align as the two terms may measure the affinity of the ligand across different receptor populations. However, based on previous work, we often observe that functional affinities derived from cAMP accumulation align well with those derived from radioligand binding, and could be used as a surrogate measure of affinity, as Gαs is the predominant effector of CTR. Therefore, for all CT agonists, changes in measured affinity for mutant receptor relative to WT (ΔpK_i) were compared to changes in functional affinities (ΔpK_A) (***Figure 4.13, Table 4.3***). Our results show that, overall, the effect of mutation on the two measures of affinity follow a similar pattern. Using this approach, we can therefore speculate an effect of our mutagenesis on the affinity of those mutants where pK_i could not be directly assessed (N286, D287, C289, W290 and I300). W290A significantly reduced functional affinity of all CT peptides. Similarly, T295A also showed a similar trend for the three CT agonists, however values reached statistical significance only in presence of pCT. Substitution of R281, D287, C289, W290 and L291 significantly reduced functional affinity of both hCT and pCT, but not of sCT.

<u>Potency and maximal response.</u> All CT peptides showed a potency at the WT receptor between 0.1-0.01 nM. When compared to WT, none of the mutations in ECL2 had a significant effect on potency of

sCT, whereas mutations C289A, W290A and T295A significantly increased E_{max} for this peptide. In contrast, the maximal response of N288A and H296A trended lower, with no effect on potency. Compared to sCT, the other two CT peptides (hCT and pCT) were more affected by alanine substitution: potency of both peptides was significantly impaired compared to WT when an alanine was introduced in position R281, C289, W290 or L291. Interestingly, all of these mutants (with the exception of R281A) significantly enhanced E_{max} relative to WT when activated by hCT, although this did not reach significance for L291A. In contrast, E_{max} was not significantly altered for C289A, W290A and L291A for pCT, but the opposite profile was observed with R281, where an increased E_{max} was observed. D287A also had a negative effect on potency of hCT and pCT, while increasing E_{max} in presence of hCT and trending lower in response to pCT. In addition, at S292A, both hCT and pCT displayed enhanced E_{max}, although this did not reach significance for hCT.

Efficacy. Operational values of efficacy of peptides for cAMP production for all mutants are listed in ***Table 4.4 and 4.5*** below. For all CT peptides, $\log(\tau_c)$ values for T280A and H296A were significantly reduced compared to WT (3-fold). All three peptides showed reduced efficacy at the N288A mutant, but this only reached significance for sCT and pCT. In contract, W290A substitution statistically enhanced efficacy of all three peptides. No other common clusters of residues were shared across all the three CT peptides, although our analysis revealed several other significant differences: T295A revealed a selective 3-fold increase efficacy for sCT, whereas R281A, S292A and L297A significantly enhanced the efficacy of pCT. These last three residues appear to have a similar effect to enhance hCT efficacy (but not sCT), however their $\Delta\log(\tau)$ values failed to reach significance (***Table 4.4***). In the mid region of ECL2, at the D287A mutation hCT displayed increased efficacy, but not sCT or pCT, while C294A enhanced efficacy of hCT and sCT, but not pCT.

4.2.3.1.2 rAmy and hαCGRP peptides

The rAmy and hαCGRP peptides have lower affinity and are less potent than CTs at the hCTR when RAMPs are not co-expressed with the receptor and their equilibrium affinity was not determined through radioligand binding. However, functional affinities (pK_A) for these two peptides at the mutants

were derived from cAMP response (***Figure 4.13***, ***Table 4.3***), with the exception of D287A for both ligands, and for C289A or W290A for hαCGRP, where no cAMP response could be detected. The pK_A values revealed that, overall, mutagenesis of ECL2 affected the affinity of these two peptides in a similar manner to the lower affinity peptides hCT and pCT, although data reached statistical significance only for W290A for rAmy, and T295A for hαCGRP.

Potency and maximal response. In our stable CV-1 cells these peptides are equipotent in cAMP accumulation assay, with a potency of about 10 nM at the WT hCTR (***Table 4.5***). Due to low potency and higher relative errors, no significant effects on potency or E_{max} were established for rAmy or hαCGRP. Nonetheless, strong trends were present for a subset of mutants, and these were noted here for comparison to CT peptides. C289A or W290A showed detectable responses only for rAmy, albeit with reduced potency relative to WT. Other select mutations that had a moderate effect on pEC_{50} or maximal response included R281A and N288A, with reduced E_{max} observed only for rAmy, whereas N286A, Y299A and I300A showed reduced E_{max} for only hαCGRP. R281A also displayed reduced potency for both peptides, whereas N286A had a decreased potency only for rAmy.

Efficacy. In terms of efficacy, similar to observed for the CT peptides, alanine substitution of T280A had a negative effect on $\log(\tau_c)$ value, although this was statistically significant only in presence of rAmy. H296A also showed a reduction in efficacy in presence of both rAmy and hαCGRP, however the values were not significant for hαCGRP. N288A showed a significantly reduced efficacy for rAmy, but not hαCGRP.

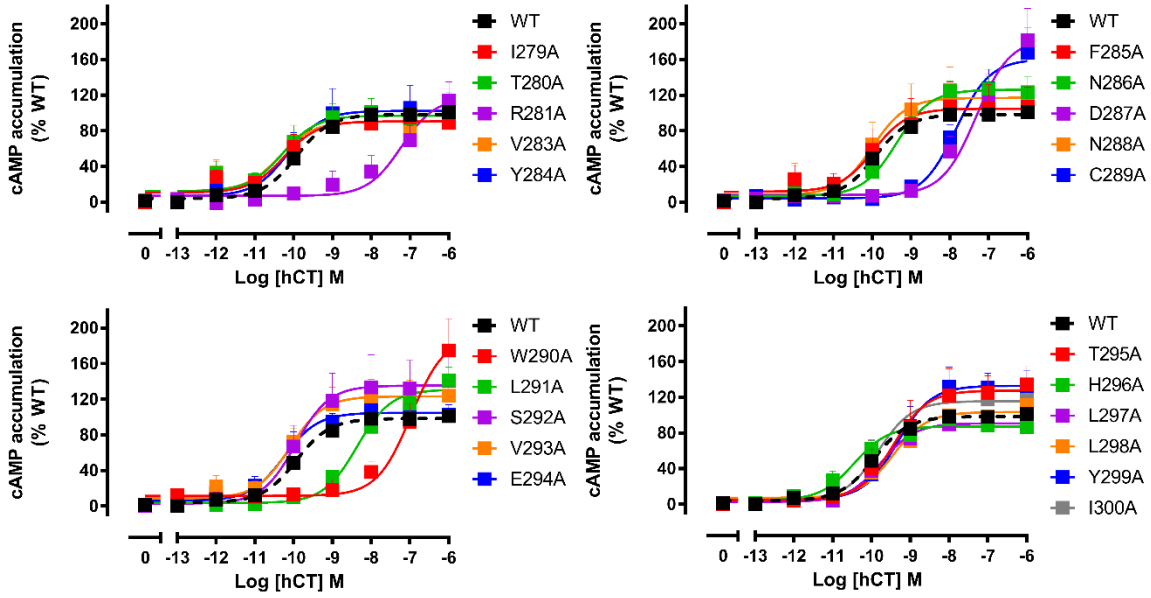

Figure 4.8 cAMP accumulation profiles elicited by hCT in CV-1-FlpIn cells stably expressing hCTR$_a$Leu ECL2 single alanine mutations. *cAMP formation in the presence of hCT was normalized to responses of the internal control (0.1 mM forskolin) and fit to a three parameter logistic equation. Data was subsequently normalised to WT receptor response. All values are mean+S.E.M. of 4 to 10 (WT N=20) independent experiments conducted in duplicate.*

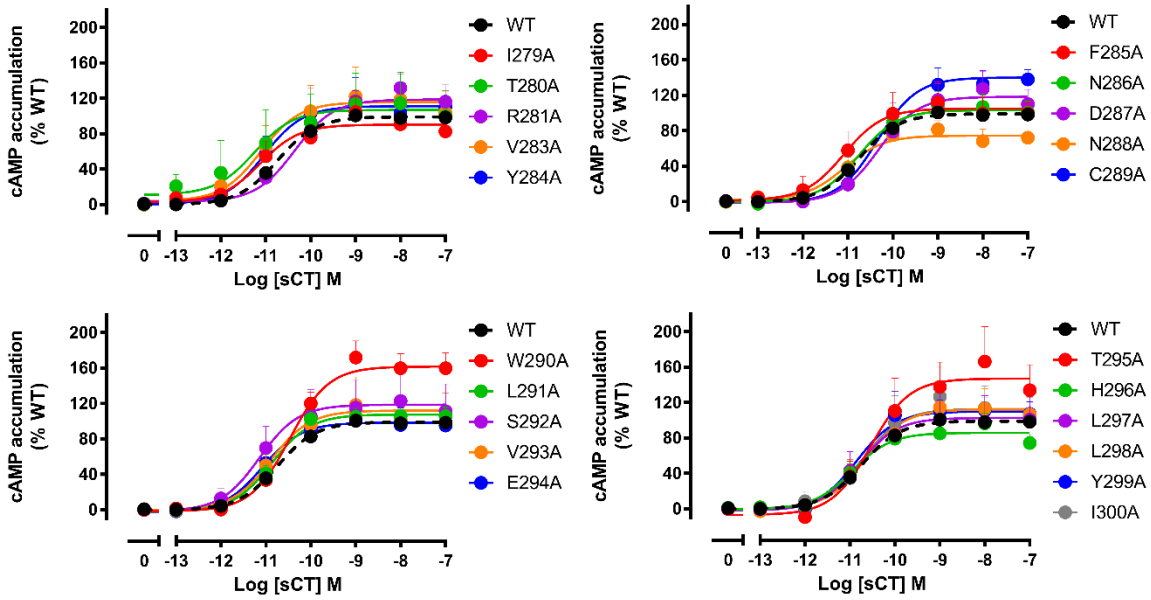

Figure 4.9 cAMP accumulation profiles elicited by sCT in CV-1-FlpIn cells stably expressing hCTR$_a$Leu ECL2 single alanine mutations *cAMP formation in the presence of sCT was normalized to responses of the internal control (0.1 mM forskolin) and fit to a three parameter logistic equation. Data was subsequently normalised to WT receptor response. All values are mean+S.E.M. of 4 to 11 (WT N=25) independent experiments conducted in duplicate.*

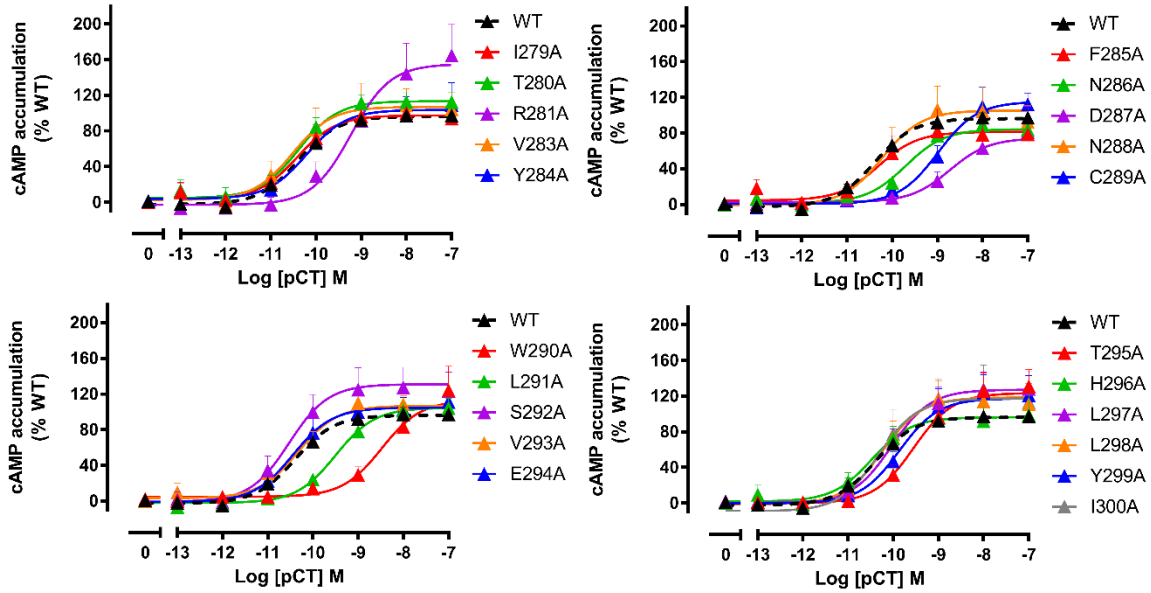

Figure 4.10 cAMP accumulation profiles elicited by pCT in CV-1-FlpIn cells stably expressing hCTR$_a$Leu ECL2 single alanine mutations. *cAMP formation in the presence of pCT was normalized to responses of the internal control (0.1 mM forskolin) and fit to a three parameter logistic equation. Data was subsequently normalised to WT receptor response. All values are mean+S.E.M. of 3 to 6 (WT N=15) independent experiments conducted in duplicate.*

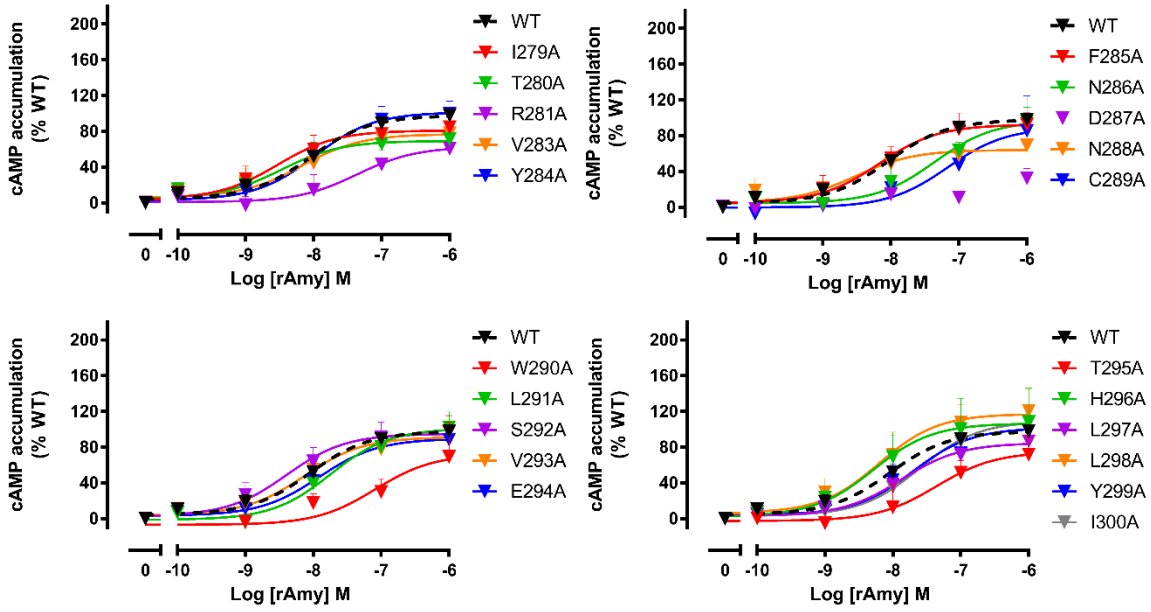

Figure 4.11 cAMP accumulation profiles elicited by rAmy in CV-1-FlpIn cells stably expressing hCTR$_a$Leu ECL2 single alanine mutations. *cAMP formation in the presence of rAmy was normalized to responses of the internal control (0.1 mM forskolin) and fit to a three parameter logistic equation. Data was subsequently normalised to WT receptor response. All values are mean+S.E.M. of 4 to 6 (WT N=11) independent experiments conducted in duplicate.*

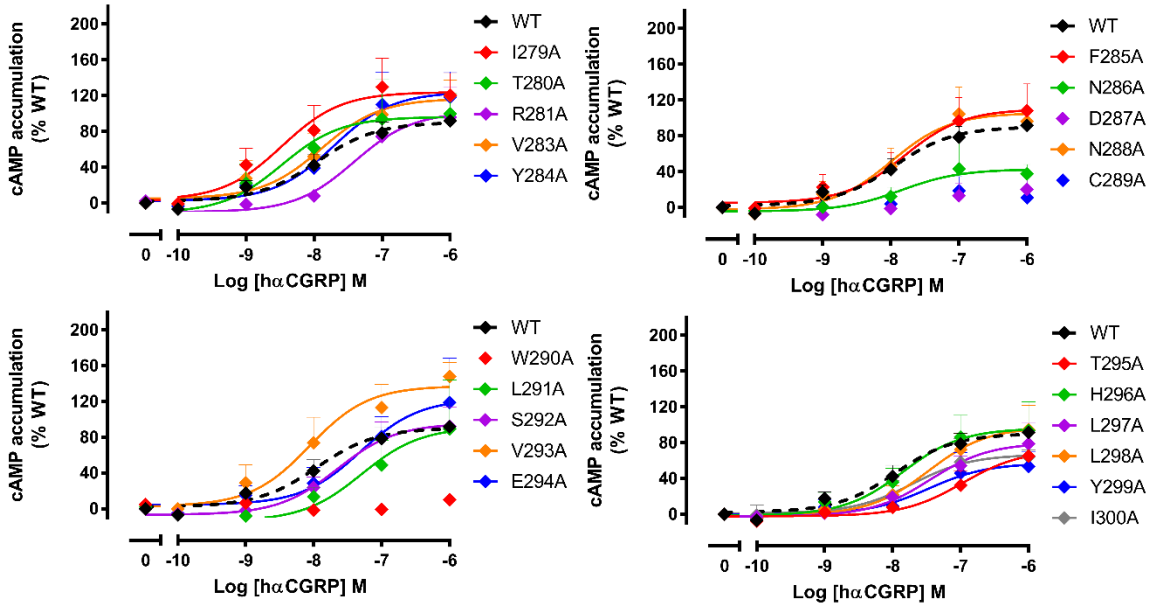

Figure 4.12 cAMP accumulation profiles elicited by hαCGRP in CV-1-FlpIn cells stably expressing hCTR$_a$Leu ECL2 single alanine mutations. *cAMP formation in the presence of hαCGRP was normalized to responses of the internal control (0.1 mM forskolin) and fit to a three parameter logistic equation. Data was subsequently normalised to WT receptor response. All values are mean+S.E.M. of 3 to 5 (WT N=8) independent experiments conducted in duplicate..*

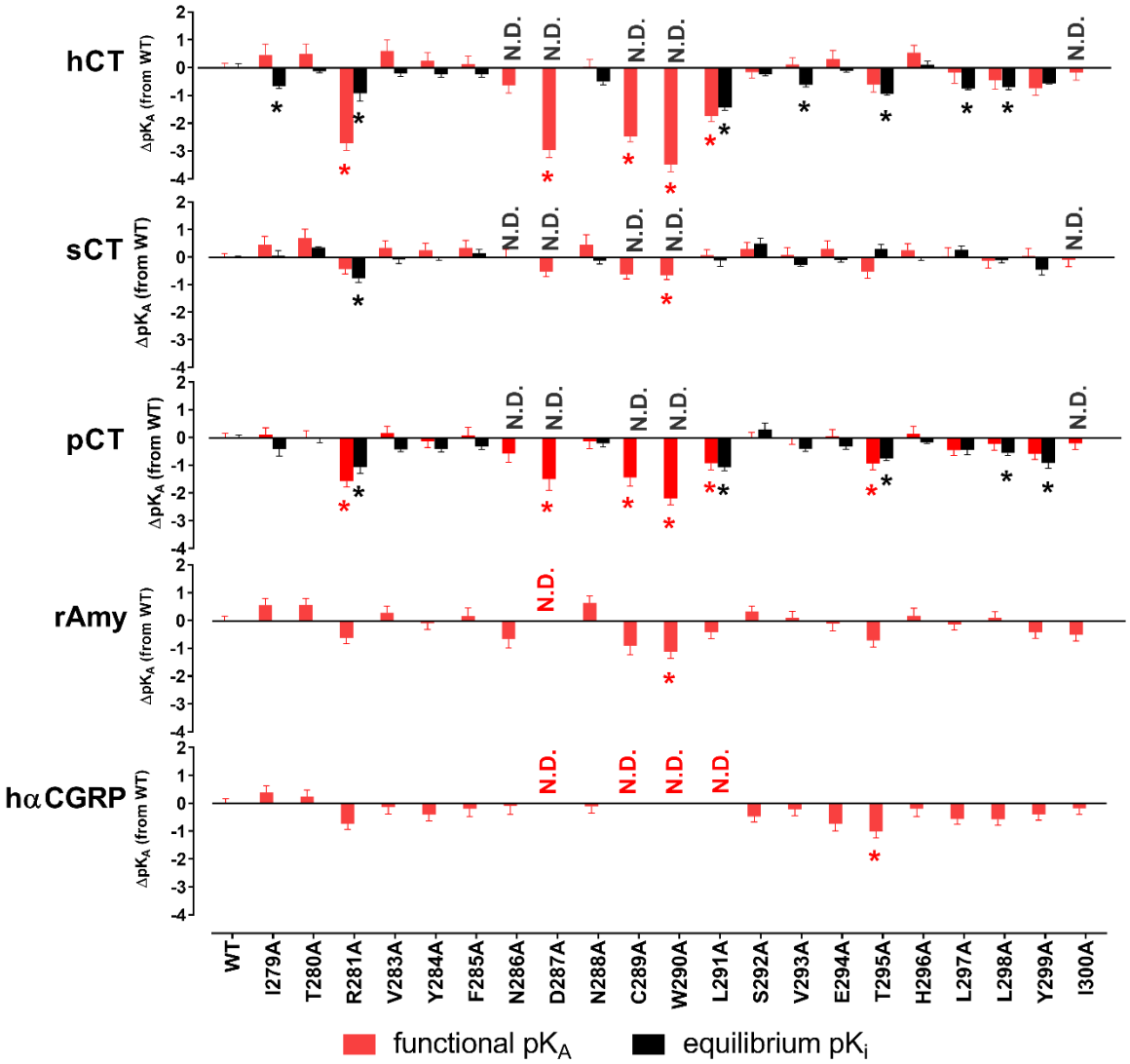

4.13 Comparison of equilibrium affinity and cAMP functional affinity (pK_A). *Functional affinity is presented as differences relative to WT (Δ pK_i, in black). Data from (Figure 4.8-12) were fit to the operational model of agonism (Black and Leff, 1983) to calculate functional affinity (pK_A) of each receptor (mutant or WT) to the cAMP signalling pathway. Graphs show the differences relative to WT (ΔpK_A, in red). All values are mean+S.E.M. of 3 to 25 independent experiments conducted in duplicate. Significance of changes was determined by comparison of the WT to the other receptor mutants in a one-way analysis of variance and Dunnett's post-test (p<0.05 represented by *). (N.D.) efficacy not determined.*

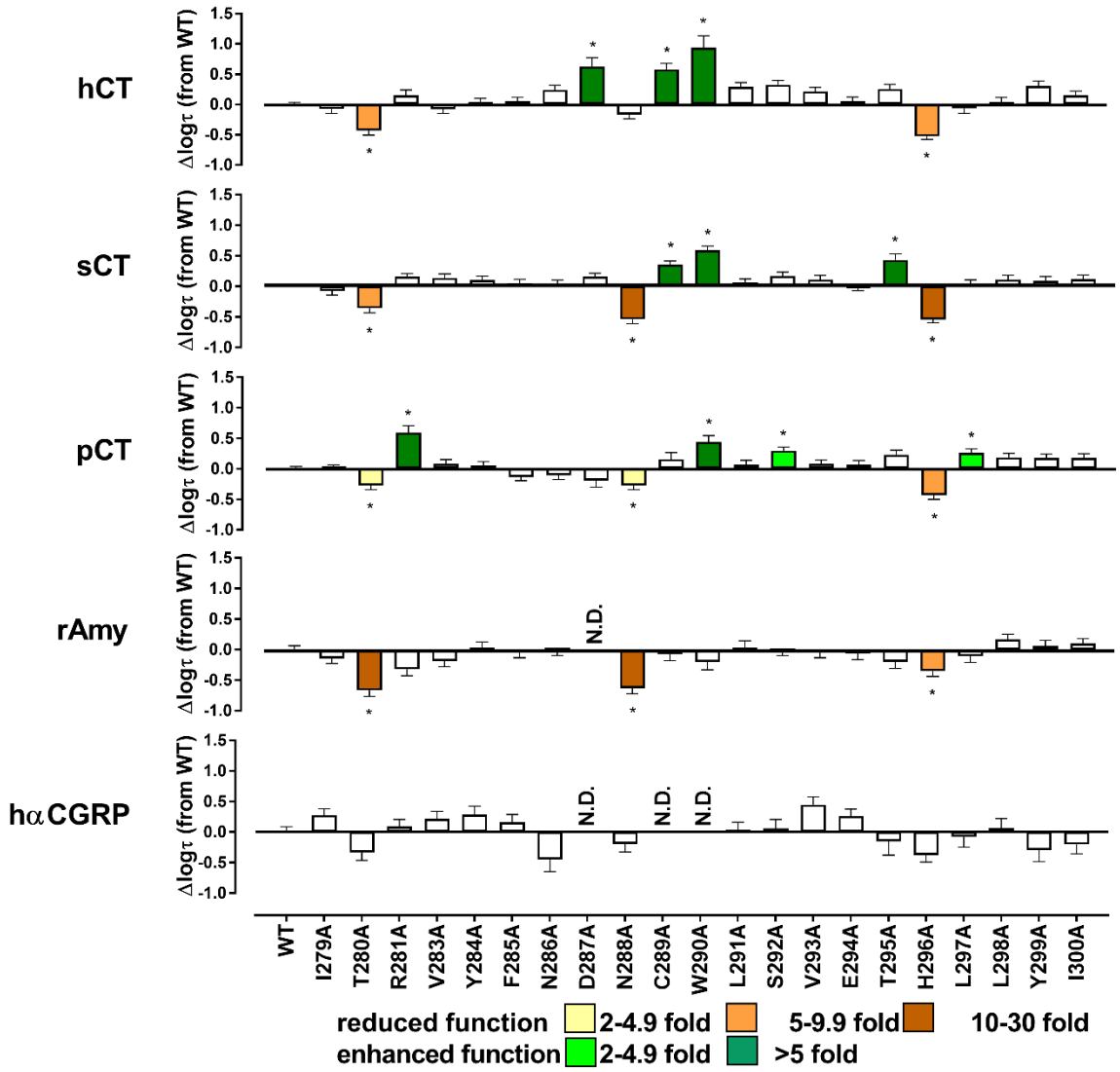

Figure 4.14 Effect of single alanine mutation in ECL2 of hCTR$_a$Leu on efficacy for cAMP accumulation. *Data from Figure 4.8-12 were fit to the operational model of agonism to calculate coupling efficacy log(τ) of each receptor (mutant or WT) to the cAMP signalling pathway. The log(τ) values of each receptor were then corrected for expression, where this was significantly different, to obtain log(τc). Graphs show the differences relative to WT. All values are mean+S.E.M. of 3 to 11 (WT 8 to 25) independent experiments conducted in duplicate. Significance of changes was determined by comparison of the WT to the other receptor mutants in a one-way analysis of variance and Dunnett's post-test (p<0.05 represented by *). (N.D.) efficacy not determined*

	hCT				sCT				pCT			
	pEC_{50}	E_{max} (% WT)	Log(τ)		pEC_{50}	E_{max} (% WT)	Log(τ)		pEC_{50}	E_{max} (% WT)	Log(τ)	
WT	9.933±0.06	100±1.6	-0.07±0.04	(20)	10.74±0.05	100±1.3	-0.04±0.03	(25)	10.39±0.1	100±2.7	-0.06±0.04	(15)
I279A	10.25±0.18	90.5±3.8	-0.14±0.08	(4)	11.12±0.25	90.2±5.8	-0.11±0.07	(5)	10.42±0.15	97.4±3.9	-0.05±0.06	(6)
T280A	10.28±0.28	96.9±6.1	-0.5±0.08*[(c)]	(4)	11.25±0.56	106.8±13.6	-0.39±0.08*[(c)]	(4)	10.38±0.17	113.3±5.2	-0.33±0.07*[(c)]	(5)
R281A	7.22±0.26*	117.2±15	0.08±0.09	(7)	10.39±0.17	114.3±5.3	0.13±0.05	(10)	9.22±0.27*	155±15.8*	0.53±0.12*	(6)
V283A	10.36±0.34	90.3±6.6	-0.15±0.07	(4)	11.11±0.38	115.6±11.6	0.1±0.07	(5)	10.52±0.32	106.9±9.1	0.03±0.06	(5)
Y284A	10.15±0.35	102.2±9.2	-0.04±0.07	(5)	11.04±0.35	111±10.5	0.06±0.07	(5)	10.21±0.29	103.5±8.5	0.0±0.06	(6)
F285A	9.97±0.42	104.8±11	-0.02±0.07	(5)	11.09±0.29	105±8.3	0.01±0.07	(5)	10.3±0.45	81.3±10	-0.19±0.06	(6)
N286A	9.37±0.17	126.1±5.9	0.17±0.08[(a)]	(5)	10.77±0.22	103.2±6.3	0.0±0.07[(a)]	(5)	9.7±0.22	84.3±5.6	-0.16±0.07[(a)]	(5)
D287A	7.33±0.23*	183.3±19.8*	0.56±0.14*[(a)]	(6)	10.32±0.22	118.3±7.1	0.13±0.05[(a)]	(10)	8.72±0.34*	74.3±9.4	-0.26±0.1[(a)]	(4)
N288A	9.99±0.32	117±9.8	-0.24±0.07[(c)]	(5)	11.07±0.26	74.5±4.8*	-0.58±0.07*[(c)]	(6)	10.22±0.31	105.2±9.9	-0.33±0.07*[(c)]	(5)
C289A	7.84±0.17*	160.5±11.5*	0.51±0.1*[(a)]	(8)	10.34±0.17	140±6.6*	0.32±0.06*[(a)]	(10)	8.99±0.16*	115.2±7.2	0.1±0.11[(a)]	(3)
W290A	6.97±0.2*	191.1±21.7*	0.87±0.2*[(a)]	(10)	10.47±0.16	161.8±6.9*	0.56±0.07*[(a)]	(11)	8.48±0.28*	113±12.5	0.37±0.11*[(a)]	(4)
L291A	8.36±0.11*	130.9±5.2	0.22±0.07	(10)	10.87±0.14	107.5±3.9	0.04±0.05	(9)	9.5±0.14*	104.5±4.9	0.01±0.07	(6)
S292A	9.95±0.35	135.3±13.1	0.26±0.07	(6)	11.14±0.38	118.6±12.1	0.13±0.07	(5)	10.53±0.26	130.9±9.2*	0.24±0.06*	(6)
V293A	10.09±0.24	123.2±7.7	0.14±0.07	(5)	10.89±0.35	112±10.8	0.07±0.07	(5)	10.33±0.18	106.8±5.4	0.02±0.06	(6)
E294A	10.25±0.2	104.8±5.2	-0.02±0.07	(5)	11.08±0.31	98.3±8.5	-0.04±0.07	(5)	10.44±0.22	104.7±6.4	0.01±0.07	(5)
T295A	9.44±0.31	127.4±11.1	0.18±0.08	(5)	10.54±0.31	147.1±13.2*	0.4±0.1*	(4)	9.55±0.21	123.4±8.1	0.17±0.08	(5)
H296A	10.45±0.19	87.3±4	-0.6±0.05*[(c)]	(10)	10.95±0.18	85.8±4.1	-0.58±0.05*[(c)]	(9)	10.47±0.29	96.2±7.6	-0.49±0.07*[(c)]	(5)
L297A	9.75±0.25	90.8±6.2	-0.14±0.08	(4)	10.81±0.4	102.6±11.5	-0.01±0.08	(4)	10.04±0.2	127.1±7.9	0.2±0.07*	(6)
L298A	9.44±0.2	103.4±5.7	-0.03±0.08	(5)	10.66±0.3	112.2±9.2	0.07±0.07	(5)	10.23±0.2	118.4±7.3	0.13±0.07	(5)
Y299A	9.33±0.22	132.9±8.6	0.23±0.08	(5)	10.85±0.25	109.9±7.2	0.06±0.07	(5)	9.87±0.23	117.3±8.5	0.12±0.07	(6)
I300A	9.83±0.18	115.6±5.8	0.08±0.07[(a)]	(5)	10.71±0.36	112.7±11.2	0.08±0.07[(a)]	(5)	10.32±0.3	117.3±11.2	0.12±0.07[(a)]	(5)

Table 4.4 Effect of single alanine mutation in ECL2 of hCTR$_a$Leu on cAMP signalling in response to CT peptides. *For each receptor and ligand, data from Figure 4.8-10 were fit to a three-parameter logistic equation to derive pEC_{50} (negative logarithm of the concentration of ligand that produces half the maximal response) and E_{max} (maximal response, as % of WT). The log(τ) reported in this table represents the operational coupling efficacy of each receptor (mutant or WT), where receptor expression was either unable to be identified on not significantly different. Where expression by radioligand binding was significantly different, values were corrected for the expression change to give log(τ_c) [(c)]. [(a)] Represents those mutation where expression could not be determined via radioligand binding. All values are mean±S.E.M. of 3 to 25 independent experiments conducted in duplicate For each ligand, significance of changes in pEC_{50}, E_{max} and log(τ) was determined by comparison of the WT to the other receptor mutants in a one-way analysis of variance and Dunnett's post-test ($p<0.05$ represented by *).*

	rAmy				hαCGRP			
	pEC_{50}	E_{max} (% WT)	Log(τ)		pEC_{50}	E_{max} (% WT)	Log(τ)	
WT	8.05±0.11	100±4.1	-0.06±0.06	(11)	7.96±0.21	100±7.3	-0.11±0.09	(8)
I279A	8.53±0.35	80.9±8.8	-0.21±0.08	(5)	8.47±0.41	123.9±16.1	0.17±0.1	(4)
T280A	8.47±0.38	69.3±8	-0.73±0.1*[(c)]	(4)	8.48±0.49	96.2±18.9	-0.45±0.13[(c)]	(4)
R281A	7.36±0.5	62.7±14.2	-0.38±0.11	(5)	7.41±0.43	101.9±21.8	0.02±0.11	(4)
V283A	8.17±0.36	76.9±9.8	-0.25±0.09	(5)	7.89±0.39	116.8±17.5	0.11±0.12	(4)
Y284A	7.99±0.25	101.4±9.8	-0.03±0.09	(5)	7.72±0.39	124.2±19.7	0.18±0.14	(4)
F285A	8.17±0.28	92.3±9.3	-0.11±0.09	(5)	7.8±0.39	109.9±16.6	0.05±0.13	(4)
N286A	7.35±0.35	96.9±15.4	-0.07±0.08[(a)]	(5)	7.85±0.75	42.7±14.3	-0.56±0.2[(a)]	(4)
D287A	N.D.	N.D.	N.D.		N.D.	N.D.	N.D.	
N288A	8.52±0.44	64±8.4	-0.7±0.09*[(c)]	(5)	7.99±0.34	105.6±15.6	-0.3±0.13[(c)]	(4)
C289A	7.17±0.48	89.1±22.7	-0.14±0.11[(a)]	(4)	N.D.	N.D.	N.D.	
W290A	7.09±0.55	72.3±25.8	-0.27±0.13[(a)]	(5)	N.D.	N.D.	N.D.	
L291A	7.74±0.31	100.9±13.3	-0.02±0.1	(5)	7.29±0.64	91.3±32.2	-0.07±0.13	
S292A	8.39±0.32	94.9±10.2	-0.08±0.08	(6)	7.65±0.3	95.4±12.6	-0.05±0.15	(4)
V293A	8.13±0.29	91.2±9.7	-0.12±0.08	(6)	8.06±0.29	137.4±15.3	0.34±0.13	(3)
E294A	7.92±0.26	89.5±9.1	-0.13±0.1	(5)	7.31±0.49	122.9±27.4	0.15±0.11	(4)
T295A	7.36±0.48	74.8±18.6	-0.27±0.11	(5)	6.97±0.42	71.9±17.9	-0.26±0.23	(4)
H296A	8.29±0.48	106.6±18.1	-0.42±0.09*[(c)]	(5)	7.85±0.41	96±16.3	-0.49±0.12[(c)]	(5)
L297A	7.87±0.3	84.6±10	-0.17±0.1	(5)	7.44±0.34	79.8±12.2	-0.19±0.17	(4)
L298A	8.21±0.3	117.2±12.7	0.1±0.09	(5)	7.47±0.36	97.6±15.4	-0.04±0.15	(4)
Y299A	7.71±0.25	101.7±0.4	0.0±0.09	(4)	7.48±0.55	57.1±13.7	-0.41±0.19	(4)
I300A	7.61±0.22	109.2±10.1	0.04±0.08[(a)]	(5)	7.71±0.45	66.7±12.1	-0.31±0.15[(a)]	(4)

Table 4.5 Effect of single alanine mutation in ECL2 of hCTR$_a$Leu on cAMP signalling in response to rAmy or hαCGRP. *For each receptor and ligand, data from Figure 4.11-12 were fit to a three-parameter logistic equation to derive pEC_{50} (negative logarithm of the concentration of ligand that produces half the maximal response) and E_{max} (maximal response as % of WT). The log(τ) reported in this table represents the operational coupling efficacy of each receptor (mutant or WT), where receptor expression was either unable to be identified on not significantly different. Where expression by radioligand binding was significantly different, values were corrected for the expression change to give log(τ_c) [(c)]. [(a)] Represents those mutation where expression could not be determined via radioligand binding. All values are mean±S.E.M. of 3 to 11 independent experiments conducted in duplicate For each ligand, significance of changes in pEC_{50}, E_{max} and log(τ) was determined by comparison of the WT to the other receptor mutants in a one-way analysis of variance and Dunnett's post-test ($p<0.05$ represented by *). (N.D.) pEC_{50}, E_{max} or efficacy not determined.*

4.2.3.2 IP_1 signalling

hCTR also couples to Gαq protein to elicit a transient intracellular calcium response through the production of DAG (di-acyl glycerol) and IP_3 (inositol-3-phosphate) (Chabre et al., 1992). The degradation of these metabolites can be prevented by LiCl treatment of the cells and IP_1 accumulation can be assessed as a surrogate of Gαq recruitment downstream of receptor activation. Due to their lower affinity (and potency), rAmy or hαCGRP responses were not detectable in this pathway at concentrations up to 1 μM of peptide. Concentration-response profiles of CT agonists were obtained after 60 minutes of accumulation, and the operational model of agonism was also applied (***Figures 4.15-17***). From these data, pEC_{50}, E_{max} and log(τ) (or log(τ_c)) were calculated for all the CT peptides (***Figure, 4.18***, ***Table 4.6***).

Potency. The three CT peptides were equipotent in this assay with a pEC_{50} value at the WT of approximately 1nM (***Table 4.6***). L291A significantly reduced potency of hCT by approximately 200 fold, but not of sCT or pCT. R281A, C289A and W290A dramatically impaired the IP_1 response, such that the potency and efficacy of hCT for these two mutants was not defined. Potency and efficacy of sCT could not be quantified for D287A and C289A, however, for all other mutations, the pEC_{50} of sCT was equivalent to WT. pCT potencies were not significantly affected for any of the mutant receptors, with the exception of I300A, which could not be quantified.

Maximal response. Maximal response to hCT, sCT and pCT peptides were significantly reduced compared to WT for Y299A. hCT and sCT E_{max} were also significantly decreased for N286A, T295A, L297A, L298A and I300A. Although pCT showed the same trend, values for this peptide at the same receptor mutants did not reach statistical significance. Y284A, F285A and L291A showed significant reductions in E_{max} only in presence of hCT. R281A showed a significant reduction of maximal response in presence of pCT. C289A and W290A, had reduced responses to all peptides, but the effect was less prominent at C281A for pCT.

Efficacy. Similar to observed for the cAMP pathway, the mid-region of ECL2 (N286-W290) was also important for efficacy in Gαq dependent signalling. Significant reductions in efficacy (compared to

WT) could be observed for N286A in presence of both hCT and sCT. In addition, the efficacy of hCT at D287A was significantly reduced, and in presence of sCT this mutant did not produce a detectable response, suggesting a more dramatic reduction in efficacy. There was a similar trend towards reduced efficacy with pCT for both these mutants, although data failed to reach statistical significance. Only a trend towards reduced efficacy was observed for pCT at C289A, a mutant that did not produce a robust response for hCT or sCT, suggesting that there is a differential effect for this peptide. While W290A substitution abolished the hCT response, it also significantly reduced pCT and sCT efficacy. Residues Y299 and I300, at the top of TM5, were extremely important to Gαq protein-dependent signalling with their substitution reducing the efficacy of all CT peptides. Substitution of R281, T295 and H296 all revealed peptide-specific effects on this pathway with mutation of the first significantly reducing pCT efficacy and abolishing hCT response; substitution of the second significantly impairing hCT and sCT efficacy, and replacement of the latter significantly reducing efficacy of both hCT and pCT, although a similar trend was also observed for sCT in this case. Although not significant, Ala mutation of L297, L298 and T280 showed a trend towards reduced efficacy for all CT peptides.

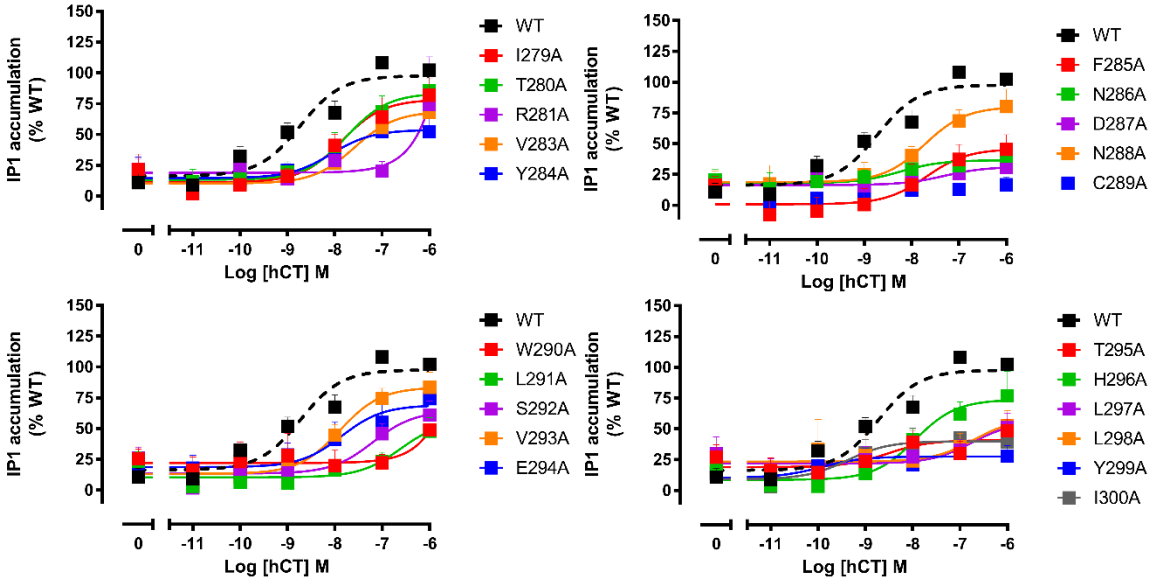

Figure 4.15 IP₁ accumulation profiles elicited by hCT in CV-1-FlpIn cells stably expressing hCTR$_a$Leu ECL2 single alanine mutations. *IP₁ formation in presence of hCT was normalized to an internal control (0.1 mM ATP) and data fit to a three parameter logistic equation. Data was subsequently normalised to WT receptor response. All values are mean+S.E.M. of 4 to 5 (WT N=10) independent experiments conducted in duplicate.*

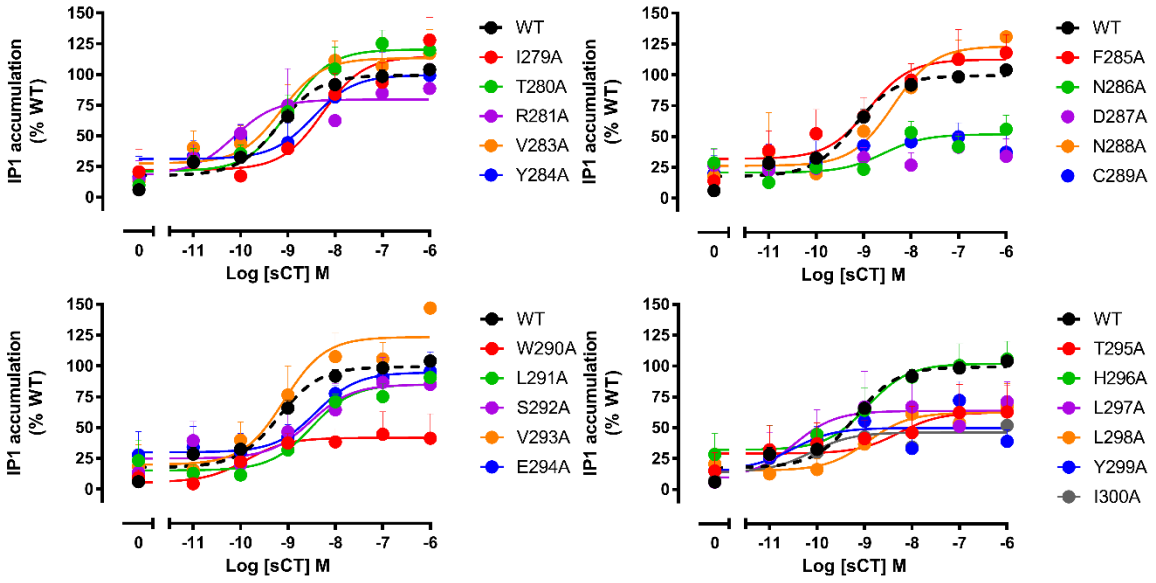

Figure 4.16 IP₁ accumulation profiles elicited by sCT in CV-1-FlpIn cells stably expressing hCTR$_a$Leu ECL2 single alanine mutations. *IP₁ formation in presence of was normalized to an internal control (0.1 mM ATP) and data fit to a three parameter logistic equation. Data was subsequently normalised to WT receptor response. All values are mean+S.E.M. of 4 to 6 (WT N=12) independent experiments conducted in duplicate.*

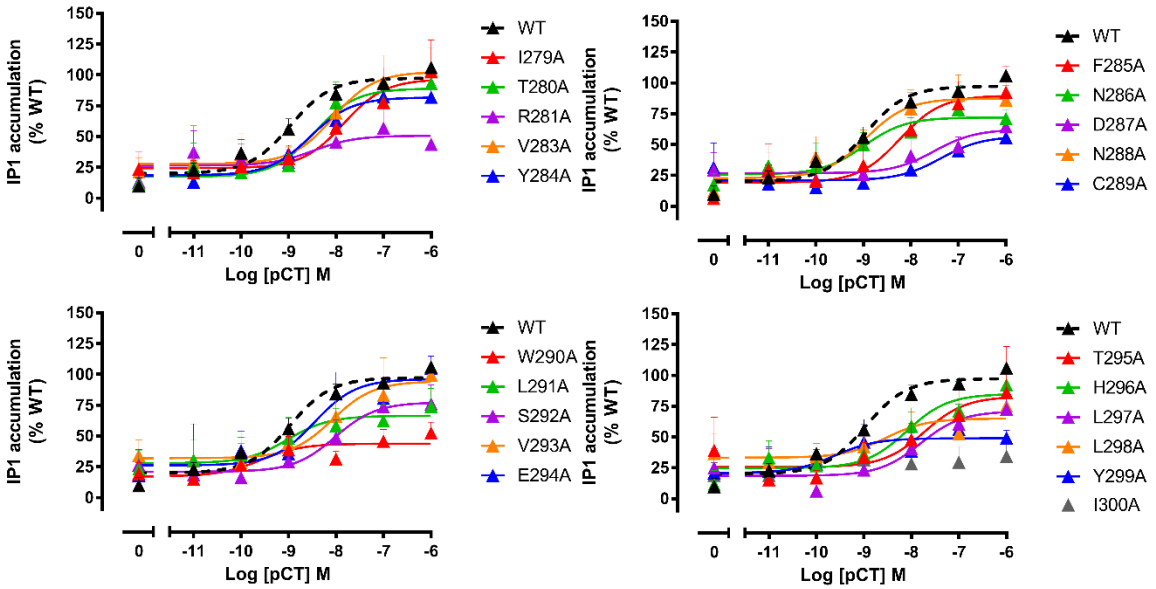

Figure 4.17 IP₁ accumulation profiles elicited by pCT in CV-1-FlpIn cells stably expressing hCTRₐLeu ECL2 single alanine mutations. *IP₁ formation in presence of pCT was normalized to an internal control (0.1 mM ATP) and data fit to a three parameter logistic equation. Data was subsequently normalised to WT receptor response. All values are mean+S.E.M. of 4 to 6 WT N=13) independent experiments conducted in duplicate.*

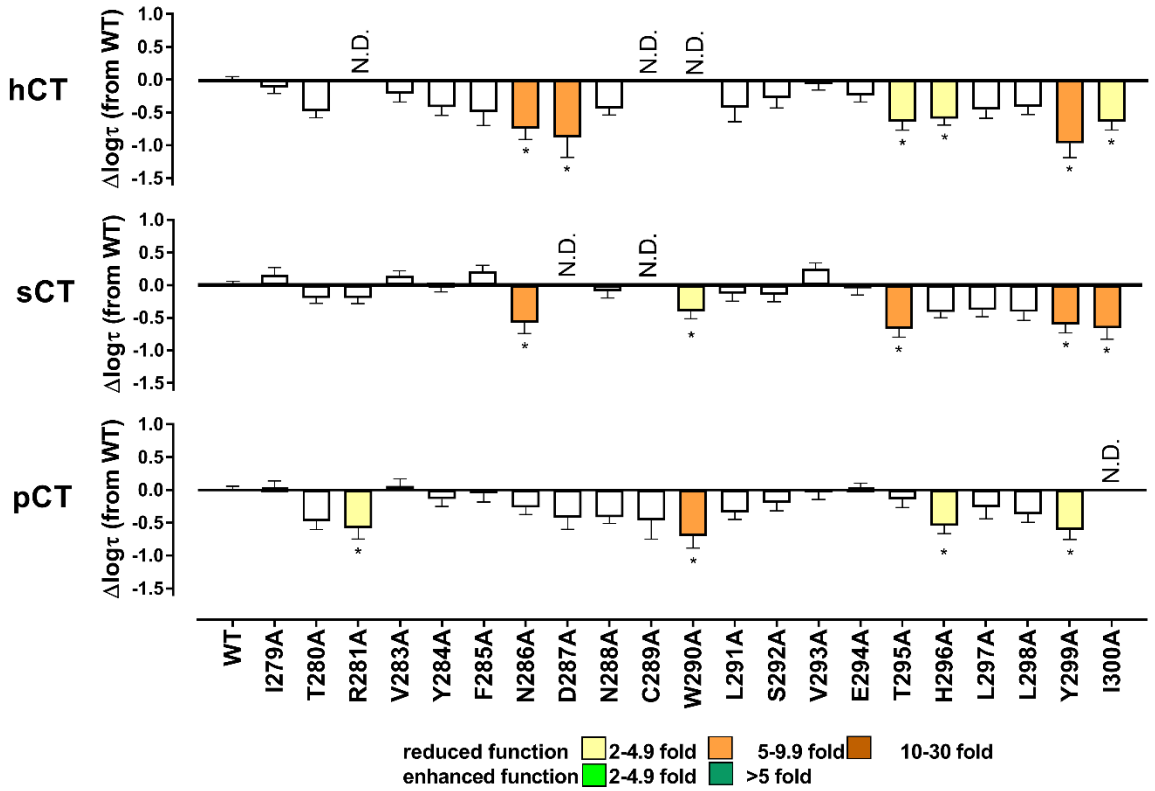

Figure 4.18 Effect of single alanine mutation in ECL2 of hCTRₐLeu on CT peptides efficacy for IP₁ accumulation. *Data from Figure 4.14-16 were fit to the operational model of agonism to calculate coupling efficacy log(τ) of each receptor (mutant or WT) to the IP₁ signalling pathway. The log(τ) values of each receptor were then corrected for expression, where this was significantly different, to obtain log(τc). Graphs show the differences relative to WT. All values are mean+S.E.M. of 4 to 6 independent experiments conducted in duplicate. Significance of changes was determined by comparison of the WT to the other receptor mutants by one-way analysis of variance and Dunnett's post-test (p<0.05 represented by *). (N.D.) efficacy not determined.*

	hCT				sCT				pCT			
	pEC_{50}	E_{max} (% WT)	Log(τ)		pEC_{50}	E_{max} (% WT)	Log(τ)		pEC_{50}	E_{max} (% WT)	Log(τ)	
WT	8.92±0.19	100±4.8	-0.15±0.05	(10)	9.23±0.13	100±3.3	-0.12±0.06	(12)	9.01±0.17	100±4.2	-0.15±0.06	(13)
I279A	7.85±0.31	78.4±8.8	-0.27±0.1	(5)	8.26±0.31	114.6±10.6	0.04±0.11	(5)	7.84±0.49	96.5±14.9	-0.15±0.13	(4)
T280A	7.75±0.32	83.5±9.6	-0.63±0.1[c]	(5)	8.98±0.22	120.3±7.1	-0.31±0.09[c]	(6)	8.46±0.36	88.9±8.8	-0.63±0.12[c]	(4)
R281A	N.D.	N.D.	N.D.		10.14±0.54	79.6±8.9	-0.31±0.09	(5)	8.51±1.15	50.6±9.7*	-0.74±0.16*	(6)
V283A	7.58±0.39	68.7±9.9	-0.37±0.12	(5)	9.15±0.39	113.3±10.5	0.02±0.08	(6)	8.07±0.46	102.5±13.8	-0.09±0.11	(5)
Y284A	8.07±0.53	53.8±8.9*	-0.57±0.13	(5)	8.46±0.58	99.5±13.8	-0.13±0.1	(5)	8.54±0.34	81.7±7.3	-0.29±0.11	(5)
F285A	7.69±0.6	45.8±11.5*	-0.65±0.2	(5)	8.9±0.39	112.5±10.8	0.09±0.09	(5)	8.23±0.48	89.8±13	-0.21±0.13	(4)
N286A	8.24±0.93	36.6±6.5*	-0.9±0.17*[a]	(5)	8.58±0.63	51.8±6.6*	-0.7±0.17*[a]	(6)	8.99±0.56	72.0±8.5	-0.42±0.11[a]	(5)
D287A	7.32±1.25	31.3±9.1*	-1.02±0.22*[a]	(5)	N.D.	N.D.	N.D. [a]		7.51±0.81	62.4±12.8	-0.58±0.18[a]	(5)
N288A	7.72±0.38	80.1±10.1	-0.6±0.09[c]	(5)	8.38±0.34	123.2±11.8	-0.21±0.1[c]	(5)	8.94±0.43	87.3±9.1	-0.57±0.09[c]	(5)
C289A	N.D.	N.D.	N.D. [a]		N.D.	N.D.	N.D. [a]		7.37±0.81	56.7±13.7*	-0.62±0.29[a]	(4)
W290A	N.D.	N.D.	N.D. [a]		9.88±0.63	41.7±6.1*	-0.89±0.24*[a]	(4)	9.59±0.72	43.8±5.2*	-0.86±0.18*[a]	(6)
L291A	6.61±0.5*	57±15.6*	-0.58±0.22	(5)	8.51±0.28	85.1±6.7	-0.25±0.11	(5)	9.02±0.73	66.4±9.1	-0.5±0.1	(6)
S292A	7.2±0.37	64.3±9.8	-0.43±0.15	(5)	8.52±0.6	84.9±12.2	-0.27±0.11	(5)	8.02±0.49	77.3±11.3	-0.35±0.12	(6)
V293A	7.9±0.23	83.5±6.7	-0.22±0.09	(5)	9.08±0.31	123.5±10.3	0.13±0.09	(5)	8.08±0.51	94.4±12.7	-0.19±0.11	(5)
E294A	7.86±0.56	69±11.9	-0.39±0.1	(5)	8.41±0.45	94.7±10.2	-0.17±0.1	(5)	8.45±0.48	96.2±11.7	-0.15±0.1	(5)
T295A	8.54±0.85	40.8±6.3*	-0.79±0.14*	(5)	8.28±1.14	62.3±14.1*	-0.62±0.13*	(6)	7.73±0.79	82.9±19.4	-0.3±0.12	(6)
H296A	7.95±0.3	73.8±8.1	-0.75±0.1*[c]	(5)	8.95±0.41	101.9±9.5	-0.53±0.09[c]	(5)	8.1±0.37	84.9±9	-0.7±0.12*[c]	(5)
L297A	6.75±0.75	55.9±16.3*	-0.61±0.13	(5)	10.48±0.78	63.7±9.7*	-0.5±0.1	(5)	7.81±0.43	71.0±9.5	-0.41±0.18	(4)
L298A	6.71±1.1	58.7±24.9*	-0.57±0.12	(5)	8.93±0.49	62.3±7.7*	-0.53±0.13	(5)	8.55±0.93	65.0±9.9	-0.53±0.12	(5)
Y299A	9.94±0.87	27.5±4.2*	-1.11±0.19*	(5)	10.51±0.78	49.8±6.2*	-0.73±0.13*	(6)	9.61±1	49.0±7.7*	-0.76±0.15*	(6)
I300A	9.38±0.58	40±5.1*	-0.79±0.13*[a]	(5)	10.12±0.71	46.2±6.*	-0.78±0.17*[a]	(5)	N.D.	N.D.	N.D. [a]	

Table 4.6 Effect of single alanine mutation in ECL2 of hCTR$_a$Leu on IP$_1$ accumulation in response to CT peptides. *For each receptor and ligand, data from Figure 4.14-16 were fit to a three-parameter logistic equation to derive pEC_{50} (negative logarithm of the concentration of ligand that produces half the maximal response) and E_{max} (maximal response as % of WT). The log(τ) reported in this table represents the operational coupling efficacy of each receptor (mutant or WT), where receptor expression was either unable to be identified on not significantly different. Where expression by radioligand binding was significantly different, values were corrected for the expression change to give log(τ_c) [c]. [a] Represents those mutation where expression could not be determined via radioligand binding. All values are mean±S.E.M. of 4 to 6 independent experiments conducted in duplicate. For each ligand, significance of changes in pEC_{50}, E_{max} and log(τ) was determined by comparison of the WT to the other receptor mutants by one-way analysis of variance and Dunnett's post-test (p<0.05 represented by *). (N.D.) pEC_{50}, E_{max} or efficacy not determined.*

4.2.3.3 ERK1/2 phosphorylation

In Chapter 3 a transient ERK1/2 phosphorylation was identified as a relevant signalling pathway for CT peptides. Agonist-dependent pERK1/2 time-courses for each receptor construct were therefore assessed in the presence of 1 μM of hCT (***Figure 4.19***), sCT (***Figure 4.20***), pCT (***Figure 4.21***), rAmy (***Figure 4.22***) or hαCGRP (***Figure 4.23***) to determine if any of the mutants altered the peak response. All peptides produced a maximal pERK1/2 response either at 6 or 8 min stimulation. Due to the limited numbers of repeats, a few of the time-courses were associated with large errors, however no significant difference between WT and all mutant receptors. Therefore the peak of maximal ERK1/2 phosphorylation of WT was selected to obtain concentration-responses curves.

hCT, rAmy or hαCGRP produced a more slow sustained pERK1/2 responses compared to a more rapid transient profile elicited by pCT and sCT (***Figure 4.24-28***). Therefore, concentration-response curves in presence of hCT, rAmy or hαCGRP were therefore measured at 8 min of ligand stimulation, while sCT and pCT were assessed at 6 min. For all receptor mutants and peptides, pEC_{50}, E_{max} and derived log(τ) from fitting the operational model to concentration-response data generated at 8 minutes of ligand stimulation (***Table 4.7 and 4.8***).

4.2.3.3.1 CT peptides

Potency. All three CT peptides produced responses in this signalling pathway, with pEC_{50}s in the nM range (8.32±0.09, 8.62±0.1 and 8.95±0.08 for hCT, sCT and pCT respectively) (***Table 4.7***). sCT potency was unaffected by any of the introduced mutations, whereas both hCT and pCT showed significantly reduced potency when D287 and L291 were replaced with alanine. Similar to other pathways, hCT was the most sensitive peptide to receptor mutation when compared to the other two CTs, as the alanine substitution of C289 also statistically reduced pEC_{50} of this peptide (15-fold) when compared to WT. Moreover, R281A and W290A dramatically reduced hCT response, and it was not possible to quantify the responses in the concentration-range assessed (up to 1 μM).

Maximal response and efficacy. Maximal responses were dramatically affected by the majority of the substitutions. Increased E_{max} for all CT peptides were observed for T280A, N288A, V293A and H296A.

Additionally, I279A and V283A also significantly enhanced the maximal response of hCT and sCT, whilst failing to show any statistical difference for pCT. E294A also showed a similar trend in increasing E_{max} for all CT peptides relative to WT, however values reached statistical significance only in presence of sCT. For these residues, when corrected for differences in cell surface expression (***Figure 4.29***, ***Table 4.7***), improved efficacy in pERK1/2 was observed for V283A for hCT and sCT (log(τ)), but not pCT. Similarly, I279A had an analogous effect on hCT and sCT efficacy, although the later was not statistically significant (p=0.06). V293A showed significantly enhanced efficacy in presence of sCT and a similar trend for the other two CT peptides. Additionally, E294A trended towards increased efficacy for all CT peptides, albeit not statistically significant. None of the other mutations altered efficacy relative to the WT for any of the CTs assessed, suggesting that for the rest of these mutant receptors the enhanced E_{max} values were a result of increased receptor expression.

A second cluster of residues significantly reduced the maximal pERK1/2 response for all CT peptides. This cluster includes R281, N286, D287, C289, W290, T295, H297, Y299 and I300 (***Figure 4.29***, ***Table 4.7***).

Operational analysis revealed that substitution of residues N286-W290 (with the exception of N288) significantly impaired efficacy for all CT ligands in pERK1/2. Outside of this segment, substitution of R281, T295, Y299 and I300 also reduced efficacy for all CT peptides. L297A also reduced efficacy for all CT peptides, however, data were only statistically significant for hCT and pCT (***Table 4.7***).

4.2.3.3.2 rAmy and hαCGRP peptides

Potency and maximal response. rAmy and hαCGRP peptides had a potency of approximately 70 nM in pERK1/2 (***Table 4.8***). D287A, C289A and W290A (for both peptides), and L291A (for hαCGRP only) showed almost no detectable pERK1/2 response (up to 1 μM of peptide). The remainder of the alanine mutations had no effect on potency, but many reduced maximal response of these receptors Statistical analysis of E_{max} values showed significant decrease (relative to WT) in maximal response for R281A, N286A, L291A, T2995A and Y299A in presence of both peptides. rAmy was more sensitive to select

ECL2 mutations than hαCGRP with significantly reduced E_{max} for Y284A, F285A, V293A, L297A and I300A mutants.

Efficacy. Mutated residues that resulted in reduced CT peptide efficacy, also significantly impaired rAmy and hαCGRP log(τ). This included R281A and T295A (and additionally D287, C289A and W290A where substitution to alanine abolished pERK1/2 response in both rAmy and hαCGRP). T286A and Y299A mutations significantly reduced hαCGRP efficacy, with a similar trend in presence of rAmy that did not reach statistical significance. Interestingly, H296A did not impair efficacy for any of the CT peptides, but significantly reduced (4-fold) hαCGRP efficacy while showing a similar (yet not significant) trend in presence of rAmy. No other mutation had any significant effect on rAmy or hαCGRP efficacy.

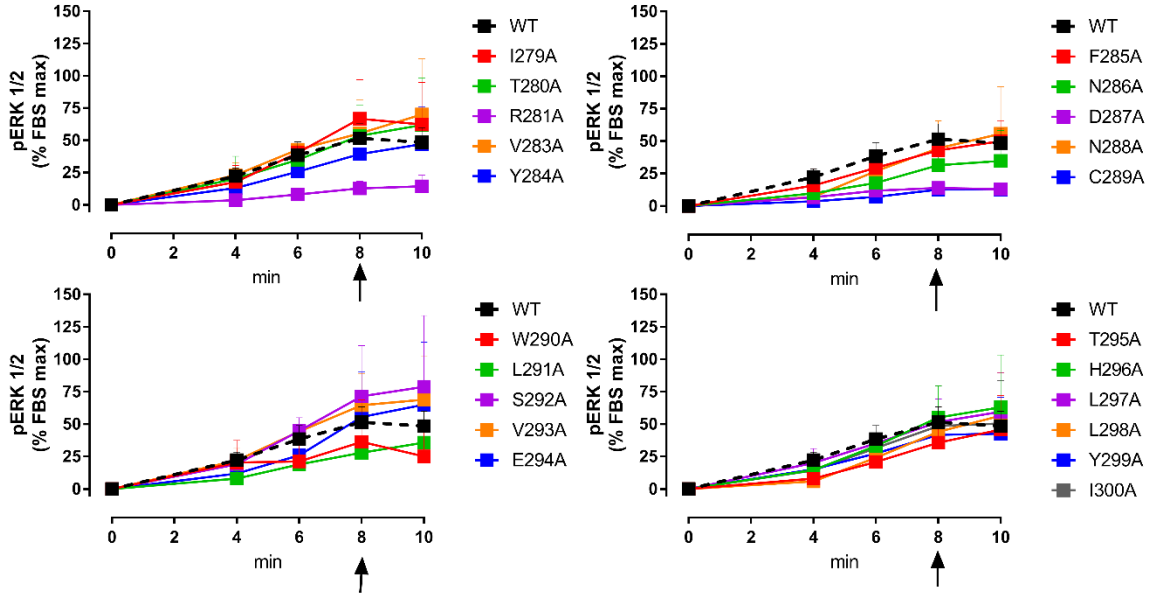

Figure 4.19 ERK1/2 phosphorylation time-course profiles elicited by hCT in CV-1-FlpIn cells stably expressing hCTR$_a$Leu ECL2 single alanine mutations. *1 μM of hCT was measured as a time-course, as indicated. Each dataset was normalised to FBS at 6 min and vehicle responses. All values are mean+S.D. of 2 (WT N=5) independent experiments conducted in duplicate. Arrows indicate where concentration-response curves where generated.*

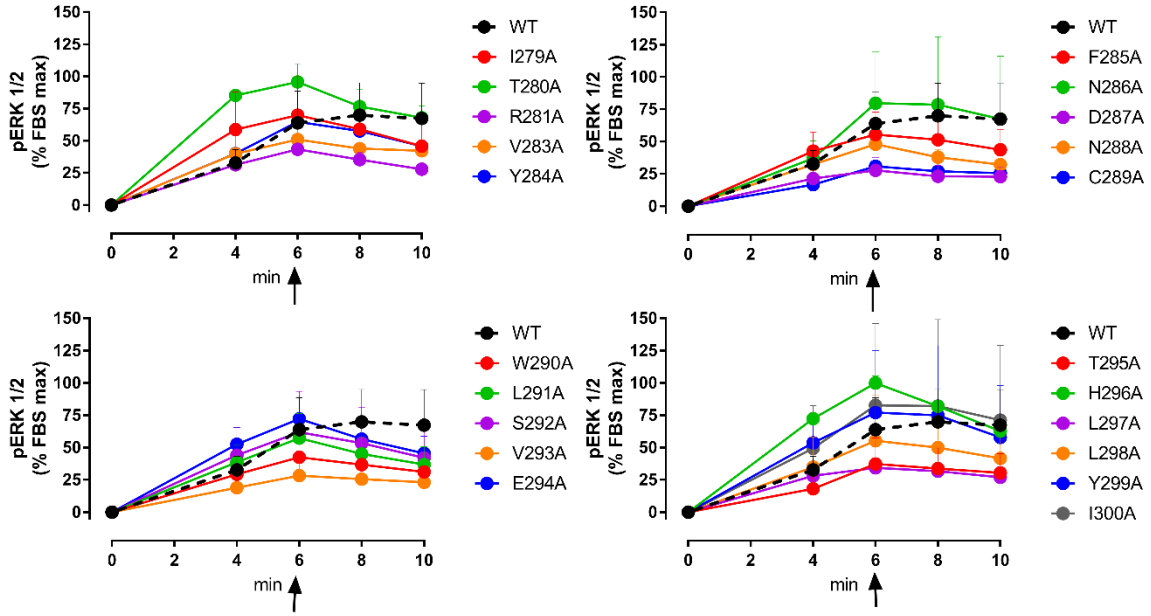

Figure 4.20 ERK1/2 phosphorylation time-course profiles elicited by sCT in CV-1-FlpIn cells stably expressing hCTR$_a$Leu ECL2 single alanine mutations. *1 μM of sCT was measured as a time-course, as indicated. Each dataset was normalised to FBS at 6 min and vehicle responses. All values are mean+S.D. of 2 (WT N=5) independent experiments conducted in duplicate. Arrows indicate where concentration-response curves where generated.*

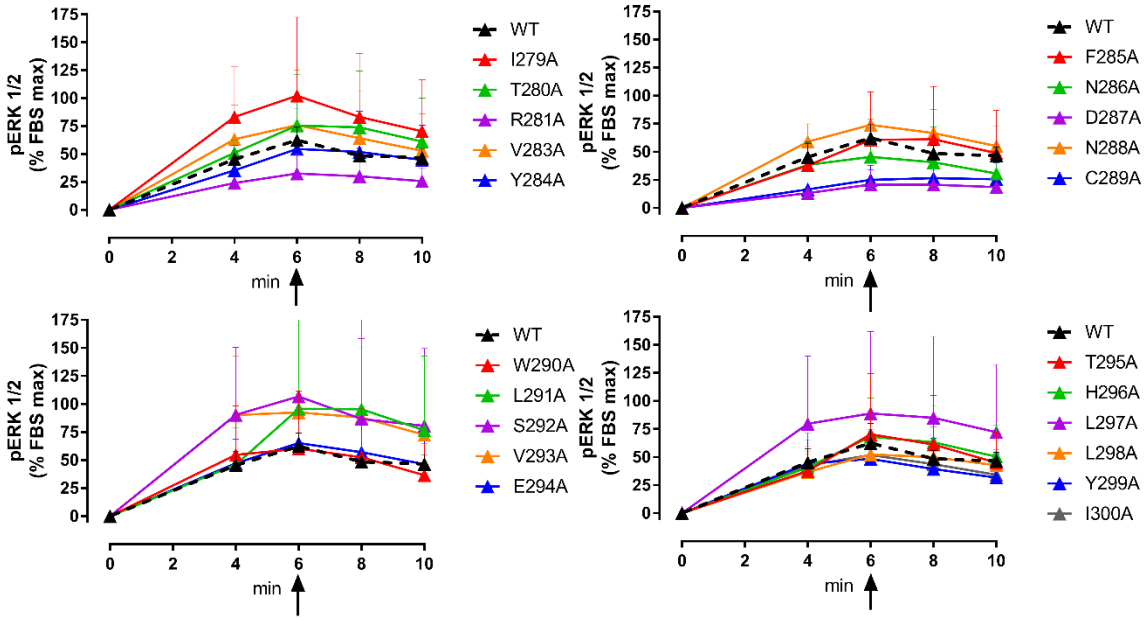

Figure 4.21 ERK1/2 phosphorylation time-course profiles elicited by pCT in CV-1-FlpIn cells stably expressing hCTR$_a$Leu ECL2 single alanine mutations. *1 µM of pCT was measured as a time-course, as indicated. Each dataset was normalised to FBS at 6 min and vehicle responses. All values are mean+S.D. of 2 (WT N=5) independent experiments conducted in duplicate. Arrows indicate where concentration-response curves where generated.*

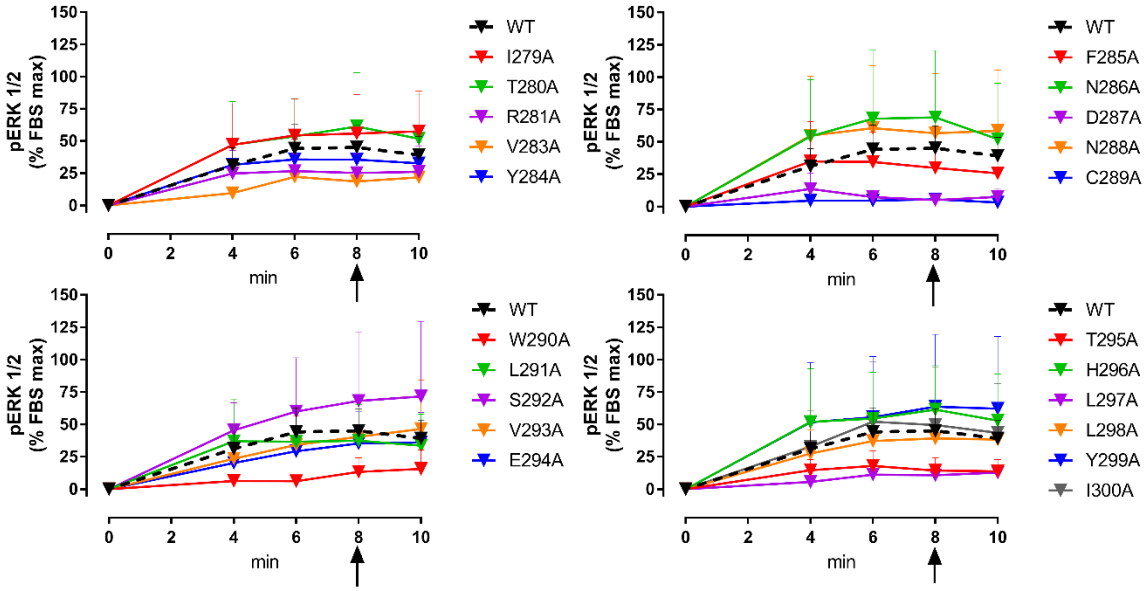

Figure 4.22 ERK1/2 phosphorylation time-course profiles elicited by rAmy in CV-1-FlpIn cells stably expressing hCTR$_a$Leu ECL2 single alanine mutations. *1 µM of rAmy was measured as a time-course, as indicated. Each dataset was normalised to FBS at 6 min and vehicle responses. All values are mean+S.D. of 2 (WT N=5) independent experiments conducted in duplicate. Arrows indicate where concentration-response curves where generated.*

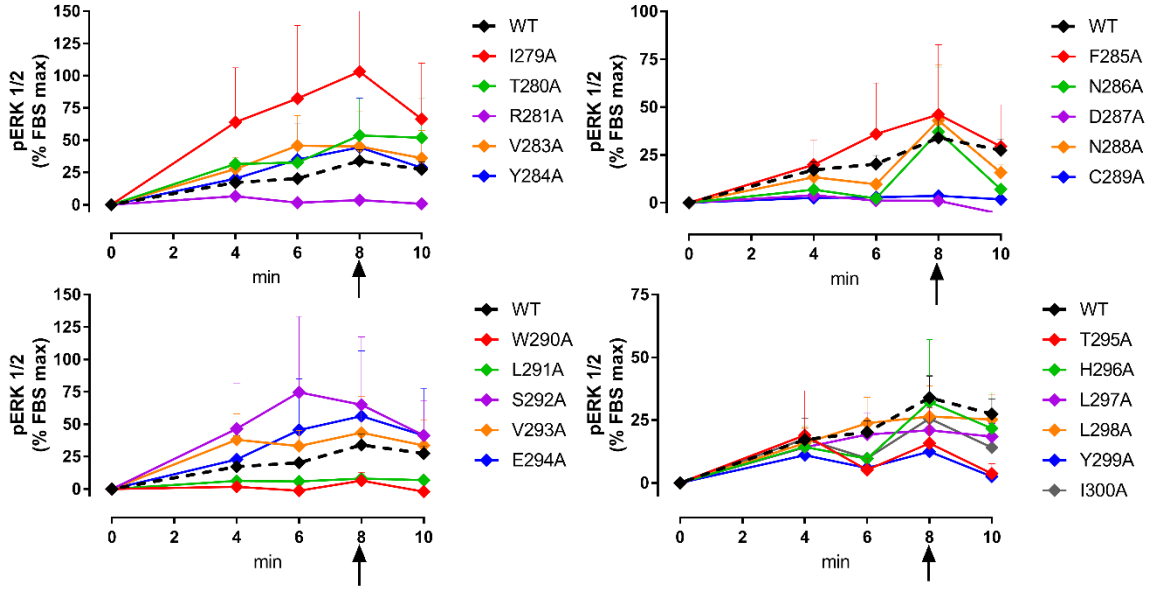

Figure 4.23 ERK1/2 phosphorylation time-course profiles elicited by hαCGRP in CV-1-FlpIn cells stably expressing hCTR$_a$Leu ECL2 single alanine mutations. *1 μM of hαCGRP was measured as a time-course, as indicated. Each dataset was normalised to FBS at 6 min and vehicle responses. All values are mean+S.D. of 2 (WT N=5) independent experiments conducted in duplicate. Arrows indicate where concentration-response curves where generated.*

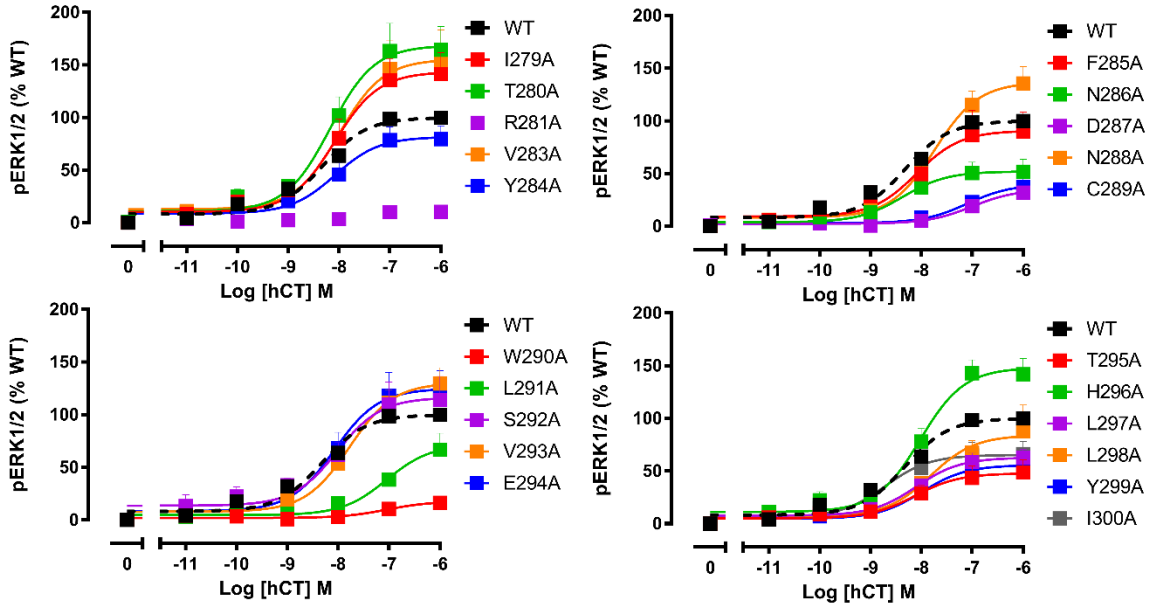

Figure 4.24 ERK1/2 phosphorylation concentration-response profiles elicited by hCT in CV-1-FlpIn cells stably expressing hCTR$_a$Leu ECL2 single alanine mutations. *pERK1/2 in response to hCT were normalized to the internal control (10% FBS measured at 6 min) and fit to a three parameter logistic equation. Data was subsequently normalised to WT receptor response. All values are mean+S.E.M. of 5 to 6 (WT N=10) independent experiments conducted in duplicate.*

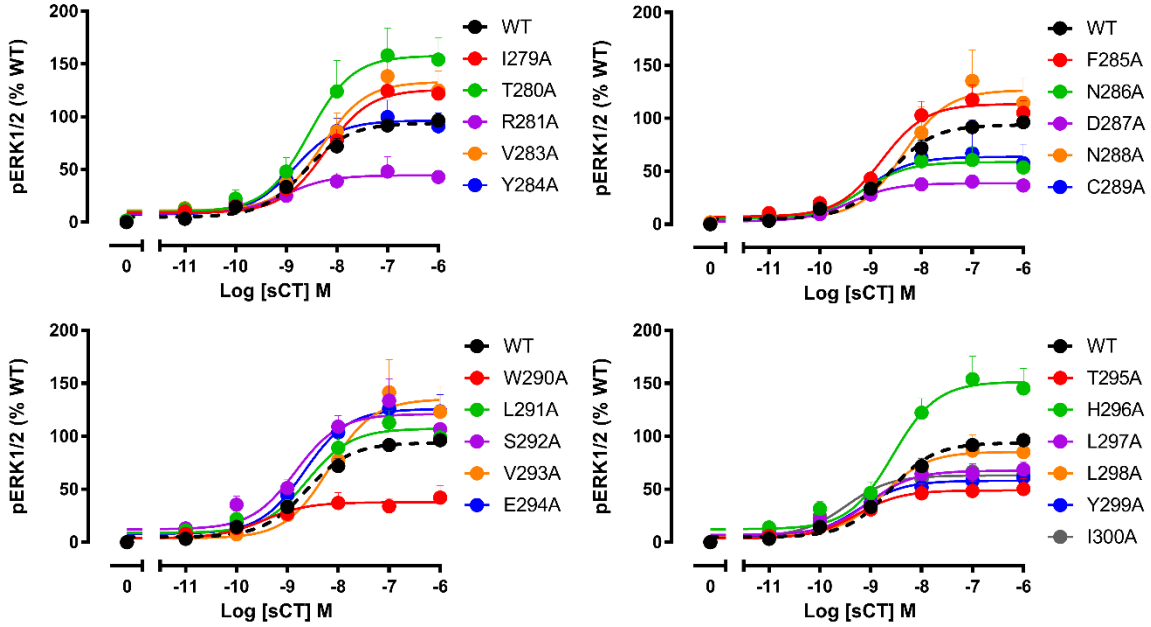

Figure 4.25 ERK1/2 phosphorylation concentration-response profiles elicited by sCT in CV-1-FlpIn cells stably expressing hCTR$_a$Leu ECL2 single alanine mutations. *pERK1/2 in response to sCT were normalized to the internal control (10% FBS measured at 6 min) and fit to a three parameter logistic equation. Data was subsequently normalised to WT receptor response. All values are mean+S.E.M. of 5 to 6 (WY N=10) independent experiments conducted in duplicate.*

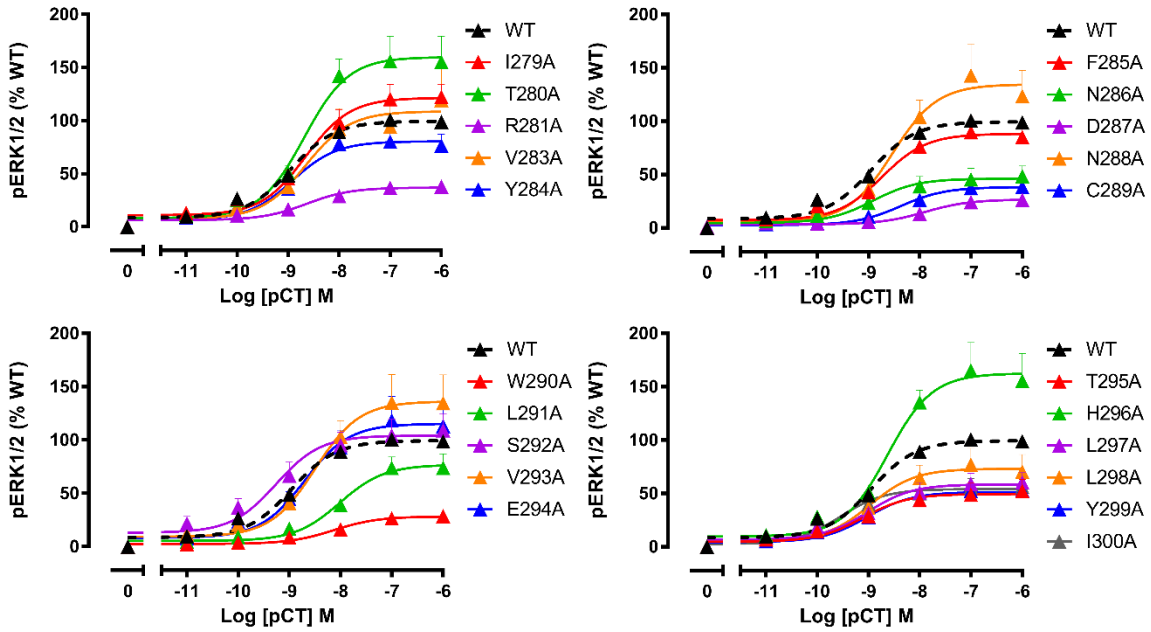

Figure 4.26 ERK1/2 phosphorylation concentration-response profiles elicited by pCT in CV-1-FlpIn cells stably expressing hCTR$_a$Leu ECL2 single alanine mutations. *pERK1/2 in response to pCT were normalized to the internal control (10% FBS measured at 6 min) and fit to a three parameter logistic equation. Data was subsequently normalised to WT receptor response. All values are mean+S.E.M. of 5 to 6 (WT N=10) independent experiments conducted in duplicate.*

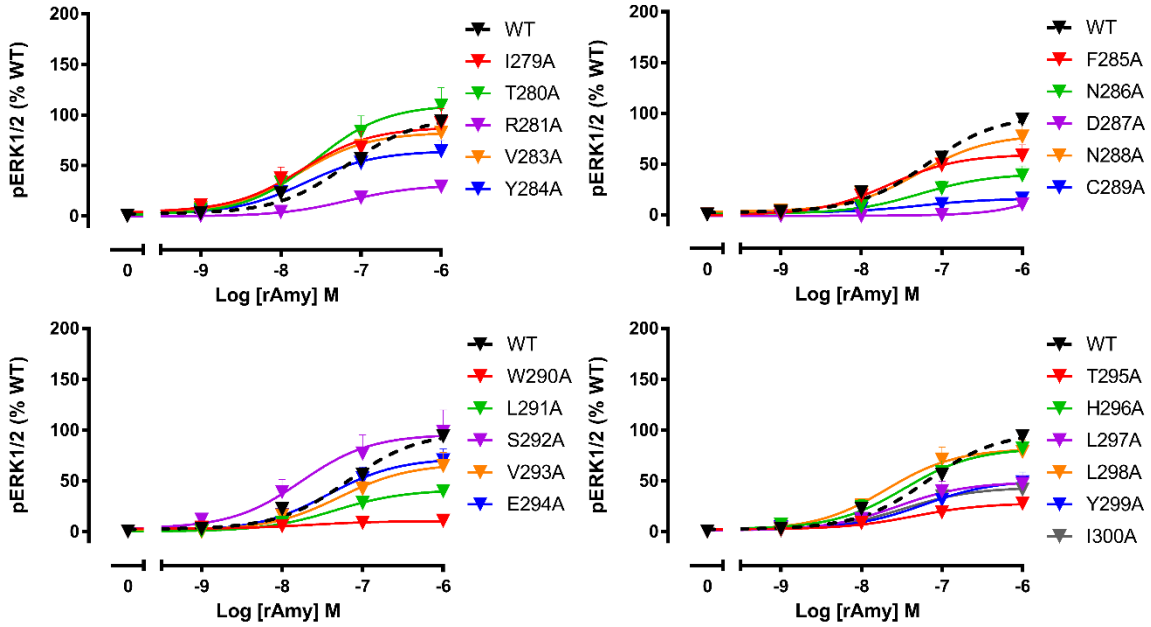

Figure 4.27 ERK1/2 phosphorylation concentration-response profiles elicited by rAmy in CV-1-FlpIn cells stably expressing hCTR$_a$Leu ECL2 single alanine mutations. *pERK1/2 in response to rAmy were normalized to the internal control (10% FBS measured at 6 min) and fit to a three parameter logistic equation. Data was subsequently normalised to WT receptor response. All values are mean+S.E.M. of 5 to 6 (WT N=8) independent experiments conducted in duplicate.*

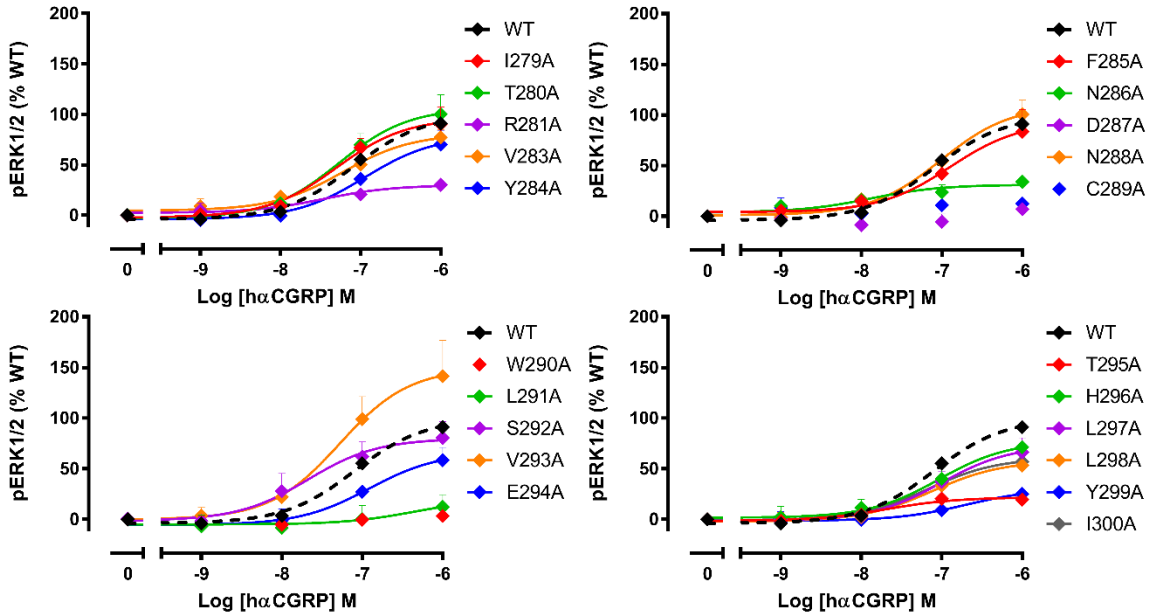

Figure 4.28 ERK1/2 phosphorylation concentration-response profiles elicited by hαCGRP in CV-1-FlpIn cells stably expressing hCTR$_a$Leu ECL2 single alanine mutations. *pERK1/2 in response to hαCGRP were normalized to the internal control (10% FBS measured at 6 min) and fit to a three parameter logistic equation. Data was subsequently normalised to WT receptor response. All values are mean+S.E.M. of 4 to 6 (WT N=8) independent experiments conducted in duplicate.*

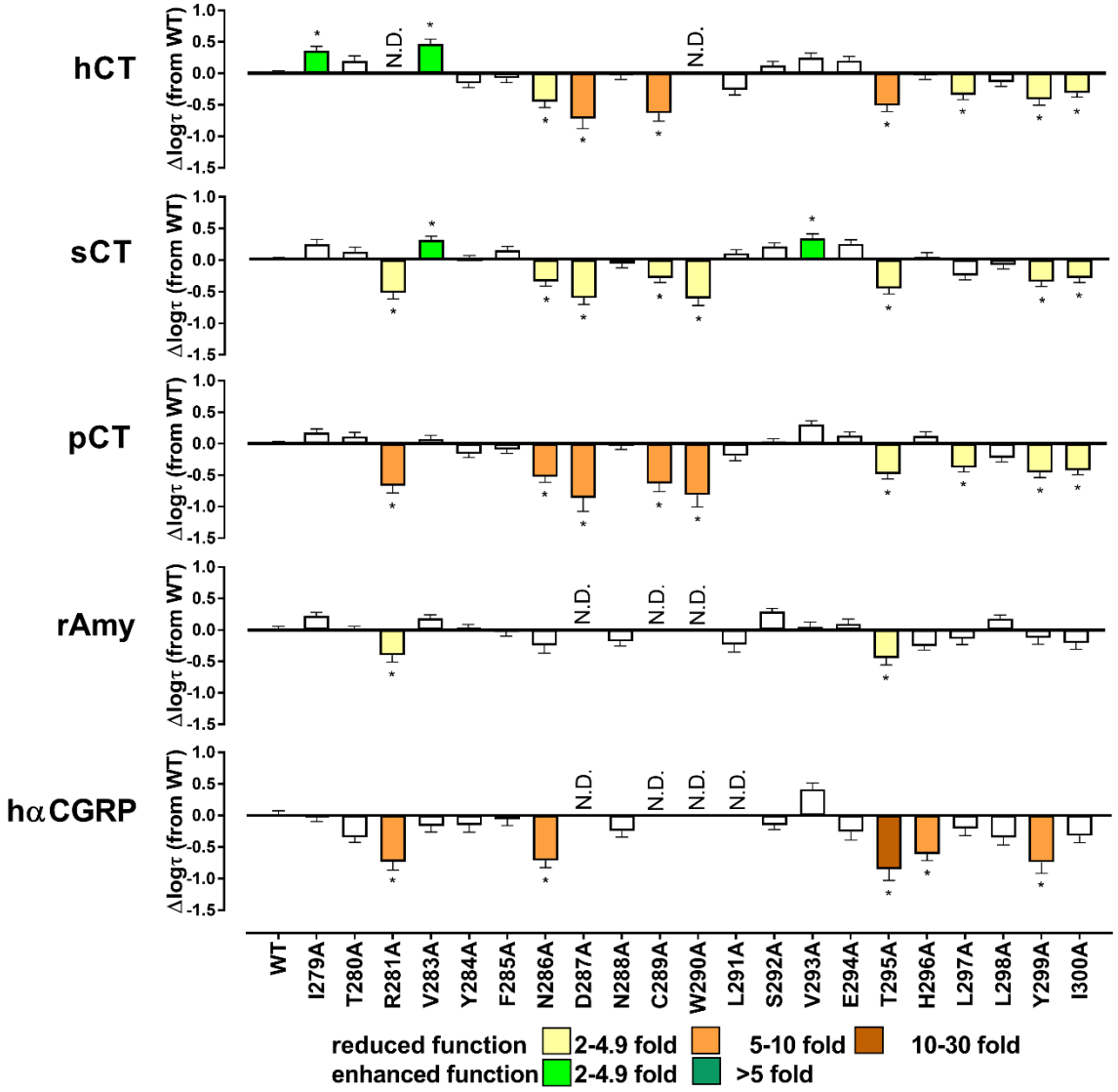

Figure 4.29 Effect of single alanine mutation in ECL2 of hCTR$_a$Leu on efficacy for ERK1/2 phosphorylation. *Data from Figure 4.23-27 were fit to the operational model of agonism to calculate coupling efficacy log(τ) of each receptor (mutant or WT) to the pERK1/2 signalling pathway. The log(τ) values of each receptor were then corrected for expression, where this was significantly different, to obtain log(τc). Graphs show the differences relative to WT. All values are mean+S.E.M. of 4 to 6 independent experiments conducted in duplicate. Significance of changes was determined by comparison of the WT to the other receptor mutants by one-way analysis of variance and Dunnett's post-test (p<0.05 represented by *). (N.D.) efficacy not determined.*

	hCT				sCT				pCT			
	pEC_{50}	E_{max} (% WT)	Log(τ)		pEC_{50}	E_{max} (% WT)	Log(τ)		pEC_{50}	E_{max} (% WT)	Log(τ)	
WT	8.32±0.09	100±3.2	-0.11±0.04	(10)	8.62±0.1	100±3.1	-0.15±0.05	(10)	8.95±0.08	100±2.5	-0.11±0.04	(10)
I279A	8.09±0.19	143.4±10.3*	0.26±0.07*	(5)	8.22±0.11	125.8±5.1*	0.11±0.07	(5)	8.66±0.17	121.5±6.3	0.01±0.07	(5)
T280A	8.17±0.19	168.4±11.7*	0.09±0.08[(c)]	(6)	8.55±0.25	157.9±12.3*	-0.02±0.07[(c)]	(6)	8.69±0.19	159.8±9.8*	0.42±0.06[(c)]	(6)
R281A	N.D.	N.D.	N.D.	(6)	9.01±0.43	44.5±5.1*	-0.67±0.1*	(5)	8.64±0.35	37±3.6*	-0.77±0.12*	(5)
V283A	8±0.24	155.4±13.8*	0.36±0.07*	(5)	8.3±0.22	133±10.1*	0.16±0.06*	(6)	8.65±0.34	108.7±11.5	-0.03±0.06	(5)
Y284A	8.08±0.23	81.6±6.7	-0.26±0.07	(5)	8.83±0.21	96.3±6.2	-0.14±0.06	(5)	8.92±0.25	80.5±6.2	-0.27±0.06	(5)
F285A	8.09±0.33	90.7±10.7	-0.19±0.06	(5)	8.78±0.16	113.6±5.8	0.01±0.06	(5)	8.74±0.2	88.2±5.4	-0.2±0.06	(5)
N286A	8.37±0.32	52±5.4*	-0.13±0.07*[(a)]	(5)	9.16±0.28	58.7±4.7*	-0.49±0.07*[(a)]	(5)	8.92±0.36	46.2±4.9*	-0.63±0.09*[(a)]	(5)
D287A	7.01±0.25*	35±4.7*	-0.83±0.16*[(a)]	(5)	9.4±0.23	38.7±2.4*	-0.75±0.11*[(a)]	(5)	7.9±0.25*	26.6±2.5*	-0.97±0.22*[(a)]	(5)
N288A	7.74±0.15	136.7±8.3*	0.2±0.07[(c)]	(5)	8.36±0.29	126.6±12.6*	-0.21±0.06[(c)]	(6)	8.53±0.26	134.6±11.2*	-0.14±0.06[(c)]	(6)
C289A	7.1±0.39*	40±7.9*	-0.74±0.13*[(a)]	(5)	9.07±0.57	63.6±10.6*	-0.44±0.07*[(a)]	(5)	8.37±0.28	38.3±3.6*	-0.74±0.12*[(a)]	(5)
W290A	N.D.	N.D.	N.D.	(5)	9.47±0.41	37.8±3.9*	-0.76±0.11*[(a)]	(5)	8.13±0.26	28. 4±2.6*	-0.92±0.19*[(a)]	(5)
L291A	7.05±0.24*	71.7±9	-0.35±0.13	(5)	8.61±0.15	107.3±5.1	-0.05±0.06	(5)	8.02±0.18*	76.8±5.3	-0.3±0.08	(5)
S292A	8.02±0.26	116.3±11	0.02±0.06	(5)	8.84±0.21	121.1±7.4	0.06±0.06	(5)	9.26±0.25	104.2±6.9	-0.08±0.05	(5)
V293A	7.78±0.15	130.2±7.9*	0.14±0.07	(5)	8.18±0.24	135.2±12.3*	0.19±0.07*	(5)	8.5±0.25	136.3±11*	0.2±0.06	(5)
E294A	8.07±0.21	124.8±10	0.1±0.06	(5)	8.67±0.17	125.8±6.8*	0.11±0.06	(5)	8.7±0.24	115.3±8.6	0.02±0.06	(5)
T295A	8.13±0.34	47.8±5.7*	-0.62±0.1*	(5)	9.27±0.3	49±4.1*	-0.6±0.09*	(5)	9.12±0.32	49.5±4.5*	-0.59±0.08*	(5)
H296A	8.02±0.14	148.1±7.9*	-0.13±0.07[(c)]	(5)	8.57±0.2	151.6±9.2*	-0.1±0.07[(c)]	(5)	8.63±0.2	162.6±10.1*	0.01±0.07[(c)]	(5)
L297A	8.1±0.22	62.7±4.8*	-0.45±0.08*	(5)	9.05±0.22	67.5±4.4*	-0.4±0.07	(5)	9.01±0.26	58.6±4.4*	-0.49±0.07*	(5)
L298A	7.82±0.29	84±9.5	-0.24±0.07	(5)	8.75±0.21	85.4±5.6	-0.23±0.06	(5)	8.96±0.28	73.2±6.1*	-0.34±0.06	(5)
Y299A	7.99±0.28	55.6±5.8*	-0.52±0.09*	(5)	9.23±0.25	58.1±4.1*	-0.49±0.07*	(5)	9.03±0.19	51.4±2.9*	-0.57±0.08*	(5)
I300A	8.71±0.29	65.3±5.7*	-0.42±0.07*[(a)]	(5)	9.49±0.21	63.1±3.3*	-0.44±0.07*[(a)]	(5)	9.55±0.22	54.2±3.2*	-0.53±0.07*[(a)]	(5)

Table 4.7 Effect of single alanine mutation in ECL2 of hCTR$_a$Leu on ERK1/2 phosphorylation in response to CT peptides. *For each receptor and ligand, data from Figure 4.23-25 were fit to a three-parameter logistic equation to derive pEC_{50} (negative logarithm of the concentration of ligand that produces half the maximal response) and E_{max} (maximal response as % of WT). The log(τ) reported in this table represents the operational coupling efficacy of each receptor (mutant or WT), where receptor expression was either unable to be identified on not significantly different. Where expression by radioligand binding was significantly different, values were corrected for the expression change to give log(τ_c) [(c)]. [(a)] Represents those mutation where expression could not be determined via radioligand binding. All values are mean±S.E.M. of 4 to 6 independent experiments conducted in duplicate For each ligand, significance of changes in pEC_{50}, E_{max} and log(τ) was determined by comparison of the WT to the other receptor mutants by one-way analysis of variance and Dunnett's post-test (p<0.05 represented by *).(N.D.) efficacy not determined.*

	rAmy				hαCGRP			
	pEC_{50}	E_{max} (% WT)	Log(τ_c)		pEC_{50}	E_{max} (% WT)	Log(τ_c)	
WT	7.19±0.1	100±4.9	-0.1±0.06	(8)	7.11±0.11	100±5.6	-0.08±0.08	(8)
I279A	7.74±0.27	87.9±9.4	-0.18±0.06	(5)	7.3±0.23	96.5±10.9	-0.09±0.09	(5)
T280A	7.57±0.23	110.1±10.5	-0.41±0.06[c]	(6)	7.27±0.23	106.4±11.8	-0.43±0.08[c]	(6)
R281A	7.16±0.27	30.9±4.5*	-0.81±0.11*	(5)	7.46±0.43	29.9±5.1*	-0.81±0.14*	(5)
V283A	7.77±0.27	82.7±9	-0.22±0.06	(5)	7.22±0.18	80.8±6.6	-0.25±0.1	(4)
Y284A	7.69±0.23	64.4±6.1*	-0.39±0.07	(5)	6.95±0.31	79±14.9	-0.23±0.11	(5)
F285A	7.66±0.28	59.5±7.1*	-0.43±0.07	(5)	6.9±0.34	93.3±17.5	-0.14±0.1	(5)
N286A	7.27±0.32	40.5±6.2*	-0.66±0.12[a]	(5)	7.89±0.47	31.1±5*	-0.79±0.11*[a]	(5)
D287A	N.D.	N.D.	N.D.	(5)	N.D.	N.D.	N.D.	(5)
N288A	7.28±0.2	79±7.3	-0.59±0.08[c]	(5)	7.01±0.16	109.6±9.9	-0.33±0.1[c]	(5)
C289A	N.D.	N.D.	N.D.	(5)	N.D.	N.D.	N.D.	(5)
W290A	N.D.	N.D.	N.D.	(5)	N.D.	N.D.	N.D.	(5)
L291A	7.35±0.22	41.2±4.3*	-0.64±0.12	(5)	N.D.	N.D.	N.D.	(5)
S292A	7.76±0.31	95.8±11.7	-0.12±0.05	(6)	7.68±0.35	79.8±11.5	-0.23±0.07	(5)
V293A	7.29±0.26	66.8±8.4*	-0.36±0.08	(5)	7.28±0.31	149.3±22	0.34±0.1	(5)
E294A	7.43±0.22	72.3±7.2	-0.31±0.08	(5)	6.91±0.36	66.3±15.3	-0.34±0.13	(5)
T295A	7.35±0.39	28±4.7*	-0.86±0.11*	(5)	7.68±0.38	21.7±3.5*	-0.93±0.18*	(5)
H296A	7.47±0.22	82.2±7.8	-0.66±0.07[c]	(5)	7.04±0.27	77.2±11.1	-0.69±0.1*[c]	(5)
L297A	7.55±0.27	48.8±5.6*	-0.55±0.09	(5)	7.01±0.29	73.2±12.1	-0.29±0.11	(5)
L298A	7.69±0.2	81.7±6.8	-0.23±0.06	(5)	7.12±0.24	58±7.7	-0.43±0.12	(5)
Y299A	7.22±0.28	50.7±6.9*	-0.54±0.1	(5)	6.69±0.56	30.4±11.2*	-0.82±0.17*	(4)
I300A	7.48±0.25	43.5±4.7*	-0.62±0.1[a]	(5)	7.17±0.42	60.9±13.3	-0.4±0.11[a]	(5)

Table 4.8 Effect of single alanine mutation in ECL2 of hCTR$_a$Leu on ERK1/2 phosphorylation in response to rAmy or hαCGRP peptides. *For each receptor and ligand, data from Figure 4.26-27 were fit to a three-parameter logistic equation to derive pEC_{50} (negative logarithm of the concentration of ligand that produces half the maximal response) and E_{max} (maximal response as % of WT). The log(τ) reported in this table represents the operational coupling efficacy of each receptor (mutant or WT), where receptor expression was either unable to be identified on not significantly different. Where expression by radioligand binding was significantly different, values were corrected for the expression change to give log(τ_c) [c]. [a] Represents those mutation where expression could not be determined via radioligand binding. All values are mean±S.E.M. of 4 to 6 independent experiments conducted in duplicate For each ligand, significance of changes in pEC_{50}, E_{max} and log(τ) was determined by comparison of the WT to the other receptor mutants by one-way analysis of variance and Dunnett's post-test (p<0.05 represented by *).(N.D.) efficacy not determined.*

4.2.3 Mapping mutational effect onto molecular models

To better visualise the effect that the alanine substitutions had on affinity and signalling efficacy of distinct peptide agonists, residues assessed in this study were mapped onto a hCTR model. This model was based on the published active Cryo-EM structure in complex with sCT (Liang et al., 2017). In this structure ECLs and the top of TM6 and TM7 had low resolution in the EM-density map, due to the flexibility of these regions. Additionally, only the backbone of the sCT agonist N-terminus was clearly resolved within the TM groove. Side chains of the peptide had poor density in the EM map. The missing regions and side chains were modelled by Prof. Christopher Reynolds (University of Essex), and the 3D surface fill map of this model of the CTR-sCT complex is presented in ***Figures 4.1, 4.31 and 4.32***. I have used this 3D model highlighted and the residues investigated in this study. The effect of mutation was mapped onto this model with colours providing a heat map of the level of effect of mutation (derived from ***Figure 4.7, 4.13, 4.18 and 4.29***).

Our data revealed that residues important for equilibrium affinity of hCT formed a continuum of residues throughout ECL2 and the top of TM5 (***Figure 4.31 A***). Although some limited differences were observed, pCT affinity was influenced by a similar cluster of residues; by comparison sCT and sCT(8-32) were less affected by mutagenesis of ECL2.

In contrast with the importance of ECL2 in affinity, alanine substitution of residues in ECL2 had limited effect on cAMP efficacy for any of the ligands assessed (sCT, hCT, pCT, rAmy or hαCGRP) (***Figure 4.31 B*** and ***Figure 4.32 A***). In our model, the CW motif that when mutated enhanced efficacy of all CT peptides, is localized at the interface with TM3-ECL1. Interestingly, mutation of these two residues had the opposite effect on rAmy and hαCGRP. Despite increased expression, substitution of H296, localised in the membrane proximal part of ECL2, reduced cAMP efficacy for all CT peptides and rAmy, while although not significant, hαCGRP also showed a similar trend.

ECL2 of CTR was important for IP_1 formation. Activation of this pathway was only measured in the presence of sCT, hCT and pCT and required a cluster of residues throughout ECL2, a pattern that partially overlaps with those important for affinity (***Figure 4.31 C***). hCT- and sCT-dependent IP_1 signalling utilised a similar network of residues, with very limited differences in the magnitude of

effects of mutations. In contrast, the effect of mutation on pCT-mediated response was less dramatic. Nonetheless, residues localized at the interface with ECL1 and in distal part of ECL3 towards the membrane adjacent portion of TM5 were important for all CT agonist peptides.

Overall, there was a similar pattern of effect for mutation on pERK1/2 efficacy for all CT peptide, with only minor differences in magnitude of effect. In general, this pattern was similar to that seen for IP_1 efficacy (***Figure 4.31 D and Figure 4.32 B***). Our mutation had less impact on rAmy efficacy, but those residues important for rAmy efficacy were a subset of those that were important for all CT peptides. The pattern of hαCGRP, while displaying partial overlap with CT peptides, revealed distinct residues important for its efficacy. For instance, a continuum cluster of residues between CW motif and the extracellular interface of TM5 was important for signalling down the IP_1 and pERK1/2 pathways for all these peptides. Additionally, substitution of V283 and V293 (residues facing the phospholipid bilayer), enhanced efficacy of this pathway for CT agonists (although data were not significant for all CT peptides), while having no effect on rAmy or hαCGRP.

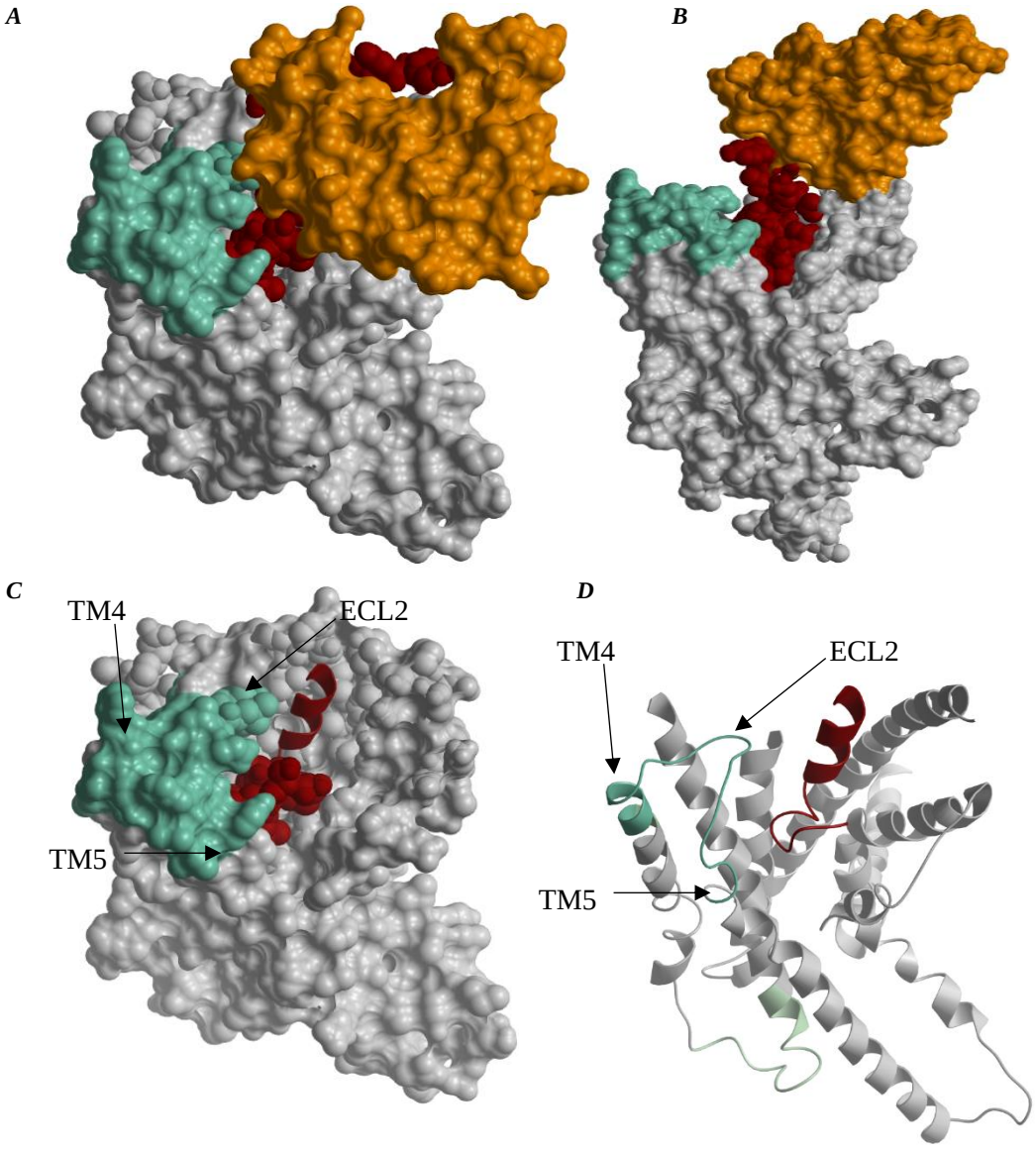

Figure 4.30. *(A)Top view and (B) side view of the active model of the hCTR in complex with the sCT ligand, based on the active Cryo-EM structure of CTR in complex with sCT and the G protein heterotrimer (pdb structure 5UZ7). Incomplete segments of the structure were modelled in by Prof. Christopher A. Reynolds to generate a complete model of the hCTR, shown here as a surface representation. The NTD (in orange) and the alanine substituted residues in ECL2 discussed in this chapter (279-300) are highlighted in green.*
To better visualise the ECLs and binding pocket within the TM bundle, the NTD, TM1-stalk region (residues 1-136) and residues 200-217 in ECL1 (that would partially cover ECL2) are not displayed. The model also shows the sCT ligand (in burgundy), with the cyclic N-terminus (residues 1-7) represented by space fill (C) or (D) ribbon. Residues 8-16 of the ligand, tightly structured in a α-helix, are shown as ribbon, while the C-terminus (residues 17-32) of the peptide is not displayed.

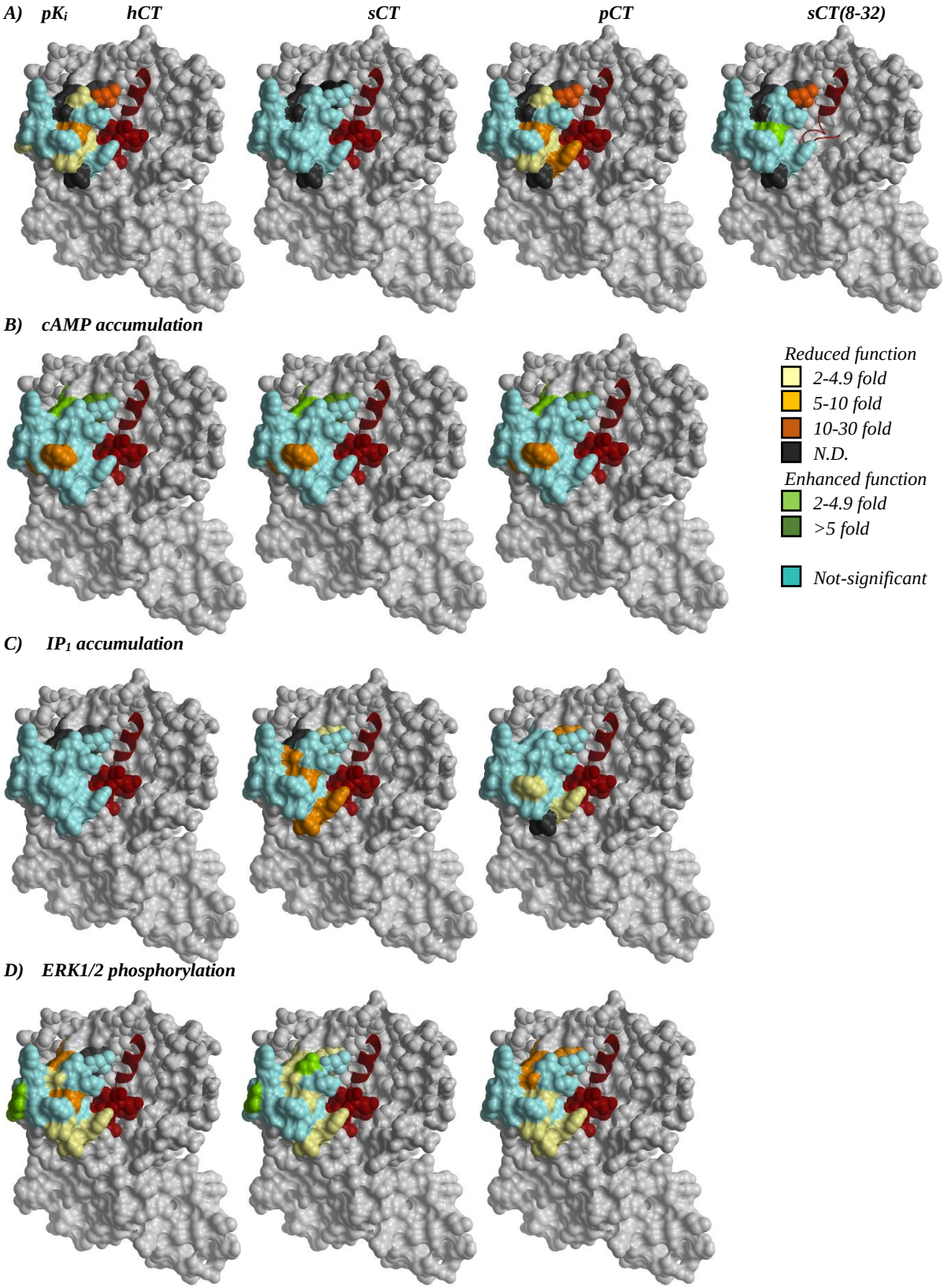

Figure 4.31 Heat-map 3D representation of ECL2 of the hCTR and the effect of alanine substitution on CT peptides equilibrium affinity and intracellular signalling. *Active model based on the active Cryo-EM structure of CTR in complex with sCT (Liang et al., 2017) into which the three ECLs were modelled as describe in Figure 4.30. Residues 1-136 and 200-217 (that would partially cover ECL2) are hidden. The model shows sCT ligand (in burgundy) where the cyclic N-terminus (residues 1-7) is represented by space fill, residues 8-16 are tightly structured in an α-helix (ribbon), while the C-terminus (residues 17-32) of the ligand is hidden. Residues that produced significant changes in binding affinity or signalling efficacy were coloured following the colour scheme for fold effect from WT in Figures 4.7, 4.13, 4.18 and 4.29.*

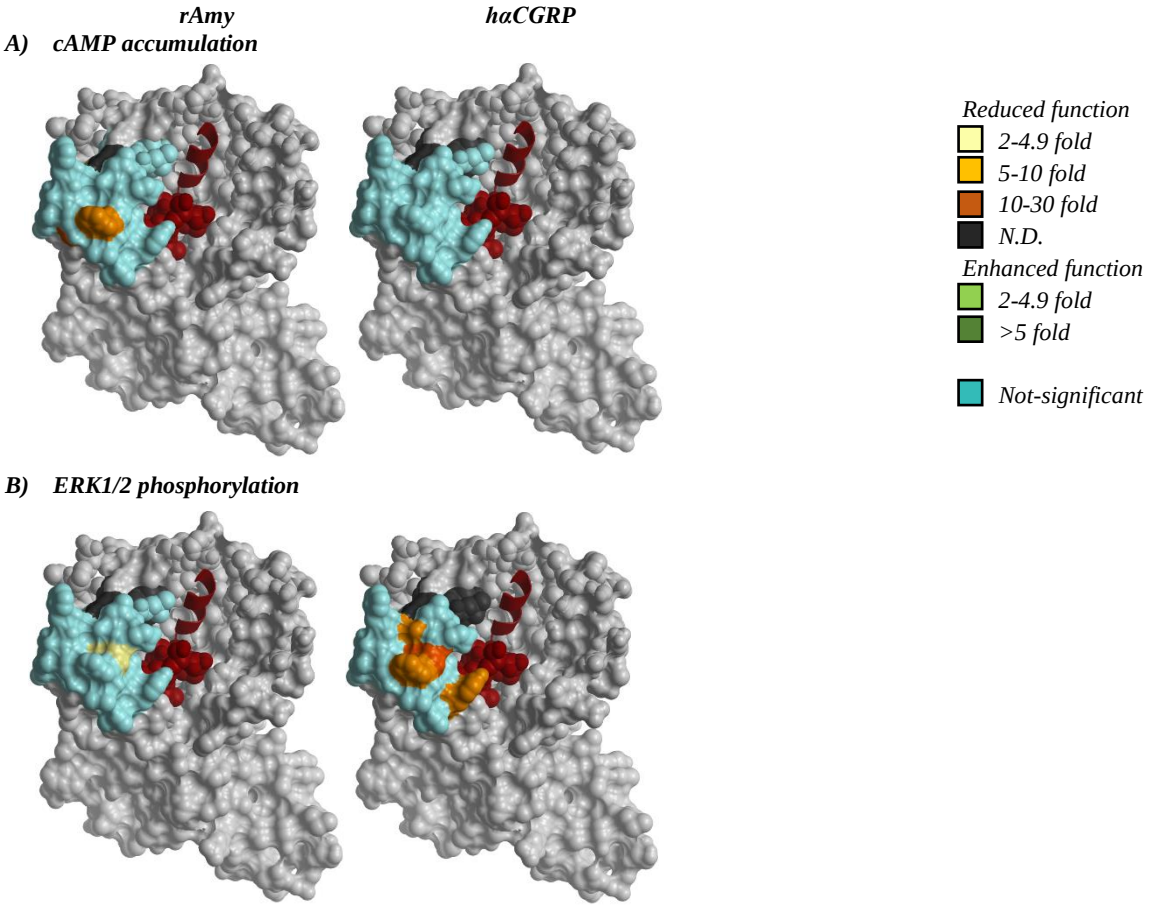

Figure 4.32 Heat-map 3D representation of ECL2 of the hCTR and the effect of alanine substitution on rAmy and hαCGRP equilibrium affinity and intracellular signalling. *Active model based on the active Cryo-EM structure of CTR in complex with sCT (Liang et al., 2017) into which the three ECLs were modelled). Residues 1-136 and 200-217 (that would partially cover ECL2) are hidden. The model shows sCT ligand (in burgundy) where the cyclic N-terminus (residues 1-7) is represented by space fill, residues 8-16 are tightly structured in an α-helix (ribbon), while the C-terminus (residues 17-32) of the ligand is hidden. Residues that produced significant changes in binding affinity or signalling efficacy were coloured following the colour scheme for fold effect from WT in Figures 4.13 and 4.29.*

4.4 Discussion

Orthosteric ligands interact with the juxta membrane portion of GPCRs to promote conformational changes within the receptor leading to effector recruitment and intracellular signalling. Like most, if not all GPCRS, Class B1 receptors pleiotropically couple to multiple effectors, and different ligands have the potential to stabilise distinct ensembles of receptor conformations, and thus produce unique signalling patterns (or biased agonism). The current literature is beginning to reveal how different biased ligands engage with these receptors to promote such heterogeneous signalling, and have begun to unravel the mechanistic basis behind this biased agonism. However, there are still significant gaps in the current understanding.

ECL2 has both direct and indirect roles, in ligand binding and signalling efficacy in different GPCR Classes (Woolley and Conner, 2017). In this study, we have performed an alanine scanning mutagenesis analysis of ECL2 and adjacent TMs (TM4 and TM5) of the $hCTR_aLeu$, to identify the role of this domain in ligand affinity and coupling efficacy to intracellular pathways (cAMP and IP_1 formation, ERK1/2 phosphorylation) for multiple different CTR peptide agonists. We have identified key networks in this region that are differentially involved in these distinct functional properties.

4.4.1 Importance of ECL2 of the hCTR for CT peptide binding

In the two domain model of activation of Class B1 GPCRs (Hoare, 2005), the initial ligand-receptor NTD interactions re-orientate the N-terminus of the peptides towards the binding groove within the receptor TM bundle. The mid-region and C-terminus of CTR agonists are critical determinants of the dissociation kinetics and affinity of binding of these ligands from the receptor, while the interactions between N-terminus of the peptide and the CTR are responsible for receptor activation, leading to recruitment and activation of intracellular effectors (Hilton et al., 2000, Furness et al., 2016, Furness et al., 2012). By mapping these residues on our 3D model, we have observed several residues that are important for the measured affinity of hCT and pCT. These residues form a continuum within ECL2, extending from the interface with TM3/ECL1 to TM5. In contrast, affinity of both sCT and the

antagonist sCT(8-32) was perturbed only by mutations to the distal part of ECL2, in particular those residues contributing to ECL1-ECL2-ligand interface (***Figure 4.31***, ***Table 4.2***) (discussed below).

Our data revealed that R281A, N286A, D287A, C289A and W290A reduced affinity of all CT peptides. These residues are highly conserved in Class B1 GPCRs, and are localised in the proximal region of ECL2, at the interface with ECL1-TM3. In our molecular model, R281 forms interactions with residues in the mid-region of ECL2, and likely plays a role in stabilising loop conformations. C289 (also completely conserved across other GPCR Classes) forms a disulphide bond with C219 at the top of TM3. D287 is predicted to form a salt bridge with R213 in ECL1, while N286, at the proximal end of ECL2, is predicted to form a hydrogen bond with the backbone of E294 within ECL2 (***Figure 4.34***). Like R281, these interactions are important for stabilising ECL2, and the surrounding residues that, in our model, may interact directly with the ligand. This is supported by the loss in affinity for all CT peptides, observed on equilibrium and/or calculated functional affinity (pK_i and pK_A) following mutation (***Figure 4.31 A***, ***Table 4.3***). We therefore hypothesise that the mutation of these residues may alter structural constraints within ECL2, rendering the loop more flexible, and/or removing important contacts required for the ligand to access to the binding pocket, thus increasing the energy barrier that these peptides need to breach to bind to their receptor or decreasing the energy barrier to dissociation of the ligand-receptor complex.

The stabilising interactions of R281A, N286A, D287A and C289A orientate W290 and L291 towards the CT peptide. The published active Cryo-EM sCT-CTR structure (Liang et al., 2017) shows that the peptide mid-region (9-17) aligns along TM1 of CTR, and both the mid-region of hCT and sCT has been reported to crosslink with TM1 (Pham et al., 2004, Dong et al., 2004b). Our 3D model (***Figure 4.34***) shows that the sCT peptide mid-region is also in close proximity to L291 and W290, of the CW motif, in ECL2. In our model, these stabilising interactions place W290 and L291 in proximity to the mid region of the peptide, where these residues may form direct interactions with the sCT peptide. These predicted interactions include a polar interaction of these receptor residues with S13, and hydrophobic stacking with L9 of the sCT peptide. W290A mutation, had dramatic effects on the affinity of all CT

ligands, albeit with larger effects on hCT and pCT than sCT; less than 5 fold reduction in sCT pK_A, but a loss ~500 fold for pCT and ~3200 fold for hCT (***Figure 4.7***, ***Table 4.3***). The L291A mutation had selective effects, reducing affinity for pCT and hCT, but not for sCT, consistent with weaker interactions. These data support previously published data, suggesting that mid-region of the hCT and sCT peptides contribute to the differences observed in the binding kinetics (Furness et al., 2016). Additionally, the important function of these conserved motifs (structural and/or direct interaction with the peptide) is also supported by the currently available Cryo-EM structure of GLP-1R in complex with GLP-1 peptide (Zhang et al., 2017b), and scanning mutagenesis studies of ECL2 on GLP-1R, CLR and CRF1R ligand pharmacology, which showed analogous reductions in the affinity of peptide agonists (Koole et al., 2012a, Koole et al., 2012b, Gkountelias et al., 2009, Woolley et al., 2017). Furthermore, a recently published study on the related CLR showed the importance of a positive charge on R274 (analogous to R281 of CTR) that was predicted to form an ionic interaction with the nearby residue D280 (analogous to D286 in CTR) (Woolley et al., 2017), and is important for CGRP mediated cAMP signalling.

Two additional residues, Y299 and I300, localised at the top of TM5, are highly conserved in Class B1. In our model, Y299 forms direct interactions with the peptide backbone of the N-terminal loop (S2 position). Interestingly, Y299 has little effect on sCT affinity, which is consistent with the fact that residues 1-3 of the peptide can be deleted without altering affinity of sCT (Hilton et al., 2000). In contrast, pCT affinity was reduced at this mutation, and hCT also trended this way, suggesting that interactions formed by Y299 may be influential on the binding of lower affinity peptides. I300 had no detectable radioligand binding, however pK_A values for hCT, sCT and pCT suggest little effect on affinity for these peptides, but a significant change in the affinity of the antagonist may occur as a consequence of more limited interaction within the TM bundle. Our model predicts I300 to be oriented towards the phospholipid bilayer, potentially stabilising membrane proximal interface. Additionally, a requirement of aromatic residues in TM5 for interaction with the N-terminus of the ligand has also been reported for some Class B1 receptor-ligand pairs (Neumann et al., 2008). For instance, an earlier GLP-1R model in complex with GLP-1 peptides (based on functional observations) suggested that H7 in the

peptide could be oriented towards W306 (analogous to Y299 of CTR) in GLP-1R (Dods and Donnelly, 2015). Although this interaction is not present in the deposited GLP-1/GLP-1R/Gαs structure (Zhang et al., 2017b), there is poor density in this region in the Cryo-EM map, and actual structure is unclear. These results are also consistent with an earlier mutagenesis study (Zhang et al., 2017b, Dods and Donnelly, 2015). A similar Ala substitution study of these amino acids of the GLP-1 caused a dramatic reduction in the affinity of different GLP-1R peptides (Koole et al., 2012a, Koole et al., 2012b). Furthermore, Y318 of PTH2R (equivalent to Y299 in CTR) is required for specific interaction with the N-terminus with TIP-39, a selective agonist of the PTH2R (but not of the PTH1R) (Weaver et al., 2017). Proximity between residues at the top of TM5 and the N-terminus of the peptide ligand is also supported by crosslinking between secretin peptide and SCTR (Dong et al., 2012, Dong et al., 2016), while the importance of these residues of the receptor for ligand binding would be supported by mutagenesis study on CLR and their effect on affinity of hαCGRP and AM peptides (Woolley et al., 2013).

Mutation of a number of additional residues within ECL2 reduced the affinity of both hCT and pCT, with no effect on sCT or sCT(8-32), including T295 and L298. hCT affinity was is also selectively affected by mutation of V293 and L297. Interestingly, our model showed that these residues (with the exception of L297) line the entrance of a deep binding groove, however they are not predicted to directly interact with sCT (***Figure 4.31***). The differential effect of mutations is suggest that they may be important for interaction of the lower affinity peptides.

sCT and hCT select distinct active conformations of G protein, presumably by stabilising distinct conformations of the CTR (Furness et al., 2016). It has been reported that scaffolding of effectors (besides G proteins) can be required to achieve the full active conformation of the receptor by allosterically modulating the affinity of a GPCR ligand (Rosenbaum et al., 2011). It is therefore possible that these CT ligands can recruit/activate effectors or scaffolding proteins in a unique manner. These in turn could affect the conformation of the receptor, influencing the affinity of different ligands in equilibrium binding assays. Although for CTR, G protein interaction has limited effect on hCT or sCT

affinities (Hilton et al., 2000), the effect of other scaffolding protein or effectors on ligand affinity have yet to be investigated.

4.4.2 Importance of ECL2 of the hCTR for CT peptide efficacy

Interestingly, the cAMP concentration-response curves obtained in CV-1 FlpIn cells better fit a three parameter logistic curve rather than a biphasic curve previously observed in COS-7 cells (Chapter 3). These differences could be attributed to the different cellular background. It is also possible that differences in expression could also play a role. In Chapter 3, a high expressing polyclonal COS-7 cells subpopulation was used, whereas in this Chapter (and also in Chapter 5) the FlpIn recombinase system was used to achieve a lower more homogeneous expression of the CTR clones. The method for expression may contribute to differential expression between cell lines, however unpublished data from our laboratory in a FlpIn background (consistent with COS-7 background) the $hCTR_a$ variant have higher expression compared to the $hCTR_b$, suggesting that the observed expression differences are likely due to post-translational processes. Nonetheless the two site profile may be in part related to the very high expression of the receptors in the COS-7 cell line or due to cell background differences.

The mapping of our results onto the 3D CTR model revealed that the activation of distinct intracellular pathways requires the engagement of different regions of the receptor structure. Specifically, our study showed that, while important for functional affinity, ECL2 had only a limited role in efficacy for cAMP production, while it was important for both IP_1 formation and pERK1/2 phosphorylation. The differential effect that our mutagenesis had on ligand affinity and on receptor signalling suggests that distinct portions of ECL2, especially those residues in proximity to ECL1, play a distinct role in the different aspects of receptor function. An analogous mutagenesis study on GLP-1R revealed that, ECL2 is also crucial for ligand binding and activation of intracellular signalling of other Class B1 GPCRs (Koole et al., 2012a, Koole et al., 2012b, Wootten et al., 2016). Nonetheless, comparison between CTR and GLP-1R revealed that ECL2 is engaged in a distinct manner in different receptors to trigger similar functions.

Mutation of R281, that stabilizes the conformation of ECL2, was the only substitution that globally altered receptor function, with reduced affinity and efficacy in all pathways and for all ligands assessed. Several other mutations had a unique impact on coupling efficacy to the different signalling pathways examined for each ligand assessed. These changes cannot simply be explained by reduction of affinity for the CT peptides. For instance, H296A substitution, which had no significant effect on ligand binding or pERK1/2, showed reduced efficacy of all CT peptides in cAMP and IP_1 formation. Conversely, mutation of C289 in the CW motif dramatically reduced radioligand binding, but significantly improving coupling efficacy to the cAMP pathway for all CT peptides (***Figure 4.7 and 4.13***). We speculate that the loss of structural constraints provided by the removal of the covalent bond between C219 (TM3) and C289 (CW motif) may facilitate activation of this pathway by lowering the energy barrier required for the activation.

Conversely, mutation of the CW motif, that enhanced efficacy in cAMP signalling reduced efficacy in both IP_1 and pERK1/2 responses for all CT peptides. As these residues are important for affinity, our results support the hypothesis that the activation of different functional pathways arises from engagement of the ligand with distinct networks within receptor structure, an observation made for other Class B1 GPCRs. For instance, an analogous study on GLP-1 revealed that ECL2 is crucial for driving both cAMP and Ca^{2+} mobilisation (an alternative method to IP_1 formation for measuring Gαq activation), but in contrast plays little part in pERK1/2 signalling pathway downstream GLP-1R stimulation (Koole et al., 2012a, Koole et al., 2012b, Wootten et al., 2016). Available structures show that Class B1 receptors have similar overall organisation of the TM bundle and recruit a common collection of intracellular effectors, while sharing less than 50% sequence homology within the TM bundle (Song et al., 2017, Zhang et al., 2017a, Zhang et al., 2017b, Liang et al., 2017, Hollenstein et al., 2013, Siu et al., 2013). The differences observed between Class B1 receptors and how they activate intracellular signalling suggests that different ligand-receptor combinations use distinct networks of residues to propagate conformational changes linked to the recruitment and activation of common effectors. At the same time, these structural differences and their impact on conformational networks could also allow the different receptors to activate signalling pathways via distinct mechanisms. For

fact, the intracellular Ca^{2+} response observed for GLP-1R involves activation of Gαi proteins (Koole et al., 2012b, Wootten et al., 2016). Work presented in Chapter 3 and other work from our laboratory exploring CTR activation in COS-7 cells would exclude a Gαi protein contribution to the peptide-mediated iCa^{2+} signalling (***Figure S1, Appendix 1***). While the contributions of Gαq or Gαi proteins to iCa^{2+} signalling or pERK1/2 responses downstream of CTR activation in either COS-7 or CV-1 cells is currently being investigated, the work presented in Chapter 3 support that Gαq protein activation, at least, is important for CTR-mediated ERK1/2 phosphorylation in both cell lines. This is consistent with the ECL2 mutational mapping for IP_1 and pERK1/2 pathways, where there is a significant overlap in the heat maps of residues required for activation of both of these pathways.

In Chapter 3 biased agonism was observed for pCT (away from cAMP and towards iCa^{2+} mobilisation and pERK1/2) when compared to hCT and sCT, while this Chapter illustrates that pCT engages less with ECL2 to activate the IP_1 pathway, while this contrasts to the similarity of important amino acids for pCT and hCT for affinity, and the pattern of key residues for cAMP and pERK1/2 profiles across all the three CT peptides (sCT, hCT and pCT). ***Table 1.1*** shows that the C-terminus and mid-region of pCT, although not completely conserved, more closely resembles the sequence of hCT than that of sCT. However, residues 11-13 of pCT are only partially conserved with hCT. This mid-region is important for both affinity and binding kinetics of CT peptides (Furness et al., 2016, Hilton et al., 2000). It is therefore not surprising that affinity of pCT is higher than hCT but lower than sCT. Interestingly, the N-terminus of pCT is highly conserved with both sCT and hCT, with the exception of residue 10 (Ser for pCT, Gly for hCT and sCT). In our model, G10 of sCT is oriented towards W290 and the deep binding pocket (***Figure 4.34***). It is therefore possible that Ser in this position could modify the pose of the pCT N-terminus, leading to distinct interactions with the receptor. This could explain the different involvement of ECL2 in pCT IP_1 signalling when compared to hCT or sCT. In these terms, it would therefore also be interesting to use cCT, which is highly homologous to sCT, with the exception of residues 2 and 3, which in our model are in close proximity of TM5, to further understand the

mechanistic role of different sub-regions of ECL2 (i.e. TM5-TM6, ECL1-ECL2 interface) in CTR function.

4.4.3 Importance of ECL2 of the hCTR for Amy/CGRP peptide binding and efficacy

In this study we have assessed the effect of our mutations on rAmy and hαCGRP peptides, Amy and CGRP peptides are low affinity agonists of the CTR alone. However, co-expression of CTR with RAMP1 or RAMP3 forms high affinity receptors for these peptides (Christopoulos et al., 1999, Tilakaratne et al., 2000, Zumpe et al., 2000, Christopoulos et al., 2003, Poyner et al., 2002, Dacquin et al., 2004, Hay et al., 2005, Morfis et al., 2008) that also strongly couple to Gαs (Lee et al., 2016b, Udawela et al., 2006b, Udawela et al., 2006a). RAMPs allosterically modulate CTR function by making extensive contacts with both the NTD and the TM bundle (Gingell et al., 2016). A separate study will investigate these same mutations in CTR function when co-expressed with RAMPs in the same cell system.

By comparing CTR with and without the presence of different RAMPs in multiple signalling pathways, it may also be possible to elucidate how RAMPs can modulate signalling efficacy of different CTR ligands, and if ligands engage with the receptor in a distinct manner in the absence or presence of RAMPs. It has indeed been shown previously that the different RAMPs can alter the signalling profiles of CTR bound to hCT, rAmy or CGRP (Udawela et al., 2006b, Udawela et al., 2006a), therefore this project will also help to understand how RAMPs and how these two structurally distinct ligands interact with the receptor to alter function.

Both rAmy and hαCGRP are characterized by low affinity at the CTR when the receptor is not co-expressed with RAMPs. For this reason, the effect of ECL2 mutations on affinity could not be robustly measured for these two peptides in traditional competition radioligand binding assay using ^{125}I-sCT(8-32) as tracer. Nonetheless, the functional pK_A values derived from cAMP could be used as a surrogate measure of affinity of both peptides (***Figure 4.14, Table 4.3***). Interestingly, the pattern of residues that had an effect on rAmy pK_A was similar in order of magnitude to sCT, whereas the hαCGRP pK_A profile

more closely resembled that of the low affinity ligand hCT. Based on our results, we hypothesise that rAmy and hαCGRP may adopt distinct poses within the binding groove, which would affect their interactions with the receptor and its activation.

The lack of RAMPs also reduces efficacy of these physiological agonists, and only cAMP and pERK1/2 signalling could be accurately measured for these ligands. Although significant IP_1 response could not be determined up to 1 μM of these peptides, we cannot exclude that the low affinity of these two peptides may have also reduced the potency of the IP_1 response.

Similar to the CT peptides, both rAmy and hαCGRP cAMP efficacy was only marginally affected by mutation of residues within ECL2 and adjacent TMs. However, notably, substitution of the CW motif significantly altered cAMP efficacy relative to WT for rAmy and hαCGRP in contrast to CT peptides, where efficacy was significantly increased by these mutations, Ala substitution of the CW motif dramatically reduced hαCGRP cAMP efficacy, while having no significant effect on rAmy. Additionally, the mutation of D287 (preceding the CW motif) significantly reduced both rAmy and hαCGRP efficacy, while having positive or no effect on CT agonists. This suggests that at the CTR, these weaker agonists activate Gαs signalling via the receptor in a distinct manner to CT peptides, where interactions involving the CW motif have been differentially modulated. Also of interest was the effect of ECL2 mutagenesis on pERK1/2 signalling. hαCGRP engaged with a network of residues that was consistent with that required for the CT agonists, although the individual mutations had more severe effects on hαCGRP efficacy. In contrast, pERK1/2 signalling downstream of rAmy interaction was minimally perturbed by the mutagenesis. Also, in contrast to the CT peptides, the majority of those residues important for cAMP signalling downstream of this rAmy were also important for ERK1/2 phosphorylation. These results suggest that rAmy, in the absence of RAMPs, may be biased away from pERK1/2 when compared to hαCGR peptide, and that rAmy and hαCGRP may trigger pERK1/2 response via the recruitment and activation of other different subset of effectors; further work will be required to confirm this hypothesis.

The absence (or presence) of RAMPs, which allosterically modulate the ligand-receptor interface (Lee et al., 2016b, Udawela et al., 2006b, Udawela et al., 2006a), could change the structure of the binding

pocket, favouring the access to or specific interaction between CTR and rAmy/hαCGRP peptides. This could be particularly important not only for Amy and CGRP, but also for the CT peptides. Indeed, a mutagenesis study conducted on the NTD of CTR that examined the effect of these mutations on both affinity and cAMP efficacy of hCT, Amy and CGRP, revealed that these three ligands interact with the NTD of CTR via a similar binding cleft, however they establish slightly different interactions (Gingell et al., 2016), supporting the hypothesis that without the presence of RAMPs (that were shown to allosterically modulate interactions of Amy and CGRP with the CTR), these three peptides may be adopting alternative poses.

4.4.4 Summary

The use of different CTR peptide agonists highlighted that distinct residue networks are differentially engaged for ligand binding or the activation of different intracellular signalling. We have shown that ECL2 is crucial for ligand binding, IP_1 formation and pERK1/2 phosphorylation, while playing little role in cAMP signalling. Our study has also revealed interesting differences in how distinct CTR ligands engage with these key networks, and this could be related to potential biased agonism described for pCT in Chapter 3. Additionally, we have also speculated that subtle changes within mid-region of the CTR peptides could not only contribute to the binding kinetics and affinity of different ligands, but also to the pose of the peptide within the binding pocket, leading to the different activation of intracellular response. Finally, by comparing our results with similar studies performed on other Class B1 GPCRs, we have shown that different receptors of this group only partially share these networks important for receptor function.

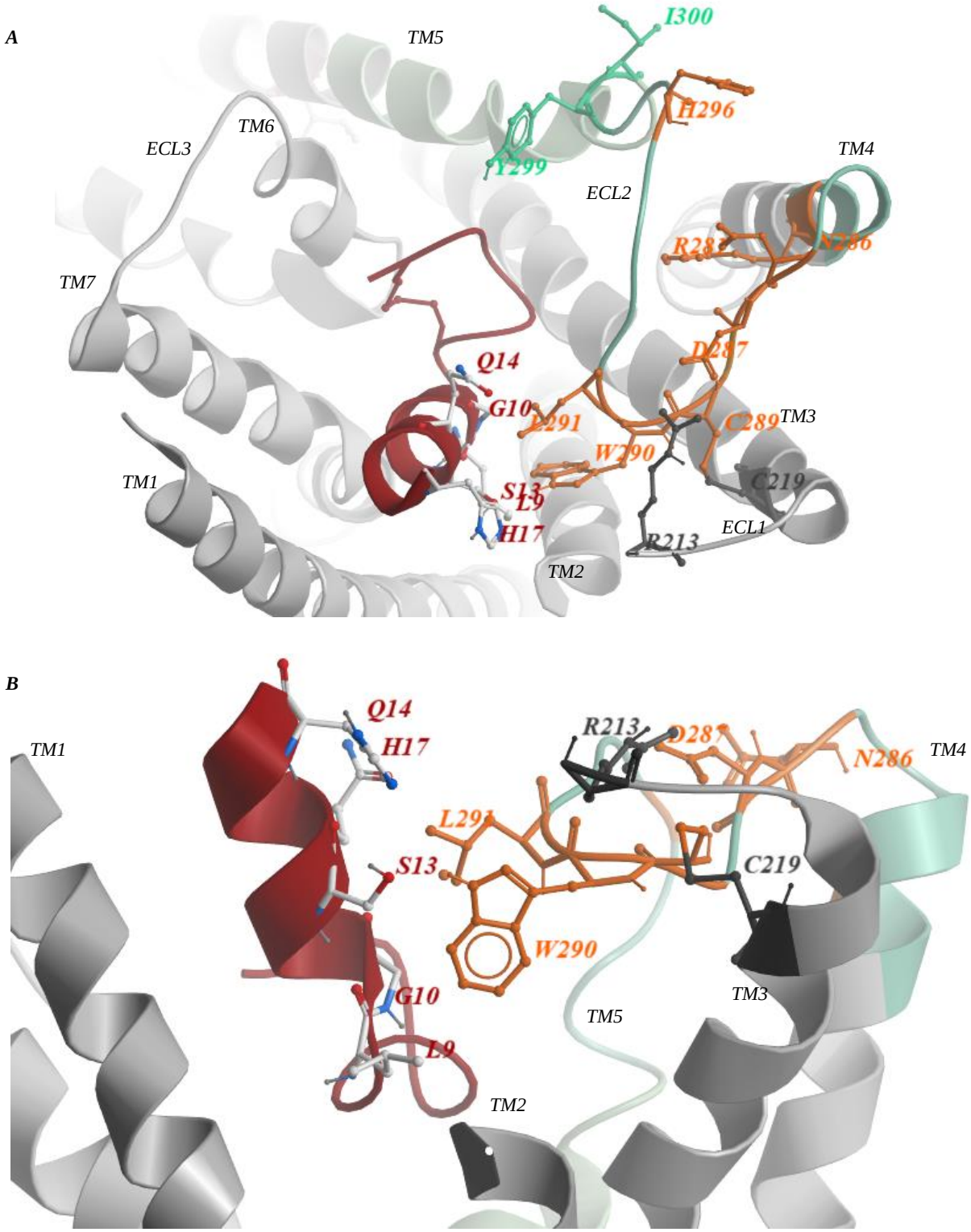

Figure 4.34 Model of the hCTR extracellular portion of the receptor in complex with sCT. *Ribbon 3D representation, A) top view and B) side view, based on the active model of hCTR in complex with sCT (Liang et al., 2017) generated as described in Figure 4.1. Relevant residues investigated for chimeric peptides are represented as sticks and highlighted in orange. C219 in TM3, that forms a disulphide bridge with C289 (part of the conserved CW motif in ECL2) is highlighted in grey. To better visualise potential interactions between receptor and peptide, side chains of the sCT ligand (shown in burgundy) were modelled and residues facing ECL2 are shown in sticks.*

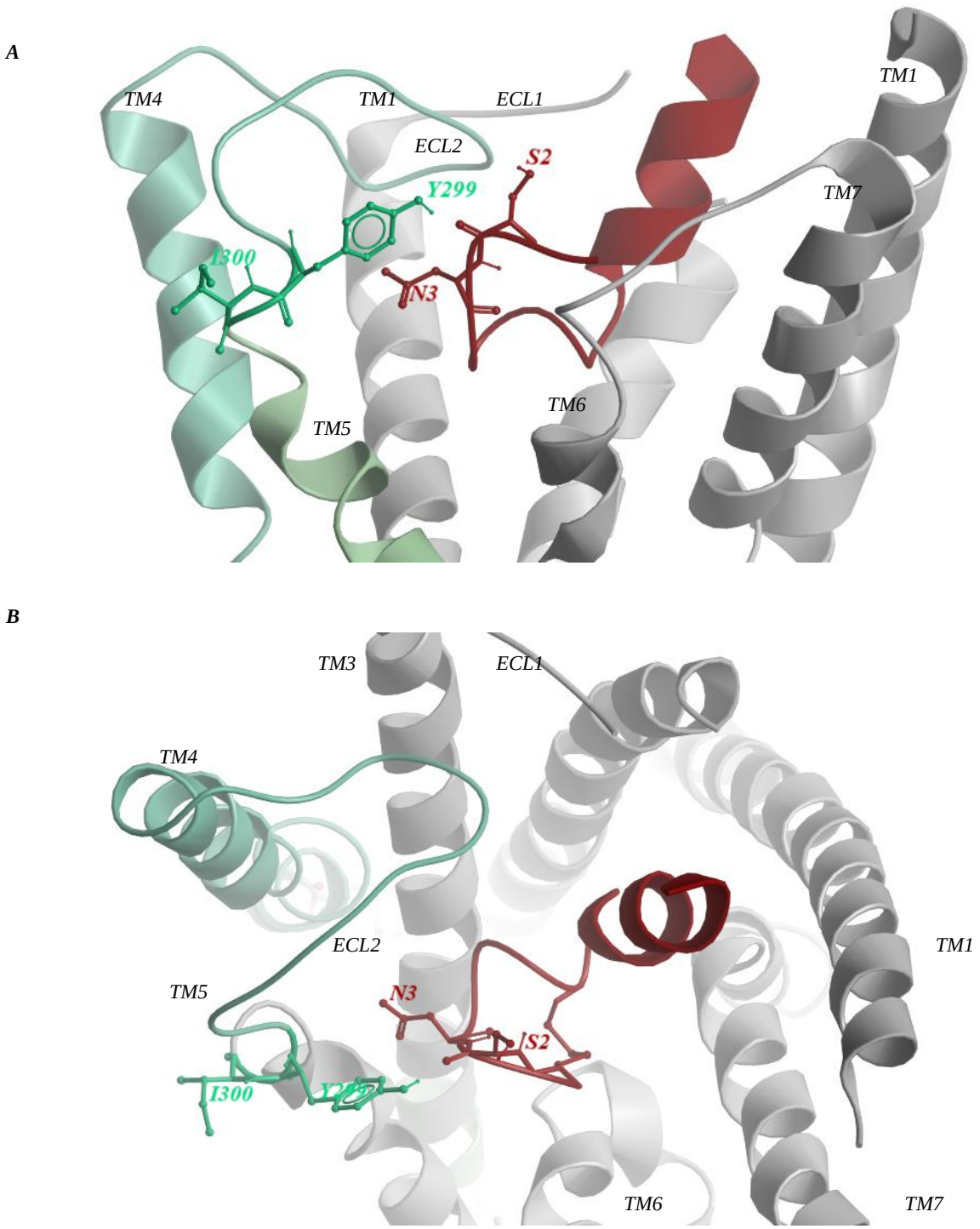

Figure 4.35 Model of the hCTR extracellular portion of the receptor in complex with sCT. *(A) Side view and (B) top view of the interaction between the extreme N-terminus of the sCT and the carboxyl terminal portion of ECL2 represented as ribbons. Peptide is highlighted in burgundy, while CTR is represented in grey. Highlighted in sticks are residues Y299 at the top of TM5 of CTR in close proximity with residues 2 and 3 or the sCT peptide agonist.*

CHAPTER 5

Structure-function study of extracellular loop 3 (ECL3) of the human calcitonin receptor (hCTR)

5.1 Introduction

Prior to the publication of 2 active Class B1 GPCR Cryo-EM structures in complex with their orthosteric ligands (Zhang et al., 2017b, Liang et al., 2017), mutagenesis and photo-crosslinking studies on several Class B1 receptors supported the hypothesis that the juxta membrane region of the TM bundle establishes interactions with both orthosteric ligands and allosteric ligands that are important for both ligand binding and receptor activation (Dong et al., 2014, Wootten et al., 2016, Barwell et al., 2011, Barwell et al., 2013, Bailey and Hay, 2007, Dong et al., 2016). Some of these findings were confirmed by the publication of structures bound to peptide agonists or small molecule inhibitors of the CTR, GLP-1R and CRF1R (Hollenstein et al., 2013, Zhang et al., 2017b, Song et al., 2017, Liang et al., 2017). Understanding of how a ligand interacts and activates its receptor is fundamental to more efficient design of improved therapeutics. In addition, knowledge regarding residues that trigger distinct signalling can aid in rational design of biased agonists to provide novel therapeutics. Recently, work by our group at the Class B1 GLP-1R, identified both ECL2 and ECL3 as crucial for ligand affinity and activation of distinct signalling pathways (Wootten et al., 2016).

Chapter 4 discussed the role of ECL2 of the CTR, in both ligand affinity and triggering intracellular signalling. This Chapter extends this study to assess the role played by ECL3 of the CTR. Photoactive cross-linking of position 8 of the hCT indicates that this residue is in close proximity of L368 of ECL3 (Dong et al., 2004b), consistent with an important role of TM6-ECL3-TM7 in CT activity. Additional work identified the importance of P360 in TM6 in receptor activation (Bailey and Hay, 2007). More recently, the publication of the Cryo-EM structure of the active CTR in complex with sCT (Liang et al., 2017) revealed that this proline is located at the top of TM6 and is oriented toward the ligand, suggesting that this residue is either involved in direct interactions with the ligand or aids the plasticity of ECL3. Due to the flexibility within the top of TM6, ECL3 and top of TM7, this Cryo-EM structure is missing details between residues W361 and N366, and to date, no detailed analysis of the role of ECL3 in CTR function has been assessed. Nonetheless, ECL3 is reported to play a role in ligand binding and receptor activation in both the calcitonin-like receptor (CLR-RAMP1) (Barwell et al., 2011), adrenomedullin receptor (CLR-RAMP2/RAMP3) (Kuwasako et al., 2012), and the GLP-1R (Wootten et al., 2016), as

well as several Class A GPCRs (Hulme, 2013). Furthermore, for the GLP-1R, ECL3 played a role in selective signalling and biased agonism, with mutation within this domain primarily influencing pERK1/2 activation, while having little effect on cAMP production and intracellular calcium mobilisation. In this Chapter a comprehensive Ala substitution study of ECL3 and the extracellular portion of adjacent TMs (F356 to M376) was performed. Similar to Chapter 4, five different agonists of the hCTR were used and the affinity and signalling efficacy was evaluated at both WT and Ala mutated receptors, and significant effects were mapped onto the CTR model, described in Chapter 4. The pattern of response for specific ligands, across different pathways, were compared, with additional comparison of the role of ECL3 for CTR-dependent signal to that mediated by peptide activation of the GLP-1R.

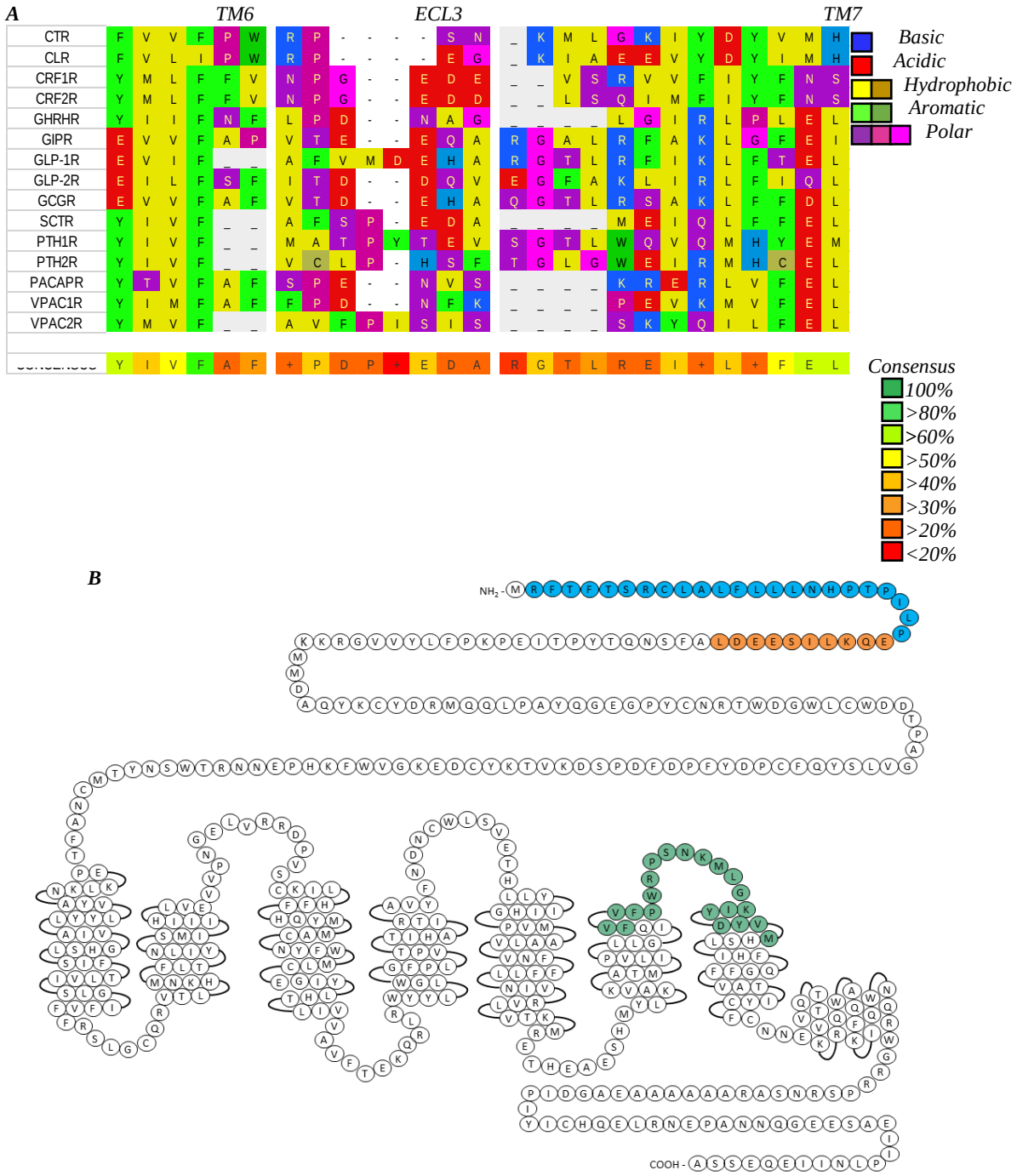

Figure 5.1 Sequence alignment of human Class B1 GPCRs, diagram and model of the hCTR$_a$Leu receptor used in this study. *Similar to Figure 4.1, (A) Sequence alignment of TM6-ECL3-TM7 of the 15 human Class B1 GPCRs, aligned and exported from gpcrdb.org. (B) Snake diagram of the hCTR: highlighted in blue are the residues that constitute the signal peptide of the receptor, in orange the cMyc tag, and in green the residues that have been mutated to alanine. 17-32) of the peptide is not displayed.*

5.2 Results

Ala mutations of residues in ECL3 and the extracellular portion of TM6 and TM7 (F356 to M376) of the hCTR$_a$Leu (***Figure 5.1 B and C***) were stably expressed in the CV-1-FlpIn recombinant cell line. For each receptor, either wild type (WT) or mutant, surface expression, affinity and signalling assays (cAMP and IP1 accumulation, and ERK1/2 phosphorylation) were assessed in the presence of hCT, sCT, pCT, rAmy or hαCGRP peptides. In all the statistical analysis, the response of each mutant receptor for each pathway and ligand, was compared to the WT in a one-way analysis of variance and Dunnett's post-test. Significance set at $p<0.05$.

5.2.1 Cell surface expression of CTR variants

Surface expression of the WT and mutant receptors was determined by whole cell radioligand binding in the presence of two different concentrations of ^{125}I-sCT(8-32) radioligand (***Figure 5.2*** and ***Table 5.1***). Mutants K370A and I371A showed no detectable binding for the radioligand used, hence their expression could not be measured. Compared to WT, P360A expression was significantly increased. The majority of the other substitutions in ECL3 were either similar to WT or displayed non-significant increases in receptor expression. F356A, displayed reduced expression, although this did not achieve significance. Due to the variance in expression estimates by binding and low specific window in independent measures of cell surface receptor expression (ELISA and western blotting), comparison of effect of mutation focused on differences in peptide response.

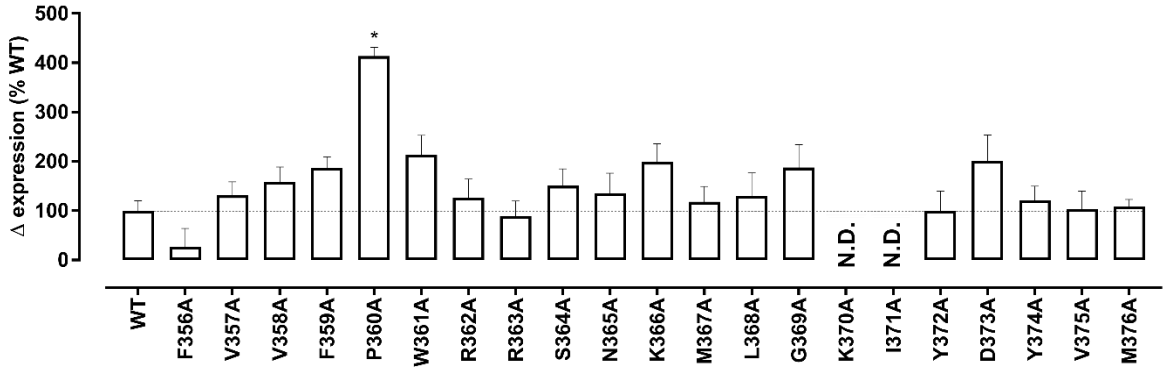

Figure 5.2 Cell surface expression of the hCTR$_a$Leu mutants stably expressed in CV-1-FlpIn cells. *Homologous competition of radioligand binding was performed in the presence of 2 concentrations of ^{125}I-sCT(8-32), with concentrations of the competing sCT(8-32) ranging between 1 μM and 1 pM. CPM data were converted to sites/cell and then normalized to WT and non-specific binding. All values are mean+S.E.M. of 4 to 5 independent experiments conducted in duplicate. (N.D.) affinity not determined as no radioligand binding was detected.*

5.2.2 Ligand affinity

The radiolabelled antagonist ^{125}I-sCT(8-32) was also used in heterologous competition binding assay to determine affinity of the CT peptides (***Table 4.1***) in whole cells, for all the hCTR$_a$Leu receptors (WT and mutants) used in this study. Affinity for sCT(8-32) was determined via homologous competition binding (***Figure 5.3***), whereas affinity of sCT (***Figure 5.4***), hCT (***Figure 5.5***) or pCT (***Figure 5.6***) was obtained via heterologous inhibition binding and corrected for radioligand occupancy using the Cheng-Prusoff equation (Equation 7, Section 2.6.1) to calculate pK$_i$ (reported in ***Table 5.2***). Changes in affinity relative to WT are shown in ***Figure 5.7***.

Similar to Chapter 4, rAmy and hαCGRP had low affinity for hCTR$_a$Leu and their pK$_i$ could not be determined via heterologous competition within the concentration range of peptide assessed. Moreover, affinities of K370A and I371A for hCT, sCT and pCT could not be determined due to the lack of detectable specific binding for the radioligand.

sCT and sCT(8-32) had highest affinity (~0.1nM) at the WT hCTR, compared to pCT or hCT whose Ki values were ~5.5nM and ~0.1 μM respectively (***Table 5.1***). Mutation of all residues (with the exception of K370A and I371A, which could not be determined) had no significant impact on the affinity of sCT(8-32). For all the CT agonist peptides (sCT, hCT and pCT), P360A statistically reduced affinity by 7-12 fold. While no other mutation had a significant effect on sCT affinity, mutation of residues located at the top of TM6 significantly reduced the affinity of hCT and pCT. Both pCT and hCT had reduced affinity for a continuous cluster of residues between F359 and R363 (F359, P360, W361, R362, P363). hCT affinity was also reduced by mutation of the adjacent residues V357A and V358A. The hCT peptide affinity was also reduced by alanine mutation of a second cluster of residues at the top of TM7 (Y372, D373 and M376). Mutations of Y372 and D373 also trended towards reduced affinity of sCT and pCT, although data failed to reach statistical significance.

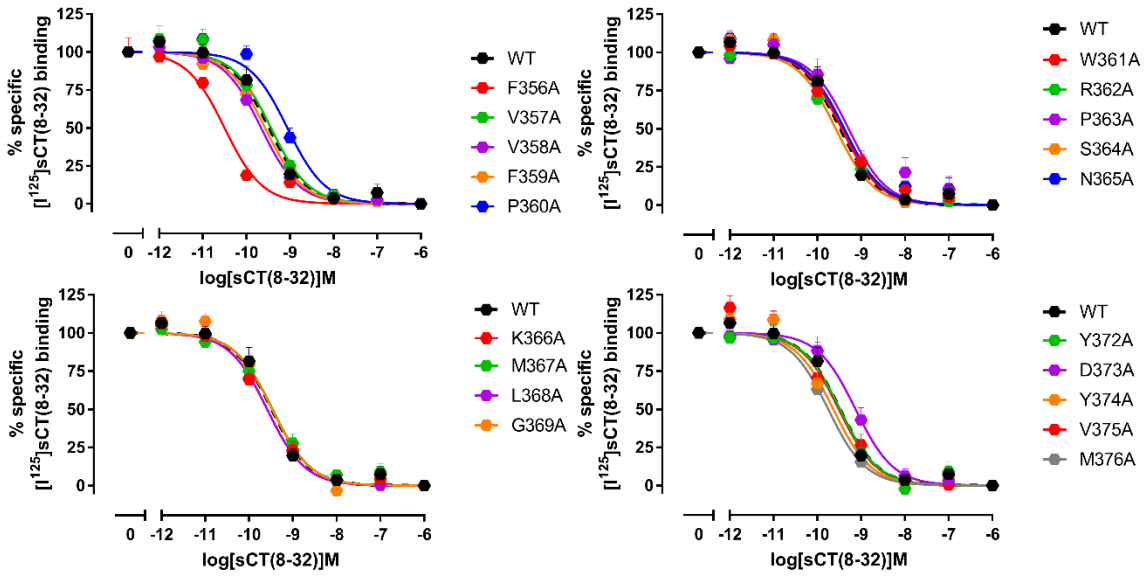

Figure 5.3 Homologous competition of ^{125}I-sCT(8-32) binding for each of the hCTR$_a$Leu mutants stably expressed in CV-1-FlpIn cells. *Whole cell radioligand binding was performed for each receptor mutant in presence of ^{125}I-sCT(8-32) and competing sCT(8-32) ranging in concentration between 1 μM and 1 pM. Non-specific binding was determined in the presence of 1 μM of sCT(8-32) and was used to calculate % of specific binding. Data were fit with a three parameter logistic equation. All values are mean+S.E.M. of 8 to 12 independent experiments conducted in duplicate.*

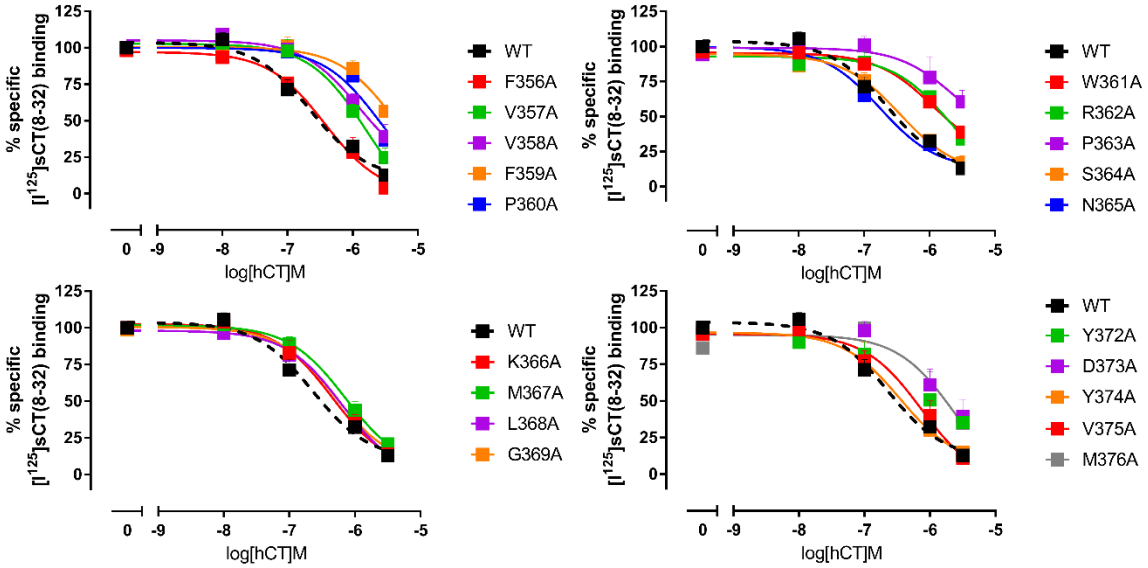

Figure 5.4 Heterologous competition binding of hCT for each of the hCTR$_a$Leu mutants stably expressed in CV-1-FlpIn cells. *Whole cell radioligand binding was performed for each receptor mutant in the presence of ^{125}I-sCT(8-32) and competing hCT ranging in concentration between 3 μM and 10 nM. Non-specific binding was determined in the presence of 1 μM of sCT(8-32) and was used to calculate % of specific binding. Data were fit with a three parameter logistic equation. All values are mean+S.E.M. of 4 to 8 independent experiments conducted in duplicate.*

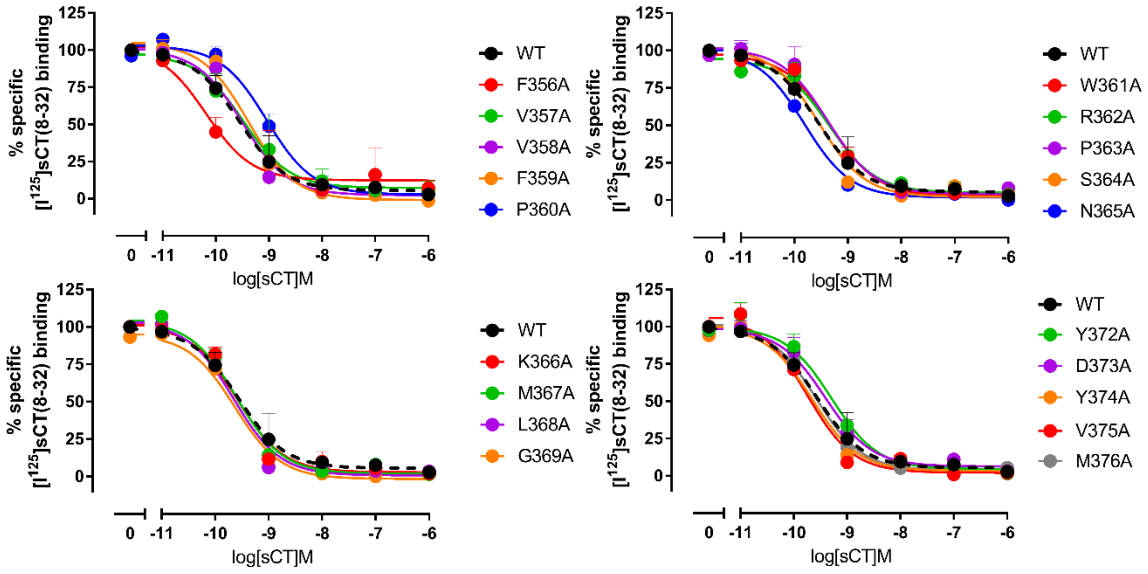

Figure 5.5 Heterologous competition binding of sCT for each of the hCTR$_a$Leu mutants stably expressed in CV-1-FlpIn cells. *Whole cell radioligand binding was performed for each receptor mutant in the presence of ^{125}I-sCT(8-32) and competing sCT ranging in concentration between 1 µM and 10 pM. Non-specific binding was determined in the presence of 1 µM of sCT(8-32) and was used to calculate % of specific binding. Data were fit with a three parameter logistic equation. All values are mean+S.E.M. of 4 to 8 independent experiments conducted in duplicate.*

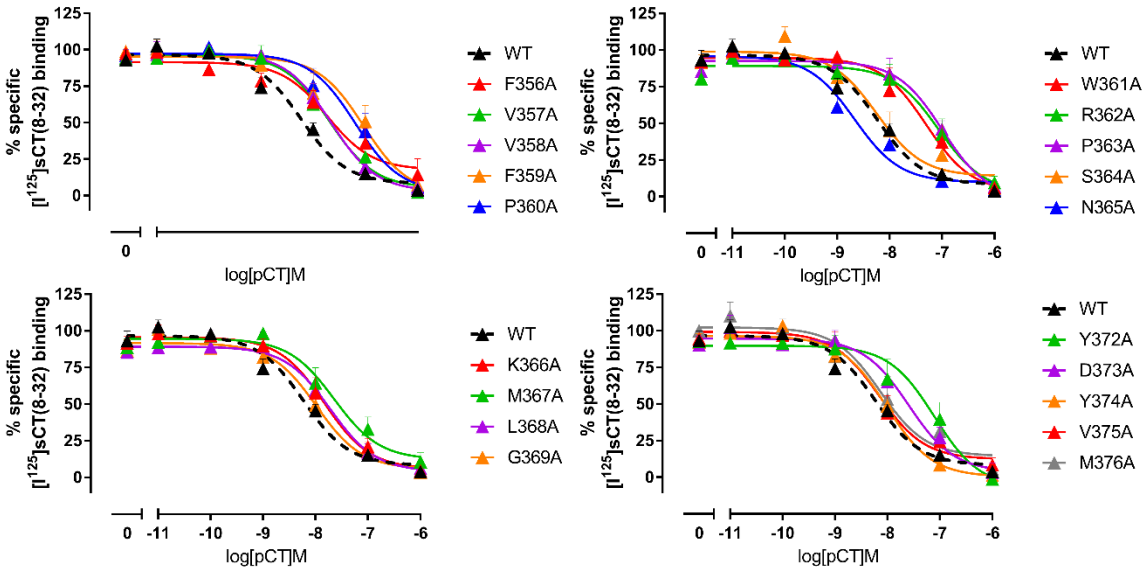

Figure 5.6 Heterologous competition binding of pCT for each of the hCTR$_a$Leu mutants stably expressed in CV-1-FlpIn cells. *Whole cell radioligand binding was performed for each receptor mutant in the presence of ^{125}I-sCT(8-32) and competing pCT ranging in concentration between 1 µM and 10 pM. Non-specific binding was determined in the presence of 1 µM of sCT(8-32) and was used to calculate % of specific binding. Data were fit with a three parameter logistic equation. All values are mean+S.E.M. of 3 to 8 independent experiments conducted in duplicate.*

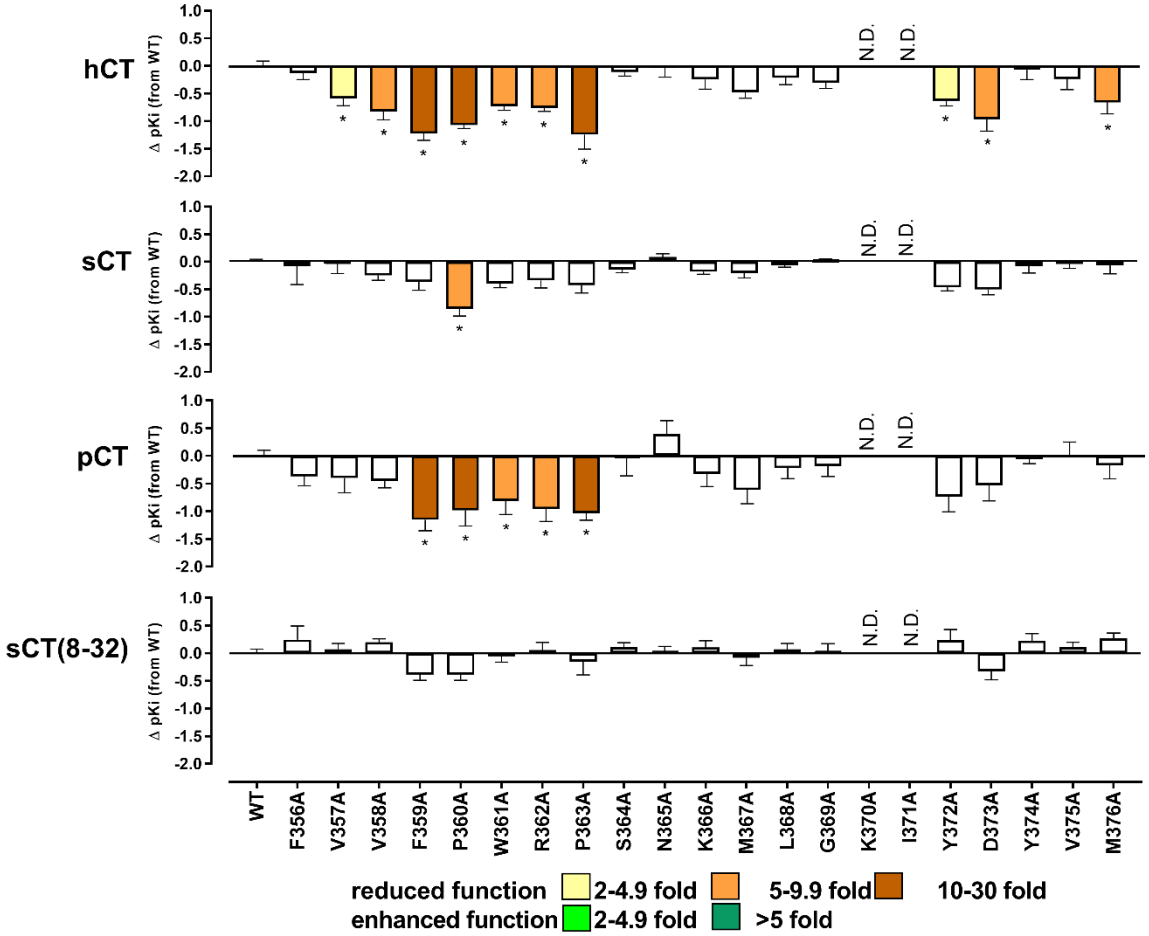

Figure 5.7 Effect of single alanine mutation in ECL3 of hCTR$_a$Leu on ligand affinity. *pK$_i$ were derived for each ligand and mutant receptor from analysis of data in Figures 5.3-6. Changes in affinity (ΔpK$_i$) for each mutant relative to WT (on a log scale) for hCT, sCT, pCT or sCT(8-32) are represented as bars. All values are mean+S.E.M. of 3 to 12 independent experiments conducted in duplicate. Significance of changes in affinity of each ligand was determined by comparison of the WT by a one-way analysis of variance and Dunnett's post-test (p<0.05 represented by *). (N.D.) affinity not determined as no radioligand binding was detected.*

	hCT pK_i		sCT pK_i		pCT pK_i		sCT(8-32) pK_i		Whole cell binding sites/cell	
WT	6.72±0.09	(8)	9.87±0.04	(8)	8.29±0.1	(8)	9.61±0.08	(10)	21,600±4,400	(5)
F356A	6.58±0.11	(5)	9.79±0.34	(5)	7.92±0.17	(4)	9.85±0.25	(12)	5,900±2,200	(5)
V357A	6.13±0.13*	(5)	9.83±0.18	(4)	7.89±0.27	(4)	9.68±0.1	(8)	28,400±7,700	(4)
V358A	5.89±0.15*	(5)	9.62±0.09	(4)	7.84±0.13	(4)	9.81±0.06	(8)	34,100±10,500	(4)
F359A	5.49±0.12*	(5)	9.5±0.15	(4)	7.13±0.19*	(3)	9.22±0.1	(10)	40,400±9,200	(4)
P360A	5.65±0.06*	(5)	9.01±0.13*	(4)	7.3±0.28*	(4)	9.22±0.1	(10)	89,400±15,800*	(5)
W361A	5.99±0.08*	(5)	9.48±0.08	(4)	7.47±0.24*	(4)	9.55±0.11	(10)	46,200±18,200	(5)
R362A	5.96±0.06*	(4)	9.53±0.13	(4)	7.33±0.22*	(4)	9.66±0.14	(8)	27,300±1,000	(4)
P363A	5.48±0.26*	(4)	9.44±0.14	(4)	7.26±0.13*	(4)	9.45±0.23	(8)	19,400±5,800	(4)
S364A	6.61±0.07	(4)	9.73±0.06	(4)	8.27±0.34	(4)	9.72±0.08	(10)	32,600±11,200	(5)
N365A	6.68±0.16	(4)	9.96±0.06	(4)	8.68±0.24	(4)	9.63±0.1	(10)	29,400±11,900	(5)
K366A	6.47±0.17	(4)	9.69±0.05	(4)	7.96±0.23	(4)	9.71±0.12	(10)	43,000±16,000	(5)
M367A	6.24±0.11	(4)	9.67±0.09	(4)	7.67±0.25	(4)	9.53±0.14	(8)	25,600±7,900	(4)
L368A	6.5±0.13	(4)	9.81±0.04	(4)	8.07±0.19	(4)	9.68±0.11	(8)	28,200±13,100	(4)
G369A	6.41±0.1	(4)	9.89±0.02	(4)	8.1±0.19	(4)	9.64±0.14	(10)	40,600±18,800	(5)
K370A	N.D.		N.D.		N.D.		N.D.		N.D.	
I371A	N.D.		N.D.		N.D.		N.D.		N.D.	
Y372A	6.09±0.09*	(4)	9.4±0.06	(4)	7.55±0.27	(4)	9.85±0.19	(8)	21,700±8,600	(4)
D373A	5.76±0.22*	(6)	9.36±0.09	(4)	7.76±0.28	(4)	9.28±0.15	(8)	43,500±22,700	(5)
Y374A	6.64±0.17	(4)	9.79±0.13	(4)	8.23±0.09	(4)	9.83±0.13	(8)	26,300±7,500	(4)
V375A	6.48±0.19	(5)	9.83±0.08	(4)	8.29±0.25	(4)	9.72±0.09	(8)	22,500±8,000	(4)
M376A	6.06±0.21*	(6)	9.8±0.15	(6)	8.11±0.24	(4)	9.88±0.1	(8)	23,600±3,200	(4)

Table 5.1 Effect of single alanine mutation in ECL3 of hCTR$_a$Leu on ligand affinity and cell surface expression. *pIC_{50} (negative logarithm of the concentration of ligand that produces half the maximal displacement of the iodinated radioligand). Data were obtained by fitting a three parameter logistic equation and data for radioligand occupancy were corrected using the Cheng-Prusoff equation (Equation 7, Section 2.6.1) to calculate pK_i. All values expressed as pK_i are mean±S.E.M. of 3 to 12 independent experiments conducted in duplicate. Homologous whole cell binding was used to determine B_{max} values by fitting (Equation 5, Section 2.6.1) to concentration-response data performed in presence of two different concentrations of the radioligand ^{125}I-sCT(8-32). B_{max} values were converted to sites/cell (Equation 6, Section 2.6.1). Significance of changes in affinity of each ligand was determined by comparison of the WT to the other receptor mutants in a one-way analysis of variance and Dunnett's post-test ($p<0.05$ represented by *). (N.D.) affinity or expression not determined as no radioligand binding was detected.*

	hCT				sCT				pCT				sCT(8-32)		rAmy		hαCGRP	
	ΔpK_i		ΔpK_A		ΔpK_i		ΔpK_A		ΔpK_i		ΔpK_A		ΔpK_i		ΔpK_A		ΔpK_A	
WT	0.0±0.09	(8)	0.0±0.08	(34)	0.0±0.04	(8)	0.0±0.07	(36)	0.0±0.1	(8)	0.0±0.11	(31)	0.0±0.08	(10)	0.0±0.15	(16)	0.0±0.15	(17)
F356A	-0.13±0.11	(5)	-1.43±0.2*	(4)	-0.08±0.34	(5)	-0.667±0.16	(5)	-0.37±0.17	(4)	-1.05±0.21	(4)	0.24±0.25	(12)	-0.6±0.27	(4)	-0.65±0.26	(5)
V357A	-0.59±0.13*	(5)	-1.01±0.18*	(4)	-0.03±0.18	(4)	-0.26±0.14	6	-0.4±0.27	(4)	-0.23±0.24	(4)	0.07±0.1	(8)	-0.41±0.32	(5)	-0.1±0.34	(5)
V358A	-0.83±0.15*	(5)	-0.3±0.26	(4)	-0.25±0.09	(4)	0.15±0.25	(4)	-0.45±0.13	(4)	-0.68±0.29	(4)	0.2±0.06	(8)	-0.25±0.32	(4)	0.02±0.36	(5)
F359A	-1.22±0.12*	(5)	-0.99±0.17*	(5)	-0.37±0.15	(4)	0.1±0.19	(5)	-1.15±0.19*	(3)	-0.41±0.25	(4)	-0.39±0.1	(10)	-0.43±0.3	(5)	0.08±0.49	(5)
P360A	-1.07±0.06*	(5)	-1.35±0.15*	(5)	-0.85±0.13*	(4)	-0.39±0.16	(5)	-0.98±0.28*	(4)	-1.25±0.24*	(4)	-0.39±0.1	(10)	-0.48±0.25	(5)	0.17±0.53	(5)
W361A	-0.73±0.08*	(5)	-0.78±0.18	(5)	-0.39±0.08	(4)	-0.11±0.2	(5)	-0.82±0.24*	(4)	-0.97±0.25	(4)	-0.05±0.11	(10)	-0.35±0.27	(5)	-0.59±0.26	(5)
R362A	-0.76±0.06*	(4)	-1.29±0.2*	(4)	-0.34±0.13	(4)	-0.64±0.21	(4)	-0.96±0.22*	(4)	-1.58±0.22*	(4)	0.06±0.14	(8)	-0.5±0.37	(4)	0.2±0.5	(5)
P363A	-1.24±0.26*	(4)	-1.27±0.23*	(4)	-0.42±0.14	(4)	-0.11±0.19	(5)	-1.03±0.13*	(4)	-1.62±0.24*	(4)	-0.16±0.23	(8)	-0.28±0.26	(6)	-0.18±0.76	(5)
S364A	-0.11±0.07	(4)	-0.03±0.21	(5)	-0.14±0.06	(4)	-0.08±0.2	(5)	-0.02±0.34	(4)	0.04±0.34	(4)	0.11±0.08	(10)	0.38±0.52	(4)	0.15±0.3	(5)
N365A	-0.04±0.16	(4)	-0.04±0.23	(5)	0.09±0.06	(4)	0.09±0.23	(5)	0.39±0.24	(4)	0.2±0.38	(4)	0.02±0.1	(10)	0.14±0.39	(4)	0.07±0.24	(5)
K366A	-0.25±0.17	(4)	0.21±0.3	(4)	-0.18±0.05	(4)	0.07±0.24	(5)	-0.33±0.23	(4)	0.36±0.41	(4)	0.1±0.12	(10)	0.04±0.4	(4)	0.62±0.34	(5)
M367A	-0.48±0.11	(4)	0.08±0.25	(5)	-0.2±0.09	(4)	0.24±0.25	(5)	-0.61±0.25	(4)	0.05±0.32	(4)	-0.08±0.14	(8)	0.26±0.32	(4)	-0.07±0.21	(7)
L368A	-0.21±0.13	(4)	0.22±0.31	(4)	-0.06±0.04	(4)	-0.07±0.18	(5)	-0.22±0.19	(4)	-0.51±0.35	(4)	0.07±0.11	(8)	-0.14±0.27	(5)	0.28±0.31	(5)
G369A	-0.31±0.1	(4)	-0.18±0.21	(4)	0.02±0.02	(4)	-0.17±0.23	(5)	-0.19±0.19	(4)	-0.13±0.29	(4)	0.03±0.14	(10)	-0.21±0.37	(4)	-0.23±0.21	(6)
K370A	N.D.		N.D.		N.D.		N.D.		N.D.		N.D.		N.D.		N.D.		N.D.	
I371A	N.D.		0.17±1.01	(4)	N.D.		0.49±0.71	(5)	N.D.		-0.2±0.98	(4)	N.D.		0.88±0.56		-0.37±0.46	(5)
Y372A	-0.63±0.09*	(4)	-2.4±0.21*	(4)	-0.46±0.06	(4)	-0.89±0.2*	(4)	-0.73±0.27	(4)	-1.83±0.23*	(4)	0.24±0.19	(8)	-1.51±0.24*	(4)	-0.49±0.81	(5)
D373A	-0.96±0.22*	(6)	-0.99±0.24*	(4)	0.5±0.09	(4)	-0.22±0.19	(4)	-.053±0.28	(4)	-1.47±0.28*	(4)	-0.33±0.15	(8)	0.02±0.39	(5)	0.29±0.74	(5)
Y374A	0.07±0.17	(4)	-0.16±0.27	(4)	-0.08±0.13	(4)	0.06±0.2	(5)	-0.06±0.09	(4)	0.26±0.37	(4)	0.23±0.13	(8)	-0.01±0.32	(4)	-0.04±0.33	(5)
V375A	-0.24±0.19	(5)	-0.3±0.17	(5)	-0.04±0.08	(4)	-0.29±0.19	(5)	0.0±0.25	(4)	-0.25±0.24	(4)	0.11±0.09	(8)	0.03±0.28	(5)	-0.07±0.24	(5)
M376A	-0.66±0.21*	(6)	-1.49±0.3*	(4)	-0.06±0.15	(6)	-0.3±0.2	(5)	-0.17±0.24	(4)	-0.84±0.36	(4)	0.27±0.1	(8)	-0.68±0.36	(5)	-0.7±0.59	(5)

Table 5.2 Comparison of the effect of single alanine mutation in ECL2 of hCTR$_a$Leu on equilibrium affinity and functional affinity. *Functional affinity (pK_A) was derived by applying the operational model of agonism (Black and Leff, 1983) to the cAMP concentration-response curves (Section 5.2.3.1). Data reported in this table (and represented in Figure 5.7) are the change from WT of functional affinity (ΔpK_A). For comparison, equilibrium affinity (calculated as described in Table 5.1) are also reported in this table as change from WT (ΔpK_i). All values are mean±S.E.M. Significance of changes in affinity of each ligand was determined by comparison of the WT to receptor mutants by one-way analysis of variance and Dunnett's post-test ($p<0.05$ represented by *). (N.D.) affinity not determined as no radioligand binding was detected.*

5.2.3 Assessment of intracellular signalling by calcitonin receptor peptides

Cells were stimulated with relevant concentrations of hCT, sCT, pCT, rAmy or hαCGRP. Concentration-response curves generated were fit to a three-parameter logistic equation to determine potency (pEC_{50}) and maximal response (E_{max}). For each mutation and ligand assessed, an operational model of partial agonism (Black and Leff, 1983) (Equation 7, Section 2.6.1) was also applied to derive functional affinities (pK_A) and efficacy of coupling of these receptors to each pathway log(τ). As P360A showed significant changes in expression when compared to WT and its efficacy was corrected for receptor expression log(τ_c).

5.2.3.1 cAMP signalling

cAMP accumulation profiles were measured following 30 min of stimulation with hCT (***Figure 5.8***), sCT (***Figure 5.9***), pCT (***Figure 5.10***), rAmy (***Figure 5.11***) or hαCGRP (***Figure 5.12***) peptides. pEC_{50}, E_{max} and derived pK_A and log(τ) (or log(τ_c)) are summarised in (***Table 5.3 and 5.4***). K370A showed no response for any of the ligand assessed in this pathway within the concentration range assessed, thus functional data could not be defined for this mutation.

5.2.3.1.1 CT peptides

From our functional characterisation of the different CT peptides (Section 5.2.3.1) we have derived functional affinity pK_A (or the equilibrium-dissociation constant) of the ligand-receptor complex, through the application of the operational model of Black and Leff (Black and Leff, 1983) to the cAMP concentration-response curves. Changes in affinity (either functional ΔpK_A or at equilibrium ΔpK_i) from WT were compared (***Figure 5.13, Table 5.2***). There was on overall correlation of the effect of mutation relative to the WT between the two measures of affinity. Interestingly F356 and Y372A showed a more pronounced and significant reduction on functional affinity relative to the pK_i determined by competition binding for all CT agonist peptides assessed. Based on a weak signalling in our functional characterisation and to the inability of detect specific binding, I371A is likely to be expressed at very low levels, and this is reflected in the high errors in the estimated pK_A. Similarly, K370A is unlikely to

be expressed at the cell surface, as it did not produce any detectable intracellular response in any of the pathways measured, nor specifically bind the radioligand used.

Potency. At the WT receptor, the CT peptides showed a potency ranging between 0.1-0.01 nM (***Table 5.3***). Statistical analysis comparing WT response to receptor mutants revealed that potency of sCT was unaffected by any of the mutations, whereas both hCT and pCT displayed reduced pEC_{50} at R362A, P363A and Y372A receptor mutants. D373A also showed a significant reduction of pEC_{50} when stimulated with pCT (with hCT sharing a similar trend). F356A, V357A, F359A, P360 and M376A significant reduced potency for hCT, but not for the other CT agonists. None of the other mutation caused significant changes in potency for any of the CT peptides.

Maximal response. When comparing E_{max}, mutation of two clusters of residues resulted in significant changes in the presence of all CT ligands; F356A, V357A and P360A increased E_{max}, whereas I371A displayed reduced maximal response. W361A, R362A, V375A, Y372A and D373A selectively enhanced maximal responses for hCT and pCT, but not for sCT. F359A and G369A increased the maximal response to hCT, but not sCT or pCT, while P363A increased E_{max} in response to pCT, but not the other two CT agonists. Interestingly, N365A and M367A significantly and selectively decreased E_{max} of the sCT response, whereas L368A reduced the maximal response to hCT only. The K366A mutation reduced the E_{max} of both hCT and sCT peptides, with a similar trend for pCT that failed to reach statistical significance.

Efficacy. Statistical analysis comparing the coupling efficacy log(τ) of each mutant receptor to WT (***Figure 5.13*** and ***Table 5.3***) revealed that I371A reduced efficacy of all CT peptides 5 to 8 fold. P360 and M367A selectively reduced efficacy for sCT, and L368A for hCT. Neither of these two mutations impacted on pCT efficacy. A second cluster of residues significantly improved CT ligand efficacy. F356A and V357A increased log(τ) for all CT ligands, while W361A, R362A, V375A, Y372A and D373A improved efficacy for hCT and pCT (but not sCT). F359A and G369A mutation enhanced hCT efficacy only, while P363A selectively augmented the response of pCT. No other substitutions had a significant effect on efficacy of any of the CT agonists.

5.2.3.1.2 rAmy and hαCGRP peptides

In the absence of equilibrium binding affinity, pK_A derived from cAMP concentration-response curves was used as a surrogate for the effects of Ala mutagenesis on affinity of rAmy and hαCGRP. Statistical analysis of changes in affinity of mutant receptors relative to the WT (ΔpK_A) (***Figure 5.14, Table 5.2***), revealed that Ala substitution had only limited effect on affinity of either peptide. Only Y372A significantly reduced the affinity of rAmy, while functional affinity of hαCGRP was not significantly altered (***Figure 5.13***).

Potency. pEC_{50} of rAmy and hαCGRP was only at the WT receptor of about 10 nM and the pEC_{50} was not significantly affected by any of the mutations introduced in ECL3 and adjacent TMs (***Figures 5.11 and 5.12, Table 5.2***).

Maximal response. On the other hand, statistical analysis of the maximal response across receptors revealed that D373A and I371A reduced E_{max} of both rAmy and hαCGRP. F359A, P360A, R362A, P363A and M376A reduced E_{max}, when compared to WT receptor response, only in presence of hαCGRP, whereas S364A revealed reduced E_{max} only for rAmy. Substitution of Y372 had opposing effects on these two peptides: increasing the maximal response for rAmy, whilst significantly reducing that of hαCGRP. No other mutations produced significant changes in either rAmy or hαCGRP maximal response.

Efficacy. The pattern of mutational effect on rAmy efficacy most closely resembled that observed for sCT, with only few mutations impacting on cAMP signalling. Of these, P360A and I371A, that reduced sCT, also reduced rAmy efficacy. S361A induced a selective, weak attenuation of rAmy efficacy, not seen with either CT peptides or hαCGRP, while Y372A increased efficacy, an effect also seen with hCT and pCT, but not sCT or hαCGRP (***Figure 5.14*** and ***Table 5.4***). In contrast, there was a broad impact of mutations on hαCGRP efficacy, but whereas many mutants increased efficacy for subsets of CT peptides, only reduced efficacy was observed. Of these, only P360A (rAmy and sCT) and I371A (all peptides) engendered effects common to other peptides, selective loss of efficacy was seen for F359A, R362A, P363A, Y372A, D373A and M376A mutants.

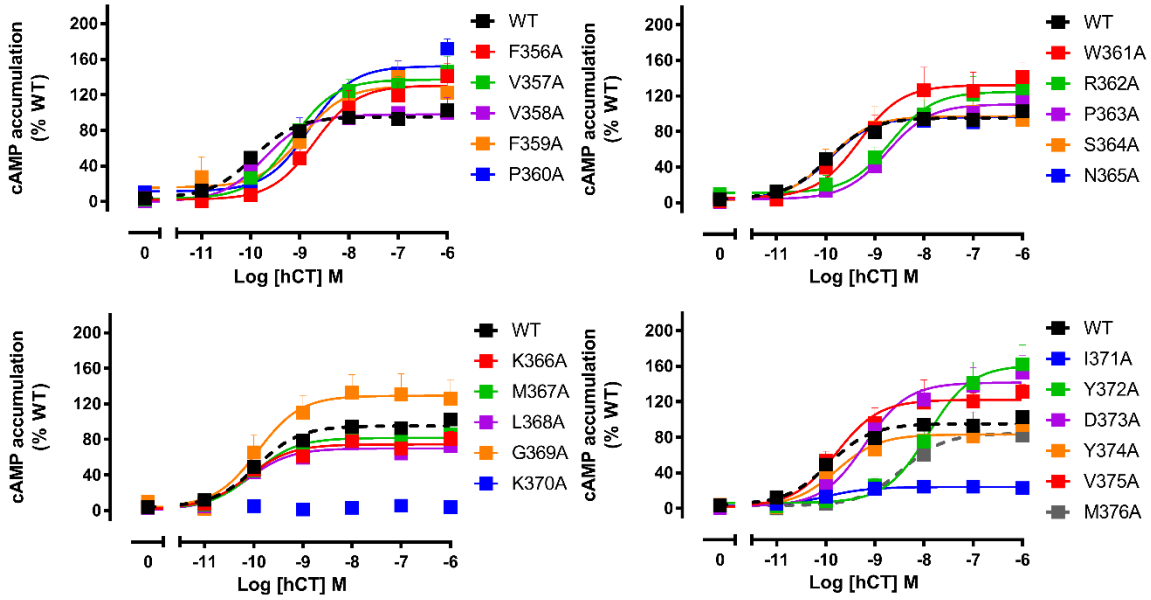

Figure 5.8 cAMP accumulation profiles elicited by hCT in CV-1-FlpIn cells stably expressing hCTR$_a$Leu ECL3 single alanine mutations. *cAMP formation in the presence of hCT was normalized to responses of the internal control (0.1 mM forskolin) and fit to a three parameter logistic equation. Data was subsequently normalised to WT receptor response. All values are mean+S.E.M. of 4 to 5 (WT N=36) independent experiments conducted in duplicate.*

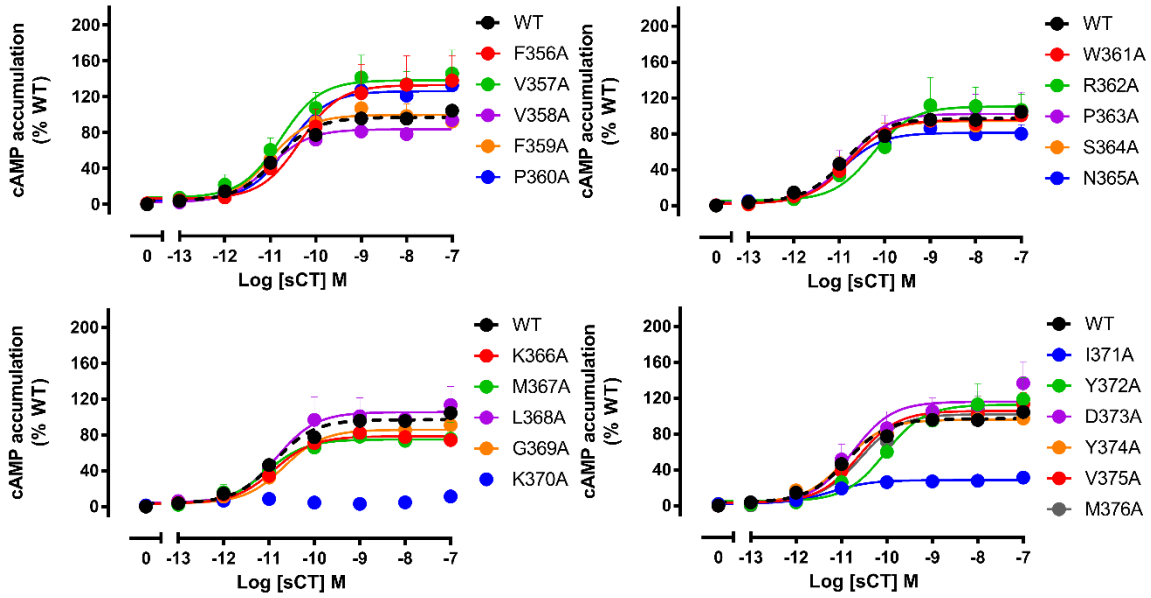

Figure 5.9 cAMP accumulation profiles elicited by sCT in CV-1-FlpIn cells stably expressing hCTR$_a$Leu ECL3 single alanine mutations. *cAMP formation in the presence of sCT was normalized to responses of the internal control (0.1 mM forskolin) and fit to a three parameter logistic equation. Data was subsequently normalised to WT receptor response. All values are mean+S.E.M. of 4 to 6 (WT N=36) independent experiments conducted in duplicate.*

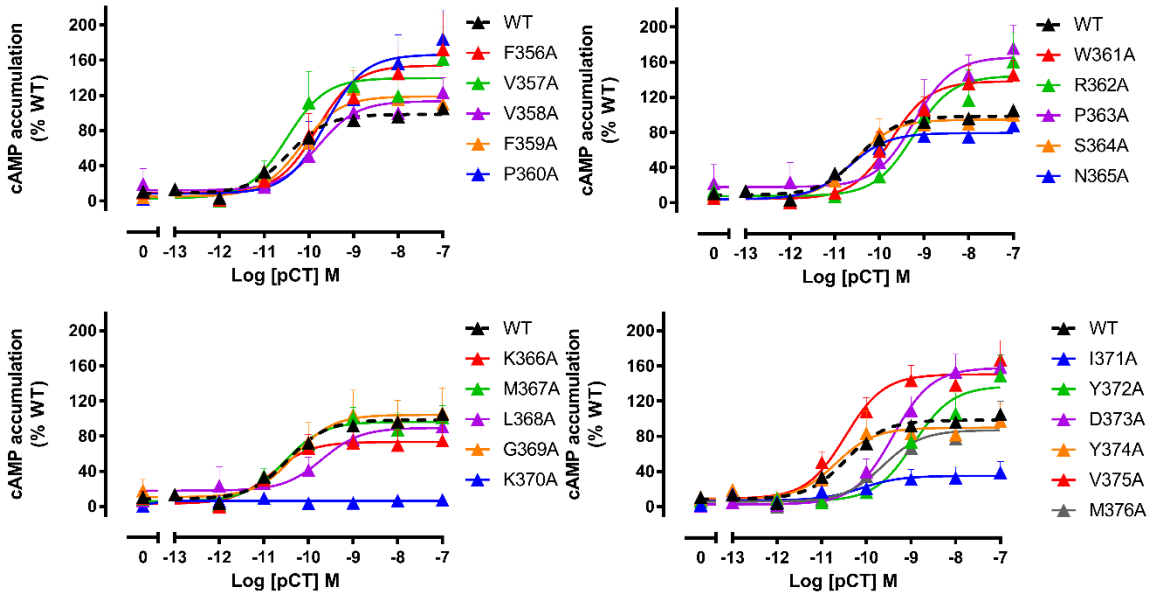

Figure 5.10 cAMP accumulation profiles elicited by pCT in CV-1-FlpIn cells stably expressing hCTR$_a$Leu ECL3 single alanine mutations. *cAMP formation in the presence of pCT was normalized to responses of the internal control (0.1 mM forskolin) and fit to a three parameter logistic equation. Data was subsequently normalised to WT receptor response. All values are mean+S.E.M. of 3 to 4 (WT N=31) independent experiments conducted in duplicate.*

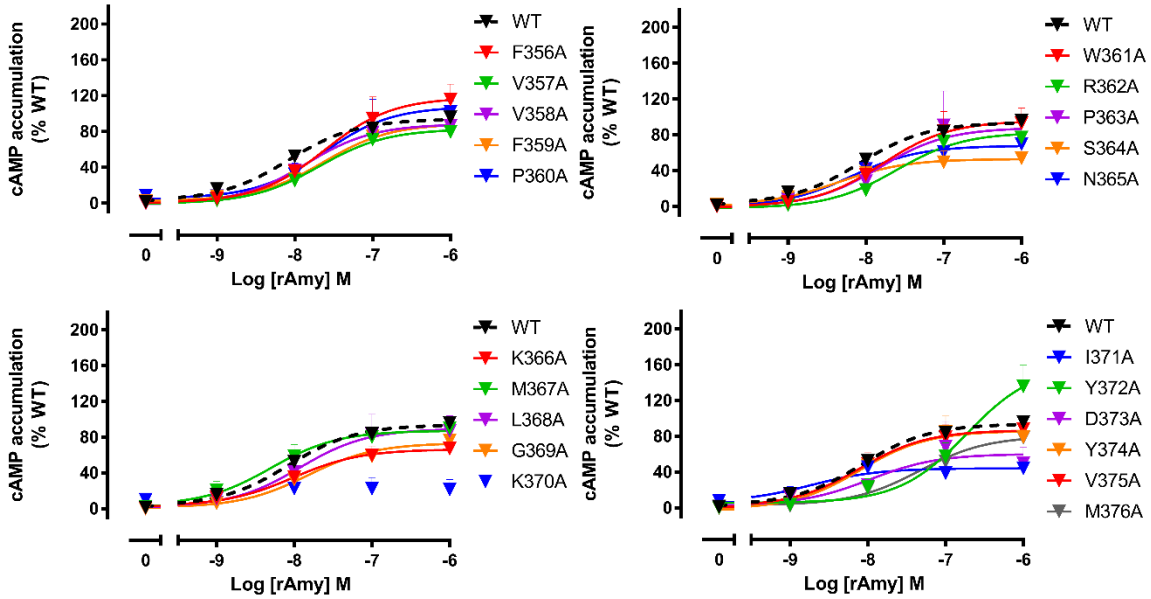

Figure 5.11 cAMP accumulation profiles elicited by rAmy in CV-1-FlpIn cells stably expressing hCTR$_a$Leu ECL3 single alanine mutations. *cAMP formation in the presence of rAmy was normalized to responses of the internal control (0.1 mM forskolin) and fit to a three parameter logistic equation. Data was subsequently normalised to WT receptor response. All values are mean+S.E.M. of 4 to 6 (WT N=16) independent experiments conducted in duplicate.*

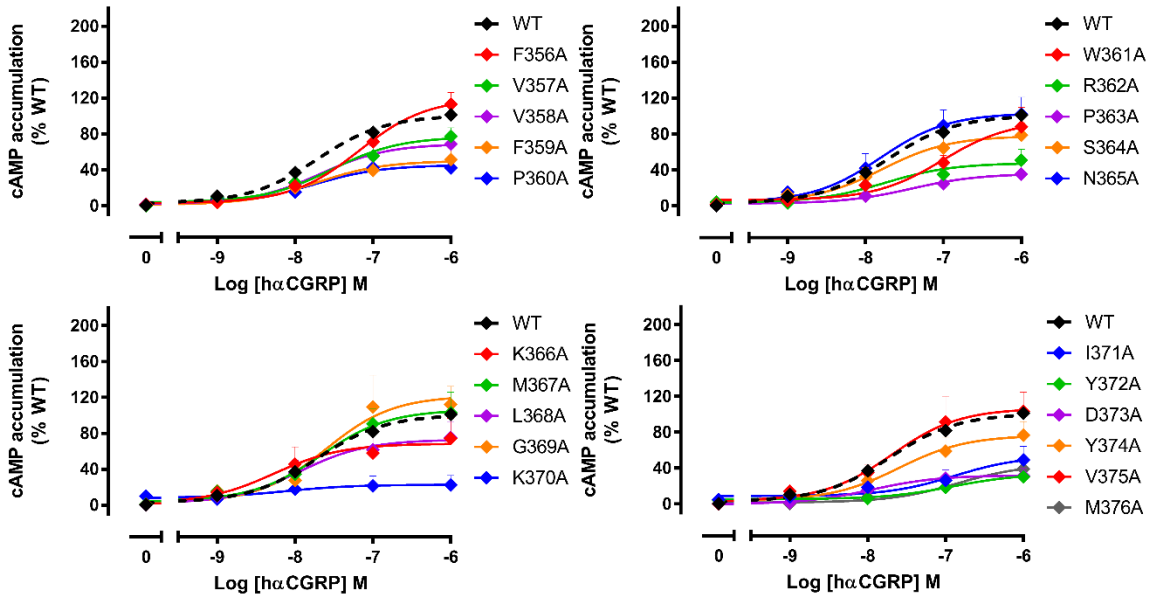

Figure 5.12 cAMP accumulation profiles elicited by hαCGRP in CV-1-FlpIn cells stably expressing hCTR$_a$Leu ECL3 single alanine mutations. *cAMP formation in the presence of hαCGRP was normalized to responses of the internal control (0.1 mM forskolin) and fit to a three parameter logistic equation. Data was subsequently normalised to WT receptor response. All values are mean+S.E.M. of 5 to 7 (WT N=17) independent experiments conducted in duplicate.*

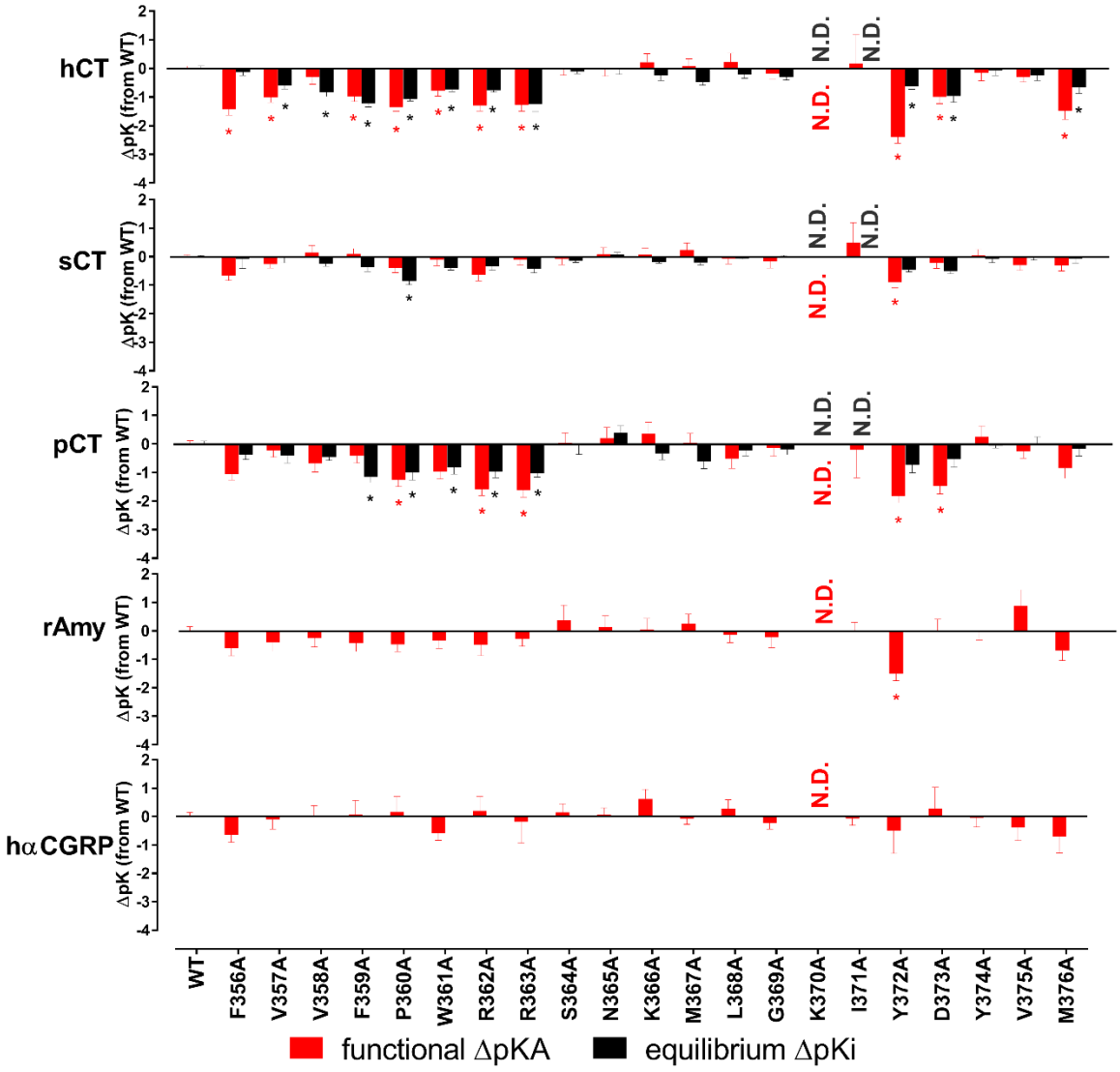

Figure 5.13 Comparison between equilibrium affinity and cAMP functional affinity (pK_A). *Functional affinity is presented as differences relative to WT (ΔpK_i, in black). Data from (Figures 5.8-12) were fit to the operational model of agonism (Black and Leff, 1983) to calculate functional affinity (pK_A) of each receptor (mutant or WT) to the cAMP signalling pathway. Graphs show the differences relative to WT (ΔpK_A, in red). All values are mean+S.E.M. Significance of changes was determined by comparison of the WT to the other receptor mutants in a one-way analysis of variance and Dunnett's post-test ($p<0.05$ represented by *). (N.D.) efficacy not determined.*

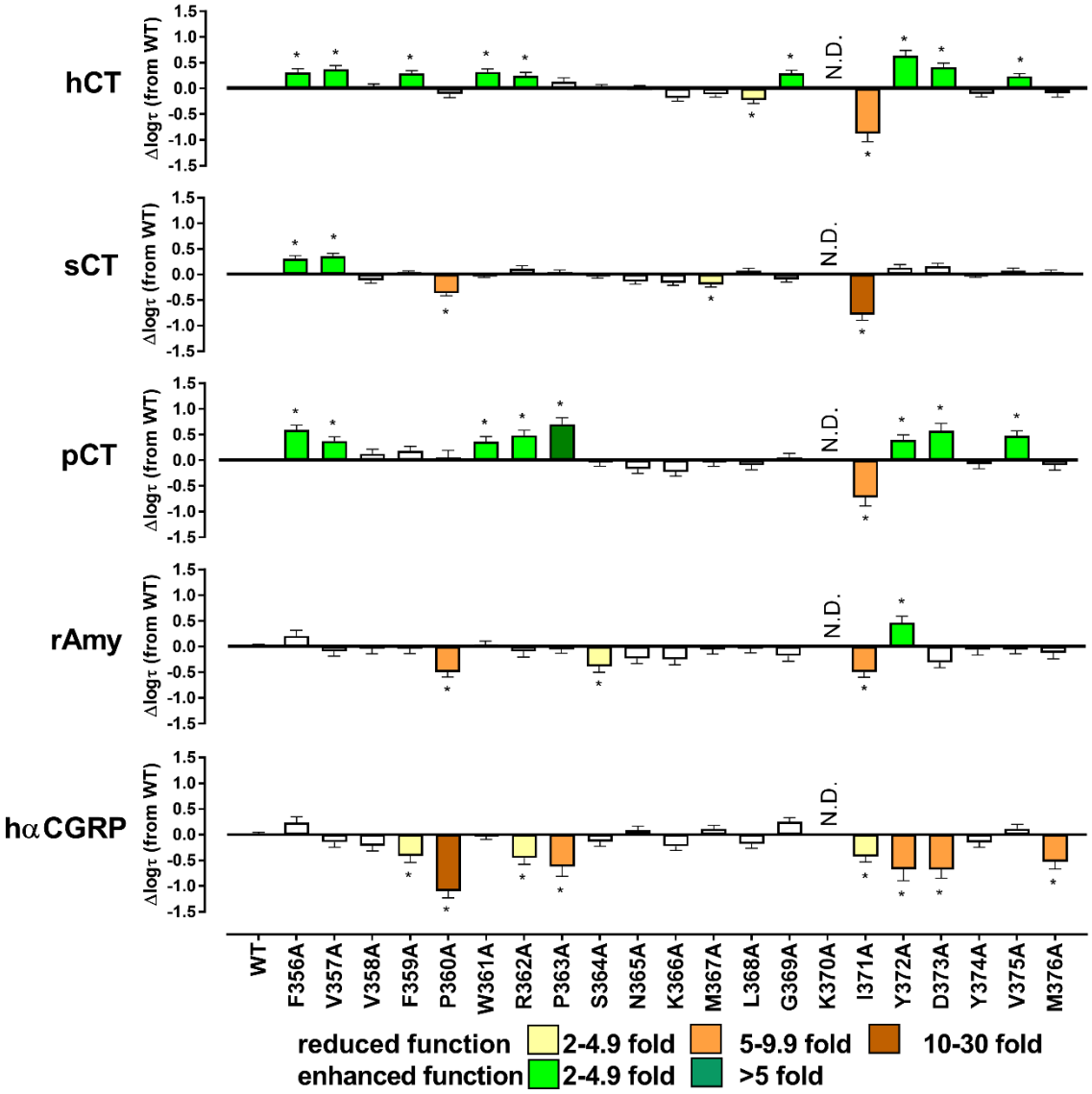

Figure 5.14 Effect of single alanine mutation in ECL3 of hCTR$_a$Leu on efficacy for cAMP accumulation. *Data from (Figures 5.8-12 were fit to the operational model of agonism to calculate coupling efficacy log(τ) of each receptor (mutant or WT) to the cAMP signalling pathway. The log(τ) values of each receptor were then corrected for expression, where this was significantly different, to obtain log(τc). Graphs show the differences relative to WT. All values are mean+S.E.M. of 3 to 7 (WT 16 to 36) independent experiments conducted in duplicate. Significance of changes was determined by comparison of the WT to the other receptor mutants in a one-way analysis of variance and Dunnett's post-test (p<0.05 represented by *). (N.D.) efficacy not determined.*

	hCT				sCT				pCT			
	pEC_{50}	E_{max}	Log(τ)		pEC_{50}	E_{max}	Log(τ)		pEC_{50}	E_{max}	Log(τ)	
WT	9.94±0.07	100±1.8	-0.09±0.02	(34)	10.88±0.05	100±1.4	-0.08±0.03	(36)	10.45±0.07	100±1.8	-0.08±0.03	(31)
F356A	8.71±0.18*	130.5±7.5*	0.22±0.07*	(4)	10.34±0.32	133.1±12.2*	0.24±0.06*	(5)	9.82±0.35	153.9±16.7*	0.51±0.1*	(4)
V357A	9.15±0.14*	137.1±5.8*	0.28±0.07*	(4)	10.77±0.24	138.5±8.9*	0.29±0.08*	6	10.49±0.38	139.6±14.5*	0.29±0.08*	(4)
V358A	9.72±0.16	97.8±4.4	-0.07±0.06	(4)	11.01±0.18	83.7±4.0	0.05±0.09	(4)	9.79±0.25	113.4±8.2	0.05±0.09	(4)
F359A	8.95±0.24*	129.9±9*	0.2±0.06*	(5)	11.01±0.18	99.7±4.9	0.1±0.09	(5)	10.18±0.31	118.8±10.9	0.10±0.09	(4)
P360A	8.8±0.17*	152.2±8.1*	-0.2±0.07[(c)]	(5)	10.61±0.19	126.2±6.7*	-0.43±0.05*[(c)]	(5)	9.63±0.27	166.3±14*	-0.03±0.14[(c)]	(4)
W361A	9.32±0.25	132.1±9.3*	0.23±0.06*	(5)	10.79±0.14	95.4±3.8	-0.28±0.1	(5)	9.74±0.21	138.3±9.3*	0.28±0.1*	(4)
R362A	8.68±0.24*	124.7±8.9*	0.16±0.07*	(4)	10.26±0.28	110.5±9.2	0.04±0.1	(4)	9.24±0.31*	144.5±15.9*	0.41±0.1*	(4)
P363A	8.74±0.13*	110.5±4.7	0.04±0.07	(4)	10.8±0.26	102.2±7.3	-0.03±0.05	(5)	9.22±0.29*	165.9±16.4*	0.62±0.13*	(4)
S364A	9.94±0.36	97.1±9.2	-0.07±0.06	(5)	10.82±0.19	94.3±5	-0.13±0.05	(5)	10.54±0.21	94.5±5.2	-0.11±0.08	(4)
N365A	9.91±0.16	95.9±4.1	-0.08±0.05	(5)	10.93±0.23	81±5.1*	-0.21±0.05	(5)	10.68±0.39	79.3±7.9	-0.25±0.09	(4)
K366A	10.11±0.17	74.4±3.3*	-0.28±0.06	(4)	10.89±0.16	78.5±3.4*	-0.23±0.05	(5)	10.81±0.34	73.4±13	-0.31±0.08	(4)
M367A	10.01±0.19	81.7±4.1	-0.21±0.05	(5)	11.06±0.33	75±6.7*	-0.27±0.05*	(5)	10.54±0.26	96.3±6.3	-0.09±0.1	(4)
L368A	10.13±0.23	69.8±4.2*	-0.32±0.06*	(4)	10.83±0.27	105.5±7.7	0.0±0.05	(5)	9.69±0.28	89.4±6.6	-0.17±0.1	(4)
G369A	9.92±0.27	129.1±9.1*	0.2±0.06*	(4)	10.66±0.16	85.8±3.7	-0.17±0.05	(5)	10.32±0.43	104.3±11.8	-0.03±0.09	(4)
K370A	N.D.	N.D.	N.D.		N.D.	N.D.	N.D.		N.D.	N.D.	N.D.	
I371A	9.99±0.47	24±2.7*	-0.97±0.15*[(a)]	(4)	11.23±0.3	28.4±2.1*	-0.86±0.11*[(a)]	(5)	10.12±0.58	34.9±5.2*	-0.8±0.17*	(4)
Y372A	7.92±0.19*	161.2±12.2*	0.54±0.1*	(4)	10.04±0.27	112.6±9.5	0.06±0.06	(4)	8.94±0.24*	137.2±12.8*	0.32±0.09*	(4)
D373A	9.2±0.19	141.6±8.2*	0.32±0.08*	(4)	10.76±0.25	116±8.1	0.09±0.05	(4)	9.41±0.16*	157.9±8.7*	0.5±0.15*	(4)
Y374A	9.78±0.23	83.2±5.1	-0.2±0.06	(4)	10.93±0.18	95.9±4.6	-0.08±0.05	(5)	10.69±0.39	89.7±8.6	-0.16±0.09	(4)
V375A	9.79±0.22	122.2±7.2*	0.14±0.05*	(5)	10.63±0.17	105.6±4.9	0.0±0.05	(5)	10.47±0.21	150.5±8.3*	0.4±0.1*	(4)
M376A	8.44±0.37*	84.3±10.4	-0.18±0.08	(4)	10.58±0.2	102±5.7	-0.03±0.05	(5)	9.63±0.4	86.9±10.7	-0.18±0.09	(4)

Table 5.3 Effect of single alanine mutation in ECL3 of hCTR$_a$Leu on cAMP signalling in response to CT peptides. *For each receptor and ligand, data from Figure 5.8-10 were fit to a three-parameter logistic equation to derive pEC_{50} (negative logarithm of the concentration of ligand that produces half the maximal response) and E_{max} (maximal response, as % of WT). The log(τ) reported in this table represents the operational coupling efficacy of each receptor (mutant or WT), where receptor expression was either unable to be identified on not significantly different. Where expression by radioligand binding was significantly different, values were corrected for the expression change to give log(τ_c) [(c)]. [(a)] Represents those mutation where expression could not be determined via radioligand binding. All values are mean+S.E.M. of 4 to 36 independent experiments conducted in duplicate For each ligand, significance of changes in pEC_{50}, E_{max} and log(τ) was determined by comparison of the WT to the other receptor mutants in a one-way analysis of variance and Dunnett's post-test ($p<0.05$ represented by *). (N.D.) pEC_{50}, E_{max} or efficacy not determined.*

	rAmy				hαCGRP			
	pEC_{50}	E_{max}	Log(τ)		pEC_{50}	E_{max}	Log(τ)	
WT	8.08±0.1	100±3.3	-0.09±0.04	(16)	7.69±0.11	100±4	-0.1±0.05	(17)
F356A	7.62±0.3	118.1±14.2	0.12±0.11	(4)	7.18±0.15	119.8±9.1	0.13±0.12	(5)
V357A	7.69±0.27	82.9±9.1	-0.18±0.1	(5)	7.53±0.32	76.9±9.7	-0.25±0.1	(5)
V358A	7.86±0.36	88.4±12.6	-0.14±0.1	(4)	7.68±0.31	68.9±8.4	-0.32±0.1	(5)
F359A	7.63±0.25	89±8.8	-0.13±0.09	(5)	7.73±0.41	50±7.9*	-0.52±0.12*	(5)
P360A	7.63±0.3	108.1±12.7	-0.59±0.09*[(c)]	(5)	7.76±0.28	45.2±4.9*	-1.2±0.13*[(c)]	(5)
W361A	7.79±0.31	95.7±12	-0.07±0.09	(5)	7.01±0.3	95.1±14.8	-0.12±0.07	(5)
R362A	7.61±0.32	82.7±11.1	-0.18±0.11	(4)	7.75±0.48	47.5±8.4*	-0.56±0.12*	(5)
P363A	7.82±0.55	87.9±19.3	-0.14±0.08	(6)	7.41±0.47	35.7±6.9*	-0.72±0.19*	(5)
S364A	8.35±0.38	52.9±6.6*	-0.48±0.11*	(4)	7.78±0.31	77.8±9.2	-0.24±0.09	(5)
N365A	8.18±0.32	67.8±7.8	-0.32±0.1	(4)	7.81±0.31	103.2±12.2	-0.02±0.08	(5)
K366A	8.02±0.26	66.3±6.3	-0.34±0.1	(4)	8.27±0.54	68.4±12.5	-0.33±0.08	(5)
M367A	8.3±0.26	87.2±7.5	-0.15±0.09	(4)	7.67±0.31	106.3±12.7	0.01±0.07	(7)
L368A	7.93±0.34	89.5±11.6	-0.13±0.08	(5)	7.94±0.4	72.9±11.3	-0.28±0.09	(5)
G369A	7.83±0.2	73.4±5.8	-0.27±0.11	(4)	7.61±0.38	121.9±18.5	0.14±0.08	(6)
K370A	N.D.	N.D.	N.D.		N.D.	N.D.	N.D.	
I371A	8.1±0.27	86.8±8.7	-0.15±0.08		7.69±0.38	106.6±15.7	0.01±0.09	(5)
Y372A	6.73±0.26	159.2±24.4*	0.38±0.12*	(4)	6.91±0.45	33.6±7.3*	-0.77±0.25*	(5)
D373A	7.98±0.7	60.2±15.5*	-0.4±0.1	(5)	7.95±0.41	32±5.1*	-0.78±0.17*	(5)
Y374A	8.1±0.24	86±8.4	-0.16±0.1	(4)	7.6±0.36	76.5±10.8	-0.25±0.1	(5)
V375A	8.73±0.6	44.2±6.8*	-0.59±0.1*[(a)]	(5)	6.88±0.54	53.9±14.2*	-0.53±0.11*[(a)]	(5)
M376A	7.33±0.34	80.2±12	-0.21±0.12	(5)	6.85±0.26	44.3±6.6*	-0.63±0.14*	(5)

Table 5.4 Effect of single alanine mutation in ECL3 of hCTR$_a$Leu on cAMP signalling. *For each receptor and ligand, data from Figures 5.11-12 were fit to a three-parameter logistic equation to derive pEC_{50} (negative logarithm of the concentration of ligand that produces half the maximal response) and E_{max} (maximal response, as % of WT). The log(τ) reported in this table represents the operational coupling efficacy of each receptor (mutant or WT), where receptor expression was either unable to be identified on not significantly different. Where expression by radioligand binding was significantly different, values were corrected for the expression change to give log(τ_c) [(c)]. [(a)] Represents those mutation where expression could not be determined via radioligand binding. All values are mean+S.E.M. of 4 to 17 independent experiments conducted in duplicate For each ligand, significance of changes in pEC_{50}, E_{max} and log(τ) was determined by comparison of the WT to the other receptor mutants in a one-way analysis of variance and Dunnett's post-test (p<0.05 represented by *).(N.D.) pEC_{50}, E_{max} or efficacy not determined.*

5.2.3.2 IP1 signalling

IP1 accumulation over 60 minutes of peptide stimulation could only be determined for hCT (***Figure 5.15***), sCT (***Figure 5.16***) and pCT (***Figure 5.17***) peptides, but not for rAmy or hαCGRP. Potency, maximal responses and efficacies for all receptors and ligands are summarised in ***Table 5.5***.

Potency. All CT peptides were equipotent for the WT receptor, with pEC_{50} ranging from 1-1.5 nM (***Table 5.5***). K370A did not produce a detectable IP1 response in response to up to 1 μM of any of the CT peptides.

Similar to cAMP, sCT potency was not significantly affected by any substitution introduced into ECL3 or the adjacent TMs. In contrast, hCT and pCT pEC_{50} were significantly reduced for R362A. hCT was the most sensitive peptide to alanine substitution, with reduced potency also observed for V357A, V358A, F359A, P360A and Y374A mutations. Additionally, although sCT and pCT potency remained unaltered, P363A showed a response only when stimulated with 1 μM of hCT, indicating loss of function for hCT. No other mutation had a significant impact on the potency of any of the CTs assessed.

Maximal response. When maximal responses were compared to WT, two main clusters of residues affecting responses could be identified (***Figure 5.17*** and ***Table 5.5***). A first cluster including F356A, V357A, Y372A and I371A showed statistically decreased maximal response in presence of all CT peptides. R362A also displayed reduced E_{max} for all CT peptides, although this value for hCT data was not significant. Mutation of M376 reduced maximal responses to hCT and pCT without having a significant effect on sCT, whereas D373A significantly reduced E_{max} of pCT and showed a similar trend (although not significant) for sCT, but was unchanged for hCT. P363A did not produce a quantifiable response for hCT, while it decreased E_{max} for pCT. N365A substitution significantly impaired sCT E_{max}, while having no effect on either hCT or pCT responses. A second cluster of residues was distinguishable with mutations affecting both hCT and sCT E_{max}, with a different effect on pCT: V358A significantly improved maximal response to sCT and hCT while significantly decreasing pCT response. F359A and M367A also showed a similar trend for sCT and hCT (however data were significant only in presence of sCT), while having no augmentation of pCT E_{max}. Additionally, P360A E_{max} was significantly

increased in response to sCT, but not other CT peptides. No other significant changes were observed for any other mutation.

Efficacy. Alanine substitutions at the extracellular portions of TM6 and 7 (with the exception of residues V358 and F359) significantly reduced efficacy in IP1 of all CT peptides although selective differences were observed (***Figure 5.18*** and ***Table 5.5***). V357A, Y372A and I371A decreased efficacy for all three CT agonists, with F356A and R362A having a similar effect, although differences were not significant for hCT. P360A and M376A statistically reduced hCT and pCT (but not sCT) efficacy. D373A had a significant effect in reducing efficacy of pCT only, while N365A had a similar effect on sCT but not on the other two CT peptides. Alanine substitution of second group of residues significantly enhanced efficacy of hCT and sCT agonists, while no mutation had any relevant positive effect on pCT efficacy. Specifically, V358A, F359A and M367A enhanced sCT and hCT efficacy. Additionally, G369A enhanced hCT efficacy, but not the other CT peptides. The substitution of the other residues had no significant effect on the efficacy of these three agonists.

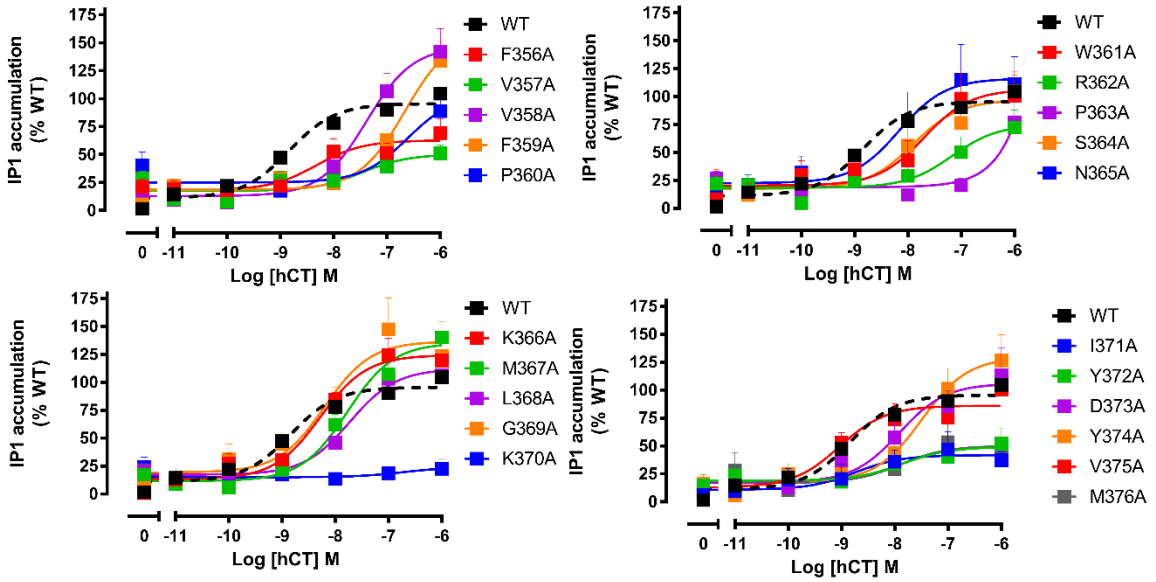

Figure 5.15 IP1 accumulation profiles elicited by hCT in CV-1-FlpIn cells stably expressing hCTR$_a$Leu ECL3 single alanine mutations. *IP1 formation in presence of hCT was normalized to an internal control (0.1 mM ATP) and data fit to a three parameter logistic equation. Data was subsequently normalised to WT receptor response. All values are mean+S.E.M. of 4 to 6 (WT N=26) independent experiments conducted in duplicate.*

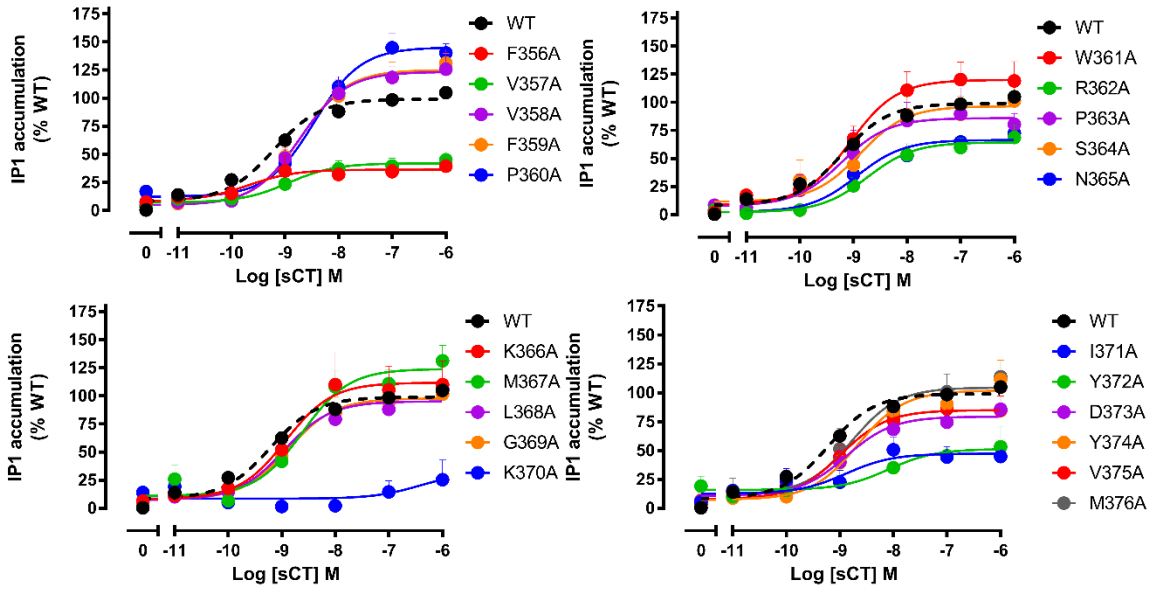

Figure 5.16 IP1 accumulation profiles elicited by sCT in CV-1-FlpIn cells stably expressing hCTR$_a$Leu ECL3 single alanine mutations. *IP1 formation in presence of sCT was normalized to an internal control (0.1 mM ATP) and data fit to a three parameter logistic equation. Data was subsequently normalised to WT receptor response. All values are mean+S.E.M. of 4 to 6 (WT N=26) independent experiments conducted in duplicate.*

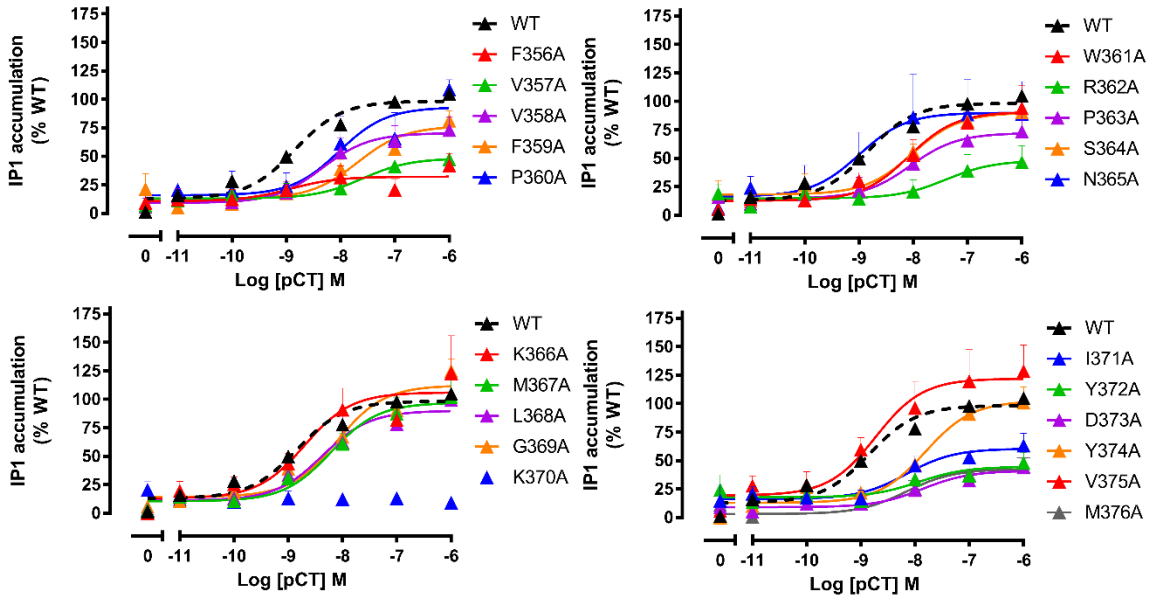

Figure 5.17 IP1 accumulation profiles elicited by pCT in CV-1-FlpIn cells stably expressing hCTR$_a$Leu ECL3 single alanine mutations. *IP1 formation in presence of pCT was normalized to an internal control (0.1 mM ATP) and data fit to a three parameter logistic equation. Data was subsequently normalised to WT receptor response. All values are mean+S.E.M. of 4 to 5 (WT N=25) independent experiments conducted in duplicate.*

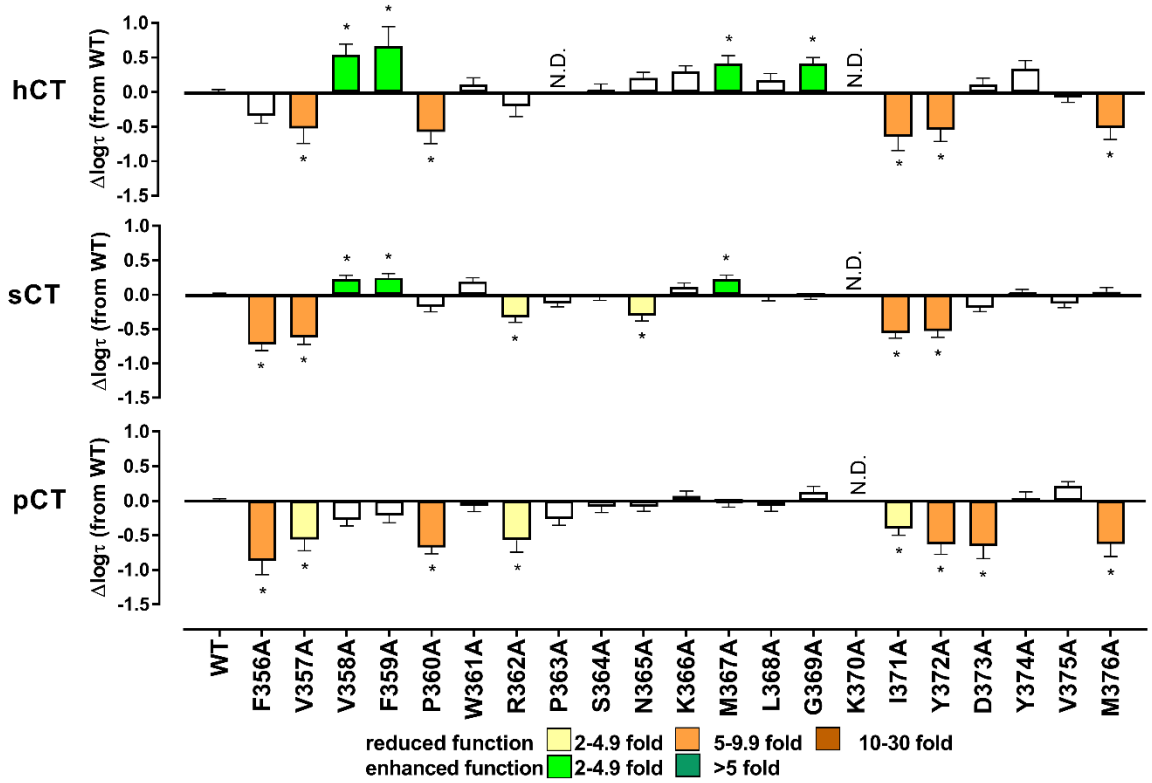

Figure 5.18 Effect of single alanine mutation in ECL3 of hCTR$_a$Leu on CT peptides efficacy for IP1 accumulation. *Data from Figure 5.14-16 were fit to the operational model of agonism to calculate coupling efficacy log(τ) of each receptor (mutant or WT) to the IP1 signalling pathway. The log(τ) values of each receptor were then corrected for expression, where this was significantly different, to obtain log(τ_c). Graphs show the differences relative to WT. All values are mean+S.E.M. of 4 to 6 independent experiments conducted in duplicate. Significance of changes was determined by comparison of the WT to the other receptor mutants by one-way analysis of variance and Dunnett's post-test (p<0.05 represented by *). (N.D.) efficacy not determined.*

	hCT				sCT				pCT			
	pEC_{50}	E_{max}	Log(τ)		pEC_{50}	E_{max}	Log(τ)		pEC_{50}	E_{max}	Log(τ)	
WT	8.76±0.09	100±2.4	-0.13±0.04	(29)	9.21±0.05	100±1.4	-0.04±0.02	(26)	8.84±0.07	100±2	-0.07±0.03	(25)
F356A	8.32±0.43	62.8±7*	-0.47±0.11	(6)	9.68±0.54	36.4±4.1*	-0.77±0.09*	(6)	8.93±0.78	32.2±5.6*	-0.94±0.2*	(4)
V357A	7.48±0.54*	50.3±8.4*	-0.66±0.22*	(5)	8.94±0.31	42.1±3.5*	-0.67±0.1*	(5)	7.59±0.4	48.3±6.2*	-0.63±0.16*	(5)
V358A	7.38±0.21*	146.9±13.1*	0.41±0.15*	(6)	8.72±0.16	123.4±6.4*	0.18±0.06*	(6)	8.34±0.31	70.4±6.8*	-0.35±0.09	(5)
F359A	6.66±0.21*	158.9±19.6	0.53±0.28*	(6)	8.71±0.14	125.1±5.5*	0.2±0.06*	(5)	7.69±0.27	76.6±7.3	-0.28±0.11	(5)
P360A	6.61±0.47*	104.4±25.1	-0.71±0.17*[(c)]	(6)	8.45±0.12	145.2±5.9*	-0.22±0.07[(c)]	(6)	8.03±0.4	93.1±12.6	-0.75±0.09*[(c)]	(4)
W361A	7.69±0.41	106.4±15	-0.02±0.1	(6)	9.06±0.2	120±7.2	0.15±0.05	(5)	8.08±0.29	90.9±9.2	-0.14±0.09	(5)
R362A	7.17±0.42*	75.1±12.6	-0.34±0.15	(6)	8.74±0.22	64.4±4.6*	-0.37±0.07*	(5)	7.4±0.66*	48±10.3*	-0.64±0.17*	(6)
P363A	N.D.	N.D.	N.D.	(6)	9.22±0.36	86±8.6	-0.16±0.05	(5)	8.06±0.42	72.3±9.8*	-0.33±0.09	(6)
S364A	7.91±0.34	97±11.4	-0.11±0.09	(6)	8.88±0.36	96.5±10.1	-0.07±0.05	(5)	8.02±0.25	90.2±7.5	-0.16±0.09	(6)
N365A	8.17±0.43	116.2±15.6	0.07±0.08	(6)	8.94±0.18	66.5±3.9*	-0.35±0.07*	(4)	9±0.6	90±14.6	-0.15±0.07	(6)
K366A	8.28±0.19	124.4±8	0.16±0.09	(6)	8.93±0.3	111.8±10.3	0.07±0.05	(5)	8.7±0.36	106.1±11.5	0.0±0.07	(6)
M367A	7.78±0.16	135.2±8.3	0.28±0.11*	(6)	8.61±0.2	124±7.6*	0.18±0.06*	(6)	8.21±0.24	97±7.8	-0.08±0.08	(6)
L368A	7.72±0.2	112±8.3	0.04±0.1	(6)	8.96±0.17	95.2±5	-0.08±0.05	(5)	8.37±0.35	90±10	-0.15±0.08	(6)
G369A	8.2±0.28	136.6±12.6	0.28±0.09*	(6)	8.88±0.23	97.8±6.9	-0.05±0.06	(5)	8.1±0.18	112.3±7.2	0.05±0.08	(6)
K370A	N.D.	N.D.	N.D.	(6)	N.D.	N.D.	N.D.	(4)	N.D.	N.D.	N.D.	(6)
I371A	8.74±0.64	41.8±6.6*	-0.78±0.2*[(a)]	(4)	8.89±0.45	47.3±5.2*	-0.6±0.08*[(a)]	(6)	8.15±0.39	60.5±6.8*	-0.47±0.1*[(a)]	(5)
Y372A	7.86±0.77	49.1±9.8*	-0.67±0.17*	(5)	8.09±0.54	51.3±7.9*	-0.57±0.09*	(5)	7.94±0.71	44.7±7.9*	-0.7±0.14*	(5)
D373A	7.92±0.33	105.9±12.2	-0.02±0.09	(6)	8.88±0.29	79.3±6.7	-0.23±0.06	(5)	7.87±0.35	41.1±4.7*	-0.72±0.19*	(6)
Y374A	7.49±0.29*	129.5±14.7	0.21±0.12	(6)	8.67±0.21	101.8±6.5	-0.02±0.05	(6)	7.81±0.19	102.5±7.2	-0.03±0.09	(6)
V375A	9.03±0.33	86.1±7.9	-0.21±0.07	(6)	8.98±0.21	84.9±5.3	-0.17±0.06	(5)	8.73±0.34	122±11.6	0.14±0.07	(6)
M376A	7.89±0.76	50.1±10.6*	-0.65±0.17*	(5)	8.78±0.26	104.5±8.1	0.0±0.06	(4)	8.16±0.35	42.5±5.4*	-0.69±0.18*	(5)

Table 5.5 Effect of single alanine mutation in ECL3 of hCTR$_a$Leu on IP1 accumulation in response to CT peptides. *For each receptor and ligand, data from Figure 5.14-16 were fit to a three-parameter logistic equation to derive pEC_{50} (negative logarithm of the concentration of ligand that produces half the maximal response) and E_{max} (maximal response as % of WT). The log(τ) reported in this table represents the operational coupling efficacy of each receptor (mutant or WT), where receptor expression was either unable to be identified on not significantly different. Where expression by radioligand binding was significantly different, values were corrected for the expression change to give $log(\tau_c)$ [(c)]. [(a)] Represents those mutation where expression could not be determined via radioligand binding. All values are mean±S.E.M. of 4 to 6 independent experiments conducted in duplicate. For each ligand, significance of changes in pEC_{50}, E_{max} and log(τ) was determined by comparison of the WT to the other receptor mutants by one-way analysis of variance and Dunnett's post-test ($p<0.05$ represented by *). (N.D.) pEC_{50}, E_{max} or efficacy not determined.*

5.2.3.3 ERK1/2 phosphorylation

To determine approximate peak response of ERK1/2 phosphorylation, time-courses were performed in presence of 1 μM of each peptide (***Figure 5.19-23***). The CT peptides and rAmy showed a transient pERK1/2 response that peaked between 6 and 7 min. In contrast, hαCGRP exhibited slower onset and were sustained over 10 min, but similar between WT and mutant receptors. Concentration-response curves were therefore measured at these peak response times (6 min for pCT, 7 min for hCT, sCT and rAmy, and 8 min for hαCGRP) and these are shown in ***Figures 5.24-28***. Derived pEC_{50}, E_{max} and log(τ) values are reported in ***Tables 5.6 and 5.7***.

As observed in both cAMP and IP1 pathways, the K370A mutant showed no detectable response for any of the peptides assessed (up to 1 μM of ligand). Additionally, the I371A substitution dramatically reduced the response to all agonist peptides, and consequently could not be quantified.

5.2.3.3.1 CT peptides

Potency. All three CT peptides had a pEC_{50} value for the WT receptor between 1.5 nM and 3.5 nM (***Table 5.6***). P360A significantly reduced the potency of all CT peptides. F356A significantly increased sCT potency, whilst reducing hCT and pCT pCE50 (although data failed to reach statistical significance for pCT). sCT potency was unaltered by any other mutation in ECL3, whereas the Y372A substitution significantly reduced pCT pEC_{50}. This last mutation also dramatically reduced hCT response to a level where quantification of the hCT effect was not possible. Similar to that observed in affinity, cAMP and IP1, hCT was the most susceptible to mutation when compared to the other CT agonists, with potency reduced by substitution of V358, F359, W361, R362, P363, D373 and M376 to Ala. None of the other mutations had a significant effect on potency of the CT peptides.

Similar to patterns observed in the other pathways, comparison of maximal responses again revealed two clusters of residues that produced divergent effects. The first cluster, including F356A, Y372A and M376A showed significant reduction in E_{max} for all CT agonists. Additionally, V357A and V375A also had reduced response for all three agonists, although data failed to reach statistical significance for pCT.

Maximal response. Compared to sCT, where E_{max} was unaltered, maximal response of both hCT and

pCT was significantly reduced by P360A, R362A, P363A and D373A substitutions. A second cluster of residues, characterised by statistical increase in E_{max} when compared to WT response for all CT agonists, included K366A, M367A and L368A. E_{max} of hCT and sCT (but not pCT) was also significantly increased by V358A and F359A, while S364A and G369A increased E_{max} of hCT and pCT without altering sCT response. Interestingly, W361A had opposing effects, with increased E_{max} in response to sCT, decreased E_{max} for pCT, and no effect on hCT E_{max}. No additional mutations had relevant effect on maximal response of these peptides.

Efficacy. ***Figure 5.29*** and ***Table 5.6*** show the effect of mutations in ECL3 and adjacent TMs on efficacy, as derived from operational modelling. Statistical analysis revealed that this region is particularly important for pERK1/2 and similar to observations in the cAMP and IP1 pathways, two clusters of residues affecting efficacy could be identified. F356A, P360A, Y372A and M376A significantly reduced efficacy of all CT ligands. hCT and pCT (but not sCT) efficacy was also significantly reduced by R362A, P363A and D373A mutation. V375A showed a significant reduction in efficacy in response to sCT and hCT, and a similar trend (although not significant) was observed for pCT. hCT efficacy was also selectively reduced at V357A. The second cluster of residues, revealed enhanced efficacy for all three CT agonists when mutated to Ala. K366A and M367A increased efficacy of all CT agonist peptides, whereas L368A enhanced sCT and pCT, with a similar trend in response to hCT. Additionally, V358 and F359 substitution significantly enhanced hCT and sCT response, while having limited effect for pCT. hCT (but not sCT or pCT) efficacy was also significantly improved at S364A and G369A mutated receptors, while W361A selectively increased sCT efficacy. No other mutation produced changes in efficacy for any of the three CT peptides assessed.

5.2.3.3 rAmy and hαCGRP peptides

Potency. rAmy and hαCGRP were also assessed in the pERK1/2 pathway. These peptides were less potent than the CT peptides, with pEC_{50} values of approximately 40 nM and 55 nM respectively (***Table 5.7***). I371A, P360A, Y372A and D373A mutations dramatically reduced pERK1/2 response for both these peptides, and substitution of V357, F359 and P363 led to loss of detectable hαCGRP response.

Functional quantification of rAmy or hαCGRP responses at these receptor mutations could not be achieved due to the limited responses. None of the other alanine substitutions had any significant impact on the potency of either peptides.

Maximal response. Statistical analysis of maximal responses revealed that V358A, W361A, R362A, S364A, N365A, Y374A and M376A significantly reduced E_{max} of both rAmy and hαCGRP responses. Although F356A and G369A had reduced maximal response of both peptides, data only reached statistical significance for rAmy. Similarly, V375A showed reduced E_{max} for both peptides, although data was significant only for hαCGRP. V357A, F359A and P363A significantly reduced rAmy maximal response, whereas E_{max} for hαCGRP concentration-response curves was not reached within the concentration range assessed, and therefore could not be defined. Interestingly, K366A, significantly increased E_{max} of hαCGRP while having no effect on rAmy. No other mutation altered the receptor mediated response these two peptides.

Efficacy. When comparing the calculated efficacy from operational analysis (***Figure 5.29***), F356A, W361A, R362A and M376A significantly reduced efficacy of both ligands relative to WT. Efficacy of rAmy was also significantly reduced at V357A, F359 and R363A receptor mutants. In addition, alanine substitution of V358, S364, N365, K366, V375 and Y374, significantly reduced efficacy of hαCGRP, and showed a similar trend for rAmy responses, but this did not reach statistical significance. No other substitutions had relevant effect on rAmy or hαCGRP efficacy.

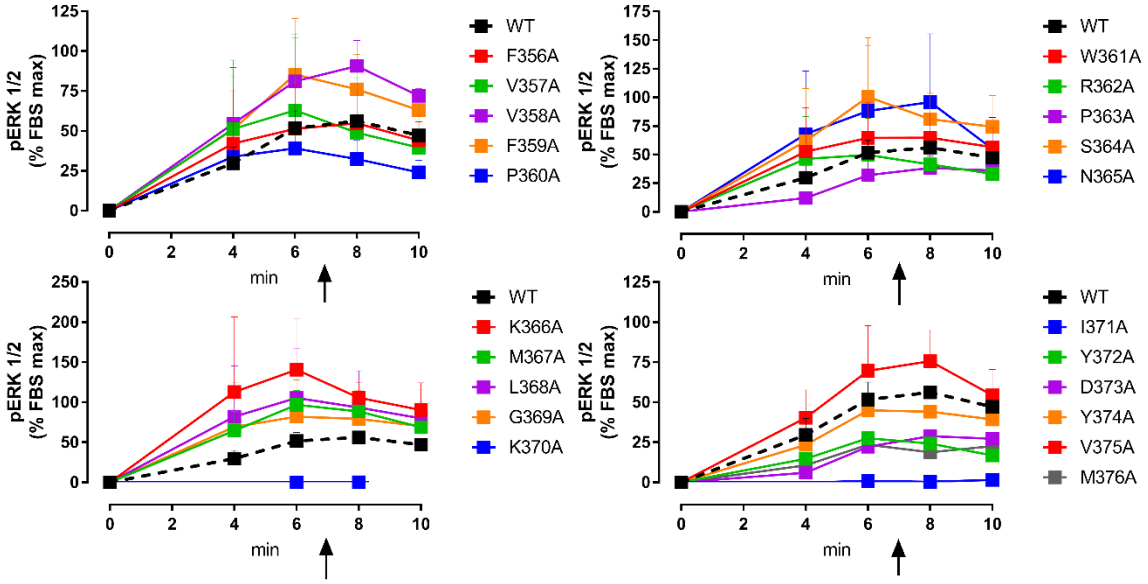

Figure 5.19 ERK1/2 phosphorylation time-course profiles elicited by hCT in CV-1-FlpIn cells stably expressing hCTR$_a$Leu ECL3 single alanine mutations. *1 µM of hCT was added at the time 0. Each dataset was normalised to FBS at 6 min and vehicle responses. All values are mean+S.D. of 2 (WT N=5) independent experiments conducted in duplicate. Arrows indicate where concentration-response curves where generated.*

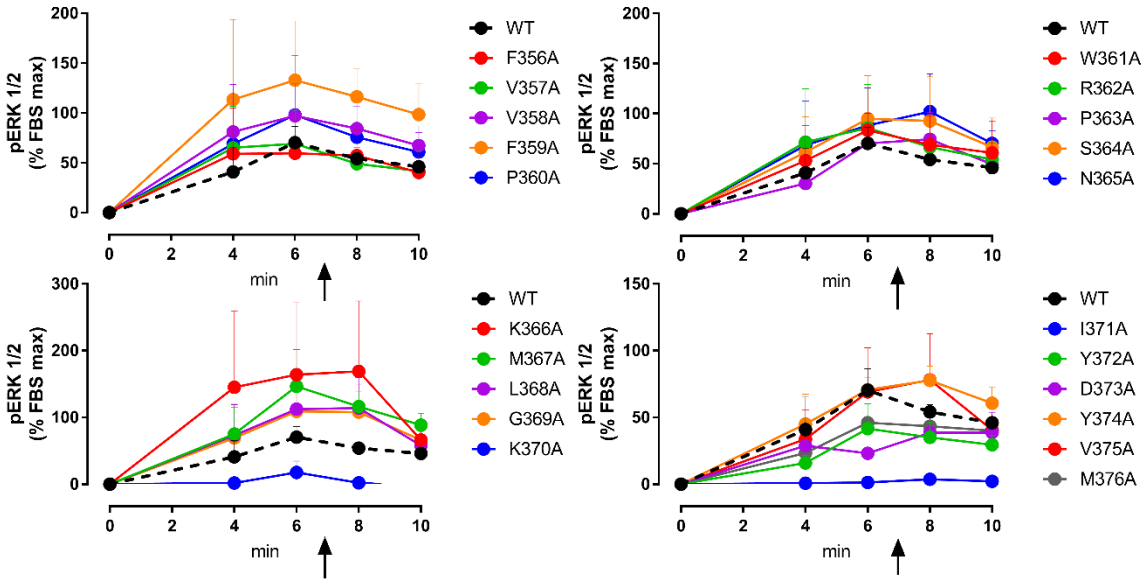

Figure 5.20 ERK1/2 phosphorylation time-course profiles elicited by sCT in CV-1-FlpIn cells stably expressing hCTR$_a$Leu ECL3 single alanine mutations. *1 µM of sCT was added at the time 0. Each dataset was normalised to FBS at 6 min and vehicle responses. All values are mean+S.D. of 2 (WT N=5) independent experiments conducted in duplicate. Arrows indicate where concentration-response curves where generated.*

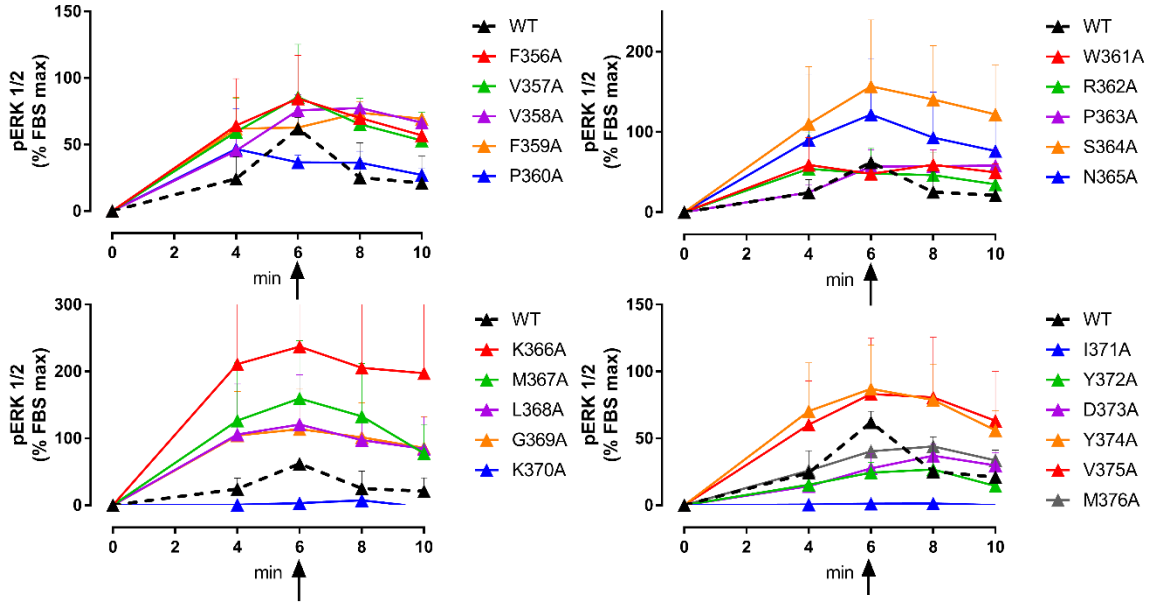

Figure 5.21 ERK1/2 phosphorylation time-course profiles elicited by pCT in CV-1-FlpIn cells stably expressing hCTR$_a$Leu ECL3 single alanine mutations. *1 μM of pCT was added at the time 0. Each dataset was normalised to FBS at 6 min and vehicle responses. All values are mean+S.D. of 2 (WT N=5) independent experiments conducted in duplicate. Arrows indicate where concentration-response curves where generated.*

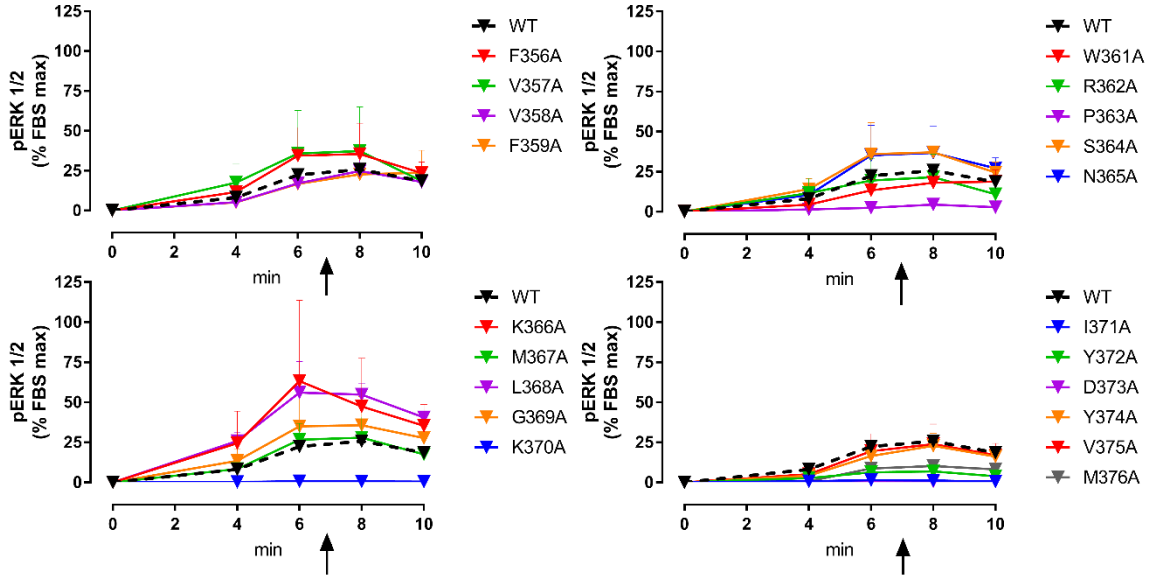

Figure 5.22 ERK1/2 phosphorylation time-course profiles elicited by rAmy in CV-1-FlpIn cells stably expressing hCTR$_a$Leu ECL3 single alanine mutations. *1 μM of rAmy was added at the time 0. Each dataset was normalised to FBS at 6 min and vehicle responses. All values are mean+S.D. of 2 (WT N=5) independent experiments conducted in duplicate. Arrows indicate where concentration-response curves where generated.*

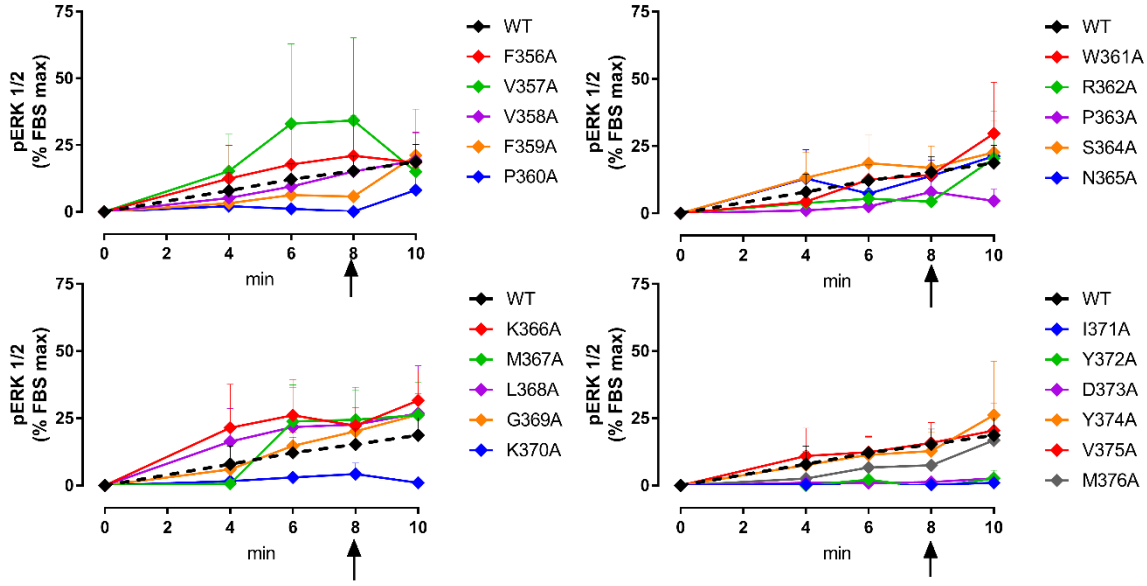

Figure 5.23 ERK1/2 phosphorylation time-course profiles elicited by hαCGRP in CV-1-FlpIn cells stably expressing hCTR$_a$Leu ECL3 single alanine mutations. *1 μM of hαCGRP was added at the time 0. Each dataset was normalised to FBS at 6 min and vehicle responses. All values are mean+S.D. of 2 (WT N=5) independent experiments conducted in duplicate. Arrows indicate where concentration-response curves where generated.*

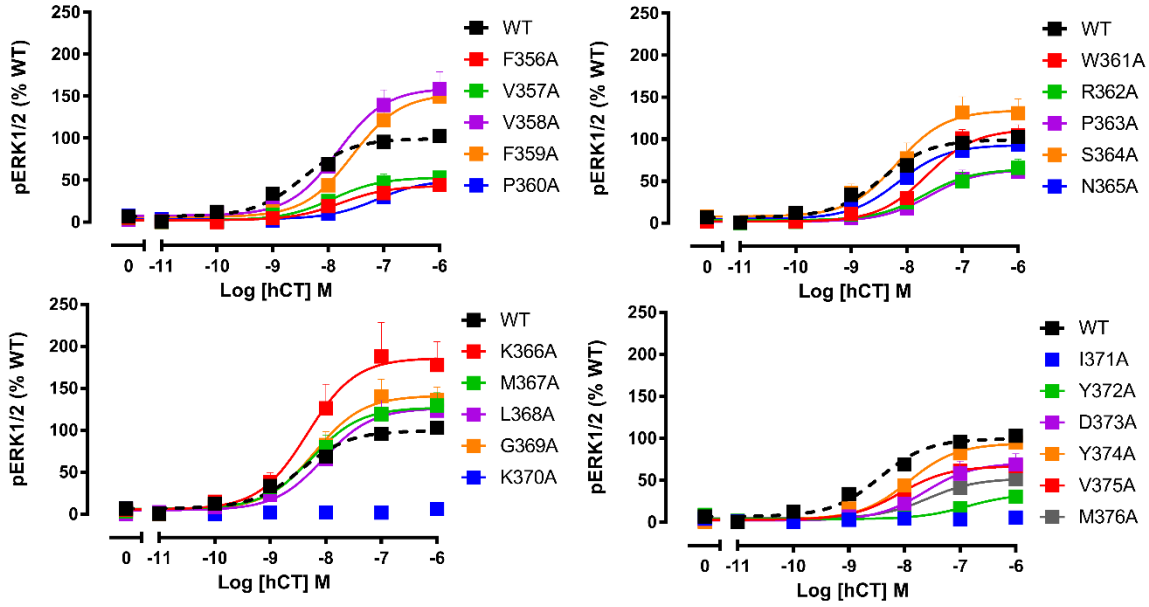

Figure 5.24 ERK1/2 phosphorylation concentration-response profiles elicited by hCT in CV-1-FlpIn cells stably expressing hCTR$_a$Leu ECL3 single alanine mutations. *pERK1/2 in response to hCT were normalized to the internal control (10% FBS measured at 6 min) and fit to a three parameter logistic equation. Data was subsequently normalised to WT receptor response. All values are mean+S.E.M. of 4 to 5 (WT N=24) independent experiments conducted in duplicate.*

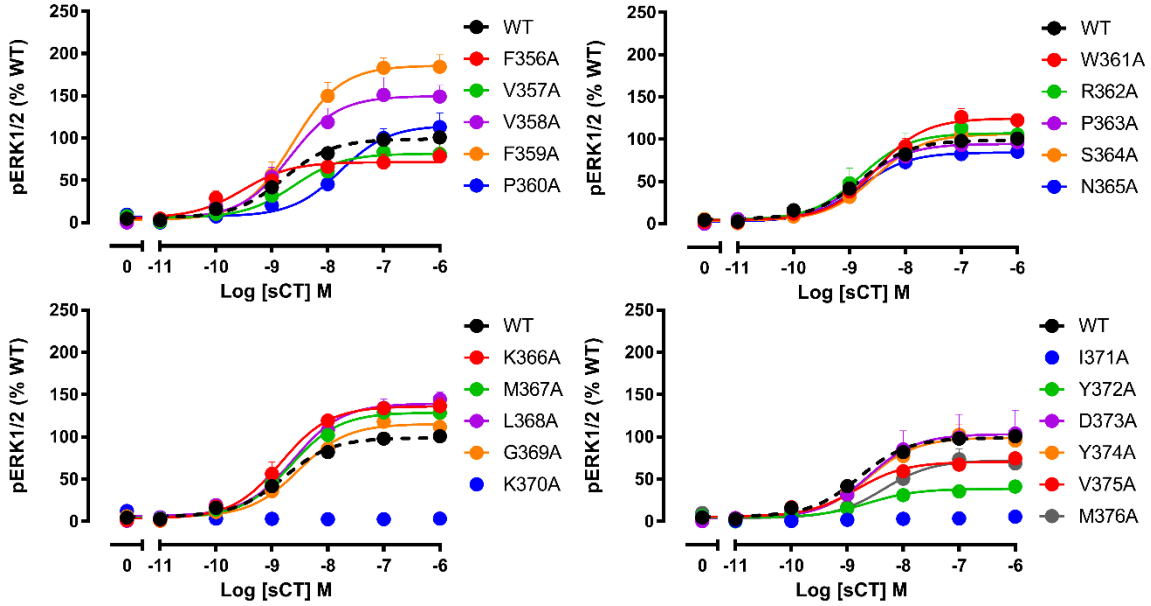

Figure 5.25 ERK1/2 phosphorylation concentration-response profiles elicited by sCT in CV-1-FlpIn cells stably expressing hCTR$_a$Leu ECL3 single alanine mutations. *pERK1/2 in response to sCT were normalized to the internal control (10% FBS measured at 6 min) and fit to a three parameter logistic equation. Data was subsequently normalised to WT receptor response. All values are mean+S.E.M. of 4 to 5 (WT N=25) independent experiments conducted in duplicate.*

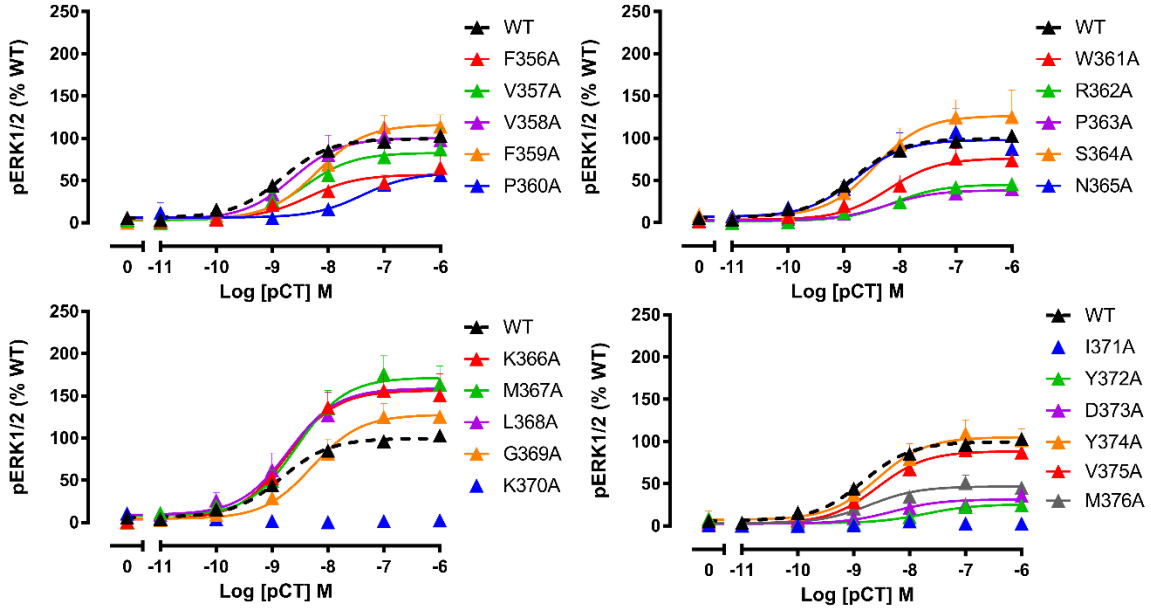

Figure 5.26 ERK1/2 phosphorylation concentration-response profiles elicited by pCT in CV-1-FlpIn cells stably expressing hCTR$_a$Leu ECL3 single alanine mutations. *pERK1/2 in response to pCT were normalized to the internal control (10% FBS measured at 6 min) and fit to a three parameter logistic equation. Data was subsequently normalised to WT receptor response. All values are mean+S.E.M. of 4 to 5 (WT N=22) independent experiments conducted in duplicate.*

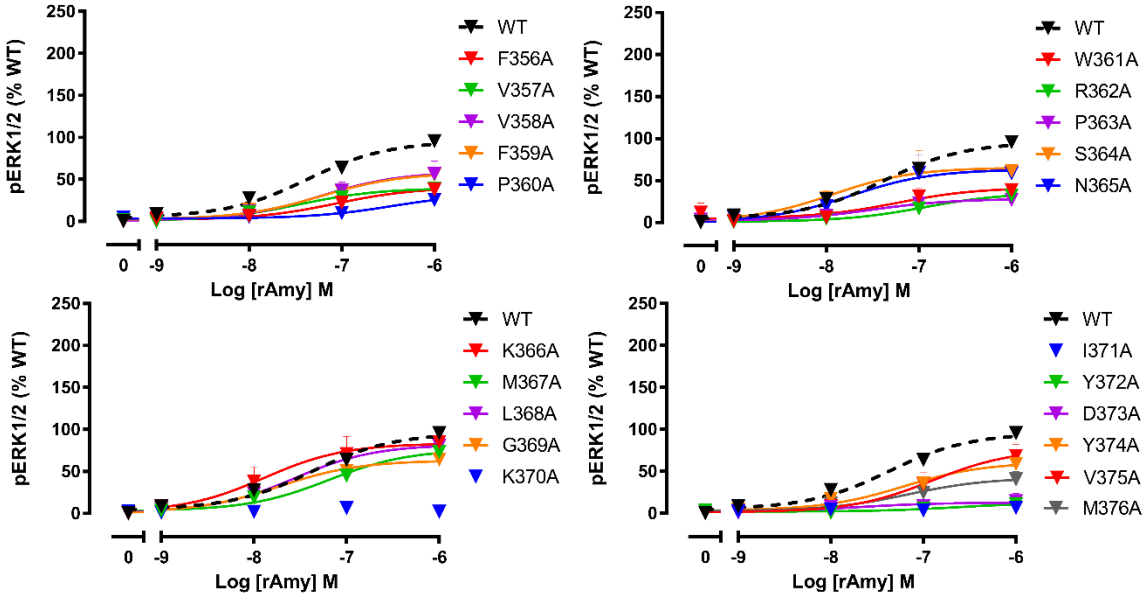

Figure 5.27 ERK1/2 phosphorylation concentration-response profiles elicited by rAmy in CV-1-FlpIn cells stably expressing hCTR$_a$Leu ECL3 single alanine mutations. *pERK1/2 in response to rAmy were normalized to the internal control (10% FBS measured at 6 min) and fit to a three parameter logistic equation. Data was subsequently normalised to WT receptor response. All values are mean+S.E.M. of 4 to 5 (WT N=16) independent experiments conducted in duplicate.*

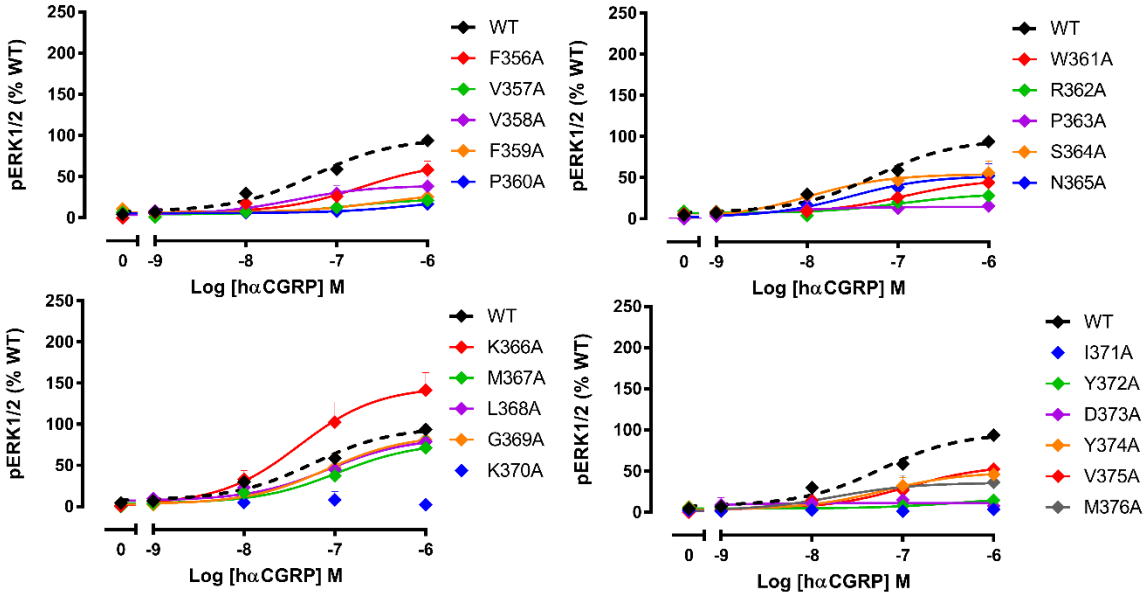

Figure 5.28 ERK1/2 phosphorylation profiles concentration-response elicited by hαCGRP in CV-1-FlpIn cells stably expressing hCTR$_a$Leu ECL3 single alanine mutations. *pERK1/2 in response to hαCGRP were normalized to the internal control (10% FBS measured at 6 min) and fit to a three parameter logistic equation. Data was subsequently normalised to WT receptor response. All values are mean+S.E.M. of 4 to 5 (WT N=17) independent experiments conducted in duplicate.*

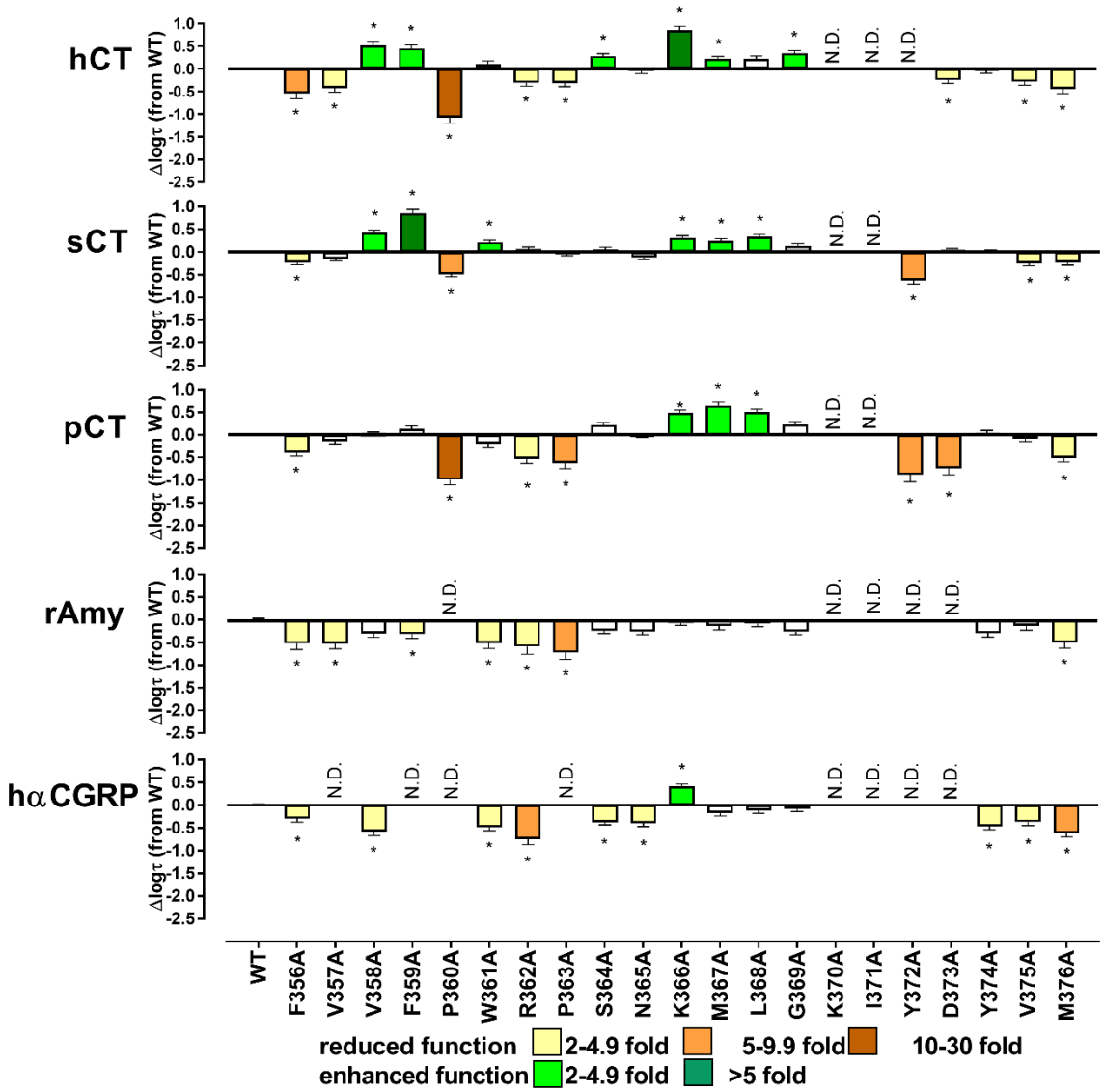

Figure 5.29 Effect of single alanine mutation in ECL3 of hCTR$_a$Leu on efficacy for ERK1/2 phosphorylation. *Data from Figures 5.23-27 were fit to the operational model of agonism to calculate coupling efficacy log(τ) of each receptor (mutant or WT) to the pERK1/2 signalling pathway. The log(τ) values of each receptor were then corrected for expression, where this was significantly different, to obtain log(τc). Graphs show the differences relative to WT. All values are mean+S.E.M. of 4 to 5 independent experiments conducted in duplicate. Significance of changes was determined by comparison of the WT to the other receptor mutants by one-way analysis of variance and Dunnett's post-test (p<0.05 represented by *. (N.D.) efficacy not determined.*

	hCT				sCT				pCT			
	pEC_{50}	E_{max}	Log(τ)		pEC_{50}	E_{max}	Log(τ)		pEC_{50}	E_{max}	Log(τ)	
WT	8.45±0.05	100±1.8	-0.1±0.02	(24)	8.79±0.04	100±1.3	-0.1±0.02	(25)	8.83±0.04	100±1.2	-0.1±0.02	(22)
F356A	7.77±0.17*	43.4±2.9*	-0.65±0.11*	(4)	9.52±0.25*	71.5±4.6*	-0.34±0.04*	(5)	8.35±0.3	57.1±5.7*	-0.49±0.08*	(4)
V357A	7.92±0.21	53.3±4.5*	-0.53±0.09*	(4)	8.61±0.27	81.6±6.9*	-0.25±0.05	(5)	8.43±0.36	83±10	-0.24±0.06	(4)
V358A	7.83±0.15*	159.7±9.8*	0.42±0.07*	(5)	8.68±0.16	149.7±7.8*	0.32±0.05*	(4)	8.65±0.26	100.5±8.3	-0.09±0.06	(4)
F359A	7.57±0.12*	153±7.6*	0.35±0.07*	(5)	8.62±0.12	185.8±7.3*	0.75±0.08*	(5)	8.2±0.15	116.3±6.2	0.04±0.06	(4)
P360A	7.12±0.24*	50.6±6.2*	-1.17±0.13*[(c)]	(5)	7.78±0.19*	115±8.8	-0.59±0.06*[(c)]	(5)	7.4±0.28*	59.1±7*	-1.09±0.11*[(c)]	(4)
W361A	7.64±0.12*	111.7±5.9	0.0±0.07	(4)	8.52±0.12	124.7±4.9*	0.11±0.05*	(4)	8.2±0.22	76.3±6*	-0.3±0.07	(4)
R362A	7.68±0.25*	64.4±6.6*	-0.41±0.08*	(5)	8.81±0.28	107.2±9.5	-0.04±0.04	(4)	8.12±0.2	45.3±3.5*	-0.63±0.11*	(4)
P363A	7.59±0.23*	63.8±6.2*	-0.41±0.08*	(5)	8.81±0.15	94.5±4.5	-0.14±0.05	(4)	8.24±0.15	38.5±2*	-0.72±0.12*	(4)
S364A	8.18±0.2	134.5±9.9*	0.18±0.05*	(5)	8.56±0.13	106.2±4.3	-0.04±0.05	(4)	8.44±0.28	126.7±11.5*	0.12±0.06	(4)
N365A	8.15±0.16	93.1±5.6	-0.15±0.05	(5)	8.82±0.12	84.4±3.3	-0.22±0.05	(4)	8.79±0.32	98.1±9.7	-0.11±0.05	(5)
K366A	8.33±0.24	186.1±15.8*	0.75±0.09*	(5)	8.84±0.11	136.2±4.7*	0.21±0.05*	(4)	8.72±0.18	156.4±9.3*	0.39±0.06*	(5)
M367A	8.26±0.15	127±7*	0.12±0.05*	(5)	8.66±0.1	128.9±4.3*	0.14±0.05*	(4)	8.56±0.19	171.8±10.4*	0.55±0.07*	(5)
L368A	8.05±0.14	126.4±6.8*	0.12±0.06	(4)	8.62±0.12	139.5±5.6*	0.23±0.05*	(4)	8.71±0.23	158.8±11.3*	0.41±0.07*	(4)
G369A	8.2±0.18	141.3±9.3*	0.25±0.05*	(5)	8.53±0.11	115.4±4	0.03±0.05	(4)	8.28±0.18	127.8±8.4*	0.13±0.06	(4)
K370A	N.D.	N.D.	N.D.		N.D.	N.D.	N.D.		N.D.	N.D.	N.D.	
I371A	N.D.	N.D.	N.D.		N.D.	N.D.	N.D.		N.D.	N.D.	N.D.	
Y372A	N.D.	N.D.	N.D.		8.64±0.26	38.6±2.9*	-0.73±0.08*	(5)	7.72±0.41*	25.7±44*	-0.98±0.16*	(4)
D373A	7.63±0.24*	70.6±7*	-0.35±0.07*	(5)	8.62±0.34	103.3±11.4	-0.07±0.04	(5)	8.31±0.35	31.6±3.7*	-0.84±0.14*	(4)
Y374A	7.92±0.09	94.1±3.5	-0.14±0.06	(5)	8.63±0.14	99.2±4.5	-0.1±0.05	(4)	8.57±0.24	105.3±88	-0.06±0.06	(4)
V375A	8.08±0.13	66.7±3.4*	-0.39±0.07*	(4)	8.83±0.14	70.4±3.1*	-0.35±0.05*	(4)	8.58±0.14	88.6±4.1	-0.19±0.06	(4)
M376A	7.58±0.21*	52.1±4.3*	-0.54±0.1*	(4)	8.35±0.2	72.3±4.8*	-0.33±0.06*	(4)	8.71±0.29	46.9±4.2*	-0.61±0.09*	(4)

Table 5.6 Effect of single alanine mutation in ECL3 of hCTR$_a$Leu on ERK1/2 phosphorylation in response to CT peptides. *For each receptor and ligand, data from Figures 5.23-25 were fit to a three-parameter logistic equation to derive pEC_{50} (negative logarithm of the concentration of ligand that produces half the maximal response) and E_{max} (maximal response as % of WT). The log(τ) reported in this table represents the operational coupling efficacy of each receptor (mutant or WT), where receptor expression was either unable to be identified on not significantly different. Where expression by radioligand binding was significantly different, values were corrected for the expression change to give log(τ_c) [(c)]. [(a)] Represents those mutation where expression could not be determined via radioligand binding. All values are mean±S.E.M. of 4 to 5 independent experiments conducted in duplicate For each ligand, significance of changes in pEC_{50}, E_{max} and log(τ) was determined by comparison of the WT to the other receptor mutants by one-way analysis of variance and Dunnett's post-test ($p<0.05$ represented by *).(N.D.) efficacy not determined.*

	rAmy				hαCGRP			
	pEC_{50}	E_{max}	Log(τ)		pEC_{50}	E_{max}	Log(τ)	
WT	7.4±0.09	100±3.7	-0.14±0.03	(16)	7.25±0.13	100±5.4	-0.14±0.03	(17)
F356A	7.06±0.23	40.8±4.8*	-0.66±0.14*	(4)	6.74±0.28	67.5±10.5	-0.43±0.08*	(4)
V357A	7.46±0.46	39.9±7.8*	-0.67±0.11*	(4)	N.D.	N.D.	N.D.	
V358A	7.23±0.35	59.4±10.1*	-0.44±0.09	(4)	7.49±0.5	39.4±7.6*	-0.71±0.09*	(4)
F359A	7.22±0.4	58.1±11.1*	-0.46±0.09*	(4)	N.D.	N.D.	N.D.	
P360A	N.D.	N.D.	N.D.		N.D.	N.D.	N.D.	
W361A	7.24±0.49	41.6±8.8*	-0.66±0.12*	(4)	6.93±0.31	48.6±7.5*	-0.62±0.08*	(5)
R362A	6.94±0.36	35.6±7.2*	-0.73±0.17*	(4)	6.95±0.61	30.9±8.3*	-0.88±0.12*	(5)
P363A	7.51±0.81	28.2±8.9*	-0.87±0.15*	(4)	N.D.	N.D.	N.D.	
S364A	7.94±0.36	65.5±9.1*	-0.38±0.06	(4)	7.97±0.29	54.4±5.9*	-0.51±0.06*	(4)
N365A	7.73±0.39	63.2±9.6*	-0.41±0.07	(4)	7.52±0.39	52.4±8.2*	-0.53±0.07*	(4)
K366A	7.89±0.33	83.6±10.5	-0.22±0.05	(5)	7.39±0.27	145.8±16.9*	0.28±0.06*	(4)
M367A	7.19±0.15	76.5±5.4	-0.29±0.08	(4)	6.97±0.27	78±11.5	-0.31±0.06	(4)
L368A	7.56±0.23	82.2±7.8	-0.23±0.06	(4)	7.07±0.37	83.7±15.5	-0.25±0.06	(4)
G369A	7.73±0.34	63.3±8.4*	-0.4±0.07	(4)	7.09±0.3	87.2±13.5	-0.22±0.06	(4)
K370A	N.D.	N.D.	N.D.		N.D.	N.D.	N.D.	
I371A	N.D.	N.D.	N.D.		N.D.	N.D.	N.D.	
Y372A	N.D.	N.D.	N.D.		N.D.	N.D.	N.D.	
D373A	N.D.	N.D.	N.D.		N.D.	N.D.	N.D.	
Y374A	7.21±0.17	60.9±4.8*	-0.44±0.09	(4)	7.21±0.31	49.1±7.5*	-0.6±0.08*	(5)
V375A	6.91±0.29	76.6±12.7	-0.28±0.1	(4)	6.96±0.24	57.5±6.8*	-0.51±0.08*	(4)
M376A	7.17±0.32	42.6±6.6*	-0.64±0.12*	(4)	7.74±0.6	35.9±8.2*	-0.75±0.08*	(5)

Table 5.7 Effect of single alanine mutation in ECL3 of hCTR$_a$Leu on ERK1/2 phosphorylation in response to rAmy or hαCGRP peptides. *For each receptor and ligand, data from Figures 5.26-27 were fit to a three-parameter logistic equation to derive pEC_{50} (negative logarithm of the concentration of ligand that produces half the maximal response) and E_{max} (maximal response as % of WT). The log(τ) reported in this table represents the operational coupling efficacy of each receptor (mutant or WT), where receptor expression was either unable to be identified on not significantly different. Where expression by radioligand binding was significantly different, values were corrected for the expression change to give log(τ_c) [(c)]. [(a)] Represents those mutation where expression could not be determined via radioligand binding. All values are mean±S.E.M. of 4 to 5 independent experiments conducted in duplicate For each ligand, significance of changes in pEC_{50}, E_{max} and log(τ) was determined by comparison of the WT to the other receptor mutants by one-way analysis of variance and Dunnett's post-test (p<0.05 represented by *).(N.D.) efficacy not determined.*

5.2.4 Mapping mutational data onto molecular models

Mapping our results onto the 3D model of the active CTR revealed regions important for different aspects of CTR function. Residues in the membrane proximal part of TM6 that reduced affinity of hCT and pCT upon mutation line up along the inside of the binding groove, whereas sCT and sCT(8-32) binding was only marginally affected by this mutagenesis (***Figure 5.31 A***). Interestingly, P360 in TM6, a residue that is conserved across the calcitonin-like family of receptors, but not other receptor of Class B1 (Liang et al., 2017) (***Figure 5.1 A*** and Appendix 1), was important for driving the affinity of the sCT agonist, but not of the sCT(8-32) antagonist.

In cAMP formation, the majority of those residues in ECL3 and adjacent TMs, where substitution reduced affinity for the CT agonists, enhanced efficacy of these agonists (***Figure 5.31 B***). Interestingly rAmy engages with a network of residues that closely resembles those used by sCT to trigger cAMP signalling (***Figure 5.31 A***). The profile efficacy effect for hαCGRP was also striking, with mapping revealing that while this peptide engages with a network that resembles the one used by hCT and pCT for cAMP formation, there were additional residues that form a distinct network profile for this peptide. For this peptide indeed, Ala substitutions across the entire region of ECL3 had a detrimental effect on efficacy for cAMP formation, whereas for the other peptides, the main effects of individual Ala substitutions were enhanced efficacy.

ECL3 was also important for IP1 formation following CT agonist stimulation of hCTR$_a$Leu (***Figure 5.29 C***). Despite some select differences, all CT peptides utilised key residues in TM6 TM7 and ECL3 that were oriented towards the entrance to the TM binding pocket. Interestingly, the hCT and sCT heat-maps show common regions where mutation enhanced efficacy, but are not important for pCT signalling down this pathway. In contrast, the regions within ECL3 that decreased efficacy in IP1 were shared by all three CT peptides, albeit that the effect of mutation (in terms of magnitude) was not always the same for each peptide.

Comparison of key networks involved in ERK1/2 phosphorylation pathway (***Figure 5.31 D*** and ***Figure 5.32 B***) revealed that ECL3 and adjacent TMs are crucial for the activation of this pathway for all peptides assessed in this study. Similar to observations in Chapter 4, residues driving pERK1/2 downstream of

CT agonist-stimulation follow a pattern more similar to IP1 and less common to cAMP formation. Similar to the pattern for IP1 efficacy, sCT and hCT appear to utilize a more similar network when compared to pCT, and the effect of mutations, in terms of magnitude of effect, are greater for the two former CT peptides.

These results are interesting because in the bias plots, presented in Chapter 3, sCT and hCT had a very similar profile, whereas pCT was more biased towards ERK, and thus differences in the way pCT engages with the receptor may be the key to its biased agonism profile. It was also interesting to observe that in pERK1/2, both rAmy and hαCGRP utilised a similar continuum of residues throughout the ECL3, with a greater degree of ECL3 surface involved in signalling to this pathway, but distinct effects on some residues for these two peptides when compared to the CT agonists in this pathway.

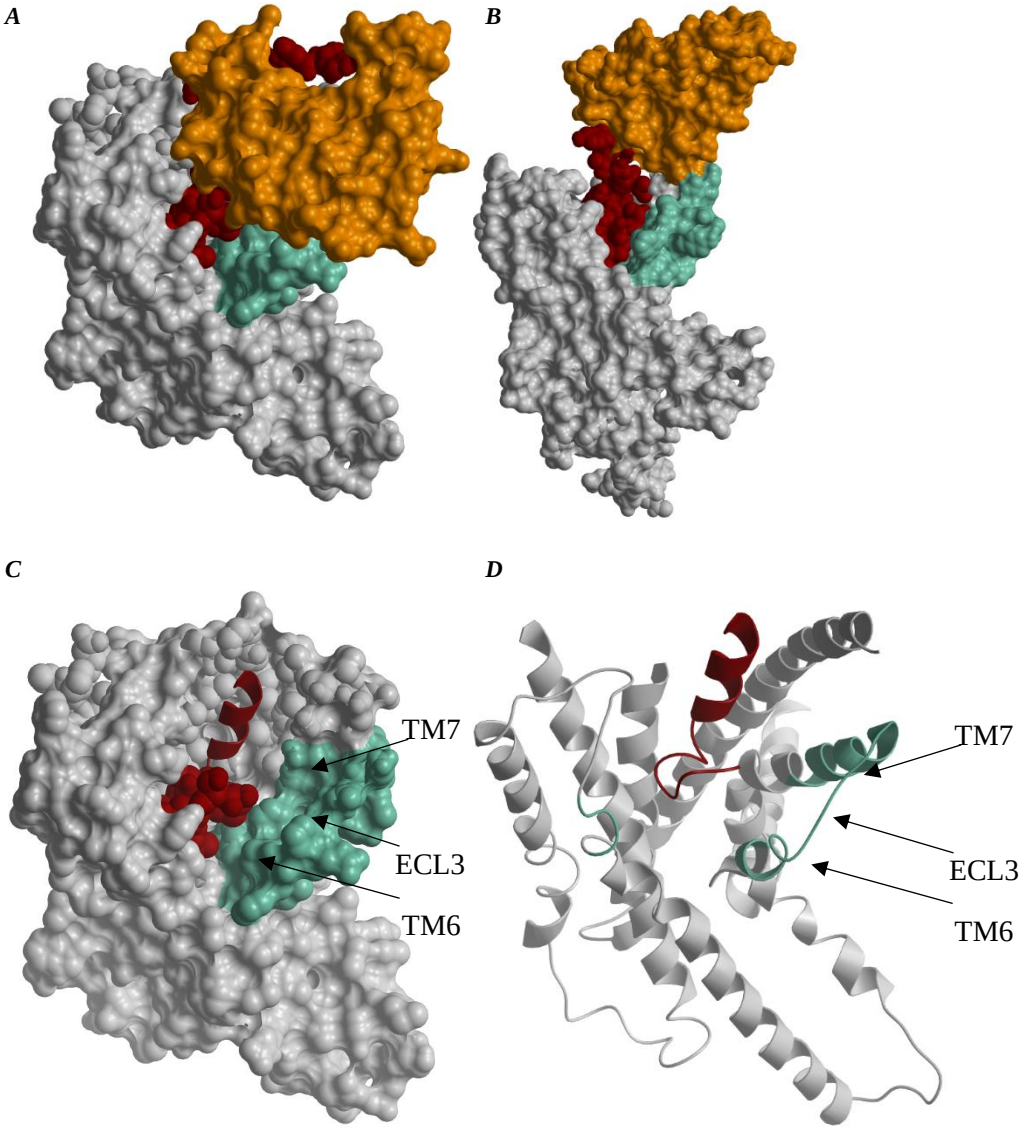

Figure 5.30. *(A)Top view and (B) side view of the active model of the hCTR in complex with the sCT ligand, based on the active Cryo-EM structure of CTR in complex with sCT and the G protein heterotrimer (pdb structure 5UZ7). Incomplete segments of the structure were modelled in by Prof. Christopher A. Reynolds to generate a complete model of the hCTR, shown here as a surface representation. The NTD (in orange) and the alanine substituted residues in ECL2 discussed in this chapter (279-300) are highlighted in green.*
To better visualise the ECLs and binding pocket within the TM bundle, the NTD, TM1-stalk region (residues 1-136) and residues 200-217 in ECL1 (that would partially cover ECL2) are not displayed. The model also shows the sCT ligand (in burgundy), with the cyclic N-terminus (residues 1-7) represented by space fill (C) or (D) ribbon. Residues 8-16 of the ligand, tightly structured in a α-helix, are shown as ribbon, while the C-terminus (residues 17-32) of the peptide is not displayed.

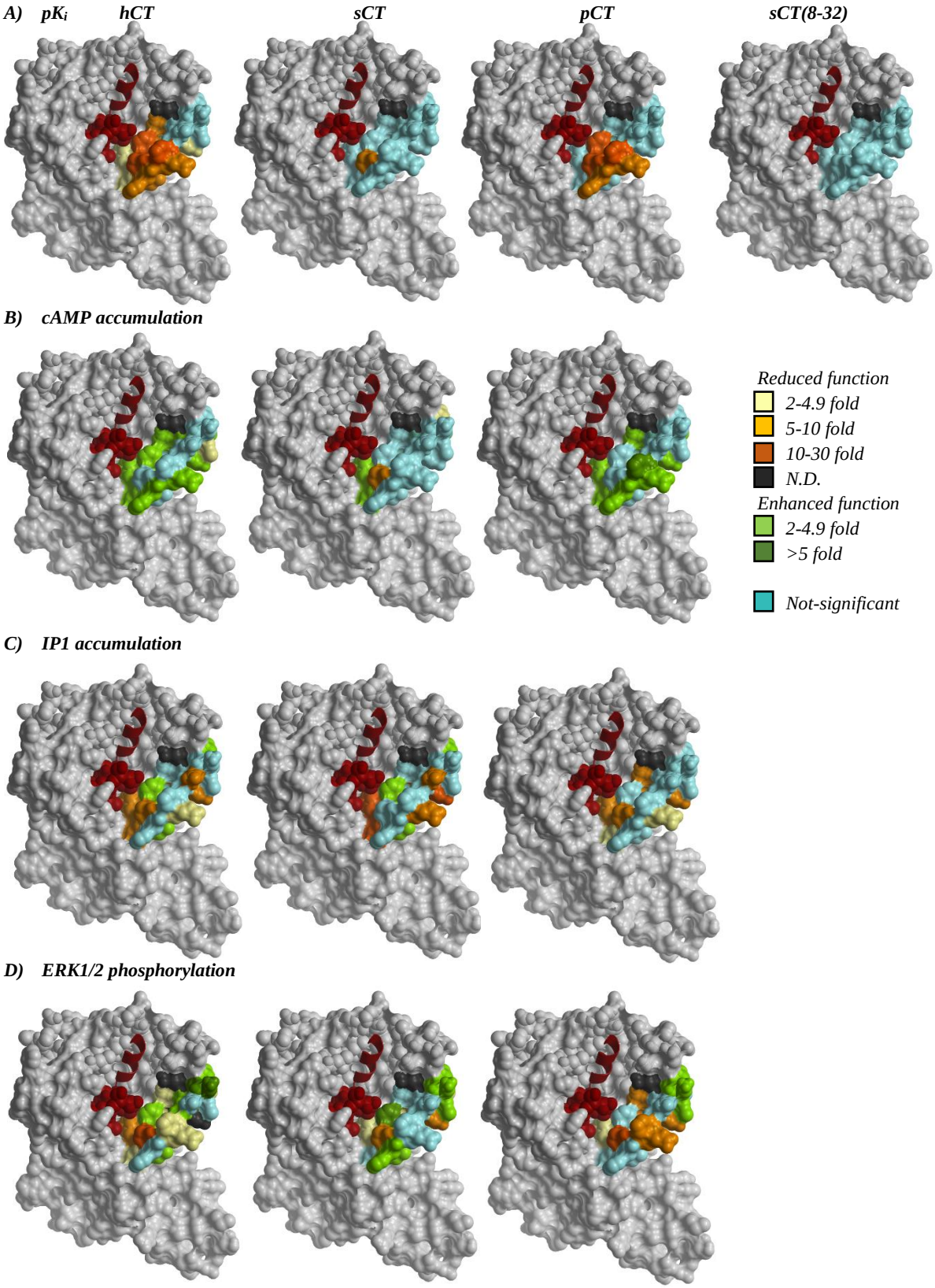

Figure 5.31 Heat-map 3D representation of ECL2 of the hCTR and the effect of alanine substitution on CT peptides equilibrium affinity and intracellular signalling. *Active model based on the active Cryo-EM structure of CTR in complex with sCT (Liang et al., 2017) into which the three ECLs were modelled as describe in Figure 5.30. Residues 1-136 and 200-217 (that would partially cover ECL2) are hidden. The model shows sCT ligand (in burgundy) where the cyclic N-terminus (residues 1-7) is represented by space fill, residues 8-16 are tightly structured in an α-helix (ribbon), while the C-terminus (residues 17-32) of the ligand is hidden. Residues that produced significant changes in binding affinity or signalling efficacy were coloured following the colour scheme for fold effect from WT in Figures 5.7, 5.13, 5.18 and 5.29.*

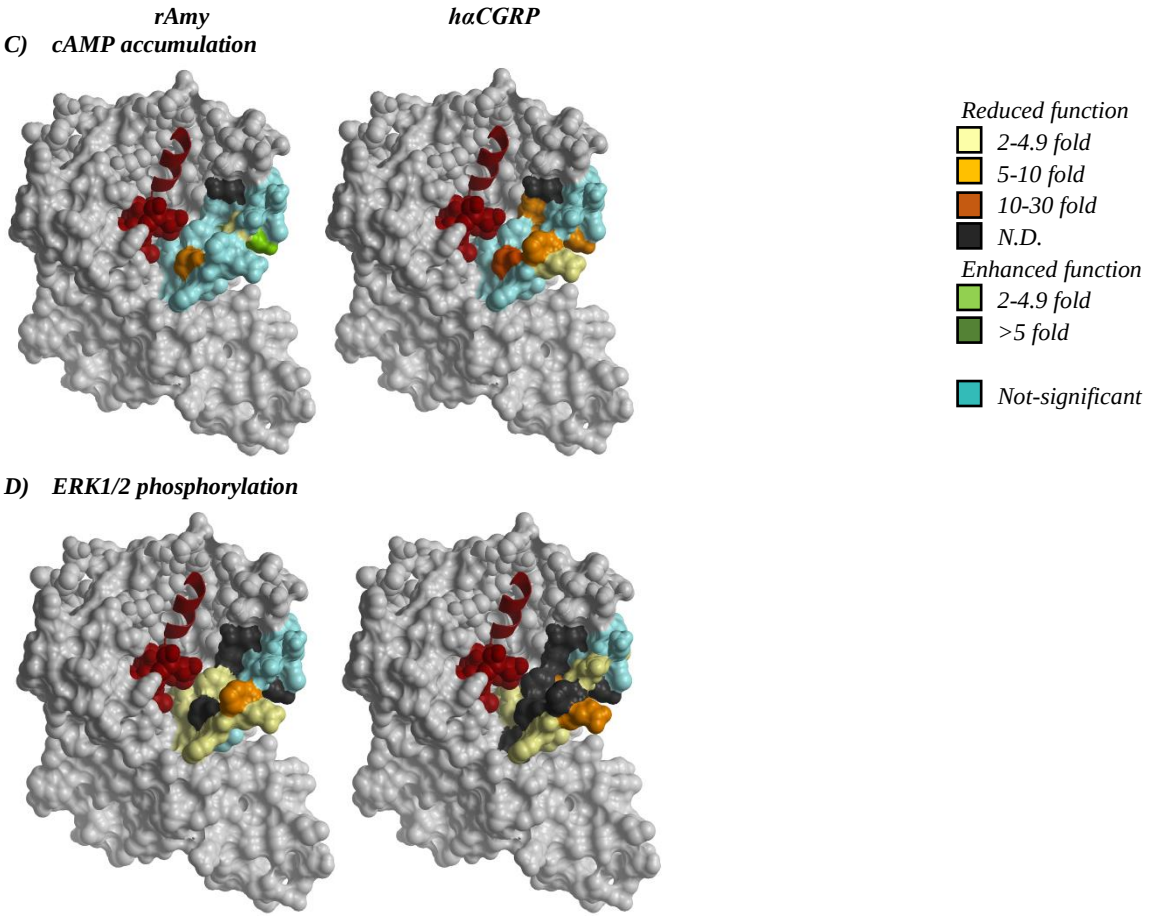

Figure 5.32 Heat-map 3D representation of ECL2 of the hCTR and the effect of alanine substitution on rAmy and hαCGRP equilibrium affinity and intracellular signalling. *Active model based on the active Cryo-EM structure of CTR in complex with sCT (Liang et al., 2017) into which the three ECLs were modelled). Residues 1-136 and 200-217 (that would partially cover ECL2) are hidden. The model shows sCT ligand (in burgundy) where the cyclic N-terminus (residues 1-7) is represented by space fill, residues 8-16 are tightly structured in an α-helix (ribbon), while the C-terminus (residues 17-32) of the ligand is hidden. Residues that produced significant changes in binding affinity or signalling efficacy were coloured following the colour scheme for fold effect from WT in Figures 4.13 and 4.29.*

5.3 Discussion

The juxta membrane region, and in particular ECL3 and adjacent TM6 and TM7 are known to be crucial for receptor activation and intracellular signalling for some GPCRs (Wheatley et al., 2012). Inactive/partially active and fully active crystal structures of the β1AR show that agonist binding triggers outward movement of ECL3 that initiates the conformational rearrangement of the TM bundle and the large twist of over 10 Å of TM6 at the intracellular face of the receptor that opens the binding pocket to intracellular effectors (Warne et al., 2008, Warne et al., 2011, Moukhametzianov et al., 2011, Lebon et al., 2011, Rasmussen et al., 2011b, Rosenbaum et al., 2011, Jaakola et al., 2008). Comparison of the available inactive and active structures of Class B1 GPCRs (Zhang et al., 2017b, Zhang et al., 2017a, Song et al., 2017, Liang et al., 2017, Hollenstein et al., 2013, Siu et al., 2013), suggest that movements at the top of TM6, TM7 and ECL3 are also associated with receptor activation. To expand the knowledge on how distinct ligands engage with the CTR to trigger distinct intracellular signalling pathways (cAMP, IP1 and pERK1/2), we have investigated the role of ECL3 and adjacent TMs (TM6 and TM7) in $hCTR_aLeu$ function. The use of different ligands, some of which exhibit biased signalling (Chapter 3), allowed us to explore the importance of this domain in binding of these ligands, and in coupling to unique signalling pathways that may be linked to the observed biased agonism profiles.

From our functional characterisation, K370A produced neither detectable specific binding of the radiolabelled antagonist nor measurable intracellular signalling, suggesting that this mutant is not functional and/or not expressed at the plasma membrane. I371A also showed no specific binding, but this CTR mutant produced a weak response in cAMP and IP1 assays (but not in pERK1/2), suggesting that this receptor was expressed but may be at a low level when compared to WT.

5.4.1 The importance of ECL3 of the hCTR for CT peptide binding

The activation of Class B1 GPCRs requires a major movement of TM6 that is facilitated by a large kink in this TM (as revealed by the recent Cryo-EM structure (Liang et al., 2017)). A movement in TM7 is also evident. Therefore it was not surprising to observe that the majority of the mutations introduced in TM6-ECL3-TM7 altered affinity of both hCT and pCT. However, hCT is affected by more residues

within this binding groove when compared to pCT, indicating that these two ligands either assume different orientations, or engage different residues in the receptor due to sequence differences in the peptides sequence (discussed in Chapter 4 and supported by photo-crosslinking studies using different CT ligands (Dong et al., 2004b, Pham et al., 2005)).

On the other hand, binding affinities of sCT and sCT(8-32) were mostly unaffected by any alanine substitutions of ECL3. This is consistent with affinity being principally driven by interactions between the receptor and the C-terminus and mid-region of these peptides, to give rise to high affinity and pseudo-irreversible binding (at least for the agonist sCT), and not the N-terminal ring structure that is adjacent to residues in TM6-ECL3-TM7 region. The exceptions to this were Y372 and D373 that have roles in affinity of all 3 CT peptides, albeit larger effects on hCT and pCT. While Y372 stabilises interactions between TM1 and TM7, D373 interacts with K11 in the sCT-CTR model (***Figure 5.32***). As noted in Chapter 4, the mid-region of the peptide is important for binding kinetic and affinity of hCT and sCT. Differences in charge/polarity and size of this important region of the ligand could account for differential interactions between peptide and receptor. Indeed, Lys 11 in sCT corresponds to Thr or Ala residues in pCT and hCT peptides, respectively. The potential salt bridge interaction that K11 of sCT establishes with D373 could be therefore substituted by a polar interaction in pCT, while A11 of hCT would not be able to form any polar contacts with the receptor. The predicted weakening of the strength of this interaction is also mirrored by a right shift in equilibrium pK_i of pCT and hCT. K11 is located within the 11-13 segment of sCT that has been implicated in the slow dissociation of this ligand compared to hCT (Hilton et al., 2000, Furness et al., 2016). However, Furness et al. (2016) has shown that affinity and potency of sCT are unaltered by the substitution of these residues with the corresponding hCT equivalent (Furness et al., 2016). As such, in sCT, K11-D373 may form a secondary interaction, not required for binding, but stabilising the peptide interaction. Interestingly, the low affinity ligands rAmy and hαCGRP (discussed in Section 5.4.3) both contain Arg residues in position 11. In these cases D373A mutation did not alter affinity, but modulated peptide efficacy for pERK1/2 (for both peptides) and cAMP (for hαCGRP). As discussed in Chapter 4, RAMPs allosterically influence the both potency and affinity of rAmy and hαCGRP, and are predicted to modify the pose of

the peptides within the binging groove, both at the level of the NTD and at the TM bundle (Barwell et al., 2011, Harikumar et al., 2009, Udawela et al., 2006a, Udawela et al., 2006b). Future work will examine the CTR ECLs mutants in the presence of RAMPs, and this will be important for elucidating of the mechanistic role of RAMP on both affinity and efficacy of rAmy and hαCGRP.

Our model predicts that the top of TM7 is in close proximity of the mid region of sCT (11-15). This would be consistent with observations made on other Class B1 GPCRs. For instance, the use of chimeric receptor between GCGR and GLP-1R showed that TM6 and TM7 are crucial for sorting/selectivity of peptide ligands (Runge et al., 2003b). Additionally, a follow up study showed that D385 (in TM7) of GCGR (equivalent to M376 of CTR) could be in close proximity of L12 of GCGR.

Previous work showed that Bpa8-hCT ligand photo-crosslinked to residue L368 of CTR (Dong et al., 2004b), while the equivalent V8 of sCT in not proximal to L368 in our model, supported by the observation that mutation of L368 to Ala does not alter sCT affinity. There are a range of possible explanations for this apparent discrepancy, including flexibility of both ECL3 and of the side chains of the ligand. Indeed, the CTR structure from which our 3D model was derived, showed low resolution density for both the side chains of the peptide and the ECL3, suggesting a high degree of flexibility of both peptides. Additionally, Bpa is a large reactive group and can cross-link residues within 6-10 Å from the peptide, bridging the distance between ligand and ECL3. While other data in Chapter 4 and the current Chapter support the potential for sCT and hCT to adopt different poses when bound to the active receptor.

Another interesting mutation, P360A, significantly reduced affinity of all CT agonists but not of the antagonist (***Figure 5.7, 5.31 A, 5.32, Table 5.1***). P360 is localised at the top of TM6, 2 turns above the absolutely conserved P350 ($P^{6.47}$) (***Figure 5.33***), that plays a fundamental for the activation of all GPCRs, and is fulcrum for large kink in TM6 in active CTR and GLP-1R structures (Liang et al., 2017, Zhang et al., 2017b). P360 is conserved in calcitonin-like receptors (***Table 5.1 A***), but not other Class B1 receptors. Previous studies where P360 was mutated to alanine in CTR showed that this mutation significantly reduced (but not abolished) affinity of hCT (but not sCT), and reduced potency (10 fold) of hCT (but had no effect on sCT) in cAMP formation (Bailey and Hay, 2007). Our data is consistent

with the hCT observations, however affinity for all CTs was reduced in the current study. The structure of the active CTR confirmed that the entire TM6-ELC3-TM7 interface undergoes a large conformational rearrangement upon agonist binding when compared to active TM models (Liang et al., 2017). Although the N-terminal loop between C1 and C7 that characterises calcitonin-like peptides is not required for sCT function (Hilton et al., 2000), we could speculate that these ligands are structurally less flexible when compared to other peptide ligands of Class B1, and may require additional contacts that alter residues within the deep portion of the binding groove. This could explain why all CT peptide are affected by P360A mutation, while the antagonist sCT(8-32), which lacks the N-terminal loop, is unaffected by this mutation.

We have already discussed in Chapter 4 the potential interactions between the N-terminus of the peptide and TM5, while data presented in the current Chapter highlights that the nearby residues of TM6 deeply buried within the TM groove (F356-E361) are also important for both affinity and/or efficacy of all CT peptides in different signalling pathways. Our model predicts that the two aromatic residues F356 and F359 are localised close to L4 and C7 of sCT (***Figure 5.34***), and mutation of these residues had both common and peptide-specific effects in different pathways. M376 in TM7 packs between F356 and F359, and also has a complex pattern of effect across peptides and pathways. Thus hydrophobic interactions between these three residues may be important for function. Mutation of surrounding V357, V358, P360, W361 and R362 are likely to influence this tight packing and alter the contacts lining the peptide binding groove. Interestingly, these residues, when mutated, did not alter sCT affinity, but had dramatic effects on hCT and pCT hydrophobic contacts with the peptides. Interestingly, in sCT, the 1-7 disulphide bond is not required for peptide affinity or potency, and indeed truncations of residues 1 and 2 does not affect sCT affinity (Hilton et al., 2000). In contrast, lack of the disulphide bond does have an impact on hCT (at elast at the rat and rabbit receptors) (Goltzman, 1980). It is therefore possible that for sCT, the slow off-rate holds sCT bound to the receptor. Even without the constraints of disulphide bond, the sCT could explore different conformations and eventually adopt the correct conformation/interactions to surpass the energy barrier to trigger receptor activation and signalling. On the other hand, for the low affinity peptide hCT (with faster K-off) the disulphide bond may be required

to constrain the N-terminal conformation such that it can bind and activate the receptor without having to explore this conformational space. Additionally, in the sCT-CTR-Gαs structure (Liang et al., 2017), residues 1 and 2 are oriented towards the extracellular vestibule and there is high flexibility in both this segment of the peptide and the proximal segment of the receptor. It is therefore possible that this receptor domain may establish weak or transient interactions with the peptide, important for correctly position of the peptide N-terminus. These interactions would be disrupted by mutation, leading to the greater impact on hCT and pCT.

5.4.2 Importance of ECL3 of the hCTR for CT peptide efficacy and biased agonism

The Class B1 active Cryo-EM structures reveal the importance of reorganisation of the extracellular face of TM6 and TM7 for conformational propagation to the intracellular face of the receptor where TM6 undergoes a large outward movement to reveal the binding pocket for the α5- helix of the Ras-like domain of Gαs. (Section 1.2.1) (Liang et al., 2017). The involvement of TM6 and TM7 in receptor activation and intracellular signalling is widely accepted for all GPCRs, and has been confirmed for some Class B1 receptors by both mutagenesis studies and the two active receptors structures (Zhang et al., 2017b, Liang et al., 2017, Wootten et al., 2016, Barwell et al., 2012, Barwell et al., 2011, Gardella and Juppner, 2001, Dong et al., 2014).

ECL3 bridges TM6 and TM7, and it is thus not surprising that this segment of the CTR playa a major role in the activation of signalling for all CT peptides, and indeed in the selective control of different signalling pathways (***Figure 5.31***).

Distinct regions of ECL3 were engaged for activation of the different signalling pathways, as revealed by broad assessment of multiple ligand across three important signalling end-points for the various mutants of CTR. For all three CT agonists, most residues that contributed to affinity were also important for cAMP signalling, although Ala substitution primarily improved efficacy (whilst decreasing affinity). This implies that, although the residues contributed to ligand binding, they were also important for maintaining networks that provide and energy barrier for Gαs engagement (***Figure 5.31 A and B***). On the

other hand, all CT agonists showed interesting similarities in terms of ECL3 residues required for the activation of both IP1 formation and ERK1/2 phosphorylation. The similarities are evident from the heat-mapping onto the model, where the overall pattern for IP1 formation and ERK1/2 phosphorylation are similar for individual ligands, with only a few minor differences between the pathways (***Figure 5.31 C and D***). This provides further support for the theory proposed in Chapter 4, that IP1 and pERK1/2 may be correlated and downstream of the same signalling effector (i.e. Gαq). Of note, although the pattern of mutational effect for individual ligands is similar for both these pathways, there are peptide specific differences between these maps. For instance, mutations across ECL3 generally enhanced sCT efficacy, and only a few mutations negatively impacted on IP1 and pERK1/2 signalling. In contrast, for hCT and pCT, Ala mutations generally reduced the ability of these peptides to induce coupling to these pathways. This suggests that while these different peptides may engage with similar regions within the receptor, the consequences of these interactions in terms of signalling propagation differ.

5.4.3 Importance of ECL3 of the hCTR for rAmy/hαCGRP peptide binding and efficacy

Our mutagenesis identified some interesting differences when comparing functional heat-maps of rAmy and hαCGRP with CT peptide agonists (***Figure 5.31*** and ***5.32***). Data in Chapter 4 suggested that rAmy and hαCGRP may adopt distinct poses within the TM groove relative to CT peptides, especially when RAMPs are not present to allosterically modulate CTR structure/function (Gingell et al., 2016, Qi et al., 2013, Qi and Hay, 2010, Morfis et al., 2008, Udawela et al., 2006b, Udawela et al., 2006a, Hay et al., 2006). Interestingly, there was a close overlap in ECL3 residues important for rAmy and sCT for cAMP pK_A and efficacy, with very few residues altering function. In contrast, hαCGRP had a distinct pattern of sensitivity to mutation, with multiple interconnected residues lining the peptide groove reducing cAMP efficacy when mutated. This enhances evidence that, in the absence of RAMPs, hαCGRP engages CTR very differently to CT peptides.

Noticeably, hαCGRP and were broadly sensitive to mutation of ECL3 in pERK1/2 signalling, further supporting the hypothesis that the pERK1/2 pathway is activated by upstream effectors other than Gαs

protein. Moreover, ECL3 mutants had a more severe impact on hαCGRP than rAmy or CT peptides. For example, mutagenesis of ECL3 reduced hαCGRP efficacy in both cAMP and pERK1/2 pathways, whereas an opposite effect on cAMP vs pERK1/2 was observed for CT peptides. To address this, further investigation of individual peptide response using selective inhibitors to block signalling cascades linked to different upstream effectors could be used to dissect the relative contribution of these effectors to ERK1/2 phosphorylation.

Select residues of the top of TM6 were globally important for functional activity of all peptides, for instance, P360 is also crucial for both hαCGRP and rAmy efficacy in both cAMP and pERK1/2 signalling. Ala mutagenesis of the P360 equivalent in CLR (P331A) led to reduced receptor function in response to CGRP (Conner et al., 2005), confirming the importance of this residues in the calcitonin-like receptors. Ala substitution of E357 and I360 of CLR (S364 and M367, respectively, in CTR) reduced cAMP potency of CGRP (Barwell et al., 2011). Interestingly, select mutation of ECL3 of CLR was important for binding AM (but not CGRP) and Gαs protein activation and signalling (Kuwasako et al., 2012), which is consistent with the differential involvement of individual receptor residues across peptides and pathways for the CTR that was revealed in the current study.

The Importance and differential involvement of ECL3 in activation of cAMP signalling pathways was also demonstrated through generation of chimeric receptor of other Class B1 GPCRs, including GLP-1R/GCGR (Runge et al., 2003b) and CLR/VPAC2 (Kuwasako et al., 2012), which showed that ligand N-terminus and TM6-ECL3-TM7 interactions may be a mechanism of different receptors to distinguish peptides with divergent N-termini sequences and this selectivity affects activation of the receptor. This may be important for the CTR activation triggered by CT peptides vs rAmy or hαCGRP.

Studies on different Class B1 receptors have suggested that the outer surface of ECL3 and TM6 could be part of the interface for RAMPs (together with the NTD), and removing these important contacts alters CLR trafficking and expression, binding affinity and cAMP signalling of Amy and CGRP, supporting a potential allosteric modulator role of RAMPs via interaction with TM6 (Barwell et al., 2011, Harikumar et al., 2009, Udawela et al., 2006a, Udawela et al., 2006b). It would therefore be

crucial to assess the role of ECL3 on rAmy, hαCGRP and CT peptide function when the CTR is in the presence of RAMPs.

5.4.3 Summary

Ala scanning of ECL3 has revealed the crucial role played by this receptor domain in both ligand binding and in the activation of intracellular signalling pathways. We have observed similar key residue network, but distinct patterns, involved in binding affinity and cAMP formation. Additionally, some interesting similarities observed in the key networks involved in both IP1 and pERK1/2 further support to the hypothesis presented in Chapter 4 about a potential link between these two pathways.

To further explore the molecular bases of biased agonism at the CTR, we use of different ligands and mapped our results onto heat-maps, revealing peptide specific differences. We attributed these differences to a combination of sequence differences across peptides, and different ligand binding affinities/kinetics that could translate into distinct pose of the peptides and interactions between peptide and receptor. Comparison between our results to published studies on other Class B1 GPCRs supports the crucial role played by TM6-ELC3-TM7 in ligand binding, receptor activation and intracellular signalling, while highlighting also some peculiar differences across receptors.

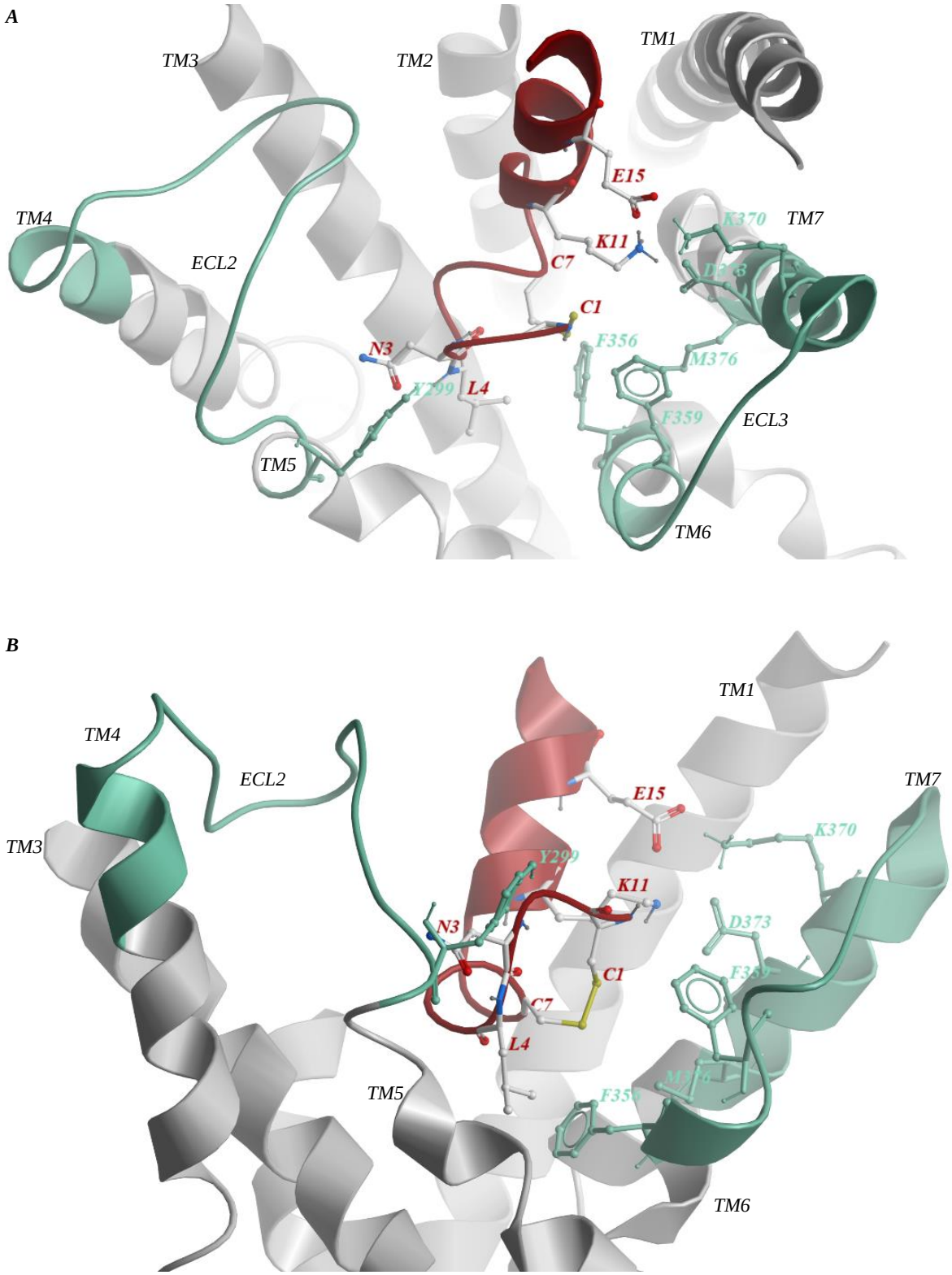

Figure 5.32 3D model showing proximity between sCT N-terminus and the top of the TM bundle of hCTR. *Ribbon representation of the (A) top view and (B) side view of the TM bundle of the sCT-CTR complex (described in Figure 5.1). Ligand is shown in burgundy, while receptor is in green. Regions highlighted in green represent residues investigated in Chapter 4 and 5. Residues F356, F359, K370 and D373 (of CTR), and C1, L4, C7, K11, E15 (of the sCT) that in this model are in close proximity were shown with sticks.*

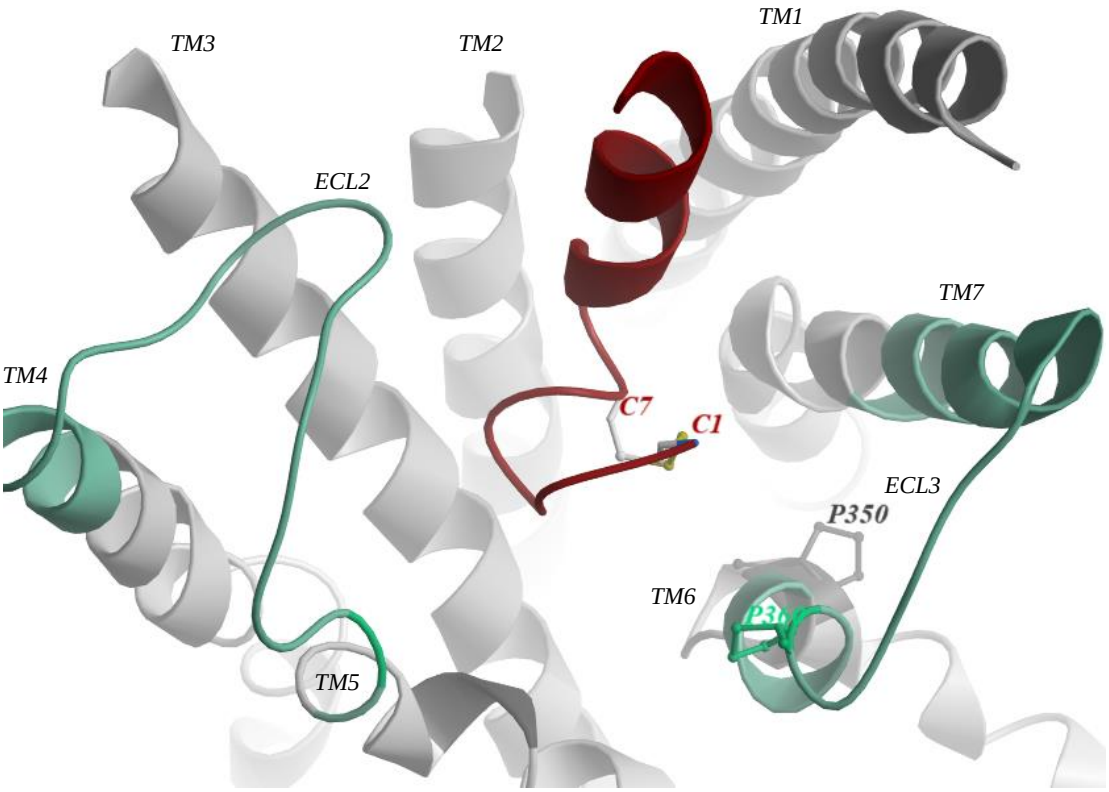

Figure 5.33 conserved Proline residues of TM6 of Calcitonin-like receptors. *Ribbon representation of the top view of the TM bundle of the sCT-CTR complex model (described in Figure 5.1). Residues in ECL3 mutated in this study (and also those in ECL2 described in Chapter 4) were highlighted in green. Conserved Pro residues of TM6 of calcitonin-like receptors and N-terminus loop characteristic of the calcitonin-like ligands are shown with sticks.*

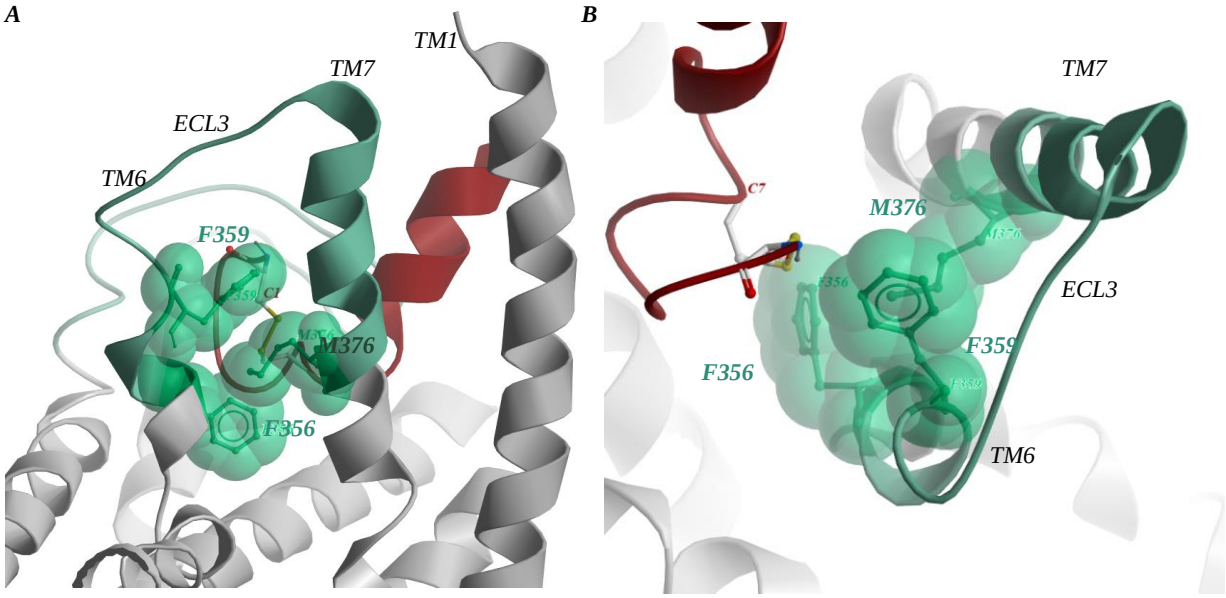

Figure 5.34 Hydrophobic stacking interactions between TM6 and TM7. *(A) Side view and (B) top view of the TM bundle of the sCT-CTR complex model, represented as ribbon. Residues in ECL3 mutated in this study were highlighted in green. Residues important for packing of TM6 and TM7 were represented by sticks and space fill.*

CHAPTER 6

General discussion and future directions

GPCRs are integral membrane proteins that can be found in all organs and tissues (Bjarnadottir et al., 2006, Fredriksson et al., 2003, Takeda et al., 2002, Venter et al., 2001). They recognise a wide variety of stimuli and are involved in almost all physiological functions, making them appealing therapeutic targets (Lagerstrom and Schioth, 2008, Rask-Andersen et al., 2014, Overington et al., 2006, Tyndall and Sandilya, 2005). Additionally, a number of these receptors have been shown to control multiple physiological outcomes via pleiotropic coupling (Bologna et al., 2017, Rajagopal et al., 2010). As a result, indiscriminate targeting can lead to on-target side effects. One example is the adenosine 1A receptor ($A_{1A}R$), a potential candidate target for cardio-protection after ischemia-reperfusion, for which drug development has been severely limited due to on-target adverse bradycardia (Mustafa et al., 2009, Valant et al., 2014).

Recently, the functional characterisation of many GPCRs has highlighted the phenomenon of biased agonism (Kenakin, 2011, Kenakin and Christopoulos, 2013) (***Figure 1.5***). Biased agonism is the ligand-dependent stabilisation of distinct ensembles of receptor conformations, which in turn differentially modulates coupling to distinct effectors (Kim et al., 2013, Furness et al., 2016). Conceptually then, it should be possible to design a biased agonist which would have the potential to differentially modulate signalling pathways and selectively trigger therapeutically beneficial pathways without triggering on-target side effects. However, to rationally design biased compounds, it is fundamental to understand the mechanism that gives rise to different signalling downstream of a particular GPCR, as well as identify which pathway activation profile leads to beneficial effects and which to adverse ones.

In this context, information available on Class B1 GPCRs, and in particular, CTR is limited. CTR is involved in bone remodelling and calcium metabolism (Fujikawa et al., 1996b, Nicholson et al., 1986, Kallio et al., 1972, Selander et al., 1996, Sexton et al., 1987, Marx et al., 1972, Carney, 1996, Cornish et al., 2001, Quinn et al., 1998, Fujikawa et al., 1996a, Wookey et al., 2010, Marx et al., 1974, Perry III et al., 1983), regulation of food intake (Eiden et al., 2002, Bello et al., 2010), central and peripheral analgesic functions (Hilton et al., 1995, Liberini et al., 2016, Fabbri et al., 1985, Bower et al., 2016, Shah et al., 1990, Rohner and Planche, 1985, Laurian et al., 1986) and is implicated in tumour proliferation (Lacroix et al., 1998, Nakamura et al., 2007, Sabbisetti et al., 2005, Thomas and Shah,

2005, Thomas et al., 2006, Thomas et al., 2007). Only a few of the known ligands of the human CTR have been pharmacologically profiled (Hilton et al., 2000, Furness et al., 2016), with limited profiling of signalling pathways for these ligands (Kuestner et al., 1994, Wolfe et al., 2003, Moore et al., 1995, Chabre et al., 1992, Raggatt et al., 2000, Thomas and Shah, 2005). Therefore, although there is potential for biased agonism at the CTR, this has not been well defined. To add further complexity, the CTR is commonly expressed in humans in at least two splice variants (Gorn et al., 1992, Kuestner et al., 1994), along with two common (non-synonymous) polymorphisms (Egerton et al., 1995, Gorn et al., 1995). These structural differences are localised at the intracellular portion of the CTR, and can impact on how the receptor engages and activates intracellular effectors; ultimately resulting in changed receptor function (Kuestner et al., 1994, Moore et al., 1995). Additionally, the CTR can also form complexes with RAMPs, accessory proteins that allosterically modulate CTR (and several other GPCRs) function (Routledge et al., 2017).

This thesis aimed to: (i) compare the effect of receptor variants on CTR function, and to specifically identify whether naturally occurring structural differences of the intracellular portion of the receptor have an effect on either ligand binding or intracellular signalling. (ii) Investigate whether biased agonism at the CTR could be identified, by performing an extended pharmacological characterisation of different CTR agonists. (iii) Once identified, to understand the mechanistic bases that drive biased agonism, by performing an Ala scanning mutagenesis study of the juxta membrane vestibule of the TM bundle.

6.1 Characterisation of the effect of hCTR variants on receptor function

In humans, alternative splicing of the calcitonin receptor transcript produces multiple variants of the CTR (Gorn et al., 1992, Kuestner et al., 1994). The two most common splice variants, $hCTR_b$ and $hCTR_a$, exhibit tissue specific expression and differ from one another by a 48 nucleotide insert encoding an additional 16 amino acids in ICL1 (Gorn et al., 1992, Kuestner et al., 1994). In whole cell binding assays this change to the intracellular portion of the CTR did not affect the affinity of any of the CT

peptides assessed. Consistent with well established knowledge, I observed that hCTR activation promotes increased intracellular cAMP (Chabre et al., 1992, Raggatt et al., 2000, Nicholson et al., 1986, Kuestner et al., 1994, Moore et al., 1995, Gorn et al., 1995, Wolfe et al., 2003, Findlay et al., 1980, Gorn et al., 1992, Frendo et al., 1994) and ERK1/2 phosphorylation (Raggatt et al., 2000, Thomas and Shah, 2005), while only $hCTR_a$ splice, but not $hCTR_b$, triggered a rapid intracellular Ca^{2+} mobilisation (Chabre et al., 1992, Kuestner et al., 1994, Moore et al., 1995). In Chapter 3, I have discussed the importance of ICLs for interaction with G proteins (Kleinau et al., 2010, Bavec et al., 2003, Iida-Klein et al., 1997, Cypess et al., 1999, Garcia et al., 2012), and hypothesised that the 16 amino acid insertion in ICL1 could modulate coupling efficiency of the effector to the different CTR variants. I observed that the $hCTR_a$ variant exhibited more efficacious coupling to all endpoints compared with $hCTR_b$, whereas ligand potency at $hCTR_b$ was much closer to ligand affinity. This reduced coupling efficacy correlates well with observations from recently solved Cryo-EM sCT-$hCTR_a$Leu-Gαs heterotrimer complex showing that ICL1 sits above both the β subunit and the N-terminal α-helical domain of the Gαs subunit (Liang et al., 2017); thus the additional insert in $hCTR_b$ is likely to interfere with effector coupling. This would be consistent with a loss of Gαq coupling, and is supported by my preliminary data demonstrating a Gαq-component of the iCa^{2+} response (***Figure S1, Appendix 1*** and Section 3.2.3).

I have also discussed that the observed pERK1/2 response is likely to be a convergent point of muliple signalling pathways. This is supported by Morfis et al. (2008) and Thomas and Shah (2005), who have shown that pERK1/2 is downstream of PLC, PKC and Akt phosphorylation. Although we have yet to investigate Akt contribution to pERK1/2 in our COS-7 cells, singalling data from Chapter 3, and heat-maps of Chapters 4 and 5 (showing a similar pattern of residues important for activation of both IP_1 and pERK1/2) (***Figure 6.1***) support a Gαq-contribution to the pERK1/2 signalling.

Despite limited evidence linking the different signalling pathways controlled by the CTR to physiological function, in Section 3.3.7 I have discussed that PKA (downstream of cAMP formation) is involved in cytoskeletal remodelling, changes in cellular metabolism and re-localisation of membrane transporters and Ca^{2+}-dependent pathways (upstream of PKC) (Morfis et al., 2008) are involved in regulating lysozyme acidification, cell shape and motility (Li et al., 2006, Suzuki et al., 1996, Li et al.,

2008). Downregulation of CTR is downstream of PKA activation (Takahashi et al., 1995, Wada et al., 1996, Wada et al., 1995), while PKC activation blocks bone remodelling (Yamamoto et al., 2005b, Sørensen et al., 2010). Understanding of how the different splice variants control these pathways and how it is linked to the different tissue expression of the two splice variants will help in understanding the physiological function of CTR.

Agonist induced internalisation is a common phenomenon for many GPCRs (Ferguson, 2001) and it is known that chronic administration of CT agonists induces CTR downregulation (Takahashi et al., 1995, Wada et al., 1996, Wada et al., 1995). In this study, in both COS-7 cells and human derived osteoclasts, both splice variants of the hCTR were shown to constitutively internalise. Internalisation of both $hCTR_a$ and $hCTR_b$ has been shown in different physiological and recombinant cell systems in presence of radioligand (Findlay et al., 1982, Lamp et al., 1981, Wada et al., 1995, Findlay et al., 1980, Michelangeli et al., 1982). The rapid internalisation of CTR I observed may have gone un-noticed in other studies, however, in contrast to our results, (Moore et al., 1995) did report that in BHK the $hCTR_b$ splice variant did not internalise. It is possible that this discrepancy in CTR trafficking could be cell background dependent. It is also possible that the two splice variants internalise at different rates (either speed or amount of receptor internalised vs receptor retained at the cell surface), an aspect of CTR trafficking that has not been assessed. In different human tissues the relative expression of the $hCTR_b$ transcript differs markedly when compared to the $hCTR_a$ variant (Kuestner et al., 1994, Frendo et al., 1994, Gorn et al., 1995, Gorn et al., 1992). Differential internalisation of these 2 variants could be a mechanism that preserves receptor at the cell surface in presence of chronic stimulation to provide a minimum CTR reserve at the cell surface (to respond to new stimuli). This would be interesting physiologically, as the $hCTR_a$ transcript is widely expressed whereas the $hCTR_b$ transcript is only present in a subset of overlapping tissues.

I also obsered that internalisation of the hCTR is ligand-independent. Similarly, (Seck et al., 2003) reported that, in HEK293 cells, rabbit CTR also constitutively internalises in a filamin dependent manner, with a mixture of degradation and recycling of the internalised receptor. In this case, agonist

stimulation was seen to protect internalised CTR from degradation while increasing receptor recycling. Although I was not able to detect ligand-induced changes in CTR internalisation, the observed rapid trafficking could be a mechanism for delivering the receptor to intracellular compartments enabling continueed CTR-dependent signalling, a phoenomenon observed for other GPCRs (Calebiro et al., 2010). We have yet to explore the whether the underlying mechanism for human CTR internalisation is the same as observed in HEK293 cells for the rabbit receptor and currently have no data to address intracellular signalling, which will be interesting to pursue in future studies.

Another family of potential intracellular effectors that can contribute to pERK1/2 signalling and receptor trafficking comprise the β-arrestins. To date only one study, conducted in U2OS cells, has shown that CT ligand addition promotes β-arrestin recruitment (Andreassen et al., 2014). In contrast, I was not able to detect any ligand-dependent β-arrestin recruitment or re-localisation for any of the CTR splice variants assessed by several methods in the COS-7 cells background, and this may be related to modification of the CTR C-terminal tail used in the former study.

I also investigated the effect that a common, non-synonymous, single-nucleotide polymorphism (SNP, SNP ID: rs1801197), at the 3' end of the coding region (residues 447 in the $hCTR_a$ splice variant), has on receptor function. This C/T polymorphism encodes either a Pro (completely conserved across species where CTR have been identified) or a Leu (identified only in humans thus far) in the C-terminal tail of the receptor (Egerton et al., 1995, Gorn et al., 1995). Interestingly, the Pro polymorphism is the predominant variant present in the Asian population (Nakamura et al., 1996), while Caucasians, Hispanics and African-Americans are either Leu homozygous or Leu/Pro heterozygous (Wolfe et al., 2003). SNPs can be associated with increased risk of developing disease (Balasubramanian et al., 2005, Braga et al., 2002, Masi et al., 1998b, Dehghan et al., 2016), and although no strong correlation has been found thus far (based on low power clinical meta-analysis), the extremely common polymorphism has been correlated with increased incidence of development of osteoporosis and kidney stone diseases (Masi et al., 1998a, Braga et al., 2002, Masi et al., 1998b, Mitra et al., 2017).

I could not measure any statistical difference attributable to this polymorphism in affinity or cAMP potency for hCT, sCT or pCT peptides. I also investigated the effect of this polymorphism on $_iCa^{2+}$ signalling and pERK1/2, downstream of CTR activation. In Section 3.2.3.4 bias plots support that this single amino acid substitution in the C-terminal terminus of hCTR can lead to peptide-dependent changes in cellular response. Specifically, the Pro polymorphism favours $_iCa^{2+}$/pERK1/2 responses over cAMP signalling when compared to the Leu variant. Although my results have yet to be extended to a more physiologically relevant system, my data suggest that the common P447L polymorphism could predispose a cohort of patient toward a pathology and/or change the response of a cohort of patients to different therapeutics.

6.2 Identification of potential biased agonists of the hCTR

The CTR exhibits promiscuous coupling, however biased agonism has yet to be explored. As a tool to understand biased signalling at the CTR I used CT peptides from different species, which are characterised by a partially conserved N-terminus with different mid-regions and C-terminus. Comparison of pharmacological response across CT agonists confirmed consolidated knowledge that hCT, pCT, cCT and sCT have distinct affinities for the CTR (Section 3.2.2) (Hilton et al., 2000, Wolfe et al., 2003), which is reflected in their binding kinetics (Furness et al., 2016).

Representation of my functional characterisation in bias plots (Section 3.2.3.4) revealed a similar functional profile of hCT and sCT, which are marketed therapeutics. Interestingly, my characterisation revealed that pCT is a potential biased agonist of the CTR, with a profile that tends away from cAMP signalling and towards $_iCa^{2+}$ and pERK1/2 response when compared to the reference ligand hCT (***Figure 3.7-9***). cCT also has a distinct response pattern that differs from the reference (hCT) peptide. This is especially true at the $hCTR_b$ polymorphic variants, where the cCT signalling profile was biased towards cAMP and away from pERK1/2 pathways at the Pro polymorphic variant, whereas it was biased towards pERK1/2 at the Leu variant.

The pharmacological characterisation also included PHM-27, an endogenous peptide structurally unrelated to CT peptides, reported to be a full agonist of the CTR in HEK293 (Ma et al., 2004). In the stable COS-7 cells, this peptide was a weak partial agonist at all variants of the hCTR. In Section 3.3.5,

we have attributed these discrepancies between our findings and published data to differences in cell background or to presence/absence of RAMPs (discussed in Section 6.5), accessory proteins that modify the CTR (and other GPCRs) function (Archbold et al., 2011).

6.3 Understanding the mechanistic basis of hCTR function

To understand molecular mechanism of CTR activation and explore how different ligands promote the biased agonism identified in Chapter 3, alanine scanning mutagenesis was performed on ECL2 (Chapter 4) and ECL3 (Chapter 5) and adjacent TMs. Binding affinity and signalling characterisation was performed on these mutants on the $hCTR_aLeu$ receptor variant in presence of hCT, sCT and pCT peptides. ***Figure 6.1*** shows the combined the data from Chapters 4 and 5 mapped onto our sCT-CTR model.

My results revealed that distinct portions of ECL2 and ECL3 are differentially engaged, by CT peptides from different species, for binding and intracellular signalling. Specifically, the TM3-TM4 interface and adjacent residues in ECL2, and the distal part of TM5 in close proximity to TM6 are important for hCT peptide binding (***Figure 6.1 A***). Interestingly, comparison of my results with a similar study on GLP-1R revealed that, analogous to CTR, ECL2 and ECL3 are both important for GLP-1 binding to GLP-1R (Wootten et al., 2016, Koole et al., 2012b, Wootten et al., 2015), suggesting that ligand binding at Class B1 occurs across overlapping regions of the receptor. Additionally, the importance of TM5 and TM6 in ligand binding and receptor activation is supported by comparison of available active/inactive structures Class B1. These show that an outward movement of the top of these two TMs is required for the access of the ligand to the binding groove (Zhang et al., 2017b, Liang et al., 2017, Rasmussen et al., 2011b). Additional residues within ECL3 of CTR are required for IP_1 and pERK1/2 signalling (***Figure 6.1 C and D***). Conversely, ECL2 plays little role in the activation of cAMP signalling pathways, where ECL3 is crucial (***Figure 6.1 B***). The comparison of my results with GLP-1R showed some interesting differences (Wootten et al., 2016); in cAMP formation, GLP-1R stimulated by GLP-1(7-36)NH_2 required more involvement of ECL2 and less of ECL3. In ERK1/2 phosphorylation, ECL3 is the main driver of GLP-1R response, while ECL2 shows limitedly involvement, which is quite different from

CTR where both ECLs are important in activation of this pathway. On the other hand, $_iCa^{2+}$ mobilisation (which, like IP_1, is downstream of Gαq activation) requires a similar network of residues in both ECL2 and ECL3. This would suggest that despite the similar overall organisation of Class B1 receptors and a number of key conserved residues, the ligands of this receptor class engage with their receptors in a distinct manner to promote the activation of analogous signalling pathways.

Interestingly, the analysis of bias plots (Chapter 3) comparing $_iCa^{2+}$ (or cAMP) and pERK1/2 pathways for the different CTR variants, in particular the $hCTR_b$, suggested that the Gαq coupling to hCTR could be one of the main drivers for the pERK1/2 signalling. This is supported by the observation that the network of residues involved in IP_1 and pERK1/2 signalling closely resemble each other (Chapter 4 and 5).

In Chapters 3, 4 and 5 I also hypothesised that activation of pERK1/2 could be convergent from signalling pathways beyond cAMP, $_iCa^{2+}$ and IP_1. Although I was not able to detect β-arrestin recruitment upon CTR activation in COS-7 cells, I cannot exclude that CTR could recruit these, or other, effectors in CV-1 cells (not yet assessed), which may contribute to the pERK1/2 response. For instance, CLR, the most closely related receptor to CTR, and also activated by αCGRP and Amy, when complexed with RAMPs, can recruit Gαi proteins in HEK293 (Weston et al., 2016). My data indicates that, in COS-7 cells, this is not the case for CTR (***Figure S1*** Appendix 1), however, this also needs to be assessed in CV-1 cells to determine if the same pattern of response is maintained across these distinct cell backgrounds.

Figure 6.1 shows that mutations in ECL2 and ECL3 had limited effect of cAMP formation induced by sCT, while the same mutations altered hCT and pCT efficacies. This indicates that other regions of the receptor vestibule, yet to be investigated (e.g. ECL1, the TM1/NTD, and deep binding pocket), contain the most important residues for the activation of this signalling pathway. Support for the involvement of these other receptor domains in cAMP response was observed for GLP-1R, where residues at the top of TM2 were important for GLP-1 binding and cAMP, $_iCa^{2+}$ and pERK1/2 signalling efficacy (Yang et al., 2016, Wootten et al., 2016).

6.4 Understanding the mechanistic basis of biased agonism of CT peptides at the hCTR

In Chapter 3 I identified that pCT is a biased agonist of the hCTR (towards $_iCa^{2+}$ and pERK1/2, and away from cAMP) when compared to hCT and sCT. Data presented in Chapter 4 highlighted that sCT and hCT engage similar networks for IP_1 formation and pERK1/2 phosphorylation (***Figure 6.1***), whereas pCT engaged less with ECL2 in IP_1 formation while still using a similar affinity, cAMP and pERK1/2 network to that utilised by hCT. This suggests that (i) ECL3 is the main driver for activation of these signalling pathways, while ECL2 has a more subtle involvement in signalling, and (ii) biased signalling relies on differential peptide engagement with the receptor.

To explain the distinct profiles of these three peptides I extend the accepted two-domain model of activation of Class B1 GPCRs. This model postulates that C-terminus of the peptide initially interacts with the NTD of the receptor; these interactions and interactions with the mid-region of the peptide orientate the N-terminus of the ligand towards the TM bundle, leading to receptor activation (Hoare, 2005, Hollenstein et al., 2014). Changes in the peptide structure could therefore affect peptide interaction and receptor activation. Hilton et al. (2000) and Furness et al. (2016) highlight that the mid-region of the CT peptides is responsible for a proportion of the distinct binding kinetics and affinity of sCT and hCT. ***Table 1.1 and 4.1*** shows that the C-terminus and mid-region of pCT (13-16), although not completely conserved, are more closely related to hCT than sCT. Because this mid-region is important for affinity of the peptide , it is not surprising that the affinity of pCT is higher than hCT but lower than sCT, and predicts that pCT has an off-rate potentially slower than hCT, without being a pseudo-irreversible ligand (like sCT).

In this two-domain binding model, the interaction of the mid-region of the peptide with the TM1-TM3-TM4 interface aids in correctly positioning the N-terminus of the peptide within the binding groove. Structural changes in this region between CT peptides may translate to subtle differences in the pose of the N-terminus of the bound peptide. Residues 11-13 of pCT are partially conserved with hCT, and therefore pCT may have more similar properties to hCT versus sCT. This is supported by results shown

in ***Figure 6.1***, where key networks for hCT and pCT are more similar to each other than to sCT. Of note, residue 10 of the pCT peptide is a Ser, whereas it is a Gly in hCT, sCT and cCT. Our model shows that S/G10 is oriented towards W290 and the deep binding pocket (***Figure 4.33***). This suggests that the N-terminal proximal residues of the pCT ligand adopt a slightly different pose in the TM binding groove, leading to distinct interactions with the receptor. This may explain the different involvement of ECL2 in the IP_1 signalling pathway and potentially correlates to the differences in signalling bias observed in Chapter 3 between pCT and hCT.

I have also previously discussed the importance of the peptide N-terminus for receptor activation and recruitment/activation of intracellular effectors (Hilton et al., 2000, Furness et al., 2016). Although the N-termini of the CTR peptides is highly conserved, I speculated, in Chapter 3, that subtle changes within N-terminus of the peptides (i.e. residues 2 and 3 differs between cCT and all the other CT ligands) may result in distinct activation of intracellular effectors. In this case, if would be interesting to use cCT in our mutagenesis study to identify whether the unique signalling profile of cCT described in Chapter 3 is reflected in different engagement of the peptide with the receptor involving these far N-terminal residues.

6.5 Understanding the role of RAMPs on CTR function

CTR can also be activated by peptides other than CTs, such as amylin (Amy) and calcitonin-like gene peptide (CGRP). Amy is involved in glucose homeostasis and food intake (Amy) (Reda et al., 2002), whereas CGRP modulates vascular tone (Russell et al., 2014). Despite low sequence homology with the CT peptides, Amy and CGRP conserve the characteristic disulphide bond at the N-terminus (between Cys 2 and 7) (***Table 4.1***).

Amy and CGRP have low affinity and low potency for the CTR alone. However, when the CTR is co-expressed with receptor activity modifying proteins (RAMPs), it forms heterocomplexes with RAMPs with distinct pharmacology (Section 1.4.6) (Routledge et al., 2017, Poyner et al., 2002). Specifically, CTR-RAMP1 complexes have high affinity and signalling potency for CGRP and Amy, whereas

complex between CTR and with any one of the three RAMPs forms high affinity and efficacy receptors for Amy (AMY receptors) (Tilakaratne et al., 2000, Hay et al., 2005, Morfis et al., 2008).

Limited evidence, principally from mutagenesis studies, suggest that RAMPs allosterically modulate CTR function (Gingell et al., 2016, Lee et al., 2016b, Udawela et al., 2006b, Udawela et al., 2006a). In the absence of a CGRP-bound (or Amy-bound) full-length CTR/RAMP structure, I investigated how Amy and CGRP peptides engage with CTR to promote cell signalling. Therefore, In Chapters 4 and 5, ECL2 and ECL3 Ala mutants of the CTR were also assessed in presence of rAmy or hαCGRP, while future studies will assess these same CTR constructs when co-expressed with RAMPs. Although still underway, this project will expand the knowledge on the role of RAMPs in modulating CTR function.

Consistent with published data, Amy and CGRP have low affinity for of CTR alone; indeed 1 μM of these peptides could not specifically compete the radioligand ^{125}I-sCT(8-32). The lack of RAMPs also reduced efficacy of these two agonists in all the signalling pathways assessed, with only cAMP and pERK1/2 giving a robust detectable response. However, functional affinities derived from cAMP accumulation studies (ΔpK_A) (***Figures 4.14 and 5.14***) showed distinct trends in the effect of mutations on affinity between rAmy and hαCGRP, suggesting that the two peptides could interact with the binding groove in a distinct manner from the CT peptides. Interestingly, my ΔpK_A data suggests that the TM5 and TM6 of the CTR are important for binding of both peptides. Therefore, based on our CTR model, and consistent with published evidence (Barwell et al., 2011, Barwell et al., 2012, Woolley et al., 2013, Hay et al., 2014), I hypothesise that, similar to the CT peptides, the N-terminus of rAmy and hαCGRP is in close proximity of this region of the CTR.

Figure 6.2 A shows heat-maps of residues important for cAMP signalling efficacy of rAmy/hαCGRP. When comparing these maps to those for CT peptides (***Figure 6.1 B***), this data reveals that CGRP engages with a pattern of residues resembling those involved in the efficacy of hCT and pCT, however, with opposing effect. With respect to rAmy, these mutants had cAMP efficacy effects more similar to sCT than any of the other ligands. I therefore hypothesise that, in the absence of RAMPs, Amy and hαCGRP

adopt distinct unique poses within the binding groove, which in turn affects their ability to activate CTR.

Interestingly, the residues important for the activation of the pERK1/2 pathway are largely conserved across all peptides (CTs, rAmy and hαCGRP) (***Figure 6.1 D*** and ***Figure 6.2 B***). I discussed that, based on our results, pERK1/2 may be downstream of Gαq activation. The IP_1 signal was below the limit for detection for rAmy and hαCGRP, however this does not preclude the possibility that Gαq is upstream of pERK1/2 for these peptides. Similarly, I can't exclude that the pERK1/2 response is triggered by the activation of other effectors not yet assessed. Therefore, further work is required to dissect this pathway. Analysis of signalling from CTR mutants co-expressed with RAMPs, will inform our understanding of how RAMPs modulate the interaction between CTR and rAmy/hαCGRP peptides that leads to binding and activation. There is initial evidence from a mutagenesis study on the NTD of the full-length CTR suggesting that RAMPs cause hCT, Amy and CGRP to establish different interactions with the NTD (Gingell et al., 2016). Additionally, RAMPs have been shown to allosterically modulate the activation of intracellular effectors (Udawela et al., 2006b, Udawela et al., 2006a). However, it is still unclear whether RAMPs convey their function by changing the orientation of the peptide within the binding pocket, by allosterically changing the structure of the binding pocket, or by allosterically influencing the interactions that transmit the activation of the receptor from the binding groove to the intracellular face of the receptor. Further experiments that probe the deep peptide binding pocket and the conserved polar networks within the TM bundle that are important for GCPRs activation (Wootten et al., 2013) will also need to be explored to understand how RAMPs alter receptor function.

6.6 Final remarks

In this study I have confirmed that receptor splicing plays a crucial role in CTR function, and also revealed that a common natural polymorphism of the CTR has the potential to change the signalling profiles of the CTR and thus, potentially effect physiological function. If confirmed, this aspect of CTR function may have to be considered in the establishment of therapeutic regimens for different patients.

The use of different agonists, some of which were revealed to be biased agonists, has started to unravel the mechanistic basis of how peptide ligands control CTR function. This thesis has shown that (i) the different CTR-effector coupling pathways are controlled by distinct portions of the receptor, and that (ii) different ligands can distinctly activate the CTR through a combination of unique interactions, potentially dictated by both kinetics of binding and/or poses within the binding groove of the receptor. (iii) Although in its early stages, this data will also help in understanding the role of RAMPs in CTR function.

This knowledge is extremely important in the development of new therapeutics, as it is may eventually allow the design of novel biased therapeutics that target specific receptor functions.

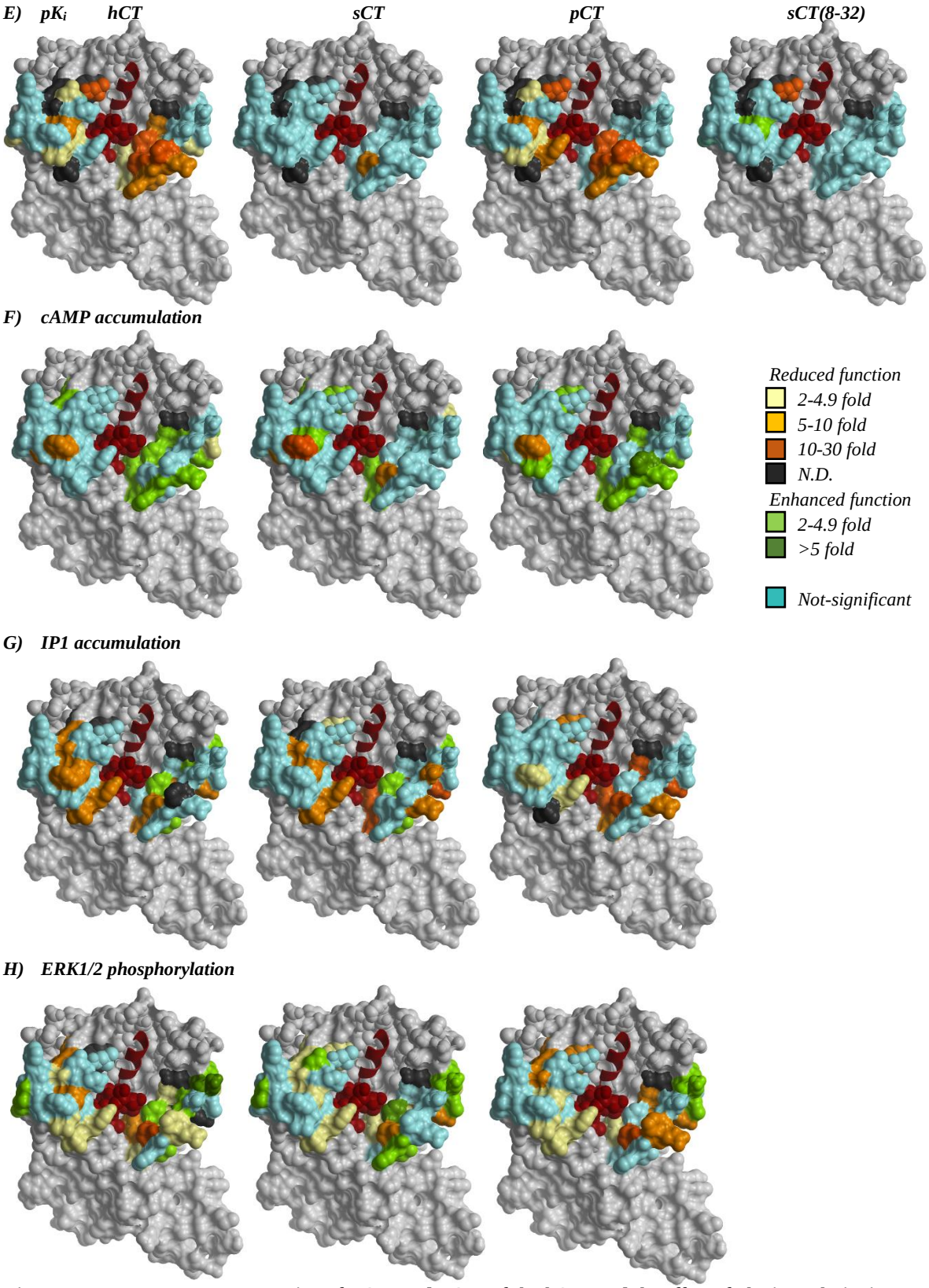

Figure 6.1 Heat-map 3D representation of ECL2 and ECL3 of the hCTR and the effect of alanine substitution on CT peptide affinity and intracellular signalling. *Active model based on the active Cryo-EM structure of CTR in complex with sCT (Liang et al., 2017) into which the three ECLs were modelled). Residues 1-136 and 200-217 (that would partially cover ECL2) are hidden. The model shows sCT ligand (in burgundy) where the cyclic N-terminus (residues 1-7) is represented by space fill, residues 8-16 are tightly structured in an α-helix (ribbon), while the C-terminus (residues 17-32) of the ligand is hidden. Residues that produced significant changes in binding affinity or signalling efficacy were coloured following the colour scheme for fold effect of from WT.*

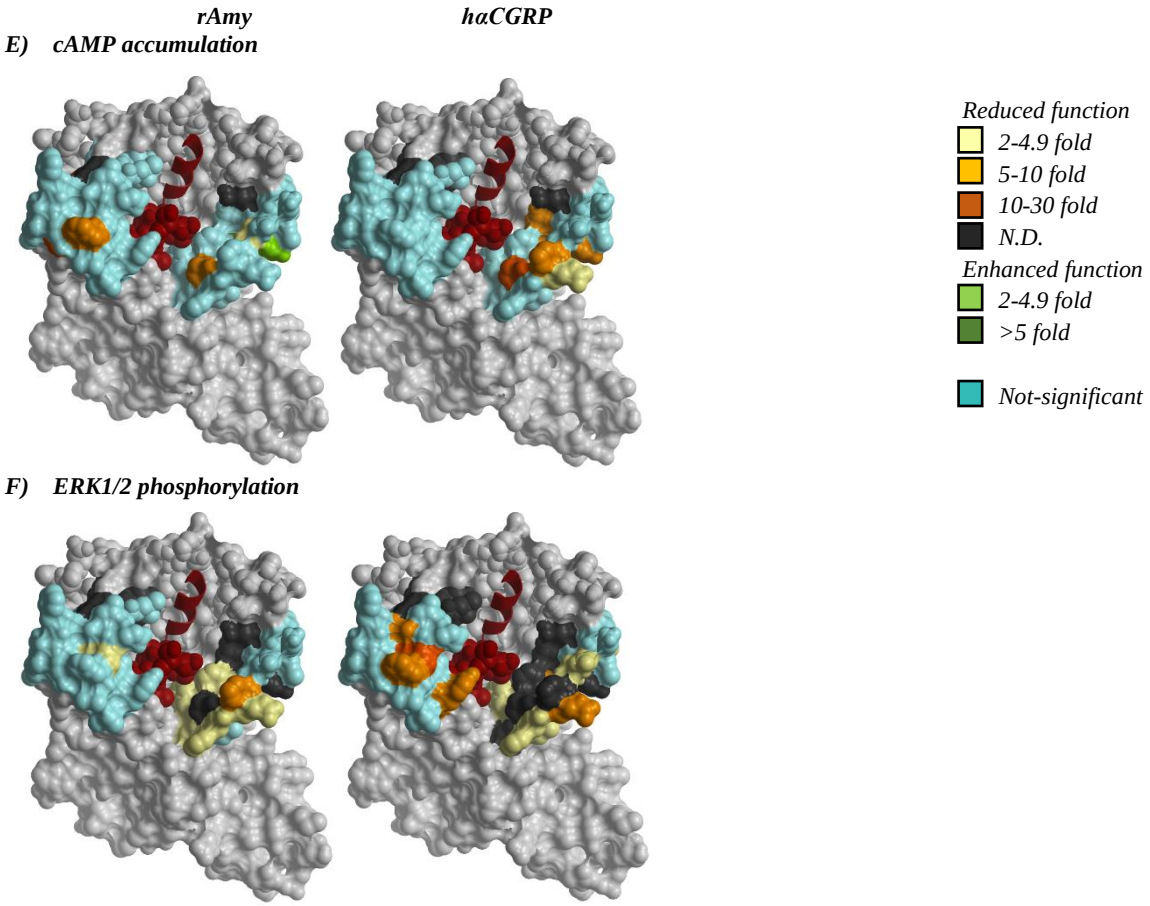

Figure 6.2 Heat-map 3D representation of ECL2 and ECL3 of the hCTR and the effect of alanine substitution on rAmy and hαCGRP intracellular signalling. *Active model based on the active Cryo-EM structure of CTR in complex with sCT (Liang et al., 2017) into which the three ECLs were modelled). Residues 1-136 and 200-217 (that would partially cover ECL2) are hidden. The model shows sCT ligand (in burgundy) where the cyclic N-terminus (residues 1-7) is represented by space fill, residues 8-16 are tightly structured in an α-helix (ribbon), while the C-terminus (residues 17-32) of the ligand is hidden. Residues that produced significant changes in binding affinity or signalling efficacy were coloured following the colour scheme for fold effect of from WT.*

CHAPTER 7

References

AL-SABAH, S. & DONNELLY, D. 2003. The positive charge at Lys-288 of the glucagon-like peptide-1 (GLP-1) receptor is important for binding the N-terminus of peptide agonists. *FEBS Lett,* 553**,** 342-6.

ALBRANDT, K., BRADY, E. M., MOORE, C. X., MULL, E., SIERZEGA, M. E. & BEAUMONT, K. 1995. Molecular cloning and functional expression of a third isoform of the human calcitonin receptor and partial characterization of the calcitonin receptor gene. *Endocrinology,* 136**,** 5377-84.

ALBRANDT, K., MULL, E., BRADY, E. M., HERICH, J., MOORE, C. X. & BEAUMONT, K. 1993. Molecular cloning of two receptors from rat brain with high affinity for salmon calcitonin. *FEBS Lett,* 325**,** 225-32.

ANDREASSEN, K. V., HJULER, S. T., FURNESS, S. G., SEXTON, P. M., CHRISTOPOULOS, A., NOSJEAN, O., KARSDAL, M. A. & HENRIKSEN, K. 2014. Prolonged calcitonin receptor signaling by salmon, but not human calcitonin, reveals ligand bias. *PloS one,* 9.

ANDREOTTI, G., MENDEZ, B. L., AMODEO, P., MORELLI, M. A., NAKAMUTA, H. & MOTTA, A. 2006. Structural determinants of salmon calcitonin bioactivity: the role of the Leu-based amphipathic alpha-helix. *J Biol Chem,* 281**,** 24193-203.

ANGEL, T. E., CHANCE, M. R. & PALCZEWSKI, K. 2009. Conserved waters mediate structural and functional activation of family A (rhodopsin-like) G protein-coupled receptors. *Proc Natl Acad Sci U S A,* 106**,** 8555-60.

APPLETON, K. M., LEE, M. H., ALELE, C., ALELE, C., LUTTRELL, D. K., PETERSON, Y. K., MORINELLI, T. A. & LUTTRELL, L. M. 2013. Biasing the parathyroid hormone receptor: relating in vitro ligand efficacy to in vivo biological activity. *Methods Enzymol,* 522**,** 229-62.

ARATAKE, Y., OKUNO, T., MATSUNOBU, T., SAEKI, K., TAKAYANAGI, R., FURUYA, S. & YOKOMIZO, T. 2012. Helix 8 of leukotriene B4 receptor 1 inhibits ligand-induced internalization. *FASEB J,* 26**,** 4068-78.

ARCHBOLD, J. K., FLANAGAN, J. U., WATKINS, H. A., GINGELL, J. J. & HAY, D. L. 2011. Structural insights into RAMP modification of secretin family G protein-coupled receptors: implications for drug development. *Trends Pharmacol Sci,* 32**,** 591-600.

ARIENS, E. J. 1954. Affinity and intrinsic activity in the theory of competitive inhibition. I. Problems and theory. *Arch Int Pharmacod T,* 99**,** 32-49.

ARLOT-BONNEMAINS, Y., FOUCHEREAU-PERON, M., MOUKHTAR, M. S. & MILHAUD, G. 1983. Characterization of target organs for calcitonin in lower and higher vertebrates. *Comp Biochem Physiol A Comp Physiol,* 76**,** 377-80.

ATTWOOD, T. K. & FINDLAY, J. B. 1994. Fingerprinting G-protein-coupled receptors. *Protein Eng,* 7**,** 195-203.

AXELROD, J., BURCH, R. M. & JELSEMA, C. L. 1988. Receptor-mediated activation of phospholipase A 2 via GTP-binding proteins: arachidonic acid and its metabolites as second messengers. *Trends Neurosci,* 11**,** 117-123.

AZRIA, M. 2002. Possible mechanisms of the analgesic action of calcitonin. *Bone,* 30**,** 80S-83S.

BAILEY, R. J. & HAY, D. L. 2007. Agonist-dependent consequences of proline to alanine substitution in the transmembrane helices of the calcitonin receptor. *Br J Pharmacol,* 151**,** 678-87.

BALASUBRAMANIAN, S., XIA, Y., FREINKMAN, E. & GERSTEIN, M. 2005. Sequence variation in G-protein-coupled receptors: analysis of single nucleotide polymorphisms. *Nucleic Acids Res,* 33**,** 1710-21.

BALLESTEROS, J. A., JENSEN, A. D., LIAPAKIS, G., RASMUSSEN, S. G. F., SHI, L., GETHER, U. & JAVITCH, J. A. 2001. Activation of the β2-adrenergic receptor involves disruption of an ionic lock between the cytoplasmic ends of transmembrane segments 3 and 6. *J Biol Chem,* 276**,** 29171-29177.

BARWELL, J., CONNER, A. & POYNER, D. R. 2011. Extracellular loops 1 and 3 and their associated transmembrane regions of the calcitonin receptor-like receptor are needed for CGRP receptor function. *Biochim Biophys Acta,* 1813**,** 1906-16.

BARWELL, J., MILLER, P. S., DONNELLY, D. & POYNER, D. R. 2010. Mapping interaction sites within the N-terminus of the calcitonin gene-related peptide receptor; the role of residues 23-60 of the calcitonin receptor-like receptor. *Peptides,* 31**,** 170-6.

BARWELL, J., WHEATLEY, M., CONNER, A. C., TADDESE, B., VOHRA, S., REYNOLDS, C. A. & POYNER, D. R. 2013. The activation of the CGRP receptor. *Biochem Soc Trans,* 41**,** 180-4.

BARWELL, J., WOOLLEY, M. J., WHEATLEY, M., CONNER, A. C. & POYNER, D. R. 2012. The role of the extracellular loops of the CGRP receptor, a family B GPCR. *Biochem Soc Trans,* 40**,** 433-7.

BAVEC, A., HALLBRINK, M., LANGEL, U. & ZORKO, M. 2003. Different role of intracellular loops of glucagon-like peptide-1 receptor in G-protein coupling. *Regul Pept,* 111**,** 137-44.

BECKER, K. L. 1993. The coming of age of a bronchial epithelial cell. *Am Rev Respir Dis,* 148**,** 1166-8.

BELLO, N. T., KEMM, M. H., OFELDT, E. M. & MORAN, T. H. 2010. Dose combinations of exendin-4 and salmon calcitonin produce additive and synergistic reductions in food intake in nonhuman primates. *Am J Physiol Regul Integr Comp Physiol,* 299**,** R945-52.

BENEMEI, S., NICOLETTI, P., CAPONE, J. G. & GEPPETTI, P. 2009. CGRP receptors in the control of pain and inflammation. *Curr Opin Pharmacol,* 9**,** 9-14.

BENOVIC, J. L., PIKE, L. J., CERIONE, R. A., STANISZEWSKI, C., YOSHIMASA, T., CODINA, J., CARON, M. G. & LEFKOWITZ, R. J. 1985. Phosphorylation of the mammalian beta-adrenergic receptor by cyclic AMP-dependent protein kinase. Regulation of the rate of receptor phosphorylation and dephosphorylation by agonist occupancy and effects on coupling of the receptor to the stimulatory guanine nucleotide regulatory protein. *J Biol Chem,* 260**,** 7094-101.

BERGWITZ, C., GARDELLA, T. J., FLANNERY, M. R., POTTS, J. T., KRONENBERG, H. M., GOLDRING, S. R. & JUPPNER, H. 1996. Full activation of chimeric receptors by hybrids between parathyroid hormone and calcitonin - Evidence for a common pattern of ligand-receptor interaction. *J Biol Chem,* 271**,** 26469-26472.

BJARNADOTTIR, T. K., GLORIAM, D. E., HELLSTRAND, S. H., KRISTIANSSON, H., FREDRIKSSON, R. & SCHIOTH, H. B. 2006. Comprehensive repertoire and phylogenetic analysis of the G protein-coupled receptors in human and mouse. *Genomics,* 88**,** 263-73.

BLACK, J. W. & LEFF, P. 1983. Operational models of pharmacological agonism. *Proc R Soc Lond B Biol Sci,* 220**,** 141-62.

BLANCHARD, J., MENK, E., RAMAMURTHY, S. & HOFFMAN, J. 1990. Subarachnoid and epidural calcitonin in patients with pain due to metastatic cancer. *J Pain Symptom Manage,* 5**,** 42-45.

BLOOM, S. R., CHRISTOFIDES, N. D., DELAMARTER, J., BUELL, G., KAWASHIMA, E. & POLAK, J. M. 1983. Diarrhoea in vipoma patients associated with cosecretion of a second active peptide (peptide histidine isoleucine) explained by single coding gene. *Lancet,* 2**,** 1163-5.

BODNER, M., FRIDKIN, M. & GOZES, I. 1985. Coding sequences for vasoactive intestinal peptide and PHM-27 peptide are located on two adjacent exons in the human genome. *Proc Natl Acad Sci U S A,* 82**,** 3548-51.

BOLOGNA, Z., TEOH, J. P., BAYOUMI, A. S., TANG, Y. & KIM, I. M. 2017. Biased G Protein-Coupled Receptor Signaling: New Player in Modulating Physiology and Pathology. *Biomol Ther (Seoul),* 25**,** 12-25.

BOOE, J. M., WALKER, C. S., BARWELL, J., KUTEYI, G., SIMMS, J., JAMALUDDIN, M. A., WARNER, M. L., BILL, R. M., HARRIS, P. W., BRIMBLE, M. A., POYNER, D. R., HAY, D. L. & PIOSZAK, A. A. 2015. Structural Basis for Receptor Activity-Modifying Protein-Dependent Selective Peptide Recognition by a G Protein-Coupled Receptor. *Mol Cell,* 58**,** 1040-52.

BOROS, E. E., COWAN, D. J., COX, R. F., MEBRAHTU, M. M., RABINOWITZ, M. H., THOMPSON, J. B. & WOLFE, L. A., 3RD 2005. Hantzsch synthesis of pyrazolo[1',2':1,2]pyrazolo[3,4-b]pyridines: partial agonists of the calcitonin receptor. *J Org Chem,* 70**,** 5331-4.

BOS, J., DE BRUYN, K., ENSERINK, J., KUIPERIJ, B., RANGARAJAN, S., REHMANN, H., RIEDL, J., DE ROOIJ, J., VAN MANSFELD, F. & ZWARTKRUIS, F. 2003. The role of Rap1 in integrin-mediated cell adhesion. Portland Press Limited.

BOWER, R. L., EFTEKHARI, S., WALDVOGEL, H. J., FAULL, R. L., TAJTI, J., EDVINSSON, L., HAY, D. L. & WALKER, C. S. 2016. Mapping the calcitonin receptor in human brain stem. *Am J Physiol Regul Integr Comp Physiol,* 310**,** R788-93.

BOYER, J. L., WALDO, G. L. & HARDEN, T. K. 1992. Beta gamma-subunit activation of G-protein-regulated phospholipase C. *J Biol Chem,* 267**,** 25451-6.

BRAGA, V., SANGALLI, A., MALERBA, G., MOTTES, M., MIRANDOLA, S., GATTI, D., ROSSINI, M., ZAMBONI, M. & ADAMI, S. 2002. Relationship among VDR (BsmI and FokI), COLIA1, and CTR polymorphisms with bone mass, bone turnover markers, and sex hormones in men. *Calcified Tissue Int,* 70**,** 457-62.

BÜHLMANN, N., LEUTHÄUSER, K., MUFF, R., FISCHER, J. A. & BORN, W. 1999. A Receptor Activity Modifying Protein (RAMP) 2-Dependent Adrenomedullin Receptor Is a Calcitonin Gene-Related Peptide Receptor when Coexpressed with Human RAMP1 1. *Endocrinology,* 140**,** 2883-2890.

BUNEMANN, M., FRANK, M. & LOHSE, M. J. 2003. Gi protein activation in intact cells involves subunit rearrangement rather than dissociation. *Proc Natl Acad Sci U S A,* 100**,** 16077-82.

CALEBIRO, D., NIKOLAEV, V. O., PERSANI, L. & LOHSE, M. J. 2010. Signaling by internalized G-protein-coupled receptors. *Trends Pharmacol Sci,* 31**,** 221-228.

CAMPS, M., CAROZZI, A., SCHNABEL, P., SCHEER, A., PARKER, P. J. & GIERSCHIK, P. 1992. Isozyme-selective stimulation of phospholipase C-beta 2 by G protein beta gamma-subunits. *Nature,* 360**,** 684-6.

CAO, J., HUANG, S., QIAN, J., HUANG, J., JIN, L., SU, Z., YANG, J. & LIU, J. 2009. Evolution of the class C GPCR Venus flytrap modules involved positive selected functional divergence. *BMC Evol Biol,* 9**,** 67.

CARNEY, S. 1996. Calcitonin and human renal calcium and electrolyte transport. *Miner Electrolyte Metab,* 23**,** 43-47.

CASTELLS, S., COLBERT, C., CHAKRABARTI, C., BACHTELL, R. S., KASSNER, E. G. & YASUMURA, S. 1979. Therapy of osteogenesis imperfecta with synthetic salmon calcitonin. *J Pediatr,* 95**,** 807-11.

CHABRE, O., CONKLIN, B. R., LIN, H. Y., LODISH, H. F., WILSON, E., IVES, H. E., CATANZARITI, L., HEMMINGS, B. A. & BOURNE, H. R. 1992. A recombinant calcitonin receptor independently stimulates 3',5'-cyclic adenosine monophosphate and Ca2+/inositol phosphate signaling pathways. *Mol Endocrinol,* 6**,** 551-6.

CHAKRABORTY, M., CHATTERJEE, D., KELLOKUMPU, S., RASMUSSEN, H. & BARON, R. 1991. Cell cycle-dependent coupling of the calcitonin receptor to different G proteins. *Science,* 251**,** 1078-82.

CHEN, W. J., ARMOUR, S., WAY, J., CHEN, G., WATSON, C., IRVING, P., COBB, J., KADWELL, S., BEAUMONT, K., RIMELE, T. & KENAKIN, T. 1997. Expression cloning and receptor pharmacology of human calcitonin receptors from MCF-7 cells and their relationship to amylin receptors. *Mol Pharmacol,* 52**,** 1164-1175.

CHEN, Y., SHYU, J. F., SANTHANAGOPAL, A., INOUE, D., DAVID, J. P., DIXON, S. J., HORNE, W. C. & BARON, R. 1998. The calcitonin receptor stimulates Shc tyrosine phosphorylation and Erk1/2 activation. Involvement of Gi, protein kinase C, and calcium. *J Biol Chem,* 273**,** 19809-16.

CHENG, X., JI, Z., TSALKOVA, T. & MEI, F. 2008. Epac and PKA: a tale of two intracellular cAMP receptors. *Acta Biochim Biophys Sin (Shanghai),* 40**,** 651-62.

CHO, Y. M., MERCHANT, C. E. & KIEFFER, T. J. 2012. Targeting the glucagon receptor family for diabetes and obesity therapy. *Pharmacol Ther,* 135**,** 247-78.

CHRISTOPOULOS, A., CHRISTOPOULOS, G., MORFIS, M., UDAWELA, M., LABURTHE, M., COUVINEAU, A., KUWASAKO, K., TILAKARATNE, N. & SEXTON, P. M. 2003. Novel receptor partners and function of receptor activity-modifying proteins. *J Biol Chem,* 278**,** 3293-7.

CHRISTOPOULOS, G., PERRY, K. J., MORFIS, M., TILAKARATNE, N., GAO, Y., FRASER, N. J., MAIN, M. J., FOORD, S. M. & SEXTON, P. M. 1999. Multiple amylin receptors arise from

receptor activity-modifying protein interaction with the calcitonin receptor gene product. *Mol Pharmacol,* 56**,** 235-42.

CHUGUNOV, A. O., SIMMS, J., POYNER, D. R., DEHOUCK, Y., ROOMAN, M., GILIS, D. & LANGER, I. 2010. Evidence that interaction between conserved residues in transmembrane helices 2, 3, and 7 are crucial for human VPAC1 receptor activation. *Mol Pharmacol,* 78**,** 394-401.

CIVELLI, O., REINSCHEID, R. K., ZHANG, Y., WANG, Z., FREDRIKSSON, R. & SCHIOTH, H. B. 2013. G protein-coupled receptor deorphanizations. *Annu Rev Pharmacol Toxicol,* 53**,** 127-46.

CLAPHAM, D. E. & NEER, E. J. 1993. New roles for G-protein beta gamma-dimers in transmembrane signalling. *Nature,* 365**,** 403-6.

CLARK, A. J. 1933. *Mode of action of drugs on cells,* Edward Arnold: London.

CLARK, R. B., KUNKEL, M. W., FRIEDMAN, J., GOKA, T. J. & JOHNSON, J. A. 1988. Activation of Camp-Dependent Protein-Kinase Is Required for Heterologous Desensitization of Adenylyl Cyclase in S49 Wild-Type Lymphoma-Cells. *Proc Natl Acad Sci U S A,* 85**,** 1442-1446.

COAST, G. M., WEBSTER, S. G., SCHEGG, K. M., TOBE, S. S. & SCHOOLEY, D. A. 2001. The Drosophila melanogaster homologue of an insect calcitonin-like diuretic peptide stimulates V-ATPase activity in fruit fly Malpighian tubules. *J Exp Biol,* 204**,** 1795-804.

CONNER, A. C., HAY, D. L., SIMMS, J., HOWITT, S. G., SCHINDLER, M., SMITH, D. M., WHEATLEY, M. & POYNER, D. R. 2005. A key role for transmembrane prolines in calcitonin receptor-like receptor agonist binding and signalling: implications for family B G-protein-coupled receptors. *Mol Pharmacol,* 67**,** 20-31.

CONNER, A. C., SIMMS, J., BARWELL, J., WHEATLEY, M. & POYNER, D. R. 2007. Ligand binding and activation of the CGRP receptor. *Biochem Soc Trans,* 35**,** 729-32.

CONNER, A. C., SIMMS, J., CONNER, M. T., WOOTTEN, D. L., WHEATLEY, M. & POYNER, D. R. 2006a. Diverse functional motifs within the three intracellular loops of the CGRP1 receptor. *Biochemistry,* 45**,** 12976-12985.

CONNER, A. C., SIMMS, J., HOWITT, S. G., WHEATLEY, M. & POYNER, D. R. 2006b. The second intracellular loop of the calcitonin gene-related peptide receptor provides molecular determinants for signal transduction and cell surface expression. *J Biol Chem,* 281**,** 1644-51.

CONNER, M., HICKS, M. R., DAFFORN, T., KNOWLES, T. J., LUDWIG, C., STADDON, S., OVERDUIN, M., GUNTHER, U. L., THOME, J., WHEATLEY, M., POYNER, D. R. & CONNER, A. C. 2008. Functional and biophysical analysis of the C-terminus of the CGRP-receptor; a family B GPCR. *Biochemistry,* 47**,** 8434-44.

CORNISH, J., CALLON, K. E., BAVA, U., KAMONA, S. A., COOPER, G. J. & REID, I. R. 2001. Effects of calcitonin, amylin, and calcitonin gene-related peptide on osteoclast development. *Bone,* 29**,** 162-8.

COSMAN, F., DE BEUR, S. J., LEBOFF, M. S., LEWIECKI, E. M., TANNER, B., RANDALL, S., LINDSAY, R. & NATIONAL OSTEOPOROSIS, F. 2014. Clinician's Guide to Prevention and Treatment of Osteoporosis. *Osteoporos Int,* 25**,** 2359-81.

COUVINEAU, A., LACAPERE, J. J., TAN, Y. V., ROUYER-FESSARD, C., NICOLE, P. & LABURTHE, M. 2003. Identification of cytoplasmic domains of hVPAC1 receptor required for activation of adenylyl cyclase. Crucial role of two charged amino acids strictly conserved in class II G protein-coupled receptors. *J Biol Chem,* 278**,** 24759-66.

CULHANE, K. J., LIU, Y., CAI, Y. & YAN, E. C. 2015. Transmembrane signal transduction by peptide hormones via family BG protein-coupled receptors. *Front Pharmacol,* 6.

CYPESS, A. M., UNSON, C. G., WU, C. R. & SAKMAR, T. P. 1999. Two cytoplasmic loops of the glucagon receptor are required to elevate cAMP or intracellular calcium. *J Biol Chem,* 274**,** 19455-64.

DACQUIN, R., DAVEY, R. A., LAPLACE, C., LEVASSEUR, R., MORRIS, H. A., GOLDRING, S. R., GEBRE-MEDHIN, S., GALSON, D. L., ZAJAC, J. D. & KARSENTY, G. 2004. Amylin inhibits bone resorption while the calcitonin receptor controls bone formation in vivo. *J Cell Biol,* 164**,** 509-14.

DALE, L. B., SEACHRIST, J. L., BABWAH, A. V. & FERGUSON, S. S. 2004. Regulation of angiotensin II type 1A receptor intracellular retention, degradation, and recycling by Rab5, Rab7, and Rab11 GTPases. *J Biol Chem,* 279**,** 13110-8.

DE LEAN, A., STADEL, J. M. & LEFKOWITZ, R. J. 1980. A ternary complex model explains the agonist-specific binding properties of the adenylate cyclase-coupled beta-adrenergic receptor. *J Biol Chem,* 255**,** 7108-17.

DE MENDOZA, A., SEBE-PEDROS, A. & RUIZ-TRILLO, I. 2014. The evolution of the GPCR signaling system in eukaryotes: modularity, conservation, and the transition to metazoan multicellularity. *Genome Biol Evol,* 6**,** 606-19.

DE ROOIJ, J., ZWARTKRUIS, F. J., VERHEIJEN, M. H., COOL, R. H., NIJMAN, S. M., WITTINGHOFER, A. & BOS, J. L. 1998. Epac is a Rap1 guanine-nucleotide-exchange factor directly activated by cyclic AMP. *Nature,* 396**,** 474-477.

DEHGHAN, M., POURAHMAD-JAKTAJI, R. & FARZANEH, Z. 2016. Calcitonin Receptor AluI (rs1801197) and Taq1 Calcitonin Genes Polymorphism in 45-and Over 45-year-old Women and their Association with Bone Density. *Acta Inform Med,* 24**,** 239.

DEL CASTILLO, J. & KATZ, B. 1957. Interaction at end-plate receptors between different choline derivatives. *Proc R Soc Lond B Biol Sci,* 146**,** 369-381.

DEROSE, J., SINGER, F. R., AVRAMIDES, A., FLORES, A., DZIADIW, R., BAKER, R. K. & WALLACH, S. 1974. Response of Paget's disease to porcine and salmon calcitonins: effects of long-term treatment. *Am J Med,* 56**,** 858-66.

DEWIRE, S. M., AHN, S., LEFKOWITZ, R. J. & SHENOY, S. K. 2007. Beta-arrestins and cell signaling. *Annu Rev Physiol,* 69**,** 483-510.

DODS, R. L. & DONNELLY, D. 2015. The peptide agonist-binding site of the glucagon-like peptide-1 (GLP-1) receptor based on site-directed mutagenesis and knowledge-based modelling. *Bioscience Rep,* 36**,** e00285.

DONG, M., COX, R. F. & MILLER, L. J. 2009. Juxtamembranous region of the amino terminus of the family B G protein-coupled calcitonin receptor plays a critical role in small-molecule agonist action. *J Biol Chem,* 284**,** 21839-21847.

DONG, M., KOOLE, C., WOOTTEN, D., SEXTON, P. M. & MILLER, L. J. 2014. Structural and functional insights into the juxtamembranous amino-terminal tail and extracellular loop regions of class B GPCRs. *Br J Pharmacol,* 171**,** 1085-1101.

DONG, M., LAM, P. C., ORRY, A., SEXTON, P. M., CHRISTOPOULOS, A., ABAGYAN, R. & MILLER, L. J. 2016. Use of Cysteine Trapping to Map Spatial Approximations between Residues Contributing to the Helix N-capping Motif of Secretin and Distinct Residues within Each of the Extracellular Loops of Its Receptor. *J Biol Chem,* 291**,** 5172-84.

DONG, M., PINON, D. I., COX, R. F. & MILLER, L. J. 2004a. Importance of the amino terminus in secretin family G protein-coupled receptors. Intrinsic photoaffinity labeling establishes initial docking constraints for the calcitonin receptor. *J Biol Chem,* 279**,** 1167-75.

DONG, M., PINON, D. I., COX, R. F. & MILLER, L. J. 2004b. Molecular approximation between a residue in the amino-terminal region of calcitonin and the third extracellular loop of the class B G protein-coupled calcitonin receptor. *J Biol Chem,* 279**,** 31177-31182.

DONG, M., XU, X., BALL, A. M., MAKHOUL, J. A., LAM, P. C., PINON, D. I., ORRY, A., SEXTON, P. M., ABAGYAN, R. & MILLER, L. J. 2012. Mapping spatial approximations between the amino terminus of secretin and each of the extracellular loops of its receptor using cysteine trapping. *FASEB J,* 26**,** 5092-105.

DONNELLY, D. 2012. The structure and function of the glucagon-like peptide-1 receptor and its ligands. *Br J Pharmacol,* 166**,** 27-41.

DORE, A. S., OKRASA, K., PATEL, J. C., SERRANO-VEGA, M., BENNETT, K., COOKE, R. M., ERREY, J. C., JAZAYERI, A., KHAN, S., TEHAN, B., WEIR, M., WIGGIN, G. R. & MARSHALL, F. H. 2014. Structure of class C GPCR metabotropic glutamate receptor 5 transmembrane domain. *Nature,* 511**,** 557-62.

DOWNES, G. B. & GAUTAM, N. 1999. The G protein subunit gene families. *Genomics,* 62**,** 544-52.

DRUCKER, D. J. 2006. The biology of incretin hormones. *Cell Metab,* 3**,** 153-65.

DUBAY, D., EPHGRAVE, K. S., CULLEN, J. J. & BROADHURST, K. A. 2003. Intracerebroventricular calcitonin prevents stress-induced gastric dysfunction. *J Surg Res,* 110**,** 188-92.

DUNHAM, T. D. & FARRENS, D. L. 1999. Conformational changes in rhodopsin. Movement of helix f detected by site-specific chemical labeling and fluorescence spectroscopy. *J Biol Chem,* 274**,** 1683-90.

EGERTON, M., NEEDHAM, M., EVANS, S., MILLEST, A., CERILLO, G., MCPHEAT, J., POPPLEWELL, M., JOHNSTONE, D. & HOLLIS, M. 1995. Identification of multiple human calcitonin receptor isoforms: heterologous expression and pharmacological characterization. *J Mol Endocrinol,* 14**,** 179-89.

EIDEN, S., DANIEL, C., STEINBRUECK, A., SCHMIDT, I. & SIMON, E. 2002. Salmon calcitonin - a potent inhibitor of food intake in states of impaired leptin signalling in laboratory rodents. *J Physiol,* 541**,** 1041-8.

ERTEL, A., VERGHESE, A., BYERS, S. W., OCHS, M. & TOZEREN, A. 2006. Pathway-specific differences between tumor cell lines and normal and tumor tissue cells. *Molecular Cancer,* 5**,** 1.

ESKOLA, A., POHJOLAINEN, T., ALARANTA, H., SOINI, J., TALLROTH, K. & SLATIS, P. 1992. Calcitonin treatment in lumbar spinal stenosis: a randomized, placebo-controlled, double-blind, cross-over study with one-year follow-up. *Calcified Tissue Int,* 50**,** 400-3.

FABBRI, A., FRAIOLI, F., PERT, C. B. & PERT, A. 1985. Calcitonin receptors in the rat mesencephalon mediate its analgesic actions: autoradiographic and behavioral analyses. *Brain Res,* 343**,** 205-15.

FARRENS, D. L., ALTENBACH, C., YANG, K., HUBBELL, W. L. & KHORANA, H. G. 1996. Requirement of rigid-body motion of transmembrane helices for light activation of rhodopsin. *Science,* 274**,** 768-70.

FERGUSON, S. S. 2001. Evolving concepts in G protein-coupled receptor endocytosis: the role in receptor desensitization and signaling. *Pharmacol Rev,* 53**,** 1-24.

FERRARI, S. L., BEHAR, V., CHOREV, M., ROSENBLATT, M. & BISELLO, A. 1999. Endocytosis of ligand-human parathyroid hormone receptor 1 complexes is protein kinase C-dependent and involves beta-arrestin2 - Real-time monitoring by fluorescence microscopy. *J Biol Chem,* 274**,** 29968-29975.

FEYEN, J. H., CARDINAUX, F., GAMSE, R., BRUNS, C., AZRIA, M. & TRECHSEL, U. 1992. N-terminal truncation of salmon calcitonin leads to calcitonin antagonists. Structure activity relationship of N-terminally truncated salmon calcitonin fragments in vitro and in vivo. *Biochem Biophys Res Commun,* 187**,** 8-13.

FINDLAY, D. M., DELUISE, M., MICHELANGELI, V. P., ELLISON, M. & MARTIN, T. J. 1980. Properties of a calcitonin receptor and adenylate cyclase in BEN cells, a human cancer cell line. *Cancer Res,* 40**,** 1311-7.

FINDLAY, D. M., HOUSSAMI, S., LIN, H. Y., MYERS, D. E., BRADY, C. L., DARCY, P. K., IKEDA, K., MARTIN, T. J. & SEXTON, P. M. 1994. Truncation of the porcine calcitonin receptor cytoplasmic tail inhibits internalization and signal transduction but increases receptor affinity. *Mol Endocrinol,* 8**,** 1691-700.

FINDLAY, D. M., NG, K. W., NIALL, M. & MARTIN, T. J. 1982. Processing of calcitonin and epidermal growth factor after binding to receptors in human breast cancer cells (T 47D). *Biochem J,* 206**,** 343-50.

FLETCHER, M. M., HALLS, M. L., CHRISTOPOULOS, A., SEXTON, P. M. & WOOTTEN, D. 2016. The complexity of signalling mediated by the glucagon-like peptide-1 receptor. *Biochem Soc Trans,* 44**,** 582-8.

FREDRIKSSON, R., LAGERSTROM, M. C., LUNDIN, L. G. & SCHIOTH, H. B. 2003. The G-protein-coupled receptors in the human genome form five main families. Phylogenetic analysis, paralogon groups, and fingerprints. *Mol Pharmacol,* 63**,** 1256-72.

FREEDMAN, N. J. & LEFKOWITZ, R. J. 1995. Desensitization of G protein-coupled receptors. *Recent Prog Horm Res,* 51**,** 319-51; discussion 352-3.

FRENDO, J. L., PICHAUD, F., MOURROUX, R. D., BOUIZAR, Z., SEGOND, N., MOUKHTAR, M. S. & JULLIENNE, A. 1994. An Isoform of the Human Calcitonin Receptor Is Expressed in Tt Cells and in Medullary Carcinoma of the Thyroid. *FEBS Lett,* 342**,** 214-216.

FUJIKAWA, Y., QUINN, J. M., SABOKBAR, A., MCGEE, J. O. & ATHANASOU, N. A. 1996a. The human osteoclast precursor circulates in the monocyte fraction. *Endocrinology,* 137**,** 4058-60.

FUJIKAWA, Y., SABOKBAR, A., NEALE, S. & ATHANASOU, N. A. 1996b. Human osteoclast formation and bone resorption by monocytes and synovial macrophages in rheumatoid arthritis. *Ann Rheum Dis,* 55**,** 816-22.

FUKUHARA, S., SAKURAI, A., SANO, H., YAMAGISHI, A., SOMEKAWA, S., TAKAKURA, N., SAITO, Y., KANGAWA, K. & MOCHIZUKI, N. 2005. Cyclic AMP potentiates vascular endothelial cadherin-mediated cell-cell contact to enhance endothelial barrier function through an Epac-Rap1 signaling pathway. *Mol Cell Biol,* 25**,** 136-46.

FURCHGOTT, R. F. 1966. The use of β-haloalkylamines in the differentiation of receptors and in the determination of dissociation constants of receptor-agonist complexes. *Adv Drug Res,* 3**,** 21-55.

FURNESS, S. G., WOOTTEN, D., CHRISTOPOULOS, A. & SEXTON, P. M. 2012. Consequences of splice variation on Secretin family G protein-coupled receptor function. *Br J Pharmacol,* 166**,** 98-109.

FURNESS, S. G. B., LIANG, Y. L., NOWELL, C. J., HALLS, M. L., WOOKEY, P. J., DAL MASO, E., INOUE, A., CHRISTOPOULOS, A., WOOTTEN, D. & SEXTON, P. M. 2016. Ligand-Dependent Modulation of G Protein Conformation Alters Drug Efficacy. *Cell,* 167**,** 739-749 e11.

GADDUM, J. H. 1957. Theories of drug antagonism. *Pharmacol Rev,* 9**,** 211-8.

GADDUM, J. H., HAMEED, K. A., HATHWAY, D. E. & STEPHENS, F. F. 1955. Quantitative studies of antagonists for 5-hydroxytryptamine. *Q J Exp Physiol Cogn Med Sci,* 40**,** 49-74.

GALANDRIN, S., DENIS, C., BOULARAN, C., MARIE, J., M'KADMI, C., PILETTE, C., DUBROCA, C., NICAISE, Y., SEGUELAS, M.-H. & N'GUYEN, D. 2016. Cardioprotective Angiotensin-(1–7) Peptide Acts as a Natural-Biased Ligand at the Angiotensin II Type 1 ReceptorNovelty and Significance. *Hypertension,* 68**,** 1365-1374.

GARCIA, G. L., DONG, M. & MILLER, L. J. 2012. Differential determinants for coupling of distinct G proteins with the class B secretin receptor. *Am J Physiol Cell Physiol,* 302**,** C1202-12.

GARDELLA, T. J. & JUPPNER, H. 2001. Molecular properties of the PTH/PTHrP receptor. *Trends Endocrinol Metab,* 12**,** 210-7.

GAUDIN, P., MAORET, J. J., COUVINEAU, A., ROUYER-FESSARD, C. & LABURTHE, M. 1998. Constitutive activation of the human vasoactive intestinal peptide 1 receptor, a member of the new class II family of G protein-coupled receptors. *J Biol Chem,* 273**,** 4990-6.

GENNARI, C., CHIERICHETTI, M. S., GONNELLI, S., VIBELLI, C., MONTAGNANI, M. & PIOLINI, M. 1986. Migraine prophylaxis with salmon calcitonin: a cross-over double-blind, placebo-controlled study. *Headache,* 26**,** 13-6.

GENSURE, R. C., GARDELLA, T. J. & JUPPNER, H. 2005. Parathyroid hormone and parathyroid hormone-related peptide, and their receptors. *Biochem Biophys Res Commun,* 328**,** 666-78.

GESTY-PALMER, D., CHEN, M., REITER, E., AHN, S., NELSON, C. D., WANG, S., ECKHARDT, A. E., COWAN, C. L., SPURNEY, R. F., LUTTRELL, L. M. & LEFKOWITZ, R. J. 2006. Distinct beta-arrestin- and G protein-dependent pathways for parathyroid hormone receptor-stimulated ERK1/2 activation. *J Biol Chem,* 281**,** 10856-64.

GETHER, U., LIN, S., GHANOUNI, P., BALLESTEROS, J. A., WEINSTEIN, H. & KOBILKA, B. K. 1997. Agonists induce conformational changes in transmembrane domains III and VI of the beta2 adrenoceptor. *EMBO J,* 16**,** 6737-47.

GETHER, U., LIN, S. & KOBILKA, B. K. 1995. Fluorescent labeling of purified beta 2 adrenergic receptor. Evidence for ligand-specific conformational changes. *J Biol Chem,* 270**,** 28268-75.

GHANOUNI, P., STEENHUIS, J. J., FARRENS, D. L. & KOBILKA, B. K. 2001. Agonist-induced conformational changes in the G-protein-coupling domain of the beta 2 adrenergic receptor. *Proc Natl Acad Sci U S A,* 98**,** 5997-6002.

GINGELL, J. J., SIMMS, J., BARWELL, J., POYNER, D. R., WATKINS, H. A., PIOSZAK, A. A., SEXTON, P. M. & HAY, D. L. 2016. An allosteric role for receptor activity-modifying proteins in defining GPCR pharmacology. *Cell Discov,* 2**,** 16020.

GKOUNTELIAS, K., TSELIOS, T., VENIHAKI, M., DERAOS, G., LAZARIDIS, I., RASSOULI, O., GRAVANIS, A. & LIAPAKIS, G. 2009. Alanine scanning mutagenesis of the second extracellular loop of type 1 corticotropin-releasing factor receptor revealed residues critical for peptide binding. *Mol Pharmacol,* 75**,** 793-800.

GLUZMAN, Y. 1981. SV40-transformed simian cells support the replication of early SV40 mutants. *Cell,* 23**,** 175-82.

GOEBELL, H., AMMANN, R., HERFARTH, C., HORN, J., HOTZ, J., KNOBLAUCH, M., SCHMID, M., JAEGER, M., AKOVBIANTZ, A., LINDER, E., ABT, K., NUESCH, E. & BARTH, E. 1979. A double-blind trial of synthetic salmon calcitonin in the treatment of acute pancreatitis. *Scand J Gastroenterol,* 14**,** 881-9.

GOLTZMAN, D. 1980. Examination of interspecies differences in renal and skeletal receptor binding and adenylate cyclase stimulation with human calcitonin. *Endocrinology,* 106**,** 510-8.

GORN, A. H., LIN, H. Y., YAMIN, M., AURON, P. E., FLANNERY, M. R., TAPP, D. R., MANNING, C. A., LODISH, H. F., KRANE, S. M. & GOLDRING, S. R. 1992. Cloning, characterization, and expression of a human calcitonin receptor from an ovarian carcinoma cell line. *J Clin Invest,* 90**,** 1726-35.

GORN, A. H., RUDOLPH, S. M., FLANNERY, M. R., MORTON, C. C., WEREMOWICZ, S., WANG, T. Z., KRANE, S. M. & GOLDRING, S. R. 1995. Expression of two human skeletal calcitonin receptor isoforms cloned from a giant cell tumor of bone. The first intracellular domain modulates ligand binding and signal transduction. *J Clin Invest,* 95**,** 2680-91.

GUREVICH, E. V., TESMER, J. J., MUSHEGIAN, A. & GUREVICH, V. V. 2012. G protein-coupled receptor kinases: more than just kinases and not only for GPCRs. *Pharmacol Ther,* 133**,** 40-69.

GUREVICH, V. V. & GUREVICH, E. V. 2013. Structural determinants of arrestin functions. *Prog Mol Biol Transl Sci,* 118**,** 57-92.

HALLS, M. L., YEATMAN, H. R., NOWELL, C. J., THOMPSON, G. L., GONDIN, A. B., CIVCIRISTOV, S., BUNNETT, N. W., LAMBERT, N. A., POOLE, D. P. & CANALS, M. 2016. Plasma membrane localization of the mu-opioid receptor controls spatiotemporal signaling. *Sci Signal,* 9**,** ra16.

HAMANN, J., AUST, G., ARAC, D., ENGEL, F. B., FORMSTONE, C., FREDRIKSSON, R., HALL, R. A., HARTY, B. L., KIRCHHOFF, C., KNAPP, B., KRISHNAN, A., LIEBSCHER, I., LIN, H. H., MARTINELLI, D. C., MONK, K. R., PEETERS, M. C., PIAO, X., PROMEL, S., SCHONEBERG, T., SCHWARTZ, T. W., SINGER, K., STACEY, M., USHKARYOV, Y. A., VALLON, M., WOLFRUM, U., WRIGHT, M. W., XU, L., LANGENHAN, T. & SCHIOTH, H. B. 2015. International Union of Basic and Clinical Pharmacology. XCIV. Adhesion G protein-coupled receptors. *Pharmacol Rev,* 67**,** 338-67.

HAMPSON, D. R., ROSE, E. M. & ANTFLICK, J. E. 2008. The structures of metabotropic glutamate receptors. *The Glutamate Receptors.* 363-386, Springer.

HAN, B., NAKAMURA, M., ZHOU, G., ISHII, A., NAKAMURA, A., BAI, Y., MORI, I. & KAKUDO, K. 2006. Calcitonin inhibits invasion of breast cancer cells: involvement of urokinase-type plasminogen activator (uPA) and uPA receptor. *Int J Oncol,* 28**,** 807-14.

HAN, S.-J., HAMDAN, F. F., KIM, S.-K., JACOBSON, K. A., BLOODWORTH, L. M., LI, B. & WESS, J. 2005. Identification of an agonist-induced conformational change occurring adjacent to the ligand-binding pocket of the M3 muscarinic acetylcholine receptor. *J Biol Chem,* 280**,** 34849-34858.

HARIKUMAR, K. G., SIMMS, J., CHRISTOPOULOS, G., SEXTON, P. M. & MILLER, L. J. 2009. Molecular basis of association of receptor activity-modifying protein 3 with the family BG protein-coupled secretin receptor. *Biochemistry,* 48**,** 11773-11785.

HARMAR, A. J. 2001. Family-B G-protein-coupled receptors. *Genome Biol,* 2**,** REVIEWS3013.

HART, M. J., JIANG, X., KOZASA, T., ROSCOE, W., SINGER, W. D., GILMAN, A. G., STERNWEIS, P. C. & BOLLAG, G. 1998. Direct stimulation of the guanine nucleotide exchange activity of p115 RhoGEF by Gα13. *Science,* 280**,** 2112-2114.

HATAKEYAMA, H., TAKAHASHI, N., KISHIMOTO, T., NEMOTO, T. & KASAI, H. 2007. Two cAMP-dependent pathways differentially regulate exocytosis of large dense-core and small vesicles in mouse beta-cells. *J Physiol,* 582**,** 1087-98.

HAUSDORFF, W. P., CARON, M. G. & LEFKOWITZ, R. J. 1990. Turning off the signal: desensitization of beta-adrenergic receptor function. *FASEB J,* 4**,** 2881-9.

HAY, D. L., CHRISTOPOULOS, G., CHRISTOPOULOS, A., POYNER, D. R. & SEXTON, P. M. 2005. Pharmacological discrimination of calcitonin receptor: receptor activity-modifying protein complexes. *Mol Pharmacol,* 67**,** 1655-65.

HAY, D. L., HARRIS, P. W., KOWALCZYK, R., BRIMBLE, M. A., RATHBONE, D. L., BARWELL, J., CONNER, A. C. & POYNER, D. R. 2014. Structure-activity relationships of the N-terminus of calcitonin gene-related peptide: key roles of alanine-5 and threonine-6 in receptor activation. *Br J Pharmacol,* 171**,** 415-26.

HAY, D. L., POYNER, D. R. & SEXTON, P. M. 2006. GPCR modulation by RAMPs. *Pharmacol Ther,* 109**,** 173-97.

HENNEN, S., KODRA, J. T., SOROKA, V., KROGH, B. O., WU, X., KAASTRUP, P., ORSKOV, C., RONN, S. G., SCHLUCKEBIER, G., BARBATESKOVIC, S., GANDHI, P. S. & REEDTZ-RUNGE, S. 2016. Structural insight into antibody-mediated antagonism of the Glucagon-like peptide-1 Receptor. *Sci Rep-Uk,* 6**,** 26236.

HILAIRET, S., FOORD, S. M., MARSHALL, F. H. & BOUVIER, M. 2001. Protein-protein interaction and not glycosylation determines the binding selectivity of heterodimers between the calcitonin receptor-like receptor and the receptor activity-modifying proteins. *J Biol Chem,* 276**,** 29575-29581.

HILDEBRANDT, J. D. 1997. Role of subunit diversity in signaling by heterotrimeric G proteins. *Biochem Pharmacol,* 54**,** 325-39.

HILTON, J. M., CHAI, S. Y. & SEXTON, P. M. 1995. In vitro autoradiographic localization of the calcitonin receptor isoforms, C1a and C1b, in rat brain. *Neuroscience,* 69**,** 1223-37.

HILTON, J. M., DOWTON, M., HOUSSAMI, S. & SEXTON, P. M. 2000. Identification of key components in the irreversibility of salmon calcitonin binding to calcitonin receptors. *J Endocrinol,* 166**,** 213-26.

HINKE, S. A., MANHART, S., PAMIR, N., DEMUTH, H., R, W. G., PEDERSON, R. A. & MCINTOSH, C. H. 2001. Identification of a bioactive domain in the amino-terminus of glucose-dependent insulinotropic polypeptide (GIP). *Biochim Biophys Acta,* 1547**,** 143-55.

HOARE, S. R. 2005. Mechanisms of peptide and nonpeptide ligand binding to Class B G-protein-coupled receptors. *Drug Discov Today,* 10**,** 417-27.

HOBBS, S., JITRAPAKDEE, S. & WALLACE, J. C. 1998. Development of a bicistronic vector driven by the human polypeptide chain elongation factor 1α promoter for creation of stable mammalian cell lines that express very high levels of recombinant proteins. *Biochem Biophys Res Commun,* 252**,** 368-372.

HOLLENSTEIN, K., DE GRAAF, C., BORTOLATO, A., WANG, M. W., MARSHALL, F. H. & STEVENS, R. C. 2014. Insights into the structure of class B GPCRs. *Trends Pharmacol Sci,* 35**,** 12-22.

HOLLENSTEIN, K., KEAN, J., BORTOLATO, A., CHENG, R. K., DORE, A. S., JAZAYERI, A., COOKE, R. M., WEIR, M. & MARSHALL, F. H. 2013. Structure of class B GPCR corticotropin-releasing factor receptor 1. *Nature,* 499**,** 438-43.

HOLTMANN, M. H., HADAC, E. M. & MILLER, L. J. 1995. Critical contributions of amino-terminal extracellular domains in agonist binding and activation of secretin and vasoactive intestinal polypeptide receptors. Studies of chimeric receptors. *J Biol Chem,* 270**,** 14394-8.

HOTZ, J. & GOEBELL, H. 1975. Long-term effects of calcitonin on gastric secretion in normals, peptic ulcer and high risk patients. *Z Gastroenterol***,** 71-77.

HUANG, H. C. & KLEIN, P. S. 2004. The Frizzled family: receptors for multiple signal transduction pathways. *Genome Biol,* 5**,** 234.

HULME, E. C. 2013. GPCR activation: a mutagenic spotlight on crystal structures. *Trends Pharmacol Sci,* 34**,** 67-84.

IIDA-KLEIN, A., GUO, J., TAKEMURA, M., DRAKE, M. T., POTTS, J. T., ABOU-SAMRA, A., BRINGHURST, F. R. & SEGRE, G. V. 1997. Mutations in the second cytoplasmic loop of the rat parathyroid hormone (PTH)/PTH-related protein receptor result in selective loss of PTH-stimulated phospholipase C activity. *J Biol Chem,* 272**,** 6882-6889.

IKEDA, S. R. 1996. Voltage-dependent modulation of N-type calcium channels by G-protein beta gamma subunits. *Nature,* 380**,** 255-8.

ITOH, N., OBATA, K., YANAIHARA, N. & OKAMOTO, H. 1983. Human preprovasoactive intestinal polypeptide contains a novel PHI-27-like peptide, PHM-27. *Nature,* 304**,** 547-9.

JAAKOLA, V. P., GRIFFITH, M. T., HANSON, M. A., CHEREZOV, V., CHIEN, E. Y., LANE, J. R., IJZERMAN, A. P. & STEVENS, R. C. 2008. The 2.6 angstrom crystal structure of a human A2A adenosine receptor bound to an antagonist. *Science,* 322**,** 1211-7.

JAEGER, H. & MAIER, C. 1992. Calcitonin in phantom limb pain: a double-blind study. *Pain,* 48**,** 21-7.

JAING, R., DUAN, J., WINDEMUTH, A., STEPHENS, J. C., JUDSON, R. & XU, C. 2003. Genome-wide evaluation of the public SNP databases. *Pharmacogenomics J,* 4**,** 779-789.

JAISWAL, B. S. & CONTI, M. 2003. Calcium regulation of the soluble adenylyl cyclase expressed in mammalian spermatozoa. *Proc Natl Acad Sci U S A,* 100**,** 10676-81.

JANZ, J. M. & FARRENS, D. L. 2004. Rhodopsin activation exposes a key hydrophobic binding site for the transducin alpha-subunit C terminus. *J Biol Chem,* 279**,** 29767-73.

JENSEN, A. D., GUARNIERI, F., RASMUSSEN, S. G., ASMAR, F., BALLESTEROS, J. A. & GETHER, U. 2001. Agonist-induced conformational changes at the cytoplasmic side of transmembrane segment 6 in the β2 adrenergic receptor mapped by site-selective fluorescent labeling. *J Biol Chem,* 276**,** 9279-9290.

JENSEN, D. D., HALLS, M. L., MURPHY, J. E., CANALS, M., CATTARUZZA, F., POOLE, D. P., LIEU, T., KOON, H. W., POTHOULAKIS, C. & BUNNETT, N. W. 2014. Endothelin-converting enzyme 1 and beta-arrestins exert spatiotemporal control of substance P-induced inflammatory signals. *J Biol Chem,* 289**,** 20283-94.

JOBERT, A. S., ZHANG, P., COUVINEAU, A., BONAVENTURE, J., ROUME, J., LE MERRER, M. & SILVE, C. 1998. Absence of functional receptors for parathyroid hormone and parathyroid hormone-related peptide in Blomstrand chondrodysplasia. *J Clin Invest,* 102**,** 34-40.

JOHANSSON, E., HANSEN, J. L., HANSEN, A. M., SHAW, A. C., BECKER, P., SCHAFFER, L. & REEDTZ-RUNGE, S. 2016. Type II Turn of Receptor-bound Salmon Calcitonin Revealed by X-ray Crystallography. *J Biol Chem,* 291**,** 13689-98.

JORGENSEN, R., MARTINI, L., SCHWARTZ, T. W. & ELLING, C. E. 2005. Characterization of glucagon-like peptide-1 receptor beta-arrestin 2 interaction: a high-affinity receptor phenotype. *Mol Endocrinol,* 19**,** 812-23.

KALLIO, D. M., GARANT, P. R. & MINKIN, C. 1972. Ultrastructural effects of calcitonin on osteoclasts in tissue culture. *J Ultrastruct Res,* 39**,** 205-16.

KANG, Y., ZHOU, X. E., GAO, X., HE, Y., LIU, W., ISHCHENKO, A., BARTY, A., WHITE, T. A., YEFANOV, O., HAN, G. W., XU, Q., DE WAAL, P. W., KE, J., TAN, M. H., ZHANG, C., MOELLER, A., WEST, G. M., PASCAL, B. D., VAN EPS, N., CARO, L. N., VISHNIVETSKIY, S. A., LEE, R. J., SUINO-POWELL, K. M., GU, X., PAL, K., MA, J., ZHI, X., BOUTET, S., WILLIAMS, G. J., MESSERSCHMIDT, M., GATI, C., ZATSEPIN, N. A., WANG, D., JAMES, D., BASU, S., ROY-CHOWDHURY, S., CONRAD, C. E., COE, J., LIU, H., LISOVA, S., KUPITZ, C., GROTJOHANN, I., FROMME, R., JIANG, Y., TAN, M., YANG, H., LI, J., WANG, M., ZHENG, Z., LI, D., HOWE, N., ZHAO, Y., STANDFUSS, J., DIEDERICHS, K., DONG, Y., POTTER, C. S., CARRAGHER, B., CAFFREY, M., JIANG, H., CHAPMAN, H. N., SPENCE, J. C., FROMME, P., WEIERSTALL, U., ERNST, O. P., KATRITCH, V., GUREVICH, V. V., GRIFFIN, P. R., HUBBELL, W. L., STEVENS, R. C., CHEREZOV, V., MELCHER, K. & XU, H. E. 2015. Crystal structure of rhodopsin bound to arrestin by femtosecond X-ray laser. *Nature,* 523**,** 561-7.

KARLIN, A. 1967. On the application of "a plausible model" of allosteric proteins to the receptor for acetylcholine. *J Theor Biol,* 16**,** 306-320.

KARSDAL, M. A., RIIS, B. J., MEHTA, N., STERN, W., ARBIT, E., CHRISTIANSEN, C. & HENRIKSEN, K. 2015. Lessons learned from the clinical development of oral peptides. *Br J Clin Pharmacol,* 79**,** 720-32.

KATAYAMA, T., FURUYA, M., YAMAICHI, K., KONISHI, K., SUGIURA, N., MURAFUJI, H., MAGOTA, K., SAITO, M., TANAKA, S. & OIKAWA, S. 2001. Discovery of a non-peptide small molecule that selectively mimics the biological actions of calcitonin. *Bba-Gen Subjects,* 1526**,** 183-190.

KELLY, E., BAILEY, C. P. & HENDERSON, G. 2008. Agonist-selective mechanisms of GPCR desensitization. *Br J Pharmacol,* 153 Suppl 1**,** S379-88.

KENAKIN, T. 2011. Functional selectivity and biased receptor signaling. *J Pharmacol Exp Ther,* 336**,** 296-302.

KENAKIN, T. & CHRISTOPOULOS, A. 2013. Signalling bias in new drug discovery: detection, quantification and therapeutic impact. *Nat Rev Drug Discov,* 12**,** 205-16.

KENAKIN, T., WATSON, C., MUNIZ-MEDINA, V., CHRISTOPOULOS, A. & NOVICK, S. 2012. A simple method for quantifying functional selectivity and agonist bias. *ACS Chem Neurosci,* 3**,** 193-203.

KENDALL, R. T. & LUTTRELL, L. M. 2009. Diversity in arrestin function. *Cell Mol Life Sci,* 66**,** 2953-73.

KIM, I. M., TILLEY, D. G., CHEN, J., SALAZAR, N. C., WHALEN, E. J., VIOLIN, J. D. & ROCKMAN, H. A. 2008. Beta-blockers alprenolol and carvedilol stimulate beta-arrestin-mediated EGFR transactivation. *Proc Natl Acad Sci U S A,* 105**,** 14555-60.

KIM, T. H., CHUNG, K. Y., MANGLIK, A., HANSEN, A. L., DROR, R. O., MILDORF, T. J., SHAW, D. E., KOBILKA, B. K. & PROSSER, R. S. 2013. The role of ligands on the equilibria between functional states of a G protein-coupled receptor. *J Am Chem Soc,* 135**,** 9465-74.

KIRCHBERG, K., KIM, T. Y., MOLLER, M., SKEGRO, D., DASARA RAJU, G., GRANZIN, J., BULDT, G., SCHLESINGER, R. & ALEXIEV, U. 2011. Conformational dynamics of helix 8 in the GPCR rhodopsin controls arrestin activation in the desensitization process. *Proc Natl Acad Sci U S A,* 108**,** 18690-5.

KIRKPATRICK, A., HEO, J., ABROL, R. & GODDARD, W. A., 3RD 2012. Predicted structure of agonist-bound glucagon-like peptide 1 receptor, a class B G protein-coupled receptor. *Proc Natl Acad Sci U S A,* 109**,** 19988-93.

KLEINAU, G., JAESCHKE, H., WORTH, C. L., MUELLER, S., GONZALEZ, J., PASCHKE, R. & KRAUSE, G. 2010. Principles and determinants of G-protein coupling by the rhodopsin-like thyrotropin receptor. *PLoS One,* 5**,** e9745.

KNUDSEN, S. M., TAMS, J. W. & FAHRENKRUG, J. 2001. Functional roles of conserved transmembrane prolines in the human VPAC1 receptor. *FEBS Lett,* 503**,** 126-130.

KOBILKA, B. 2013. The structural basis of G-protein-coupled receptor signaling (Nobel Lecture). *Angew Chem Int Ed Engl,* 52**,** 6380-8.

KOLAKOWSKI JR, L. F. 1993. GCRDb: a G-protein-coupled receptor database. *Recept Channels,* 2**,** 1-7.

KOOISTRA, M. R., DUBE, N. & BOS, J. L. 2007. Rap1: a key regulator in cell-cell junction formation. *J Cell Sci,* 120**,** 17-22.

KOOLE, C., WOOTTEN, D., SIMMS, J., MILLER, L. J., CHRISTOPOULOS, A. & SEXTON, P. M. 2012a. Second Extracellular Loop of Human Glucagon-like Peptide-1 Receptor (GLP-1R) Has a Critical Role in GLP-1 Peptide Binding and Receptor Activation. *J Biol Chem,* 287**,** 3642-3658.

KOOLE, C., WOOTTEN, D., SIMMS, J., SAVAGE, E. E., MILLER, L. J., CHRISTOPOULOS, A. & SEXTON, P. M. 2012b. Second extracellular loop of human glucagon-like peptide-1 receptor (GLP-1R) differentially regulates orthosteric but not allosteric agonist binding and function. *J Biol Chem,* 287**,** 3659-73.

KOOLE, C., WOOTTEN, D., SIMMS, J., VALANT, C., SRIDHAR, R., WOODMAN, O. L., MILLER, L. J., SUMMERS, R. J., CHRISTOPOULOS, A. & SEXTON, P. M. 2010. Allosteric ligands of the glucagon-like peptide 1 receptor (GLP-1R) differentially modulate endogenous

and exogenous peptide responses in a pathway-selective manner: implications for drug screening. *Mol Pharmacol,* 78**,** 456-65.

KOTH, C. M., MURRAY, J. M., MUKUND, S., MADJIDI, A., MINN, A., CLARKE, H. J., WONG, T., CHIANG, V., LUIS, E., ESTEVEZ, A., RONDON, J., ZHANG, Y., HOTZEL, I. & ALLAN, B. B. 2012. Molecular basis for negative regulation of the glucagon receptor. *Proc Natl Acad Sci U S A,* 109**,** 14393-8.

KOZASA, T., JIANG, X., HART, M. J., STERNWEIS, P. M., SINGER, W. D., GILMAN, A. G., BOLLAG, G. & STERNWEIS, P. C. 1998. p115 RhoGEF, a GTPase activating protein for Gα12 and Gα13. *Science,* 280**,** 2109-2111.

KRISHNA, A. G., MENON, S. T., TERRY, T. J. & SAKMAR, T. P. 2002. Evidence that helix 8 of rhodopsin acts as a membrane-dependent conformational switch. *Biochemistry,* 41**,** 8298-8309.

KUESTNER, R. E., ELROD, R. D., GRANT, F. J., HAGEN, F. S., KUIJPER, J. L., MATTHEWES, S. L., O'HARA, P. J., SHEPPARD, P. O., STROOP, S. D. & THOMPSON, D. L. 1994. Cloning and characterization of an abundant subtype of the human calcitonin receptor. *Mol Pharmacol,* 46**,** 246-55.

KUNA, R. S., GIRADA, S. B., ASALLA, S., VALLENTYNE, J., MADDIKA, S., PATTERSON, J. T., SMILEY, D. L., DIMARCHI, R. D. & MITRA, P. 2013. Glucagon-like peptide-1 receptor-mediated endosomal cAMP generation promotes glucose-stimulated insulin secretion in pancreatic beta-cells. *Am J Physiol Endocrinol Metab,* 305**,** E161-70.

KUSANO, S., KUKIMOTO-NIINO, M., HINO, N., OHSAWA, N., OKUDA, K. I., SAKAMOTO, K., SHIROUZU, M., SHINDO, T. & YOKOYAMA, S. 2012. Structural basis for extracellular interactions between calcitonin receptor-like receptor and receptor activity-modifying protein 2 for adrenomedullin-specific binding. *Protein Sci,* 21**,** 199-210.

KUWASAKO, K., HAY, D. L., NAGATA, S., HIKOSAKA, T., KITAMURA, K. & KATO, J. 2012. The third extracellular loop of the human calcitonin receptor-like receptor is crucial for the activation of adrenomedullin signalling. *Br J Pharmacol,* 166**,** 137-150.

LABURTHE, M., COUVINEAU, A. & TAN, V. 2007. Class II G protein-coupled receptors for VIP and PACAP: structure, models of activation and pharmacology. *Peptides,* 28**,** 1631-9.

LACROIX, M., SIWEK, B. & BODY, J. J. 1998. Breast cancer cell response to calcitonin: modulation by growth-regulating agents. *Eur J Pharmacol,* 344**,** 279-86.

LAFOND, J., SIMONEAU, L., SAVARD, R. & LAJEUNESSE, D. 1994. Calcitonin receptor in human placental syncytiotrophoblast brush border and basal plasma membranes. *Mol Cell Endocrinol,* 99**,** 285-92.

LAGERSTROM, M. C. & SCHIOTH, H. B. 2008. Structural diversity of G protein-coupled receptors and significance for drug discovery. *Nat Rev Drug Discov,* 7**,** 339-57.

LAMBRIGHT, D. G., NOEL, J. P., HAMM, H. E. & SIGLER, P. B. 1994. Structural determinants for activation of the alpha-subunit of a heterotrimeric G protein. *Nature,* 369**,** 621-8.

LAMP, S. J., FINDLAY, D. M., MOSELEY, J. M. & MARTIN, T. J. 1981. Calcitonin induction of a persistent activated state of adenylate cyclase in human breast cancer cells (T 47D). *J Biol Chem,* 256**,** 12269-74.

LANGER, I. & ROBBERECHT, P. 2007. Molecular mechanisms involved in vasoactive intestinal peptide receptor activation and regulation: current knowledge, similarities to and differences from the A family of G-protein-coupled receptors. *Biochemical Society Transactions,* 35**,** 724-8.

LANGSTON, A. L. & RALSTON, S. H. 2004. Management of Paget's disease of bone. *Rheumatology (Oxford),* 43**,** 955-9.

LASMOLES, F., JULLIENNE, A., DAY, F., MINVIELLE, S., MILHAUD, G. & MOUKHTAR, M. S. 1985. Elucidation of the nucleotide sequence of chicken calcitonin mRNA: direct evidence for the expression of a lower vertebrate calcitonin-like gene in man and rat. *EMBO J,* 4**,** 2603-7.

LAURIAN, L., OBERMAN, Z., GRAF, E., GILAD, S., HOERER, E. & SIMANTOV, R. 1986. Calcitonin induced increase in ACTH, beta-endorphin and cortisol secretion. *Horm Metab Res,* 18**,** 268-71.

LEBON, G., WARNE, T., EDWARDS, P. C., BENNETT, K., LANGMEAD, C. J., LESLIE, A. G. & TATE, C. G. 2011. Agonist-bound adenosine A2A receptor structures reveal common features of GPCR activation. *Nature,* 474**,** 521-5.

LEE, A., RANA, B. K., SCHIFFER, H. H., SCHORK, N. J., BRANN, M. R., INSEL, P. A. & WEINER, D. M. 2003. Distribution analysis of nonsynonymous polymorphisms within the G-protein-coupled receptor gene family. *Genomics,* 81**,** 245-248.

LEE, M. H., APPLETON, K. M., STRUNGS, E. G., KWON, J. Y., MORINELLI, T. A., PETERSON, Y. K., LAPORTE, S. A. & LUTTRELL, L. M. 2016a. The conformational signature of beta-arrestin2 predicts its trafficking and signalling functions. *Nature,* 531**,** 665-8.

LEE, S.-M., HAY, D. L. & PIOSZAK, A. A. 2016b. Calcitonin and Amylin Receptor Peptide Interaction Mechanisms insights into peptide-binding modes and allosteric modulation of the calcitonin receptor by receptor activity-modifying proteins. *J Biol Chem,* 291**,** 8686-8700.

LEE, S. M., BOOE, J. M. & PIOSZAK, A. A. 2015. Structural insights into ligand recognition and selectivity for classes A, B, and C GPCRs. *Eur J Pharmacol,* 763**,** 196-205.

LEFKOWITZ, R. J. & SHENOY, S. K. 2005. Transduction of receptor signals by ß-arrestins. *Science,* 308**,** 512-517.

LI, H. Y., SHEN, J. T., CHANG, S. P., HSU, W. L. & SUNG, Y. J. 2008. Calcitonin promotes outgrowth of trophoblast cells on endometrial epithelial cells: involvement of calcium mobilization and protein kinase C activation. *Placenta,* 29**,** 20-9.

LI, Q., BAGCHI, M. K. & BAGCHI, I. C. 2006. Identification of a signaling pathway involving progesterone receptor, calcitonin, and tissue tranglutaminase in Ishikawa endometrial cells. *Endocrinology,* 147**,** 2147-54.

LIANG, Y. L., KHOSHOUEI, M., RADJAINIA, M., ZHANG, Y., GLUKHOVA, A., TARRASCH, J., THAL, D. M., FURNESS, S. G. B., CHRISTOPOULOS, G., COUDRAT, T., DANEV, R., BAUMEISTER, W., MILLER, L. J., CHRISTOPOULOS, A., KOBILKA, B. K., WOOTTEN, D., SKINIOTIS, G. & SEXTON, P. M. 2017. Phase-plate cryo-EM structure of a class B GPCR-G-protein complex. *Nature,* 546**,** 118-123.

LIBERINI, C. G., BOYLE, C. N., CIFANI, C., VENNIRO, M., HOPE, B. T. & LUTZ, T. A. 2016. Amylin receptor components and the leptin receptor are co-expressed in single rat area postrema neurons. *Eur J Neurosci,* 43**,** 653-61.

LIN, H. Y., HARRIS, T. L., FLANNERY, M. S., ARUFFO, A., KAJI, E. H., GORN, A., KOLAKOWSKI, L. F., JR., LODISH, H. F. & GOLDRING, S. R. 1991. Expression cloning of an adenylate cyclase-coupled calcitonin receptor. *Science,* 254**,** 1022-4.

LUTTRELL, L. M. & GESTY-PALMER, D. 2010. Beyond desensitization: physiological relevance of arrestin-dependent signaling. *Pharmacol Rev,* 62**,** 305-30.

LUTTRELL, L. M. & LEFKOWITZ, R. J. 2002. The role of beta-arrestins in the termination and transduction of G-protein-coupled receptor signals. *J Cell Sci,* 115**,** 455-65.

LUTTRELL, L. M., ROUDABUSH, F. L., CHOY, E. W., MILLER, W. E., FIELD, M. E., PIERCE, K. L. & LEFKOWITZ, R. J. 2001. Activation and targeting of extracellular signal-regulated kinases by beta-arrestin scaffolds. *Proc Natl Acad Sci U S A,* 98**,** 2449-54.

MA, J. N., CURRIER, E. A., ESSEX, A., FEDDOCK, M., SPALDING, T. A., NASH, N. R., BRANN, M. R. & BURSTEIN, E. S. 2004. Discovery of novel peptide/receptor interactions: identification of PHM-27 as a potent agonist of the human calcitonin receptor. *Biochem Pharmacol,* 67**,** 1279-84.

MA, Y. C., HUANG, J. Y., ALL, S., LOWRY, W. & HUANG, X. Y. 2000. Src tyrosine kinase is a novel direct effector of G proteins. *Cell,* 102**,** 635-646.

MACREZ-LEPRÊTRE, N., KALKBRENNER, F., SCHULTZ, G. & MIRONNEAU, J. 1997. Distinct functions of Gq and G11 proteins in coupling α1-adrenoreceptors to Ca2+ release and Ca2+ entry in rat portal vein myocytes. *J Biol Chem,* 272**,** 5261-5268.

MANN, R. J., AL-SABAH, S., DE MATURANA, R. L., SINFIELD, J. K. & DONNELLY, D. 2010. Functional coupling of Cys-226 and Cys-296 in the glucagon-like peptide-1 (GLP-1) receptor indicates a disulfide bond that is close to the activation pocket. *Peptides,* 31**,** 2289-93.

MARX, S. J., AURBACH, G. D., GAVIN, J. R., 3RD & BUELL, D. W. 1974. Calcitonin receptors on cultured human lymphocytes. *J Biol Chem,* 249**,** 6812-6.

MARX, S. J., WOODWARD, C. J. & AURBACH, G. D. 1972. Calcitonin receptors of kidney and bone. *Science,* 178**,** 999-1001.

MASI, L., BECHERINI, L., COLLI, E., GENNARI, L., MANSANI, R., FALCHETTI, A., BECORPI, A. M., CEPOLLARO, C., GONNELLI, S., TANINI, A. & BRANDI, M. L. 1998a. Polymorphisms of the calcitonin receptor gene are associated with bone mineral density in postmenopausal Italian women. *Biochem Biophys Res Commun,* 248**,** 190-5.

MASI, L., BECHERINI, L., GENNARI, L., COLLI, E., MANSANI, R., FALCHETTI, A., CEPOLLARO, C., GONNELLI, S., TANINI, A. & BRANDI, M. L. 1998b. Allelic variants of human calcitonin receptor: distribution and association with bone mass in postmenopausal Italian women. *Biochem Biophys Res Commun,* 245**,** 622-6.

MCLATCHIE, L. M., FRASER, N. J., MAIN, M. J., WISE, A., BROWN, J., THOMPSON, N., SOLARI, R., LEE, M. G. & FOORD, S. M. 1998. RAMPs regulate the transport and ligand specificity of the calcitonin-receptor-like receptor. *Nature,* 393**,** 333-9.

MICHELANGELI, V., FINDLAY, D., MOSELEY, J. & MARTIN, T. 1982. Mechanisms of calcitonin induction of prolonged activation of adenylate cyclase in human cancer cells. *J Cyclic Nucleotide Protein Phosphor Res,* 9**,** 129-141.

MICIELI, G., CAVALLINI, A., MARTIGNONI, E., COVELLI, V., FACCHINETTI, F. & NAPPI, G. 1988. Effectiveness of salmon calcitonin nasal spray preparation in migraine treatment. *Headache,* 28**,** 196-200.

MINHAS, P. S. & VIRDI, J. K. 2017. Hypercalcemia in Inpatient Setting: Diagnostic Approach and Management. *Curr Emerg Hosp Med Rep,* 5**,** 5-10.

MIRALLES, F. S., LOPEZ-SORIANO, F., PUIG, M. M., PEREZ, D. & LOPEZ-RODRIGUEZ, F. 1987. Postoperative analgesia induced by subarachnoid lidocaine plus calcitonin. *Anesth Analg,* 66**,** 615-8.

MITRA, P., GUHA, M., GHOSH, S., MUKHERJEE, S., BANKURA, B., PAL, D. K., MAITY, B. & DAS, M. 2017. Association of calcitonin receptor gene (CALCR) polymorphism with kidney stone disease in the population of West Bengal, India. *Gene,* 622**,** 23-28.

MOORE, E. E., KUESTNER, R. E., STROOP, S. D., GRANT, F. J., MATTHEWES, S. L., BRADY, C. L., SEXTON, P. M. & FINDLAY, D. M. 1995. Functionally different isoforms of the human calcitonin receptor result from alternative splicing of the gene transcript. *Mol Endocrinol,* 9**,** 959-68.

MOREIRA, I. S. 2014. Structural features of the G-protein/GPCR interactions. *Biochim Biophys Acta,* 1840**,** 16-33.

MORFIS, M., TILAKARATNE, N., FURNESS, S. G., CHRISTOPOULOS, G., WERRY, T. D., CHRISTOPOULOS, A. & SEXTON, P. M. 2008. Receptor activity-modifying proteins differentially modulate the G protein-coupling efficiency of amylin receptors. *Endocrinology,* 149**,** 5423-31.

MOSCAT, J., DIAZ-MECO, M. T. & RENNERT, P. 2003. NF-κB activation by protein kinase C isoforms and B-cell function. *EMBO Rep,* 4**,** 31-36.

MOUKHAMETZIANOV, R., WARNE, T., EDWARDS, P. C., SERRANO-VEGA, M. J., LESLIE, A. G. W., TATE, C. G. & SCHERTLER, G. F. X. 2011. Two distinct conformations of helix 6 observed in antagonist-bound structures of a β1-adrenergic receptor. *Proc Natl Acad Sci USA,* 108**,** 8228-8232.

MOULD, R. & PONDEL, M. D. 2003. Calcitonin receptor gene expression in K562 chronic myelogenous leukemic cells. *Cancer Cell Int,* 3**,** 6.

MUKUND, S., SHANG, Y., CLARKE, H. J., MADJIDI, A., CORN, J. E., KATES, L., KOLUMAM, G., CHIANG, V., LUIS, E., MURRAY, J., ZHANG, Y., HOTZEL, I., KOTH, C. M. & ALLAN, B. B. 2013. Inhibitory mechanism of an allosteric antibody targeting the glucagon receptor. *J Biol Chem,* 288**,** 36168-78.

MURTHY, K., GRIDER, J. & MAKHLOUF, G. 2000. Heterologous desensitization of response mediated by selective PKC-dependent phosphorylation of Gi-1 and Gi-2. *Am J Physiol Cell Physiol,* 279**,** C925-C934.

MUSTAFA, S. J., MORRISON, R. R., TENG, B. & PELLEG, A. 2009. Adenosine receptors and the heart: role in regulation of coronary blood flow and cardiac electrophysiology. *Handb Exp Pharmacol,* 193**,** 161-188.

NABHAN, C., XIONG, Y., XIE, L. Y. & ABOUSAMRA, A. B. 1995. The alternatively spliced type II corticotropin-releasing factor receptor, stably expressed in LLCPK-1 cells, is not well coupled to the G protein (s). *Biochem Biophys Res Commun,* 212**,** 1015-1021.

NAKAMURA, M., HAN, B., NISHISHITA, T., BAI, Y. & KAKUDO, K. 2007. Calcitonin targets extracellular signal-regulated kinase signaling pathway in human cancers. *J Mol Endocrinol,* 39**,** 375-84.

NAKAMURA, M., HASHIMOTO, T., NAKAJIMA, T., ICHII, S., FURUYAMA, J., ISHIHARA, Y. & KAKUDO, K. 1995. A new type of human calcitonin receptor isoform generated by alternative splicing. *Biochem Biophys Res Commun,* 209**,** 744-51.

NAKAMURA, M., ZHANG, Z.-Q., SHAN, L., HISA, T., SASAKI, M., TSUKINO, R., YOKOI, T., KANAME, A. & KAKUDO, K. 1996. Allelic variants of human calcitonin receptor in the Japanese population. *Hum Genet,* 99**,** 38-41.

NEUMANN, J.-M., COUVINEAU, A., MURAIL, S., LACAPERE, J.-J., JAMIN, N. & LABURTHE, M. 2008. Class-B GPCR activation: is ligand helix-capping the key? *Trends Biochem Sci,* 33**,** 314-319.

NG, S. Y., CHOW, B. K., KASAMATSU, J., KASAHARA, M. & LEE, L. T. 2012. Agnathan VIP, PACAP and their receptors: ancestral origins of today's highly diversified forms. *PLoS One,* 7**,** e44691.

NICHOLSON, G. C., MOSELEY, J. M., SEXTON, P. M., MENDELSOHN, F. A. & MARTIN, T. J. 1986. Abundant calcitonin receptors in isolated rat osteoclasts. Biochemical and autoradiographic characterization. *J Clin Invest,* 78**,** 355-60.

NICKERSON, M. 1956. Receptor occupancy and tissue response. *Nature,* 178**,** 697-8.

NIELSEN, S. M., NIELSEN, L. Z., HJORTH, S. A., PERRIN, M. H. & VALE, W. W. 2000. Constitutive activation of tethered-peptide/corticotropin-releasing factor receptor chimeras. *Proc Natl Acad Sci U S A,* 97**,** 10277-81.

NISHIZUKA, Y. 1992. Intracellular signaling by hydrolysis of phospholipids and activation of protein kinase C. *Science,* 258**,** 607-14.

NISHIZUKA, Y. 1995. Protein kinase C and lipid signaling for sustained cellular responses. *FASEB J,* 9**,** 484-96.

NOMA, T., LEMAIRE, A., PRASAD, S. V. N., BARKI-HARRINGTON, L., TILLEY, D. G., CHEN, J., LE CORVOISIER, P., VIOLIN, J. D., WEI, H., LEFKOWITZ, R. J. & ROCKMAN, H. A. 2007. b-arrestin-mediated beta(1)-adrenergic receptor transactivation of the EGFR confers cardioprotection. *J Clin Invest,* 117**,** 2445-2458.

NYGAARD, R., ZOU, Y., DROR, R. O., MILDORF, T. J., ARLOW, D. H., MANGLIK, A., PAN, A. C., LIU, C. W., FUNG, J. J., BOKOCH, M. P., THIAN, F. S., KOBILKA, T. S., SHAW, D. E., MUELLER, L., PROSSER, R. S. & KOBILKA, B. K. 2013. The dynamic process of beta(2)-adrenergic receptor activation. *Cell,* 152**,** 532-42.

OAKLEY, R. H., LAPORTE, S. A., HOLT, J. A., BARAK, L. S. & CARON, M. G. 1999. Association of beta-arrestin with G protein-coupled receptors during clathrin-mediated endocytosis dictates the profile of receptor resensitization. *J Biol Chem,* 274**,** 32248-57.

OAKLEY, R. H., OLIVARES-REYES, J. A., HUDSON, C. C., FLORES-VEGA, F., DAUTZENBERG, F. M. & HAUGER, R. L. 2007. Carboxyl-terminal and intracellular loop sites for CRF1 receptor phosphorylation and beta-arrestin-2 recruitment: a mechanism regulating stress and anxiety responses. *Am J Physiol Regul Integr Comp Physiol,* 293**,** R209-22.

OLDHAM, W. M. & HAMM, H. E. 2008. Heterotrimeric G protein activation by G-protein-coupled receptors. *Nat Rev Mol Cell Biol,* 9**,** 60-71.

ORLOWSKI, R. C., EPAND, R. M. & STAFFORD, A. R. 1987. Biologically potent analogues of salmon calcitonin which do not contain an N-terminal disulfide-bridged ring structure. *Eur J Biochem,* 162**,** 399-402.

OVERINGTON, J. P., AL-LAZIKANI, B. & HOPKINS, A. L. 2006. How many drug targets are there? *Nat Rev Drug Discov,* 5**,** 993-996.

PAL, K., MELCHER, K. & XU, H. E. 2012. Structure and mechanism for recognition of peptide hormones by Class B G-protein-coupled receptors. *Acta Pharmacol Sin,* 33**,** 300-11.

PARTHIER, C., REEDTZ-RUNGE, S., RUDOLPH, R. & STUBBS, M. T. 2009. Passing the baton in class B GPCRs: peptide hormone activation via helix induction? *Trends Biochem Sci,* 34**,** 303-10.

PERRY III, H., KAHN, A., CHAPPEL, J., KOHLER, G., TEITELBAUM, S. & PECK, W. 1983. Calcitonin Response in Circulating Human Lymphocytes. *Endocrinology,* 113**,** 1568-1573.

PHAM, V., DONG, M., WADE, J. D., MILLER, L. J., MORTON, C. J., NG, H. L., PARKER, M. W. & SEXTON, P. M. 2005. Insights into interactions between the alpha-helical region of the salmon calcitonin antagonists and the human calcitonin receptor using photoaffinity labeling. *J Biol Chem,* 280**,** 28610-22.

PHAM, V., WADE, J. D., PURDUE, B. W. & SEXTON, P. M. 2004. Spatial proximity between a photolabile residue in position 19 of salmon calcitonin and the amino terminus of the human calcitonin receptor. *J Biol Chem,* 279**,** 6720-9.

PISEGNA, J. R., MOODY, T. W. & WANK, S. A. 1996. Differential Signaling and Immediate-Early Gene Activation by Four Splice Variants of the Human Pituitary Adenylate CyclaseActivating Polypeptide Receptor (hPACAP-R). *Ann N Y Acad Sci,* 805**,** 54-64.

PITCHER, J. A., INGLESE, J., HIGGINS, J. B., ARRIZA, J. L., CASEY, P. J., KIM, C., BENOVIC, J. L., KWATRA, M. M., CARON, M. G. & LEFKOWITZ, R. J. 1992. Role of beta gamma subunits of G proteins in targeting the beta-adrenergic receptor kinase to membrane-bound receptors. *Science,* 257**,** 1264-7.

PLOSKER, G. L. & MCTAVISH, D. 1996. Intranasal salcatonin (salmon calcitonin). A review of its pharmacological properties and role in the management of postmenopausal osteoporosis. *Drugs Aging,* 8**,** 378-400.

POYNER, D. R., SEXTON, P. M., MARSHALL, I., SMITH, D. M., QUIRION, R., BORN, W., MUFF, R., FISCHER, J. A. & FOORD, S. M. 2002. International Union of Pharmacology. XXXII. The mammalian calcitonin gene-related peptides, adrenomedullin, amylin, and calcitonin receptors. *Pharmacol Rev,* 54**,** 233-46.

QI, T., DONG, M., WATKINS, H. A., WOOTTEN, D., MILLER, L. J. & HAY, D. L. 2013. Receptor activity-modifying protein-dependent impairment of calcitonin receptor splice variant Delta(1-47)hCT((a)) function. *Br J Pharmacol,* 168**,** 644-57.

QI, T. & HAY, D. L. 2010. Structure-function relationships of the N-terminus of receptor activity-modifying proteins. *Br J Pharmacol,* 159**,** 1059-68.

QIAO, J., MEI, F. C., POPOV, V. L., VERGARA, L. A. & CHENG, X. 2002. Cell cycle-dependent subcellular localization of exchange factor directly activated by cAMP. *J Biol Chem,* 277**,** 26581-6.

QUINN, J. M., NEALE, S., FUJIKAWA, Y., MCGEE, J. O. & ATHANASOU, N. A. 1998. Human osteoclast formation from blood monocytes, peritoneal macrophages, and bone marrow cells. *Calcified Tissue Int,* 62**,** 527-31.

RAGGATT, L. J., EVDOKIOU, A. & FINDLAY, D. M. 2000. Sustained activation of Erk1/2 MAPK and cell growth suppression by the insert-negative, but not the insert-positive isoform of the human calcitonin receptor. *J Endocrinol,* 167**,** 93-105.

RAJAGOPAL, S., RAJAGOPAL, K. & LEFKOWITZ, R. J. 2010. Teaching old receptors new tricks: biasing seven-transmembrane receptors. *Nat Rev Drug Discov,* 9**,** 373-86.

RANGARAJAN, S., ENSERINK, J. M., KUIPERIJ, H. B., DE ROOIJ, J., PRICE, L. S., SCHWEDE, F. & BOS, J. L. 2003. Cyclic AMP induces integrin-mediated cell adhesion through Epac and Rap1 upon stimulation of the β2-adrenergic receptor. *J Cell Biol,* 160**,** 487-493.

RASK-ANDERSEN, M., MASURAM, S. & SCHIOTH, H. B. 2014. The druggable genome: Evaluation of drug targets in clinical trials suggests major shifts in molecular class and indication. *Annu Rev Pharmacol Toxicol,* 54**,** 9-26.

RASMUSSEN, S. G., CHOI, H.-J., FUNG, J. J., PARDON, E., CASAROSA, P., CHAE, P. S., DEVREE, B. T., ROSENBAUM, D. M., THIAN, F. S. & KOBILKA, T. S. 2011a. Structure of a nanobody-stabilized active state of the [bgr] 2 adrenoceptor. *Nature,* 469**,** 175-180.

RASMUSSEN, S. G., DEVREE, B. T., ZOU, Y., KRUSE, A. C., CHUNG, K. Y., KOBILKA, T. S., THIAN, F. S., CHAE, P. S., PARDON, E., CALINSKI, D., MATHIESEN, J. M., SHAH, S. T., LYONS, J. A., CAFFREY, M., GELLMAN, S. H., STEYAERT, J., SKINIOTIS, G., WEIS, W. I., SUNAHARA, R. K. & KOBILKA, B. K. 2011b. Crystal structure of the beta2 adrenergic receptor-Gs protein complex. *Nature,* 477**,** 549-55.

REDA, T. K., GELIEBTER, A. & PI-SUNYER, F. X. 2002. Amylin, food intake, and obesity. *Obes Res,* 10**,** 1087-91.

REITER, E. & LEFKOWITZ, R. J. 2006. GRKs and beta-arrestins: roles in receptor silencing, trafficking and signaling. *Trends Endocrinol Metab,* 17**,** 159-65.

RESSLER, K. J., MERCER, K. B., BRADLEY, B., JOVANOVIC, T., MAHAN, A., KERLEY, K., NORRHOLM, S. D., KILARU, V., SMITH, A. K. & MYERS, A. J. 2011. Post-traumatic stress disorder is associated with PACAP and the PAC1 receptor. *Nature,* 470**,** 492.

RHEE, S. G. & CHOI, K. D. 1992. Regulation of inositol phospholipid-specific phospholipase C isozymes. *J Biol Chem,* 267**,** 12393-6.

RING, A. M., MANGLIK, A., KRUSE, A. C., ENOS, M. D., WEIS, W. I., GARCIA, K. C. & KOBILKA, B. K. 2013. Adrenaline-activated structure of [bgr] 2-adrenoceptor stabilized by an engineered nanobody. *Nature,* 502**,** 575-579.

RIVIER, J., RIVIER, C. & VALE, W. 1984. Synthetic competitive antagonists of corticotropin-releasing factor: effect on ACTH secretion in the rat. *Science,* 224**,** 889-91.

ROHNER, J. & PLANCHE, D. 1985. Mechanism of the analgesic effect of calcitonin evidence for a twofold effect: morphine-like and cortisone-like. *Clin Rheumatol,* 4**,** 218-9.

ROSENBAUM, D. M., RASMUSSEN, S. G. & KOBILKA, B. K. 2009. The structure and function of G-protein-coupled receptors. *Nature,* 459**,** 356-63.

ROSENBAUM, D. M., ZHANG, C., LYONS, J. A., HOLL, R., ARAGAO, D., ARLOW, D. H., RASMUSSEN, S. G. F., CHOI, H. J., DEVREE, B. T. & SUNAHARA, R. K. 2011. Structure and function of an irreversible agonist-[bgr] 2 adrenoceptor complex. *Nature,* 469**,** 236-240.

ROUTLEDGE, S. J., LADDS, G. & POYNER, D. R. 2017. The effects of RAMPs upon cell signalling. *Mol Cell Endocrinol,* 449**,** 12-20.

ROVATI, G. E., CAPRA, V. & NEUBIG, R. R. 2007. The highly conserved DRY motif of class AG protein-coupled receptors: beyond the ground state. *Mol Pharmacol,* 71**,** 959-964.

RUI, L. 2014. Energy metabolism in the liver. *Compr Physiol,* 4**,** 177-97.

RUNGE, S., GRAM, C., BRAUNER-OSBORNE, H., MADSEN, K., KNUDSEN, L. B. & WULFF, B. S. 2003a. Three distinct epitopes on the extracellular face of the glucagon receptor determine specificity for the glucagon amino terminus. *J Biol Chem,* 278**,** 28005-10.

RUNGE, S., WULFF, B. S., MADSEN, K., BRAUNER-OSBORNE, H. & KNUDSEN, L. B. 2003b. Different domains of the glucagon and glucagon-like peptide-1 receptors provide the critical determinants of ligand selectivity. *Br J Pharmacol,* 138**,** 787-94.

RUSSELL, F. A., KING, R., SMILLIE, S. J., KODJI, X. & BRAIN, S. D. 2014. Calcitonin gene-related peptide: physiology and pathophysiology. *Physiol Rev,* 94**,** 1099-142.

SABBISETTI, V. S., CHIRUGUPATI, S., THOMAS, S., VAIDYA, K. S., REARDON, D., CHIRIVA-INTERNATI, M., ICZKOWSKI, K. A. & SHAH, G. V. 2005. Calcitonin increases invasiveness of prostate cancer cells: role for cyclic AMP-dependent protein kinase A in calcitonin action. *Int J Cancer,* 117**,** 551-60.

SAMAMA, P., COTECCHIA, S., COSTA, T. & LEFKOWITZ, R. J. 1993. A mutation-induced activated state of the beta 2-adrenergic receptor. Extending the ternary complex model. *J Biol Chem,* 268**,** 4625-36.

SANTOS, N. M. D., GARDNER, L. A., WHITE, S. W. & BAHOUTH, S. W. 2006. Characterization of the residues in helix 8 of the human β1-adrenergic receptor that are involved in coupling the receptor to G proteins. *J Biol Chem,* 281**,** 12896-12907.

SCHANK, J. R., RYABININ, A. E., GIARDINO, W. J., CICCOCIOPPO, R. & HEILIG, M. 2012. Stress-related neuropeptides and addictive behaviors: beyond the usual suspects. *Neuron,* 76**,** 192-208.

SCHEERER, P., PARK, J. H., HILDEBRAND, P. W., KIM, Y. J., KRAUSS, N., CHOE, H. W., HOFMANN, K. P. & ERNST, O. P. 2008. Crystal structure of opsin in its G-protein-interacting conformation. *Nature,* 455**,** 497-502.

SCHEUER, T. Regulation of sodium channel activity by phosphorylation. Seminars in cell & developmental biology, 2011. Elsevier, 160-165.

SCHIPANI, E., LANGMAN, C. B., PARFITT, A. M., JENSEN, G. S., KIKUCHI, S., KOOH, S. W., COLE, W. G. & JUPPNER, H. 1996. Constitutively activated receptors for parathyroid hormone and parathyroid hormone-related peptide in Jansen's metaphyseal chondrodysplasia. *N Engl J Med,* 335**,** 708-14.

SCHNEIDER, H.-G., RAUE, F., ZINK, A., KOPPOLD, A. & ZIEGLER, R. 1988. Down-regulation of calcitonin receptors in T 4 7D cells by internalization of calcitonin-receptor complexes. *Mol Cell Endocrinol,* 58**,** 9-15.

SCHRAGE, R., SCHMITZ, A. L., GAFFAL, E., ANNALA, S., KEHRAUS, S., WENZEL, D., BULLESBACH, K. M., BALD, T., INOUE, A., SHINJO, Y., GALANDRIN, S., SHRIDHAR, N., HESSE, M., GRUNDMANN, M., MERTEN, N., CHARPENTIER, T. H., MARTZ, M., BUTCHER, A. J., SLODCZYK, T., ARMANDO, S., EFFERN, M., NAMKUNG, Y., JENKINS, L., HORN, V., STOSSEL, A., DARGATZ, H., TIETZE, D., IMHOF, D., GALES, C., DREWKE, C., MULLER, C. E., HOLZEL, M., MILLIGAN, G., TOBIN, A. B., GOMEZA, J., DOHLMAN, H. G., SONDEK, J., HARDEN, T. K., BOUVIER, M., LAPORTE, S. A., AOKI, J., FLEISCHMANN, B. K., MOHR, K., KONIG, G. M., TUTING, T. & KOSTENIS, E. 2015. The experimental power of FR900359 to study Gq-regulated biological processes. *Nat Commun,* 6**,** 10156.

SCHULTE, G. 2010. International Union of Basic and Clinical Pharmacology. LXXX. The class Frizzled receptors. *Pharmacol Rev,* 62**,** 632-67.

SCHULTE, G. & BRYJA, V. 2007. The Frizzled family of unconventional G-protein-coupled receptors. *Trends Pharmacol Sci,* 28**,** 518-25.

SECK, T., BARON, R. & HORNE, W. C. 2003. Binding of filamin to the C-terminal tail of the calcitonin receptor controls recycling. *J Biol Chem,* 278**,** 10408-16.

SECK, T., PELLEGRINI, M., FLOREA, A. M., GRIGNOUX, V., BARON, R., MIERKE, D. F. & HORNE, W. C. 2005. The delta e13 isoform of the calcitonin receptor forms a six-transmembrane domain receptor with dominant-negative effects on receptor surface expression and signaling. *Mol Endocrinol,* 19**,** 2132-44.

SEGRE, G. V. & GOLDRING, S. R. 1993. Receptors for secretin, calcitonin, parathyroid hormone (PTH)/PTH-related peptide, vasoactive intestinal peptide, glucagonlike peptide 1, growth hormone-releasing hormone, and glucagon belong to a newly discovered G-protein-linked receptor family. *Trends Endocrinol Metab,* 4**,** 309-314.

SEKIGUCHI, T., SUZUKI, N., FUJIWARA, N., AOYAMA, M., KAWADA, T., SUGASE, K., MURATA, Y., SASAYAMA, Y., OGASAWARA, M. & SATAKE, H. 2009. Calcitonin in a protochordate, Ciona intestinalis–the prototype of the vertebrate calcitonin/calcitonin gene-related peptide superfamily. *FEBS J,* 276**,** 4437-4447.

SELANDER, K. S., HARKONEN, P. L., VALVE, E., MONKKONEN, J., HANNUNIEMI, R. & VAANANEN, H. K. 1996. Calcitonin promotes osteoclast survival in vitro. *Mol Cell Endocrinol,* 122**,** 119-29.

SEXTON, P. M., ADAM, W. R., MOSELEY, J. M., MARTIN, T. J. & MENDELSOHN, F. A. 1987. Localization and characterization of renal calcitonin receptors by in vitro autoradiography. *Kidney Int,* 32**,** 862-8.

SEXTON, P. M., HOUSSAMI, S., HILTON, J. M., O'KEEFFE, L. M., CENTER, R. J., GILLESPIE, M. T., DARCY, P. & FINDLAY, D. M. 1993. Identification of brain isoforms of the rat calcitonin receptor. *Mol Endocrinol,* 7**,** 815-21.

SHAH, G., WANG, W., GROSVENOR, C. & CROWLEY, W. 1990. Calcitonin Inhibits Basal and Thyrotropin-Releasing Hormone-Induced Release of Prolactin from Anterior Pituitary Cells:

Evidence for a Selective Action Exerted Proximal To Secretagogue-Induced Increases in Cytosolic Ca2+. *Endocrinology,* 127**,** 621-628.

SHAYWITZ, A. J. & GREENBERG, M. E. 1999. CREB: a stimulus-induced transcription factor activated by a diverse array of extracellular signals. *Annu Rev Biochem,* 68**,** 821-61.

SHEIKH, S. P., VILARDARGA, J. P., BARANSKI, T. J., LICHTARGE, O., IIRI, T., MENG, E. C., NISSENSON, R. A. & BOURNE, H. R. 1999. Similar structures and shared switch mechanisms of the beta2-adrenoceptor and the parathyroid hormone receptor. Zn(II) bridges between helices III and VI block activation. *J Biol Chem,* 274**,** 17033-41.

SHEIKH, S. P., ZVYAGA, T. A., LICHTARGE, O., SAKMAR, T. P. & BOURNE, H. R. 1996. Rhodopsin activation blocked by metal-ion-binding sites linking transmembrane helices C and F. *Nature,* 383**,** 347-50.

SHEN, S., GEHLERT, D. R. & COLLIER, D. A. 2013. PACAP and PAC1 receptor in brain development and behavior. *Neuropeptides,* 47**,** 421-30.

SHETZLINE, M. A., WALKER, J. K., VALENZANO, K. J. & PREMONT, R. T. 2002. Vasoactive intestinal polypeptide type-1 receptor regulation. Desensitization, phosphorylation, and sequestration. *J Biol Chem,* 277**,** 25519-26.

SHI, L., LIAPAKIS, G., XU, R., GUARNIERI, F., BALLESTEROS, J. A. & JAVITCH, J. A. 2002. β2 Adrenergic Receptor Activation modulation of the proline kink in transmembrane 6 by a rotamer toggle switch. *J Biol Chem,* 277**,** 40989-40996.

SHUKLA, A. K., XIAO, K. & LEFKOWITZ, R. J. 2011. Emerging paradigms of beta-arrestin-dependent seven transmembrane receptor signaling. *Trends Biochem Sci,* 36**,** 457-69.

SHYU, J. F., INOUE, D., BARON, R. & HORNE, W. C. 1996. The deletion of 14 amino acids in the seventh transmembrane domain of a naturally occurring calcitonin receptor isoform alters ligand binding and selectively abolishes coupling to phospholipase C. *J Biol Chem,* 271**,** 31127-34.

SIGISMUND, S. & POLO, S. 2016. Strategies to Detect Endogenous Ubiquitination of a Target Mammalian Protein. *Proteostasis: Methods and Protocols***,** 143-151.

SIU, F. Y., HE, M., DE GRAAF, C., HAN, G. W., YANG, D., ZHANG, Z., ZHOU, C., XU, Q., WACKER, D., JOSEPH, J. S., LIU, W., LAU, J., CHEREZOV, V., KATRITCH, V., WANG, M. W. & STEVENS, R. C. 2013. Structure of the human glucagon class B G-protein-coupled receptor. *Nature,* 499**,** 444-9.

SMALL, K. M., TANGUAY, D. A., NANDABALAN, K., ZHAN, P., STEPHENS, J. C. & LIGGETT, S. B. 2003. Gene and protein domain-specific patterns of genetic variability within the G-protein coupled receptor superfamily. *Am J Pharmacogenomics,* 3**,** 65-71.

SMRCKA, A. V. 2008. G protein betagamma subunits: central mediators of G protein-coupled receptor signaling. *Cell Mol Life Sci,* 65**,** 2191-214.

SMRCKA, A. V. & STERNWEIS, P. C. 1993. Regulation of purified subtypes of phosphatidylinositol-specific phospholipase C beta by G protein alpha and beta gamma subunits. *J Biol Chem,* 268**,** 9667-74.

SONG, G., YANG, D., WANG, Y., DE GRAAF, C., ZHOU, Q., JIANG, S., LIU, K., CAI, X., DAI, A., LIN, G., LIU, D., WU, F., WU, Y., ZHAO, S., YE, L., HAN, G. W., LAU, J., WU, B., HANSON, M. A., LIU, Z. J., WANG, M. W. & STEVENS, R. C. 2017. Human GLP-1 receptor transmembrane domain structure in complex with allosteric modulators. *Nature,* 546**,** 312-315.

SONODA, N., IMAMURA, T., YOSHIZAKI, T., BABENDURE, J. L., LU, J. C. & OLEFSKY, J. M. 2008. Beta-Arrestin-1 mediates glucagon-like peptide-1 signaling to insulin secretion in cultured pancreatic beta cells. *Proc Natl Acad Sci U S A,* 105**,** 6614-9.

SØRENSEN, M. G., KARSDAL, M. A., DZIEGIEL, M. H., BOUTIN, J. A., NOSJEAN, O. & HENRIKSEN, K. 2010. Screening of protein kinase inhibitors identifies PKC inhibitors as inhibitors of osteoclastic acid secretion and bone resorption. *BMC musculoskeletal disorders,* 11**,** 250.

SPENGLER, D., WAEBER, C., PANTALONI, C., HOLSBOER, F., BOCKAERT, J., SEEBURG, P. H. & JOURNOT, L. 1993. Differential signal transduction by five splice variants of the PACAP receptor. *Nature,* 365**,** 170-5.

STEELE, A. D., SZABO, I., BEDNAR, F. & ROGERS, T. J. 2002. Interactions between opioid and chemokine receptors: heterologous desensitization. *Cytokine Growth Factor Rev,* 13**,** 209-222.

STEPHENS, L., SMRCKA, A., COOKE, F. T., JACKSON, T. R., STERNWEIS, P. C. & HAWKINS, P. T. 1994. A Novel Phosphoinositide-3 Kinase-Activity in Myeloid-Derived Cells Is Activated by G-Protein Beta-Gamma-Subunits. *Cell,* 77**,** 83-93.

STEPHENSON, R. P. 1956. A modification of receptor theory. *Br J Pharmacol Chemother,* 11**,** 379-93.

STEVENS, R. C., CHEREZOV, V., KATRITCH, V., ABAGYAN, R., KUHN, P., ROSEN, H. & WUTHRICH, K. 2013. The GPCR Network: a large-scale collaboration to determine human GPCR structure and function. *Nat Rev Drug Discov,* 12**,** 25-34.

STORK, P. J. S. & SCHMITT, J. M. 2002. Crosstalk between cAMP and MAP kinase signaling in the regulation of cell proliferation. *Trends Cell Biol,* 12**,** 258-266.

STROOP, S. D., KUESTNER, R. E., SERWOLD, T. F., CHEN, L. & MOORE, E. E. 1995. Chimeric human calcitonin and glucagon receptors reveal two dissociable calcitonin interaction sites. *Biochemistry,* 34**,** 1050-7.

STROOP, S. D., THOMPSON, D. L., KUESTNER, R. E. & MOORE, E. E. 1993. A recombinant human calcitonin receptor functions as an extracellular calcium sensor. *J Biol Chem,* 268**,** 19927-19930.

SUN, C., SONG, D., DAVIS-TABER, R. A., BARRETT, L. W., SCOTT, V. E., RICHARDSON, P. L., PEREDA-LOPEZ, A., UCHIC, M. E., SOLOMON, L. R., LAKE, M. R., WALTER, K. A., HAJDUK, P. J. & OLEJNICZAK, E. T. 2007. Solution structure and mutational analysis of pituitary adenylate cyclase-activating polypeptide binding to the extracellular domain of PAC1-RS. *Proc Natl Acad Sci U S A,* 104**,** 7875-80.

SUNAHARA, R. K., DESSAUER, C. W. & GILMAN, A. G. 1996. Complexity and diversity of mammalian adenylyl cyclases. *Annu Rev Pharmacol Toxicol,* 36**,** 461-80.

SUZUKI, H., NAKAMURA, I., TAKAHASHI, N., IKUHARA, T., MATSUZAKI, K., ISOGAI, Y., HORI, M. & SUDA, T. 1996. Calcitonin-induced changes in the cytoskeleton are mediated by a signal pathway associated with protein kinase A in osteoclasts. *Endocrinology,* 137**,** 4685-90.

TAKAHASHI, S., GOLDRING, S., KATZ, M., HILSENBECK, S., WILLIAMS, R. & ROODMAN, G. D. 1995. Downregulation of calcitonin receptor mRNA expression by calcitonin during human osteoclast-like cell differentiation. *J Clin Invest,* 95**,** 167-71.

TAKEDA, S., KADOWAKI, S., HAGA, T., TAKAESU, H. & MITAKU, S. 2002. Identification of G protein-coupled receptor genes from the human genome sequence. *FEBS Lett,* 520**,** 97-101.

TAUSSIG, R., INIGUEZLLUHI, J. A. & GILMAN, A. G. 1993. Inhibition of Adenylyl-Cyclase by G(I-Alpha). *Science,* 261**,** 218-221.

TAYLOR, M. M., BAGLEY, S. L. & SAMSON, W. K. 2005. Intermedin/adrenomedullin-2 acts within central nervous system to elevate blood pressure and inhibit food and water intake. *Am J Physiol Regul Integr Comp Physiol,* 288**,** R919-27.

TETSUKA, M., SAITO, Y., IMAI, K., DOI, H. & MARUYAMA, K. 2004. The basic residues in the membrane-proximal C-terminal tail of the rat melanin-concentrating hormone receptor 1 are required for receptor function. *Endocrinology,* 145**,** 3712-23.

THOMAS, S., CHIGURUPATI, S., ANBALAGAN, M. & SHAH, G. 2006. Calcitonin increases tumorigenicity of prostate cancer cells: evidence for the role of protein kinase A and urokinase-type plasminogen receptor. *Mol Endocrinol,* 20**,** 1894-911.

THOMAS, S., MURALIDHARAN, A. & SHAH, G. V. 2007. Knock-down of calcitonin receptor expression induces apoptosis and growth arrest of prostate cancer cells. *Int J Oncol,* 31**,** 1425-37.

THOMAS, S. & SHAH, G. 2005. Calcitonin induces apoptosis resistance in prostate cancer cell lines against cytotoxic drugs via the Akt/survivin pathway. *Cancer Biol Ther,* 4**,** 1226-33.

THOMAS, S. M. & BRUGGE, J. S. 1997. Cellular functions regulated by Src family kinases. *Annu Rev Cell Dev Biol,* 13**,** 513-609.

THRON, C. D. 1973. On the analysis of pharmacological experiments in terms of an allosteric receptor model. *Mol Pharmacol,* 9**,** 1-9.

TILAKARATNE, N., CHRISTOPOULOS, G., ZUMPE, E. T., FOORD, S. M. & SEXTON, P. M. 2000. Amylin receptor phenotypes derived from human calcitonin receptor/RAMP coexpression exhibit pharmacological differences dependent on receptor isoform and host cell environment. *J Pharmacol Exp Ther,* 294**,** 61-72.

TSENG, C. C. & LIN, L. 1997. A point mutation in the glucose-dependent insulinotropic peptide receptor confers constitutive activity. *Biochem Biophys Res Commun,* 232**,** 96-100.

TURNER, P. R., BAMBINO, T. & NISSENSON, R. A. 1996. Mutations of neighboring polar residues on the second transmembrane helix disrupt signaling by the parathyroid hormone receptor. *Mol Endocrinol,* 10**,** 132-9.

TYNDALL, J. D. & SANDILYA, R. 2005. GPCR agonists and antagonists in the clinic. *Med Chem,* 1**,** 405-21.

UDAWELA, M., CHRISTOPOULOS, G., MORFIS, M., CHRISTOPOULOS, A., YE, S., TILAKARATNE, N. & SEXTON, P. M. 2006a. A critical role for the short intracellular C terminus in receptor activity-modifying protein function. *Mol Pharmacol,* 70**,** 1750-60.

UDAWELA, M., CHRISTOPOULOS, G., TILAKARATNE, N., CHRISTOPOULOS, A., ALBISTON, A. & SEXTON, P. M. 2006b. Distinct receptor activity-modifying protein domains differentially modulate interaction with calcitonin receptors. *Mol Pharmacol,* 69**,** 1984-9.

UEDA, Y., HIRAI, S., OSADA, S., SUZUKI, A., MIZUNO, K. & OHNO, S. 1996. Protein kinase C activates the MEK-ERK pathway in a manner independent of Ras and dependent on Raf. *J Biol Chem,* 271**,** 23512-9.

UHLEN, M., FAGERBERG, L., HALLSTROM, B. M., LINDSKOG, C., OKSVOLD, P., MARDINOGLU, A., SIVERTSSON, A., KAMPF, C., SJOSTEDT, E., ASPLUND, A., OLSSON, I., EDLUND, K., LUNDBERG, E., NAVANI, S., SZIGYARTO, C. A., ODEBERG, J., DJUREINOVIC, D., TAKANEN, J. O., HOBER, S., ALM, T., EDQVIST, P. H., BERLING, H., TEGEL, H., MULDER, J., ROCKBERG, J., NILSSON, P., SCHWENK, J. M., HAMSTEN, M., VON FEILITZEN, K., FORSBERG, M., PERSSON, L., JOHANSSON, F., ZWAHLEN, M., VON HEIJNE, G., NIELSEN, J. & PONTEN, F. 2015. Proteomics. Tissue-based map of the human proteome. *Science,* 347**,** 1260419.

VALANT, C., MAY, L. T., AURELIO, L., CHUO, C. H., WHITE, P. J., BALTOS, J.-A., SEXTON, P. M., SCAMMELLS, P. J. & CHRISTOPOULOS, A. 2014. Separation of on-target efficacy from adverse effects through rational design of a bitopic adenosine receptor agonist. *Proc Natl Acad Sci U S A,* 111**,** 4614-4619.

VAUDRY, D., GONZALEZ, B. J., BASILLE, M., YON, L., FOURNIER, A. & VAUDRY, H. 2000. Pituitary adenylate cyclase-activating polypeptide and its receptors: from structure to functions. *Pharmacol Rev,* 52**,** 269-324.

VENKATAKRISHNAN, A. J., DEUPI, X., LEBON, G., TATE, C. G., SCHERTLER, G. F. & BABU, M. M. 2013. Molecular signatures of G-protein-coupled receptors. *Nature,* 494**,** 185-94.

VENTER, J. C., ADAMS, M. D., MYERS, E. W., LI, P. W., MURAL, R. J., SUTTON, G. G., SMITH, H. O., YANDELL, M., EVANS, C. A., HOLT, R. A., GOCAYNE, J. D., AMANATIDES, P., BALLEW, R. M., HUSON, D. H., WORTMAN, J. R., ZHANG, Q., KODIRA, C. D., ZHENG, X. H., CHEN, L., SKUPSKI, M., SUBRAMANIAN, G., THOMAS, P. D., ZHANG, J., GABOR MIKLOS, G. L., NELSON, C., BRODER, S., CLARK, A. G., NADEAU, J., MCKUSICK, V. A., ZINDER, N., LEVINE, A. J., ROBERTS, R. J., SIMON, M., SLAYMAN, C., HUNKAPILLER, M., BOLANOS, R., DELCHER, A., DEW, I., FASULO, D., FLANIGAN, M., FLOREA, L., HALPERN, A., HANNENHALLI, S., KRAVITZ, S., LEVY, S., MOBARRY, C., REINERT, K., REMINGTON, K., ABU-THREIDEH, J., BEASLEY, E., BIDDICK, K., BONAZZI, V., BRANDON, R., CARGILL, M., CHANDRAMOULISWARAN, I., CHARLAB, R., CHATURVEDI, K., DENG, Z., DI FRANCESCO, V., DUNN, P., EILBECK, K., EVANGELISTA, C., GABRIELIAN, A. E., GAN, W., GE, W., GONG, F., GU, Z., GUAN, P., HEIMAN, T. J., HIGGINS, M. E., JI, R. R., KE, Z., KETCHUM, K. A., LAI, Z., LEI, Y., LI, Z., LI, J., LIANG, Y., LIN, X., LU, F., MERKULOV, G. V., MILSHINA, N., MOORE, H. M., NAIK, A. K., NARAYAN, V. A., NEELAM, B., NUSSKERN, D., RUSCH, D. B., SALZBERG, S., SHAO, W., SHUE, B., SUN,

J., WANG, Z., WANG, A., WANG, X., WANG, J., WEI, M., WIDES, R., XIAO, C., YAN, C., et al. 2001. The sequence of the human genome. *Science,* 291**,** 1304-51.

VILARDAGA, J. P., ROMERO, G., FRIEDMAN, P. A. & GARDELLA, T. J. 2011. Molecular basis of parathyroid hormone receptor signaling and trafficking: a family B GPCR paradigm. *Cell Mol Life Sci,* 68**,** 1-13.

VOHRA, S., TADDESE, B., CONNER, A. C., POYNER, D. R., HAY, D. L., BARWELL, J., REEVES, P. J., UPTON, G. J. & REYNOLDS, C. A. 2013. Similarity between class A and class B G-protein-coupled receptors exemplified through calcitonin gene-related peptide receptor modelling and mutagenesis studies. *J R Soc Interface,* 10**,** 20120846.

WADA, S., MARTIN, T. J. & FINDLAY, D. M. 1995. Homologous regulation of the calcitonin receptor in mouse osteoclast-like cells and human breast cancer T47D cells. *Endocrinology,* 136**,** 2611-21.

WADA, S., UDAGAWA, N., NAGATA, N., MARTIN, T. J. & FINDLAY, D. M. 1996. Physiological levels of calcitonin regulate the mouse osteoclast calcitonin receptor by a protein kinase Alpha-mediated mechanism. *Endocrinology,* 137**,** 312-20.

WANG, J., ROUT, U. K., BAGCHI, I. C. & ARMANT, D. R. 1998. Expression of calcitonin receptors in mouse preimplantation embryos and their function in the regulation of blastocyst differentiation by calcitonin. *Development,* 125**,** 4293-4302.

WARD, S. D., HAMDAN, F. F., BLOODWORTH, L. M., SIDDIQUI, N. A., LI, J. H. & WESS, J. 2006. Use of an in situ disulfide cross-linking strategy to study the dynamic properties of the cytoplasmic end of transmembrane domain VI of the M3 muscarinic acetylcholine receptor. *Biochemistry,* 45**,** 676-685.

WARD, S. D., HAMDAN, F. F., BLOODWORTH, L. M. & WESS, J. 2002. Conformational Changes That Occur during M3Muscarinic Acetylcholine Receptor Activation Probed by the Use of an in Situ Disulfide Cross-linking Strategy. *J Biol Chem,* 277**,** 2247-2257.

WARNE, T., MOUKHAMETZIANOV, R., BAKER, J. G., NEHME, R., EDWARDS, P. C., LESLIE, A. G., SCHERTLER, G. F. & TATE, C. G. 2011. The structural basis for agonist and partial agonist action on a beta(1)-adrenergic receptor. *Nature,* 469**,** 241-4.

WARNE, T., SERRANO-VEGA, M. J., BAKER, J. G., MOUKHAMETZIANOV, R., EDWARDS, P. C., HENDERSON, R., LESLIE, A. G., TATE, C. G. & SCHERTLER, G. F. 2008. Structure of a beta1-adrenergic G-protein-coupled receptor. *Nature,* 454**,** 486-91.

WEAVER, R. E., MOBAREC, J. C., WIGGLESWORTH, M. J., REYNOLDS, C. A. & DONNELLY, D. 2017. High affinity binding of the peptide agonist TIP-39 to the parathyroid hormone 2 (PTH 2) receptor requires the hydroxyl group of Tyr-318 on transmembrane helix 5. *Biochem Pharmacol,* 127**,** 71-81.

WESTON, C., POYNER, D., PATEL, V., DOWELL, S. & LADDS, G. 2014. Investigating G protein signalling bias at the glucagon-like peptide-1 receptor in yeast. *Br J Pharmacol,* 171**,** 3651-3665.

WESTON, C., WINFIELD, I., HARRIS, M., HODGSON, R., SHAH, A., DOWELL, S. J., MOBAREC, J. C., WOODLOCK, D. A., REYNOLDS, C. A., POYNER, D. R., WATKINS, H. A. & LADDS, G. 2016. Receptor Activity-modifying Protein-directed G Protein Signaling Specificity for the Calcitonin Gene-related Peptide Family of Receptors. *J Biol Chem,* 291**,** 21925-21944.

WHALEN, E. J., RAJAGOPAL, S. & LEFKOWITZ, R. J. 2011. Therapeutic potential of beta-arrestin- and G protein-biased agonists. *Trends Mol Med,* 17**,** 126-39.

WHEATLEY, M., WOOTTEN, D., CONNER, M. T., SIMMS, J., KENDRICK, R., LOGAN, R. T., POYNER, D. R. & BARWELL, J. 2012. Lifting the lid on GPCRs: the role of extracellular loops. *Br J Pharmacol,* 165**,** 1688-1703.

WICKMAN, K. D., INIQUEZ-LIUHI, J., DAVENPORT, P., TAUSSIG, R., KRAPIVINSKY, G., LINDER, M., GILMAN, A. & CLAPHAM, D. 1994. Recombinant G protein ßy subunits activate the muscarinic gated atrial potassium channel. *Nature,* 368**,** 255-257.

WOLF, S. & GRUNEWALD, S. 2015. Sequence, structure and ligand binding evolution of rhodopsin-like G protein-coupled receptors: a crystal structure-based phylogenetic analysis. *PLoS One,* 10**,** e0123533.

WOLFE, L. A., 3RD, FLING, M. E., XUE, Z., ARMOUR, S., KERNER, S. A., WAY, J., RIMELE, T. & COX, R. F. 2003. In vitro characterization of a human calcitonin receptor gene polymorphism. *Mutat Res,* 522**,** 93-105.

WOOKEY, P., ZULLI, A., LO, C., HARE, D., SCHWARER, A., DARBY, I. & LEUNG, A. 2010. Calcitonin Receptor Expression in Embryonic, Foetal and Adult Tissues: Developmental and Pathophysiological Implications. *The calcitonin gene-related peptide family.* 199-233, Springer Netherlands.

WOOLLEY, M. J. & CONNER, A. C. 2017. Understanding the common themes and diverse roles of the second extracellular loop (ECL2) of the GPCR super-family. *Mol Cell Endocrinol,* 449**,** 3-11.

WOOLLEY, M. J., SIMMS, J., MOBAREC, J. C., REYNOLDS, C. A., POYNER, D. R. & CONNER, A. C. 2017. Understanding the molecular functions of the second extracellular loop (ECL2) of the calcitonin gene-related peptide (CGRP) receptor using a comprehensive mutagenesis approach. *Mol Cell Endocrinol*.

WOOLLEY, M. J., WATKINS, H. A., TADDESE, B., KARAKULLUKCU, Z. G., BARWELL, J., SMITH, K. J., HAY, D. L., POYNER, D. R., REYNOLDS, C. A. & CONNER, A. C. 2013. The role of ECL2 in CGRP receptor activation: a combined modelling and experimental approach. *J R Soc Interface,* 10**,** 20130589.

WOOTTEN, D., REYNOLDS, C. A., SMITH, K. J., MOBAREC, J. C., KOOLE, C., SAVAGE, E. E., PABREJA, K., SIMMS, J., SRIDHAR, R., FURNESS, S. G. B., LIU, M., THOMPSON, P. E., MILLER, L. J., CHRISTOPOULOS, A. & SEXTON, P. M. 2016. The Extracellular Surface of the GLP-1 Receptor Is a Molecular Trigger for Biased Agonism. *Cell,* 165**,** 1632-1643.

WOOTTEN, D., SIMMS, J., MILLER, L. J., CHRISTOPOULOS, A. & SEXTON, P. M. 2013. Polar transmembrane interactions drive formation of ligand-specific and signal pathway-biased family B G protein-coupled receptor conformations. *Proc Natl Acad Sci U S A,* 110**,** 5211-6.

WOOTTEN, D. M., REYNOLDS, C. A., KOOLE, C., SMITH, K. J., MOBAREC, J. C., SIMMS, J., QUON, T., COUDRAT, T., FURNESS, S. G. & MILLER, L. J. 2015. A hydrogen-bonded polar network in the core of the glucagon-like peptide-1 receptor is a fulcrum for biased agonism: lessons from class B crystal structures. *Mol Pharmacol***,** mol. 115.101246.

WYMAN, J. & ALLEN, D. W. 1951. The Problem of the Heme Interactions in Hemoglobin and the Basis of the Bohr Effect. *J Polym Sci A,* 7**,** 499-518.

XIONG, T., ZHAO, Y., HU, D., MENG, J., WANG, R., YANG, X., AI, J., QIAN, K. & ZHANG, H. 2012. Administration of calcitonin promotes blastocyst implantation in mice by up-regulating integrin β3 expression in endometrial epithelial cells. *Hum Reprod,* 27**,** 3540-3551.

YAMAMOTO, Y., NOGUCHI, T. & TAKAHASHI, N. 2005a. Effects of calcitonin on osteoclast. *Clin Calcium,* 15**,** 147-51.

YAMAMOTO, Y., UDAGAWA, N., OKUMURA, S., MIZOGUCHI, T., TAKE, I., YAMAUCHI, H., NOGUCHI, T. & TAKAHASHI, N. 2005b. Effects of calcitonin on the function of human osteoclast-like cells formed from CD14-positive monocytes. *Cell Mol Biol (Noisy-le-grand),* 52**,** 25-31.

YAMIN, M., GORN, A. H., FLANNERY, M. R., JENKINS, N. A., GILBERT, D. J., COPELAND, N. G., TAPP, D. R., KRANE, S. M. & GOLDRING, S. R. 1994. Cloning and characterization of a mouse brain calcitonin receptor complementary deoxyribonucleic acid and mapping of the calcitonin receptor gene. *Endocrinology,* 135**,** 2635-43.

YANG, D., DE GRAAF, C., YANG, L., SONG, G., DAI, A., CAI, X., FENG, Y., REEDTZ-RUNGE, S., HANSON, M. A., YANG, H., JIANG, H., STEVENS, R. C. & WANG, M. W. 2016. Structural Determinants of Binding the Seven-transmembrane Domain of the Glucagon-like Peptide-1 Receptor (GLP-1R). *J Biol Chem,* 291**,** 12991-3004.

YANG, L., YANG, D., DE GRAAF, C., MOELLER, A., WEST, G. M., DHARMARAJAN, V., WANG, C., SIU, F. Y., SONG, G., REEDTZ-RUNGE, S., PASCAL, B. D., WU, B., POTTER, C. S., ZHOU, H., GRIFFIN, P. R., CARRAGHER, B., YANG, H., WANG, M. W., STEVENS, R. C. & JIANG, H. 2015. Conformational states of the full-length glucagon receptor. *Nat Commun,* 6**,** 7859.

YAO, X., PARNOT, C., DEUPI, X., RATNALA, V. R., SWAMINATH, G., FARRENS, D. & KOBILKA, B. 2006. Coupling ligand structure to specific conformational switches in the beta2-adrenoceptor. *Nat Chem Biol,* 2**,** 417-22.

YAO, X. J., VELEZ RUIZ, G., WHORTON, M. R., RASMUSSEN, S. G., DEVREE, B. T., DEUPI, X., SUNAHARA, R. K. & KOBILKA, B. 2009. The effect of ligand efficacy on the formation and stability of a GPCR-G protein complex. *Proc Natl Acad Sci U S A,* 106**,** 9501-6.

YIN, Y., ZHOU, X. E., HOU, L., ZHAO, L. H., LIU, B., WANG, G., JIANG, Y., MELCHER, K. & XU, H. E. 2016. An intrinsic agonist mechanism for activation of glucagon-like peptide-1 receptor by its extracellular domain. *Cell Discov,* 2**,** 16042.

ZANDAWALA, M., LI, S., HAUSER, F., GRIMMELIKHUIJZEN, C. J. & ORCHARD, I. 2013. Isolation and functional characterization of calcitonin-like diuretic hormone receptors in Rhodnius prolixus. *PLoS One,* 8**,** e82466.

ZHANG, H., QIAO, A., YANG, D., YANG, L., DAI, A., DE GRAAF, C., REEDTZ-RUNGE, S., DHARMARAJAN, V., ZHANG, H., HAN, G. W., GRANT, T. D., SIERRA, R. G., WEIERSTALL, U., NELSON, G., LIU, W., WU, Y., MA, L., CAI, X., LIN, G., WU, X., GENG, Z., DONG, Y., SONG, G., GRIFFIN, P. R., LAU, J., CHEREZOV, V., YANG, H., HANSON, M. A., STEVENS, R. C., ZHAO, Q., JIANG, H., WANG, M. W. & WU, B. 2017a. Structure of the full-length glucagon class B G-protein-coupled receptor. *Nature,* 546**,** 259-264.

ZHANG, Y., SUN, B., FENG, D., HU, H., CHU, M., QU, Q., TARRASCH, J. T., LI, S., SUN KOBILKA, T., KOBILKA, B. K. & SKINIOTIS, G. 2017b. Cryo-EM structure of the activated GLP-1 receptor in complex with a G protein. *Nature,* 546**,** 248-253.

ZHAO, L.-H., YIN, Y., YANG, D., LIU, B., HOU, L., WANG, X., PAL, K., JIANG, Y., FENG, Y. & CAI, X. 2016. Differential requirement of the extracellular domain in activation of class BG protein-coupled receptors. *J Biol Chem,* 291**,** 15119-15130.

ZINDEL, D., ENGEL, S., BOTTRILL, A. R., PIN, J. P., PREZEAU, L., TOBIN, A. B., BUNEMANN, M., KRASEL, C. & BUTCHER, A. J. 2016. Identification of key phosphorylation sites in PTH1R that determine arrestin3 binding and fine-tune receptor signaling. *Biochem J,* 473**,** 4173-4192.

ZUMPE, E. T., TILAKARATNE, N., FRASER, N. J., CHRISTOPOULOS, G., FOORD, S. M. & SEXTON, P. M. 2000. Multiple ramp domains are required for generation of amylin receptor phenotype from the calcitonin receptor gene product. *Biochem Biophys Res Commun,* 267**,** 368-72.

APPENDIX 1

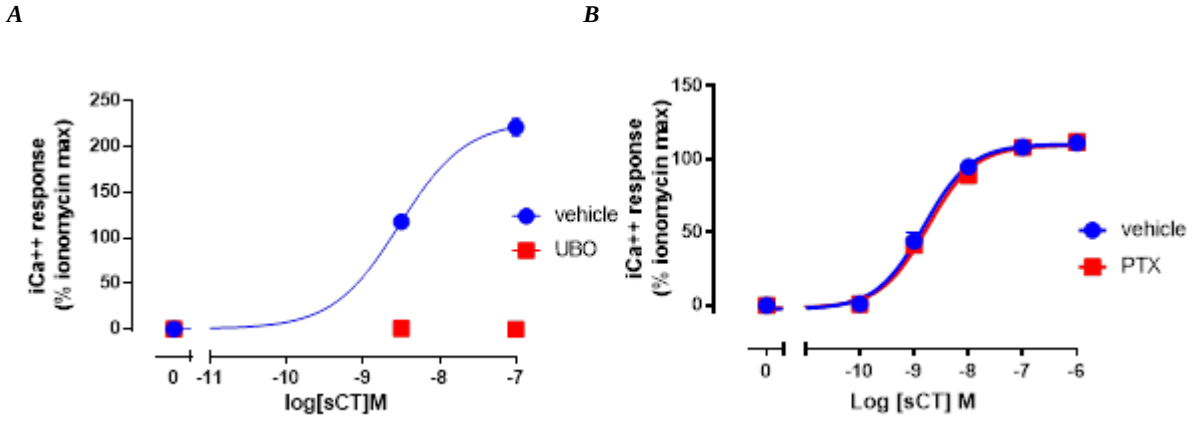

Figure S1: Effect of UBO and PTX on intracellular Ca^{2+} signalling triggered by sCT at the $hCTR_aLeu$ variant. *Cells were incubated for 30 minutes with either vehicle or (A) 100 nM of UBO-QIC (also known as FR900359), a Gαq/11/14 inhibitor (Schrage et al., 2015) or (B) 100 ng/ml of PTX. Cells were stimulated with saturating (0.1 μM) or pEC_{50} (3 nM) concentration of sCT and iCa^{2+} mobilisation data was calculated at the peak of response. Data were analysed by non-linear regression using a three-parameter logistic equation. All values are (A) mean+S.D. of 1 experiments conducted in duplicate or (B) mean+S.E.M. of 3 experiments conducted in duplicate. Experiments using to PTX (B) were conducted by Dr. Caroline Hick.*

ATGAGGTTCACATTTACAAGCCGGTGCTTGGCACTGTTTCTTCTTCTAAATCACCCAACCCCAATTCT
GCCTGAGCAGAAGCTTATCAGCGAGGAGGACCTGGCCTTTTCAAATCAAACCTATCCAACAATAGAGC
CCAAGCCATTTCTTTACGTCGTAGGACGAAAGAAGATGATGGATGCACAGTACAAATGCTATGACCGA
ATGCAGCAGTTACCCGCATACCAAGGAGAAGGTCCATATTGCAATCGCACCTGGGATGGATGGCTGTG
CTGGGATGACACACCGGCTGGAGTATTGTCCTATCAGTTCTGCCCAGATTATTTTCCGGATTTTGATC
CATCAGAAAAGGTTACAAAATACTGTGATGAAAAAGGTGTTTGGTTTAAACATCCTGAAAACAATCGA
ACCTGGTCCAACTATACTATGTGCAATGCTTTCACTCCTGAGAAACTGAAGAATGCATATGTTCTGTA
CTATTTGGCTATTGTGGGTCATTCTTTGTCAATTTTCACCCTAGTGATTTCCCTGGGGATTTTCGTGT
TTTTCAGGAGCCTTGGCTGCCAAAGGGTAACCCTGCACAAGAACATGTTTCTTACTTACATTCTGAAT
TCTATGATTATCATCATCCACCTGGTTGAAGTAGTACCCAATGGAGAGCTCGTGCGAAGGGACCCGGT
GAGCTGCAAGATTTTGCATTTTTTCCACCAGTACATGATGGCCTGCAACTATTTCTGGATGCTCTGTG
AAGGGATCTATCTTCATACACTCATTGTCGTGGCTGTGTTTACTGAGAAGCAACGCTTGCGGTGGTAT
TATCTCTTGGGCTGGGGGTTCCCGCTGGTGCCAACCACTATCCATGCTATTACCAGGGCCGTGTACTT
CAATGACAACTGCTGGCTGAGTGTGGAAACCCATTTGCTTTACATAATCCATGGACCTGTCATGGCGG
CACTTGTGGTCAATTTCTTCTTTTTGCTCAACATTGTCCGGGTGCTTGTGACCAAAATGAGGGAAACC
CATGAGGCGGAATCCCACATGTACCTGAAGGCTGTGAAGGCCACCATGATCCTTGTGCCCCTGCTGGG
AATCCAGTTTGTCGTCTTTCCCTGGAGACCTTCCAACAAGATGCTTGGGAAGATATATGATTACGTGA
TGCACTCTCTGATTCATTTCCAGGGCTTCTTTGTTGCGACCATCTACTGCTTCTGCAACAATGAGGTC
CAAACCACCGTGAAGCGCCAATGGGCCCAATTCAAAATTCAGTGGAACCAGCGTTGGGGGAGGCGCCC
CTCCAACCGCTCTGCTCGCGCTGCAGCCGCTGCTGCGGAGGCTGGCGACATCCCAATTTACATCTGCC
ATCAGGAGCTGAGGAATGAACCAGCCAACAACCAAGGCGAGGAGAGTGCTGAGATCATCCCTTTGAAT
ATCATAGAGCAAGAGTCATCTGCTTGA

Table S1 CALCR gene. *DNA sequence hCTR$_a$Leu variant. Highlighted in green the signalling peptide of the CALCR gene, in yellow the cMyc tag, in blue and red the residues of ECL2 and ECL3, respectively, Ala-substituted to and reported in Chapter 4 and 5.*

MRFTFTSRCLALFLLLNHPTPILPEQKLISEEDLAFSNQTYPTIEPKPFLYVVGRKKMMDAQYKCYDR
MQQLPAYQGEGPYCNRTWDGWLCWDDTPAGVLSYQFCPDYFPDFDPSEKVTKYCDEKGVWFKHPENNR
TWSNYTMCNAFTPEKLKNAYVLYYLAIVGHSLSIFTLVISLGIFVFFRSLGCQRVTLHKNMFLTYILN
SMIIIIHLVEVVPNGELVRRDPVSCKILHFFHQYMMACNYFWMLCEGIYLHTLIVVAVFTEKQRLRWY
YLLGWGFPLVPTTIHAITRAVYFNDNCWLSVETHLLYIIHGPVMAALVVNFFFLLNIVRVLVTKMRET
HEAESHMYLKAVKATMILVPLLGIQFVVFPWRPSNKMLGKIYDYVMHSLIHFQGFFVATIYCFCNNEV
QTTVKRQWAQFKIQWNQRWGRRPSNRSARAAAAAAEAGDIPIYICHQELRNEPANNQGEESAEIIPLN
IIEQESSA

Table S2 Amino acid sequence of the hCTR$_a$Leu variant. *Similar to Table S1, residues of the receptor were highlighted as follows: in green the signalling peptide of the CTR that is cleaved during post translational modifications, in yellow the cMyc tag, in blue and red the residues of ECL2 and ECL3, respectively, Ala-substituted to and reported in Chapter 4 and 5.*

Sequencing primer	**Nucleotide sequences**
pENTR11 forward	AGGCTTCGAAGGAGATAGAACC
pENTR11 reverse	GTGCAATGTAACATCAGAGATTTTGAG
BGH	CAACTAGAAGGCACAGTCGAGGCTGAT
T7	TAATACGACTCACTATAGGG

Table S3 Sequencing primers nucleotide sequence*. As part of the study presented in Chapter 4 and 5, primers were used to confirm the introduction of single Ala substitutions in CALCR gene sequence (reported in Table S1).*

Residue	Nucleotide sequences
Extracellular loop 2 (ECL_2)	
I279A	S : CAACCACTATCCATGCTGCTACCAGGGCCGTGTAC AS: GTACACGGCCCTGGTAGCAGCATGGATAGTGGTTG
T280A	S : CTATCCATGCTATTGCCAGGGCCGTGTAC AS: GTACACGGCCCTGGCAATAGCATGGATAG
R281A	S : CTATCCATGCTATTACCGCGGCCGTGTACTTCAATG AS: CATTGAAGTACACGGCCGCGGTAATAGCATGGATAG
V283A	S : CTATTACCAGGGCCGCGTACTTCAATGACAAC AS: GTTGTCATTGAAGTACGCGGCCCTGGTAATAG
Y284A	S : CTATTACCAGGGCCGTGGCCTTCAATGACAACTGC AS: GCAGTTGTCATTGAAGGCCACGGCCCTGGTAATAG
F285A	S : CTATTACCAGGGCCGTGTACGCCAATGACAACTGCTGGCTG AS: CAGCCAGCAGTTGTCATTGGCGTACACGGCCCTGGTAATAG
N286A	S : GGCCGTGTACTTCGCTGACAACTGCTGG AS: CCAGCAGTTGTCAGCGAAGTACACGGCC
D287A	S : CGTGTACTTCAATGCCAACTGCTGGCTG AS: CAGCCAGCAGTTGGCATTGAAGTACACG
N288A	S : GTGTACTTCAATGACGCCTGCTGGCTGAGTG AS: CACTCAGCCAGCAGGCGTCATTGAAGTACAC
C289A	S : GTGTACTTCAATGACAACGCCTGGCTGAGTGTGGAAAC AS: GTTTCCACACTCAGCCAGGCGTTGTCATTGAAGTACAC
W290A	S : CTTCAATGACAACTGCGCGCTGAGTGTGGAAAC AS: GTTTCCACACTCAGCGCGCAGTTGTCATTGAAG
L291A	S : CTTCAATGACAACTGCTGGGCGAGTGTGGAAACCCATTTG AS: CAAATGGGTTTCCACACTCGCCCAGCAGTTGTCATTGAAG
S292A	S : GACAACTGCTGGCTGGCTGTGGAAACCCATTTG AS: CAAATGGGTTTCCACAGCCAGCCAGCAGTTGTC
V293A	S : GCTGGCTGAGTGCGGAAACCCATTTG AS: CAAATGGGTTTCCGCACTCAGCCAGC
E294A	S : CTGGCTGAGTGTGGCCACCCATTTGCTTTAC AS: GTAAAGCAAATGGGTGGCCACACTCAGCCAG
T295A	S : GGCTGAGTGTGGAAGCCCATTTGCTTTAC AS: GTAAAGCAAATGGGCTTCCACACTCAGCC
H296A	S : GCTGAGTGTGGAAACCGCTTTGCTTTACATAATCC AS: GGATTATGTAAAGCAAAGCGGTTTCCACACTCAGC
L297A	S : GAGTGTGGAAACCCATGCGCTTTACATAATCCATG AS: CATGGATTATGTAAAGCGCATGGGTTTCCACACTC
L298A	S : GTGTGGAAACCCATTTGGCCTACATAATCCATGGACC AS: GGTCCATGGATTATGTAGGCCAAATGGGTTTCCACAC
Y299A	S : GGAAACCCATTTGCTTGCCATAATCCATGGACCTG AS: CAGGTCCATGGATTATGGCAAGCAAATGGGTTTCC
I300A	S : GAAACCCATTTGCTTTACGCCATCCATGGACCTGTCATG AS: CATGACAGGTCCATGGATGGCGTAAAGCAAATGGGTTTC

Table S4: Primer used to generate CTR constructs containing single Ala substituted residues in ECL2 and adjacent TM4 and TM5 assessed in Chapter 4.

Residue	Nucleotide sequences
Extracellular loop 3 (ECL_3)	
F356A	S : CTGCTGGGAATCCAGGCTGTCGTCTTTCCCTG AS: CAGGGAAAGACGACAGCCTGGATTCCCAGCAG
V357A	S : GGAATCCAGTTTGCCGTCTTTCCCTGG AS: CCAGGGAAAGACGGCAAACTGGATTCC
V358A	S : GAATCCAGTTTGTCGCCTTTCCCTGGAGAC AS: GTCTCCAGGGAAAGGCGACAAACTGGATTC
F359A	S : GAATCCAGTTTGTCGTCGCTCCCTGGAGACCTTCC AS: GGAAGGTCTCCAGGGAGCGACGACAAACTGGATTC
P360A	S : GTTTGTCGTCTTTGCCTGGAGACCTTCC AS: GGAAGGTCTCCAGGCAAAGACGACAAAC
W361A	S : GTTTGTCGTCTTTCCCGCGAGACCTTCCAACAAG AS: CTTGTTGGAAGGTCTCGCGGGAAAGACGACAAAC
R362A	S : GTCGTCTTTCCCTGGGCACCTTCCAACAAGATG AS: CATCTTGTTGGAAGGTGCCCAGGGAAAGACGAC
P363A	S : GTCTTTCCCTGGAGAGCTTCCAACAAGATG AS: CATCTTGTTGGAAGCTCTCCAGGGAAAGAC
S364A	S : CCCTGGAGACCTGCCAACAAGATGC AS: GCATCTTGTTGGCAGGTCTCCAGGG
N365A	S : CCTGGAGACCTTCCGCGAAGATGCTTGGGAAG AS: CTTCCCAAGCATCTTCGCGGAAGGTCTCCAGG
K366A	S : GGAGACCTTCCAACGCGATGCTTGGGAAG AS: CTTCCCAAGCATCGCGTTGGAAGGTCTCC
M367A	S : GAGACCTTCCAACAAGGCGCTTGGGAAGATATATG AS: CATATATCTTCCCAAGCGCCTTGTTGGAAGGTCTC
L368A	S : GAGACCTTCCAACAAGATGGCCGGGAAGATATATGATTAC AS: GTAATCATATATCTTCCCGGCCATCTTGTTGGAAGGTCTC
G369A	S : CCTTCCAACAAGATGCTTGCGAAGATATATGATTACGTG AS: CACGTAATCATATATCTTCGCAAGCATCTTGTTGGAAGG
K370A	S : CCAACAAGATGCTTGGGGCGATATATGATTACGTG AS: CACGTAATCATATATCGCCCCAAGCATCTTGTTGG
I371A	S : CAAGATGCTTGGGAAGGCATATGATTACGTGATGC AS: GCATCACGTAATCATATGCCTTCCCAAGCATCTTG
Y372A	S : GATGCTTGGGAAGATAGCCGATTACGTGATGCACTC AS: GAGTGCATCACGTAATCGGCTATCTTCCCAAGCATC
D373A	S : CTTGGGAAGATATATGCTTACGTGATGCACTC AS: GAGTGCATCACGTAAGCATATATCTTCCCAAG
Y374A	S : GCTTGGGAAGATATATGATGCCGTGATGCACTCTCTGATTC AS: AATCAGAGAGTGCATCACGGCATCATATATCTTCCCAAGC
V375A	S : GAAGATATATGATTACGCGATGCACTCTCTGATTC AS: GAATCAGAGAGTGCATCGCGTAATCATATATCTTC
M376A	S : GAAGATATATGATTACGTGGCGCACTCTCTGATTCATTTC AS: GAAATGAATCAGAGAGTGCGCCACGTAATCATATATCTTC

Table S5: Primer used to generate CTR constructs containing single Ala substituted residues in ECL3 and adjacent TM6 and TM7 assessed in Chapter 5.

APPENDIX 2

Ligand-Dependent Modulation of G Protein Conformation Alters Drug Efficacy

Furness, S.G.B., Liang, Y.L., Nowell, C.J., Halls. M.L., Wookey, P.J., Dal Maso, E., Inoue, A., Christopoulos, A., Wootten, D. AND Sexton, P.M.

Cell 167, 739–749, 2016.

Article

Cell

Ligand-Dependent Modulation of G Protein Conformation Alters Drug Efficacy

Sebastian George Barton Furness,[1,*] Yi-Lynn Liang,[1] Cameron James Nowell,[1] Michelle Louise Halls,[1] Peter John Wookey,[2] Emma Dal Maso,[1] Asuka Inoue,[3,4] Arthur Christopoulos,[1] Denise Wootten,[1] and Patrick Michael Sexton[1,5,*]

[1]Drug Discovery Biology, Monash Institute of Pharmaceutical Sciences and Department of Pharmacology, Monash University, Parkville, 3052 VIC, Australia

[2]Department of Medicine, Austin Health, University of Melbourne, Austin Campus, Heidelberg, VIC 3084, Australia

[3]Graduate School of Pharmaceutical Sciences, Tohoku University, 6-3, Aoba, Aramaki, Aoba-ku, Sendai 980-0065, Japan

[4]Japan Science and Technology Agency (JST), Precursory Research for Embryonic Sciences and Technology (PRESTO), 4-1-8 Honcho, Kawaguchi, Saitama 332-0012, Japan

[5]Lead Contact

*Correspondence: [redacted] S.G.B.F.), [redacted] (P.M.S.)

http://dx.doi.org/10.1016/j.cell.2016.09.021

SUMMARY

G protein-coupled receptor (GPCR) signaling, mediated by hetero-trimeric G proteins, can be differentially controlled by agonists. At a molecular level, this is thought to occur principally via stabilization of distinct receptor conformations by individual ligands. These distinct conformations control subsequent recruitment of transducer and effector proteins. Here, we report that ligand efficacy at the calcitonin GPCR (CTR) is also correlated with ligand-dependent alterations to G protein conformation. We observe ligand-dependent differences in the sensitivity of the G protein ternary complex to disruption by GTP, due to conformational differences in the receptor-bound G protein hetero-trimer. This results in divergent agonist-dependent receptor-residency times for the hetero-trimeric G protein and different accumulation rates for downstream second messengers. This study demonstrates that factors influencing efficacy extend beyond receptor conformation(s) and expands understanding of the molecular basis for how G proteins control/influence efficacy. This has important implications for the mechanisms that underlie ligand-mediated biased agonism.

INTRODUCTION

G protein-coupled receptors (GPCRs) are the largest family of cell-surface receptors, sensing a diverse array of stimuli from the extracellular environment and transmitting these signals to evoke cellular responses. This fundamental function is encapsulated by the concept of efficacy, which relates receptor occupancy by an agonist to the magnitude of the cellular response (Kenakin, 2002). The existence of ligands displaying different efficacies and, in particular, ligands displaying preferential signaling to different effectors has led to a model in which GPCRs can adopt multiple active states (Kenakin, 2002; Kim et al., 2013). Such ligand-directed signaling bias (biased agonism) is now an important focus in drug discovery (Kenakin and Christopoulos, 2013), but there are limited data addressing the mechanisms by which such differential efficacy occurs.

GPCRs are highly dynamic proteins that rapidly sample a range of both active and inactive conformations (Deupi and Kobilka, 2010). Activation of GPCRs occurs due to changes in the proportion of time the receptor spends in one or more active states upon agonist binding. This is due to a relative decrease in the energy state of the active receptor in the receptor:agonist complex (Deupi and Kobilka, 2010). The principal driver for differential efficacy is thought to be distinct receptor conformations stabilized by different ligands. For example, ligands with distinct efficacies show divergent sampling of conformational space for the β_2-adrenoceptor (ADRB2) (Nygaard et al., 2013), the ghrelin (GHSR) (Mary et al., 2012), serotonin (HTR2B) (Wacker et al., 2013), and the glucagon-like peptide 1 (GLP1R) receptors (Wootten et al., 2013). These divergent active conformations are thought to have different affinities for their cognate G protein hetero-trimer, providing a mechanism by which agonists could achieve differential receptor activation.

Early work by Seifert et al. (1999, 2001), however, provided the first hint that the ligand-receptor complex may also distinctly affect G protein conformations, and this has been supported by G protein fluorescence resonance energy transfer (FRET) in the presence of partial versus full agonists (Nikolaev et al., 2006). Additionally, recent work by Goricanec et al. (2016) has shown that the Gα subunit itself is highly dynamic, sampling a number of conformations in both GDP-bound and nucleotide-free states. Nonetheless, these data on differences in receptor:G protein complexes have principally been interpreted as differences in G protein recruitment to the receptor due to distinct ligand-receptor conformations. At the most basic level, the role of the GPCR is as a guanine nucleotide exchange factor (GEF), responsible for stimulating the exchange of GDP for GTP at the G_α subunit of hetero-trimeric G proteins resulting in their activation. By extension therefore, the formation of an agonist:receptor complex potentiates the receptor's GEF activity; thus, the agonist is a positive allosteric modulator of the GPCRs GEF

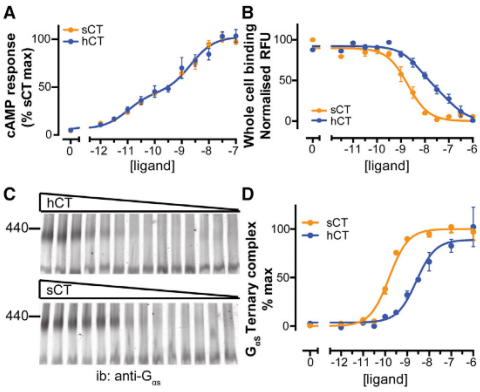

Figure 1. Functional Characterization of the Relative Efficacy of CTR Agonists and Identification of the receptor:agonist:Gαs Affinity State

(A) cAMP accumulation assay in COS-7 cells stably expressing CTR with cells stimulated for 30 min in the presence of IBMX with the indicated concentrations of hCT or sCT. Both agonist response curves are best described by a biphasic curve (F test, $p < 0.0001$) with a common fit (F test, $p = 0.979$, $n = 8$, each n in triplicate with different drug dilutions on different days, data are mean ± SEM) with log EC_{50} values of −11.00 ± 0.18 and −8.67 ± 0.12.

(B) Whole-cell competition ligand binding in which cells were incubated overnight at 4°C with 10 nM sCT8-32:AF568 (antagonist, affinity defined by saturation binding; Figure S1B) in the presence of the indicated concentrations of cold competing agonist. sCT competition is best described by a single-site fit with a log Ki of −9.10 ± 0.07; hCT competition fits to a two-site model (F test, $p = 0.0007$) with log Ki values of −7.30 ± 0.31 and −8.64 ± 0.26 ($n = 6$, each n in triplicate with different drug dilutions on different days, data are mean ± SEM).

(C and D) Plasma-membrane preparations from COS-7 cells expressing CTR were treated with various concentrations of agonists prior to solubilization in Lauryl Maltose Neopentyl Glycol (MNG)/Cholesterol Hemisuccinate (CHS) and separation on a 6%–11% clear native page and transfer. The ternary complex was identified by probing for mobility shift in $G_{\alpha s}$ with a representative blot (from $n = 4$, each n with different plasma-membrane preparations and different drug dilutions on different days) shown in (C) and quantified densitometry (Fiji) shown in (D) (data are mean ± SEM). Estimated log EC_{50} values for ternary complex formation are −8.58 ± 0.13 for hCT and −9.80 ± 0.08 for sCT (F test, p value for different EC_{50} of <0.0001).

See also Figure S1.

activity. As such, we posit that efficacy differences must translate into differential GEF activity of the GPCR. This could be due to differences in GPCR affinity for G protein but potentially also due to agonist-dependent conformational differences in G proteins, resulting in changes to nucleotide exchange rate.

The human calcitonin receptor (CTR) is the most ancient of class B GPCRs (Fredriksson et al., 2003; Nag et al., 2007). It is widely expressed in adults and during development and has complex roles in bone metabolism, brain function, cell cycle, and cancer (Clarke et al., 2015; Davey and Findlay, 2013; Venkatanarayan et al., 2015; Yamaguchi et al., 2015), including an anti-apoptotic role in osteoclasts (Selander et al., 1996) and thymic lymphomas (Venkatanarayan et al., 2015). CTR is a clinical target for the treatment of multiple diseases including Paget's disease, osteoporosis, and hypercalcemia of malignancy, with both human and salmon calcitonins (hCT and sCT, respectively) used clinically. These two peptides display distinct potency/efficacy for guanine nucleotide-binding protein G(s) subunit alpha isoforms short ($G_{\alpha s}$)-mediated cyclic AMP (cAMP) production, in a cell-dependent manner (Andreassen et al., 2014; Hilton et al., 2000; Kuestner et al., 1994). We sought to understand the mechanistic basis of the differential efficacy displayed by hCT and sCT at the CTR. Here, we demonstrate that variations in cellular efficacy are correlated with agonist-dependent, conformational differences promoted in G proteins. This current work extends the concept of conformational selection at the level of the agonist:receptor complex to one that includes conformation selection at the level of the agonist:receptor:G protein complex.

RESULTS

CTR Ligands Have Distinct Potencies for G Protein Recruitment

The CTR is most strongly coupled to the stimulatory G alpha subunit, $G_{\alpha s}$, upstream of adenylate-cyclase-mediated cAMP production. To define the cellular efficacy of hCT and sCT, we performed cAMP accumulation and ligand binding assays (Figures 1A, 1B, and S1A–S1E). Consistent with previous publications (Andreassen et al., 2014; Hilton et al., 2000), in cAMP accumulation assays (Figure 1A) the concentration response curves to both ligands were not significantly different, with similar EC_{50} and E_{max} values. We performed competition binding on whole cells and isolated plasma membranes to determine the affinity constants for both ligands (Figures 1B and S1A–S1E). sCT had high affinity for the receptor that could be defined by a single binding constant. In contrast, hCT had lower affinity with two discernible affinity states, both of which are lower than that of sCT. Similar to certain chemokine GPCRs (Di Salvo et al., 2000), and, in contrast to GPCRs for small molecules such as biogenic amines and acetylcholine (Brodde et al., 1982; Kellar et al., 1985), we found that the distribution of CTR affinity states was unaffected by the non-hydrolysable GTP analog GppNHp (Figures S1D and S1E), suggesting that binding of G protein to the CTR is not a major driver of conformational selection for this receptor, unlike recent data for the β_2 adrenergic receptor (DeVree et al., 2016).

The observed affinity represents a composite of all the interchangeable affinity states of the receptor at equilibrium (Liu et al., 2012; Nygaard et al., 2013). To define the particular affinity state(s) associated with the ternary complex containing native $G_{\alpha s}$, we explicitly identified this complex using native PAGE (Wittig et al., 2006, 2007) (Figures 1C, 1D, S2, and 2B). This allowed us to directly establish concentration-response curves for agonist promoted recruitment of $G_{\alpha s}$ protein (Figures 1C and 1D). Similar to measures of ligand affinity (Figure 1B), sCT had an ~10-fold greater potency over hCT for promotion of $G_{\alpha s}$ recruitment (Figure 1D). This suggests that the equivalent efficacy of the ligands in cAMP accumulation (Figure 1A) was not purely driven by efficiency of G protein recruitment (Figures 1A versus 1D). To better understand the nature of the agonist:receptor:G protein (ternary) complex, the relative stoichiometry of receptor and G protein was defined by using Fab fragments to induce discrete mobility shifts (Figures 2A–2C). The presence of a single shift in mobility of the ternary complex with increasing

concentrations of Fab against the receptor indicated a monomeric receptor in the G protein-bound complex (Figure 2A). In contrast, in the absence of agonist, the two different receptor bands undergo either single or double Fab-induced mobility shifts, suggesting both monomeric and dimeric receptor species (Figure 2C). Taken together with the loss of dimeric receptor with increasing G protein interaction (Figure 2B), this indicated that the ligand-responsive receptor species is dimeric, but, upon G protein binding, the dimeric interface weakens and G protein activation occurs in *cis* (Figure 2A and compare with Figure S2). This is consistent with a proposed model for β1 adrenergic receptor activation where the dimer interface partially overlaps the G protein-binding interface (Huang et al., 2013) and is depicted in the cartoon in Figure 2H. The apparent mobility observed for the ternary complex by native PAGE was lower than predicted from the molecular weight of the individual components. As an additional confirmation, the same relative mobility (~440 kDa) and stoichiometry (1:1:1:1 [molecular weight divided by intensity]) of the ternary complex was observed when expressed and purified from insect cells (Figures 2D and 2E).

CT Ligands Promote Distinct G Protein Conformations Linked to Guanine Nucleotide Exchange and Signaling

To understand how $G_{\alpha s}$ activation might differ between hCT and sCT, we defined the transduction mechanism of the

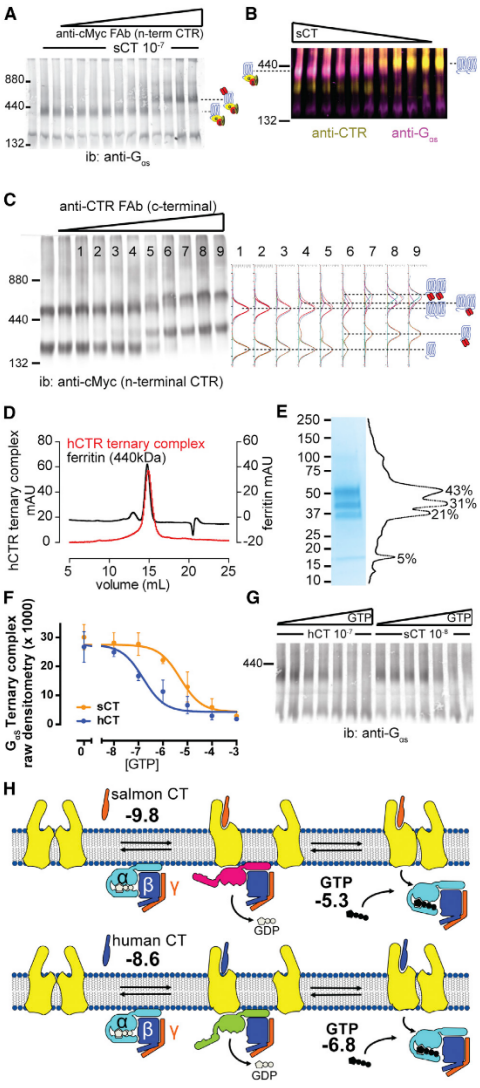

Figure 2. CTR Activates Gαs in *cis* and the GTP Affinity of the Ternary Complex Is Agonist Dependent

All n numbers for all experiments were performed with different (plasma) membrane preparations on different days.

(A) A representative mobility shift assay (n = 3) using an Fab directed against the N-terminal epitope tag of CTR shows that the ternary complex contains only one CTR protomer, which is shown in cartoon with CTR in blue.

(B) A representative two-color blot (n = 4) of ligand-dependent transition of CTR (yellow) and $G_{\alpha s}$ (magenta) to the ternary complex indicating the mobility of CTR increases as it transitions to the ternary complex, consistent with a transition from the dimeric complex (Figure S2).

(C) Plasma-membrane preparations from COS-7 cells expressing CTR were incubated with increasing amounts of anti-CTR C-terminal Fab (1H10, IgG_{2a}) during solubilization in digitonin at 6 g/g for 50 min at 4°C, separation on a 4%–13.5% blue native page and transfer. Solubilization in digitonin followed by blue native PAGE preserves the 1H10 Fab interaction with CTR but results in relatively poor solubilization of CTR. The shift in CTR mobility was identified using anti-cMyc (9E10, IgG_1) followed by an isotype-specific secondary; the quantified densitometry was fitted to Gaussian distributions indicating a single shift in the lower-molecular-weight complex and two shifts in the higher molecular weight complex (n = 3).

(D and E) (D) A representative size exclusion chromatography trace comparing the relative mobility of insect cell-expressed and purified sCT/CTR/$G_{\alpha s}$/G_{β}/G_{γ} ternary complex with that of a known standard, ferritin, with the purified material shown on a Coomassie-stained gel in (E) and quantified by densitometry supportive of a 1:1:1:1 stoichiometry (representative of more than five experiments).

(F) Extensively washed plasma-membrane preparations from COS-7 cells stably expressing CTR were treated with various concentrations of GTP in the presence of (saturating) equi-occupant concentrations of agonist prior to solubilization and separation on a 6%–11% native page and transfer.

(G) The ternary complex was identified by probing for mobility shift in $G_{\alpha s}$ with a representative blot (from n = 3) shown in (G) and quantified densitometry shown in (F) (data are mean ± SEM). Estimated log EC_{50} values for GTP-dependent disruption of ternary complexes are −6.84 ± 0.16 for hCT and −5.32 ± 0.19 for sCT (F test, p value for different EC_{50} for GTP sensitivity <0.0001). Maximum recruitment of $G_{\alpha s}$ did not differ between ligands (F test, p value for different maximum = 0.42).

(H) A cartoon depiction of the differences in receptor:G protein coupling in the presence of salmon and human calcitonin. sCT has higher affinity for the ternary complex, but the resulting ternary complex has a lower sensitivity to GTP, causing lower efficacy (shown in bold are the log EC_{50} values for each step). See also Figure S2.

receptor:agonist:$G_{\alpha s}$ ternary complex. Using equi-occupant ligand concentrations, with respect to $G_{\alpha S}$ recruitment (Figures 1C and 1D), we determined the susceptibility of the different ternary complexes, containing native G-protein, gamma subunit (G_{γ}):$G_{\alpha S}$: G-protein, beta subunit (G_{β}), to GTP by native-PAGE (Figures 2F and 2G). Both ligands were analyzed on the same gel, which revealed that, although there was no difference in the amount of G protein recruited (Figure 2G, E_{max} not significantly different), the hCT-occupied complex was disrupted by GTP at ~10-fold lower GTP concentration than for sCT-occupied complexes (Figures 2F and 2G). Thermodynamically, binding of GTP to disrupt the ternary complex must be the same if the target (G protein) conformation is the same. As this differs for the two ligand-occupied complexes upon equivalent levels of G protein recruitment, it is indicative of a ligand-specific conformational difference in the recruited G protein. To test this model, we used bioluminescent resonance energy transfer (BRET) to measure rearrangement between G_{γ}, N-terminally labeled with Venus (G_{γ}:Venus), and $G_{\alpha s}$ with Rluc8 inserted at position 72 ($G_{\alpha s}^{72}$:Rluc8) (Figure 3A). $G_{\alpha s}^{72}$:Rluc8 coupled to both CTR and adenylate cyclase with sCT or hCT potencies similar to wild-type $G_{\alpha s}$, when transfected into cells genetically engineered to lack $G_{\alpha s}$ (HEK293A $\Delta G_{\alpha s}$, see STAR Methods; Schrage et al., 2015; and Figure S3A) and responded to agonist stimulation in COS7 cells in live-cell BRET experiments (Figure S3C).

We performed BRET assays on washed membrane preparations in which the nucleotide concentration could be controlled. At high agonist concentrations (100 nM), we observed a rapid and sustained increase in BRET ratio (Figure 3B) with a greater magnitude apparent in the presence of sCT, consistent with a different conformational rearrangement of the G protein in the presence of sCT versus hCT. The release of G protein (and consequent rearrangement of the G_{α} and G_{γ} subunits) from agonist-receptor complex requires binding of GTP to the receptor-bound nucleotide-free G protein. The addition of 300 μM GTP caused a rapid decrease in BRET signal. This decrease in BRET could be reversed by addition of high concentrations of agonist (Figures 3C and S3B). We interpreted these ratio changes as a conformation shift from the apo to the nucleotide-bound form of the $G_{\gamma 2}$Venus:$G_{\alpha s}^{72}$Rluc8:$G_{\beta 1}$ hetero-trimer, consistent with previous reports of subunit rearrangement (Bünemann et al., 2003; Galés et al., 2006). Supporting this model of subunit rearrangement, subsequent agonist addition led to a BRET increase above that of vehicle (Figures 3C and S3B). The rate of change in BRET signal following addition of 100 nM ligand was significantly faster ($p < 0.0001$) for sCT compared to hCT (Figure 3D), which we believe to be driven principally by the rate of agonist binding. In contrast, at approximate EC_{50} concentrations, the rate of change in BRET was significantly faster for hCT compared to sCT ($p = 0.0007$) (Figure 3E). These data are inconsistent with a model in which increased efficacy is merely driven by increased transducer (i.e., G protein) affinity.

To further evaluate the differences in agonist-induced changes to G protein BRET, concentration-dependent time-course assays were performed (Figure S3D), and normalized area under curve (AUC) was used to plot concentration response curves (Figure 3F). The potency for driving conformational rearrangement was lower for hCT compared with sCT (Figure 3F), consistent with the lower potency of hCT to induce ternary complex formation by native PAGE (Figures 1C and 1D). The maxima of the agonist concentration response curves were also significantly different by AUC ($p < 0.0001$ Figure 3F) with hCT showing a lower maximum, supportive of different G protein hetero-trimer conformation in the agonist:receptor:G protein complex. The saturable and significant difference in the E_{max} for this signal is consistent with different receptor-bound G protein states for these agonists (see time courses in Figure S3D). This finding is in contrast to previous reports that activation of the same hetero-trimeric G protein complex by different receptors results in similar rearrangements (Galés et al., 2006). While the assay design should ensure full occupancy of the agonist receptor complex by G protein at saturating concentrations of ligand (e.g., Figure 2B), we directly tested whether there is an agonist-dependent difference in receptor-bound G protein conformation using in-gel FRET by native PAGE. HEK293A $\Delta G_{\alpha s}$ stably expressing CTR were transiently transfected with two different G protein FRET pairs using myristoylation-positive $G_{\alpha s}$, with the fluorescent protein inserted at position 72 and N-terminally tagged $G_{\gamma 2}$ ($^{Myr+}G_{\alpha s}^{72}$-mCherry:$G_{\gamma 2}$-Venus or $^{Myr+}G_{\alpha s}^{72}$-Venus:$G_{\gamma 2}$-mCherry) and used to prepare washed membranes. Using saturating ligand concentrations, the in-gel fluorescence of the receptor-bound G protein hetero-trimer (arrows, Figure 3H) was directly quantitated. Consistent with the native PAGE experiments in Figure 2, equivalent levels of G protein were recruited to the hCT- and sCT-induced complexes as determined by direct excitation of the acceptor ($G_{\alpha s}$-mCherry [circles] or $G_{\gamma 2}$-mCherry [squares]; Figure 3I). In contrast, a small and significant difference in FRET between the $G_{\alpha s}$ and $G_{\gamma 2}$ was observed between the agonist:receptor:G protein complexes with the hCT-bound complex exhibiting a lower FRET signal than the equivalent sCT-occupied complex (Figure 3J). This provides corroborating evidence of a difference in conformational rearrangement of the hetero-trimeric G protein in the sCT- versus hCT-occupied complexes.

To accommodate these data, the agonist-dependent receptor-bound G protein state needs to be more sensitive to GTP concentration for the more efficacious agonist, hCT, allowing for faster G protein turnover and more effective activation of adenylate cyclase. In a cellular context, GTP is present in the 200- to 400-μM range; we therefore performed BRET on extensively washed membranes containing G_{γ}:Venus/$G_{\alpha S}^{72}$Rluc8 pair with the addition of GTP prior to agonist stimulation (Figures 3G and S3E). We observed a significant reduction in EC_{50} for ligand-induced BRET for hCT in the presence of GTP, but not for sCT. This is consistent with a greater sensitivity of the hCT ternary complex to GTP in native PAGE (Figures 2F and 2G). Collectively, these data support that the hCT-occupied ternary complex has a different receptor-bound G protein conformation that is more sensitive to disruption by GTP.

To correlate the differences in GTP sensitivity from native PAGE (Figures 2F and 2G) and G protein BRET (Figure 3G) with the apparent conformational differences by BRET (e.g., Figure 3F) and in-gel FRET by Native PAGE (Figure 3J), we measured the rate of association of GTP to $G_{\alpha s}$ in pre-formed ternary complex. HEK293A $\Delta G_{\alpha s}$ stably expressing CTR were transiently transfected with $^{Myr+}G_{\alpha s}^{72}$-mCherry and used to

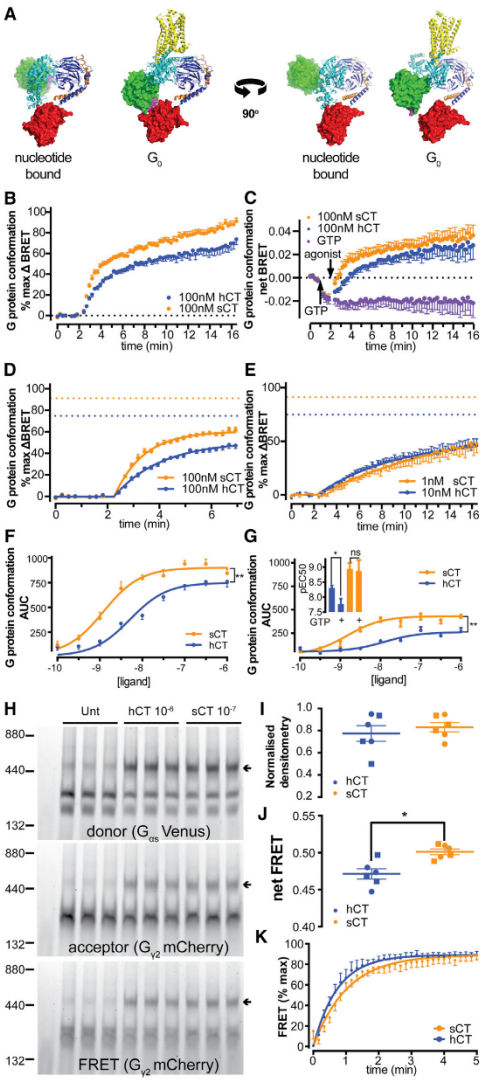

Figure 3. Agonist Promoted Changes in Hetrotrimeric G Protein Conformation

(A) A cartoon illustrating the change in relative position of the BRET donor and acceptor was generated in PyMOL using PDB structures for the β_2 adrenergic receptor (yellow) in complex with $G_{\alpha s}$ (cyan) β_1 (blue) γ_2 (orange) (PDB: 3SN6), GDP-bound conformation of $G_{\alpha s}$ (cyan) (PDB: 1AZT), Rluc8 (green) (PDB: 2SPSD), and eYFP (red) (PDB: 3V3D); residues 156–171 of the Rluc8 cap are colored magenta to highlight the rotation and translation Rluc8 must undergo to accommodate the opening of $G_{\alpha s}$.

prepare washed membranes. These were pre-incubated with saturating concentrations of either hCT or sCT before mixing with 30 nM of ATTO488-γ-(6-Aminohexyl)-GTP and the rate of association measured by FRET transfer between GTP and $G_{\alpha s}$. The fitted rate was significantly faster in the presence of hCT (Figure 3K).

In (B)–(G), each n was conducted with different plasma-membrane preparations from independent transfections and different drug dilutions on different days.

(B and C) COS-7 cells stably expressing CTR were transfected with $G_{\gamma 2}$:Venus/$G_{\alpha s}^{72}$:Rluc8/$G_{\beta 1}$ 16 hr before preparation of extensively washed, crude membranes. Membranes were equilibrated and baseline BRET measured for 1 min prior to addition of vehicle or 300 μM GTP and measured for another 45 s prior to addition of ligand (baseline BRET indicated by black dotted line). (B) Time course for ligand-induced change in BRET at 100 nM (n = 9, data are mean ± SEM). (C) Time course for ligand-induced change in BRET at 100 nM after the addition of 300 μM GTP (n = 4, data are mean ± SEM).

(D and E) Rate of change in BRET signal fitted to an exponential curve (the maximum sCT- and hCT-induced BRET signal is shown by orange and blue dotted lines, respectively), (D) 100 nM, $p < 0.0001$ for faster ΔBRET in the presence of sCT, and (E) 1 nM sCT c.f. 10 nM hCT, with hCT showing faster ΔBRET $p = 0.0007$.

(F and G) Normalized AUC for the indicated ligand concentrations is plotted as a concentration response curve. (F) The log EC_{50} values for ligand-induced changes in BRET are −8.30 ± 0.08 for hCT and −8.94 ± 0.08 for sCT (n = 9, F test, p value for different EC_{50} for ligand-induced change in BRET < 0.0001) with AUC top of 744 ± 24 for hCT and 900 ± 22 for hCT (n = 9 F test, *p value for different top for ligand-induced change in BRET < 0.0001, data are presented as mean ± SEM). (G) Log EC_{50} values for ligand-induced change in BRET in the presence of 300 μM GTP are −7.77 ± 0.17 for hCT and −8.87 ± 0.18 for sCT (n = 4, F test, p value for different EC_{50} for ligand-induced change in BRET = 0.0001), with an AUC top of 304 ± 19 for hCT and 472 ± 21 for sCT (n = 4, F test, *p value for different top for ligand-induced change in BRET <0.0001, data are mean ± SEM). GTP-induced change in pEC_{50} is shown in inset with a significant decrease for hCT (n = 4–9, t test, p value for different pEC_{50} in the absence of GTP = 0.0069) but no change for sCT (n = 4–9, t test, p value for different pEC_{50} in the absence of GTP = 0.68).

(H–J) Extensively washed plasma-membrane preparations from HEK293A $\Delta G_{\alpha s}$ cells (stably expressing CTR and transiently transfected with $G_{\gamma 2}$:Venus/$^{Myr+}G_{\alpha s}^{72}$:mCherry/$G_{\beta 1}$ (circles) OR $G_{\gamma 2}$:mCherry/$^{Myr+}G_{\alpha s}^{72}$:Venus/$G_{\beta 1}$ (squares) 36 hr before preparation) were either untreated or treated with (saturating) equi-occupant concentrations of hCT (1 μM) or sCT (100 nM) prior to solubilization and separation on a 6%–11% native page. The ternary complex was identified by direct in-gel fluorescence, and data are presented as individual determinations ±SEM with FRET swap shown in circles and squares and representative gel (from n = 6, each n conducted with triplicate lanes with different plasma-membrane preparations from independent transfections and different drug dilutions on different days) shown in (H). Quantified densitometry of the acceptor only channel is shown in (I), with no difference in densitometry between hCT- and sCT-induced G protein recruitment (n = 6, t test, *p value for different densitometry = 0.51). (J) Calculated net-FRET from quantified densitometry; 0.471 ± 0.007 for hCT and 0.501 ± 0.004 for sCT (n = 6, t test, *p value for different FRET = 0.0036).

(K) HEK293A $\Delta G_{\alpha s}$ cells stably expressing CTR were transiently transfected with $G_{\gamma 2}$ /$^{Myr+}G_{\alpha s}^{72}$:mCherry/$G_{\beta 1}$ 16 hr before preparation of extensively washed crude membranes. Membranes were pre-equilibrated with 1 μM of either hCT or SCT before the association of fluorescently labeled GTP (ATTO-488-γ-[6-Aminohexyl]-GTP) was measured by FRET. (K) Time course for increase in FRET signal upon mixing of membranes with 30 nM labeled GTP as mean ± SEM; the observed k for hCT is 1.35 ± 0.08 min^{-1} ($t_{1/2}$ ~0.51 min) and for sCT is 0.97 ± 0.05 min^{-1} ($t_{1/2}$ ~0.71 min) (n = 6, two independent transfections, six independent drug dilutions, F test, p value for different $k < 0.0001$).

See also Figure S3.

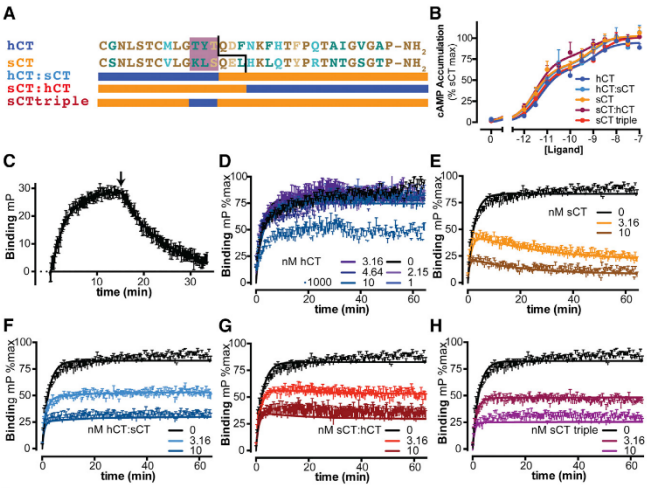

I

sCT8-32	hCT	sCT	hCT:sCT	sCT:hCT	sCT triple
6.6±0.3 mins	4.4±0.5 mins	41±2 mins	9.7±0.4 mins	16.3±0.9 mins	11.7±0.5 mins

Figure 4. Agonist Structural Determinants of Dissociation Rates

(A) Alignment of hCT and sCT; identical residues shown in brown, conserved in light brown, weakly conserved in light cyan and non-conserved in dark cyan. Cartoon illustrating the chimeric peptides used in this study is shown underneath.

(B) cAMP accumulation assay in COS-7 cells stably expressing CTR with cells stimulated for 30 min in the presence of IBMX with the indicated concentrations of hCT, sCT, and chimeric peptides. All agonist response curves are biphasic (F test, p better than 0.03 for all curves) and are best described by a common fit (F test, p = 0.762, n = 3, each n conducted in triplicate with different drug dilutions on different days, data are mean ± SEM) with shared log EC_{50} values of −11.4 ± 0.13 and −8.85 ± 0.23.

(C) Homogeneous association and dissociation of sCT8-32:AF568 by fluorescence polarization on membranes from COS-7 cells stably expressing CTR, $K_{on} = 1.91 \pm 0.19 \times 10^7\ M^{-1}\ min^{-1}$ and $K_{off} = 0.1043 \pm 0.005\ min^{-1}$ (n = 9, each n conducted with different plasma-membrane preparations and different drug dilutions on different days, K_d = 5.3 nM, consistent with equilibrium binding; Figures S1B and S1C) corresponding to a $t_{1/2}$ of 6.6 min.

(D–H) Homogenous kinetic competition between sCT-8-23:AF568 and indicated ligands by fluorescence polarization on membranes from COS-7 cells stably expressing CTR (hCT n = 8, all other peptides n = 6, data are mean ± SEM, each n conducted with different plasma-membrane preparations and different drug dilutions on different days).

(I) Calculated $t_{1/2}$ values for all ligands.

To exclude the possibility that these differences in apparent efficacy and G protein conformation were the result of kinetic effects due to the slow dissociation rate of sCT, chimeric peptides (Hilton et al., 2000), as shown in Figure 4A, were generated and tested. In cAMP accumulation assays, these chimeric peptides displayed concentration response curves that overlayed with those of the parental peptides (Figure 4B). Association and dissociation rates were determined using kinetic competition against a fluorescently labeled antagonist (Figure 4C). As expected, wild-type sCT had a very slow off rate (Andreassen et al., 2014; Hilton et al., 2000), with a $T_{1/2}$ of >40 min, whereas all chimeric peptides displayed significantly faster off rate kinetics (Figures 4D–4I), demonstrating that observed potencies in the cAMP assay are not correlated with peptide binding kinetics. The potency of ligands to cause changes in G protein conformation was then assessed by BRET assays, as described above (Figures 5A–5C). The hCT:sCT chimera, containing the amino terminal 13 amino acids of hCT and the last 19 amino acids of sCT, induced a maximal change in BRET (G protein conformational rearrangement) that was similar to that induced by hCT but significantly different from that induced by sCT. In contrast, the EC_{50} was similar to that of sCT (Figure 5D). These data are consistent with the peptide amino terminus driving receptor activation, while the affinity for the complex is driven by interactions of the peptide C terminus with the receptor extracellular domain (Wootten et al., 2016). Similarly, the sCT(1-16):hCT(17-32) chimera, elicited a maximal change in BRET equivalent to that of sCT, and significantly different to that of hCT, while the EC_{50} of the response was intermediate between that of sCT and hCT (Figure 5E). Finally the sCT triple chimera, containing three amino acids from the central portion of hCT, promoted a conformational rearrangement yielding a potency and maximal effect similar to those of sCT (Figure 5F) in spite of its significantly faster off rate (c.f. Figures 4E with 4H). Collectively, these data demonstrate that cellular efficacy results from a complex interplay between G protein recruitment affinity and the subsequent G protein conformation in the ternary complex, and that this is independent of ligand dissociation rates.

CT Ligands Differentially Stabilize Receptor-G Protein Complexes at the Cell Surface

To accommodate the equivalent cellular potency of the lower-affinity agonist, hCT, with the higher-affinity agonist sCT, and taking into account the difference in GTP binding, we reasoned that the turnover of G protein at the hCT-bound receptor would be faster than that at the sCT-bound receptor. We therefore imaged fluorescent G protein mobility at the apical surface by total internal reflection (TIRF) microscopy as depicted schematically in Figure S4. Using a fluorescently tagged sCT analog, we established that the mobility of agonist-bound CTR is limited (data not shown) at the timescale of tens-to-hundreds of milliseconds (at 20°C). We observed two distinct, mutually exclusive, distributions of fluorescently tagged G proteins (both $G_{\alpha s}$ and $G_{\gamma 2}$), either rapidly mobile G proteins with latency in the

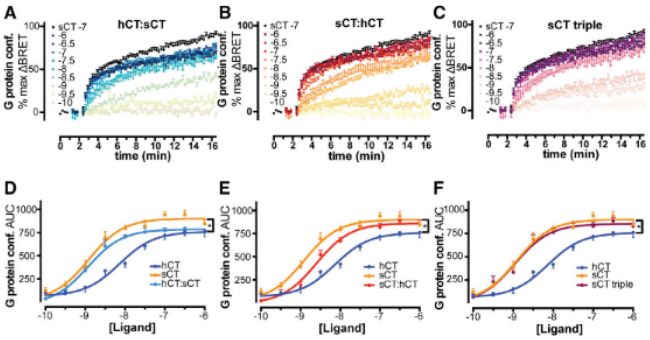

Figure 5. Agonist Structural Determinants of Differential Effects on Heterotrimeric G Protein Conformation

(A–C) Full kinetic responses, using washed, crude membranes, at all concentrations tested of hCT:sCT chimera (A), sCT:hCT (B), and sCT triple mutant (C) (all data are n = 4, each n conducted in triplicate with different plasma-membrane preparations from independent transfections and different drug dilutions on different days and are shown as mean ± SEM; sCT maximum response curve is in black).

(D–F) The normalized AUC for the indicated ligand concentrations is plotted as a concentration response curve and shown as mean ± SEM (D) the log EC_{50} for hCT:sCT-induced changes in BRET is −8.89 ± 0.05 (n = 4, F test, p value for different EC_{50} c.f. hCT < 0.001 and sCT = 0.667) with AUC top of 785 ± 15 (n = 4, F test, p value for different top c.f. hCT = 0.187 and sCT = 0.0006). (E) The log EC_{50} for sCT:hCT-induced changes in BRET is −8.59 ± 0.05 (n = 4, F test, p value for different EC_{50} c.f. hCT = 0.0111 and sCT = 0.0007) with AUC top of 864 ± 18 (n = 4, F test, p value for different top c.f. hCT = 0.0008 and sCT = 0.288). (F) The log EC_{50} for sCT triple-induced changes in BRET is −8.95 ± 0.06 (n = 4, F test, p value for different EC_{50} c.f. hCT < 0.0001 and sCT = 0.856) with AUC top of 854 ± 20 (n = 4, F test, p value for different top c.f. hCT = 0.0019 and sCT = 0.166).

evanescent field on the tens of millisecond timescale or those that remained essentially immobile over timescales in the minutes (at 20°C). Cells transiently overexpressing $G_{\gamma2}$Venus and native $G_{\alpha s}$ and exhibiting rapid G protein mobility (Movie S1) were imaged. The latency of individual $G_{\gamma2}$Venus events in the evanescent field was extracted prior to and after stimulation with saturating concentrations of agonist and fitted to an exponential decay curve. Both ligands increased the half-life of $G_{\gamma2}$ Venus at the plasma membrane, with a significantly longer (p = 0.005) half-life in the presence of sCT (24.1 ± 1.2 versus 20.8 ± 1.1 ms for hCT and 17.9 ± 0.5 ms for unstimulated at 20°C, n = 3, Figure 6A). This is consistent with proportionately faster G protein turnover in response to hCT versus sCT. To confirm this, we also visualized the $G_{\alpha s}$ subunit; the biological activity of $G_{\alpha s}{}^{72}$mCherry was confirmed by transient transfection into cells genetically engineered to lack $G_{\alpha s}$ (see STAR Methods; Schrage et al., 2015; and Figure S5A). Cells transiently overexpressing $G_{\gamma2}$:$G_{\alpha s}{}^{72}$mCherry:$G_{\beta1}$ and exhibiting rapid G protein mobility (Movie S2) were imaged. Only sCT produced a significant increase in the latency of individual $G_{\alpha s}{}^{72}$mCherry events in the evanescent field over vehicle (p < 0.0001) (Figure 6A and representative 3D histograms from a small subset of data in Figure 6B). This slower G protein mobility suggests slower GTP turnover and therefore that the GTP binding step is rate limiting when sCT is bound at the receptor. These data are consistent with native PAGE, in which hCT shows greater GTP sensitivity (Figures 2F and 2G), and the GTP induced change in G protein BRET EC_{50} for hCT and not sCT (Figures 3F and 3G). Importantly, they further support a model in which hCT promotes a receptor-bound G protein conformation that is less open than the sCT conformation. This results in faster GTP binding and more rapid G protein turnover (Figure 6C), potentially allowing more rapid signaling.

CT Ligands Display Differential cAMP Production Rates in Live Cells

To test the latter prediction, we used a cAMP biosensor to measure the rates at which cAMP accumulates in response to these ligands. At saturating concentrations, we saw no difference in the rate or magnitude of cAMP accumulation (Figure 7A, p = 0.215), but at 10 pM we observed a significantly faster (p = 0.018) accumulation of cAMP in response to hCT compared with sCT (Figure 7B). This was confirmed in a cell line that endogenously expresses CTR (Figures 7C and 7D) and supports our model (Figure 6C) in which the hCT-occupied CTR is capable of promoting more G protein activation per time compared with the sCT-occupied receptor.

DISCUSSION

Differential efficacy at GPCRs has already been exploited clinically with the use of partial agonists, for example, at adrenergic and opioid receptors (Cowan, 2003; Lipworth and Grove, 1997). In spite of this, and the emergence of biased agonism as another means to tailor the clinical efficacy of drugs, there are few data that address the underlying molecular basis of differential efficacy. There is now a broad appreciation that different ligands acting at a single GPCR can alter the sampling of the conformational landscape explored by the GPCR (Deupi and Kobilka, 2010; Kim et al., 2013; Mary et al., 2012; Nygaard et al., 2013; Wacker et al., 2013; Wootten et al., 2013). In general, it is thought that the consequence of ligand-dependent conformational selection is to alter the affinity of the receptor for particular transducers and thus alter signaling efficacy and/or bias. Although distinct G protein conformations linked to individual receptor complexes have been alluded to (Seifert et al., 1999, 2001), collectively, our work provides evidence of *ligand*-dependent ternary complexes controlling guanine nucleotide exchange, via promotion of distinct changes in G protein conformation. We were able to show that binding of the high-affinity ligand, sCT, results in a ternary complex that has a lower tendency to dissociate in the presence of GTP. This is analogous to the concept that a G protein that has disproportionately high affinity for a GPCR can act in a physiologically and/or clinically relevant, "dominant-negative" fashion (Berlot, 2002; Grishina and Berlot,

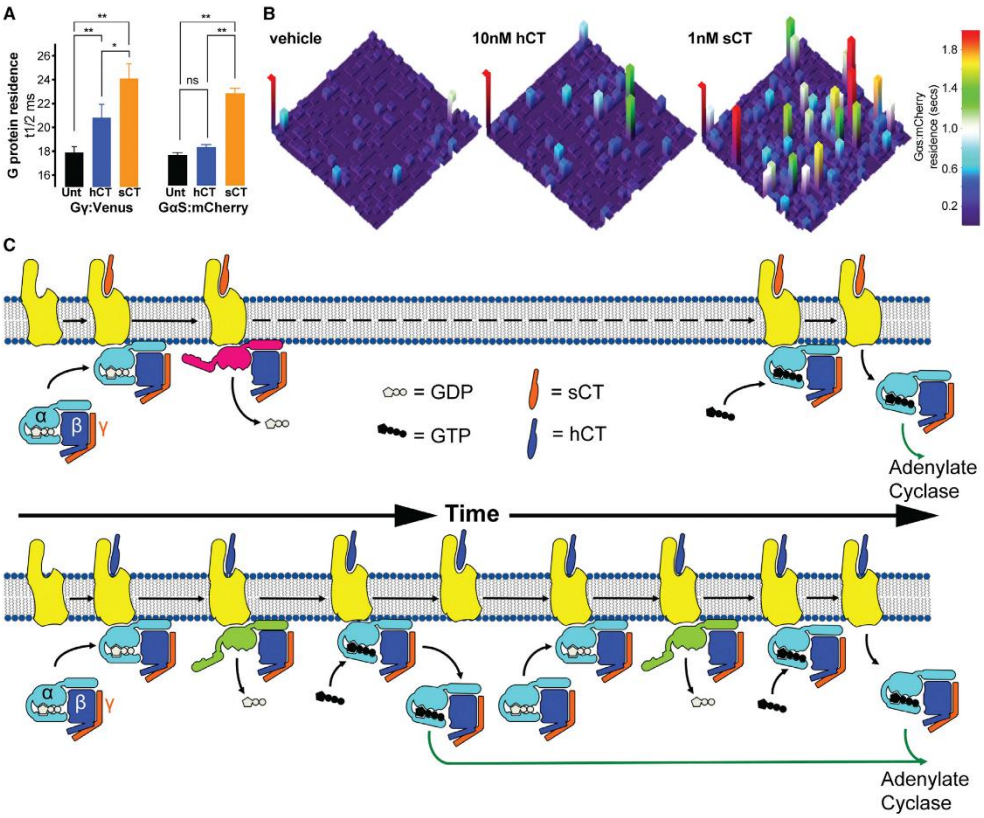

Figure 6. Agonist-Promoted G Protein Residency in Live Cells

(A) COS-7 cells stably expressing CTR were transfected with either $G_{\gamma 2}$:Venus or $G_{\gamma 2}/G_{\alpha s}^{72}$:mCherry/$G_{\beta 1}$ 16 hr before assay. Ligand-induced changes in $G_{\gamma 2}$ or $G_{\alpha s}^{72}$:mCherry residence were measured on live cells under TIRF at 33 or 40 frames/second with the addition of equi-occupant concentrations of sCT (1 nM) and hCT (10 nM) after 2 min of baseline data collection at 20°C. For $G_{\gamma 2}$:Venus residency three independent experiments were performed with three to five different cell areas imaged with at least 3,000 spots of two or more frames per ligand per experiment (total of 11 cells per ligand). Spot sizes were not significantly different between hCT- and sCT-treated cells. For $G_{\alpha s}^{72}$:mCherry residency, four independent experiments were performed with three different cell areas imaged with at least 3,000 spots of two or more frames per ligand per experiment (total of 12 cells per ligand). G protein latency in the TIRF field was fitted to an exponential decay curve and derived half-lives plotted (mean ± SEM p value for difference between unstimulated and ligand-induced decay rate of $G_{\gamma 2}$:Venus <0.0001 (**) and for difference between sCT and hCT = 0.0046 (*), one-way ANOVA (n = 3, unstimulated k = 38.3 ± 1.1, hCT k = 33.0 ± 1.9 and sCT k = 28.5 ± 0.6), p value for difference between unstimulated sCT decay rate of $G_{\alpha s}^{72}$:mCherry < 0.0001 (**) no significant difference between unstimulated and hCT (ns), one-way ANOVA (n = 4, unstimulated k = 39.2 ± 0.5, hCT k = 38.3 ± 0.5 and sCT k = 30.7 ± 0.6).

(B) The residence time of 625 representative spots (of >10,000 of two or more frames) was plotted in 2D with the length of residence plotted in the z dimension (as shown on scale).

(C) Cartoon indicating the relative efficacy of sCT (orange) compared with hCT (blue) in which the rate-limiting step for agonist-induced G protein activation is GTP association to the receptor-bound G protein complex. The rate at which this occurs is faster in the presence of hCT allowing for quantitatively more G protein and adenylate cyclase activation per unit time in spite of lower receptor occupancy.

See also Figure S4 and Movies S1 and S2.

2000; Iiri et al., 1994, 1999). We therefore argue that, as different ligands acting at the same receptor engender differences in the sampling of conformational space by the receptor, this differential sampling extends to the heterotrimeric G protein bound in the ternary complex. Distinct, ligand-dependent conformations of transducer proteins has recently been proposed for arrestins and may control secondary signaling from these key scaffolding proteins (Lee et al., 2016; Nuber et al., 2016). Since the prime,

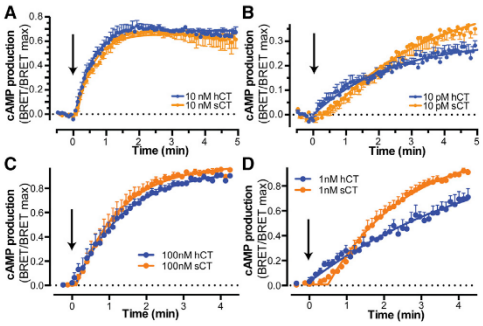

Figure 7. Agonist-Promoted Rates of cAMP Accumulation in Live Cells

(A and B) Rate of increase of intracellular cAMP as measured by a BRET cAMP sensor (CAMYEL) in COS-7 cells transiently transfected with CTR. cAMP formation data were fitted using an exponential one phase model with the rate of production in response to 10 pM hCT being significantly faster than 10 pM sCT (B) (F test, $p = 0.018$), whereas no statistical difference in formation rate was seen at 10 nM (A) (F test, $p = 0.215$, $n = 4$, each n conducted in triplicate from independent transfections and different drug dilutions on different days; data are mean ± SEM).

(C and D) Rate of increase of intracellular cAMP as measured by a BRET cAMP sensor (CAMYEL) in CHO-K1 cells expressing endogenous CTR. cAMP formation data were fitted using an exponential one phase model with the onset of production in response to 1 nM hCT being significantly faster than 1 nM sCT (D) (F test, $p < 0.0001$), whereas no statistical difference in formation rate was seen at 100 nM (C) (F test, $p = 0.0687$, $n = 3$, each n conducted in triplicate on separate days with separate drug dilutions; data are mean ± SEM).

See also Figure S5.

orthodox, role of a ligand-bound GPCR is to accelerate the rate of nucleotide exchange at G_{α}, we would argue that there is a fine balance between the affinity that the ligand-bound receptor has for its cognate G protein and its ability to release this G protein once nucleotide exchange has occurred. Indeed, for GPCRs that possess more than one endogenous agonist, this could provide another means by which their different physiological effects are engendered. Moreover, it provides an additional mechanism through which biased agonism, at the level of the G protein, can occur. Our work thus extends the understanding of the molecular basis of G protein-dependent efficacy.

STAR★METHODS

Detailed methods are provided in the online version of this paper and include the following:

- KEY RESOURCES TABLE
- CONTACT FOR REAGENT AND RESOURCE SHARING
- EXPERIMENTAL MODEL AND SUBJECT DETAILS
  - Cell Lines
- METHOD DETAILS
  - Fluorescently labeled peptides
  - Cell Culture
  - CTR and G protein expression and purification from insect cells
  - cAMP accumulation assay
  - Competition fluorescent binding assay
  - Kinetic ligand binding
  - Membrane preparations
  - Native PAGE
  - G protein BRET
  - GTP association
  - G protein residency
  - Modeling G protein rearrangement
  - BRET CAMYEL assay
- QUANTIFICATION AND STATISTICAL ANALYSIS
  - cAMP accumulation assay analysis
  - Ligand binding analysis
  - Analysis of Native PAGE
  - G protein BRET analysis
  - GTP association analysis
  - G protein residency analysis
- DATA AND SOFTWARE AVAILABILITY
  - TIRF residency script
  - In gel FRET quantitation script

SUPPLEMENTAL INFORMATION

Supplemental Information includes five figures and two movies and can be found with this article online at http://dx.doi.org/10.1016/j.cell.2016.09.021.

A video abstract is available at http://dx.doi.org/10.1016/j.cell.2016.09.021#mmc3.

AUTHOR CONTRIBUTIONS

Conceptualization, S.G.B.F. and P.M.S.; Methodology, S.G.B.F.; Software, C.J.N.; Formal Analysis, S.G.B.F. and C.J.N.; Investigation, S.G.B.F., L.L., M.L.H., D.W., and E.D.M.; Resources, P.J.W.; Writing – Original Draft, S.G.B.F.; Writing – Review & Editing, P.J.W., C.J.N., D.W., A.C., and P.M.S.; Visualization, S.G.B.F. and P.M.S.; Supervision, P.M.S. and S.G.B.F.; Funding Acquisition, P.M.S. and A.C.

ACKNOWLEDGMENTS

This work was funded by National Health and Medical Research Council (NHMRC) Project Grant APP1061044 and NHMRC Program Grant APP1055134. P.M.S. is an NHMRC Principal Research Fellow and A.C. an NHMRC Senior Principal Research Fellow. M.L.H. is a NHMRC RD Wright Fellow (1061687). D.W. is an NHMRC Career Development Fellow. A.I. was funded by JST, PRESTO. We thank N.A. Lambert for the constructs encoding $G_{\alpha s}^{72}$:RLuc8 and $G_{\alpha s}^{72}$:mCherry and for critiquing the manuscript. We thank B.K. Kobilka for the construct encoding Nb35 and for advice on expression and purification of the CTR ternary complex from insect cells. We thank P. Zhao and J.R. Lane for discussions. We also thank J.B. Furness and M.L. Whitelaw for critiquing the manuscript.

Received: June 14, 2016
Revised: July 28, 2016
Accepted: September 8, 2016
Published: October 6, 2016

REFERENCES

Andreassen, K.V., Hjuler, S.T., Furness, S.G., Sexton, P.M., Christopoulos, A., Nosjean, O., Karsdal, M.A., and Henriksen, K. (2014). Prolonged calcitonin

receptor signaling by salmon, but not human calcitonin, reveals ligand bias. PLoS ONE *9*, e92042.

Berlot, C.H. (2002). A highly effective dominant negative alpha s construct containing mutations that affect distinct functions inhibits multiple Gs-coupled receptor signaling pathways. J. Biol. Chem. *277*, 21080–21085.

Brodde, O.E., Hardung, A., Ebel, H., and Bock, K.D. (1982). GTP regulates binding of agonists to alpha 2-adrenergic receptors in human platelets. Arch. Int. Pharmacodyn. Ther. *258*, 193–207.

Bünemann, M., Frank, M., and Lohse, M.J. (2003). Gi protein activation in intact cells involves subunit rearrangement rather than dissociation. Proc. Natl. Acad. Sci. USA *100*, 16077–16082.

Clarke, M.V., Russell, P.K., Findlay, D.M., Sastra, S., Anderson, P.H., Skinner, J.P., Atkins, G.J., Zajac, J.D., and Davey, R.A. (2015). A role for the calcitonin receptor to limit bone loss during lactation in female mice by inhibiting osteocytic osteolysis. Endocrinology *156*, 3203–3214.

Cowan, A. (2003). Buprenorphine: New pharmacological aspects. Int. J. Clin. Pract. Suppl., 3–8, discussion, 23–24.

Davey, R.A., and Findlay, D.M. (2013). Calcitonin: Physiology or fantasy? J. Bone Miner. Res. *28*, 973–979.

Deupi, X., and Kobilka, B.K. (2010). Energy landscapes as a tool to integrate GPCR structure, dynamics, and function. Physiology (Bethesda) *25*, 293–303.

DeVree, B.T., Mahoney, J.P., Vélez-Ruiz, G.A., Rasmussen, S.G.F., Kuszak, A.J., Edwald, E., Fung, J.J., Manglik, A., Masureel, M., Du, Y., et al. (2016). Allosteric coupling from G protein to the agonist-binding pocket in GPCRs. Nature *535*, 182–186.

Di Salvo, J., Koch, G.E., Johnson, K.E., Blake, A.D., Daugherty, B.L., DeMartino, J.A., Sirotina-Meisher, A., Liu, Y., Springer, M.S., Cascieri, M.A., and Sullivan, K.A. (2000). The CXCR4 agonist ligand stromal derived factor-1 maintains high affinity for receptors in both Galpha(i)-coupled and uncoupled states. Eur. J. Pharmacol. *409*, 143–154.

Fredriksson, R., Lagerström, M.C., Lundin, L.-G., and Schiöth, H.B. (2003). The G-protein-coupled receptors in the human genome form five main families. Phylogenetic analysis, paralogon groups, and fingerprints. Mol. Pharmacol. *63*, 1256–1272.

Galés, C., Van Durm, J.J.J., Schaak, S., Pontier, S., Percherancier, Y., Audet, M., Paris, H., and Bouvier, M. (2006). Probing the activation-promoted structural rearrangements in preassembled receptor-G protein complexes. Nat. Struct. Mol. Biol. *13*, 778–786.

Goricanec, D., Stehle, R., Egloff, P., Grigoriu, S., Plückthun, A., Wagner, G., and Hagn, F. (2016). Conformational dynamics of a G-protein α subunit is tightly regulated by nucleotide binding. Proc. Natl. Acad. Sci. USA *113*, E3629–E3638.

Grishina, G., and Berlot, C.H. (2000). A surface-exposed region of G(salpha) in which substitutions decrease receptor-mediated activation and increase receptor affinity. Mol. Pharmacol. *57*, 1081–1092.

Hilton, J.M., Dowton, M., Houssami, S., and Sexton, P.M. (2000). Identification of key components in the irreversibility of salmon calcitonin binding to calcitonin receptors. J. Endocrinol. *166*, 213–226.

Hobbs, S., Jitrapakdee, S., and Wallace, J.C. (1998). Development of a bicistronic vector driven by the human polypeptide chain elongation factor 1alpha promoter for creation of stable mammalian cell lines that express very high levels of recombinant proteins. Biochem. Biophys. Res. Commun. *252*, 368–372.

Huang, J., Chen, S., Zhang, J.J., and Huang, X.-Y. (2013). Crystal structure of oligomeric β1-adrenergic G protein-coupled receptors in ligand-free basal state. Nat. Struct. Mol. Biol. *20*, 419–425.

Iiri, T., Herzmark, P., Nakamoto, J.M., van Dop, C., and Bourne, H.R. (1994). Rapid GDP release from Gs alpha in patients with gain and loss of endocrine function. Nature *371*, 164–168.

Iiri, T., Bell, S.M., Baranski, T.J., Fujita, T., and Bourne, H.R. (1999). A Gsalpha mutant designed to inhibit receptor signaling through Gs. Proc. Natl. Acad. Sci. USA *96*, 499–504.

Jiang, L.I., Collins, J., Davis, R., Lin, K.-M., DeCamp, D., Roach, T., Hsueh, R., Rebres, R.A., Ross, E.M., Taussig, R., et al. (2007). Use of a cAMP BRET sensor to characterize a novel regulation of cAMP by the sphingosine 1-phosphate/G13 pathway. J. Biol. Chem. *282*, 10576–10584.

Kellar, K.J., Martino, A.M., Hall, D.P., Jr., Schwartz, R.D., and Taylor, R.L. (1985). High-affinity binding of [3H]acetylcholine to muscarinic cholinergic receptors. J. Neurosci. *5*, 1577–1582.

Kenakin, T. (2002). Drug efficacy at G protein-coupled receptors. Annu. Rev. Pharmacol. Toxicol. *42*, 349–379.

Kenakin, T., and Christopoulos, A. (2013). Signalling bias in new drug discovery: Detection, quantification and therapeutic impact. Nat. Rev. Drug Discov. *12*, 205–216.

Kim, T.H., Chung, K.Y., Manglik, A., Hansen, A.L., Dror, R.O., Mildorf, T.J., Shaw, D.E., Kobilka, B.K., and Prosser, R.S. (2013). The role of ligands on the equilibria between functional states of a G protein-coupled receptor. J. Am. Chem. Soc. *135*, 9465–9474.

Kuestner, R.E., Elrod, R.D., Grant, F.J., Hagen, F.S., Kuijper, J.L., Matthewes, S.L., O'Hara, P.J., Sheppard, P.O., Stroop, S.D., Thompson, D.L., et al. (1994). Cloning and characterization of an abundant subtype of the human calcitonin receptor. Mol. Pharmacol. *46*, 246–255.

Lee, M.-H., Appleton, K.M., Strungs, E.G., Kwon, J.Y., Morinelli, T.A., Peterson, Y.K., Laporte, S.A., and Luttrell, L.M. (2016). The conformational signature of β-arrestin2 predicts its trafficking and signalling functions. Nature *531*, 665–668.

Lipworth, B.J., and Grove, A. (1997). Evaluation of partial beta-adrenoceptor agonist activity. Br. J. Clin. Pharmacol. *43*, 9–14.

Liu, J.J., Horst, R., Katritch, V., Stevens, R.C., and Wüthrich, K. (2012). Biased signaling pathways in β2-adrenergic receptor characterized by 19F-NMR. Science *335*, 1106–1110.

Mary, S., Damian, M., Louet, M., Floquet, N., Fehrentz, J.-A., Marie, J., Martinez, J., and Banères, J.-L. (2012). Ligands and signaling proteins govern the conformational landscape explored by a G protein-coupled receptor. Proc. Natl. Acad. Sci. USA *109*, 8304–8309.

Motulsky, H.J., and Mahan, L.C. (1984). The kinetics of competitive radioligand binding predicted by the law of mass action. Mol. Pharmacol. *25*, 1–9.

Nag, K., Kato, A., Sultana, N., Ogoshi, M., Takei, Y., and Hirose, S. (2007). Fish calcitonin receptor has novel features. Gen. Comp. Endocrinol. *154*, 48–58.

Nikolaev, V.O., Hoffmann, C., Bünemann, M., Lohse, M.J., and Vilardaga, J.-P. (2006). Molecular basis of partial agonism at the neurotransmitter alpha2A-adrenergic receptor and Gi-protein heterotrimer. J. Biol. Chem. *281*, 24506–24511.

Nuber, S., Zabel, U., Lorenz, K., Nuber, A., Milligan, G., Tobin, A.B., Lohse, M.J., and Hoffmann, C. (2016). β-Arrestin biosensors reveal a rapid, receptor-dependent activation/deactivation cycle. Nature *531*, 661–664.

Nygaard, R., Zou, Y., Dror, R.O., Mildorf, T.J., Arlow, D.H., Manglik, A., Pan, A.C., Liu, C.W., Fung, J.J., Bokoch, M.P., et al. (2013). The dynamic process of β(2)-adrenergic receptor activation. Cell *152*, 532–542.

Schindelin, J., Arganda-Carreras, I., Frise, E., Kaynig, V., Longair, M., Pietzsch, T., Preibisch, S., Rueden, C., Saalfeld, S., Schmid, B., et al. (2012). Fiji: An open-source platform for biological-image analysis. Nat. Methods *9*, 676–682.

Schrage, R., Schmitz, A.-L., Gaffal, E., Annala, S., Kehraus, S., Wenzel, D., Büllesbach, K.M., Bald, T., Inoue, A., Shinjo, Y., et al. (2015). The experimental power of FR900359 to study Gq-regulated biological processes. Nat. Commun. *6*, 10156.

Seifert, R., Gether, U., Wenzel-Seifert, K., and Kobilka, B.K. (1999). Effects of guanine, inosine, and xanthine nucleotides on β(2)-adrenergic receptor/G(s) interactions: Evidence for multiple receptor conformations. Mol. Pharmacol. *56*, 348–358.

Seifert, R., Wenzel-Seifert, K., Gether, U., and Kobilka, B.K. (2001). Functional differences between full and partial agonists: Evidence for ligand-specific receptor conformations. J. Pharmacol. Exp. Ther. *297*, 1218–1226.

Selander, K.S., Härkönen, P.L., Valve, E., Mönkkönen, J., Hannuniemi, R., and Väänänen, H.K. (1996). Calcitonin promotes osteoclast survival in vitro. Mol. Cell. Endocrinol. *122*, 119–129.

Venkatanarayan, A., Raulji, P., Norton, W., Chakravarti, D., Coarfa, C., Su, X., Sandur, S.K., Ramirez, M.S., Lee, J., Kingsley, C.V., et al. (2015). IAPP-driven metabolic reprogramming induces regression of p53-deficient tumours in vivo. Nature *517*, 626–630.

Verzijl, D., Storelli, S., Scholten, D.J., Bosch, L., Reinhart, T.A., Streblow, D.N., Tensen, C.P., Fitzsimons, C.P., Zaman, G.J.R., Pease, J.E., et al. (2008). Noncompetitive antagonism and inverse agonism as mechanism of action of nonpeptidergic antagonists at primate and rodent CXCR3 chemokine receptors. J. Pharmacol. Exp. Ther. *325*, 544–555.

Wacker, D., Wang, C., Katritch, V., Han, G.W., Huang, X.-P., Vardy, E., McCorvy, J.D., Jiang, Y., Chu, M., Siu, F.Y., et al. (2013). Structural features for functional selectivity at serotonin receptors. Science *340*, 615–619.

Wittig, I., Braun, H.-P., and Schägger, H. (2006). Blue native PAGE. Nat. Protoc. *1*, 418–428.

Wittig, I., Karas, M., and Schägger, H. (2007). High resolution clear native electrophoresis for in-gel functional assays and fluorescence studies of membrane protein complexes. Mol. Cell. Proteomics *6*, 1215–1225.

Wookey, P.J., McLean, C.A., Hwang, P., Furness, S.G.B., Nguyen, S., Kourakis, A., Hare, D.L., and Rosenfeld, J.V. (2012). The expression of calcitonin receptor detected in malignant cells of the brain tumour glioblastoma multiforme and functional properties in the cell line A172. Histopathology *60*, 895–910.

Wootten, D., Simms, J., Miller, L.J., Christopoulos, A., and Sexton, P.M. (2013). Polar transmembrane interactions drive formation of ligand-specific and signal pathway-biased family B G protein-coupled receptor conformations. Proc. Natl. Acad. Sci. USA *110*, 5211–5216.

Wootten, D., Miller, L.J., Koole, C., Christopoulos, A., and Sexton, P.M. (2016). Allostery and biased agonism at class B G protein-coupled receptors. Chem. Rev. Published online April 4, 2016. http://dx.doi.org/10.1021/acs.chemrev.6b00049.

Yamaguchi, M., Watanabe, Y., Ohtani, T., Uezumi, A., Mikami, N., Nakamura, M., Sato, T., Ikawa, M., Hoshino, M., Tsuchida, K., et al. (2015). Calcitonin receptor signaling inhibits muscle stem cells from escaping the quiescent state and the niche. Cell Rep. *13*, 302–314.